

**Series: Mechanics of Space Flight**

NASA  
TT  
F-429  
e.1

**V.V. Beletskii** LOAN COPY: RETURN TO  
AFWL (WLIL-2)  
KIRTLAND AFB, N MEX

# MOTION OF AN ARTIFICIAL SATELLITE ABOUT ITS CENTER OF MASS

TECH LIBRARY KAFB, NM



0068786

## **TRANSLATED FROM RUSSIAN**



Published for the National Aeronautics and Space Administration U.S.A.

and the National Science Foundation, Washington, D.C.

by the Israel Program for Scientific Translations

TECH LIBRARY KAFB, NM



0068786

Series: *Mechanics of Space Flight*

V. V. BELETSKII

# Motion of an Artificial Satellite About Its Center of Mass

(Dvizhenie iskusstvennogo sputnika otnositel no tsentra mass)

Izdatel'stvo Nauka  
Glavnaya Redaktsiya  
Fiziko-Matematicheskoi  
Literatury  
Moskva 1965

Translated from Russian

Israel Program for Scientific Translations  
Jerusalem 1966

NASA TT F-429  
TT 67-51366

Published Pursuant to an Agreement with  
THE NATIONAL AERONAUTICS AND SPACE ADMINISTRATION, U.S.A.  
and  
THE NATIONAL SCIENCE FOUNDATION, WASHINGTON, D.C.

Copyright © 1966  
Israel Program for Scientific Translations Ltd.  
IPST Cat. No. 1815

Translated by Z. Lerman

Printed in Jerusalem by S. Monson  
Binding: Wiener Bindery Ltd., Jerusalem

Price: \$ 6.00

Available from the  
U.S. DEPARTMENT OF COMMERCE  
Clearinghouse for Federal Scientific and Technical Information  
Springfield, Va. 22151

## TABLE OF CONTENTS

PREFACE . . . . .	v
INTRODUCTION . . . . .	vi
CHAPTER 1. ANALYSIS OF TORQUES ON A SATELLITE . . . . .	1
§ 1. Systems of coordinates. Preliminary analysis of a rigid body in a Newtonian force field . . . . .	1
§ 2. Torques on an arbitrary rigid body in a Newtonian force field . . . . .	9
§ 3. Aerodynamic torques and their approximations . . . . .	13
§ 4. Torques produced by the magnetic field . . . . .	19
§ 5. Solar radiation torques and their approximations . . . . .	23
§ 6. Estimating the relative influence of the various torques . . . . .	26
CHAPTER 2. STABILIZATION AND LIBRATION OF THE SATELLITE IN A NEWTONIAN FORCE FIELD . . . . .	28
§ 1 The equations of motion of a satellite around its mass center in the limited problem. Jacobi integral. Stable relative equilibrium . . . . .	28
§ 2. Plane oscillations in a circular orbit . . . . .	32
§ 3. Plane oscillations of a satellite in an elliptical orbit. Nonlinear and linear equations. Preliminary analysis . . . . .	37
§ 4. Eccentricity oscillations . . . . .	39
§ 5. Small plane oscillations in an elliptical orbit with a small eccentricity . . . . .	41
§ 6. Some nonlinear oscillations in a slightly elliptical orbit . . . . .	43
§ 7. Nonlinear plane oscillations in an elliptical orbit . . . . .	48
§ 8. Small space oscillations of a satellite about a position of relative equilibrium in a circular orbit . . . . .	58
§ 9. Small space oscillations in an elliptical orbit . . . . .	64
§ 10. Gravity attitude stabilization of artificial satellites . . . . .	66
CHAPTER 3. ADDITIONAL FACTORS INFLUENCING STABILIZATION AND LIBRATION OF A SATELLITE . . . . .	70
§ 1. The influence of aerodynamic torques on stabilization and libration of a satellite . . . . .	70
§ 2. The influence of the Earth's flattening on the libration of a satellite in a field of gravity . . . . .	77
§ 3. Magnetic attitude stabilization. Passive attitude stabilization to the Sun . . . . .	82
CHAPTER 4. THE RELATIONS BETWEEN TRANSLATIONAL AND ROTATIONAL MOTIONS OF A RIGID BODY IN A NEWTONIAN FORCE FIELD . . . . .	85
§ 1. Equations of motion and their first integrals . . . . .	85
§ 2. Particular solution of the equations of motion – relative equilibrium . . . . .	87
§ 3. On bodies satisfying the conditions of existence of relative equilibrium . . . . .	90
§ 4. Stability of relative equilibrium . . . . .	93
§ 5. Analysis of the conditions of stability of relative equilibrium . . . . .	96
§ 6. One particular case of translational–rotational motion . . . . .	102
CHAPTER 5. PERTURBED ROTATIONAL MOTION OF A SATELLITE AND EQUATIONS IN OSCULATING ELEMENTS . . . . .	105
§ 1. Perturbed rotational motion and a method of its analysis . . . . .	105
§ 2. Some probability characteristics of unperturbed motion . . . . .	106
§ 3. Perturbed motion. Equations in osculating elements . . . . .	108
§ 4. The case of perturbations having a force function . . . . .	110
§ 5. Equations for a dynamically asymmetric body . . . . .	114

CHAPTER 6. GRAVITATIONAL PERTURBATIONS IN ROTATIONAL MOTION . . . . .	116
§ 1. Permitted and forbidden motions of a dynamically symmetric satellite. Regular precessions in a gravitational field . . . . .	116
§ 2. Secular gravitational perturbations . . . . .	127
§ 3. General properties of motion . . . . .	129
§ 4. The case of a circular orbit. Preliminary analysis . . . . .	131
§ 5. The case of a circular orbit. Integration of the equations of motion . . . . .	132
§ 6. The case of an elliptical orbit . . . . .	134
§ 7. Gravitational perturbations on a satellite with a triaxial ellipsoid of inertia /71/. . . . .	138
CHAPTER 7. AERODYNAMIC PERTURBATIONS IN ROTATIONAL MOTION . . . . .	142
§ 1. Restoring aerodynamic torques. Secular effects . . . . .	142
§ 2. Atmospheric rotation and its effect on secular perturbations . . . . .	148
§ 3. Periodic perturbations. Analysis of motion in a circular orbit . . . . .	149
§ 4. The effect of aerodynamic dissipative torques . . . . .	151
CHAPTER 8. ANALYSIS OF SECULAR PERTURBATIONS UNDER THE COMBINED INFLUENCE OF GRAVITY AND AERODYNAMIC TORQUES AND ORBIT EVOLUTION . . . . .	157
§ 1. Motion of the angular momentum vector relative to an evolving orbit . . . . .	157
§ 2. Equations of secular motion of the angular momentum vector relative to an evolving orbit with gravity and aerodynamic perturbations . . . . .	158
§ 3. Preliminary analysis. Equations of secular motion. Integrable cases . . . . .	162
§ 4. Interaction of aerodynamic and gravitational perturbations. Classification of motions . . . . .	164
§ 5. The influence of orbital regression . . . . .	174
§ 6. Mean aerodynamic drag coefficient . . . . .	177
CHAPTER 9. THE INFLUENCE OF MAGNETIC FIELDS AND OF SOLAR RADIATION TORQUES ON SATELLITE SPIN AND ATTITUDE . . . . .	181
§ 1. The interaction of the satellite's magnetic field with the geomagnetic field . . . . .	181
§ 2. The influence of eddy currents on satellite spin and attitude . . . . .	185
§ 3. The influence of solar radiation torques on the spin and the attitude of an artificial Sun satellite . . . . .	190
§ 4. Interaction of the fundamental perturbations . . . . .	195
CHAPTER 10. THE MOTION OF SOME ORBITED ARTIFICIAL EARTH SATELLITES AROUND THE CENTER OF MASS . . . . .	199
§ 1. Sputnik III . . . . .	199
§ 2. Explorer XI and Explorer IV . . . . .	214
CHAPTER 11. USES OF AN EARTH-ORIENTED SATELLITE IN SOLAR RESEARCH /59/ . . . . .	221
§ 1. Insolation time for a constant orientation of the orbit relative to the Sun . . . . .	221
§ 2. Variation of orbital orientation in time . . . . .	226
§ 3. Determining the total insolation time . . . . .	228
§ 4. Supplements . . . . .	234
APPENDIX 1. MOTION OF A RIGID BODY ABOUT A FIXED POINT IN A NEWTONIAN FORCE FIELD . . . . .	236
§ 1. Equations of motion. First integrals . . . . .	236
§ 2. Stability of steady-state spin /16/ . . . . .	238
§ 3. Some cases of integrable equations and analysis of motion . . . . .	243
APPENDIX 2. THE ORBIT OF AN EQUATORIAL EARTH SATELLITE . . . . .	250
BIBLIOGRAPHY . . . . .	257

## PREFACE

The interest in various topics of space science has greatly increased since the launching of the first artificial Earth satellite, as man has advanced toward the conquest of space. Of particular interest are the various aspects of the theory of flight of artificial space vehicles.

The subject matter of this book is one aspect of the dynamics of space flight — the motion of an artificial space vehicle about its center of mass. The main aim of the book is to describe the research tools and to bring out the principal properties of this motion. The discussion is confined to problems which fall within the scope of the dynamics of rigid bodies.

The book has been written on the basis of some of my previously published papers /6—18, 59/ and lectures at the Department of Mechanics and Mathematics of the Moscow State University during the 1962—1963 academic year. Some results of other authors have also been used.

The topics treated in the book have been discussed repeatedly with D. E. Okhotsimskii, M. L. Lidov, V. A. Sarychev, and Yu. V. Zonov. Lecture notes taken down by K. S. Zhigalovskii were of great help in the preparation of this book. A. I. Lur'e and T. V. Kharitonova carefully read the manuscript and offered some valuable suggestions. To these colleagues of mine, my deepest thanks.

V. Beletskii

## **INTRODUCTION**

Some problems of geophysics and dynamics connected with space research require detailed analysis of the rotational motion of artificial space vehicles about the center of mass. For example, solar radiation can be investigated from a satellite only if the relevant instruments are illuminated by the Sun, whereas the conditions of illumination clearly depend on the satellite's motion about its mass center. The satellite attitude relative to the oncoming air stream is highly significant for the readings of various instruments which measure the composition and the structure of the upper atmosphere; the attitude with respect to the Earth's magnetic field influences magnetometer readings. The motion about the center of mass also affects the mean aerodynamic drag coefficient, and hence the orbital parameters and the satellite's lifetime. The orientation of the satellite in space is also indispensable in various other problems.

Another class of topics which require detailed analysis of the satellite's motion about its mass center is concerned with the possibility of passive attitude control of satellites, i. e., attitude control by space-environment torques. The basic aim here is to find the natural equilibrium attitudes of the satellite, to analyze their stability, and to investigate the motion in the vicinity of these equilibria.

The motion of a satellite about its center of mass is also of independent interest as a problem in mechanics. These motions can be broadly classified in two groups. If the kinetic energy of the satellite spin is small in comparison with the work done by the external environment forces, the satellite will librate, oscillating about a certain mean attitude in a frame of reference connected with some fixed direction in space (orbit's radius-vector, geomagnetic field vector, etc.). This motion is attributable to the attitude stabilizing effect of the space-environment torques. A classical example of libration is provided by the motion of the Moon under the Earth's gravitational torques.

If now the kinetic energy of the satellite spin is large in comparison with the work done by space-environment forces, the motion over small time intervals is nearly unperturbed, an analog of the Euler motion of a free body. The external torques produce small perturbations, which may, however, build up in time leading to secular effects. For example, the precession of the Earth's spin axis is attributable to the attraction of the Moon and the Sun. When we say rotation, we generally mean this case of perturbed motion (as distinct from libration).

In classical celestial mechanics, the theory of motion about the center of mass is developed in application to particular heavenly bodies (Moon, Earth) /94/, and this has obviously resulted in various simplifications which do not hold true in the general case; the main factor considered is the contribution of gravitational torques. The rotational motion of artificial

space vehicles is highly complex: the geometry and the mass distribution are quite general, the initial data are arbitrary, and the motion is significantly influenced by a multiplicity of factors. Aside from gravity torques, we must also consider aerodynamic and electromagnetic torques, dissipative effects attributable to the friction of the satellite's shell with the atmosphere and the interaction of the metallic body with the Earth's magnetic field, contribution from orbit evolution, solar radiation pressure on a space vehicle moving in an interplanetary orbit, etc. Furthermore, the modern research tools (theory of stability, theory of oscillations, asymptotic methods) provide new paths of attack and yield various novel results even for topics which have been previously considered by classical celestial mechanics.

This book, comprising eleven chapters and two appendices, analyzes the rotational motion of artificial space vehicles and touches upon some related problems. Chapter 1 is mainly concerned with an analysis of torques on a satellite. Gravity torques are considered both for a central Newtonian field and, following /63/, for noncentral fields also. The torques due to aerodynamic pressure and friction are derived for a certain simplified model; some simplifications are also introduced in the analysis of torques attributable to the interaction of the satellite's magnetic field with the magnetic field of the Earth; approximation expressions are given for the dissipative torques produced by eddy currents in the satellite's metallic shell. Solar radiation torques are treated following /41/.

This chapter also describes the various systems of axes and the corresponding direction cosines, which are used throughout the book.

Chapters 2 and 3 deal with satellite librations. It is shown that gravity torques ensure a stable relative equilibrium of a satellite in a circular orbit, provided the largest axis of the satellite's ellipsoid of inertia points along the radius-vector, the least axis along the normal to the orbital plane, and the medium axis along the tangent to the orbit. Plane and space oscillations about this equilibrium attitude are considered. In elliptical orbits, however, this equilibrium attitude is not allowed. An analysis of nonlinear oscillations in elliptical orbits reveals the existence of stable periodic ("eccentricity") oscillations about the radius-vector. The conditions of resonance in plane and space oscillations are investigated. Practical application of the effects discussed in Chapter 2 is illustrated by a description (following /60/) of a system for gravity attitude stabilization of artificial satellites. The effect of aerodynamic torques on satellite librations about a relative equilibrium is also considered. The existence of some "oblique" equilibrium attitudes should be especially noted, with the satellite axis making a certain constant (nonzero) angle with the radius-vector. These attitudes may arise under the combined application of gravity and aerodynamic torques. The influence of the Earth's flattening on satellite librations is analyzed. It is shown that a satellite can be stabilized relative to the Earth's magnetic field and, in virtue of solar radiation torques, relative to the Sun also.

Strictly speaking, the orbit of a satellite depends on its motion about the center of mass. In Chapter 4 we consider the relation between the translational and the rotational motions of a satellite in a Newtonian force field. A rigorous proof is offered for the existence of the previously mentioned stable equilibrium attitude of a satellite in a gravitation field.

An analysis of the general conditions of stability provides a criterion for estimating the allowed perturbations. The influence of satellite geometry on the orbital motion and some other problems are considered in a restricted setting, for various particular examples.

Chapters 5—9 develop the general theory of perturbed rotational motion of a satellite. In Chapter 5 the equations in osculating elements are introduced and investigated; these equations are found to be most convenient for the analysis of perturbed rotation. These equations describe the evolution of the angular momentum vector in space and the evolution of the Euler motion relative to the angular momentum vector. Perturbed motion is conveniently treated by the various asymptotic techniques of the theory of oscillations. Averaging over the fast spin and over the orbital motion of the satellite's mass center brings out the secular effects. A higher ("second") approximation is obtained by averaging over the fast spin only (without averaging over the orbital motion). It is shown that in the case of a dynamically symmetric satellite with perturbations which have a potential function, the perturbed motion "in the second approximation" can be resolved into quasiregular precession around the angular momentum vector and precession-nutation of this vector, which remains constant in magnitude. The equations of motion of the angular momentum vector are independent of other equations, and in some highly relevant cases they are actually integrable. Analogous techniques can be applied to analyze the effect of arbitrary torques (dissipative torques included) on an arbitrary satellite with a triaxial ellipsoid of inertia.

Some probability characteristics of perturbed motion are also considered in this chapter.

Chapter 6 deals with gravitational perturbations. The Jacobi integral is applied to map the permitted regions of motion for the axis of a dynamically symmetric satellite in a circular orbit. It is shown, in particular, that the axis of a dynamically prolate satellite will execute bounded oscillations in the vicinity of the radius-vector, whereas the axis of a dynamically oblate satellite will oscillate about the normal to the orbital plane. If the axial component of the absolute angular velocity is always zero, the axis of a dynamically oblate satellite may oscillate in the neighborhood of the tangent to the orbit. If the kinetic energy of the satellite spin is fairly high, the permitted region of motion covers the entire unit sphere, and bounded oscillations give way to continuous rotation. Secular gravitational perturbations and general properties of motion in circular and elliptical orbits are considered for this case; a solution "in the second approximation" in elliptical functions is derived, following Chapter 5, for a circular orbit; an analogous approximate solution is also constructed for an elliptical orbit. Comparison with the results of numerical integration of the exact equations shows that the "second approximation" is highly accurate.

The principal contribution from gravitational perturbations amounts to secular precession of the angular momentum vector around the normal to the orbital plane. Periodic nutations of the angular momentum vector (with a period comparable to the satellite's orbital period) are superimposed on this secular precession. On the whole, the angular momentum vector moves so that, say, in a circular orbit it describes a closed conical surface in the orbital system of axes (which rotates together with the radius-vector).

Analogous effects have been shown /71/ to obtain for a satellite with a triaxial ellipsoid of inertia.

Chapter 7 proceeds with a similar analysis for aerodynamic torques. Here the main effect is secular precession of the angular momentum vector around the tangent at the perigee point; in a circular orbit, the angular momentum vector in the orbital system of axes seeks the direction of the current velocity vector: as the aerodynamic torques increase, it approaches nearer and nearer to this direction. The aerodynamic torques thus have a distinct stabilizing influence on a spinning satellite. Aerodynamic dissipative torques on a dynamically prolate satellite make it "tumble", while a dynamically oblate satellite is stabilized spinning around its axis of symmetry. The angular momentum vector (in the limit, the spin axis) orients itself along the tangent at the perigee point, so that the satellite is maintained in an attitude of maximum aerodynamic resistance (within the framework of the approximate theory of rotational motion; for fairly small kinetic energies, the satellite may start librating).

Chapter 8 analyzes the combined influence of secular gravitational and aerodynamic perturbations, taking into consideration the contribution from orbit evolution due to the Earth's flattening. A classification of various motions is given.

The slow-down of a satellite in the atmosphere and the resulting orbit evolution enter the equations of satellite's motion about its mass center in the form of the aerodynamic drag coefficient; for a fast spinning satellite, the mean aerodynamic drag coefficient is substituted. The determination of this mean drag coefficient and its dependence on satellite attitude are also considered in Chapter 8.

Chapter 9 deals with the secular effects attributable to the interaction of the satellite's magnetic field with the magnetic field of the Earth. These effects mainly reduce to precession-nutation of the angular momentum vector relative to directions which depend on the orientation of the orbit with respect to the geomagnetic dipole. Dissipative effects produced by eddy currents in the satellite shell lead to tumble or stabilization (according as the satellite is prolate or oblate), the angular momentum vector seeking a certain direction which is fixed relative to the orbit and the geomagnetic dipole.

An analysis of solar radiation torques on an artificial Sun satellite shows that these torques have a distinct stabilizing influence on a spinning satellite: in the orbital system of axes, the angular momentum vector seeks a certain direction, which approaches the radius-vector as the magnitude of the radiation torques increases. In the orbital system, the angular momentum vector describes a closed conical surface. This chapter also analyzes the combined influence of the fundamental perturbations: the main part of aerodynamic and magnetic perturbations, gravitational perturbations, and orbit evolution.

Chapter 10 summarizes various data on the actual motion of some satellites around the center of mass; the satellites under discussion are Sputnik III and the two American satellites Explorer XI and Explorer IV /84, 85/. The analysis shows that the observed motion is in satisfactory agreement with the theory.

Chapter 11 deals with a strictly applied problem. It investigates the insulation of instruments in a satellite oriented with respect to the Earth. For a given instrumental angle of view, total insulation time of a few tens

of hours can be achieved by optimizing the angle of setting of the spaceborne instrument, the day and the hour of launch, and the orbit of the satellite. This insulation, attainable even for narrow-angle instruments, is quite sufficient for various scientific purposes.

Appendix 1 deals with the general problem of motion of a rigid body around a fixed point in a Newtonian force field. The results of this Appendix are partly utilized in Chapters 1 and 2 to interpret the gravitational effects in satellite motion. The problem, however, is of independent interest. The appendix states the problem, gives the first integrals of motion, and describes the integrable cases; the stability of particular solutions (steady-state spin) is analyzed and some modes of motion are considered, for which the various effects produced by Newtonian field perturbations are most pronounced.

Appendix 2 investigates the motion of an equatorial Earth satellite. The results of this Appendix are applied in Chapters 3 and 4.

## Chapter 1

### ANALYSIS OF TORQUES ON A SATELLITE

#### § 1. SYSTEMS OF COORDINATES. PRELIMINARY ANALYSIS OF A RIGID BODY IN A NEWTONIAN FORCE FIELD

1. Systems of coordinates. We shall use the following fundamental systems of coordinates (Figure 1):

$CXYZ$  — the system of fixed axes (absolute system), with its origin at the Earth's center  $C$ ; the axis  $\bar{Y}$  points along the Earth's axis,  $\bar{X}$  and  $\bar{Z}$  lie in the equatorial plane of the Earth, the axis  $\bar{z}$  directed to the point of vernal equinox (Figure 1a).

$OXYZ$  — a system with axes parallel to the corresponding axes of the absolute system, its origin coinciding with the mass center  $O$  of the satellite.

$OXYZ$  — the "perigee" system: the axis  $Z$  is parallel to the radius-vector of the perigee, the axis  $Y$  is perpendicular to the orbital plane, and the axis  $X$  is tangent to the orbit at the perigee, pointing in the direction of motion of the satellite's mass center  $O$  (Figure 1a).

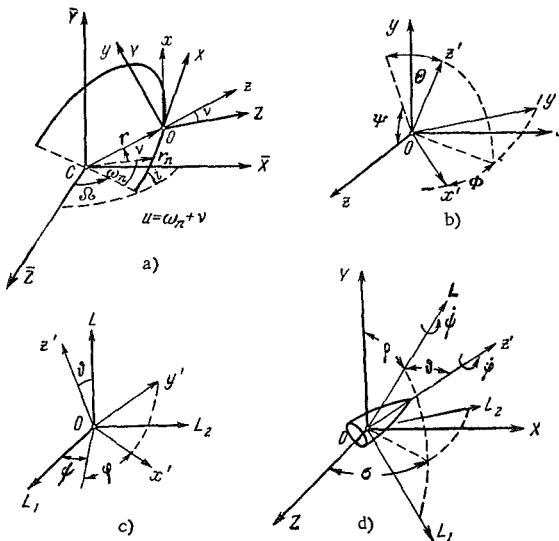


FIGURE 1. The fundamental systems of coordinates.

$Oxyz$  — the "orbital" system: the axis  $z$  is parallel to the current radius-vector, the axis  $x$  perpendicular to the orbital plane, and the axis  $y$  parallel to the transversal. An osculating orbit may be assumed (Figure 1a, b).

$OL_1L_2L$  — a system connected with the angular momentum  $L$  of satellite's rotation. The axis  $OL$  points along  $L$ ;  $OL_1$  lies in the plane  $OLY$  at right angles to  $OL$ , making an obtuse angle with  $Y$ ; the axis  $OL_2$  completes the triad to a right-handed system (Figure 1c, d).

$Ox'y'z'$  — a moving system with its axes parallel to the principal central axes of inertia of the satellite (Figure 1b, c).

$Ox_Hy_Hz_H$  — a system connected with the geomagnetic field; the axis  $Oy_H$  is parallel to the magnetic field vector  $H$ .

The relative position of these systems is defined by the following tables of direction cosines:

$x' y' z'$	$x' y' z'$	$x' y' z'$
$x \alpha \alpha' \alpha''$	$\bar{X} \tilde{\alpha}_1 \tilde{\alpha}_2 \tilde{\alpha}_3$	$X \alpha_1 \alpha_2 \alpha_3$
$y \beta \beta' \beta''$	$\bar{Y} \tilde{\beta}_1 \tilde{\beta}_2 \tilde{\beta}_3$	$Y \beta_1 \beta_2 \beta_3$
$z \gamma \gamma' \gamma''$	$\bar{Z} \tilde{\gamma}_1 \tilde{\gamma}_2 \tilde{\gamma}_3$	$Z \gamma_1 \gamma_2 \gamma_3$
$x' y' z'$	$x' y' z'$	$x y z$
$L_1 \alpha_{11} \alpha_{12} \alpha_{13}$	$x_H \alpha_H \alpha'_H \alpha''_H$	$\bar{X} a_1 b_1 c_1$
$L_2 \alpha_{21} \alpha_{22} \alpha_{23}$	$y_H \beta_H \beta'_H \beta''_H$	$\bar{Y} a_2 b_2 c_2$
$L \alpha_{31} \alpha_{32} \alpha_{33}$	$z_H \gamma_H \gamma'_H \gamma''_H$	$\bar{Z} a_3 b_3 c_3$
$L_1 L_2 L$	$L_1 L_2 L$	
$X m_1 m_2 m$	$\bar{X} a_1^0 a_2^0 a_3^0$	
$Y n_1 n_2 n$	$\bar{Y} \beta_1^0 \beta_2^0 \beta_3^0$	
$Z k_1 k_2 k$	$\bar{Z} \gamma_1^0 \gamma_2^0 \gamma_3^0$	

We note the following three properties of the matrices of direction cosines:

- 1) The sum of the squares of the elements in one row (column) is equal to unity. E.g.,  $\alpha^2 + \beta^2 + \gamma^2 = 1$ .
- 2) The sum of pair products of the elements in two rows (columns) is zero. E.g.,  $\alpha\beta + \alpha'\beta' + \alpha''\beta'' = 0$ .
- 3) Each matrix element is equal to its algebraic complement. E.g.,  $\alpha' = \beta''\gamma - \beta\gamma''$ .

The following expressions are satisfied by some of the foregoing direction cosines:

$$\left. \begin{aligned} a_1 &= -\sin u \sin \Omega + \cos u \cos \Omega \cos i, \\ b_1 &= -\cos \Omega \sin i, \\ c_1 &= \cos u \sin \Omega + \sin u \cos \Omega \cos i, \\ a_2 &= \cos u \sin i, \\ b_2 &= \cos i, \\ c_2 &= \sin u \sin i, \\ a_3 &= -\cos \Omega \sin u - \sin \Omega \cos u \cos i, \\ b_3 &= \sin \Omega \sin i, \\ c_3 &= \cos \Omega \cos u - \sin \Omega \sin u \cos i. \end{aligned} \right\} \quad (1.1.1)$$

Here  $u = \omega_\pi + v$ , where  $\omega_\pi$  is the argument of perigee, i.e., the angular distance of the perigee from the line of nodes (Figure 1a),  $v$  the true anomaly,  $\Omega$  the

longitude of the ascending node from the point of vernal equinox, which by assumption lies on the axis  $\bar{Z}$ ;  $i$  the inclination of the orbit to the equator.

Also clearly

$$\left. \begin{array}{l} \tilde{\alpha}_1 = \alpha a_1 + \beta b_1 + \gamma c_1, \quad \tilde{\alpha}_2 = \alpha' a_1 + \beta' b_1 + \gamma' c_1, \\ \tilde{\beta}_1 = \alpha a_2 + \beta b_2 + \gamma c_2, \quad \tilde{\beta}_2 = \alpha' a_2 + \beta' b_2 + \gamma' c_2, \\ \tilde{\gamma}_1 = \alpha a_3 + \beta b_3 + \gamma c_3, \quad \tilde{\gamma}_2 = \alpha' a_3 + \beta' b_3 + \gamma' c_3, \\ \tilde{\alpha}_3 = \alpha'' a_1 + \beta'' b_1 + \gamma'' c_1, \\ \tilde{\beta}_3 = \alpha'' a_2 + \beta'' b_2 + \gamma'' c_2, \\ \tilde{\gamma}_3 = \alpha'' a_3 + \beta'' b_3 + \gamma'' c_3. \end{array} \right\} \quad (1.1.2)$$

Let further  $\Psi$  be the angle between the projection of  $Oz'$  on the plane  $Oyz$  and the axis  $Oz$ ;  $\Theta$  the angle between the axis  $Oz'$  and the plane  $Oyz$ ;  $\Phi$  the angle between the axis  $Ox'$  and the plane  $Oz'x$ . The trihedrons  $Oxyz$  and  $Ox'y'z'$  can be made to coincide by three successive rotations through angles  $\Psi$ ,  $\Theta$ ,  $\Phi$  about the axes  $Ox$ ,  $Oy$ ,  $Oz'$  (Figure 1b). Then

$$\left. \begin{array}{l} \alpha = \cos \Theta \cos \Phi, \\ \alpha' = -\cos \Theta \sin \Phi, \\ \alpha'' = \sin \Theta, \\ \beta = \cos \Psi \sin \Phi + \sin \Psi \sin \Theta \cos \Phi, \\ \beta' = \cos \Psi \cos \Phi - \sin \Psi \sin \Theta \sin \Phi, \\ \beta'' = -\sin \Psi \cos \Theta, \\ \gamma = \sin \Psi \sin \Phi - \cos \Psi \sin \Theta \cos \Phi, \\ \gamma' = \sin \Psi \cos \Phi + \cos \Psi \sin \Theta \sin \Phi, \\ \gamma'' = \cos \Psi \cos \Theta. \end{array} \right\} \quad (1.1.3)$$

Let  $\rho$  be the angle between the vector  $L$  and the axis  $OY$ ,  $\sigma$  the angle reckoned from the axis  $OZ$  to the projection of the vector  $L$  onto the plane  $OZX$  (Figure 1d). Then

$$\left. \begin{array}{l} m_1 = \cos \rho \sin \sigma, \quad m_2 = \cos \sigma, \quad m = \sin \rho \sin \sigma, \\ n_1 = -\sin \rho, \quad n_2 = 0, \quad n = \cos \rho, \\ k_1 = \cos \rho \cos \sigma, \quad k_2 = -\sin \sigma, \quad k = \sin \rho \cos \sigma. \end{array} \right\} \quad (1.1.4)$$

The direction cosines  $\alpha_{ij}$  are expressible in terms of the Eulerian angles  $\vartheta$ ,  $\psi$ ,  $\varphi$  (Figure 1c):

$$\left. \begin{array}{l} \alpha_{11} = \cos \varphi \cos \psi - \cos \vartheta \sin \varphi \sin \psi, \\ \alpha_{21} = \cos \varphi \sin \psi + \cos \vartheta \sin \varphi \cos \psi, \\ \alpha_{31} = \sin \vartheta \sin \varphi, \\ \alpha_{12} = -\sin \varphi \cos \psi - \cos \vartheta \cos \varphi \sin \psi, \\ \alpha_{22} = -\sin \varphi \sin \psi + \cos \vartheta \cos \varphi \cos \psi, \\ \alpha_{32} = \sin \vartheta \cos \varphi, \\ \alpha_{13} = \sin \vartheta \sin \psi, \\ \alpha_{23} = -\sin \vartheta \cos \psi, \\ \alpha_{33} = \cos \vartheta. \end{array} \right\} \quad (1.1.5)$$

We shall often use the expressions of  $\alpha_3$ ,  $\beta_3$ ,  $\gamma_3$  in terms of  $\rho$ ,  $\sigma$ ,  $\vartheta$ ,  $\psi$ . Applying

(1.1.4) and (1.1.5), we find

$$\left. \begin{aligned} \alpha_3 &= \sin \psi \sin \vartheta \cos \rho \sin \sigma - \cos \psi \sin \vartheta \cos \sigma + \\ &\quad + \cos \vartheta \sin \rho \sin \sigma, \\ \beta_3 &= -\sin \psi \sin \vartheta \sin \rho + \cos \vartheta \cos \rho, \\ \gamma_3 &= \sin \psi \sin \vartheta \cos \rho \cos \sigma + \cos \psi \sin \vartheta \sin \sigma + \\ &\quad + \cos \vartheta \sin \rho \cos \sigma. \end{aligned} \right\} \quad (1.1.6)$$

The coordinates  $\rho, \sigma$  will sometimes be replaced with  $\theta, \lambda$ :  $\theta$  is the angle between  $L$  and  $OX$ ,  $\lambda$  is reckoned from the axis  $OZ$  to the projection of the vector  $L$  onto the plane  $OZY$ . Then, e.g.,

$$m = \cos \theta, \quad n = -\sin \theta \sin \lambda, \quad k = \sin \theta \cos \lambda \quad (1.1.4a)$$

and (1.1.6) are correspondingly modified.

In the analysis of particular problems, we shall also use the values of  $\alpha_3, \beta_3, \gamma_3$  averaged over  $\psi$ . Some combinations of these averages are given below (averaging is denoted with a bar):

$$\left. \begin{aligned} \bar{\alpha}_3 &= \cos \vartheta \sin \rho \sin \sigma, \quad \bar{\beta}_3 = \cos \vartheta \cos \rho, \\ \bar{\gamma}_3 &= \cos \vartheta \sin \rho \cos \sigma, \\ \bar{\alpha}_3^2 &= \frac{1}{2} \sin^2 \vartheta + \left(1 - \frac{3}{2} \sin^2 \vartheta\right) \sin^2 \rho \sin^2 \sigma, \\ \bar{\beta}_3^2 &= \frac{1}{2} \sin^2 \vartheta + \left(1 - \frac{3}{2} \sin^2 \vartheta\right) \cos^2 \rho, \\ \bar{\gamma}_3^2 &= \frac{1}{2} \sin^2 \vartheta + \left(1 - \frac{3}{2} \sin^2 \vartheta\right) \sin^2 \rho \cos^2 \sigma, \\ \bar{\alpha}_3 \bar{\beta}_3 &= \left(1 - \frac{3}{2} \sin^2 \vartheta\right) \sin \rho \cos \rho \sin \sigma, \\ \bar{\alpha}_3 \bar{\gamma}_3 &= \left(1 - \frac{3}{2} \sin^2 \vartheta\right) \sin^2 \rho \sin \sigma \cos \sigma, \\ \bar{\beta}_3 \bar{\gamma}_3 &= \left(1 - \frac{3}{2} \sin^2 \vartheta\right) \sin \rho \cos \rho \cos \sigma, \\ \bar{\alpha}_3^3 &= \frac{3}{2} \cos \vartheta \sin^2 \vartheta \sin \rho \sin \sigma + \\ &\quad + \cos \vartheta \left(1 - \frac{5}{2} \sin^2 \vartheta\right) \sin^3 \rho \sin^3 \sigma, \\ \bar{\alpha}_3 \bar{\gamma}_3^2 &= \cos \vartheta \sin \rho \sin \sigma \left[ \frac{1}{2} \sin^2 \vartheta + \right. \\ &\quad \left. + \left(1 - \frac{5}{2} \sin^2 \vartheta\right) \sin^2 \rho \cos^2 \sigma \right]. \end{aligned} \right\} \quad (1.1.7)$$

Also note that

$$\gamma'' = \gamma_3 \cos v + \alpha_3 \sin v, \quad \beta'' = \beta_3, \quad \alpha'' = \alpha_3 \cos v - \gamma_3 \sin v, \quad (1.1.8)$$

and similarly for the direction cosines of the axes  $x', y'$ . The values of  $a_i, b_i, c_i$  for  $v=0$  (i.e., for  $u=\omega_\pi$ ) will be denoted by  $\bar{a}_i, \bar{b}_i, \bar{c}_i$ . Then

$$\left. \begin{aligned} \bar{a}_3^0 &= m \bar{a}_1 + n \bar{b}_1 + k \bar{c}_1, \quad \bar{\beta}_3^0 = m \bar{a}_2 + n \bar{b}_2 + k \bar{c}_2, \\ \bar{\gamma}_3^0 &= m \bar{a}_3 + n \bar{b}_3 + k \bar{c}_3. \end{aligned} \right\} \quad (1.1.9)$$

We introduce the angles  $\rho_1$  and  $\sigma_1$  specifying the position of  $L$  relative to  $OXYZ$ , by analogy with the angles  $\rho$  and  $\sigma$  specifying the position of  $L$

relative to  $OXYZ$ . Then

$$\alpha_3^0 = \sin \rho_1 \sin \sigma_1, \quad \beta_3^0 = \cos \rho_1, \quad \gamma_3^0 = \sin \rho_1 \cos \sigma_1. \quad (1.1.10)$$

the direction cosines  $\tilde{\alpha}_3, \tilde{\beta}_3, \tilde{\gamma}_3$  take the form (1.1.6) on substitution  $\rho, \sigma \rightarrow \rho_1, \sigma_1$ .

**2. Preliminary analysis of gravity torques.** Gravity torques constitute one of the main factors influencing the motion of artificial space vehicles and they are apparently the principal factor affecting the rotation of artificial satellites. We shall start with an elementary analysis of a rigid body in a field of gravity.

Let us first consider the influence of a Newtonian central field of force, neglecting the motion of the satellite's mass center. Let the mass center of the satellite be distant  $R$  from the center of attraction, and consider a right-hand rectangular orbital system  $xyz$  with its origin at the satellite's mass center. A particle of the satellite having the mass  $dm$  and the coordinates  $x, y, z$  experiences a Newtonian force  $F$  toward the center of attraction:

$$F = -\frac{\mu dm}{x^2 + y^2 + (z + R)^2} \cdot r_0, \quad (1.1.11)$$

where  $\mu$  is the gravitational constant (for the Earth,  $\mu \approx 398,602 \text{ km}^3/\text{sec}^2$ ), and the unit vector  $r_0$  is defined by the direction cosines

$$\left. \begin{aligned} \cos(\hat{x}, r_0) &= \frac{x}{r}, & \cos(\hat{y}, r_0) &= \frac{y}{r}, \\ \cos(\hat{z}, r_0) &= \frac{z + R}{r}, \\ r &= \sqrt{x^2 + y^2 + (z + R)^2}. \end{aligned} \right\} \quad (1.1.12)$$

The satellite is small in comparison with the distance  $R$  from the center of attraction. This implies that the action of the force  $F$  on the particles of the satellite should be considered only for  $x, y, z$  which are small in comparison with  $R$ . Then, to within terms of second order of smallness, the components of the force  $F$  along the axes  $x, y, z$  are given by

$$\left. \begin{aligned} F_x &= -\frac{\mu dm}{R^2} \cdot \frac{x}{R}, \\ F_y &= -\frac{\mu dm}{R^2} \cdot \frac{y}{R}, \\ F_z &= -\frac{\mu dm}{R^2} + 2 \frac{\mu dm}{R^2} \cdot \frac{z}{R} = F_z^{(0)} + F_z^{(1)}. \end{aligned} \right\} \quad (1.1.13)$$

The resultant of the elementary forces  $-\mu dm/R^2$  entering the expression for  $F_z$  is applied to the satellite's center of mass, pointing along its radius-vector. This resultant drives the mass center in a Kepler orbit. The second term in the expression for  $F_z$ , as well as the elementary forces  $F_x$  and  $F_y$ , when summed for all the particles, produce a resultant torque which rotates the satellite about its mass center. Consider, for example, the lines of force of the corresponding field pattern in the orbital plane  $zx$  (the field pattern will be the same in any other plane containing the axis  $z$ ). The differential equation of the lines of force

$$\frac{dz}{dx} = \frac{F_z^{(1)}}{F_x} = -\frac{2z}{x}$$

gives, on integration, a family of force lines

$$z = \frac{c}{x^2}.$$

They are plotted in Figure 2. The direction in which the force acts is marked with arrows. A particle moving in this field will approach the axis  $z$ , i. e., the radius-vector of the mass center. Consider a liquid mass immersed in the force field shown in Figure 2. The particles of the liquid will then tend to move in the direction of the axis  $z$ . This is the well-known phenomenon which on the Earth causes worldwide tidal motions due to the attraction of the Moon and the Sun.

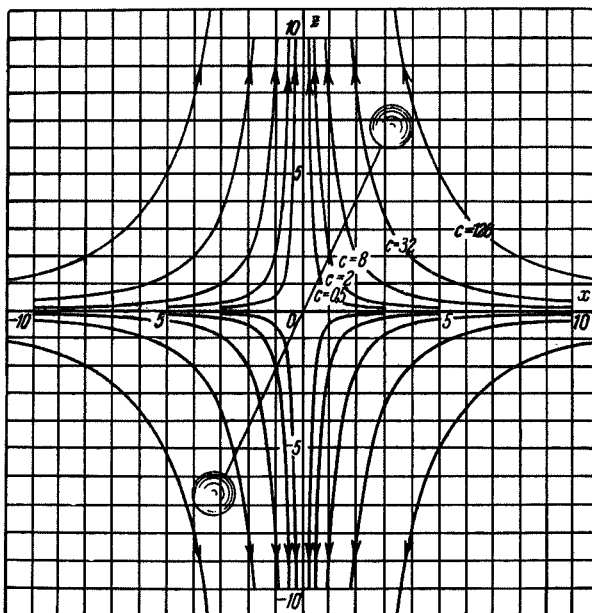


FIGURE 2. Field of perturbation forces.

If an ideally rigid body is immersed in this force field, its mass center coinciding with the center of the field, the body will rotate about its center of mass. To illustrate this point, consider an oblong axisymmetric figure, e.g., a dumbbell (two equal point masses at the ends of a long rod of negligible mass). We then easily see that if initially the body axis is close to the axis  $z$ , small perturbations will produce libration (oscillation) of the dumbbell. The effect of the Newtonian force field is thus to set apart one of the axes, namely the axis  $z$ , as the line of stable equilibrium; this preferred axis points along the radius-vector joining the center of force with the mass center of the body. The axis  $x$  perpendicular to the radius-vector and lying in the orbital plane constitutes the line of unstable equilibrium.

Applying the foregoing expressions for the components  $F_x$ ,  $F_y$ ,  $F_z^{(1)}$  of the perturbation force field, we can calculate the torque produced by this field

relative to the origin for any point  $x, y, z$ . We have

$$M_x = +3yz \frac{\mu dm}{R^3}, \quad M_y = -3xz \frac{\mu dm}{R^3}, \quad M_z = 0. \quad (1.1.14)$$

For a circular orbit  $\frac{\mu}{R^3} = \omega^2$ , where  $\omega$  is the angular velocity of the mass center in the orbit. For a dumbbell with a halflength  $l$  and a halfmass  $m_0$  lying in the orbital plane, the restoring torque is

$$M_y = -3m_0 l^2 \omega^2 \sin 2\alpha_0,$$

while in the plane through the radius-vector, at right angles to the orbital plane, the restoring torque (as it follows from the pattern of the lines of force) is

$$M_x = -3m_0 l^2 \omega^2 \sin 2\beta_0,$$

where  $\alpha_0$  and  $\beta_0$  are the angles between the positive direction of the axis  $z$  and the dumbbell axis, reckoned counterclockwise in the corresponding planes (as viewed from the positive ends of the axes  $y$  and  $x$ , respectively). In the plane perpendicular to the radius-vector, the torque is zero. An oblong body in a Newtonian force field thus shows a tendency to orient itself along the orbital radius-vector.

In our analysis we neglected the motion of the satellite's mass center. The orbital motion of the center of mass superimposes centrifugal forces on the Newtonian field. The combined effect can be easily investigated for the simple dumbbell model.

For simplicity let us consider a circular orbit, the mass center of the satellite moving with an angular velocity  $\omega$ . Then each point  $m(x, y, z)$  experiences a centrifugal force  $\Phi = \omega^2 r_1 dm$ , where  $r_1$  is the distance from the point  $m$  to the axis of revolution, i.e., the axis through the center of attraction at right angles to the orbital plane. Clearly,

$$\cos(\widehat{r_1, x}) = \frac{x}{r_1}, \quad \cos(\widehat{r_1, y}) = 0, \quad \cos(\widehat{r_1, z}) = \frac{R+z}{r_1},$$

where  $r_1 = \sqrt{x^2 + (R+z)^2}$ , and the components of the centrifugal force are

$$\Phi_x = x\omega^2 dm, \quad \Phi_y = 0, \quad \Phi_z = (R+z)\omega^2 dm.$$

The torque of  $\Phi$  about the mass center of the dumbbell satellite has the components

$$M_x = -m_0 l^2 \omega^2 \sin 2\beta_0, \quad M_y = 0, \quad M_z = -m_0 l^2 \omega^2 \sin 2\gamma_0,$$

where  $\gamma_0$  is the angle between the axis  $x$  and the dumbbell axis, reckoned in the same sense as the angles  $\alpha_0$  and  $\beta_0$ . By inspecting the lines of force in a plane perpendicular to the radius-vector, we see that the torque  $M_z$  tends to stabilize the dumbbell along the axis  $x$ . In a plane perpendicular to the plane of the orbit, the centrifugal forces produce a restoring torque  $M_x$  which, as it follows from an examination of the field pattern in the plane

$y, z$ , tends to orient the dumbbell axis along the radius-vector. In the orbital plane, the centrifugal force produces no torque.

The combined action of gravity and centrifugal forces will thus produce the following restoring torques along the three axes:

along the normal to the orbit

$$M_y = -3m_0 l^2 \omega^2 \sin 2\alpha_0,$$

along the tangent to the orbit

$$M_x = -4m_0 l^2 \omega^2 \sin 2\beta_0,$$

along the radius-vector

$$M_z = -m_0 l^2 \omega^2 \sin 2\gamma_0.$$

For a three-dimensional dumbbell, the gravity and centrifugal torques tend to orient the dumbbell axes along the axes  $x, y, z$ . Passing to the general case of an arbitrary rigid body, we conclude, by analogy, that the Newtonian and centrifugal forces tend to stabilize the body in an attitude where two of the principal central axes of inertia, like the axes of the three-dimensional dumbbell, point respectively along the radius-vector of the orbit and the line perpendicular to it in the orbital plane. We shall refer to this orbital attitude of a body as a state of relative equilibrium. A question arises: exactly which of the various states of relative equilibrium is stable?

By intuition, we would suggest that the major axis of the ellipsoid of inertia should point along the radius-vector, since, by analogy with the dumbbell, "prolateness" in the direction of the radius-vector is most conducive to the restoring effect of the Newtonian force field. Indeed, in Appendix 1 it is shown that in a Newtonian field at rest the absolute equilibrium is stable if and only if the largest axis of the ellipsoid of inertia points along the line to the center of attraction. But then the second axis in the orbital plane (in the case of a circular orbit, the tangent to the trajectory) should coincide with the medium axis of the ellipsoid of inertia. Indeed, this attitude is the most expedient for utilizing the residual dynamic "prolateness" of the body for its stabilization along the tangent to the orbit under the action of centrifugal forces. This orientation of the medium axis is also deduced from the following: it cannot point along the binormal to the orbit, since absolute rotation of the body about the binormal is a state of relative equilibrium, and rotation about the medium axis of inertia is inherently unstable; Newtonian and centrifugal forces do not eliminate this instability.

Tisserand /94/ also gives this orientation of the axes of the ellipsoid of inertia. He arrived at this result by means of an approximate analysis of the equations of motion and qualitative considerations.

In the following chapters, Lyapunov—Chetaev techniques /54, 74/ will be applied to show that the preliminary considerations of this section lead to correct conditions for the stability of relative equilibrium: the attitude of the ellipsoid of inertia that we have described is found to be a sufficient condition for the stability of relative equilibrium.

## § 2. TORQUES ON AN ARBITRARY RIGID BODY IN A NEWTONIAN FORCE FIELD

**1. Central Newtonian field of force.** We have shown that a point mass  $dm$  experiences an elementary torque (1.1.14). Summing over the entire volume of the satellite gives the torques on the whole body. Let us find the components of the elementary gravity torque along the satellite's own axes, e.g., the component  $dm_{x'}$  along the axis  $x'$ . Applying property 3 of the matrix of direction cosines (see § 1), we find substituting  $M_x$ ,  $M_y$ ,  $M_z$  from (1.1.14)

$$dm_{x'} = M_x \alpha + M_y \beta + M_z \gamma = 3 \frac{\mu}{R^3} dm (x' \gamma + y' \gamma' + z' \gamma'') (y' \gamma'' - z' \gamma').$$

Since the axes in a rigid body point along the principal central axes of inertia, we have

$$\int_V x' y' dm = 0, \quad \int_V x' z' dm = 0, \quad \int_V y' z' dm = 0.$$

We also introduce the principal central moments of inertia

$$\left. \begin{aligned} J_{x'x'} &= A = \int_V (y'^2 + z'^2) dm, \\ J_{y'y'} &= B = \int_V (x'^2 + z'^2) dm, \\ J_{z'z'} &= C = \int_V (x'^2 + y'^2) dm. \end{aligned} \right\} \quad (1.2.1)$$

Integrating the elementary torque  $dm_{x'}$  over the entire volume of the body, we find the total torque  $M_{x'}$ ; the torque components  $M_{y'}$ ,  $M_{z'}$  are similarly calculated, so that

$$\left. \begin{aligned} M_{x'} &= 3 \frac{\mu}{R^3} (C - B) \gamma' \gamma'', \\ M_{y'} &= 3 \frac{\mu}{R^3} (A - C) \gamma'' \gamma, \\ M_{z'} &= 3 \frac{\mu}{R^3} (B - A) \gamma \gamma'. \end{aligned} \right\} \quad (1.2.2)$$

that is

$$\mathbf{M} = 3 \frac{\mu}{R^3} \mathbf{e}_r \times [A(\mathbf{e}_r \cdot \mathbf{i}') \mathbf{i}' + B(\mathbf{e}_r \cdot \mathbf{j}') \mathbf{j}' + C(\mathbf{e}_r \cdot \mathbf{k}') \mathbf{k}'],$$

where  $\mathbf{e}_r$ ,  $\mathbf{i}'$ ,  $\mathbf{j}'$ ,  $\mathbf{k}'$  are unit vectors in the direction of the radius-vector and the principal central axes of inertia of the body, respectively. From the last formula we see that  $\mathbf{M} \perp \mathbf{e}_r$ .

These torques were obtained assuming that the body was sufficiently small in comparison with the distance to the center of attraction.

If no such assumption is imposed, the force function  $U$  on a satellite of arbitrary form is given by the relations

$$\left. \begin{aligned} U &= \int_V \varphi^*(r) dm, \\ r^2 &= R^2 + 2R(x' \gamma + y' \gamma' + z' \gamma'') + \rho'^2, \\ \rho'^2 &= x'^2 + y'^2 + z'^2. \end{aligned} \right\} \quad (1.2.3)$$

Here  $\varphi^*(r)$  is a force function on the element  $dm$  of the body, which depends only on the distance between the point of the body and the center of attraction. The integral is taken over the entire volume  $V$  of the body. A system of fixed axes  $X\bar{Y}\bar{Z}$  is placed at the center of force  $C$  (located outside the body). The mutual position of the coordinate system  $CX\bar{Y}\bar{Z}$  and  $Ox'y'z'$  is described by a table of direction cosines (§ 1) and the coordinates  $\bar{X}_0\bar{Y}_0\bar{Z}_0$  of the satellite's mass center. Then

$$\left. \begin{aligned} \gamma &= \frac{\bar{X}_0}{R} \tilde{a}_1 + \frac{\bar{Y}_0}{R} \tilde{b}_1 + \frac{\bar{Z}_0}{R} \tilde{v}_1, \\ \gamma' &= \frac{\bar{X}_0}{R} \tilde{a}_2 + \frac{\bar{Y}_0}{R} \tilde{b}_2 + \frac{\bar{Z}_0}{R} \tilde{v}_2, \\ \gamma'' &= \frac{\bar{X}_0}{R} \tilde{a}_3 + \frac{\bar{Y}_0}{R} \tilde{b}_3 + \frac{\bar{Z}_0}{R} \tilde{v}_3. \end{aligned} \right\} \quad (1.2.3')$$

The expression for  $r$  entering (1.2.3) takes the form

$$\begin{aligned} r^2 = & \bar{X}_0^2 + \bar{Y}_0^2 + \bar{Z}_0^2 + 2\bar{X}_0(x'\tilde{a}_1 + y'\tilde{a}_2 + z'\tilde{a}_3) + \\ & + 2\bar{Y}_0(x'\tilde{b}_1 + y'\tilde{b}_2 + z'\tilde{b}_3) + \\ & + 2\bar{Z}_0(x'\tilde{v}_1 + y'\tilde{v}_2 + z'\tilde{v}_3) + x'^2 + y'^2 + z'^2. \end{aligned} \quad (1.2.3'')$$

Let us write the components of the elementary force of attraction along the axes  $x', y', z'$  for the case (1.2.3):

$$\begin{aligned} f_{x'} &= \frac{\partial \varphi^*}{\partial r} \cdot \frac{R\gamma + x'}{r} dm, \quad f_{y'} = \frac{\partial \varphi^*}{\partial r} \cdot \frac{R\gamma' + y'}{r} dm, \\ f_{z'} &= \frac{\partial \varphi^*}{\partial r} \cdot \frac{R\gamma'' + z'}{r} dm. \end{aligned}$$

The components of the elementary torque are

$$m_{x'} = y'f_{z'} - z'f_{y'} = \frac{\partial \varphi^*}{\partial r} \cdot \frac{R}{r} (y'\gamma'' - z'\gamma') dm,$$

and similarly for  $m_{y'}$ ,  $m_{z'}$ . The total torque projected onto the axis  $x'$  is found by integrating  $m_{x'}$  over the entire volume  $V$ :

$$M_{x'} = \gamma'' \int_V \frac{\partial \varphi^*}{\partial r} \cdot \frac{R}{r} y' dm - \gamma' \int_V \frac{\partial \varphi^*}{\partial r} \cdot \frac{R}{r} z' dm.$$

Applying (1.2.3), we see that the first integral in this expression is equal to  $\frac{\partial U}{\partial \gamma'}$  and the second to  $\frac{\partial U}{\partial \gamma''}$ .  $M_{y'}$  and  $M_{z'}$  are found similarly. The Newtonian torque components on a satellite of an arbitrary shape thus have the form

$$\left. \begin{aligned} M_{x'} &= \gamma'' \frac{\partial U}{\partial \gamma'} - \gamma' \frac{\partial U}{\partial \gamma''}, \\ M_{y'} &= \gamma \frac{\partial U}{\partial \gamma''} - \gamma'' \frac{\partial U}{\partial \gamma}, \\ M_{z'} &= \gamma' \frac{\partial U}{\partial \gamma} - \gamma \frac{\partial U}{\partial \gamma'}. \end{aligned} \right\} \quad (1.2.4)$$

Assuming that the distance from the center of attraction is much greater than the size of the satellite, we can derive the approximate expressions (1.2.2) from the general expressions (1.2.4). Let the integrand  $\varphi^*$  be a

Newtonian force function

$$\varphi^* = \frac{\mu}{r} = \frac{\mu}{R \sqrt{1 + \frac{2(x'y + y'z + z'y')}{R} + \frac{\rho'^2}{R^2}}}. \quad (1.2.5)$$

The radicand can be series-expanded in powers of the small terms  $\frac{x'}{R}, \frac{y'}{R}, \frac{z'}{R}$ , omitting all terms above the second order of smallness. Then

$$\begin{aligned} \varphi^* dm &= \frac{\mu dm}{R} \left\{ 1 - \frac{x'y + y'z + z'y'}{R} - \frac{1}{2} \frac{\rho'^2}{R^2} + \right. \\ &\quad \left. + \frac{3}{4} \frac{(x'y + y'z + z'y')^2}{R^2} \right\} + o\left[\left(\frac{\rho'}{R}\right)^3\right]. \end{aligned} \quad (1.2.6)$$

Let us calculate the torque about the origin of a system  $x'y'z'$  which does not coincide with the mass center (the axes  $x'$ ,  $y'$ ,  $z'$ , however, point along the principal axes of inertia of the satellite). Integrating (1.2.3) over the entire volume  $V$ , substituting (1.2.5), and applying (1.2.1), we find

$$\begin{aligned} U &= \frac{\mu M}{R} - \frac{\mu M}{R^2} (x'_0 y + y'_0 z + z'_0 y') + \\ &\quad + \frac{1}{2} \frac{\mu}{R^3} (A + B + C) - \frac{3}{2} \frac{\mu}{R^3} (Ay^2 + By^2 + Cy^2). \end{aligned} \quad (1.2.7)$$

Here  $x'_0, y'_0, z'_0$  are the coordinates of the satellite's mass center. The first term in (1.2.7) is a Newtonian force function for the case of a body with its entire mass concentrated at a single point. All the other terms are attributable to the satellite having measurable geometrical dimensions.

The motions of a rigid body due to the force function (1.2.7) can be classified in three categories:

1. Motion around a fixed point. The origin of the system  $x'y'z'$  is assumed to be at rest. This is a generalization of the classical problem of motion of a heavy body. The classical problem is obtained if we formally set  $A=B=C=0$  in (1.2.7).

2. Motion of a satellite around its mass center for a given orbit of the mass center. Here  $x'_0 = y'_0 = z'_0 = 0$ , and the center of mass is assumed to follow a known Kepler orbit (i.e., in (1.2.7)  $R$  is a known function of time). This, so to say, limited statement of the problem is ideally suited for the apparatus of celestial mechanics.

3. The motion around the mass center, as well as the proper motion of the mass center, are both defined by the force function  $U$  in (1.2.7) ( $x'_0 = y'_0 = z'_0 = 0$ ) or (1.2.3); the translation and the rotation are then related and, strictly speaking, the orbit is non-Keplerian. Note that the moments of inertia  $J$  can be written as  $J=M\rho'^2$ , where  $M$  is the mass of the satellite,  $\rho^*$  the radius of gyration ( $\rho^*$  is comparable with the size of the satellite). Since  $\rho^* \ll R$ , and the non-Newtonian terms in the function  $U$  (1.2.7) are of the order of  $(\frac{\rho^*}{R})^2$ , the shape of the satellite has a negligible effect on the orbit. The most reasonable statement of the problem of satellite motion is therefore the classical limited problem 2. In some cases, however, separate analysis of the more rigorous problem 3 is not meaningless.

2. Fields deviating from central. Until now, we have always assumed a central Newtonian field of force. The actual field of the Earth deviates from the ideal central field: the Earth's figure is close to a spheroid.

Gravity torques allowing for the Earth's oblateness can be obtained, say, by a technique proposed by V. A. Sarychev /63/. Consider three right-hand rectangular systems of axes (see § 1):  $CXYZ$  — the absolute system;  $Oxyz$  — the orbital system;  $Ox'y'z'$  — a system with axes parallel to the principal central axes of inertia of the artificial satellite.

The force function describing the influence of the Earth's field of gravity, with terms of first order of smallness in oblateness, is written

$$U = \mu \int \int \int_M \left[ \frac{1}{R} - \bar{\varepsilon} \frac{R_e^2}{3R^3} \left( 3 \frac{\bar{Y}^2}{R} - 1 \right) \right] dM, \quad (1.2.8)$$

where

$$\begin{aligned} \mu &= M_0 f, \quad \bar{\varepsilon} = a_R - \frac{m}{2}, \quad a = \frac{R_e - R_p}{R_e}, \quad m = \frac{\omega^2 R_e}{g_e}; \\ \bar{X} &= \bar{X}_0 + x' \tilde{a}_1 + y' \tilde{a}_2 + z' \tilde{a}_3, \\ \bar{Y} &= \bar{Y}_0 + x' \tilde{b}_1 + y' \tilde{b}_2 + z' \tilde{b}_3, \\ \bar{Z} &= \bar{Z}_0 + x' \tilde{c}_1 + y' \tilde{c}_2 + z' \tilde{c}_3, \\ R^2 &= \bar{X}^2 + \bar{Y}^2 + \bar{Z}^2. \end{aligned}$$

Here the cosines  $\tilde{a}_i$ ,  $\tilde{b}_i$ ,  $\tilde{c}_i$  are defined by (1.1.1)–(1.1.2);  $M_0$  the Earth's mass,  $f$  the gravitational constant,  $M$  the mass of the satellite,  $R_e$  the equatorial radius of the earth,  $R_p$  the polar radius,  $a_R$  the oblateness,  $\omega$  the angular velocity of the Earth,  $g_e$  gravitational acceleration on the equator,  $x'$ ,  $y'$ ,  $z'$  the coordinates of a variable point of the satellite in the system  $Ox'y'z'$ ;  $\bar{X}_0$ ,  $\bar{Y}_0$ ,  $\bar{Z}_0$  the absolute coordinates of the satellite's mass center.

In evaluating the integral (1.2.8), we make use of the smallness of the linear size  $l$  of the satellite relative to the distance  $R$  between the mass centers of the satellite and the Earth. Series-expanding the integrand in (1.2.8) in powers of  $\frac{x'}{R}$ ,  $\frac{y'}{R}$ ,  $\frac{z'}{R}$  and neglecting terms above the second order of smallness relative to unity, we find on integration the following expression for the force function:

$$\begin{aligned} U = \frac{\mu M}{R} &\left[ 1 - \frac{\bar{\varepsilon}}{3} \cdot \frac{R_e^2}{R^2} \left( 3 \frac{\bar{Y}_0^2}{R^2} - 1 \right) \right] - \\ &- \frac{1}{4} \frac{\mu}{R^3} \left[ 1 - \bar{\varepsilon} \frac{R_e^2}{R^2} \left( 5 \frac{\bar{Y}_0^2}{R^2} - 1 \right) \right] (A + B + C) + \\ &+ \frac{1}{4} \frac{\mu}{R^3} \left[ 3 - 5\bar{\varepsilon} \frac{R_e^2}{R^2} \left( 7 \frac{\bar{Y}_0^2}{R^2} - 1 \right) \right] [(B + C - A)\gamma^2 + \\ &+ (C + A - B)\gamma^2 + (A + B - C)\gamma'^2] + \\ &+ 5\bar{\varepsilon} \frac{\mu}{R^3} \cdot \frac{\bar{Y}_0}{R} \cdot \frac{R_e^2}{R^2} [(B + C - A)\tilde{b}_1 + \\ &+ (C + A - B)\tilde{b}_2 + (A + B - C)\tilde{b}_3] - \\ &- \frac{1}{2} \bar{\varepsilon} \frac{\mu}{R^3} \cdot \frac{R_e^2}{R^2} [(B + C - A)\tilde{b}_1^2 + \\ &+ (C + A - B)\tilde{b}_2^2 + (A + B - C)\tilde{b}_3^2], \quad (1.2.9) \end{aligned}$$

where  $A$ ,  $B$ ,  $C$  are the principal central moments of inertia of the satellite.

\* Roberson /89/ was apparently the first to consider gravity torques with allowance for the oblateness of the Earth. See also the note by Lur'e /53/.

The torque components projected onto the satellite's axes are

$$\left. \begin{aligned} M_{x'} &= (C-B) \frac{\mu}{R^3} \left\{ \left[ 3 - 5\varepsilon \frac{R_e^2}{R^2} \left( 7 \frac{Y_0^2}{R^2} - 1 \right) \right] \gamma' \gamma'' + \right. \\ &\quad \left. + 10\varepsilon \frac{Y_0}{R} \frac{R_e^2}{R^2} (\gamma \tilde{\beta}_3 + \gamma' \tilde{\beta}_2) - 2\varepsilon \frac{R_e^2}{R^2} \tilde{\beta}_2 \tilde{\beta}_3 \right\}, \\ M_{y'} &= (A-C) \frac{\mu}{R^3} \left\{ \left[ 3 - 5\varepsilon \frac{R_e^2}{R^2} \left( 7 \frac{Y_0^2}{R^2} - 1 \right) \right] \gamma'' \gamma + \right. \\ &\quad \left. + 10\varepsilon \frac{Y_0}{R} \frac{R_e^2}{R^2} (\gamma' \tilde{\beta}_1 + \gamma \tilde{\beta}_3) - 2\varepsilon \frac{R_e^2}{R^2} \tilde{\beta}_3 \tilde{\beta}_1 \right\}, \\ M_{z'} &= (B-A) \frac{\mu}{R^3} \left\{ \left[ 3 - 5\varepsilon \frac{R_e^2}{R^2} \left( 7 \frac{Y_0^2}{R^2} - 1 \right) \right] \gamma \gamma' + \right. \\ &\quad \left. + 10\varepsilon \frac{Y_0}{R} \frac{R_e^2}{R^2} (\gamma \tilde{\beta}_2 + \gamma' \tilde{\beta}_1) - 2\varepsilon \frac{R_e^2}{R^2} \tilde{\beta}_1 \tilde{\beta}_2 \right\}. \end{aligned} \right\} \quad (1.2.10)$$

### § 3. AERODYNAMIC TORQUES AND THEIR APPROXIMATIONS

When a satellite moves in the tenuous layers of the upper atmosphere, the interactions of the molecular stream with the satellite hull give rise to certain effects influencing the motion of the satellite about its center of mass. We list here some of these effects:

1. The center of pressure does not coincide with the center of mass. This produces a restoring (pitch-over) torque. The velocity vector of the incident stream does not lie in the orbital plane, since the Earth rotates entraining the atmosphere, while the orbit may be assumed stationary. This torque tends to stabilize the satellite in the direction of the incident stream.

2. The spin of the satellite produces spin-damping dissipative torques and some other effects.

3. The density of the atmosphere is variable over the satellite surface (being higher on the side facing the Earth), which produces an additional small torque (pressure gradient effect) /87/.

4. Another small effect is associated with the proper thermal motion of the molecules.

The thermal velocities of the molecules can be neglected (on the average, they are small in comparison with the orbital velocity of the satellite); the pressure gradient effect will also be ignored. We shall only deal with the effects listed under 1 and 2. The components of the aerodynamic torque along the satellite's axes in general depend on the orientation of these axes relative to the incident stream and the components  $p, q, r$  of the satellite's spin relative to the stream. Since the linear velocity of rotation of the satellite hull is small in comparison with the orbital velocity of the satellite's mass center, the torque may be assumed to vary linearly with  $p, q, r$ . Let  $i', j', k'$  be unit vectors along the principal central axes of the satellite. The aerodynamic torque vector may be written in the general form\*

$$\begin{aligned} \mathbf{M} &= \frac{1}{2} \rho_a V_0^2 e_v \times \mathbf{C}^m + \frac{1}{2} \rho_a V_0 P, \\ \mathbf{C}^m &= C_1^m i' + C_2^m j' + C_3^m k', \quad \mathbf{P} = P_1 i' + P_2 j' + P_3 k', \end{aligned}$$

\* The derivation of these formulas for a more particular case is given below.

$$\begin{pmatrix} P_1 \\ P_2 \\ P_3 \end{pmatrix} = \begin{pmatrix} I_{11} & I_{12} & I_{13} \\ I_{21} & I_{22} & I_{23} \\ I_{31} & I_{32} & I_{33} \end{pmatrix} \times \begin{pmatrix} p \\ q \\ r \end{pmatrix}$$

Here  $V_0$  is the velocity of the mass center relative to the stream;  $e_V$  a unit vector in the direction of this velocity;  $\rho_a$  stream density. The coefficients  $C_i^m$ ,  $I_{jk}$  depend on the satellite's attitude relative to the stream.

In the particular case of a symmetric configuration (the axis of symmetry pointing along  $\mathbf{k}'$ ), we have  $C_1^m = C_2^m = 0$ . The coefficient  $C_3^m$  and the coefficients  $I_{jk}$  (some of which may vanish) depend only on the angle of attack, the angle between  $e_V$  and  $\mathbf{k}'$ . The explicit angular dependence of the coefficients is determined by the nature of the collisions of the impinging molecules with the hull.

The following mechanism is generally accepted for the interaction of the incident molecules with the surface of the satellite. The colliding particle practically gives off its entire energy and reaches a temperature equilibrium with the site of collision (which is slightly heated by the impact). When the surface cools, the particle escapes with a thermal velocity equal to the thermal speed of the hull molecules. Since this thermal velocity is essentially less than the thermal velocity of the gas molecules, the collision pattern can be idealized by the model of plastic impact, the particles losing their entire energy on collision with the satellite (without reflection).

The elementary force  $dF$  acting in this case on a surface element  $dS$  is

$$dF = -f \frac{V}{V}, \quad f = \frac{1}{2} c \rho_a V^2 \cos \gamma_V dS. \quad (1.3.1)$$

Here  $V$  is the velocity of the surface element relative to the incident stream;  $\rho_a$  stream density;  $c$  a coefficient;  $\gamma_V$  the local angle of attack (the angle between the outer normal to the surface element and the vector  $V$ ). The elementary torque

$$dM = \mathbf{r}_s \times dF, \quad (1.3.2)$$

where  $\mathbf{r}_s$  is the radius-vector joining the center of the surface element  $dS$  with the satellite's mass center. Substituting (1.3.1) in (1.3.2) and seeing that

$$\cos \gamma_V = \frac{\mathbf{n} \cdot \mathbf{V}}{|\mathbf{n}| |\mathbf{V}|} = \frac{\mathbf{n} \cdot \mathbf{V}}{V}, \quad (1.3.3)$$

we find

$$dM = \frac{1}{2} c \rho_a (\mathbf{n} \cdot \mathbf{V}) \mathbf{V} \times \mathbf{r}_s dS, \quad (1.3.4)$$

where

$$\mathbf{V} = \mathbf{V}_0 + \boldsymbol{\Omega} \times \mathbf{r}_s, \quad (1.3.5)$$

$\mathbf{V}_0$  being the velocity of the mass center relative to the incident stream,  $\boldsymbol{\Omega}$  the angular velocity vector of the satellite. (Strictly speaking,  $\boldsymbol{\Omega}$  is the vector of the angular velocity of rotation of the satellite relative to the

atmosphere, which in turn rotates with the earth; but for fast spinning satellites,  $\Omega$  can be taken as the vector of the absolute angular velocity, since the angular velocity of transportation (the rotation of the atmosphere) is small in comparison with  $|\Omega|$ .

The linear velocity of the surface  $|\Omega r_s|$  is very small in comparison with  $V_0$ . Therefore, substituting (1.3.5) in (1.3.4), we neglect terms of the order of  $\Omega^2$ . Integrating over the surface of attack  $S^*$ , we obtain an expression for the total aerodynamic torque on the satellite:

$$\begin{aligned} M = & \frac{1}{2} c\rho_a V_0^2 \int_{S^*} (\mathbf{n} \cdot \mathbf{e}_V) \mathbf{e}_V \times \mathbf{r}_s dS + \\ & + \frac{1}{2} c\rho_a V_0 \int_{S^*} ((\mathbf{n} \cdot |\Omega \times \mathbf{r}_s|) (\mathbf{e}_V \times \mathbf{r}_s) + \\ & + (\mathbf{n} \cdot \mathbf{e}_V) [\Omega \times \mathbf{r}_s] \times \mathbf{r}_s) dS; \end{aligned} \quad (1.3.6)$$

here  $\mathbf{e}_V = \frac{\mathbf{V}_0}{V_0}$  is a unit vector in the direction of the translational velocity of the mass center relative to the incident stream. The domain of integration  $S^*$ , strictly speaking, is defined by the inequality  $\mathbf{V} \cdot \mathbf{n} \geq 0$ , but the second term in (1.3.5) being small in comparison with the first term, we shall take the domain of integration to be independent of the satellite spin; it is thus defined by the inequality  $\mathbf{V}_0 \cdot \mathbf{n} > 0$ . For an axisymmetric satellite,  $S^* = S^*(\delta_V)$ , where  $\delta_V$  is the angle of attack, i.e., the angle between  $\mathbf{V}_0$  and the axis of symmetry.

Let  $\Phi(z, \rho^2) = 0$ ,  $\rho^2 = x^2 + y^2$ , be the equation of the surface of a satellite which is symmetric about its axis  $z$ . The components of the unit vector  $\mathbf{n}$  are then

$$n_z = \frac{\Phi_z}{\sqrt{\Phi_z^2 + 4\rho^2 \Phi_{\rho}^2}}, \quad n_x = \sigma_n x, \quad n_y = \sigma_n y, \quad (1.3.7)$$

where

$$\sigma_n = \frac{2\Phi_{\rho^2}}{\sqrt{\Phi_z^2 + 4\rho^2 \Phi_{\rho}^2}}, \quad \Phi_z = \frac{\partial \Phi}{\partial z}, \quad \Phi_{\rho^2} = \frac{\partial \Phi}{\partial \rho^2}.$$

Let the coordinate system  $xyz$  be chosen so that the axis  $y$  always lies in the plane  $zV_0$  (Figure 3); we shall call this a semiconstrained system. The position of a surface point of the satellite in the system  $xyz$  will be further

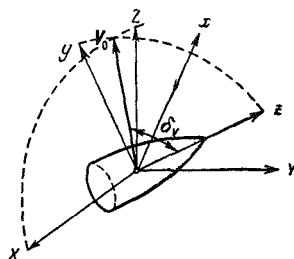


FIGURE 3. A system of coordinates connected with the velocity vector and the satellite.

specified by the cylindrical coordinates  $\bar{z}$ ,  $\bar{p}$ ,  $\bar{\varphi}$ , where  $\bar{\varphi}$  is reckoned from the axis  $y$  in a plane perpendicular to  $z$ , so that

$$y = \bar{p} \cos \bar{\varphi}, \quad x = -\bar{p} \sin \bar{\varphi}. \quad (1.3.8)$$

$\Phi$ ,  $n_z$ , and  $\sigma_n$  are independent of  $\bar{\varphi}$ . The integration domain  $S^*$  depends only on the angle of attack  $\delta_V$ ; since this domain is symmetric about the plane  $zy$ , the integral with respect to  $\bar{\varphi}$  is taken between some  $\bar{\varphi}_0(\delta_V)$  and  $-\bar{\varphi}_0(\delta_V)$ . The system  $xyz$  can be described by a triad of unit vectors  $i$ ,  $j$ ,  $k$ . Then  $r = xi + yj + zk$ ;

$$\left. \begin{aligned} e_V \times k &= \sin \delta_V i, & e_V \times j &= -\cos \delta_V i, \\ e_V \times i &= -k \sin \delta_V + j \cos \delta_V, \\ e_V \times k &= -\operatorname{tg} \delta_V e_V \times j. \end{aligned} \right\} \quad (1.3.9)$$

From vector algebra

$$\left. \begin{aligned} n \cdot (\Omega \times r) &= \begin{vmatrix} \bar{p} & \bar{q} & \bar{r} \\ x & y & z \\ n_x & n_y & n_z \end{vmatrix} \\ (\Omega \times r) \times r &= -r^2(i\bar{p} + j\bar{q} + k\bar{r}) + (x\bar{p} + y\bar{q} + z\bar{r})(ix + jy + kz), \end{aligned} \right\} \quad (1.3.10)$$

where  $\bar{p}$ ,  $\bar{q}$ ,  $\bar{r}$  are the components of  $\Omega$  along  $x$ ,  $y$ ,  $z$ . Applying (1.3.7) – (1.3.10) and omitting all terms with  $\sin \bar{\varphi}$  in the integrand (these terms vanish on integration from  $\bar{\varphi}_0(\delta_V)$  to  $-\bar{\varphi}_0(\delta_V)$ ), we write (1.3.6) as

$$\left. \begin{aligned} M &= \frac{1}{2} \rho_a V_0^2 \bar{c}(\delta_V) e_V \times k + \frac{1}{2} c \rho_a V_0 [i[-\bar{p}\tilde{I}_3 + \bar{r}\tilde{I}_4] + \\ &+ j[-\tilde{I}_5\bar{q}] + k[-\tilde{I}_1\bar{r} + \tilde{I}_2\bar{p}]]. \quad \bar{c}(\delta_V) = c[W_1 \cos \delta_V + W_2 \sin \delta_V - W_3 \cos \delta_V \operatorname{ctg} \delta_V]. \end{aligned} \right\} \quad (1.3.11)$$

The first term in this formula gives the restoring torque produced by aerodynamic pressure, while the remaining terms constitute the dissipative torque of aerodynamic friction.

In (1.3.11),  $W_i$  ( $i = 1, 2, 3$ ) and  $\tilde{I}_j$  ( $j = 1, 2, 3, 4, 5$ ) depend on  $\delta_V$  only; they are defined by the following formulas, in terms of integrals over the surface of attack  $S^*(\delta_V)$ :

$$\left. \begin{aligned} W_1 &= \int [zn_z - \sigma_n \bar{p}^2 \cos^2 \bar{\varphi}] dS, \\ W_2 &= \int z \sigma_n \bar{p} \cos \bar{\varphi} dS, \\ W_3 &= \int n_z \bar{p} \cos \bar{\varphi} dS, \\ \tilde{I}_1 &= \cos \delta_V \int n_x \bar{p}^2 dS + \sin \delta_V \int \sigma_n \bar{p}^3 \cos \bar{\varphi} dS, \\ \tilde{I}_2 &= \cos \delta_V \int zn_z \bar{p} \cos \bar{\varphi} dS + \sin \delta_V \int [\sigma_n z \bar{p}^2 \cos^2 \bar{\varphi} + \bar{p}^2 \sin^2 \bar{\varphi} (n_z - \sigma_n z)] dS, \\ \tilde{I}_3 &= \cos \delta_V \int [(n_z - \sigma_n z) \bar{p}^2 \sin^2 \bar{\varphi} + n_z (z^2 + \bar{p}^2 \sin^2 \bar{\varphi})] dS + \\ &+ \sin \delta_V \int (z^2 + \bar{p}^2 \sin^2 \bar{\varphi}) \sigma_n \bar{p} \cos \bar{\varphi} dS, \\ \tilde{I}_4 &= \sin \delta_V \int z \sigma_n \bar{p}^2 \cos^2 \bar{\varphi} dS + \cos \delta_V \int n_z \bar{p} \cos \bar{\varphi} dS, \\ \tilde{I}_5 &= \cos \delta_V \int [(z^2 + \bar{p}^2 \cos^2 \bar{\varphi}) n_z + (n_z - \sigma_n z) \bar{p}^2 \cos^2 \bar{\varphi}] dS + \\ &+ \sin \delta_V \int [(z^2 + \bar{p}^2 \cos^2 \bar{\varphi}) \sigma_n \bar{p} \cos \bar{\varphi} - z(n_z - \sigma_n z) \bar{p} \cos \bar{\varphi}] dS. \end{aligned} \right\} \quad (1.3.12)$$

Strictly speaking, these integrals should be evaluated separately for each particular body. However, the principal quantitative and qualitative effects, which are common for various bodies, are conveniently described by assuming some approximation formulas for  $W_i$  and  $I_j$  which correctly reflect the structure of these integrals.

Let us first consider the restoring torque, i.e., the approximation of the coefficient  $\bar{c}(\delta_v)$ . Applying the Gauss—Ostrogradskii formula to the first integral in (1.3.6) (see /41/, and also § 5 of this chapter), we can show that the coefficient  $\bar{c}(\delta_v)$  has the following simple meaning:

$$\bar{c}(\delta_v) = cS_0(\delta_v)z_0(\delta_v), \quad (1.3.13)$$

where  $S_0(\delta_v)$  is the stream cross section, defined in what follows, and  $z_0(\delta_v)$  is the distance from the center of pressure on the satellite's axis of symmetry to the center of mass.

Indeed, let us concentrate on the  $\Omega$ -independent part of the torque  $M$  in (1.3.6). The surface of attack  $S^*$  is completed to a closed surface, comprising  $S^*$  and a cylindrical surface  $S_1$  with its generatrix parallel to the stream and its directrix following the boundary of  $S^*$ ; the surface is closed by a plane bottom  $S_0$  perpendicular to the stream (Figure 4).

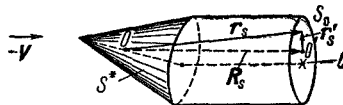


FIGURE 4. Illustrating the calculation of aerodynamic and solar radiation torques.

From the Gauss—Ostrogradskii formula,

$$\iint_{S_0+S_1+S^*} r_s (\mathbf{n} \cdot \mathbf{e}_v) dS = \iiint_{\tau} e_v d\tau,$$

where  $\tau$  is the volume enclosed by the surface  $S_0+S_1+S^*$ . Seeing that on  $S_1$   $\mathbf{n} \cdot \mathbf{e}_v = 0$ , and on  $S_0$   $\mathbf{n} \cdot \mathbf{e}_v = 1$ , we find (reversing the direction of the normal to  $S_0$ )

$$\iint_{S^*} r_s (\mathbf{n} \cdot \mathbf{e}_v) dS = \iint_{S_0} r_s dS + \tau e_v.$$

Substituting in the material part of (1.3.6), we have

$$M = \frac{1}{2} \rho_a V_0^2 e_v \times \iint_{S_0} r_s dS.$$

Let  $O$  be the mass center of the satellite,  $O'$  its projection on  $S_0$ ;  $OO' = |R_s|$ ;  $r_s = R_s + r'_s$ , where  $r'_s$  is in the plane  $S_0$ ; as  $e_v \times R_s = 0$ , we have  $M = \frac{1}{2} \rho_a V_0^2 e_v \times \iint_{S_0} r'_s dS$ . The last integral is  $r_{0s} S_0$ , where  $r_{0s}$  is the vector of the center of mass  $C$  of the bottom relative to  $O'$ . Thus,

$$M = \frac{1}{2} \rho_a V_0^2 \iint_{S_0} e_v \times r_{0s} dS.$$

We may clearly introduce  $z_0$ — the coordinate of the "center of pressure" on the axis  $z$  ( $C$  being its projection on  $S_0$ ). Taking a unit vector  $i$  at right angles to  $e_V$  and  $r_{0S}$ , we find

$$M = \frac{1}{2} c\rho_a V_0^2 S_0(\delta_V) r_{0S}(\delta_V) i = \frac{1}{2} c\rho_a V_0^2 S_0(\delta_V) z_0(\delta_V) \sin \delta_V i,$$

and finally (seeing that  $z_0 = z'_0$ ,  $k = k'$ )

$$M = \frac{1}{2} c\rho_a V_0^2 S_0(\delta_V) z'_0(\delta_V) e_V \times k'. \quad (1.3.14)$$

Comparing with (1.3.11), we find (1.3.13).

Obviously,

$$\bar{c}(\pi - \delta_V) = \bar{c}(\delta_V). \quad (1.3.15)$$

This is a reflection of the properties of ideally inelastic collision: the torque depends only on the size and the position (relative to the satellite) of the section  $S(\delta_V)$ , and  $\bar{c}(\delta_V)$  therefore remains constant under this rotation. From (1.3.12) for  $W_2$  and  $W_3$  we see that when  $\delta_V = 0, \pi$ ,  $W_3(0) = W_2(0) = 0$ , since the integral is taken over the entire lateral surface of the body, i.e., over  $\bar{\varphi}$  from 0 to  $2\pi$ . We may therefore take  $W_2 = \sin \delta_V f_2(\delta_V)$ ,  $W_3 = \sin \delta_V f_3(\delta_V)$ , and then  $\bar{c}(\delta_V)$  from (1.3.11) is written as

$$\bar{c}(\delta_V) = c [W_1(\delta_V) \cos \delta_V + f_2(\delta_V) - [f_2(\delta_V) + f_3(\delta_V)] \cos^2 \delta_V]. \quad (1.3.16)$$

We shall seek  $\bar{c}(\delta_V)$  in the form of a series in powers of  $\cos \delta_V$ . Applying (1.3.15), we see that the simplest approximation of (1.3.16) is

$$c [W_1(\delta_V) \cos \delta_V + f_2(\delta_V)] = a_0^b, \quad -c [f_2(\delta_V) + f_3(\delta_V)] = a_2^b,$$

where  $a_0^b$  and  $a_2^b$  are constants. Then

$$\bar{c}(\delta_V) = a_0^b + a_2^b \cos^2 \delta_V. \quad (1.3.17)$$

Now, according to (1.3.13), we can easily calculate the coefficients  $a_0^b$  and  $a_2^b$  in terms of the constants  $S(0)z_0(0)$  and  $S(\pi/2)z_0(\pi/2)$ , but  $a_0^b$  and  $a_2^b$  may also be selected by an alternative technique, so that the approximation formula (1.3.17) gives the best description of the true dependence  $\bar{c}(\delta_V)$ . For an oblong body, e.g., we may take  $a_0^b > 0$ ,  $a_2^b < 0$ . In the simplest case we may even set

$$a_2^b = 0, \quad \bar{c}(\delta_V) = a_0^b. \quad (1.3.18)$$

According to (1.3.13),  $a_0^b > 0$  then signifies that the center of pressure is "in front" of the center of mass ( $z_0 > 0$ ), and  $a_0^b < 0$  indicates that the center of pressure is "behind" the center of mass ( $z_0 < 0$ ) for  $\delta_V < \pi/2$ . If the collision is not ideally inelastic, and part of the molecules are reflected, condition (1.3.15) need not apply, since now there is a distinct difference between the previously indistinguishable cases of "leading nose" and "leading tail". Although we do not derive the general formulas for this

case, we may assume an approximation formula

$$\bar{c}(\delta_v) = a_0^b + a_1^b \cos \delta_v + a_2^b \cos^2 \delta_v, \quad (1.3.19)$$

which provides the simplest expression of the fact that

$$\bar{c}(\pi - \delta_v) \neq \bar{c}(\delta_v). \quad (1.3.20)$$

We shall principally operate with approximation formula (1.3.17), whereas additional effects attributable to condition (1.3.20) will be introduced by approximation formula (1.3.19). Note that if the satellite is also symmetric about some other plane perpendicular to the spin axis (e.g., a satellite in the shape of an ellipsoid of revolution, etc.), then  $c(\pi - \delta_v) = c(\delta_v)$  irrespective of the molecular motions. In this case we should also set  $a_1^b = 0$  in the approximation formula. Also note that for small angles of attack we may take  $c(0) = c(0) = a_0^b + a_1^b + a_2^b = \text{const.}$

We now proceed with the approximation of  $I_j$ . The main terms entering  $I_j$  will be assumed as approximation formulas. The integrals containing the factor  $\cos \varphi$  in their integrands may be written, as we have observed, in the form  $\sin \delta_v / (\delta_v)$ . Hence we see that  $I_1$ , as well as  $I_3$  and  $I_5$ , may be regarded as positive quantities for any  $\delta_v$ ; the main part of these functions is therefore a certain constant (which is positive on account of physical considerations). As regards  $I_3$  and  $I_5$ , we should also note that the difference  $I_3 - I_5$  is zero on integration over the entire lateral surface (i.e., for  $\delta_v = 0, \pi$ ). The main parts of  $I_3$  and  $I_5$  are therefore approximated by constants of equal value.  $I_2$  and  $I_4$ , however, cannot be approximated with constant numbers; they vary in proportion in the sine of the angle of attack. To sum up, we set

$$\left. \begin{aligned} \tilde{I}_1 &\approx I_1, & \tilde{I}_3 &\approx I_3, & \tilde{I}_5 &\approx I_3, & \tilde{I}_2 &\approx I_2 \sin \delta_v, \\ \tilde{I}_4 &\approx I_4 \sin \delta_v, & I_k &= \text{const.}, & k &= 1, 2, 3, 4. \end{aligned} \right\} \quad (1.3.21)$$

We see from (1.3.12) that, in general, the assumption  $I_2 = I_4$  is inadmissible; this is, however, of no significance in the analysis of motion.

The quantities (1.3.21) can be calculated from (1.3.12) by setting, say,  $\delta_v = 0$  and  $\delta_v = \pi/2$  and taking the arithmetic average of the two extreme values of  $I_k$ ; other approximate estimates for  $I_k$  can also be sought; all  $I_k$  have the dimension [cm<sup>4</sup>]. The calculation of  $I_k$  is essentially simplified when a particular body geometry is assumed (e.g., cylinder, cone, sphere, etc.). Anyhow,  $I_k$  are assumed to be known.

The aerodynamic torques are of greatest significance for satellites flying at a comparatively low altitude. Comparison of aerodynamic torques with gravity torques (see Chapter 3 and § 6 of the present chapter) shows that in typical cases aerodynamic torques prevail at altitudes of up to 300 km, while gravity torques take over at altitudes above 600 km.

#### § 4. TORQUES PRODUCED BY THE MAGNETIC FIELD

Artificial satellites in orbit around the Earth interact with the geo-magnetic field. This interaction is attributable to the current-carrying

devices and the permanent magnets in the satellite payload, as well as the magnetization of the hull and the induction of eddy currents in the metal, etc.

We know /50/ that the torque  $\mathbf{M}$  produced by the interaction of an external magnetic field of strength  $\mathbf{H}$  with the intrinsic magnetic field of a body with a magnetic moment  $\mathbf{I}$  is defined as the vector product

$$\mathbf{M} = \mathbf{H} \times \mathbf{I}. \quad (1.4.1)$$

Among the factors contributing to the magnetic moment of the satellite we shall first consider the following:

a) Current-carrying devices and permanent magnets in instruments. For simplicity, we shall assume that all these factors jointly produce a constant magnetic moment  $I_0$  along the axis of symmetry of the satellite:

$$\mathbf{I}_0 = \mathbf{k}' I_0. \quad (1.4.2)$$

Here  $\mathbf{k}'$  is a unit vector in the direction of the symmetry axis.

b) Magnetization of the satellite hull in the geomagnetic field. For fairly ablong bodies, the resulting magnetic moment  $\mathbf{I}_1$  points along the axis of symmetry, its magnitude being proportional to the component of the external field on this axis:

$$\mathbf{I}_1 = \frac{\mu_0 - 1}{4\pi} v (\mathbf{H} \cdot \mathbf{k}') \mathbf{k}'. \quad (1.4.3)$$

Here  $\mu_0$  is the magnetic permeability,  $v$  the volume of the hull. The total magnetic moment is thus taken in the form

$$\mathbf{I} = \left\{ \mathbf{I}_0 + \frac{\mu_0 - 1}{4\pi} v (\mathbf{H} \cdot \mathbf{k}') \right\} \mathbf{k}'. \quad (1.4.4)$$

According to (1.4.4) the magnetic moment vector points along the longitudinal axis of the satellite. We have thus neglected the transverse component  $\mathbf{I}_{\perp}$  of the vector  $\mathbf{I}$ .

In a more general case, we may assume different magnetic permeabilities along ( $\mu_{||}$ ) and across ( $\mu_{\perp}$ ) the hull. The expression for the couple of magnetic forces is then

$$\mathbf{M} = \mathbf{H} \times \left\{ \mathbf{I}_0 + \frac{v}{4\pi} [(\mu_{||} - 1) \mathbf{H}_{||} + (\mu_{\perp} - 1) \mathbf{H}_{\perp}] \right\}. \quad (1.4.5)$$

Here the magnetic moment  $\mathbf{I}_0$  of the intrinsic satellite field has an arbitrary orientation relative to the satellite. If  $\mu_{\perp} \ll \mu_{||}$ , the transverse component of the magnetization vector is negligible; if we further assume that the direction "along the hull" is parallel to the axis of symmetry of the satellite, and that  $\mathbf{I}_0$  is defined by (1.4.2), we return to formula (1.4.4).\*

The vector  $\mathbf{H}$  of the geomagnetic field is taken in the form /51/

$$\mathbf{H} = \frac{\mu_E}{R^3} [\mathbf{k}_E - 3(\mathbf{k}_E \mathbf{e}_r) \mathbf{e}_r], \quad (1.4.6)$$

\* Formula (1.4.4) adopted in /78/ is equivalent to the assumption  $\mu_{\perp} - 1 = 0$ . A different formula is assumed in /79/, where  $\mu_{\perp} = 0$ . Both formulas are qualitatively identical, apart from a constant factor. Strictly speaking, the components  $I_i$  of the induced magnetic moment and the components  $H_h$  of the external magnetic field are related by  $I_i = \frac{v}{4\pi} \alpha_{ih} H_h$ , where  $\alpha_{ih}$  is a symmetric tensor /50/.

where  $k_E$  is a unit vector in the direction of the geomagnetic dipole axis,  $e$ , a unit vector along the radius-vector  $R$  of the orbit,  $\mu_E$  the magnetic moment of the terrestrial dipole ( $\mu_E \approx 8 \cdot 10^{25}$  oersted  $\cdot$  cm $^3$ ). For simplicity we shall take  $k_E$  to coincide with the Earth's axis. Consider a system of fixed axes  $XZY$ , with the axis  $Y$ , as in § 1, pointing along the Earth's axis, while the axis  $Z$  points to the orbital node. The components of the field  $H$  (1.4.6) are then

$$\left. \begin{aligned} H_Z &= -\frac{\mu_E}{R^3} 3 \sin i \sin u \cos u, \\ H_X &= -\frac{\mu_E}{R^3} 3 \sin i \cos i \sin^2 u, \\ H_Y &= \frac{\mu_E}{R^3} [1 - 3 \sin^2 i \sin^2 u]. \end{aligned} \right\} \quad (1.4.7)$$

Let us now consider the torques produced by eddy currents in the hull. Exact calculation of these torques involves formidable difficulties and cannot be performed unless a particular satellite geometry is assumed. However, proceeding from the fundamental properties of the torque produced by eddy currents, we can derive approximate formulas which provide a satisfactory model of the actual torque pattern. We shall not go beyond the derivation of these approximate models.

Eddy currents are induced when the satellite spins in a magnetic field. The following reasonable assumptions can be made concerning the torques produced by these eddy currents:

- a) When a body spins around a line of force in the external magnetic field, no eddy currents are induced in the hull; eddy currents arise only when the body spins across lines of force. Let  $\Omega$  be the angular velocity of the body,  $H$  the magnetic strength of the external field; eddy currents are then induced by the component  $\Omega_{\perp}$  of the angular velocity, where  $\Omega_{\perp}$  is the projection of  $\Omega$  on a direction which lies in the plane  $(\Omega H)$ , at right angles to  $H$ .
- b) Eddy currents cause dissipation of energy and they consequently reduce the angular velocity  $\Omega$  (in point of fact, only the component  $\Omega_{\perp}$  decreases, while the other component  $\Omega_{\parallel}$  parallel to  $H$  remains unaffected: it induces no eddy currents). This implies that a torque  $M$  is produced, which is directed opposite to the vector  $\Omega_{\perp}$  and is in all probability proportional to  $\Omega_{\perp}$ ,  $|\Omega_{\perp}| = |\Omega \sin \delta_H|$ .
- c) The torque should have the form (1.4.1), while the magnetic moment  $I$  contributed by the eddy currents is determined by the strength  $H$  of the external magnetic field. Thus taking  $I$  to be proportional to  $H$ , we find from (1.4.1) that  $M$  is proportional to  $H^2$ .

According to our remarks under a, b, c, the torque produced by eddy currents has the form

$$M = -k_s H^2 \Omega \sin \delta_H e_{\perp H}, \quad (1.4.8)$$

where  $\delta_H$  is the angle between  $\Omega$  and  $H$ ,  $e_{\perp H}$  a unit vector along  $\Omega_{\perp}$ ;  $k_s$  a dissipation coefficient depending on hull parameters, and also on the satellite attitude. Let  $x'y'z'$  be the fixed axes of a satellite, which has a symmetric hull and correspondingly displays dynamic symmetry; the axis of symmetry is the axis  $z'$ . The torque components along axes perpendicular to  $x'$ ,  $y'$ ,  $z'$

and lying in the planes  $x'H$ ,  $y'H$ ,  $z'H$ , respectively, are then given by

$$\left. \begin{aligned} M_{Hx'} &= -k_s H^2 p \sin(\widehat{x', H}) e_{Hx'}, \\ M_{Hy'} &= -k_s H^2 q \sin(\widehat{y', H}) e_{Hy'}, \\ M_{Hz'} &= -k_s H^2 r \sin(\widehat{z', H}) e_{Hz'} \end{aligned} \right\} \quad (1.4.9)$$

Here  $p, q, r$  are the components of the angular velocity of the body along the axes  $x', y', z'$ ;  $e_{Hx'}, e_{Hy'}, e_{Hz'}$  unit vectors along  $p_\perp, q_\perp, r_\perp$ , defined by analogy with  $\Omega_\perp$ . Let  $\delta_0$  be the angle between  $z'$  and  $H$ ; also  $\delta_1 = (\widehat{x', H})$ ,  $\delta_2 = (\widehat{y', H})$ . The matrix of the direction cosines of the axes  $x', y', z'$  and  $e_{Hx'}, e_{Hy'}, e_{Hz'}$  has the form

$$\begin{matrix} & e_{Hx'} & e_{Hy'} & e_{Hz'} \\ x' & \sin \delta_1 & -\cos \delta_1 \operatorname{ctg} \delta_2 & -\cos \delta_1 \operatorname{ctg} \delta_0 \\ y' & -\cos \delta_2 \operatorname{ctg} \delta_1 & \sin \delta_2 & -\cos \delta_2 \operatorname{ctg} \delta_0 \\ z' & -\cos \delta_0 \operatorname{ctg} \delta_1 & -\cos \delta_0 \operatorname{ctg} \delta_2 & \sin \delta_0 \end{matrix} \quad (1.4.10)$$

Consider a right-hand system of coordinates  $Ox_H y_H z_H$ , the axis  $y_H$  pointing along  $H$ ; the axes  $x_H$  and  $z_H$  are arbitrary for the time being (see § 1). The total torque

$$M = M_{Hz'} + M_{Hx'} + M_{Hy'}, \quad (1.4.11)$$

made up from the components (1.4.9) can now be resolved along the axes  $x', y', z'$  applying the matrix (1.4.10) and the cosine matrix from § 1, and also seeing that  $\sin^2 \delta_1 = 1 - \beta_H^2$ , etc. The components of  $M$  along the axes  $x', y', z'$ :

$$\left. \begin{aligned} M_{x'} &= -H^2 \{ k_s p - k_s \beta_H (\beta_H p + \beta'_H q) - k_s \beta_H \beta''_H r \}, \\ M_{y'} &= -H^2 \{ k_s q - k_s \beta'_H (\beta_H p + \beta'_H q) - k_s \beta'_H \beta''_H r \}, \\ M_{z'} &= -H^2 \{ k_s r - k_s \beta''_H (\beta_H p + \beta'_H q) - k_s \beta''_H r \}, \\ M &= -k_s \{ H^2 \Omega - (H \cdot \Omega) H \} = \\ &= k_s H \times [H \times \Omega]^*. \end{aligned} \right\} \quad (1.4.12)$$

The dissipation coefficient  $k_s$ , in general, depends on the shape of the satellite and its attitude relative to  $H$ . The coefficient cannot be determined unless we choose a particular satellite geometry. Since  $k_s$  is a nonzero positive number, we shall approximate it with a certain known, attitude-independent constant, having the following structure:

$$k_s = a_{0,1}^* J_{0,1} \frac{h_{\text{hull}}}{\mathfrak{R}},$$

where  $J_{0,1}$  is the longitudinal or the transverse moment of inertia of the satellite hull,  $h_{\text{hull}}$  the thickness of the hull,  $\mathfrak{R}$  specific volume resistance of the hull material. If  $H$  and  $\Omega$  are given in electromagnetic units, then  $a_{0,1}^*$  are dimensionless coefficients. For a spherical hull of radius  $a_{\text{sph}}$ ,

\* More precisely,  $M = k_s H \times (H \times \Omega + \dot{H})$ , but for fairly large  $\Omega$ ,  $\dot{H}$  can be neglected. This formula is derived as follows: in (1.4.12),  $\Omega = \Omega_{\text{abs}} - \Omega_{\text{tr}}$ , where  $\Omega_{\text{tr}} \times H = H \cdot \frac{d\mathbf{e}_H}{dt} = \dot{H} - \frac{\dot{H}}{H} H$ . Vector-multiplying by  $H$ , we obtain the above expression for  $M$  (where  $\Omega_{\text{abs}}$  is again denoted by  $\Omega$ ).

we have /38/

$$k_s = \frac{2\pi a_{\text{sph}}^4 h_{\text{hull}}}{3\Re}. \quad (1.4.13)$$

In a more general case,  $k = k_0 f(\beta_H, \beta'_H, \beta''_H)$ ; we may take, e.g.,

$$k_s = k_{0s} \left( 1 + a_0^s \beta_H^2 + a_1^s \beta_H'^2 + a_2^s \beta_H''^2 \right).$$

Let us write the components of the eddy-current torques along the fixed axes  $\bar{X}, \bar{Y}, \bar{Z}$  of the geomagnetic dipole field. The direction cosines  $\beta_H, \beta'_H, \beta''_H$  of the satellite axes relative to the magnetic field  $H$  are

$$\left. \begin{aligned} \beta_H &= (\tilde{\alpha}_1 H_x + \tilde{\beta}_1 H_y + \tilde{\gamma}_1 H_z) \frac{1}{H}, \\ \beta'_H &= (\tilde{\alpha}_2 H_x + \tilde{\beta}_2 H_y + \tilde{\gamma}_2 H_z) \frac{1}{H}, \\ \beta''_H &= (\tilde{\alpha}_3 H_x + \tilde{\beta}_3 H_y + \tilde{\gamma}_3 H_z) \frac{1}{H}. \end{aligned} \right\} \quad (1.4.14)$$

Writing the torque components  $M_{\bar{X}}, M_{\bar{Y}}, M_{\bar{Z}}$ , we apply (1.4.12), (1.4.14), and relations of the form  $p\tilde{\alpha}_1 + q\tilde{\alpha}_2 = \frac{L_{\bar{X}} - C r \tilde{\alpha}_3}{A}$  (where  $L_{\bar{X}}$  is a component of the angular momentum). After simple manipulations, we find

$$\left. \begin{aligned} M_{\bar{X}} &= -H^2 \left\{ k_s \frac{L_{\bar{X}}}{A} + \left( k_s - \frac{C}{A} k_s \right) r \tilde{\alpha}_3 - \frac{H_{\bar{X}}}{H} F \right\}, \\ M_{\bar{Y}} &= -H^2 \left\{ k_s \frac{L_{\bar{Y}}}{A} + \left( k_s - \frac{C}{A} k_s \right) r \tilde{\beta}_3 - \frac{H_{\bar{Y}}}{H} F \right\}, \\ M_{\bar{Z}} &= -H^2 \left\{ k_s \frac{L_{\bar{Z}}}{A} + \left( k_s - \frac{C}{A} k_s \right) r \tilde{\gamma}_3 - \frac{H_{\bar{Z}}}{H} F \right\}, \\ F &= \frac{H_{\bar{X}}}{H} \left[ k_s \frac{L_{\bar{X}}}{A} + \left( k_s - \frac{C}{A} k_s \right) r \tilde{\alpha}_3 \right] + \\ &\quad + \frac{H_{\bar{Y}}}{H} \left[ k_s \frac{L_{\bar{Y}}}{A} + \left( k_s - \frac{C}{A} k_s \right) r \tilde{\beta}_3 \right] + \\ &\quad + \frac{H_{\bar{Z}}}{H} \left[ k_s \frac{L_{\bar{Z}}}{A} + \left( k_s - \frac{C}{A} k_s \right) r \tilde{\gamma}_3 \right]. \end{aligned} \right\} \quad (1.4.15)$$

## § 5. SOLAR RADIATION TORQUES AND THEIR APPROXIMATIONS

When an artificial space vehicle moves in orbit around the Earth or especially around the Sun, its motion can be substantially influenced by the light pressure of the solar radiation. Solar radiation torques are among the more significant factors influencing the motion of a satellite around its mass center.

Following A. A. Karymov /41, 42/, we shall derive integral expressions for the forces and torques produced by the impact of a luminous flux on the surface of a satellite.

**1. Forces and torques on a satellite of arbitrary shape.** The light pressure  $p$ , at a distance  $R$  from the center of the Sun is given by

$$p_r = \frac{E_0}{c} \left( \frac{R_0}{R} \right)^2.$$

where  $c$  the velocity of light,  $E_0$  the flux of luminous energy at a distance  $R_0$  from the center of the sun. Let  $R_0$  be the radius of the Earth's orbit, then  $E_0 = 1200 \text{ kcal/m}^2 \cdot \text{hour} = 1.39 \cdot 10^6 \text{ erg} \cdot \text{sec/cm}^2$ , and  $p_{r0} = E_0/c = 4.64 \cdot 10^{-5}$  dyne/cm<sup>2</sup> =  $4.72 \cdot 10^{-8} \text{ g/cm}^2$ .

Let us examine the interaction of a luminous flux with a surface element  $dS$ . The angle of incidence is assumed to be equal to the angle of reflection, the incident and the reflected fluxes lying in one plane, at right angles to  $dS$  (Figure 5). The elementary force  $df$  acting on the surface element  $dS$  is

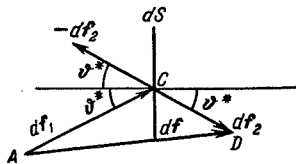


FIGURE 5. Illustrating the calculations of solar radiation torques.

made up from the force  $df_1$  exerted by the incident flux and the force  $df_2$  produced by the reflected flux. Let  $\epsilon_0$  be the reflection coefficient, i.e., the ratio of the reflected to incident energy density. The elementary force  $df_i = df_i^{(1)} + df_i^{(2)}$ , where  $df_i^{(1)}$  is attributable to the absorbed flux and  $df_i^{(2)}$  to the reflected flux. The force  $df_i^{(1)}$  clearly points along the direction of the flux. Let  $\tau$  be a unit vector in the opposite direction, and  $n$  a unit vector along the outer normal, so that  $n \cdot \tau = \cos \theta^*$  (Figure 5). Since the radiation pressure on a surface element  $\Delta S$  perpendicular to the flux is  $p_r \Delta S$ , a surface element making an angle with the flux experiences a force

$$df_i^{(1)} = df_\tau = p_r(n \cdot \tau) \tau dS (1 - \epsilon_0), \quad (1.5.1)$$

where the factor  $(1 - \epsilon_0)$  implies that we consider the absorbed, and not the reflected, part of the flux. The reflected part produces a force  $df_i^{(2)}$  when hitting the surface element  $dS$ , and an additional force  $df_2$  on reflection; the resultant of these two forces clearly points along the inner normal to the surface element (specular reflection). Each of the elementary forces  $df_i^{(2)}$  and  $df_2$  is equal to  $p_r(n \cdot \tau) dS \epsilon_0$ , while their projections on  $n$  are  $p_r(n \cdot \tau)^2 n dS \epsilon_0$ , so that

$$\left. \begin{aligned} df_i^{(2)} + df_2 &= df_n = -2p_r(n \cdot \tau)^2 n dS \epsilon_0, \\ df &= df_\tau + df_n. \end{aligned} \right\} \quad (1.5.2)$$

Let  $S_i$  be the illuminated part of the body surface, i.e., the part satisfying the inequality  $\tau \cdot n > 0$ . The resultant force of light pressure applied to the body is then

$$\left. \begin{aligned} F &= (1 - \epsilon_0) F^+ + \epsilon_0 F^-, \\ F^+ &= -p_r \tau \int_{S_i} (\tau \cdot n) dS, \\ F^- &= -2p_r \int_{S_i} n (\tau \cdot n)^2 dS. \end{aligned} \right\} \quad (1.5.3)$$

The resultant torque produced by this light pressure is

$$\left. \begin{aligned} M &= (1 - \epsilon_0) M^+ + \epsilon_0 M^- \\ M^+ &= p_r \mathbf{e} \times \int_{S_1} \mathbf{r}_s (\mathbf{e} \cdot \mathbf{n}) dS, \\ M^- &= 2p_r \int_{S_1} \mathbf{n} \times \mathbf{r}_s (\mathbf{e} \cdot \mathbf{n})^2 dS, \end{aligned} \right\} \quad (1.5.4)$$

where  $\mathbf{r}_s$  is the radius-vector (relative to the mass center of the body) of a current point on the body surface. The integrands and the domain of integration depend on the surface parameters and the attitude of the body. Calculation of forces and torques therefore involves certain difficulties and, in general, requires knowledge of the particular body geometry. However, the expression for  $M^+$  in (1.5.4) is analogous to the expression for the aerodynamic torques in the case of ideally inelastic impact (the first term in (1.3.6)), and it can be simplified like the expression for  $F^+$ . The exact procedure is a repetition of the techniques applied in § 3 for the aerodynamic torques. The result is

$$F^+ = p_r S_2 \mathbf{e}, \quad M^+ = p_r S_2 \mathbf{e} \times \mathbf{r}_{0S}. \quad (1.5.5)$$

Here  $S_2$  is the projection of the illuminated surface onto a plane perpendicular to the flux;  $\mathbf{r}_{0S}$  the radius-vector of the center of gravity of the domain  $S_2$  relative to the projection of the satellite's mass center on the plane containing the domain  $S_2$ .  $F^-$  and  $M^-$ , however, must be evaluated by direct integration for particular bodies. Some results of these calculations are given in /41/.

**2. Formulas for a symmetric satellite.** For a body with an axisymmetric surface, the solar radiation torque only depends on the position of the axis of symmetry in space, since rotation about the axis of symmetry clearly does not affect the situation. Nevertheless, exact calculation of the radiation torques involves the same difficulties which we have encountered in the calculation of aerodynamic torques. In the present case, however, we cannot select one particular mode of reflection of light quanta by the surface for purposes of our analysis, since the reflection is determined by the specific properties of each body. It is therefore advisable to adopt approximation formulas similar to those applied for the aerodynamic torques. From (1.5.4), for axisymmetric bodies we may find /13, 42/

$$M = \frac{a_r(\epsilon_s) R_0^2}{R^2} \mathbf{e}_r \times \mathbf{k}'. \quad (1.5.6)$$

For the case of total absorption

$$a_r(\epsilon_s) \frac{R_0^2}{R^2} = p_r S(\epsilon_s) z'_0(\epsilon_s). \quad (1.5.7)$$

Here  $\mathbf{e}_r$  is a unit vector along the radius-vector (a satellite of the Sun is considered);  $\mathbf{k}'$  a unit vector along the axis of symmetry of the satellite;  $\epsilon_s$  the angle between these unit vectors, so that  $|\mathbf{e}_r \times \mathbf{k}'| = \sin \epsilon_s$ ;  $R$  the current distance from the center of the Sun to the satellite's mass center;  $R_0$  a fixed (e.g., initial) value of  $R$ ;  $a_r(\epsilon_s)$  a coefficient of solar radiation torque;  $S$  "shadow" area on a plane perpendicular to the flux;  $z'_0$  the distance from

the center of mass to the center of pressure.  $a_r$  and  $M$  have the same dimensions. We shall take  $a_r = a_r(\cos \epsilon_s)$ , approximating  $a_r$  with polynomials in powers of  $\cos \epsilon_s$ . Particular expressions for  $a_r(\cos \epsilon_s)$  will be considered in Chapter 9.\*

## § 6. ESTIMATING THE RELATIVE INFLUENCE OF THE VARIOUS TORQUES

Let us estimate the relative magnitudes of the various torques on a satellite /96/. We shall evaluate the maximum values of gravity  $M_g$ , aerodynamic  $M_a$ , magnetic  $M_H$ , and solar radiation  $M_r$ ; torques on an Earth's satellite with the following characteristic parameters: aerodynamic torque coefficients  $C^m = C_x S = 3 m^3 = 3 \cdot 10^6 \text{ cm}^3$  (which for  $C_x = 2$  corresponds to a characteristic area  $S = 3 \text{ m}^2$  and center of mass to center of pressure distance  $z = 0.5 \text{ m}$ ); difference in moments of inertia  $A - C = 3 \cdot 10^9 \text{ g} \cdot \text{cm}^2$ ; intrinsic magnetic moment  $I = 3.5 \cdot 10^3 \text{ g}^{1/2} \cdot \text{cm}^{5/2}/\text{sec}$ .

These characteristics are indicatory of space vehicles of the type of Sputnik III.

The density of the atmosphere for our purposes can be borrowed from /56, 57, and others/. The magnetic moment of the terrestrial dipole  $\mu_E = 8 \cdot 10^{25} \text{ g}^{1/2} \cdot \text{cm}^{5/2}/\text{sec}$ ; solar radiation pressure in the Earth's orbit  $p_{ro} = 4.64 \cdot 10^{-5} \text{ dyne/cm}^2$ . We shall also estimate the torque  $M_m$  produced by the impact of micrometeorites, assuming  $\rho_m = 1.5 \cdot 10^{-20} \text{ g/cm}^3$  for the density of meteoric matter near the Earth /96/, and 7–8 km/sec for the velocity of the satellite relative to the meteoric matter.

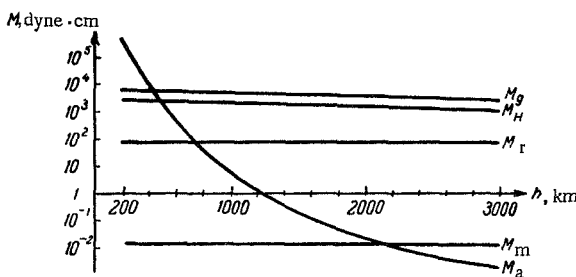


FIGURE 6. Torques on a satellite of the Earth as a function of the orbit height  $h$ :  $M_g$  gravity torque;  $M_a$  aerodynamic torque;  $M_H$  magnetic torque;  $M_r$  solar radiation torque;  $M_m$  micrometeorite impact torque.

The results of these calculations are plotted in Figure 6. We see that for altitudes of up to 200–300 km above the surface of the Earth, aerodynamic torques predominate, while gravity torques prevail at altitudes over 500 km. Magnetic torques are always comparable with gravity torques.

\* A rigorous derivation of (1.5.6) for a symmetric satellite and exact expressions for  $a_r(\cos \epsilon_s)$  (in integral form) are given in /42/.

Note that in /77/ not only the solar radiation pressure is considered, but also the pressure due to the radiation reflected and emitted by the Earth, and the motion around a center of mass is analyzed for the combined influence of all these factors.

Note, however, that the magnetic torques may be much higher (by two or three orders of magnitude) if the satellite carries strong permanent magnets, powerful current-carrying devices, etc. Solar radiation torques are one-tenth to one-hundredth of the gravity torques in the range of altitudes up to 3000 km, but already for  $h > 700$  km these torques are comparable with, and even greater than, the aerodynamic torques. Solar radiation torques will exceed the gravity torques at altitudes above  $h \approx 35,000 - 40,000$  km. In the range between 300 and 500 km, gravity, aerodynamic, and magnetic torques are all of comparable magnitude. The torque produced by the impact of micrometeorites is always negligible.

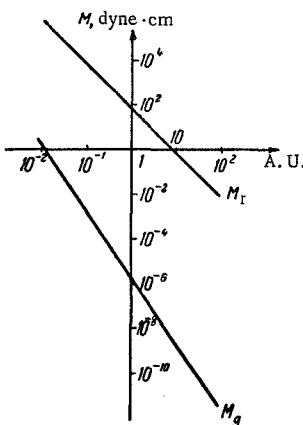


FIGURE 7. Solar radiation  $M_r$  and gravity  $M_g$  torques on a satellite of the Sun as a function of the distance from the Sun (in astronomical units).

The relative magnitudes of the torques are quite different for the satellite of the Sun. The magnetic torques are apparently negligible; gravity torques are probably also small. Solar radiation torques prevail, as we easily see from Figure 7, which plots the gravity and the radiation torques for a space vehicle in orbit around the Sun. Solar radiation torques in this case are greater than the gravity torques by several orders of magnitude. Solar radiation torques will retain their dominant position even for space vehicles with inertia characteristics greater by two or three magnitudes than the figures assumed in our calculations.

## Chapter 2

### STABILIZATION AND LIBRATION OF THE SATELLITE IN A NEWTONIAN FORCE FIELD

If the rotational kinetic energy of a satellite is fairly small in comparison with the work of external torques, the motion of the satellite will be libratory: the satellite will oscillate about a position of stable relative equilibrium. The determination of these equilibrium positions and the study of libration is of particular significance with a view to attitude stabilization of space vehicles with the aid of external torques.

#### § 1. THE EQUATIONS OF MOTION OF A SATELLITE AROUND ITS MASS CENTER IN THE LIMITED PROBLEM. JACOBI INTEGRAL. STABLE RELATIVE EQUILIBRIUM

We shall assume that the motion of a satellite around its center of mass has no influence on the orbit, so that the mass center moves in an elliptical Kepler orbit. This assumption is justified since the satellite is small in comparison with the dimensions of the orbit. This statement of the so-called limited problem is often applied in the classical analysis of the Earth's precession and the libration of the Moon /94/.

Substituting expressions (1.2.2) of the gravity torques in Euler's equations, we find

$$\left. \begin{aligned} A \frac{dp}{dt} + (C - B)qr &= 3\frac{\mu}{R^3}(C - B)\gamma\gamma'', \\ B \frac{dq}{dt} + (A - C)pr &= 3\frac{\mu}{R^3}(A - C)\gamma''\gamma, \\ C \frac{dr}{dt} + (B - A)qp &= 3\frac{\mu}{R^3}(B - A)\gamma\gamma'. \end{aligned} \right\} \quad (2.1.1)$$

For the relative direction cosines, we have

$$\left. \begin{aligned} \frac{dy}{dt} &= \gamma'r - \gamma''q + \omega a, & \frac{da}{dt} &= a'r - a''q - \omega y, \\ \frac{d\gamma'}{dt} &= \gamma''p - \gamma r + \omega a', & \frac{da'}{dt} &= a''p - ar - \omega \gamma', \\ \frac{d\gamma''}{dt} &= \gamma q - \gamma' p + \omega a'', & \frac{da''}{dt} &= aq - a'p - \omega \gamma''. \end{aligned} \right\} \quad (2.1.2)$$

Here  $\omega$  is the angular orbital velocity of the mass center. The set (2.1.1)–(2.1.2) is a closed system of differential equations: there are 9 equations in 9 unknowns. Note that not all the variables are independent (in virtue of the properties of the matrix of direction cosines). The set

can be supplemented with equations for  $\beta$ ,  $\beta'$ ,  $\beta''$ :

$$\frac{d\beta}{dt} = \beta' r - \beta'' q, \quad \frac{d\beta'}{dt} = \beta'' p - \beta r, \quad \frac{d\beta''}{dt} = \beta q - \beta' p. \quad (2.1.3)$$

The set (2.1.1)–(2.1.3) apparently is not integrable in a finite form. Indeed, according to the theory of Jacobi's last multiplier, the integration of this set requires knowledge of four first integrals which are time-independent and nontrivial (relations between the cosines). And yet, even in the most favorable case, we can write two integrals only: if the ellipsoid of inertia is an ellipsoid of revolution, i.e., if  $A=B$ , we have the first integral

$$r=r_0, \quad (2.1.4)$$

and then, for a circular orbit, with arbitrary moments of inertia, we have the Jacobi-type integral

$$\begin{aligned} \frac{1}{2}(Ap^2 + Bq^2 + Cr^2) + \frac{3}{2}\omega^2(A\gamma^2 + B\gamma'^2 + C\gamma''^2) - \\ - \omega(Ap\beta + Bq\beta' + Cr\beta'') = h \end{aligned} \quad (2.1.5)$$

(the existence of this integral can be easily verified by, say, substituting in equations (2.1.1)–(2.1.3) and remembering that for a circular orbit  $\frac{\mu}{R^3} = \omega^2 = \text{const}$ ).

Let us express this integral in terms of relative angular velocities

$$\bar{p} = p - \omega\beta, \quad \bar{q} = q - \omega\beta', \quad \bar{r} = r - \omega\beta''. \quad (2.1.6)$$

Substituting (2.1.6) in (2.1.5), we find

$$\begin{aligned} \frac{1}{2}(\bar{A}\bar{p}^2 + \bar{B}\bar{q}^2 + \bar{C}\bar{r}^2) + \frac{3}{2}\omega^2(A\gamma^2 + B\gamma'^2 + C\gamma''^2) - \\ - \frac{1}{2}\omega^2(A\beta^2 + B\beta'^2 + C\beta''^2) = h. \end{aligned} \quad (2.1.7)$$

The integral (2.1.7) gives the law of conservation of energy in the form

$$T + V_1 + V_2 = h;$$

here  $T$  is the kinetic energy of relative motion,  $V_1$  the potential energy of Newtonian forces,  $V_2$  the potential energy of centrifugal forces. Applying this integral, we can easily derive the conditions for the stability of relative equilibrium.

A relative equilibrium, as we see from the equations of motion, does exist; the matrix of the relative direction cosines in this case (see § 1, Chapter 1) reduces to a unit matrix.

The components of the angular velocity of the satellite in relative equilibrium are  $p=r=0$ ,  $q=\omega$ . In relative equilibrium, the satellite always turns to the Earth one face only.

A particular solution of the equations of motion describing relative equilibrium of a body in a circular orbit is written as

$$\left. \begin{aligned} \bar{p} = \bar{q} = \bar{r} = 0, \quad \alpha = \beta' = \gamma'' = 1, \\ \alpha' = \alpha'' = \beta = \beta'' = \gamma = \gamma' = 0. \end{aligned} \right\} \quad (2.1.8)$$

For these values of the direction cosines, the axis  $y'$  is perpendicular to the plane of the orbit, the axis  $z'$  points along the radius-vector, and the axis  $x'$  is tangential to the circular orbit of the satellite.

Let us apply Lyapunov's theory to establish under what conditions this solution is stable.

Before Lyapunov, stability was generally investigated with linearized equations. But linearized equations may give a wrong answer to the question of stability. The investigation of stability on the basis of non-linear equations reduces to the determination of a certain Lyapunov function. If integrals of motion are known, then, following N.G. Chetaev, we may try to construct the Lyapunov function by the method of matching of integrals. This approach to Lyapunov's theory and the proof of theorems of stability and instability can be found in the books of A.M. Lyapunov /54/, N.G. Chetaev /74/, I.G. Malkin /55/, G.N. Duboshin /33/, and others.

If (2.1.8) is taken to represent unperturbed motion, perturbed motion may be written as

$$\bar{p}, \bar{q}, \bar{r}, 1 + \Delta_1, \alpha', \alpha'', \beta, 1 + \Delta_2, \beta'', \gamma, \gamma', 1 + \Delta_3; \quad (2.1.9)$$

$\Delta_1, \Delta_2, \Delta_3$  and the other quantities characterize the deviation of the perturbed from the unperturbed motion; they are all different from zero.

According to the 1st property of the cosine matrix, we have

$$\gamma'^2 = 1 - \gamma^2 - \gamma'^2, \quad \beta'^2 = 1 - \beta^2 - \beta'^2. \quad (2.1.10)$$

Inserting these  $\gamma''$  and  $\beta'$  in the integral (2.1.7) and collecting the constants in the right-hand side, we have

$$V = \frac{1}{2}(A\bar{p}^2 + B\bar{q}^2 + C\bar{r}^2) + \frac{3}{2}\omega^2[(A-C)\gamma^2 + (B-C)\gamma'^2] + \\ + \frac{1}{2}\omega^2[(B-A)\beta^2 + (B-C)\beta'^2] = h_0. \quad (2.1.11)$$

Here  $h_0$  is a new constant.

The left-hand side of this equality vanishes only in the case of unperturbed motion (2.1.8). For

$$B > A > C \quad (2.1.12)$$

this function is positive. The integral (2.1.11) is thus positive definite when (2.1.12) applies.

The derivative of  $V$  is zero by definition (this is an integral of motion). Hence, according to Lyapunov's theorem, conditions (2.1.12) are sufficient for the stability of relative equilibrium.

The meaning of these conditions emerges from the table (2.1.13), which lists the values of the direction cosines in relative equilibrium and the symbols of the moments of inertia corresponding to the three axes of the body:

	$A$	$B$	$C$
	$x'$	$y'$	$z'$
Tangent to the orbit	$x$	1	0
Normal to the orbital plane	$y$	0	1
Radius-vector of the orbit	$z$	0	0

(2.1.13)

Our analysis thus leads to the following conclusion: a sufficient condition for the stability of relative equilibrium of a satellite in a circular orbit is that the major axis of the ellipsoid of inertia of the satellite should point along the radius-vector, the minor axis along the normal to the orbital plane, and the medium axis along the tangent to the orbit (Figure 8).

Note that we have only considered the stability of motion around the center of mass, while the circular orbit remains unperturbed. In Chapter 4 we shall analyze the general problem and prove that conditions (2.1.12) are sufficient for the stability of unperturbed motion with respect to perturbations about the center of mass and also with respect to extremely small perturbations of the orbit.

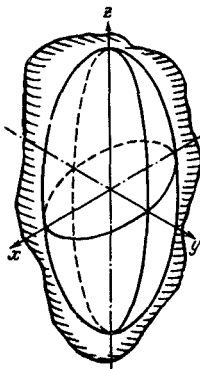


FIGURE 8. Stable position of the ellipsoid of inertia of a satellite in orbit (the axis  $z$  points along the radius-vector,  $y$  perpendicular to the orbital plane,  $x$  along the tangent to the orbit;  $B > A > C$ ).

Conditions (2.1.12) maximize the force function of Newtonian and centrifugal forces; these conditions can be illustrated following the considerations at the end of § 1 in Chapter 1.

The existence of a stable state of relative equilibrium of an orbiting satellite can be applied to devise a system of passive gravity attitude stabilization /60/. This problem is discussed in some detail in § 10 of this chapter.

For the satellite to oscillate about a position of relative equilibrium (without pitching over), the kinetic energy of the satellite's motion around its mass center should be fairly small (this aside from conditions (2.1.12)).

The terms in the left-hand side of (2.1.11) are nonzero positive quantities, and we can therefore estimate the amplitudes of perturbed motion. For the direction cosines we have the obvious estimates

$$\left. \begin{aligned} \gamma^2 &\leq \frac{2h_0}{3\omega^2(A-C)}, & \gamma'^2 &\leq \frac{2h_0}{3\omega^2(B-C)}, \\ \beta^2 &\leq \frac{2h_0}{\omega^2(B-A)}, & \beta''^2 &\leq \frac{2h_0}{\omega^2(B-C)}. \end{aligned} \right\} \quad (2.1.14)$$

The constant  $h_0$  is calculated by substituting the initial data in the left-hand side of the energy integral (2.1.11). From these estimates we can determine the oscillation boundaries of the satellite. If  $h_0$  is fairly large, the body may spin at an arbitrary speed; to prevent this spin, it is necessary that

$$\left. \begin{aligned} \frac{2h_0}{3\omega^2(A-C)} &< 1, \\ \frac{2h_0}{3\omega^2(B-C)} &< 1, \\ \frac{2h_0}{\omega^2(B-A)} &< 1, \\ \frac{2h_0}{\omega^2(B-C)} &< 1. \end{aligned} \right\} \quad (2.1.14')$$

These four conditions of "no pitch-over" can be reduced to a single condition. The second and the fourth conditions are satisfied if  $2h_0 < \omega^2(B-C)$ . Since, however,  $B-A < B-C$ , this condition is satisfied if the third condition in (2.1.14') applies:  $2h_0 < \omega^2(B-A)$ . Conditions (2.1.14) therefore reduce to the 1st and the 3rd inequality in (2.1.14'), which can be combined in a relation

$$h_0 < \min \left\{ \frac{3}{2} \omega^2(A-C), \frac{1}{2} \omega^2(B-A) \right\}. \quad (2.1.15)$$

This condition imposed on the initial data ensures bounded oscillation of the satellite. Also note that for  $h_0 \rightarrow 0$ , we have  $\gamma \rightarrow 0$ ,  $\gamma' \rightarrow 0$ ,  $\beta \rightarrow 0$ ,  $\beta'' \rightarrow 0$ , as is seen from (2.1.14).

The direction cosines  $\gamma, \gamma', \beta, \beta''$  completely define the position of the body, and the angular velocities  $\bar{p}, \bar{q}, \bar{r}$  completely define the spin of the body. The stability of motion with respect to these particular variables, proved by (2.1.11), is therefore equivalent to the stability of the body with respect to all the variables describing its motion.

## § 2. PLANE OSCILLATIONS IN A CIRCULAR ORBIT

The only case when the integration of equations (2.1.1)–(2.1.3) can be completed is the case of plane motion in a circular orbit.

In the plane case, the components of the relative angular velocities  $\bar{p} = \bar{r} = 0$ ,  $\bar{q} \neq 0$ . Consider the angle  $\Theta$  between the axis  $z'$  of the satellite and the radius-vector. In terms of this angle,

$$\bar{q} = \dot{\Theta}, \quad \gamma' = \cos \Theta, \quad \gamma = -\sin \Theta, \quad \beta = \beta'' = 0.$$

Substituting these variables in the integral (2.1.11), we find the energy integral of plane oscillations in the form

$$\frac{1}{2} B \dot{\Theta}^2 + \frac{3}{2} \omega^2(A-C) \sin^2 \Theta = h_0. \quad (2.2.1)$$

Hence,

$$\dot{\Theta} = \pm \sqrt{\frac{2h_0}{B} - 3\omega^2 \frac{A-C}{B} \sin^2 \Theta}. \quad (2.2.2)$$

This equation is integrable. Let us first consider the motion in the phase plane  $(\dot{\Theta}, \Theta)$ . We select three values of  $h_0$ , such that

$$\left. \begin{array}{l} 1^{\circ}. \frac{2h_0}{B} > 3\omega^2 \frac{A-C}{B}, \\ 2^{\circ}. \frac{2h_0}{B} = 3\omega^2 \frac{A-C}{B}, \\ 3^{\circ}. \frac{2h_0}{B} < 3\omega^2 \frac{A-C}{B}, \end{array} \right\} \quad (2.2.3)$$

and for each of these  $h_0$  we plot a phase path  $\dot{\Theta}(\Theta)$  according to (2.2.2). Let  $A > C$ . We obtain the pattern of phase paths shown in Figure 9. We see that the points  $\Theta = 0, \pi$  are points of stable equilibrium, while the points  $\Theta = \pi/2, 3\pi/2$  are points of unstable equilibrium. In other words, in stable equilibrium the larger of the two axes  $x'$ ,  $z'$  of the ellipsoid of inertia — the axis  $z'$  — points along the radius-vector. For large  $h_0$  satisfying inequality 1° in (2.2.3), the satellite spins continuously in one direction. For small  $h_0$  (inequality 3° in (2.2.3)), the motion is periodic. The case of limiting motion is observed on the separatrix where  $h_0$  satisfies equality 2° of (2.2.3): for  $t \rightarrow \infty$ , the phase point on the separatrix approaches the point of (unstable) equilibrium. Spin and periodic motion are the typical modes. Limiting motion is exceptional.

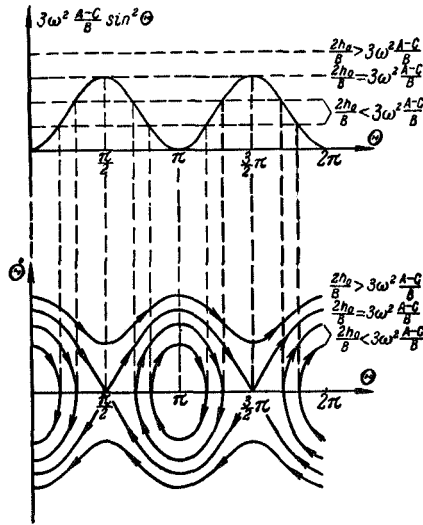


FIGURE 9. Oscillations of a satellite in a circular orbit (phase plane).

Let us now consider the case  $A < C$ ; the stable equilibrium occurs for  $\Theta = \pi/2, 3\pi/2$ . Physically, this means that in the state of stable relative equilibrium the major axis of the ellipsoid of inertia (the axis  $x'$  for once) points toward the center of attraction.

The condition of bounded oscillations 3° in (2.2.3) can now be written as

$$|\dot{\Theta}_0| < \omega \sqrt{3 \frac{A-C}{B} |\cos \Theta_0|}.$$

Since physical considerations invariably lead to the inequalities  $\frac{A-C}{B} \leq 1$ ,  $|\cos \theta_0| \leq 1$ , we find  $|\dot{\theta}_0| < \omega \sqrt{3}$ . Here  $\dot{\theta}_0$  is the initial perturbation of the angular velocity of the satellite around its center of mass. For ordinary orbits of artificial satellites,  $\dot{\theta}_0 \sim 0.05 - 0.1 \text{ deg} \cdot \text{sec}^{-1}$ . This implies that libration is possible only for very small initial perturbations of the angular velocity of rotation about the mass center.

Separating the variables in (2.2.2) and integrating, we find

$$t - t_0 = \int_{\theta_0}^{\theta} \frac{d\theta}{\sqrt{\frac{2h_0}{B} - 3\omega^2 \frac{A-C}{B} \sin^2 \theta}}. \quad (2.2.4)$$

This is an elliptical integral. Let us write it in a normal form. We introduce the modulus of the elliptical integral  $k$ :

$$k^2 = \frac{2h_0}{3\omega^2(A-C)} = \frac{\dot{\theta}_0^2}{3 \frac{A-C}{B} \omega^2} + \sin^2 \theta_0. \quad (2.2.5)$$

We shall consider the case  $k^2 < 1$ , which, according to 3° of (2.2.3), corresponds to bounded oscillation of the satellite. A new variable  $\varphi$  is defined by

$$\sin \theta = k \sin \varphi. \quad (2.2.6)$$

The integral (2.2.4) is now written as

$$\omega \sqrt{3 \frac{A-C}{B}} (t - t_0) = \int_{\varphi_0}^{\varphi} \frac{d\varphi}{\sqrt{1 - k^2 \sin^2 \varphi}}. \quad (2.2.7)$$

The right-hand side of this equality is an elliptical integral in a normal form. Setting

$$F = \int_0^{\varphi} \frac{d\varphi}{\sqrt{1 - k^2 \sin^2 \varphi}} \quad (2.2.8)$$

and inverting (2.2.7), we find

$$\sin \theta = k \cdot \operatorname{sn} \left\{ \omega \sqrt{3 \frac{A-C}{B}} (t - t_0) + F; k^2 \right\}. \quad (2.2.9)$$

From (2.2.9), we have

$$|\sin \theta| \leq k, \quad \max |\sin \theta| = k.$$

The amplitude of oscillation can be obtained from the last equality.

The period  $T$  of oscillations through an angle  $\Theta$  is given by

$$T = \frac{4K(k^2)}{\omega \sqrt{3 \frac{A-C}{B}}} = \frac{T_0}{\sqrt{3 \frac{A-C}{B}}} \cdot \frac{K(k^2)}{\frac{\pi}{2}}, \quad (2.2.10)$$

where  $K$  is a complete elliptical integral of the first kind:

$$K(k^2) = \int_0^{\frac{\pi}{2}} \frac{d\varphi}{\sqrt{1 - k^2 \sin^2 \varphi}}, \quad (2.2.11)$$

and  $T_0 = \frac{2\pi}{\omega}$  is the orbital period of the mass center. If  $k$  is not too large, the elliptical integral may be expanded in terms of  $k^2$ :

$$\begin{aligned} K(k^2) &= \frac{\pi}{2} \left\{ 1 + \left(\frac{1}{2}\right)^2 k^2 + \left(\frac{1 \cdot 3}{2 \cdot 4}\right)^2 k^4 + \dots \right. \\ &\quad \left. \dots + \left[\frac{(2n-1)!!}{2n!!}\right]^2 k^{2n} + \dots \right\}. \end{aligned} \quad (2.2.12)$$

Substituting (2.2.12) in (2.2.10), we find

$$\begin{aligned} T &= \frac{T_0}{\sqrt{3 \frac{A-C}{B}}} \left\{ 1 + \left(\frac{1}{2}\right)^2 k^2 + \left(\frac{1 \cdot 3}{2 \cdot 4}\right)^2 k^4 + \dots \right. \\ &\quad \left. \dots + \left[\frac{(2n-1)!!}{2n!!}\right]^2 k^{2n} + \dots \right\}. \end{aligned} \quad (2.2.13)$$

For small oscillations,  $k^2 \ll 1$  and it can be neglected; then

$$T = \frac{T_0}{\sqrt{3 \frac{A-C}{B}}}. \quad (2.2.14)$$

Note that since  $K(k^2) > \pi/2$ , we have from (2.2.10) that  $T > \frac{T_0}{\sqrt{3 \frac{A-C}{B}}}$ ,

i.e., the period of finite oscillations is always longer than the period of small oscillations. Further, since physically  $\frac{A-C}{B} \ll 1$ , we have  $T > \frac{T_0}{\sqrt{3}}$ . It is easily seen that  $\frac{T_0}{\sqrt{3}}$  is the period of small oscillations of a dumbbell in a circular orbit, since for a dumbbell we may take  $C=0$ ,  $A=B$ . The least possible period of oscillation is thus  $T_{\min} = \frac{T_0}{\sqrt{3}} \approx 0.577 T_0$ . If the orbital period of the satellite  $T_0 = 90$  min, then  $T_{\min} = 61$  min 10 sec. Since the largest period of oscillation is clearly infinite, we always have  $\frac{T_0}{\sqrt{3}} < T < \infty$ . This, in particular, signifies that we can always choose suitable parameters  $A, B, C$  of the satellite and suitable initial values  $\theta_0, \dot{\theta}_0$  so that the period of oscillation  $T$  should be equal to the orbital period  $T_0$ . From (2.2.10) we see that the corresponding values of the parameters satisfy the transcendental equation  $K(k^2) = \frac{\pi}{2} \sqrt{3 \frac{A-C}{B}}$ .

A specimen calculation of the period and the amplitude of oscillations for plane motion. The parameters of this example are close to the parameters of Sputnik III. With fair accuracy, we may take  $A=B$ ,  $\frac{A-C}{C} \approx 2.5$ ,  $\frac{A-C}{B} = 0.6$ .

The starting orbital period of the mass center around the Earth was  $T_0 = 106$  min, which corresponds to  $\omega = 0.056 \text{ deg} \cdot \text{sec}^{-1}$ . We shall assume

various initial angular velocities of rotation around the center of mass and two initial angles of nutation,  $\theta_0 = 0$  and  $\theta_0 = 10^\circ$ . The results of period and amplitude calculations are listed in Table 1.

TABLE 1

$\dot{\theta}_0$ , deg/sec	$\theta_0 = 0$		$\theta_0 = 10^\circ$	
	$\theta_{\max}$	$T$ , min	$\theta_{\max}$	$T$ , min
0.00	0	—	10°	79.5
0.01	7°40'	79.5	12°35'	80
0.02	15°25'	80.5	18°30'	81
0.05	41°40'	91	43°25'	92
0.07	68°35'	122	—	—
0.074	—	—	90°	—
0.075	90°	$\infty$	—	$\infty$

The rows of the table containing  $\theta_{\max} = 90^\circ$  and  $T = \infty$  correspond to the case of limiting motion.

All the preceding applies to the region of motion which is enclosed by the separatrix in the phase space (Figure 9). If  $k^2 > 1$ , we obtain the region of the phase space located outside the separatrix. The integral (2.2.4) in this case is conveniently written in the form

$$\sqrt{\frac{2h_0}{B}}(t - t_0) = \int_{\theta_0}^{\Theta} \frac{d\theta}{\sqrt{1 - k_1^2 \sin^2 \theta}}; \quad k_1^2 = \frac{1}{k^2} < 1,$$

Transforming this elliptical integral as before and inverting, we find

$$\left. \begin{aligned} \Theta &= \operatorname{am} \left\{ \sqrt{\frac{2h_0}{B}}(t - t_0) + F_1; \ k_1^2 \right\}, \\ F_1 &= \int_0^{\theta_0} \frac{d\theta}{\sqrt{1 - k_1^2 \sin^2 \theta}}. \end{aligned} \right\} \quad (2.2.15)$$

Depending on the initial conditions,  $\Theta$  will monotonically increase or decrease, with some oscillations in the angular velocity of rotation. The greater  $h$ , the smaller the amplitude of these oscillations and the nearer  $\Theta(t)$  to a linear dependence.  $\Theta$  varies through  $2\pi$  with a period

$$T = \frac{4K(k_1^2)}{\sqrt{3\frac{A-C}{B}}} \cdot \frac{k_1}{\omega}, \quad k_1^2 = \frac{3\frac{A-C}{B}\omega^2}{\dot{\theta}_0^2 + 3\frac{A-C}{B}\omega^2 \sin^2 \theta_0}. \quad (2.2.16)$$

Consider, for example, a satellite spinning in a sense opposite to the motion of its center of mass. Relative to a system of fixed axes, it will rotate with a mean angular velocity  $\omega^* = \omega \left[ 1 - \frac{\sqrt{3\frac{A-C}{B}}}{k_1 \frac{K(k_1^2)}{\left(\frac{\pi}{2}\right)}} \right]$ . Hence we see

that if the initial values are chosen so that the transcendental equation

$k_1 K(k_1^2) = \frac{\pi}{2} \sqrt{3 \frac{A-C}{B}}$  is satisfied, the mean angular velocity of the satellite's absolute rotation is zero. The satellite thus assumes a certain attitude in space, slightly oscillating about the fixed direction. It is easily seen, however, that this attitude in the absolute space is unstable.

In conclusion we note that the plane relative motion of a satellite in a circular orbit is completely equivalent to the plane motion of a rigid body about a fixed center of mass in a Newtonian force field (see Appendix 1).

### § 3. PLANE OSCILLATIONS OF A SATELLITE IN AN ELLIPTICAL ORBIT. NONLINEAR AND LINEAR EQUATIONS. PRELIMINARY ANALYSIS

The equations of motion in elliptical orbits are qualitatively different from the equations for a circular orbit, since the coefficients are variable (periodic) quantities.

Let us consider the equation of plane oscillations in an elliptical orbit. Here  $p=r=0$ ,  $\gamma''=\cos \Theta$ ,  $\gamma'=-\sin \Theta$ ,  $q=\omega+\dot{\theta}$ , where  $\omega$  is the angular velocity of transportation, i.e., the orbital velocity of the center of mass. Equations (2.1.1) then give

$$\ddot{\theta} + 3 \frac{\mu}{R^3} \frac{A-C}{B} \sin \Theta \cos \Theta = -\dot{\omega}. \quad (2.3.1)$$

If the orbit is circular, we have  $\dot{\omega}=0$ ,  $\frac{\mu}{R^3}=\text{const}=\omega^2$ . In general, however,  $\dot{\omega}\neq 0$ . Let us substitute the true anomaly  $v$  as the independent variable. To this end, we add the equation of motion of the mass center:

$$R = \frac{P}{1+e \cos v}, \quad \frac{dv}{dt} = \omega = \frac{\sqrt{\mu P}}{R^2} = \frac{\sqrt{\mu P}}{P^2} (1+e \cos v)^2. \quad (2.3.2)$$

Here  $e$  is the eccentricity,  $P$  the focal parameter of the orbit. Hence

$$\zeta = \frac{\mu}{R^3}, \quad \dot{\omega} = -2e \sin v \zeta, \quad \ddot{\theta} = (1+e \cos v) \zeta \dot{\theta}'' - 2e \sin v \dot{\theta}' \quad (2.3.3)$$

(primes denote differentiation by  $v$ ). Substituting (2.3.3) in (2.3.1) and dividing through by  $\zeta$ , we find

$$(1+e \cos v) \dot{\theta}'' - 2e \sin v \dot{\theta}' + 3 \frac{A-C}{B} \sin \Theta \cos \Theta = 2e \sin v. \quad (2.3.4)$$

This is the required equation of plane oscillations in an elliptical orbit.

Let  $\bar{\delta}=2\theta$ , and the equation takes the form

$$\left. \begin{aligned} (1+e \cos v) \ddot{\delta}'' - 2e \sin v \ddot{\delta}' + n^2 \sin \bar{\delta} &= 4e \sin v, \\ n^2 &= 3 \frac{A-C}{B}. \end{aligned} \right\} \quad (2.3.5)$$

Without loss of generality, we may take  $n^2>0$  (the substitution of variables  $\bar{\delta}=\bar{\delta}_1+\pi$  only changes the sign of the last term in the left-hand side of (2.3.5)).

The non-linear equation (2.3.5) contains periodic coefficients and its right-hand side is also periodic. If  $e=0$ , we obtain the equation of oscillations in a circular orbit.

Equation (2.3.5) has the following particular solution: if the natural frequency  $n$  satisfies the equality  $n^2=6e$ , then  $\delta=v$ , i.e.,  $\theta=\frac{v}{2}$ , is a solution of the equation. In perigee,  $v=0$ ,  $\theta=0$ , and the axis of the satellite "seeks" the center of attraction. In apogee,  $v=\pi$ ,  $\theta=\pi/2$ , and the axis of the satellite points along the tangent to the orbit. In a subsequent perigee passage,  $v=2\pi$ ,  $\theta=\pi$ , i.e., the satellite has turned around, so that its opposite side now "faces" the center of attraction. In other words, the satellite rotates continuously (but uniformly in time) in one direction, so as to assume the initial attitude every two orbital periods of the mass center.

Let us consider small plane oscillations in an elliptical orbit. Linearizing equation (2.3.4), we find

$$(1+e \cos v)\theta'' - 2e \sin v \theta' + n^2 \theta = 2e \sin v. \quad (2.3.6)$$

Let us introduce a new variable  $\Theta$ , related with  $z$  by the expression

$$\Theta = \frac{z}{1+e \cos v}. \quad (2.3.7)$$

Equation (2.3.6) then takes the form

$$z'' + \left\{ \frac{n^2 + e \cos v}{1+e \cos v} \right\} z = 2e \sin v. \quad (2.3.8)$$

Equation (2.3.8) is a Hill-type equation (with periodic coefficients) with a periodic right-hand side. If we omit the elementary integrable case  $n^2=1$ , which is later identified with a resonance, we see that equation (2.3.8) is no longer integrable for  $e \neq 0$ . Equation (2.3.8) should therefore be solved by approximate methods. For  $e \ll n^2$ , it can be conveniently solved by the method of Krylov—Bogolyubov [19], taking the orbital eccentricity  $e$  as the small parameter.

We know from previous sections that for zero initial conditions, relative equilibrium is always maintained in a circular orbit. In an elliptical orbit, the right-hand sides of (2.3.8) and (2.3.5) result in forced oscillations, which we call eccentricity oscillations. To evaluate these eccentricity oscillations, we drop the terms with  $e$  in the left-hand side of (2.3.8), leaving its right-hand side unchanged; then

$$z'' + n^2 z = 2e \sin v.$$

The forced oscillations are easily seen to have the form

$$z_e = \frac{2e}{n^2 - 1} \sin v. \quad (2.3.9)$$

More exact formulas for forced (eccentricity) oscillations will be derived in later sections.

For  $n^2 \approx 1$ , equation (2.3.9) points to a resonance. An investigation of the nonlinear equation (see below) shows that for small  $e$ , the resonant

oscillations are large, but bounded. For large  $e$ , the nonlinear equation may have a solution which increases indefinitely near the resonance, i.e., for large  $e$ , the satellite may actually change over from an oscillating mode to a spin.

Note that this resonance is physically significant, since for the physically admissible values of the parameters  $A, B, C$ , we have the inequality

$$\left| \frac{A-C}{B} \right| < 1, \text{ and the resonant value } \frac{A-C}{B} = \frac{1}{3} \text{ lies within the physical region.}$$

A solution neglecting all powers higher than  $e$  will be called a first-order solution (first approximation); that neglecting all powers higher than  $e^2$ , a second-order solution (second approximation), etc. The third-order solution of the linear equation does not satisfy the nonlinear equation with quite the same accuracy, since  $\sin \bar{\delta} = \bar{\delta} - \frac{\bar{\delta}^3}{3!} + \dots$ , and if  $\bar{\delta} \sim e$ , the term  $\bar{\delta}^3$  gives in the nonlinear solution terms of the order of  $e^3$  which are different from the terms of the same order in the linear solution. Solutions of the linear equation are therefore meaningful on first and second approximation only.

#### § 4. ECCENTRICITY OSCILLATIONS

We shall seek a particular solution of the inhomogeneous equation (2.3.8) in the form

$$z_e = 2e \sin v \varphi_e \quad (2.4.1)$$

Then for  $\varphi_e$  we have the equation

$$(1-x^2)(1+ex)\varphi_e'' - 3(1+ex)x\varphi_e' + (n^2-1)\varphi_e = 1+ex, \quad (2.4.2)$$

where primes denote derivatives with respect to

$$x = \cos v. \quad (2.4.3)$$

A particular solution of equation (2.4.2) may be sought as a series in terms of a small parameter  $e$ . The series will converge, according to the theory of Poincaré, for fairly small  $e$ . Let

$$\varphi_e = \varphi_{e0} + e\varphi_{e1} + e^2\varphi_{e2} + \dots + e^k\varphi_{ek} + \dots \quad (2.4.4)$$

Substituting in (2.4.2) and equating terms of the same degree  $k$ , we obtain a system of equations

$$\left. \begin{aligned} (1-x^2)\varphi_{e0}'' - 3x\varphi_{e0}' + (n^2-1)\varphi_{e0} &= 1, \\ (1-x^2)\varphi_{e1}'' - 3x\varphi_{e1}' + (n^2-1)\varphi_{e1} &= x - x(1-x^2)\varphi_{e0}'' + 3x^2\varphi_{e0}', \\ (1-x^2)\varphi_{e2}'' - 3x\varphi_{e2}' + (n^2-1)\varphi_{e2} &= -x(1-x^2)\varphi_{e1}'' + 3x^2\varphi_{e1}', \\ \dots & \dots \dots \dots \dots \dots \dots \\ (1-x^2)\varphi_{ek}'' - 3x\varphi_{ek}' + (n^2-1)\varphi_{ek} &= -x(1-x^2)\varphi_{e(k-1)}'' + 3x^2\varphi_{e(k-1)}' \end{aligned} \right\} \quad (2.4.5)$$

From this system we can successively find particular solutions for  $\varphi_{ek}$ , in the form of polynomials of  $k$ -th degree:

$$\varphi_{e0} = \frac{1}{n^2 - 1}, \quad \varphi_{e1} = \frac{1}{n^2 - 4} x, \dots, \quad (2.4.6)$$

$$\varphi_{e(k-1)} = \sum_{m=0}^{m=k-1} a_m x^m, \quad \varphi_{ek} = \sum_{m=0}^{m=k} b_m x^m. \quad (2.4.7)$$

Here, to avoid confusion, the coefficients of the  $(k-1)$ -th polynomial are denoted by  $a_m$ , and the coefficients of the  $k$ -th polynomial by  $b_m$ . These coefficients are defined by recursion:

$$b_m = \frac{m^2 - 1}{n^2 - (m+1)^2} a_{m-1} \text{ for } m = k \text{ and } m = k-1, \quad (2.4.8)$$

$$(m+2)(m+1)b_{m+2} + [n^2 - (m+1)^2]b_m = (m^2 - 1)a_{m-1} - m(m+1)a_{m+1} \quad (2.4.9)$$

for  $m = 0, 1, 2, \dots, k-2$ .

We see that the two leading terms ( $k$ -th and  $(k-1)$ -th) of the  $k$ -th polynomial are determined from (2.4.8) with the aid of the corresponding leading terms ( $(k-1)$ -th and  $(k-2)$ -th) of the  $(k-1)$ -th polynomial. The successive terms of the  $k$ -th polynomial are determined from (2.4.9) making use of the leading terms that we have just found and of the previously known terms ( $(k-3)$ -th and  $(k-1)$ -th) of the preceding,  $(k-1)$ -th polynomial.

For example, the coefficients of the polynomial

$$\varphi_{e2} = b_0 + b_1 x + b_2 x^2$$

are determined in terms of the coefficients of the polynomial

$$\varphi_{e1} = a_0 + a_1 x, \quad a_0 = 0, \quad a_1 = \frac{1}{n^2 - 4}$$

in the following way: from (2.4.8) we have

$$b_2 = \frac{3}{n^2 - 9} \cdot \frac{1}{n^2 - 4}, \quad b_1 = 0,$$

and from (2.4.9), seeing that  $a_{-1} \equiv 0$ , we find

$$2b_2 + (n^2 - 1)b_0 = 0, \quad b_0 = -\frac{6}{(n^2 - 9)(n^2 - 4)(n^2 - 1)}.$$

The solution (2.4.1), (2.4.4), (2.4.6)–(2.4.8) that we have constructed is of some interest as an example of an exact solution of an inhomogeneous Hill-type equation. In our particular case of oscillations of a satellite in an elliptical orbit, we need only consider the first terms of this solution, namely the terms (2.4.6), which give the required formula for the forced oscillations. In virtue of (2.3.7), (2.4.3), and (2.4.1), the terms (2.4.6) give eccentricity oscillations in the form

$$\begin{aligned} \Theta_e &= \frac{2e \sin v}{(1 + e \cos v)} \left\{ \frac{1}{n^2 - 1} + \frac{e}{n^2 - 4} \cos v \right\} \approx \\ &\approx \frac{2e}{n^2 - 1} \sin v + \frac{3e^2}{(n^2 - 4)(n^2 - 1)} \sin 2v. \end{aligned} \quad (2.4.10)$$

The terms with  $e^k$ ,  $k \geq 3$ , need not be considered, in compliance with our remarks at the end of the previous section.

For  $n^2 \approx 1$ , solution (2.4.10) is meaningless (the resonance). Resonant oscillations will be considered later. No other resonance is physically possible for the case of eccentricity oscillations, since  $n^2 = 3 \frac{A-C}{B} < 3$ , so that the second term in braces in (2.4.10) is always bounded.

## § 5. SMALL PLANE OSCILLATIONS IN AN ELLIPTICAL ORBIT WITH A SMALL ECCENTRICITY

For small  $e$ , equation (2.3.8) reduces to a Mathieu equation, so that apart from terms of higher order in  $e$ , we have

$$\frac{n^2 + e \cos v}{1 + e \cos v} \approx n^2 - (n^2 - 1)e \cos v. \quad (2.5.1)$$

Equation (2.3.8) can be approximately solved for small  $e$  by the method of Krylov—Bogolyubov [19]. Applying (2.5.1), we write equation (2.3.8) as

$$z'' + n^2 z = e [2 \sin v + (n^2 - 1) z \cos v]. \quad (2.5.2)$$

For  $e = 0$ , we find the zero-order solution

$$z = a \cos \Psi, \quad \Psi = nv + \Psi^*. \quad (2.5.3)$$

The phase  $\Psi^*$  and the amplitude  $a$  of the oscillations are determined from the initial conditions. We shall seek a solution of (2.5.2) in the form

$$z = a \cos \Psi + eu_1(\Psi, v, a), \quad (2.5.4)$$

where  $a, \Psi$  should satisfy the equations

$$\frac{da}{dv} = eA_1(a), \quad \frac{d\Psi}{dv} = n + eB_1(a). \quad (2.5.5)$$

Substituting (2.5.4) in (2.5.2) and applying (2.5.5), we find after some transformations

$$\begin{aligned} & -2en(A_1 \sin \Psi + B_1 a \cos \Psi) + \\ & + e \left\{ \frac{\partial^2 u_1}{\partial \Psi^2} n^2 + 2 \frac{\partial^2 u_1}{\partial \Psi \partial v} n + \frac{\partial^2 u_1}{\partial v^2} \right\} + n^2 eu_1 = \\ & = e \left\{ 2 \sin v + \frac{a(n^2 - 1)}{2} [\cos(v + \Psi) + \cos(v - \Psi)] \right\}. \end{aligned} \quad (2.5.6)$$

This equation can be divided through by  $e$ .

The right-hand side, as we see, contains the harmonics  $\cos(v + \Psi)$ ,  $\cos(v - \Psi)$ , but the harmonics  $\sin \Psi$  and  $\cos \Psi$  enter the left-hand side only. Thus

$$A_1 = 0, \quad B_1 = 0. \quad (2.5.7)$$

Applying (2.5.7), we proceed to choose  $u_1$  so that the left- and the right-hand sides of (2.5.6) are equal. We seek  $u_1$  in the form

$$u_1 = \gamma_u \sin v + a_u \cos(v - \Psi) + \beta_u \cos(v + \Psi).$$

Substituting in (2.5.6) and equating the coefficients of identical harmonics, we find

$$\left. \begin{aligned} \gamma_u &= \frac{2}{n^2 - 1}, & a_u &= \frac{1}{2} a (n^2 - 1) \frac{1}{2n - 1}, \\ \beta_u &= -\frac{1}{2} a (n^2 - 1) \frac{1}{2n + 1}. \end{aligned} \right\} \quad (2.5.8)$$

The term with  $\gamma_u$  appears since the right-hand side of (2.3.8) is not zero; it is equivalent to the first term in (2.4.10). In the first approximation, the solution has the following final form

$$\begin{aligned} z = & \frac{2e}{n^2 - 1} \sin v + a \cos \Psi + e \frac{a(n^2 - 1)}{2} \times \\ & \times \left\{ \frac{1}{2n - 1} \cos(v - \Psi) - \frac{1}{2n + 1} \cos(v + \Psi) \right\}. \end{aligned} \quad (2.5.9)$$

Here, in virtue of (2.5.7),  $a = \text{const}$ ,  $\Psi = nv + \Psi^*$ , where  $a$  and  $\Psi^*$  are determined from the initial conditions.

We see that, aside from the resonance at  $n^2 = 1$ , the eccentricity oscillations now display a so-called parametric resonance at  $n^2 = 1/4$ . All terms with the factor  $a$  in the solution (2.5.9) constitute a first-order solution of the Mathieu equation.

We shall consider, without derivation, the solution of (2.3.8) in the next higher approximation, i.e., with terms of the order of  $e^2$ . The coefficient entering (2.3.8) should then be written in the form

$$\frac{n^2 + e \cos v}{1 + e \cos v} \approx n^2 - (n^2 - 1)e \cos v + (n^2 - 1)e^2 \cos^2 v.$$

A second-order solution is sought in the form

$$z = a \cos \Psi + eu_1 + e^2 u_2, \quad (2.5.10)$$

where

$$\frac{da}{dv} = eA_1 + e^2 A_2, \quad \frac{d\Psi}{dv} = n + eB_1 + e^2 B_2. \quad (2.5.11)$$

It turns out that  $A_1 = A_2 = 0$ ;  $B_1 = 0$ ;  $B_2 \neq 0$ , so that

$$\left. \begin{aligned} \frac{d\Psi}{dv} &= n + e^2 \frac{3}{4} n \frac{n^2 - 1}{4n^2 - 1}, & \Psi &= \frac{d\Psi}{dv} v + \Psi^*, \\ u_1 &= \frac{a(n^2 - 1)}{2} \left\{ \frac{1}{2n - 1} \cos(v - \Psi) - \right. \\ &\quad \left. - \frac{1}{2n + 1} \cos(v + \Psi) \right\} + \frac{2}{n^2 - 1} \sin v, \\ u_2 &= \frac{a}{16} \left\{ \frac{n(n+1)(n-2)}{2n-1} \cos(\Psi - 2v) + \right. \\ &\quad \left. + \frac{n(n-1)(n+2)}{2n+1} \cos(\Psi + 2v) \right\} + \frac{1}{n^2 - 4} \sin 2v. \end{aligned} \right\} \quad (2.5.12)$$

The last terms in  $u_1$  and  $u_2$  constitute a periodic solution of the equation (2.3.8); these are eccentricity oscillations equivalent to (2.4.10). The second approximation, as we see, does not introduce new parametric resonances. This is a distinctive property of the solution (2.5.10), since the solution of the Mathieu equation introduces a new resonance in the second approximation. Also note that on third approximation  $A_3=B_3=0$ , a resonance appears near  $n^2=9/4/37$ . Since  $n^2 \leq 3$ , no other resonances are possible. The solution (2.5.10)–(2.5.12) applies for arbitrary initial conditions, defining the constants  $a, \Psi^*$ . The solution with zero initial conditions is of some interest. For a circular orbit, this solution is identically zero (relative equilibrium). In an elliptical orbit, however, this is not so on account of eccentricity oscillations. Thus, let  $\theta_0=0, \theta'_0=0$  for  $v=0$ . Then, to terms of the order of  $e^2$  inclusive, we have

$$\left. \begin{aligned} \theta &= \frac{z}{1+e \cos v} \\ z &= \frac{2e}{n^2-1} \left\{ \sin v - \frac{1}{\omega} \sin \omega v \right\} + \\ &\quad + e^2 \left\{ \frac{1}{n^2-4} \sin 2v - \frac{2}{(n^2-4)\omega} \sin \omega v + \right. \\ &\quad \left. + \frac{2}{(n^2-1)\omega^2} [k_1(\omega-1) + m_1(\omega+1)] \sin \omega v - \right. \\ &\quad \left. - \frac{2}{(n^2-1)\omega} [k_1 \sin(\omega-1)v + m_1 \sin(\omega+1)v] \right\}, \\ \omega &= n + e^2 \frac{3}{4} n \frac{n^2-1}{4n^2-1}, \quad k_1 = \frac{n^2-1}{2(2n-1)}, \\ m_1 &= -\frac{n^2-1}{2(2n+1)}. \end{aligned} \right\} \quad (2.5.13)$$

## § 6. SOME NONLINEAR OSCILLATIONS IN A SLIGHTLY ELLIPTICAL ORBIT

**1. Periodic oscillations.** Let us find a periodic solution of the equation (2.3.5), i.e., oscillations contributed by the nonzero right-hand side of this equation. We seek the solution as a Fourier series in terms of  $v$ , and we proceed to determine the first harmonic of this series. Let

$$\bar{\delta}=a \cos \Psi, \quad \Psi=v+\Psi_0, \quad (2.6.1)$$

where  $\Psi_0$  is the constant phase of the oscillations, and  $a$  the constant amplitude, both unknown

Note that  $\sin(a \cos \Psi)$  is Fourier-expandable in a series

$$\sin(a \cos \Psi) = 2 \sum_{k=0}^{k=\infty} (-1)^k J_{2k+1}(a) \cos(2k+1)\Psi \approx 2J_1(a) \cos \Psi. \quad (2.6.2)$$

Here  $J_{2k+1}(a)$  is Bessel's function of first kind of the order  $2k+1$ ; in the last approximate equality, only the first harmonic of the series has been retained. Substituting (2.6.1) and (2.6.2) in (2.3.5) and seeing that  $\Psi=v+\Psi_0$ , we collect and equate to zero the coefficients of the nonharmonic term and of the terms with the first harmonics  $\cos v, \sin v$ :

$$\left. \begin{aligned} \frac{1}{2}ea \cos \Psi_0 &= 0, \quad [2n^2J_1 - a] \cos \Psi_0 = 0, \\ a \sin \Psi_0 - 2n^2J_1(a) \sin \Psi_0 - 4e &= 0. \end{aligned} \right\} \quad (2.6.3)$$

From (2.6.3) we have  $\Psi_0 = \pi/2$  or  $\Psi_0 = -\pi/2$ , and correspondingly,

$$n^2 = \frac{a \mp 4e}{2J_1(a)}, \quad (2.6.4)$$

while from (2.6.1) we respectively have

$$\bar{\delta} = \mp a \sin v. \quad (2.6.5)$$

Note that for small amplitudes  $a$ , we have  $J_1(a) \approx \frac{a}{2}$ ; then from (2.6.4),  $n^2 = \frac{a \mp 4e}{a}$ , and applying (2.6.5),

$$a = \mp \frac{4e}{n^2 - 1}, \quad \bar{\delta} = \frac{4e}{n^2 - 1} \sin v,$$

i.e., the formula for the first harmonic of the eccentricity oscillations is the same as with linear equations (see (2.4.10)).

The signs  $\mp$  in (2.6.4) correspond to two branches of one curve, which plots the amplitude-frequency characteristic of the first harmonic of forced periodic oscillations.

**Example.** Let  $e = 0.01$ . Applying (2.6.4), we plot the amplitude-frequency characteristic (Figure 10). In this graph, the amplitude  $a$  of the angle  $\bar{\delta}$  has been replaced with the amplitude  $\frac{a}{2}$  of the angle  $\theta$ . The signs + and - mark the corresponding branches of the curve (2.6.4).

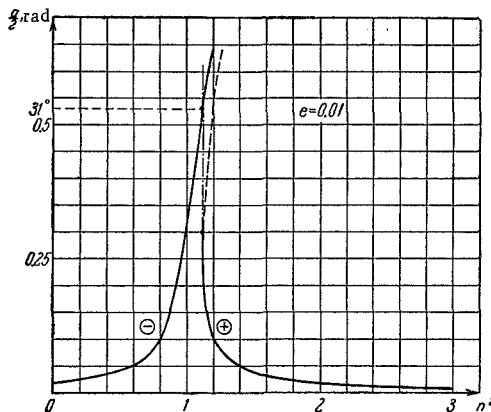


FIGURE 10. Periodic oscillations of a satellite in an elliptical orbit; amplitude-frequency characteristic.

For  $n^2 < n_*^2 \approx 1.12$ , there is one periodic solution, while for  $n^2 > n_*^2$ , there are three periodic solutions; one of these is unstable, namely the solution corresponding to the dashed section on the plus-branch (this will be proved in the next section).

We see that in the region with a single periodic solution, the peak amplitude  $\alpha_{\max} = 31^\circ$  (for  $n^2 = n_*^2$ ), while for  $n^2$  far from the resonance, the amplitude of the oscillations is of the order of  $\sim 1^\circ$ .

Let us now consider forced oscillations, retaining the second harmonic. The previous analysis of the linear and the nonlinear problems suggests that we seek these oscillations in the form

$$\bar{\delta} = \pm a \sin v + a_1 \sin 2v. \quad (2.6.6)$$

Let us consider the case  $+a$ ; the case  $-a$  is obtained simply by reversing the sign.

Substituting (2.6.6) in (2.3.5), we denote all the trigonometric terms, with the exception of  $n^2 \sin \bar{\delta}$ , by  $S$ ; then, collecting the terms with equal harmonics, we find

$$S = -(a + 4e) \sin v - \left(4a_1 + \frac{3}{2}ea\right) \sin 2v + (\dots) \sin 3v. \quad (2.6.7)$$

Consider the term  $\sin \bar{\delta}$ . Expanding

$$\left. \begin{aligned} \sin(a \sin \Psi) &= 2 \sum_{k=0}^{\infty} J_{2k+1}(a) \sin(2k+1)\Psi, \\ \cos(a \sin \Psi) &= J_0(a) + 2 \sum_{k=1}^{\infty} J_{2k}(a) \cos 2k\Psi, \end{aligned} \right\} \quad (2.6.8)$$

and applying (2.6.6), we obtain after some transformations

$$\begin{aligned} \sin \bar{\delta} &= J_0(a_1) \cdot 2 \sum_{k=0}^{\infty} J_{2k}(a) \sin(2k+1)v + \\ &+ 2 \sum_{k=0}^{\infty} \sum_{m=1}^{\infty} J_{2m}(a_1) J_{2k+1}(a) [\sin(2k+1-4m)v + \\ &+ \sin(2k+1+4m)v] + J_0(a) \cdot 2 \sum_{k=0}^{\infty} J_{2k+1}(a_1) \sin 2(2k+1)v + \\ &+ 2 \sum_{k=0}^{\infty} \sum_{m=1}^{\infty} J_{2k+1}(a_1) J_{2m}(a) [\sin 2(2k+1-m)v + \\ &+ \sin 2(2k+1+m)v]. \end{aligned} \quad (2.6.9)$$

Let us pick out the terms with the first harmonic. It may only enter the first half of (2.6.9), and in the double sum it obviously corresponds to  $2k+1-4m=\pm 1$ . In other words, the first harmonic obtains when the following conditions are imposed on  $k$  and  $m$ :

$$2k = 4m, \quad 2k+1 = 4m-1. \quad (2.6.10)$$

Aside from the double sum, the first harmonic enters only the first sum in (2.6.9). Let  $S_1$  denote the collective coefficient of the first harmonic. Then

$$S_1 = 2J_0(a_1)J_1(a) + 2 \sum_{m=1}^{\infty} J_{2m}(a_1) [J_{4m+1}(a) - J_{4m-1}(a)]. \quad (2.6.11)$$

The second harmonic only enters the second half of (2.6.9). The conditions imposed on  $k$  and  $m$  in the coefficients of the second harmonic are found in a similar way; they are given by

$$2k = m, \quad 2k = m-2,$$

so that the collective coefficient  $S_2$  of the second harmonic is

$$S_2 = 2 \sum_{k=0} J_{2k+1}(a_1) [J_{4k}(a) - J_{4k+4}(a)]. \quad (2.6.12)$$

Applying (2.6.7) and setting the coefficients of the first and the second harmonics equal to zero, we finally obtain

$$-a - 4e + n^2 S_1 = 0, \quad -4a_1 - \frac{3}{2}ea + n^2 S_2 = 0. \quad (2.6.13)$$

These transcendental equations cannot be solved exactly. We shall seek an approximate solution. Assuming that  $a_1$  is a small quantity, we have

$$J_1(a_1) = \frac{a_1}{2}, \quad J_0(a_1) = 1, \quad J_s(a_1) \sim a_1^s \approx 0 \quad (s > 1).$$

The set (2.6.13) is now written as

$$\left. \begin{aligned} -a - 4e + n^2 2J_1(a) &= 0, \\ -4a_1 - \frac{3}{2}ea + n^2 a_1 [J_0(a) - J_4(a)] &= 0. \end{aligned} \right\} \quad (2.6.14)$$

Note that  $J_1(-a) = -J_1(a)$ ,  $J_0(-a) = J_0(a)$ . Then from the first equation in (2.6.14) we obtain the formula (2.6.4) for the two branches of the amplitude-frequency characteristic of the first harmonic, while from the second equation in (2.6.14) we correspondingly find a formula for  $a_1$ :

$$a_1 = \pm \frac{3}{2} e \frac{a}{[J_0(a) - J_4(a)] n^2 - 4}. \quad (2.6.15)$$

Our assumption of a small  $a_1$  was clearly justified (the factor  $e$ ). For example, for  $e = 0.01$  and  $n \approx 1$ , we had  $a \approx 30^\circ$ ; then  $a_1 \approx 0.3^\circ$ . For small  $a$ ,  $J_4(a)$  can be neglected in comparison with  $J_0(a)$ . For very small  $a$ , we may approximately take

$$J_0(a) = 1, \quad J_1(a) = \frac{a}{2}, \quad J_4(a) = 0.$$

Then

$$a \approx \frac{4e}{n^2 - 1}, \quad a_1 \approx \frac{3 \cdot 2e^2}{(n^2 - 1)(n^2 - 4)},$$

i.e., the amplitudes of the linear problem are recovered (see (2.4.10)).

**2. Sustained oscillations in the case of parametric resonance.** We have already observed that the periodicity of the coefficients results in a parametric resonance in the oscillations of a satellite about its center of mass. This resonance occurs for  $n^2 \approx 1/4$ . Let us consider the sustained oscillations.

The oscillations near the parametric resonance are represented by a Fourier series in terms of arcs which are multiples of  $\pi/2$ . We shall seek the first harmonic of the oscillations near the parametric resonance in the form

$$\bar{\delta} = a \cos \left( \frac{1}{2}v + \Psi_0 \right). \quad (2.6.16)$$

Substituting in (2.3.5) and proceeding as before, we obtain two cases:

$$1) \quad \sin \Psi_0 = 0, \quad n^2 = a \frac{\frac{1}{4} - \frac{3}{8}e}{2J_1(a)}; \quad (2.6.17)$$

$$2) \quad \cos \Psi_0 = 0, \quad n^2 = a \frac{\frac{1}{4} + \frac{3}{8}e}{2J_1(a)}. \quad (2.6.18)$$

From these formulas we may conclude that the amplitude is uniquely defined in the region

$$\frac{1}{4} - \frac{3}{8}e \leq n^2 \leq \frac{1}{4} + \frac{3}{8}e. \quad (2.6.19)$$

If  $n^2$  falls in this interval, resonance oscillations occur; if  $n^2$  lies outside the interval (2.6.19), no resonance is observed. Inside the interval (2.6.19), the amplitude of the actual resonant oscillations is determined by the branch

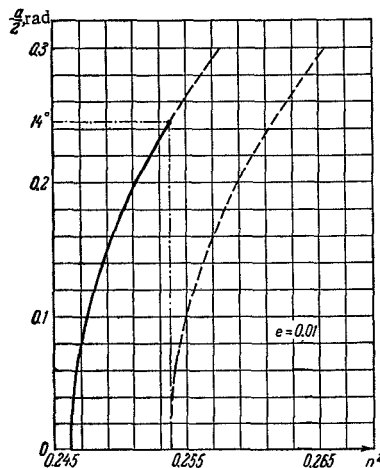


FIGURE 11. Parametric resonance in the oscillations of a satellite in an elliptical orbit; amplitude-frequency characteristic.

(2.6.17) only (Figure 11). In the region of single-valued  $a$ , i.e., in the interval (2.6.19), the resonant oscillations are cosinusoidal:

$$\bar{\delta} = a \cos \frac{\nu}{2}.$$

**Example.** Let  $e = 0.01$ . The region of resonant  $n^2$  is then  $0.245 \leq n^2 \leq 0.255$ . The peak amplitude  $\theta \sim 14^\circ$  (see Figure 11).

On the resonance near  $n^2 = 9/4$ , see § 7, 3 in this chapter.

## § 7. NONLINEAR PLANE OSCILLATIONS IN AN ELLIPTICAL ORBIT

**1. Quasiharmonic oscillations.** In the previous section we considered the particular case of periodic oscillations resulting from the nonzero right-hand side of equation (2.3.5). Let us now consider, on first approximation, the influence of this factor (i.e., the presence of a sinusoidal perturbation) on the oscillations as a whole, both in and near the resonance. This analysis will enable us, among other things, to "place" the particular periodic solutions in the set of all solutions.

We shall assume that the oscillations are nearly harmonic, writing equation (2.3.5) in the form

$$\ddot{\delta} + n^2 \bar{\delta} = e [4 \sin v + 2 \bar{\delta}' \sin v - \bar{\delta}'' \cos v] + n^2 [\bar{\delta} - \sin \bar{\delta}] \equiv f(v, \bar{\delta}, \bar{\delta}', \bar{\delta}''). \quad (2.7.1)$$

According to the method of Bogolyubov—Krylov /19/, if  $f$  is small, the first-order solution of equation (2.7.1) is sought in the form

$$\bar{\delta} = a \cos \Psi, \quad \Psi = v + \kappa, \quad (2.7.2)$$

where the amplitude  $a$  and the phase  $\kappa$  satisfy the equations

$$\frac{da}{dv} = A_1(a, \kappa), \quad \frac{d\kappa}{dv} = n - 1 + B_1(a, \kappa), \quad (2.7.3)$$

$A_1$  and  $B_1$  being particular,  $\kappa$ -periodic solutions of the set

$$\left. \begin{aligned} \frac{1}{2}(n-1) \frac{\partial A_1}{\partial \kappa} - anB_1 &= \frac{1}{2\pi} \int_0^{2\pi} f_0 \cos \Psi d\Psi, \\ \frac{1}{2}(n-1)a \frac{\partial B_1}{\partial \kappa} + nA_1 &= -\frac{1}{2\pi} \int_0^{2\pi} f_0 \sin \Psi d\Psi, \end{aligned} \right\} \quad (2.7.4)$$

where

$$\begin{aligned} f_0 &= f(\Psi - \kappa, a \cos \Psi, -an \sin \Psi, an^2 \cos \Psi) = \\ &= e [4 \sin(\Psi - \kappa) - 2 \sin(\Psi - \kappa) an \sin \Psi - \\ &- \cos(\Psi - \kappa) an^2 \cos \Psi] + n^2 [a \cos \Psi - \sin(a \cos \Psi)]. \end{aligned} \quad (2.7.5)$$

Substituting (2.7.5) in the integrands in the right-hand sides of (2.7.4) and integrating, we can easily find from (2.7.4)  $\kappa$ -periodic expressions for  $A_1$ ,  $B_1$ . The set (2.7.3) takes the form

$$\left. \begin{aligned} \frac{da}{dv} &= -\frac{4e}{n+1} \cos \kappa = -\frac{1}{a} \frac{\partial \Phi}{\partial \kappa}, \\ \frac{d\kappa}{dv} &= \left[ \frac{n}{2} + \frac{n}{a} J_1(a) \right] - 1 + \frac{4e}{a(n+1)} \sin \kappa = \frac{1}{a} \frac{\partial \Phi}{\partial a}, \end{aligned} \right\} \quad (2.7.6)$$

where  $J_1(a)$  is Bessel's function of first order, and

$$\Phi = \frac{4e}{n+1} a \sin \kappa + n \left[ \frac{a^2}{4} - (J_0(a) - 1) \right] - \frac{a^2}{2}. \quad (2.7.7)$$

Here  $J_0(a)$  is a zeroth-order Bessel function. Hence it follows immediately that equations (2.7.6) have a first integral

$$\Phi = \Phi_0, \quad (2.7.8)$$

so that the problem reduces to quadratures, and the dependences  $a(\nu)$ ,  $\kappa(\nu)$  can be analyzed. The analysis of the integral curves (2.7.8) is more profitable, however, if carried out in the  $(a, \kappa)$  plane. To this end, (2.7.8) may be written as

$$\sin \kappa = \frac{C_0 - (n^2 - 1) \frac{a^2}{2} + n(n+1)f(a)}{4ea}, \quad (2.7.9)$$

where  $C_0$  is an integration constant, and

$$f(a) = J_0(a) + \frac{a^2}{4} - 1 = \frac{a^4}{2^4} - \dots \quad (2.7.10)$$

Figure 12 plots the integral curves for  $n^2 < 1$  ( $n^2 = 0.8$ ) and  $e = 0.01$ . We see that for  $\kappa = \pi/2$  there is but one stable steady-state mode  $a = \text{const}$ , corresponding to the periodic solution of the previous section. For all other initial values (of course within the framework of our statement of the problem),  $a$  varies periodically between finite limits: the maximum  $a$ , as we see from Figure 12, is always greater than the steady-state  $a$ .

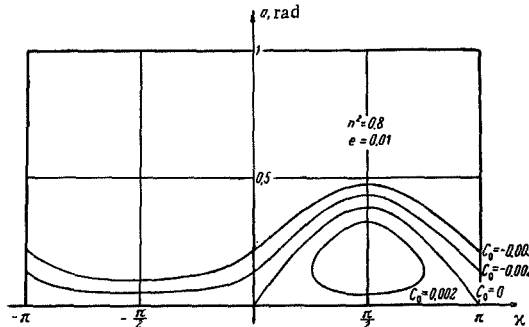


FIGURE 12. Oscillations of a satellite in an elliptical orbit; phase-amplitude characteristic for  $n^2 = 0.8$ .

Hence follows a conclusion which is of considerable importance for gravity attitude stabilization of a satellite in an elliptical orbit: we must try to satisfy the conditions of the steady-state periodic oscillations, since this mode ensures minimum deviation of the satellite from the position of relative equilibrium (as compared with any other mode of oscillations).

Note that as  $n$  increases from 0 to 1, the pattern of the integral curves in the plane  $(a, \kappa)$  evolves so that the maximum values of  $a$  increase.

Figure 13 plots the integral curves for  $n^2 > 1$  ( $n^2 = 1.2$ ) and  $e = 0.01$ . We see that, besides the steady-state mode with an amplitude  $a_1^*(\kappa = \pi/2)$ , there are two additional time-independent modes with amplitudes  $a_2^*$ ,  $a_3^*$  for  $\kappa = -\pi/2$ ; here  $a_1^* > a_2^* > a_3^*$ , the modes with  $a_1^*$  and  $a_3^*$  are stable, while the mode with  $a_2^*$  is unstable.

As  $n$  increases above 1, the pattern of integral curves evolves so that the steady-state amplitudes  $a = a_1^*$ ,  $a = a_2^*$  increase, while the amplitude  $a = a_3^*$  decreases.

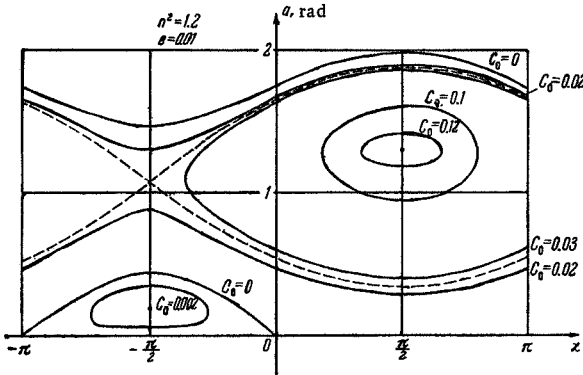


FIGURE 13. Oscillations of a satellite in an elliptical orbit: phase-amplitude characteristic for  $n^2 = 1.2$ .

The steady-state amplitudes  $a_{1,2,3}^*$  are determined directly from (2.7.6) by setting the right-hand sides equal to zero. This gives

$$\left. \begin{aligned} \kappa &= +\frac{\pi}{2}, -\frac{1}{2}\pi; \\ 2n^2J_1(a) + n(n-1)\left(\frac{a}{2} - J_1(a)\right) &= a \mp 4e. \end{aligned} \right\} \quad (2.7.11)$$

Since for small  $a$ ,  $\frac{a}{2} \approx J_1(a)$ , while for moderately large  $a$  we have  $n \approx 1$ , equation (2.7.11) is approximately equivalent to (2.6.4). Also note that the value  $n = 1$  corresponds to a branching point of the periodic solutions (for  $e \sim 0$  and  $n > 1$ , there are three periodic solutions, while for  $n < 1$ , one only) [66].

For  $n = 1$ , in accordance with (2.7.11), we have  $2J_1(a) = a \mp 4e$ ; seeing that  $J_1(a) = \frac{a}{2} - \frac{a^3}{24}$ , we approximately have

$$a = \sqrt[3]{2^8 e} = 2\sqrt[3]{4e}. \quad (2.7.12)$$

This formula gives an expression of the resonant amplitude in terms of the orbit's eccentricity.

There is another important formula. For arbitrary initial conditions, the amplitude  $a$  reaches its maximum for  $\kappa = \pi/2$  (and  $\kappa = -3\pi/2$ ). In particular, from (2.7.9) and (2.7.10) we see that oscillations with a zero initial amplitude ( $a_0 = 0$ ) grow to a peak amplitude  $a_{\max}$  determined from the relation ( $\kappa = \pi/2$  is assumed)

$$4e = -(n^2 - 1) \frac{a_{\max}}{2} + (n + 1)n \frac{a_{\max}^3}{2^8},$$

which in resonance ( $n = 1$ ) gives

$$a_{\max} = 4\sqrt{2e}. \quad (2.7.13)$$

Figure 14 plots the comparative values of the maximal amplitudes calculated from (2.7.13) and determined by direct numerical integration of the starting equation (2.3.5). We see that the agreement is satisfactory for small eccentricities ( $e \leq 0.02 - 0.03$ ).

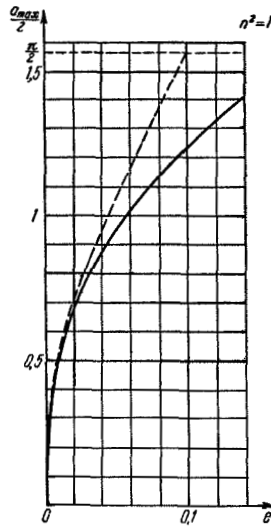


FIGURE 14. Maximal amplitude of oscillations in an elliptical orbit; exact values (dashed curve) and approximate calculations (solid line).

Let us now approximately determine the branching curve. In (2.6.4), Bessel's function  $J_1(a)$  is series-expanded in  $a$ , and only the first two terms are retained. This gives a cubic in  $a$ :

$$a^3 - \frac{8(n^2 - 1)}{n^2} a \pm \frac{32e}{n^2} = 0, \quad (2.7.14)$$

with a discriminant

$$D = -\left[\frac{8(n^2 - 1)}{3n^2}\right]^3 + \left[\frac{16e}{n^2}\right]^2.$$

Equation (2.7.14) has one real solution if  $D > 0$ , and three real solutions if  $D < 0$ . The equation of the branching curve is thus  $D = 0$ , i.e.,

$$e = \left(\frac{2}{3}\right)^{\frac{1}{n^2}} \frac{(n^2 - 1)^{\frac{1}{n^2}}}{2n}. \quad (2.7.15)$$

If  $e > \left(\frac{2}{3}\right)^{\frac{1}{n^2}} \frac{(n^2 - 1)^{\frac{1}{n^2}}}{2n}$ , equation (2.3.5) has one  $2\pi$ -periodic solution; otherwise, for  $e < \left(\frac{2}{3}\right)^{\frac{1}{n^2}} \frac{(n^2 - 1)^{\frac{1}{n^2}}}{2n}$ , there are three such solutions. The branching curve,

as we easily see from (2.7.15), monotonically increases in the entire interval of definition  $1 < n < \sqrt{3}$ , rising from  $e = 0$  for  $n = 1$  (here the curve touches the  $n$  axis) to  $e = e_*$  for  $n = \sqrt{3}$ . We see from (2.7.15) that  $e_* = 4/9 = 0.444\dots$ . For  $e > e_*$ , there is always a single periodic solution for any physically permissible  $n$ . (On this subject, see also [66, 37, 72/].) Note that equation (2.7.15) of the branching curve has been obtained by analyzing the first harmonic of the periodic solution only; nevertheless, the curve (2.7.15) is apparently very close to the true branching curve, as it reflects all the principal characteristics discovered in [66, 37] and gives satisfactory numerical estimates. For example, the exact value  $e_* = 0.446/37$ , while (2.7.15) gives, as we have mentioned,  $e_* = 0.444\dots$

A detailed analysis of the periodic solutions of (2.3.5) will be found in [66, 37/]. The solutions of equation (2.3.5) which are close to arbitrary solutions for a circular orbit are considered in [72/]. This equation is also dealt with in [43/].

**2. Periodic oscillations of an almost symmetric satellite for arbitrary eccentricities.** F. L. Chernous'ko [72] investigated motions close to an arbitrary motion in a circular orbit. The asymptotic solution for small eccentricities is based on harmonic (linear) oscillations, as in our analysis, and also on nonlinear oscillations described by equation (2.3.5) for  $e = 0$ . This approach makes it possible to consider the behavior of both spinning and wobbling satellites.

Another case, analyzed by Chernous'ko in the same reference, proceeds from the assumption  $n^2 \ll 1$ , i.e., the body is close to a dynamically symmetric figure; an arbitrary eccentricity is assumed ( $0 \leq e < 1$ ). As an independent variable in this case, we choose the time  $\tau$  reckoned from the perigee and related to the orbital period of the satellite divided by  $2\pi$ :

$$\left. \begin{aligned} \tau &= 2 \operatorname{arctg} \sqrt{\frac{1-e}{1+e}} \operatorname{tg} \frac{v}{2} - \frac{e \sqrt{1-e^2} \sin v}{1+e \cos v}, \\ \tau(v+2\pi) &= \tau(v)+2\pi. \end{aligned} \right\} \quad (2.7.16)$$

As a new unknown function, we take the angle  $\Theta_1$  between one of the principal central axes of inertia ( $C$  being the moment of inertia about this axis) and the radius-vector of the perigee:

$$\Theta_1 = v + \theta = v + \frac{\delta}{2}.$$

Equation (2.3.5) takes the form

$$\frac{d^2\Theta_1}{d\tau^2} + \frac{n^2}{2} \cdot \frac{(1+e \cos v)^3}{(1-e^2)^3} \sin 2(\Theta_1 - v) = 0, \quad (2.7.17)$$

where  $v$  is treated as a function of  $\tau$ , defined by (2.7.16). From (2.7.17) we see that a dynamically symmetric satellite uniformly rotates around its center of inertia. For small  $n$ , the motion of the satellite is close to uniform rotation, and the solution of equation (2.7.17) may be sought in the form

$$\Theta_1 = \Omega\tau + \varphi_\theta, \quad (2.7.18)$$

where  $\Omega$  is a constant and  $\varphi_\theta$  is the unknown function. An approximate solution can be obtained by asymptotic techniques. If  $2\Omega$  is not an integer,

the first-order motion remains uniform rotation. Of greater interest are the resonances  $2\Omega=m$ , where  $m$  is a whole number, and particularly the principal resonance  $m=2$ , when the rotation period of the satellite is close to its orbital period, which clearly corresponds to  $2\pi$ -periodic oscillations in the orbital system of coordinates. We substitute (2.7.18) in (2.7.17). Then for any integer  $m$ , the coefficients of (2.7.17) are  $\tau$ -periodic with a period of  $2\pi$ ; to obtain a first-order solution, the coefficients of the equation should be averaged over this period. Then

$$\left. \begin{aligned} & \frac{d^2(2\Phi_\theta)}{d\tau^2} + n^2\Phi_m(e) \sin 2\Phi_\theta = 0, \\ & \Phi_m = \frac{1}{\pi(1-e^2)^{1/2}} \int_0^\pi (1+e \cos v) \cos [m\tau(v)-2v] dv, \end{aligned} \right\} \quad (2.7.19)$$

where  $\tau(v)$  is defined by (2.7.16).

Equation (2.7.19), as we know, is solvable in elliptical functions. Comparing (2.7.18) with the solutions of (2.7.19) we see that the satellite rotates with an angular velocity  $\Omega=m/2$ , on which slow rotations or oscillations are superimposed. This asymptotic solution holds true to within quantities of the order of  $n$  over time periods of the order of  $1/n$  (much longer than the orbital period of the satellite). The equilibria in equation (2.7.19) correspond to the points  $\varphi_\theta=k\pi/2$  ( $k=0, \pm 1, \pm 2, \dots$ ); they represent rotation with a constant angular velocity. Since at the time of perigee passage  $\varphi_\theta$  is equal to the angle between the principal axis of inertia (with the moment  $C$ ) and the radius-vector, rotation with a constant angular velocity  $\Omega=m/2$  is possible only if in perigee one of the principal central axes of inertia points along the radius vector.

If  $\Phi_m(e)>0$ , the equilibria  $\varphi_\theta=k\pi$  are stable: the least moment of inertia  $C$  points along the radius-vector in perigee; the other states are unstable. If  $\Phi_m(e)<0$ , conversely, only those motions are stable when the least moment of inertia points along the tangent to the orbit in perigee. The frequency of small oscillations relative to the stable rotation is equal to  $n\sqrt{|\Phi_m(e)|}$ . From the formula for  $\Phi_m$  we have

$$\begin{aligned} \Phi_1(e) &= -\frac{1}{2}e + O(e^2), \quad \Phi_2(e) = 1 - \frac{5}{2}e^2 + O(e^4), \\ \Phi_3(e) &= \frac{7}{2}e + O(e^2), \quad \Phi_4(e) = \frac{17}{2}e^2 + O(e^4), \\ \Phi_m(e) &= O(e^2) \quad (m \geq 5). \end{aligned}$$

The case of the principal resonance ( $m=2$ ) is the most significant; in other cases, the rotation of the satellite moving in a nearly circular orbit is almost uniform. With a circular orbit and  $m=2$ , the averaged equation (2.7.19) coincides with the exact equation of oscillations in the orbital system. For any  $e$ , the case  $m=2$  corresponds to a periodic solution of equation (2.3.5) for oscillations in the orbital system.

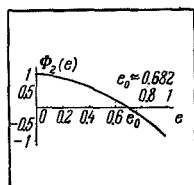


FIGURE 15. The graph of  $\Phi_2(e)$ .

The change in the steady-state mode of oscillation is connected with the function  $\Phi_2(e)$  reversing its sign.  $\Phi_2(e)$  can be calculated numerically. It is found to decrease monotonically, passing through zero for  $e \approx 0.682$  (Figure 15). The periodic solution — steady-

state rotation with a period equal to the orbital period of the satellite — is thus stable if in perigee the axis of the least moment of inertia is directed

along the radius-vector for  $e < e_0 \approx 0.682$ ;

along the tangent to the orbit for  $e > e_0 \approx 0.682$ .

**3. Periodic oscillations of an arbitrary satellite with arbitrary eccentricities.** If the two parameters in (2.3.5) —  $n^2$  and  $e$  — are arbitrary (not small), the analysis of motion is a formidable task; this analysis, however, can be carried out on a computer. V. A. Zlatoustov, D. E. Okhotsimskii, V. A. Sarychev, and A. P. Torzhevskii made the necessary calculations, and their joint results are described in [37]. As we have already observed, the periodic solutions are of greatest interest, since stable periodic motions can be regarded as the basic modes for a system of gravity attitude stabilization in elliptical orbits. In [37], odd periodic solutions are investigated, with a period equal to the orbital period of the satellite.

The following is known on the  $2\pi$ -periodic solutions of equation (2.3.5). It has been proved [66] that for all values of the parameters  $n^2$  and  $e$  filling a region  $E(|n^2| \leq 3; 0 \leq e < 1)$ , there exists at least one odd  $2\pi$ -periodic solution. The region  $E$  is divided by the branching curve (bifurcation curve) into two subregions  $E_1$  and  $E_3$ . The branching curve has the axis  $n^2$  as its tangent at the point of principal resonance ( $n^2 = 1, e = 0$ ). In the region  $E_3$ , there are three periodic solutions  $\Theta_0, \Theta_+, \Theta_-$ , of which  $\Theta_0$  and  $\Theta_+$  merge on the branching curve and disappear upon transition into the region  $E_1$ . In  $E_1$  exists a single periodic solution  $\Theta_-$  (in our notations,  $\Theta = \bar{\delta}/2$ ).

In a circular orbit ( $e = 0$ ), equation (2.3.5) reduces to the equation of free oscillations of a mathematical pendulum, which is integrable in elliptical functions (see § 2 of this chapter). The foregoing  $2\pi$ -periodic solutions have the following form for  $e = 0$ :

in  $E_3$  ( $3 \geq n^2 \geq 1$ ),

$$\left. \begin{array}{ll} (1) & \Theta_0 = 0; \\ (2) & \Theta_+ = \arcsin(k \operatorname{sn} nv), \quad k^2 = \frac{1}{n^2} \left( \frac{d\Theta}{dv} \right)_{v=0}^2, \\ & n = \sqrt{3 \frac{A-C}{B}}, \\ (3) & \Theta_- = -\arcsin(k \operatorname{sn} nv); \end{array} \right\}$$

in  $E_1$  ( $-3 \leq n^2 \leq 1$ ),

$$\Theta_- = 0.$$

In these formulas,  $k^2$ , and therefore  $\left( \frac{d\Theta}{dv} \right)_{v=0}$ , are determined from the equation

$$2K(k^2) = \pi \sqrt{\frac{3(A-C)}{B}}$$

For nonzero eccentricities, these are generating solutions. In a circular orbit, trivial solutions for positive  $n^2$  define the position of relative equilibrium.

Seeking odd  $2\pi$ -periodic solutions of (2.3.5) is equivalent to solving a boundary-value problem for this equation with the boundary conditions

$$\Theta(0) = \Theta(\pi) = 0,$$

i.e., finding all  $\dot{\theta}(0)$  for which  $\theta(\pi) = 0$ ; this was in fact the approach adopted in the numerical techniques. The solution of the boundary-value problem shows, in particular, that the branching curve starting at the point  $n^2 = 1$ ,  $e = 0$  passes through the point  $n^2 = 3$ ,  $e = 0.446$ .

Figure 16 plots the initial angular velocity  $\dot{\theta}(0)$  as a function of the parameter  $e$  for some  $n^2$ . Periodic solutions  $\theta_+$  and  $\theta_-$  correspond to positive, and  $\theta_-$  to negative values of  $\dot{\theta}(0)$ . The initial data for the solution  $\theta_+$  in the figure lie above the branching curve (the dashed line). Positive values of  $\dot{\theta}(0)$  below the branching curve correspond to the solution  $\theta_-$ .

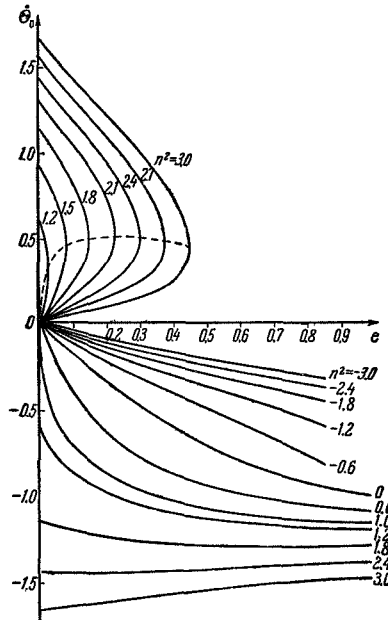


FIGURE 16. The initial velocity  $\dot{\theta}(0)$  corresponding to periodic solutions as a function of  $e$  for various  $n^2$ . The dashed line marks the branching curve.

To investigate the stability of these numerically obtained periodic solutions, we write equation (2.3.5) in the variational form

$$(1 + e \cos v) \frac{d^2x}{dv^2} - 2e \sin v \frac{dx}{dv} + n^2 x \cos 2\theta^* = 0, \quad (2.7.20)$$

where  $\theta^*$  is the periodic solution with whose stability we are concerned,  $x$  a small deviation from this solution.

Substituting  $x = \frac{z}{1 + e \cos v}$ , we obtain

$$\frac{d^2z}{dv^2} + \left\{ \frac{n^2 \cos 2\theta^* + e \cos v}{1 + e \cos v} \right\} z = 0$$

(compare with (2.3.8)).

The characteristic equation of (2.7.20) has the form

$$\lambda^2 - 2A\lambda + 1 = 0. \quad (2.7.21)$$

Here

$$A = \frac{1}{2} [x_1(2\pi) + \dot{x}_2(2\pi)];$$

$x_1$  and  $x_2$  are the solutions of the variational equation which constitute a fundamental system and satisfy the initial conditions

$$\begin{cases} x_1(0) = 1, & x_2(0) = 0, \\ \dot{x}_1(0) = 0, & \dot{x}_2(0) = 1. \end{cases}$$

If  $|A| < 1$ , the roots of the characteristic equation are complex conjugates, and on-first approximation, the periodic solution is stable. The equation  $|A|=1$  defines the boundary of the region of stability of the periodic solution. If  $|A| > 1$ , the periodic solution is unstable.

The values  $x_1(2\pi)$  and  $\dot{x}_2(2\pi)$  are determined by numerical integration of the variational equation (2.7.20). The results concerning the roots of the characteristic equation (2.7.21) are plotted in Figure 17, where the boundaries of stability of the periodic solutions (thin lines) and the branching curve (thick line) issuing from the point ( $n^2=1$ ,  $e=0$ ) are marked in the plane  $n^2$ ,  $e$ . The region  $E_3$  where three periodic solutions exist is located in Figure 17 above and to the left from the branching curve. One periodic solution exists in the region  $E_1$ , located below and to the right from the branching curve.

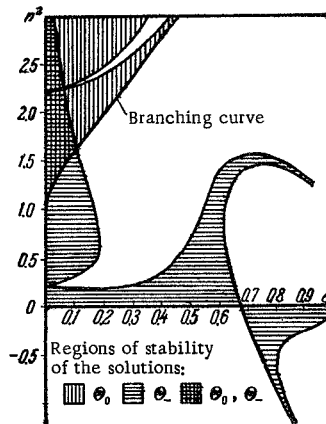


FIGURE 17. Regions of existence of one and three periodic solutions and the regions of stability of the solutions  $\Theta_0$  and  $\Theta_1$ .

The analysis shows that the solution  $\Theta_1$  is always unstable, while  $\Theta_0$  is stable in  $E_3$ , with the exception of the region of parametric resonance starting at the point ( $n^2 = 9/4$ ,  $e = 0$ ). The boundaries of the region of parametric resonance (for small  $e$ ) are defined by the relation

$$n^2 = \frac{9}{4} + \frac{1227}{200} e^2 \pm \frac{74853}{51200} e^3 + \dots$$

The region of stability of the periodic solution  $\Theta_0$  is more complex. For this solution, the point ( $n^2 = 1/4$ ,  $e = 0$ ) is the origin of parametric resonance, the boundaries of the resonance region being defined by (2.6.19) in the first approximation. The transition of the stability region from positive to negative  $n^2$  through the point ( $n^2 = 0$ ,  $e = 0.682$ ) is of considerable interest. When the motion is stable,  $n^2 > 0$  corresponds to the oscillation of the small moment of inertia about the radius-vector, while for  $n^2 < 0$  it is the large moment of inertia which oscillates (see also [72] and the previous subsection of this section).

The calculation of the limits of stability of the solution  $\Theta_0$  for  $e \rightarrow 1$  involves considerable difficulties, since (2.3.5) has singularities for  $e = 1$ ,  $v = (2k+1)\pi$  ( $k = 0, \pm 1, \pm 2, \dots$ ). For  $n^2 > 0$ , the two boundary curves apparently merge approaching the vertical tangent at the point ( $n^2 = 0$ ,  $e = 1$ ), while for  $n^2 < 0$  they asymptotically approach the line  $e = 1$ .

It follows from the results of [2, 58] that the necessary conditions of stability of the periodic solutions of (2.3.5) obtained on first approximation are also sufficient, almost for all values of the parameters  $n^2, e$ .

Let us now consider the behavior of solutions near the fundamental periodic solutions. Autonomous systems with one degree of freedom are conveniently described by their phase paths. For nonautonomous systems with periodic coefficients, the equivalent of the phase pattern is provided by the stroboscopic pattern, which is a plot of the phase paths taken at discrete times, at intervals which are multiples of the system period. The points of the phase plane are transformed during each period. A periodic solution obviously corresponds to a fixed point under this transformation. A periodic solution is stable if the image of a sufficiently small neighborhood of the fixed point remains small after any number of successive mappings; the stroboscopic pattern of almost periodic phase trajectories gives closed curves around the fixed point.

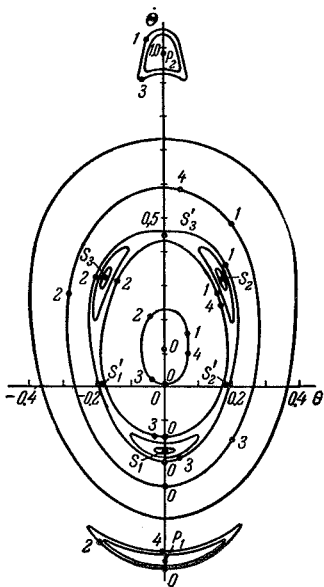


FIGURE 18. A stroboscopic pattern of phase paths near the periodic solution  $\Theta_0$  for  $n^2=3$  and  $e=0.2$ .

$n^2 = 3$ ,  $e = 0.2$ . The angle  $\Theta$  and the angular velocity  $\dot{\Theta}$  in perigee are laid off along the axes. The fixed point  $O$  corresponds to the stable periodic solution  $\Theta_0$ . The points tagged with  $n = 0, 1, 2, \dots$  are images of  $n$  mappings (periods). The initial position of the phase points has been chosen on the axis  $\dot{\Theta}$ . The figure shows the closed curves surrounding the fixed point. The stable subharmonic with a period  $4\pi$  also emerges from this pattern: these are the points  $P_1$  and  $P_2$  which are swapped over once every  $2\pi$ . The points  $S_1, S_2, S_3$  which are swapped over with a period of  $2\pi$  correspond to the stable  $6\pi$  subharmonic, while the points  $S'_1, S'_2, S'_3$  correspond to the unstable subharmonic with a period of  $6\pi$ . The closed curves surrounding

the points  $P_1$ ,  $P_2$  and  $S_1$ ,  $S_2$ ,  $S_3$  are also distinctly outlined. The curves around different fixed points of one subharmonic are mapped into one another with a period of  $2\pi$ .

Aside from the periodic motions about the radius-vector, we must also consider the periodic motions about a fixed line in the absolute space, e.g., the line parallel to the major axis of the elliptical orbit. There is, however, but one such  $2\pi$ -periodic solution in the entire  $E$  region of the parameters  $(n^2, e)$ . Its generating solution is  $\Theta_1 = 0$ , which obtains for  $n^2 = 0$  and corresponds to translational motion in the absolute space ( $\Theta_1$  is the angle between the axis of inertia of the satellite and the radius-vector to the perigee). The stability of these solutions is determined by the coefficient  $A$  of the characteristic equation.

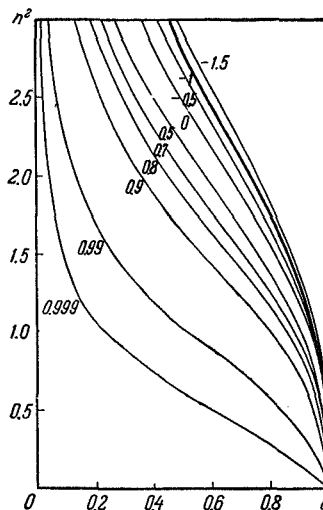


FIGURE 19.  $A = \text{const}$  lines and the region of stability of periodic solutions corresponding to oscillations about the direction of the major axis.

Figure 19 plots the lines of equal values of  $A$  in the  $(n^2, e)$  plane. The region of stability corresponds to the part of this plane where  $|A| < 1$ . The boundary of this region is marked in Figure 19 by a thick line: it comprises segments of the coordinate axes ( $A = 1$ ), part of the upper boundary of the region  $E$ , and the line  $A = -1$ , which emerges from the point  $(n^2 = 0, e = 1)$  where it has a vertical tangent. Part of the region  $E$  above and to the right from the curve  $A = -1$  corresponds to unstable solutions.

## § 8. SMALL SPACE OSCILLATIONS OF A SATELLITE ABOUT A POSITION OF RELATIVE EQUILIBRIUM IN A CIRCULAR ORBIT

In § 1 of the present chapter we gave the dynamic (2.1.1) and the kinematic (2.1.2)–(2.1.3) equations of motion of a satellite about its center of mass

under gravity forces; these equations can be applied to derive the form of small space oscillations of the satellite. For small oscillations,  $\alpha=1+\eta$ ,  $\beta'=1+\chi$ ,  $\gamma''=1+\xi$ , where  $\eta$ ,  $\chi$ ,  $\xi$ , as well as  $\alpha'$ ,  $\alpha''$ ,  $\beta$ ,  $\beta''$ ,  $\gamma$ ,  $\gamma'$ , are small in comparison with unity. Trivial integrals give  $\eta = -\frac{1}{2}(\eta^2 + \alpha'^2 + \alpha''^2)$ , and similar expressions for  $\chi$ ,  $\xi$ . We see that  $\eta$ , and also  $\chi$  and  $\xi$ , are of second order of smallness; we may therefore take  $\alpha=\beta'=\gamma''=1$ . Also  $q=\omega+x$ , where  $x$  is of the first order of smallness; the components  $p$ ,  $r$  are also of the first order of smallness. Linearizing equations (2.1.2)–(2.1.3) for the direction cosines, we have

$$r = -\dot{\alpha}' - \omega\gamma', \quad \dot{\alpha}'' = x, \quad p = \dot{\gamma}' - \omega\alpha', \quad \dot{\gamma} = -x, \quad \alpha'' = -\gamma. \quad (2.8.1)$$

The set (2.1.1) of dynamic equations can now be written as

$$\left. \begin{aligned} \ddot{\alpha}'' + 3\xi \frac{A-C}{B} \alpha'' &= -\dot{\omega}, \quad \xi = \frac{\mu}{R^3}, \\ \ddot{\gamma}' + (3\xi + \omega^2) \frac{B-C}{A} \gamma' + \omega \left( \frac{B-C}{A} - 1 \right) \dot{\alpha}' - \dot{\omega}\alpha' &= 0, \\ \ddot{\alpha}' + \frac{B-A}{C} \omega^2 \alpha' + \omega \left( 1 - \frac{B-A}{C} \right) \dot{\gamma}' + \dot{\omega}\gamma' &= 0. \end{aligned} \right\} \quad (2.8.2)$$

Small plane oscillations, as we see, are described by a separate equation, not dependent on transverse oscillations. This justifies the approach of previous sections, where plane oscillations were treated as an independent phenomenon. The transverse modes ( $\gamma'$  and  $\alpha'$ ) are interdependent.

The three equations (2.8.2) have variable coefficients, which are determined making use of relations (2.3.2) of the elliptical theory of motion of the satellite's mass center.

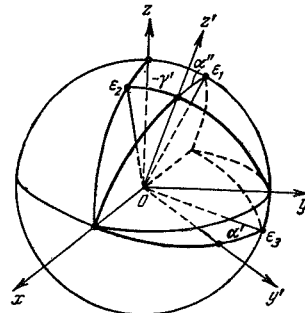


FIGURE 20. Illustrating the angles of small oscillations.

Let us consider the physical meaning of the small angles  $\alpha'$ ,  $\gamma'$ ,  $\alpha''$  (Figure 20). Consider the orbital system  $xyz$  and the satellite's system  $x'y'z'$  of the principal central axes of inertia. Since  $\alpha''$  is small, we have from Figure 20, where  $Oe_1$  is the projection of  $Oz'$  on the plane  $xy$ ,

$$\alpha'' = \cos \angle xOz' = \sin \angle z'Oe_1 \approx \angle z'Oe_1.$$

Thus  $\alpha''$  describes the oscillations of the axis  $z'$  "along" the orbital plane  $xy$ .

From the integral  $\beta\gamma + \beta'\gamma' + \beta''\gamma'' = 0$  of the direction cosines, we have for small oscillations  $\gamma' = -\beta''$ . Then, from Figure 20,  $\beta'' = -\gamma' = \sin \angle e_2 O z' \approx \angle e_2 O z'$ , where  $Oe_2$  is the projection of  $Oz'$  on the plane  $xz$ . Thus  $\gamma'$  describes the oscillations of the axis  $z'$  "across" the orbital plane. Let  $Oe_3$  be the projection of  $Oy'$  on the plane  $zy$ ; then  $\alpha' = \angle y' O e_3$ . For a fixed axis  $z'$ , the angle  $\alpha'$  describes the rotation of the satellite around the axis  $z'$ . The physical meaning of the small angles emerges from this discussion. The angle  $\alpha''$  is the pitch, while  $\alpha'$  and  $\gamma'$  are the roll and the yaw, respectively. Now  $\alpha'' = \theta$ ,  $\gamma' = -\Psi$ ,  $\alpha' = \Phi$ , where  $\theta$ ,  $\Psi$ ,  $\Phi$  are the angles defined in § 1 of Chapter 1.

For a circular orbit, we have  $\omega = 0$ ,  $\zeta = \omega^2 = \text{const}$ . Equations (2.8.2) then take the form

$$\left. \begin{aligned} \ddot{\alpha}'' + 3\omega^2 \frac{A-C}{B} \alpha'' &= 0, \\ \ddot{\gamma}' + 4\omega^2 \frac{B-C}{A} \gamma' + \omega \left( \frac{B-C}{A} - 1 \right) \dot{\alpha}' &= 0, \\ \ddot{\alpha}' + \omega^2 \frac{B-A}{C} \alpha' + \omega \left( 1 - \frac{B-A}{C} \right) \dot{\gamma}' &= 0, \end{aligned} \right\} \quad (2.8.3)$$

i.e., a system of linear equations with constant coefficients. The characteristic equation of the set (2.8.3) is

$$\left. \begin{aligned} (\lambda^2 + n^2)(\lambda^4 + \tilde{a}\lambda^2 + \tilde{b}) &= 0, \\ n^2 &= 3\omega^2 \frac{A-C}{B}, \\ \tilde{a} &= \omega^2 \left\{ 1 + 3 \frac{B-C}{A} + \frac{B-A}{C} \cdot \frac{B-C}{A} \right\}, \\ \tilde{b} &= 4\omega^4 \frac{B-C}{A} \cdot \frac{B-A}{C}. \end{aligned} \right\} \quad (2.8.4)$$

The motion is stable only if all the roots of the characteristic equation (2.8.4) are pure imaginary quantities, which is in turn possible if and only if  $n^2$ ,  $\tilde{a}$ ,  $\tilde{b}$ ,  $\tilde{a}^2 - 4\tilde{b}$  are all positive, i.e.,

$$\left. \begin{aligned} \text{(i)} \quad 1-\varepsilon &> 0; \\ \text{(ii)} \quad \varepsilon + 3(\delta-\varepsilon)\varepsilon + (\delta-1)(\delta-\varepsilon) &> 0; \\ \text{(iii)} \quad (\delta-\varepsilon)(\delta-1) &> 0; \\ \text{(iv)} \quad \{ \varepsilon + 3(\delta-\varepsilon)\varepsilon + (\delta-1)(\delta-\varepsilon) \}^2 - \\ &\quad - 16\varepsilon(\delta-\varepsilon)(\delta-1) > 0; \quad \varepsilon = \frac{C}{A}, \quad \delta = \frac{B}{A}. \end{aligned} \right\} \quad (2.8.5)$$

If any of these conditions does not hold true, the motion is unstable. If all the conditions hold true, the motion is stable, but only in the linear approximation. Equations (2.8.3) and conditions (2.8.5) are encountered in the classical theory of the libration of the Moon; in this theory, which is presented, e.g., by Tisserand /94/, the analysis is confined to bodies of nearly spherical dynamic figure. This restriction substantially simplifies the conditions (2.8.5).

Let us analyze the conditions (2.8.5) in some detail.

Consider the plane  $\delta$ ,  $\varepsilon$  (Figure 21). By examining the physical meaning of the moments of inertia, we see that

$$1+\delta < \varepsilon, \quad 1+\varepsilon > \delta, \quad \varepsilon + \delta > 1. \quad (2.8.6)$$

We need only consider the part of the plane  $\epsilon, \delta$  where inequalities (2.8.6) are satisfied (the hatched strip in Figure 21).

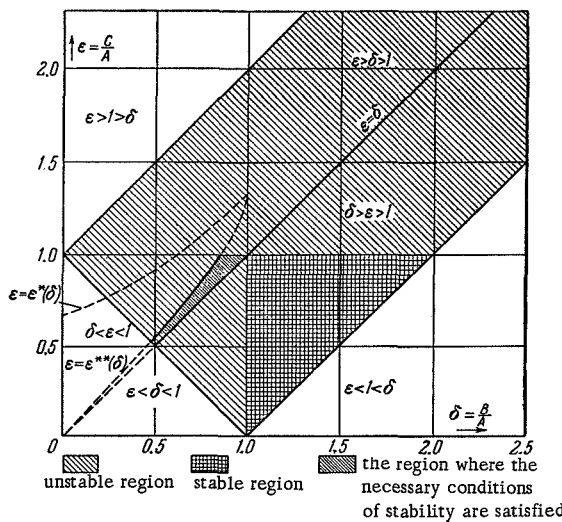


FIGURE 21. Regions of stability and instability.

- Let the 1st condition in (2.8.5) be false. Then  $\epsilon > 1$ ; the motion (relative equilibrium) is unstable in this region (the range of instability is the sparsely cross-hatched region of the  $\epsilon, \delta$  plane in Figure 21).
- Consider the 3rd condition in (2.8.5). If  $(\delta - \epsilon)(\delta - 1) < 0$ , the motion is unstable. This inequality obtains in two cases:  $\epsilon > \delta > 1$ ;  $\epsilon < \delta < 1$ . Only the second of these inequalities defines a new range of instability.
- The 4th condition in (2.8.5) may be written as  $F(\epsilon, \delta) > 0$ . The ranges of stability and instability extend on the two sides of the curve  $F(\epsilon, \delta) = 0$ . This is a curve of fourth order. The corresponding dependence  $\epsilon(\delta)$  may be calculated numerically in any relevant region. The results are listed in Table 2.

TABLE 2

$\delta$	0	0.1	0.2	0.3	0.4	0.5	0.6	0.7	0.8	0.854	0.9	1.0
$\epsilon$	0	0.11	0.22	0.33	0.44	0.55	0.67	0.79	0.92	1.00	1.07	1.33 = 4/3

Let this curve be denoted by  $\epsilon^{**}(\delta)$ . Above this curve,  $F(\epsilon, \delta) < 0$  and the motion is unstable. In the narrow region wedging between the curve  $\epsilon^{**}(\delta)$  and the straight line  $\epsilon = \delta$ , the 1st, 3rd, and 4th conditions of (2.8.5) are satisfied; let us check that the 2nd condition of (2.8.5) is also satisfied. In the left-hand side of the 2nd condition in (2.8.5), we add and subtract  $(\delta - \epsilon)\epsilon$ .

Then, after simple manipulations, we write this condition in the form

$$4(\delta - \varepsilon)\varepsilon + (\delta - 1) + (1 - \delta + \varepsilon)^2 > 0 \quad (2.8.7)$$

and this inequality, as is easily seen, is satisfied in the narrow wedge-shaped region covered with dense cross-hatching in Figure 21. Indeed, if inequality (2.8.7) reduces to equality, the resulting curve, which we denote by  $\varepsilon^*(\delta)$ , is a hyperbola through the points

$$\delta = 1, \varepsilon = \frac{4}{3} \text{ and } \delta = 0, \varepsilon = \frac{2}{3}.$$

Below the hyperbola, all the way to the straight line  $\varepsilon = \delta$ , inequality (2.8.7) holds true; therefore all the necessary conditions of stability are satisfied in the narrow region between the curves  $\varepsilon^{**}(\delta)$ ,  $\varepsilon = \delta$ ,  $\varepsilon = 1$ ,  $\delta + \varepsilon = 1$ . According to Lyapunov's theorem, if the motion is unstable to first approximation, it is unstable to any other approximation, so that the diagonally hatched region of Figure 21 represents the range of unstable motion. The necessary conditions of stability (2.8.5) are not sufficient. There is therefore no certainty that the motion is stable if the parameters lie in the densely hatched region of Figure 21, where the conditions (2.8.5) hold true.

Conditions (2.8.5), as we shall show presently, are also satisfied in the triangle between the straight lines  $\delta = 1$ ,  $\varepsilon = 1$ ,  $1 + \varepsilon = \delta$ . In this region, the motion is truly stable according to Lyapunov, since a point lying in this region corresponds to the inequalities  $B > A > C$ , which have been proved to be a sufficient condition of stability.

We shall now prove that conditions (2.8.5) are satisfied in this triangle (the triangle which is square-hatched in Figure 21). Condition (i) ( $\varepsilon < 1$ ) is obviously satisfied. Condition (ii) is also seen to apply if it is written in the form (2.8.7), since in our triangle  $\delta > 1$ ,  $\delta > \varepsilon$ . Condition (iii)  $((\delta - 1)(\delta - \varepsilon) > 0)$  clearly holds true. It now remains to check the fourth condition of (2.8.5). The expression in braces in this condition is written in a form similar to the left-hand side of inequality (2.8.7). Then,

$$[4(\delta - \varepsilon)\varepsilon + (\delta - 1) + (1 - \delta + \varepsilon)^2]^2 > [4(\delta - \varepsilon)\varepsilon + (\delta - 1)]^2.$$

On the other hand,

$$[4(\delta - \varepsilon)\varepsilon + (\delta - 1)]^2 > 16\varepsilon(\delta - \varepsilon)(\delta - 1),$$

since this is equivalent to

$$[4(\delta - \varepsilon)\varepsilon - (\delta - 1)]^2 > 0.$$

We thus see that the fourth condition in (2.8.5) is satisfied.

Some addition to the analysis of the conditions of stability will be found in § 1 of Chapter 6.

Writing the solution of the small oscillation equations, we shall now assume that all the parameters take their values in the region  $\delta > 1 > \varepsilon$ ,  $1 + \varepsilon > \delta$ , since this is sufficient for the relative equilibrium to be stable.

For the angle of pitch we have

$$\alpha'' = A_0 \sin(n\omega t + \alpha^*), \quad n = \sqrt{3 \frac{1-\varepsilon}{\delta}}, \quad (2.8.8)$$

where  $A_0$  and  $\alpha^*$  are integration constants defined by the initial conditions. Let

$$\left. \begin{aligned} \lambda_1 &= \pm i\omega\bar{\lambda}_1, \quad \lambda_2 = \pm i\omega\bar{\lambda}_2, \\ \bar{\lambda}_1 &= \sqrt{\frac{a}{2} + \sqrt{\frac{a^2}{4} - b}}, \\ \bar{\lambda}_2 &= \sqrt{\frac{a}{2} - \sqrt{\frac{a^2}{4} - b}}, \\ a &= 1 + 3(\delta - \varepsilon) + (\delta - 1)\left(\frac{\delta}{\varepsilon} - 1\right), \\ b &= 4(\delta - 1)\left(\frac{\delta}{\varepsilon} - 1\right). \end{aligned} \right\} \quad (2.8.9)$$

Then

$$\left. \begin{aligned} \gamma &= A_1 \sin(\bar{\lambda}_1 \omega t + \kappa_1) + A_2 \sin(\bar{\lambda}_2 \omega t + \kappa_2), \\ a' &= A_1 k_1 \cos(\bar{\lambda}_1 \omega t + \kappa_1) + A_2 k_2 \cos(\bar{\lambda}_2 \omega t + \kappa_2), \\ k_1 &= \frac{1}{\left(1 - \frac{B-C}{A}\right) \bar{\lambda}_1} \left(4 \frac{B-C}{A} - \bar{\lambda}_1^2\right); \\ k_2 &= \frac{1}{\left(1 - \frac{B-C}{A}\right) \bar{\lambda}_2} \left(4 \frac{B-C}{A} - \bar{\lambda}_2^2\right). \end{aligned} \right\} \quad (2.8.10)$$

Here  $A_1$ ,  $A_2$ ,  $\kappa_1$ ,  $\kappa_2$  are integration constants defined by the initial conditions. We see that the roll and the yaw are a superposition of two oscillations of different frequencies.

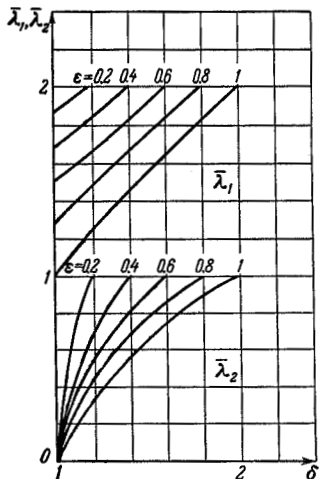


FIGURE 22. The dimensionless frequencies  $\bar{\lambda}_1$ ,  $\bar{\lambda}_2$  of space oscillations as a function of  $\varepsilon = C/A$  and  $\delta = B/A$ .

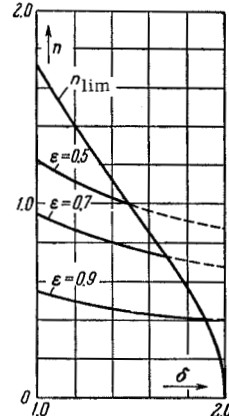


FIGURE 23. The dimensionless frequency  $n$  as a function of  $\varepsilon = C/A$  and  $\delta = B/A$ .

Let us consider the behavior of  $\bar{\lambda}_1$  and  $\bar{\lambda}_2$ . We shall restrict the analysis to the region where the sufficient conditions of stability are satisfied,  $\delta > 1 > \varepsilon$ ,  $1 + \varepsilon > \delta$ . Figure 22 plots  $\bar{\lambda}_1$  and  $\bar{\lambda}_2$  as a function of  $\delta$  for  $\varepsilon = \text{const}$ . From (2.8.9) we see that  $\bar{\lambda}_1 > \bar{\lambda}_2$ ,  $\bar{\lambda}_2 < 1$  ( $\bar{\lambda}_2 = 1$  when  $1 + \varepsilon = \delta$ ). The sufficient conditions of stability are satisfied, therefore  $1 \leq \bar{\lambda}_1 \leq 2$ . The dimensionless

frequencies of the space oscillations are thus bounded:

$$0 \leq \bar{\lambda}_2 \leq 1 \leq \bar{\lambda}_1 \leq 2. \quad (2.8.11)$$

The period corresponding to  $\bar{\lambda}_2$  may be arbitrarily large (for small  $\bar{\lambda}_2$ ).

Let us also consider the frequency  $n$  (2.8.8). It is meaningful if  $1+\epsilon > \delta$ .

The frequency  $n$  is therefore bounded by  $n_{\lim} < n < n_{\lim}$ ; here  $\frac{n_{\lim}}{\sqrt{3}} = \sqrt{\frac{2-\delta}{\delta}}$ ,

$1 < \delta < 2$ . Figure 23 plots  $n$  as a function of  $\delta$  for  $\epsilon = \text{const}$ , as well as the limiting curve  $n_{\lim}(\delta)$ . The solid sections of the curves in this figure are physically meaningful, while the dashed segments have no physical meaning. The maximum possible frequency of pitch, as we see from Figure 23, is  $n_{\max} = \sqrt{3}$ .

## § 9. SMALL SPACE OSCILLATIONS IN AN ELLIPTICAL ORBIT

We shall now deal with transverse oscillations (roll and yaw) only, since they are independent of the previously considered oscillations in the orbital plane. We substitute  $v$  — the true anomaly — for  $t$  as a new independent variable. Applying equations (2.3.2) and (2.3.3), we substitute in (2.8.2)

$$\gamma' = \frac{\tilde{\gamma}}{1+e \cos v}, \quad \alpha' = \frac{\tilde{\alpha}}{1+e \cos v}, \quad \alpha'' = \frac{z}{1+e \cos v}, \quad (2.9.1)$$

where  $\tilde{\gamma}$  and  $\tilde{\alpha}$  are new variables. Then

$$\left. \begin{aligned} \frac{d^2\tilde{\gamma}}{dv^2} + \frac{e \cos v + \bar{a}_1 (4 + e \cos v)}{1 + e \cos v} \tilde{\gamma} - \bar{a}_2 \frac{d\tilde{\alpha}}{dv} + \\ + \frac{e \sin v}{1 + e \cos v} \bar{a}_3 \tilde{\alpha} = 0, \\ \frac{d^2\tilde{\alpha}}{dv^2} + \frac{e \cos v + \bar{b}_1 (1 + e \cos v)}{1 + e \cos v} \tilde{\alpha} + \\ + \bar{b}_2 \frac{d\tilde{\gamma}}{dv} - \frac{e \sin v}{1 + e \cos v} \bar{b}_3 \tilde{\gamma} = 0, \\ \bar{a}_1 = \frac{B-C}{A}, \quad \bar{a}_2 = \frac{A+C-B}{A}, \quad \bar{a}_3 = \frac{B-C+A}{A}, \\ \bar{b}_1 = \frac{B-A}{C}, \quad \bar{b}_2 = \frac{A+C-B}{C}, \quad \bar{b}_3 = \frac{B+C-A}{C}. \end{aligned} \right\} \quad (2.9.2)$$

The first equation in (2.8.2) reduces to (2.3.8) which has already been investigated. Equations (2.9.2) contain no free terms, so that no forced oscillations will occur. However, parametric resonances are possible, the coefficients being periodic.

As the zero-order approximation for the solution of equations (2.9.2) we may take the circular orbit solution ( $e=0$ ). Then for small  $e$ , we may construct an approximate solution. Let us write the equations series-expanding the coefficients in  $e$  and retaining terms of the first order of

smallness only. Then

$$\left. \begin{aligned} \frac{d^2\tilde{\gamma}}{dv^2} + 4\bar{a}_1\tilde{\gamma} - \bar{a}_2 \frac{d\tilde{\alpha}}{dv} &= eF_\gamma, \\ \frac{d^2\tilde{\alpha}}{dv^2} + \bar{b}_1\tilde{\alpha} + \bar{b}_2 \frac{d\tilde{\gamma}}{dv} &= eF_\alpha, \\ F_\gamma &= -[\bar{a}_3\tilde{\alpha} \sin v + (1 - 3\bar{a}_1)\tilde{\gamma} \cos v], \\ F_\alpha &= -[\tilde{\alpha} \cos v - \bar{b}_3\tilde{\gamma} \sin v]. \end{aligned} \right\} \quad (2.9.3)$$

The solution of this set of equations should be properly sought only to first order in  $e$ . If  $e = 0$ , we obtain the circular orbit solution. The set (2.9.3) is solved by successive approximations. Substituting the circular orbit solution in the right-hand sides, we integrate the inhomogeneous system of linear differential equations with constant coefficients.

The circular orbit solution is symbolically written as

$$\tilde{\gamma} = A_i \sin \Psi_i, \quad \tilde{\alpha} = k_i A_i \cos \Psi_i, \quad \Psi_i = \bar{\lambda}_i v + \kappa_i. \quad (2.9.4)$$

( $\Sigma$  denoting summation over  $i = 1, 2$  has been omitted). Substituting (2.9.4) in (2.9.3), we find  $F_\gamma$  and  $F_\alpha$ :

$$\left. \begin{aligned} F_\gamma &= \frac{A_i}{2} [(3\bar{a}_1 - 1) - \bar{a}_3 k_i \delta] \sin(\Psi_i + \delta v) \equiv \\ &\qquad\qquad\qquad \equiv \Gamma_{i,\delta} \sin(\Psi_i + \delta v), \\ F_\alpha &= -\frac{A_i}{2} [k_i + \delta \bar{b}_3] \cos(\Psi_i + \delta v) \equiv \\ &\qquad\qquad\qquad \equiv B_{i,\delta} \cos(\Psi_i + \delta v). \end{aligned} \right\} \quad (2.9.3')$$

(The same symbolic notations again. This is in fact a sum of four terms, taken over  $i = 1, 2$  and  $\delta = -1, +1$ .) The equations of motion now take the form

$$\left. \begin{aligned} \frac{d^2\tilde{\gamma}}{dv^2} + 4\bar{a}_1\tilde{\gamma} - \bar{a}_2 \frac{d\tilde{\alpha}}{dv} &= e\Gamma_{i,\delta} \sin(\Psi_i + \delta v), \\ \frac{d^2\tilde{\alpha}}{dv^2} + \bar{b}_1\tilde{\alpha} + \bar{b}_2 \frac{d\tilde{\gamma}}{dv} &= eB_{i,\delta} \cos(\Psi_i + \delta v). \end{aligned} \right\} \quad (2.9.5)$$

It is easily seen that a particular solution of the inhomogeneous system (2.9.5) may be sought in the form

$$\tilde{\gamma} = eM_{i,\delta} \sin(\Psi_i + \delta v), \quad \tilde{\alpha} = eN_{i,\delta} \cos(\Psi_i + \delta v). \quad (2.9.6)$$

To find  $M_{i,\delta}$  and  $N_{i,\delta}$ , we substitute (2.9.6) in (2.9.5) and obtain a system of algebraic equations

$$\left. \begin{aligned} [4\bar{a}_1 - (\bar{\lambda}_i + \delta)^2] M_{i,\delta} + \bar{a}_2 (\bar{\lambda}_i + \delta) N_{i,\delta} &= \Gamma_{i,\delta}, \\ \bar{b}_2 (\bar{\lambda}_i + \delta) M_{i,\delta} + [\bar{b}_1 - (\bar{\lambda}_i + \delta)^2] N_{i,\delta} &= B_{i,\delta}. \end{aligned} \right\} \quad (2.9.7)$$

This is a set of eight equations in eight unknowns. Each pair of coefficients  $M_{i,\delta}$ ,  $N_{i,\delta}$  is easily determined from the set of the two corresponding linear algebraic equations in (2.9.7). The sum of solutions (2.9.4) and (2.9.6) (taken in conjunction with (2.9.1)) describes the transverse oscillations in an elliptical orbit. For the amplitudes  $M_{i,\delta}$  and  $N_{i,\delta}$  we obtain linear-fractional expressions with an arbitrary numerator (since the integration constants  $A_i$  are arbitrary) whose denominator is the determinant  $D$  of the

set (2.9.7). The parameters for which  $D$  is zero constitute the resonance values of the system. If the parameters are close to the resonance values, parametric resonance of transverse oscillations occurs. The equation  $D = 0$  has the form

$$D \equiv x^4 - x^2 \{4\bar{a}_1 + \bar{b}_1 + \bar{b}_2 \bar{a}_2\} + 4\bar{a}_1 \bar{b}_1 = 0, \quad x = (\bar{\lambda}_i + \delta)^2. \quad (2.9.8)$$

But the roots of this equation are  $x_j = \bar{\lambda}_j^2$ ,  $j = 1, 2$ , as we see from a comparison with (2.8.4). The resonance values of the parameters therefore satisfy one of the relations

$$(\bar{\lambda}_i \pm 1)^2 = \bar{\lambda}_j^2; \quad i = 1, 2, \quad j = 1, 2. \quad (2.9.9)$$

Let us examine the graph of  $\bar{\lambda}_1, \bar{\lambda}_2$  as a function of  $\delta$  for  $\varepsilon = \text{const}$ , (Figure 22), picking out the resonance values of  $\bar{\lambda}_i$ .

i) Consider the case  $i \neq j$ . Then from (2.9.8) we have  $\bar{\lambda}_i \pm 1 = \pm \bar{\lambda}_j$ ;  $\bar{\lambda}_2 \pm 1 = \pm \bar{\lambda}_1$ , whence it follows that (2.9.8) is satisfied only for  $\bar{\lambda}_1$  and  $\bar{\lambda}_2$  lying on the very boundary of the domain of their definition (Figure 22), where the ellipsoid of inertia degenerates; this case is of little significance. For example,  $\bar{\lambda}_1 - 1 = \bar{\lambda}_2$  is possible only for  $\bar{\lambda}_2 = 1, \bar{\lambda}_1 = 2$ .

ii) The case  $i = j$ . (a)  $\bar{\lambda}_i \pm 1 = \pm \bar{\lambda}_i$ . The solution  $\bar{\lambda}_i = 1/2$  is physically meaningless, since  $\bar{\lambda}_i > 1$ . (b)  $\bar{\lambda}_2 \pm 1 = \pm \bar{\lambda}_2$ . The solution  $\bar{\lambda}_2 = 1/2$  is the only real resonance of space oscillations in an elliptical orbit. Parametric resonance thus occurs for  $\bar{\lambda}_2$  close to  $1/2$ .

## § 10. GRAVITY ATTITUDE STABILIZATION OF ARTIFICIAL SATELLITES

Artificial satellites will mostly be useless as a research tool in space unless effective uniaxial or even triaxial orientation relative to the Earth can be achieved. The application of active attitude control systems involves considerable difficulties in long-lived satellites: energy requirements become formidable, the weight and the complexity of design of these systems also constitute a serious obstacle.

Passive stabilization systems can be devised, utilizing the properties of magnetic and gravitational fields, the effects of radiation pressure, atmospheric drag, etc. An important advantage of passive systems is that they may function for a long time without consuming power. The main shortcoming of the passive systems, however, is that the regulating torques are comparatively small.

D. E. Okhotsimskii and V. A. Sarychev /60/ considered the possibility of stabilizing a satellite relative to the trihedron formed by the radius-vector, the transversal, and the binormal of the orbit, i.e., relative to the orbital system of axes. Their approach is based on the property of the Newtonian force field, described and analyzed in previous sections, according to which a body with a triaxial ellipsoid of inertia orients itself in a certain way in orbit. The basic conclusions of /60/ are presented in what follows.

If a satellite moves in a circular orbit in a Newtonian central field, it has four stable positions of relative equilibrium, the largest axis of its ellipsoid of inertia coinciding with the radius-vector and the least axis

pointing along the binormal to the orbit (Figure 8). The different positions of relative equilibrium succeed one another as the satellite rotates through  $180^\circ$  around the radius-vector and the binormal. In the absolute system of coordinates, the position of relative equilibrium corresponds to the rotation of the satellite around the binormal with an angular velocity equal to the angular orbital velocity of the satellite's mass center.

If the energy is not dissipated internally, the amplitude of the small oscillations of the satellite about the state of relative equilibrium is constant in time. The precision of attitude stabilization is determined by the initial values of the axial angles and the angular velocities of the satellite. Introduction of dissipative forces in the system reduces the states of stable relative equilibrium of the satellite to asymptotically stable states. The amplitudes of the natural oscillations determined by the initial angles and angular velocities will approach zero.

The simplest scheme for the introduction of dissipative forces and the stabilization of an artificial satellite in a circular orbit relative to the orbital system of axes is the following. A central cavity filled with a viscous fluid is provided inside a gravitationally stable satellite. The oscillatory motion of the satellite displaces the viscous fluid relative to the hull, causing dissipation of energy. A sphere may be redesigned as a cavity between two spherical envelopes. For a given thickness and density of the viscous fluid layer enclosed between the spherical envelopes, there exists an optimal viscosity ensuring maximal rate of energy dissipation.

The main disadvantage of the oscillation damping system by means of a viscous fluid is that comparatively fast dissipation of oscillatory energy requires a large amount of fluid to achieve optimal damping, the moment of inertia of the fluid must be comparable in magnitude with the largest moment of inertia of the

satellite. This system will be somewhat more effective if the fluid is enclosed in a toroidal shell mounted outside the satellite.

In 1956, D. E. Okhotsimskii proposed a more effective system of damping and stabilization. This system is schematically shown in Figure 24. A second body, a so-called stabilizer, is attached to the satellite proper by means of a spherical hinge. The stabilizer comprises two booms of equal length rigidly connected with each other and carrying equal weights at their ends. The coordinate systems  $O_1x_1y_1z_1$  and  $O_2x_2y_2z_2$  are the principal central trihedra connected with the satellite and the stabilizer, respectively. The position of the stabilizer relative to the satellite proper is maintained by centering springs.

The parameters of the stabilizer (boom length, weight, angle between booms) are chosen so as to ensure gravitational stability of the satellite—stabilizer system when the stabilizer is rigidly fixed to the satellite. In a position of stable equilibrium of the satellite—stabilizer system, the booms lie in the orbital plane  $O_1x_1 \parallel O_2x_2, O_1y_1 \parallel O_2y_2$ , parallel to the tangent to the circular orbit,  $O_1z_1 \parallel O_2z_2$ .

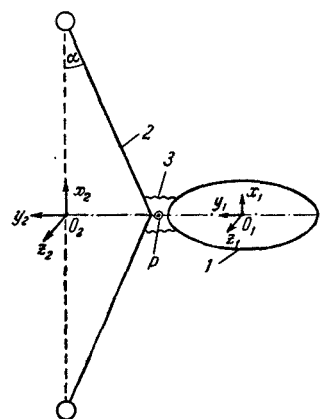


FIGURE 24. A satellite with a stabilizer:  
1) satellite; 2) stabilizer; 3) centering  
springs; P spherical hinge.

The stabilizer and the satellite are articulated by an elastic joint so as to introduce linear damping terms in the system, resulting from the relative displacement of the satellite and the stabilizer. Linear damping in the satellite-stabilizer system is feasible, e.g., with the aid of a magnetic damper, utilizing eddy currents, or a fluid damper. These damping devices are very common in various instruments.

The system proposed ensures attitude stabilization of the satellite relative to the orbital system of axes, irrespective of the particular inertia parameters. The shape of the satellite is of no significance in a drag-free medium. The motion of the system is determined by the inertia characteristics of the satellite and the stabilizer and by the coordinates of the spherical hinge relative to the axes  $O_1x_1y_1z_1$  and  $O_2x_2y_2z_2$ .

The moments of inertia of the stabilizer are proportional to the square of the length of the booms, whereas the maximum span of the booms is limited by rigidity requirements only. An adequate relation between the moments of inertia of the satellite and the stabilizer, necessary to achieve a satisfactory transient behavior, can therefore be easily ensured by attaching small masses at the ends of appropriately long booms. Telescopic booms or booms fabricated from metallic bands which roll up into a tube under the action of elastic forces are apparently the most convenient from the engineer's point of view.

No elastic coupling between the satellite and the stabilizer is needed, if the satellite without the stabilizer is gravitationally stable and the hinge is provided on the satellite's principal central axis with the medium moment of inertia. Gravity torques will provide the necessary elastic coupling in this case.

The satellite-stabilizer system shown in Figure 24 is the simplest and also the most general, since it provides a successful solution to the problem of stabilization for a satellite with quite arbitrary parameters. Introduction of more complex stabilizer geometries does not add to the results of this analysis.

Until now we have discussed the motion of a satellite-stabilizer system in a circular orbit in a drag-free medium. In an elliptical orbit, aside from the damped natural oscillations, there are also the forced eccentricity oscillations resulting from the nonuniform rotation of the orbital system of axes. Eccentricity oscillations occur in the orbital plane.

The amplitude of eccentricity oscillations is proportional to the eccentricity of the orbit and it depends on the inertia parameters of the satellite and the stabilizer. The frequency of eccentricity oscillations coincides with the orbital frequency of the center of mass of the satellite-stabilizer system, so that the angle of deviation of the satellite relative to the orbital system of axes varies very slowly in time. Eccentricity oscillations are easily calculated, and they can be taken into consideration when treating the results of experiments carried out on board satellites.

Atmospheric effects cannot be neglected for satellites orbiting at altitudes of less than 600 km; these effects mainly amount to drag forces applied to the centers of pressure of the satellite and the stabilizer and resisting the motion of the center of mass of the satellite-stabilizer system.

A gravitationally stable satellite-stabilizer system is also aerodynamically stable for a fixed position of equilibrium of the satellite and the stabilizer relative to the orbital system of axes if the following conditions are satisfied:

- 1) the axes  $O_1P$  and  $O_2P$  (Figure 24) are axes of geometrical symmetry of the satellite and the stabilizer;
- 2) the satellite and the stabilizer are each aerodynamically stable;
- 3) the aerodynamic stopping (drag to mass ratio) of the stabilizer is not greater than the aerodynamic stopping of the satellite, i.e., the satellite acts as a parachute of sorts relative to the stabilizer.

The above conditions are sufficient. If the satellite—stabilizer system is gravitationally stable and an elastic coupling is provided, weaker conditions will suffice.

In a circular orbit, atmospheric drag forces increase the frequency of natural oscillations of the satellite—stabilizer system. Another atmospheric effect influencing the oscillations of the system is connected with the entrainment of the atmosphere by the Earth's diurnal rotation and depends on the obliquity and the altitude of the orbit and the position of the centers of pressure of the satellite and the stabilizer.

Calculations show that the maximum amplitude of the forced oscillations resulting from the rotation of the atmosphere does not exceed a few degrees, falling off with altitude. The frequency of these oscillations coincides with the orbital frequency of the system's mass center. The rotation of the atmosphere does not influence the oscillations in the orbital plane: it is felt only for oscillations at right angles to the plane of the orbit.

The atmospheric effects for a satellite—stabilizer system moving in an elliptical orbit are more complex, since the density of the atmosphere varies with altitude.

If the aerodynamic forces on the satellite and the stabilizer are known with fair accuracy, the oscillations attributable to atmospheric effects can be computed and taken into consideration.

It is noteworthy that in principle, the influence of the atmospheric drag on the oscillations can be eliminated. To this end, it suffices to make the satellite and the stabilizer aerodynamically neutral, ensuring equal aerodynamic stopping for both. If these conditions are satisfied, the drag forces affect the translational motion only.

If a satellite is to be stabilized in a certain attitude, i.e., in a certain state of stable equilibrium, the initial conditions after its separation from the last stage of the launching rocket must comply with some restrictions. The angles and the angular velocities of the satellite must be such that any transition between different stable states of equilibrium is ruled out in the process of oscillation damping. If such transitions are possible, special active despun systems should be actuated in order to reduce the initial amplitudes to a manageable level and to permit the gravity stabilization system to take over. The initial spin of the system may also be killed by increasing its moment of inertia, i.e., unfolding the booms which remained hidden during the launching.

The proposed system for gravity attitude stabilization will function for a very long time without consuming any power. The stabilization precision is determined by the precision with which the satellite—stabilizer system has been assembled and is in principle unlimited. The weight of a stabilizer ensuring an optimal transient process, with booms equal to twice the largest linear dimension of the satellite, does not exceed a few percent of the satellite weight.

A detailed analysis of this attitude stabilization system is given in V. A. Sarychev's works (see /64, 65/, etc.).

## Chapter 3

### ADDITIONAL FACTORS INFLUENCING STABILIZATION AND LIBRATION OF A SATELLITE

#### § 1. THE INFLUENCE OF AERODYNAMIC TORQUES ON STABILIZATION AND LIBRATION OF A SATELLITE

**1. Conditions of stability of relative equilibrium.** Plane oscillations. Let us consider the influence of restoring aerodynamic torques (the first term in (1.3.14)) on the oscillation of a satellite about its center of mass. In the present section, we shall analyze the combined influence of aerodynamic and gravity torques, assuming the axis  $x'$  as the axis of symmetry of the satellite's surface; then  $\mathbf{k}$  in expression (1.3.11) is a unit vector in the direction of  $x'$ .

In the orbital system  $xyz$ , the components of the velocity vector of the satellite's mass center relative to the atmosphere, which rotates with an angular velocity  $\omega$  with the Earth, are written in the form

$$\left. \begin{aligned} V_x &= V_0(1 + e \cos \nu) - \omega R \cos i, \\ V_y &= \omega R \sin i \cos u, \quad V_z = V_0 e \sin \nu, \\ V_0 &= \sqrt{\frac{\mu}{P}}, \quad R = \frac{P}{1 + e \cos \nu}. \end{aligned} \right\} \quad (3.1.1)$$

The torque components (1.3.11) (without the dissipative terms) along the satellite's axes  $x'y'z'$  expressed in terms of the direction cosines of the axes  $x'y'z'$  and  $xyz$  (see § 1 of Chapter 1) have the form

$$\left. \begin{aligned} M_{x'} &= \frac{1}{2} \rho c (\delta_V) V [V_x \alpha'' + V_y \beta'' + V_z \gamma''], \\ M_{y'} &= -\frac{1}{2} \rho c (\delta_V) V [V_x \alpha' + V_y \beta' + V_z \gamma'], \\ M_{z'} &= 0, \quad V = \sqrt{V_x^2 + V_y^2 + V_z^2}, \\ \cos \delta_V &= \frac{1}{V} (V_x \alpha + V_y \beta + V_z \gamma). \end{aligned} \right\} \quad (3.1.2)$$

In a resistive medium,  $P$  and  $e$  vary in time. The variation of the parameters  $P, e$ , however, is very slow, and for the duration of one or several revolutions we may take  $P=\text{const}$ ,  $e=\text{const}$ . Since the velocity of rotation of the atmosphere  $R\omega \sim 0.5 \text{ km/sec}$  is roughly one tenth of the orbital velocity  $V_0 \sim 8 \text{ km/sec}$ , we may assume  $\omega \sim 0$  on first approximation. Also let  $e = 0$  (a circular orbit). Under these assumptions,  $\cos \delta_V = \alpha$ . The total aerodynamic and gravity torque then has the following components along

the axes  $x'y'z'$ :

$$\left. \begin{aligned} M_x^{\Sigma} &= 3\omega^2(C-B)\gamma'\gamma'', \\ M_y^{\Sigma} &= 3\omega^2(A-C)\gamma''\gamma + \frac{1}{2}\rho V^2 \bar{c}(a) \alpha'', \\ M_z^{\Sigma} &= 3\omega^2(B-A)\gamma\gamma' - \frac{1}{2}\rho V^2 \bar{c}(a) \alpha', \\ \alpha &= \text{const}, \quad \rho = \text{const}, \quad V = \text{const}. \end{aligned} \right\} \quad (3.1.3)$$

A Jacobi integral exists in this case:

$$\begin{aligned} \frac{1}{2}(A\bar{p}^2 + B\bar{q}^2 + C\bar{r}^2) + \frac{1}{2}\omega^2[(B-A)\beta^2 + (B-C)\beta''^2] + \\ + \frac{3}{2}\omega^2[(A-C)\gamma^2 + (B-C)\gamma'^2] + U(a) = h_0, \end{aligned} \quad (3.1.4)$$

$$U(a) = \frac{1}{2}\rho V^2 \int \bar{c}(a) da. \quad (3.1.5)$$

Here  $\bar{p}, \bar{q}, \bar{r}$  are the components (along the axes  $x'y'z'$ ) of the relative angular velocity of the satellite's rotation. Since

$$U(a) = U(1) - \frac{1}{2} \frac{\partial U}{\partial a} \Big|_{a=1} (\alpha'^2 + \alpha''^2 + \zeta^2) + \dots,$$

where  $\zeta = 1 - \alpha$ , the function  $h_0 - U(1)$  vanishes only in a state of relative equilibrium

$$\bar{p} = \bar{q} = \bar{r} = \beta = \beta'' = \gamma = \gamma' = \alpha' = \alpha'' = \zeta = 0;$$

it is positive if the condition (2.1.12) of gravitational stability is satisfied and if

$$\frac{\partial U}{\partial a} \Big|_{a=1} < 0. \quad (3.1.6)$$

Condition (3.1.6) yields

$$\bar{c}(1) < 0. \quad (3.1.7)$$

In other words, a sufficient condition for the stability of relative equilibrium of a satellite is the following: the satellite should be gravitationally stable and the aerodynamic torque coefficient in unperturbed motion should be negative. We may take  $\bar{c} = x'_0 S c_x$ , where  $x'_0$  the coordinate of the center of pressure;  $S$  a characteristic area;  $c_x$  the drag coefficient. Condition (3.1.7) is then equivalent to the condition  $x'_0 < 0$ , i.e., for a relative equilibrium to be stable it is sufficient that the center of pressure should lie behind the center of mass, relative to the oncoming stream.

Note that this state of equilibrium is not the only possible stable position. Setting the total aerodynamic and gravity torque equal to zero, we obtain new conditions of equilibrium:

$$\alpha' = 0, \gamma' = 0, 3\omega^2(A-C)\gamma''\gamma + \frac{1}{2}\rho V^2 \bar{c}(a) \alpha'' = 0.$$

There exists a  $\gamma'' = \text{const} \neq 1$ , and corresponding values of  $\gamma, \alpha, \alpha''$ , which satisfy this condition; new states of equilibrium can thus be found. In this case, one of the satellite's axes points along the normal to the orbital plane,

the other two axes being oriented at an angle to the radius-vector and the tangent of the orbit.

Figure 25 shows a satellite for which the "ordinary" stable state of relative equilibrium does not obtain. In Figure 25a, the satellite is gravitationally stable, but aerodynamically unstable. In Figure 25c, on the other hand, it is aerodynamically stable, but gravitationally unstable. The stable state in this case corresponds to a certain "oblique" orientation (Figure 25b), intermediate to the orientations illustrated in Figure 25a and Figure 25c.

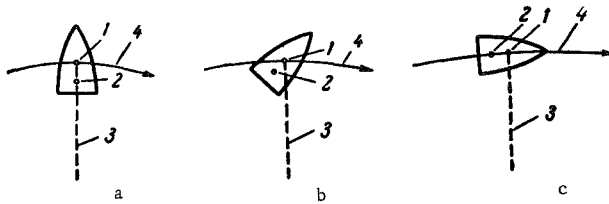


FIGURE 25. The interaction of aerodynamic and gravity torques:  
1) center of mass, 2) center of pressure, 3) to the Earth's center,  
4) flight trajectory.

Let  $\Theta$  be the angle between the axis  $z'$  of the satellite and the radius-vector. The equation of plane oscillations is then written as

$$\ddot{\Theta} + n^2 \sin \Theta \cos \Theta - b_V \sin \Theta = 0, \quad (3.1.8)$$

$$n^2 = 3 \frac{A - C}{B}, \quad b_V = \frac{1}{2} \rho \frac{V^2}{\omega^3 B} \bar{c} (\cos \Theta). \quad (3.1.9)$$

( $\tau = \omega t$  being the independent variable). The following states of relative equilibrium  $\Theta = \Theta^*$  obtain from this equation:

i)  $\Theta^* = 0, \pi$ : these are the conventional equilibria, which also exist in the case of gravity torques, without any aerodynamic factors.

ii)  $\cos \Theta^* = \frac{b_V}{n^2}$ : these are new states of relative equilibrium which, in the absence of aerodynamic torques ( $b_V = 0$ ), reduce to  $\cos \Theta^* = 0, \Theta^* = \pm \pi/2$ , i.e., the second pair of gravitational equilibria. This new relative equilibrium obtains when  $\left| \frac{b_V}{n^2} \right| \equiv |\xi_V| < 1$ . Note that  $|b_V|$  is the magnitude of the aerodynamic torque vector, while  $|n^2|$  is the magnitude of the gravity torque, so that  $\xi_V = \frac{b_V}{n^2}$  is the magnitude of the aerodynamic torque relative to the gravity torque. Let us estimate the numerical value of this parameter for various altitudes  $h$  above the Earth's surface.

If  $\bar{c} = \text{const}$ , we may take  $\bar{c} = x'_0 c_x' S$ . Then, seeing that  $V = \omega R$ , we have from

$$(3.1.9) \quad \xi_V = k \rho (R_E + h)^2, \quad k = \frac{c_x' S x'_0}{6(A - C)}. \quad \text{Here } R_E \text{ is the radius of the Earth, } h \text{ the height of the orbit above the Earth's surface, } \rho \text{ the density of the atmosphere.}$$

Table 3 gives the variation of  $\xi_V$  with altitude for a satellite having the parameters  $c_x = 2$ ;  $x'_0 = 0.5 \text{ m}$ ,  $S = 3 \text{ m}^2$ ,  $A - C = 30 \text{ kg} \cdot \text{m} \cdot \text{sec}^2$ ,  $k = 1/18 \text{ m}^2 \cdot \text{kg}^{-1} \cdot \text{sec}^{-2} \approx 0.05 \text{ m}^2 \cdot \text{kg}^{-1} \cdot \text{sec}^{-2}$ . In the table, for each  $h$ , the

density  $\rho$  is given in technical ( $\text{kg} \cdot \text{sec}^2/\text{m}^4$ ) and in physical ( $\text{g}/\text{cm}^3$ ) units; when the absolute value of  $\xi_V$  is less than unity, the table also lists the equilibria  $\Theta^*$  corresponding to these  $\xi_V$ .

TABLE 3

$h, \text{ km}$	$\rho, \text{ kg} \cdot \text{sec}^2/\text{m}^4$	$\rho, \text{ g}/\text{cm}^3$	$\xi_V$	$\Theta^*$
200	$4.52 \cdot 10^{-11}$	$4.43 \cdot 10^{-13}$	97.5	
225	$2.18 \cdot 10^{-11}$	$2.12 \cdot 10^{-13}$	47.4	
250	$1.12 \cdot 10^{-11}$	$1.10 \cdot 10^{-13}$	24.5	
300	$3.61 \cdot 10^{-12}$	$3.53 \cdot 10^{-14}$	8.0	
400	$6.75 \cdot 10^{-13}$	$6.60 \cdot 10^{-15}$	1.55	
500	$2.245 \cdot 10^{-13}$	$2.21 \cdot 10^{-15}$	0.530	58°
600	$6.95 \cdot 10^{-14}$	$6.80 \cdot 10^{-16}$	0.169	80°
720	$1.02 \cdot 10^{-14}$	$1.00 \cdot 10^{-16}$	0.026	88°.5
800	$3.74 \cdot 10^{-15}$	$3.67 \cdot 10^{-17}$	0.01	89°.3
900	$1.99 \cdot 10^{-15}$	$1.95 \cdot 10^{-17}$	0.005	89°.5

Note that in the case of zero aerodynamic torque the relative equilibrium is  $\Theta^* = 90^\circ$ , while in the gravity-free case  $\Theta^* = 0$ .

The height dependence of density for altitudes above 700 km is borrowed from Mitra's book /56/, while the data up to 600 km have been obtained with artificial satellites /57/. It follows from the table that at heights of 200–250 km the aerodynamic torques prevail; for  $h = 300$ –500 km, the aerodynamic and the gravity torques are comparable; at 600 km it is the gravity torques which predominate, while at heights above 700 km the aerodynamic torques are negligible.

Let us write the Jacobi integral in the plane case, taking for simplicity  $\bar{c} = \text{const}$ :

$$\dot{\Theta}^2 = h - n^2 \sin^2 \Theta - 2b_V \cos \Theta. \quad (3.1.10)$$

Here  $b_V = \text{const}$ .

The motion can be conveniently analyzed in the phase plane  $(\Theta, \dot{\Theta})$ . Let us consider the different cases possible.

i)  $n^2 > 0$ ,  $b_V < 0$ . Let  $n^2 > |b_V|$ , i.e., the aerodynamic torque is less than the gravity torque. In this case, the satellite is aerodynamically and gravitationally stable for  $\Theta^* = 0$  (Figure 26).  $\Theta^* = \pi$  is gravitationally stable, but aerodynamically unstable, so that near this point the region of stability narrows down. The point  $P$  in Figure 26a is a state of unstable equilibrium;

here  $\cos \Theta^* = \frac{b_V}{n^2}$ . The periods of oscillation near  $\Theta = 0$  are larger than with

gravity torques alone. The amplitude of the oscillations may even be greater than  $\pi$ . The larger the gravity torques in comparison with the aerodynamic torques, the broader the region near the point  $\Theta = \pi$ . As the aerodynamic torques increase, the region near the point  $\pi$  narrows down.

In the limit, for  $\frac{|b_V|}{n^2} \rightarrow 1$ , the region near  $\Theta = \pi$  vanishes. In the case  $|b_V| \gg n^2$ , the phase paths have the form shown in Figure 26b; the oscillations are distinctly "aerodynamic".

If  $n^2 > 0$ ,  $b_V > 0$ , we have a physically similar case, but the center of pressure is symmetrically displaced to its image point relative to the center of mass.

ii)  $n^2 < 0$ ,  $b_v < 0$ . For  $\Theta = 0$  the satellite is gravitationally unstable, but aerodynamically stable. In this case (see Figure 25c), the phase paths have the form shown in Figure 26c. The new state of equilibrium  $\cos \Theta^* = \frac{b_v}{n^2}$  is stable. The states  $\Theta = 0, \pi$  are unstable. For  $b_v \rightarrow 0$ , the stable equilibria approach  $\pi/2$  and  $3\pi/2$  (the case of gravity oscillations about  $\Theta = \pi/2$ ,  $\Theta = 3\pi/2$ ). If  $b_v$  increases, then for  $b_v = n^2$ , the pattern of Figure 26b is recovered.

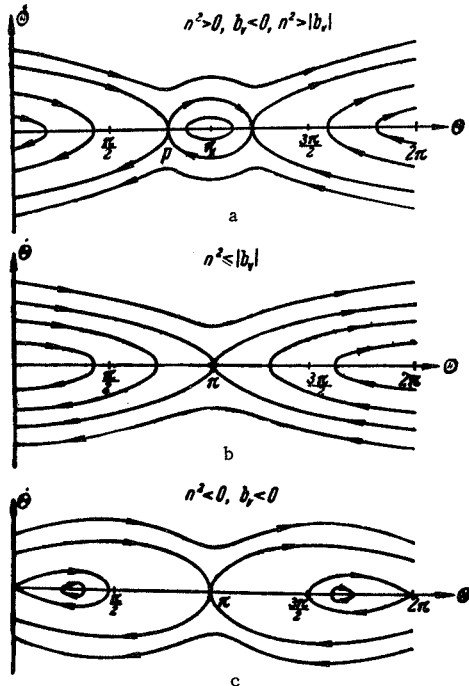


FIGURE 26. Interaction of aerodynamic and gravity torques:  
the phase plane.

We see that if the aerodynamic torques are less than the gravity torques (in absolute values), gravity oscillations are distorted by aerodynamic oscillations. If the aerodynamic torques are larger, the oscillations are essentially aerodynamic. In other words, the qualitative influence of the aerodynamic torques is much more noticeable than that of the gravity torques. This, as we shall show in Chapter 8, also holds true in the case of fast space motion about the mass center.

The case  $n^2 < 0$ ,  $b_v > 0$  is entirely analogous, the center of pressure being symmetrically displaced to its image point relative to the center of mass.

From (3.1.10) it also follows that if  $\dot{\Theta}_0^2 < n^2 \cos^2 \Theta_0 + \frac{b_v^2}{n^2} - 2b_v \cos \Theta_0$  in case (i) and  $\dot{\Theta}_0^2 + n^2 \sin^2 \Theta_0 + 2b_v \cos \Theta_0 < 2b_v < 0$  in case (ii), the motion is oscillatory.

**2. Small space oscillations due to aerodynamic and gravity torques.**  
 It is clear from the foregoing that the parameters of the satellite and the initial conditions can be chosen so as to achieve one of the stable equilibria  $\Theta = \Theta^*$ , where  $\Theta^* = 0, \pi$ , or  $\cos \Theta^* = \frac{b^2}{n^2}$ . Let us now consider small oscillations about the principal stable equilibrium  $\Theta = 0$ . The equations of small oscillations in an elliptical orbit are obtained by linearizing the torques (3.1.2) and adding them to equations (2.8.2), while simultaneously changing over from the time  $t$  to the true anomaly  $v$  as the independent variable and substituting new dependent variables from (2.9.1). We then obtain a system of inhomogeneous linear equations with  $v$ -periodic coefficients:

$$\left. \begin{aligned} \frac{d^2\tilde{\gamma}}{dv^2} + \frac{e \cos v + \bar{a}_1 (4 + e \cos v)}{1 + e \cos v} \tilde{\gamma} - \bar{a}_2 \frac{d\tilde{\alpha}}{dv} + \\ + \bar{a}_3 \frac{e \sin v}{1 + e \cos v} \tilde{\alpha} = 0, \\ \frac{d^2z}{dv^2} + \left\{ \frac{n^2 + e \cos v}{1 + e \cos v} + \frac{1}{2} \rho (\cos v) \frac{|\bar{c}_0| V}{\zeta B} \frac{V_x}{1 + e \cos v} \right\} z - \\ - \frac{1}{2} \rho (\cos v) \frac{|\bar{c}_0| V}{\zeta B} \cdot \frac{V_y}{1 + e \cos v} \tilde{\gamma} = \\ = e \sin v \left\{ 2 - \frac{1}{2} \rho (\cos v) \frac{|\bar{c}_0| V V_0}{\zeta B} \right\}, \\ \frac{d^2\tilde{\alpha}}{dv^2} + \left\{ \frac{e \cos v + \bar{b}_1 (1 + e \cos v)}{1 + e \cos v} + \right. \\ \left. + \frac{1}{2} \rho (\cos v) \frac{|\bar{c}_0|}{\zeta C} \frac{V V_x}{1 + e \cos v} \right\} \tilde{\alpha} + \\ + \bar{b}_2 \frac{d\tilde{\gamma}}{dv} - \left\{ \bar{b}_3 - \frac{1}{2} \rho (\cos v) \frac{|\bar{c}_0|}{\zeta C} V V_0 \right\} \frac{e \sin v}{1 + e \cos v} \tilde{\gamma} = \\ = - \frac{1}{2} \rho (\cos v) \frac{|\bar{c}_0|}{\zeta C} V \frac{w R \sin t}{1 + e \cos v} \cos(\omega_n + v). \end{aligned} \right\} \quad (3.1.11)$$

Here  $\zeta = \frac{\mu}{R^3} = \frac{\mu (1 + e \cos v)^3}{P^3}$ ,  $n^2 = 3 \frac{A - C}{B}$ , the constants  $\bar{a}_{1,2,3}$ ,  $\bar{b}_{1,2,3}$  are defined by formula (2.9.2),  $V_x(v)$ ,  $V_y(v)$ ,  $V_z(v)$ ,  $V_0$  by formulas (3.1.1), (3.1.2) (these formulas have been partly used in writing equations (3.1.11)). We may take  $\rho = \rho_\pi \exp(R - R_\pi)$ , where the subscript  $\pi$  marks the corresponding values in perigee. For small aerodynamically stable oscillations  $\bar{c}_0 = \text{const} < 0$ .

Equations (3.1.11) describe small oscillations in the orbital system of axes for a satellite moving in an elliptical orbit and acted upon by gravity and aerodynamic torques (with allowance for the rotation of the atmosphere).

In these equations,  $\tilde{\gamma}$ ,  $z$ ,  $\tilde{\alpha}$  are proportional, according to (2.9.1), to the yaw, pitch, and roll relative to the axis  $z'$ , which is not the axis of geometrical symmetry of the satellite (this being the axis  $x'$ ). The yaw for the axis  $z'$  is equivalent in a certain sense to the roll about the axis  $x'$ ; therefore, the surface of the satellite being symmetric about the axis  $x'$ , the first of the equations above contains no aerodynamic terms.

The homogeneous parts of the first and third equations in (3.1.11) are in principle equivalent to equations without aerodynamic terms (only the periodic coefficients are somewhat more complex). The right-hand side of the third equation in (3.1.11) contains a term attributable to the rotation of the atmosphere: this term is responsible for forced oscillations of the satellite. As regards the second equation in (3.1.11), the forced oscillations in the pitch angle produced by aerodynamic factors are qualitatively equivalent, at least to the first order in  $e$ , to the forced (eccentricity)

oscillations analyzed in the previous chapter. When the forced aerodynamic oscillations are considered to second and higher approximations (to powers of  $e^2$  and higher), the eccentricity  $e$  must be treated as varying with the atmospheric density  $\rho$  and the velocity  $V$ . Note that this equation contains a term  $V_y \dot{\gamma}$  attributable to the rotation of the atmosphere; the pitch is thus related with the yaw. This relation, however, is extremely weak, since both  $V_y$  (the angular velocity of the atmosphere) and  $\dot{\gamma}$  (oscillations in attitude) are small. This term produces additional forced oscillations, but their amplitude is of a relatively high order of smallness in comparison with the amplitude of the principal oscillations. The term  $V_y \dot{\gamma}$  is therefore ignored.

These equations can be solved and investigated by the same techniques that we have used in the case of pure gravity torques.

For example, let us neglect the rotation of the atmosphere; the orbit is elliptic. Forced oscillations in the pitch angle, as it follows from the second equation in (3.1.11), are described on first approximation by the expression

$$a''_e = e \sin v \frac{\frac{2\omega^2 - \frac{1}{2} \rho_\pi |\bar{c}_0| \frac{V_0^2}{B}}{3\omega^2 \frac{A-C}{B} + \frac{1}{2} \rho_\pi \frac{|\bar{c}_0| V_0^2}{B} - \omega^2}}{(3.1.12)}$$

(approximately  $\xi \approx \omega^2 = \text{const}$ ,  $V_0^2 \approx \text{const}$ ,  $\rho \approx \rho_\pi$ ). We see that the aerodynamic factors somewhat modify the amplitude and the resonant values of the parameters. It is remarkable that aerodynamic and gravity forced

oscillations may mutually cancel: for  $2\omega^2 \approx \frac{1}{2} \rho_\pi |\bar{c}_0| \frac{V_0^2}{B}$  no forced oscillations are observed to first approximation.

If we do not ignore the rotation of the atmosphere, and assume a spherical orbit ( $\omega = \text{const}$ ), equations (3.1.11) can be written as

$$\left. \begin{aligned} \frac{d^2\gamma'}{dt^2} + 4\bar{a}_1 \omega^2 \gamma' - \bar{a}_2 \omega \frac{da'}{dt} &= 0, \\ \frac{d^2a'}{dt^2} + (\bar{b}_1 \omega^2 + \beta_w) a' + \bar{b}_2 \omega \frac{d\gamma'}{dt} &= k_1^w \cos u, \\ \frac{d^2a''}{dt^2} + n_1 \omega^2 a'' &= k^w \gamma' \cos u, \\ \beta_w &= -\frac{1}{2} \rho \frac{\bar{c}_0}{C} V_0 (V_0 - wR \cos i), \\ k_1^w &= -\frac{1}{2} \rho \frac{\bar{c}_0}{C} V_0 \omega R \sin i, \quad u = \omega_\pi + \omega t, \\ n_1 &= n^2 - \frac{1}{2} \rho \frac{\bar{c}_0 V_0}{B \omega^2} (V_0 - wR \cos i), \\ k^w &= -\frac{1}{2} \rho \frac{\bar{c}_0}{B} V_0 wR \sin i. \end{aligned} \right\} \quad (3.1.13)$$

Here  $\omega_\pi$  is the argument of perigee.

The equations of transverse oscillations are analogous to the equations with zero aerodynamic torques, and the rotation of the atmosphere only introduces an additional term with  $k^w$  which produces forced oscillations. The pitch is moreover related with the yaw (the third equation).

Forced transverse oscillations have the form

$$a'_f = M \cos u, \quad \gamma'_f = N \sin u.$$

Then in the right-hand side of the equation for  $\alpha''$  we have  $\frac{1}{2}kN \sin 2u$ , and the amplitude of the forced oscillations in  $\alpha''$  is proportional to  $kN \sim \omega^2$ , i.e., it is a quantity of second order of smallness. The forced oscillations in  $\alpha''$  may therefore be ignored.

To find  $M$  and  $N$ , we proceed in an ordinary way to derive a system of algebraic equations. The determinant  $D$  of this system and the expressions for  $M$  and  $N$  are

$$D = \left\{ 1 - \left[ 4\bar{a}_1 + \bar{b}_1 + \frac{\beta_w}{\omega^2} + \bar{a}_2 \bar{b}_2 \right] + 4\bar{a}_1 \left( \bar{b}_1 + \frac{\beta_w}{\omega^2} \right) \right\},$$

$$M = \frac{k_1^w (4\bar{a}_1 - 1)}{\omega^2 D}, \quad N = -\frac{k_1^w \bar{a}_2}{\omega^2 D}.$$

If  $D \neq 0$ , the amplitudes of forced oscillations are small (of the order of  $k_1^w / \omega^2$ ). The cases with  $D$  close to zero are the resonances. For a satellite with parameters close to the parameters of Sputnik III, we have the following estimate for the amplitudes of these forced oscillations:

$N \approx 0.3^\circ$ ,  $M \sim 2.5^\circ$ . The equation for the roll  $\alpha'$  (i.e., for the yaw relative to the axis of symmetry of the satellite) contains an independent "driving force", and the roll amplitude  $M$  is therefore much greater than the amplitude  $N$  of the yaw  $\gamma'$  (i.e., of the roll relative to the axis  $x'$ ), which is influenced by the "driving force" only indirectly, via pitch.

Since the aerodynamic torques stabilize the axis  $x'$  of geometrical symmetry of the satellite along the oncoming stream, and in low orbits (up to  $\sim 400$  km) they may exceed by one or two orders of magnitude the gravity torques, it is advisable in this case to apply the aerodynamic torques for purposes of passive attitude stabilization. The most natural and expedient system of passive attitude stabilization should obviously combine gravity and aerodynamic mechanisms, since our analysis shows that satellites can be designed where the two effects complement and amplify each other (see /60, 65/, and also § 10 of Chapter 2).

A more detailed analysis of aerodynamic factors and their influence on the oscillations of a satellite will be found in /60, 67, 91/.

## § 2. THE INFLUENCE OF THE EARTH'S FLATTENING ON THE LIBRATION OF A SATELLITE IN A FIELD OF GRAVITY

**1. Equations of motion and their analysis.** The flattening of the Earth is responsible for slow rotation of the orbital plane /61/. If considered in conjunction with the stabilizing (relative to the orbit) effect of the gravity torques, the rotation of the orbital plane is seen to produce forced oscillations of the satellite relative to this plane. These oscillations, however, are very small.

The problem of the Earth's flattening and its influence on the librations of a satellite has been considered in /63/. Applying the direction cosines (§ 1 of Chapter 1) between the orbital and the absolute systems of axes and Poisson's kinematic relations for these direction cosines, and then writing, in osculating elements, the equation of motion of a satellite's mass center in the field of an oblate spheroid /61/, we can derive expressions for the components  $p_1, q_1, r_1$  of the absolute angular velocity of

rotation of the orbital system along the orbital axes  $x, y, z$ :

$$\left. \begin{aligned} p_1 &= a_2 \frac{d\delta}{dt} - \sin u \frac{di}{dt} = 0, \\ q_1 &= b_2 \frac{d\delta}{du} + \frac{du}{dt} = \frac{\sqrt{\mu P}}{R^2}, \\ r_1 &= c_2 \frac{d\delta}{dt} + \cos u \frac{di}{dt} = -\bar{\epsilon} \sqrt{\frac{\mu}{P}} \cdot \frac{R_e^2}{R^3} \sin 2i \sin u. \end{aligned} \right\} \quad (3.2.1)$$

The attitude of a satellite relative to the orbital system of axes can be defined in terms of three independent angles  $\Psi, \Theta, \Phi$  (see § 1, Chapter 1). The position of the moving system  $Ox'y'z'$  relative to the orbital system is defined by the direction cosines (1.1.3), and the components of the absolute angular velocity along the axes of  $Ox'y'z'$  are

$$\left. \begin{aligned} p &= \dot{\Psi} a + \dot{\Theta} \sin \Phi + r_1 \gamma + p_1 \alpha + q_1 \beta, \\ q &= \dot{\Psi} a' + \dot{\Theta} \cos \Phi + r_1 \gamma' + p_1 \alpha' + q_1 \beta', \\ r &= \dot{\Psi} a'' + \dot{\Phi} + p_1 \alpha'' + q_1 \beta'' + r_1 \gamma''. \end{aligned} \right\} \quad (3.2.2)$$

The rotation of the satellite can be described by Euler's equations (2.1.1), substituting the gravity torque components  $M_x, M_y, M_z$  (1.2.10) in their right-hand sides. Euler's equations, together with (1.2.10), (3.2.1), (3.2.2), (1.1.1)–(1.1.3), then give a closed system of equations for the rotation of a satellite in the Earth's gravitational field.

For the particular case of a satellite's mass center moving in an equatorial orbit ( $i = 0$ ), the equations of rotation are simplified, taking the form

$$\left. \begin{aligned} A \frac{dp}{dt} + (C - B) qr &= \\ &= (C - B) \frac{\mu}{R^3} \left[ \left( 3 + 5\bar{\epsilon} \frac{R_e^2}{R^2} \right) \gamma' \gamma'' - 2\bar{\epsilon} \frac{R_e^2}{R^2} \beta' \beta'' \right], \\ B \frac{dq}{dt} + (A - C) rp &= \\ &= (A - C) \frac{\mu}{R^3} \left[ \left( 3 + 5\bar{\epsilon} \frac{R_e^2}{R^2} \right) \gamma'' \gamma - 2\bar{\epsilon} \frac{R_e^2}{R^2} \beta'' \beta \right], \\ C \frac{dr}{dt} + (B - A) pq &= \\ &= (B - A) \frac{\mu}{R^3} \left[ \left( 3 + 5\bar{\epsilon} \frac{R_e^2}{R^2} \right) \gamma \gamma' - 2\bar{\epsilon} \frac{R_e^2}{R^2} \beta \beta' \right], \\ r &= \dot{\Psi} a'' + \dot{\Phi} + \frac{\sqrt{\mu P}}{R^2} \beta'', \\ p &= \dot{\Psi} a + \dot{\Theta} \sin \Phi + \frac{\sqrt{\mu P}}{R^2} \beta, \\ q &= \dot{\Psi} a' + \dot{\Theta} \cos \Phi + \frac{\sqrt{\mu P}}{R^2} \beta'. \end{aligned} \right\} \quad (3.2.3)$$

For a circular equatorial orbit, equations (3.2.3) have the Jacobi integral

$$\begin{aligned} \frac{1}{2} \frac{\mu}{R^3} \left( 1 + 3\bar{\epsilon} \frac{R_e^2}{R^2} \right) [(B - C) \beta''^2 + (B - A) \beta^2] + \\ + \frac{1}{2} \frac{\mu}{R^3} \left( 3 + 5\bar{\epsilon} \frac{R_e^2}{R^2} \right) [(A - C) \gamma^2 + (B - C) \gamma'^2] + \\ + \frac{1}{2} [C(\dot{\Psi} a'' + \dot{\Phi})^2 + A(\dot{\Psi} a + \dot{\Theta} \sin \Phi)^2 + \\ + B(\dot{\Psi} a' + \dot{\Theta} \cos \Phi)^2] = h. \end{aligned} \quad (3.2.4)$$

From the integral (3.2.4) it follows that the relative equilibrium of a satellite in a circular orbit defined by the solution  $\Psi=\Theta=\Phi=\dot{\Psi}=\dot{\Theta}=\dot{\Phi}=0$  is stable if  $B>A>C$ . These inequalities are independent of  $e$  and do not coincide with the previously derived sufficient conditions of stability (2.1.12), which have been obtained for the motion in a Newtonian central field.

Applying the integral (3.2.4) inside the region of stability (2.1.12), we find the following estimates for the direction cosines:

$$\left. \begin{aligned} \gamma^2 &\leq \frac{2h}{\frac{\mu}{R^3} \left( 3 + 5\bar{\varepsilon} \frac{R_e^2}{R^2} \right) (A - C)}, \\ \gamma'^2 &\leq \frac{2h}{\frac{\mu}{R^3} \left( 3 + 5\bar{\varepsilon} \frac{R_e^2}{R^2} \right) (B - C)}, \\ \beta''^2 &\leq \frac{2h}{\frac{\mu}{R^3} \left( 1 + 3\bar{\varepsilon} \frac{R_e^2}{R^2} \right) (B - C)}, \\ \beta^2 &\leq \frac{2h}{\frac{\mu}{R^3} \left( 1 + 3\bar{\varepsilon} \frac{R_e^2}{R^2} \right) (B - A)}. \end{aligned} \right\} \quad (3.2.5)$$

For the Earth  $\bar{\varepsilon}=0.0016$ , and the effect of flattening on these estimates does not exceed 0.5%.

Let us consider small oscillations of a satellite relative to the orbital system of axes for the case of an arbitrary orientation of the orbit in space. The equations of these oscillations are derived from the exact equations by linearizing the trigonometric functions:

$$\left. \begin{aligned} A\ddot{\Psi} + (B - C)\left(q_1^2 + 3\frac{\mu}{R^3}\right)\Psi + (C + A - B)q_1\dot{\Phi} + \\ + A\dot{q}_1\Phi + f_2 = (B - C)\left(r_1q_1 - 8\frac{\mu}{R^3}\frac{R_e^2}{R^2}\bar{\varepsilon}c_2b_2\right), \\ B\ddot{\Theta} + 3(A - C)\frac{\mu}{R^3}\Theta + Bq_1 + f_3 = \\ = 8(A - C)\frac{\mu}{R^3}\frac{R_e^2}{R^2}\bar{\varepsilon}c_2a_2, \\ C\ddot{\Phi} + (B - A)q_1^2\Phi - (C + A - B)q_1\dot{\Psi} - Cq_1\Psi + f_1 = \\ = -Cr_1 - 2(B - A)\frac{\mu}{R^3}\frac{R_e^2}{R^2}\bar{\varepsilon}a_2b_2, \\ f_1 = -(B - A)\left\{r_1q_1\Theta + \frac{\mu}{R^3}\frac{R_e^2}{R^2}\bar{\varepsilon}[8c_2a_2\Psi - \right. \\ \left. - 8c_2b_2\Theta - 2(b_2^2 - a_2^2)\Phi]\right\}, \\ f_2 = -A(\dot{r}_1\Theta + r_1\dot{\Theta}) + (B - C)\left\{-r_1^2\Psi - r_1\dot{\Theta} + \right. \\ \left. + \frac{\mu}{R^3}\frac{R_e^2}{R^2}\bar{\varepsilon}[(5 - 17c_2^2 + 2b_2^2)\Psi - 2a_2b_2\Theta - 8c_2a_2\Phi]\right\}, \\ f_3 = B(\dot{r}_1\Psi + r_1\dot{\Psi}) + (A - C)\left\{r_1(\dot{\Psi} - r_1\Theta + q_1\Phi) - \right. \\ \left. - \frac{\mu}{R^3}\frac{R_e^2}{R^2}\bar{\varepsilon}[2a_2b_2\Psi - (5 - 17c_2^2 + 2a_2^2)\Theta + 8c_2b_2\Phi]\right\}. \end{aligned} \right\} \quad (3.2.6)$$

We shall only investigate the forced solution of the set (3.2.6) inside the stability region (2.1.12) of the satellite's equilibrium attitude in a circular orbit; we shall seek this solution to first order in  $\bar{\varepsilon}$  and  $e$ . This approximate

solution is in fact a sum of the eccentricity oscillations (2.3.9) and the functions  $\Psi_{10}$ ,  $\Phi_{10}$ ,  $\Theta_{10}$  which constitute the forced solution of the following set of equations:

$$\left. \begin{aligned} C\ddot{\Phi}_{10} + (B - A)\omega^2\Phi_{10} - (C + A - B)\omega\Psi_{10} &= \\ &= -\bar{\varepsilon}(C + A - B)\omega^2 \frac{R_e^2}{R^2} \sin 2i \cos \omega t, \\ A\ddot{\Psi}_{10} + 4(B - C)\omega^2\Psi_{10} + (C + A - B)\omega\dot{\Phi}_{10} &= \\ &= -5\bar{\varepsilon}(B - C)\omega^2 \frac{R_e^2}{R^2} \sin 2i \sin \omega t, \\ B\ddot{\Theta}_{10} + 3(A - C)\omega^2\Theta_{10} &= \\ &= 4\bar{\varepsilon}(A - C)\omega^2 \frac{R_e^2}{R^2} \sin^2 i \sin 2\omega t; \\ \omega = \text{const}, \quad R = \text{const}. \end{aligned} \right\} \quad (3.2.7)$$

In calculating  $\Theta_{10}$ ,  $\Psi_{10}$ ,  $\Phi_{10}$ , we should set  $e = 0$  in the right-hand sides of (3.2.7). Having solved (3.2.7) for  $\Psi_{10}$ ,  $\Theta_{10}$ ,  $\Phi_{10}$ , we find the desired expressions for  $\Psi$ ,  $\Theta$ ,  $\Phi$ :

$$\left. \begin{aligned} \Psi &= -\bar{\varepsilon} \frac{4(B - C) + A}{3(B - C)} \frac{R_e^2}{R^2} \sin 2i \sin \omega t, \\ \Theta &= \bar{\varepsilon} \frac{4(A - C)}{3(A - C) - 4B} \frac{R_e^2}{R^2} \sin^2 i \sin 2\omega t + \\ &\quad + e \frac{2B}{3(A - C) - B} \sin \omega t, \\ \Phi &= \bar{\varepsilon} \frac{(B - C) + A}{3(B - C)} \frac{R_e^2}{R^2} \sin 2i \cos \omega t. \end{aligned} \right\} \quad (3.2.8)$$

Fairly far from the boundaries of the region of stability of the trivial circular orbit solution ( $B > A > C$ ), the influence of  $\bar{\varepsilon}$  on the forced solution is small.

Table 4 gives the amplitudes of the angles  $\Psi$ ,  $\Theta$ ,  $\Phi$  contributed by flattening, for various values of  $\frac{\varepsilon}{\delta} = \frac{C}{B}$ , with  $i = 65^\circ$  and  $\frac{1}{\delta} = \frac{A}{B} = 0.9$ . In calculations  $\frac{R_e}{R}$  was assumed equal to unity. We see from the table that the amplitude of the oscillations does not exceed  $12'$  in a wide range of  $\varepsilon/\delta$ .

TABLE 4

$\varepsilon/\delta$	0.8	0.7	0.6	0.5	0.4	0.3	0.2	0.1
$\Psi$ , min of arc	-11.9	-9.8	-8.8	-8.2	-7.7	-7.4	-7.2	-7.0
$\Theta$ , min of arc	-0.5	-1.1	-1.8	-2.6	-3.6	-4.9	-6.7	-9.0
$\Phi$ , min of arc	7.7	5.6	4.6	3.9	3.5	3.2	3.0	2.8

The first terms in (3.2.8) are inherently nonresonant inside the region  $B > A > C$ , since  $B > C$  and  $3(A - C) - 4B < -B$ .

The second term in the expression for the angle  $\Theta$ , attributable to the ellipticity of the orbit, has been investigated in the previous chapter.

For  $B > A > C$  the satellite rotates with a constant angular velocity about a fixed axis in the absolute space. Linearized equations (3.2.6) do not apply in this case.

**2. Plane oscillations of an equatorial satellite.** Let us consider the case of plane oscillations in a noncircular equatorial orbit, comparing these oscillations with the case of an elliptical orbit. The equations of motion of the center of mass in an equatorial orbit in the gravitational field of the flattened Earth are given in Appendix 2.

Substituting the variables  $t \rightarrow v$  and applying the areal integral (A2.2) and the equation of the trajectory (A2.5a) from Appendix 2, we obtain from the second equation in (3.2.3) for  $\beta' = 1$ ,  $\beta = \beta'' = 0$ ,  $\Phi = \pi/2$ ,  $\Psi = 0$  an equation of plane oscillations

$$\left. \begin{aligned} & [1 + \tilde{e}(\operatorname{cn}^2 u - \operatorname{sn}^2 u)] \frac{d^2 \bar{\delta}}{dv^2} - \\ & - 2\tilde{e} \cdot 4\tilde{a}_* \operatorname{cn} u \operatorname{sn} u \operatorname{dn} u \frac{d\bar{\delta}}{dv} + \bar{n}^2 \sin \bar{\delta} = \\ & = 4\tilde{e} \cdot 4\tilde{a}_* \operatorname{cn} u \operatorname{sn} u \operatorname{dn} u, \quad u = \tilde{a}_* v, \\ & \bar{n}^2 = 3 \frac{A - C}{B} \left\{ 1 + \frac{5}{3} \tilde{e} \frac{R_0^2}{P^2} [1 + \tilde{e}(\operatorname{cn}^2 u - \operatorname{sn}^2 u)]^2 \right\}, \\ & \bar{\delta} = 2\theta, \end{aligned} \right\} \quad (3.2.9)$$

which in the limit, for  $\tilde{e} \rightarrow 0$  ( $\tilde{a}_* \rightarrow \frac{1}{2}$ ,  $\operatorname{cn} u \rightarrow \cos \frac{v}{2}$ ,  $\operatorname{sn} u \rightarrow \sin \frac{v}{2}$ ,  $\operatorname{dn} u \rightarrow 1$ ), reduces to equation (2.3.5) of plane oscillations in an elliptical orbit. From (3.2.9) we see that for a circular equatorial orbit ( $e = 0$ ) the solution is the same as for a circular orbit around a spherical Earth.

Linearizing equation (3.2.9) for the case of small oscillations, we replace the angle  $\bar{\delta}$  with  $\Theta = \frac{\bar{\delta}}{2}$  and make the substitution

$$\Theta = \frac{z}{1 + \tilde{e}[\operatorname{cn}^2 u - \operatorname{sn}^2 u]}. \quad (3.2.10)$$

For  $z$  we then have a linear inhomogeneous Hill-type equation

$$\frac{d^2 z}{dv^2} + \frac{\bar{n}^2 - 4\tilde{e}\tilde{a}_*^2 [\operatorname{cn}^2 u \operatorname{sn}^2 u k^2 - (\operatorname{cn}^2 u - \operatorname{sn}^2 u) \operatorname{dn}^2 u]}{1 + \tilde{e}(\operatorname{cn}^2 u - \operatorname{sn}^2 u)} z = 2\tilde{e} \cdot 4\tilde{a}_* \operatorname{cn} u \operatorname{sn} u \operatorname{dn} u. \quad (3.2.11)$$

Here  $k$  is the modulus of the elliptical integral (see Appendix 2). In the limit, for  $\tilde{e} \rightarrow 0$  ( $k \rightarrow 0$ ,  $\tilde{a}_* \rightarrow 1/2$ , etc.), equation (3.2.11) reduces to equation (2.3.8) for small oscillations in an elliptical orbit. Let us now proceed with approximate calculation of forced (eccentricity) oscillations. We shall only seek the first term in the series-expansion in  $e$  of the particular solution of (3.2.11). Since the Earth's flattening  $\tilde{e}$  is small, the elliptical functions can be replaced with their approximate values:  $\operatorname{sn} u \approx \sin \frac{\pi u}{2K}$ ,  $\operatorname{cn} u \approx \cos \frac{\pi u}{2K}$ ,  $\operatorname{dn} u \approx 1$ , where  $K$  is the complete elliptical integral of the first kind. The eccentricity oscillations are then obtained from the equation

$$\frac{d^2 z}{dv^2} + n^2 z = 2\tilde{e} \cdot 2\tilde{a}_* \sin \frac{\pi \tilde{a}_* v}{K}, \quad n^2 = 3 \frac{A - C}{B}.$$

Now applying (3.2.10), we find for the eccentricity oscillations

$$\Theta_e = \frac{4\tilde{\epsilon}\tilde{a}_*}{n^2 - \left(\frac{\pi\tilde{a}_*}{K}\right)^2} \frac{\sin \frac{\pi\tilde{a}_* v}{K}}{1 + \tilde{\epsilon} \cos \frac{\pi\tilde{a}_* v}{K}}. \quad (3.2.12)$$

From the formulas of Appendix 2,  $\tilde{a}_*$  is representable as

$$\tilde{a}_* = \frac{1}{2} \sqrt{1 - \frac{2}{3} \tilde{\epsilon} \frac{R_e^2}{P^2} (3 - \tilde{\epsilon})}.$$

In the limit, for  $\tilde{\epsilon} \rightarrow 0$ ,  $\tilde{a}_* \rightarrow 1/2$ ,  $2K \rightarrow \pi$ , we obtain the first term of (2.3.9) for eccentricity oscillations in an elliptical orbit. We see that the Earth's flattening has somewhat modified the resonant value of the parameter  $n^2$ . Formula (3.2.12) is more exact for the case of an equatorial orbit than the second formula in (3.2.8).

### § 3. MAGNETIC ATTITUDE STABILIZATION. PASSIVE ATTITUDE STABILIZATION TO THE SUN

**1. Magnetic attitude stabilization.** If the satellite has an intrinsic magnetic moment  $I$  which is parallel to the vector  $H$  of the external magnetic field, then, as we see from (1.4.1), the torque on the satellite is zero. Hence it follows that, in principle, a satellite can be oriented and stabilized relative to the geomagnetic field in the same way as a magnetic needle. Seeing, however, that the vector  $H$  rotates nonuniformly along the satellite's orbit, no precise orientation can be expected in general, since the axis  $I$  will execute forced oscillations about the direction of  $H$ . Let us consider this effect in the simple case of plane oscillations in a polar ( $i = 90^\circ$ ) circular orbit (assuming the geomagnetic poles to coincide with the geographical poles of the Earth). Incidentally, note that according to (1.4.7),  $H = \text{const}$  for an equatorial orbit, and in this case precise magnetic attitude stabilization can be achieved.

For a polar orbit, we have the following equation of plane oscillations

$$B \frac{dq}{dt} = -[I_0 + a_H H \cos \varphi_H] H \sin \varphi_H, \quad a_H = \frac{\mu_0 - 1}{4\pi} v. \quad (3.3.1)$$

Here  $\varphi_H$  is the angle between the axis of symmetry of the satellite ( $z'$ ) and the vector  $H$ ; the strength  $H$ , as it follows from (1.4.7) is given by (for  $i = 90^\circ$ ,  $R = R_0$ )

$$H = \frac{\mu_E}{R_0^3} \sqrt{1 + 3 \sin^2 u}. \quad (3.3.2)$$

Let us consider the motion in a rotating system, where one of the axes points along  $H$ . The relative ( $q_{\text{rel}}$ ) and the transportation ( $q_{\text{tr}}$ ) angular velocities are then given by

$$q_{\text{rel}} = \dot{\varphi}_H, \quad q_{\text{tr}} = 3\omega \frac{1 + \sin^2 u}{1 + 3 \sin^2 u}, \quad (3.3.3)$$

where  $\omega = \text{const}$  is the angular velocity of the satellite's mass center.

Substituting  $q = q_{\text{rel}} + q_{\text{tr}}$  in (3.3.1) and applying (3.3.3), we obtain an equation of plane oscillations of a satellite about a magnetic line of force in the form

$$\ddot{\Phi}_H + \frac{1}{B} [I_0 H \sin \varphi_H + a_H H^2 \sin \varphi_H \cos \varphi_H] = 6\omega^2 \frac{\sin 2u}{(1+3\sin^2 u)^2}. \quad (3.3.4)$$

In our case,  $u = \omega(t - t^*)$ , where  $t^*$  is the time of equator passage. We see that even for a circular orbit, the equation of oscillations contains variable (periodic) coefficients (since  $H(u)$  is periodic along the orbit) and a nonzero right-hand side contributed by the nonuniform rotation of  $H$  along the orbit. This periodic right-hand side makes the satellite's axis oscillate about a magnetic line of force.

To estimate the characteristics of these forced oscillations, we linearize the equation (3.3.4) and substitute certain constants for the variable coefficients. Then

$$\left. \begin{aligned} \ddot{\Phi}_H + n_H^2 \Phi_H &= \zeta_0 \omega^2 \sin 2u, & n_H^2 &= \frac{1}{B} [I_0 \bar{H} + a_H \bar{H}^2], \\ \zeta_0 &= \max \left\{ \frac{6 \sin 2u}{(1+3\sin^2 u)^2} \right\} \approx 2.12. \end{aligned} \right\} \quad (3.3.5)$$

In (3.3.5), the bar on  $H$  and  $H^2$  denotes averaging over  $u$ . The right-hand side of (3.3.4) is approximated with a sine function having the same frequency and maximum amplitude. It is easily seen from (3.3.5) that the forced oscillations are described by the formula

$$\Phi_{Hf} = A_H \sin 2u, \quad A_H = \frac{\zeta_0 \omega^2}{n_H^2 - 4\omega^2}. \quad (3.3.6)$$

The period of these forced oscillations is thus equal to half the orbital period of the satellite; resonance occurs for  $n_H \approx 2\omega$ . If the parameters are not close to the resonance, the oscillations of the satellite about the magnetic line of force are fairly small. For example, let the satellite carry a permanent magnet with  $I_0 = 10^4 \text{ G} \cdot \text{cm}^3$  (which is quite probable); let  $H = 0.3 \text{ G}$ ,  $B = 10 \text{ kgm} \cdot \text{sec}^2$ , the radius of the orbit  $R_0 = 7000 \text{ km}$ . Then  $A_H \approx 0.1 \approx 6^\circ$ . This proves that at least crude orientation of the satellite along the geomagnetic field is actually feasible. The axis of a magnetically stabilized satellite seeks a direction which completes two revolutions during one orbital period of the satellite.

**2. Attitude stabilization to the Sun by solar radiation torques.** The solar radiation torques considered in Chapter 1 may stabilize the satellite in a sunward attitude. For example, let us consider a space vehicle orbiting around the Sun. We shall assume that the orbital perturbations are negligible, so that the orbit is circular. The torque on this satellite of the Sun is assumed to have the form (1.5.6), (1.5.7), and we proceed to consider the plane motion of the satellite due to this torque. The equation of plane oscillations has the form

$$B \frac{d^2 \epsilon_s}{dt^2} + p_r S(\cos \epsilon_s) z'_0(\cos \epsilon_s) \sin \epsilon_s = 0. \quad (3.3.7)$$

To estimate the stabilizing effect, we take  $Sz'_0 = \text{const}$ . Integrating (3.3.7), we then obtain the energy integral in the form

$$\frac{\dot{\varepsilon}_s^2}{2} - \frac{p_r Sz'_0}{B} \cos \varepsilon_s = c_0. \quad (3.3.8)$$

Hence in an ordinary way we find the maximum permissible value of the initial angular velocity:

$$\dot{\varepsilon}_{s\max}^0 = \sqrt{\frac{2p_r Sz'_0}{B}}.$$

If  $\dot{\varepsilon}_s^0 > \dot{\varepsilon}_{s\max}^0$ , the satellite will spin continuously in one sense. If  $\dot{\varepsilon}_s^0 < \dot{\varepsilon}_{s\max}^0$ , attitude stabilization can be achieved: the satellite will oscillate about the axis pointing to the Sun.

Let us assume for the solar radiation pressure its value on the Earth's orbit,  $p_r = 4.72 \cdot 10^{-8} \text{ g/cm}^2$ ; the satellite's parameters:  $Sz'_0 = 1 \text{ m}^3$ ,  $B = \text{kgm} \cdot \text{sec}^2$ . Then  $\dot{\varepsilon}_{s\max}^0 = 0.0186 \text{ deg} \cdot \text{sec}^{-1}$ , which is a fairly substantial figure, so that we can discuss in practice the possibility of harnessing the light pressure for satellite attitude stabilization. One of the schemes for this attitude stabilization was considered by O. V. Gurko and L. I. Slabkii /26/, who proposed to utilize the combined effect of gravity and solar radiation torques. A. A. Karymov /42/ investigated the conditions of stability of relative equilibrium of an axisymmetric satellite in the field of solar radiation pressure.

## *Chapter 4*

### *THE RELATIONS BETWEEN TRANSLATIONAL AND ROTATIONAL MOTIONS OF A RIGID BODY IN A NEWTONIAN FORCE FIELD*

If a body moving in a Newtonian central field is not a point mass, but actually a rigid body of finite dimensions, its translational and rotational motions, strictly speaking, are not independent; the center of mass of the body describes a non-Keplerian trajectory.

For real satellites, this translation—rotation dependence is very weak. When studying the motion of a satellite about its center of mass, we may naturally assume that the translational and the rotational motions are independent, and that the mass center moves in a Kepler orbit. This so-called limited statement of the problem is generally adopted when analyzing the rotation of heavenly bodies. We also follow this approach in other chapters of this book.

And yet, the question of translation—rotation dependence is of considerable theoretical interest with a view to the general rigorous statement of the problem, and further advances in this field may prove to be useful for the development and the improvement of some theories in celestial mechanics, in particular, the theory of motion of the Moon. Various estimates of the effects associated with the translation—rotation dependence for artificial Earth satellites are of course also important.

The problem of translational—rotational motion has recently attracted the attention of various researchers in the USSR /10, 11, 29, 30, 44, 45/ and elsewhere /83, 92/.

#### **§ 1. EQUATIONS OF MOTION AND THEIR FIRST INTEGRALS**

Let us consider the motion of a rigid body in a Newtonian central field in its most general form.

Let  $C$  be a fixed center of attraction situated outside the rigid body. A system of fixed axes  $X_0Y_0Z_0$  is introduced, with its origin at the point  $C$ ; another system has its origin at the mass center of the body, and its axes  $x'y'z'$  point along the principal central axes of inertia of the body. The mutual orientation of these systems is specified by a table of direction cosines (see § 1, Chapter 1) and the coordinates  $\bar{X}_0\bar{Y}_0\bar{Z}_0$  of the center of mass. The force function  $U$  representing the action of the center of attraction on the rigid body is defined by the integral (1.2.3), (1.2.5). If the body is small in comparison with the distance to the center of force, i.e., if  $\ell = \sqrt{x'^2 + y'^2 + z'^2} \ll R$ , the force function may be written in the form (1.2.7)

for  $x'_0 = y'_0 = z'_0 = 0$ . Note that in practice approximation (1.2.7) is quite sufficient for  $U$ , since the ignored terms are very small. For the Moon  $\frac{l}{R} = 0.0045$ , for artificial satellites  $\frac{l}{R} = 10^{-4} - 10^{-6}$ . The various effects, such as the size of the regions of stability in stable motion, the magnitude of the perturbations disturbing the steady oscillations about the stable equilibrium, etc., estimated by the approximate technique differ by terms of the order of  $\frac{l}{R}$  from the exact figures, and this difference is nearly always negligible. If higher accuracy is required (as, e.g., in the theory of motion of the Moon, where the truncated terms constitute  $\sim 0.5\%$  of the principal terms), more exact expressions for  $U$  should be considered, e.g., those defined by formulas (1.2.3), (1.2.5). Keeping this in mind, we shall henceforth operate with the exact expression (1.2.3) for  $U$ , or with the approximate formula (1.2.7) (assuming  $x'_0 = y'_0 = z'_0 = 0$  in the latter case).

The equations of motion have the form

$$M \frac{d^2 \tilde{X}_0}{dt^2} = \frac{\partial U}{\partial \tilde{X}_0}, \quad M \frac{d^2 \tilde{Y}_0}{dt^2} = \frac{\partial U}{\partial \tilde{Y}_0}, \quad M \frac{d^2 \tilde{Z}_0}{dt^2} = \frac{\partial U}{\partial \tilde{Z}_0}, \quad (4.1.1)$$

$$\left. \begin{aligned} A \frac{dp}{dt} + (C - B) qr &= M_{x'}, \\ B \frac{dq}{dt} + (A - C) pr &= M_{y'}, \\ C \frac{dr}{dt} + (B - A) pq &= M_{z'} \end{aligned} \right\} \quad (4.1.2)$$

If the force function  $U$  depends on all the absolute direction cosines, then the torque components are written as

$$\left. \begin{aligned} M_{x'} &= \frac{\partial U}{\partial \tilde{\alpha}_2} \tilde{\alpha}_3 - \frac{\partial U}{\partial \tilde{\alpha}_3} \tilde{\alpha}_2 + \frac{\partial U}{\partial \tilde{\beta}_2} \tilde{\beta}_3 - \frac{\partial U}{\partial \tilde{\beta}_3} \tilde{\beta}_2 + \\ &\quad + \frac{\partial U}{\partial \tilde{\gamma}_2} \tilde{\gamma}_3 - \frac{\partial U}{\partial \tilde{\gamma}_3} \tilde{\gamma}_2, \\ M_{y'} &= \frac{\partial U}{\partial \tilde{\alpha}_3} \tilde{\alpha}_1 - \frac{\partial U}{\partial \tilde{\alpha}_1} \tilde{\alpha}_3 + \frac{\partial U}{\partial \tilde{\beta}_3} \tilde{\beta}_1 - \frac{\partial U}{\partial \tilde{\beta}_1} \tilde{\beta}_3 + \\ &\quad + \frac{\partial U}{\partial \tilde{\gamma}_3} \tilde{\gamma}_1 - \frac{\partial U}{\partial \tilde{\gamma}_1} \tilde{\gamma}_3, \\ M_{z'} &= \frac{\partial U}{\partial \tilde{\alpha}_1} \tilde{\alpha}_2 - \frac{\partial U}{\partial \tilde{\alpha}_2} \tilde{\alpha}_1 + \frac{\partial U}{\partial \tilde{\beta}_1} \tilde{\beta}_2 - \frac{\partial U}{\partial \tilde{\beta}_2} \tilde{\beta}_1 + \\ &\quad + \frac{\partial U}{\partial \tilde{\gamma}_1} \tilde{\gamma}_2 - \frac{\partial U}{\partial \tilde{\gamma}_2} \tilde{\gamma}_1. \end{aligned} \right\} \quad (4.1.3)$$

In terms of the relative direction cosines ( $\gamma$ ,  $\gamma'$ ,  $\gamma''$ ), these torque components take the form (1.2.4), or (1.2.2) if the approximate force function (1.2.7) is assumed (taking  $x'_0 = y'_0 = z'_0 = 0$ ). Equations (4.1.2) are completed to a closed system by Poisson's kinematic relations

$$\left. \begin{aligned} \frac{d\tilde{\alpha}_1}{dt} &= r\tilde{\alpha}_2 - q\tilde{\alpha}_3, & \frac{d\tilde{\beta}_1}{dt} &= r\tilde{\beta}_2 - q\tilde{\beta}_3, & \frac{d\tilde{\gamma}_1}{dt} &= r\tilde{\gamma}_2 - q\tilde{\gamma}_3, \\ \frac{d\tilde{\alpha}_2}{dt} &= p\tilde{\alpha}_3 - r\tilde{\alpha}_1, & \frac{d\tilde{\beta}_2}{dt} &= p\tilde{\beta}_3 - r\tilde{\beta}_1, & \frac{d\tilde{\gamma}_2}{dt} &= p\tilde{\gamma}_3 - r\tilde{\gamma}_1, \\ \frac{d\tilde{\alpha}_3}{dt} &= q\tilde{\alpha}_1 - p\tilde{\alpha}_2, & \frac{d\tilde{\beta}_3}{dt} &= q\tilde{\beta}_1 - p\tilde{\beta}_2, & \frac{d\tilde{\gamma}_3}{dt} &= q\tilde{\gamma}_1 - p\tilde{\gamma}_2 \end{aligned} \right\} \quad (4.1.4)$$

Equations (4.1.1)–(4.1.4) have four first integrals, which can be derived without difficulty (see, e.g., [11]).

The kinetic energy of the translational motion of the mass center and the kinetic energy of the body in its motion about the mass center are inseparably connected by a single energy integral, so that there is continuous "pumping" of translational kinetic energy into rotational kinetic energy and back (always allowing, of course, for their relation with the potential energy  $U$ ). The energy integral is

$$\left. \begin{aligned} \frac{1}{2}MV^2 + \frac{1}{2}(Ap^2 + Bq^2 + Cr^2) - U = h, \\ V^2 = \dot{X}_0^2 + \dot{Y}_0^2 + \dot{Z}_0^2. \end{aligned} \right\} \quad (4.1.5)$$

There are also the three angular momentum integrals:

$$M(\bar{Y}_0\dot{\bar{Z}}_0 - \bar{Z}_0\dot{\bar{Y}}_0) + Ap\tilde{\alpha}_1 + Bq\tilde{\alpha}_2 + Cr\tilde{\alpha}_3 = L_1, \quad (4.1.6)$$

$$M(\bar{Z}_0\dot{\bar{X}}_0 - \bar{X}_0\dot{\bar{Z}}_0) + Ap\tilde{\beta}_1 + Bq\tilde{\beta}_2 + Cr\tilde{\beta}_3 = L_2, \quad (4.1.7)$$

$$M(\bar{X}_0\dot{\bar{Y}}_0 - \bar{Y}_0\dot{\bar{X}}_0) + Ap\tilde{\gamma}_1 + Bq\tilde{\gamma}_2 + Cr\tilde{\gamma}_3 = L_3. \quad (4.1.8)$$

The equations of motion of course have the usual trivial integrals, namely the relations between the direction cosines. We shall require the following two trivial integrals:

$$V_3 = \tilde{\beta}_1^2 + \tilde{\beta}_2^2 + \tilde{\beta}_3^2 - 1 = 0, \quad (4.1.9)$$

$$V_2 = \gamma^2 + \gamma'^2 + \gamma''^2 - 1 = 0. \quad (4.1.10)$$

## § 2. PARTICULAR SOLUTION OF THE EQUATIONS OF MOTION — RELATIVE EQUILIBRIUM

Let us now seek the following particular solution of the set (4.1.1) — (4.1.4): the satellite's mass center moves in a circular orbit of radius  $R$  with a constant angular velocity  $\omega$  and the body is maintained in relative equilibrium, i.e., the principal central axes of inertia of the body invariably point along the radius-vector, the tangent, and the binormal of the circular orbit.

This motion should be considered because, among other things, it constitutes an idealized model of real motions observed in nature, e.g., the motion of the Moon about the Earth.

If the axis  $z'$  (with the moment of inertia  $C$ ) points along the radius-vector, and the axis  $y'$  (with the moment of inertia  $B$ ) is directed along the normal to the orbital plane, this motion can be written as

$$\left. \begin{aligned} p = r = 0, & \quad q = \omega, \\ \gamma = \gamma' = \tilde{\beta}_1 = \tilde{\beta}_3 = 0, & \quad \gamma'' = \tilde{\beta}_2 = 1, \end{aligned} \right\} \quad (4.2.1)$$

$$R = R_0, \quad \psi_R = 0, \quad \dot{\psi}_R = 0, \quad \dot{\varphi}_R = 0, \quad \dot{R} = 0, \quad (4.2.2)$$

where (4.2.2) is expressed in terms of the spherical coordinates of the mass center,  $R, \varphi_R, \psi_R$ , so that  $\bar{X}_0 = R \cos \psi_R \sin \varphi_R$ ,  $\bar{Y}_0 = R \sin \psi_R \sin \varphi_R$ ,  $\bar{Z}_0 = R \cos \varphi_R$ . The motion occurs in the plane  $X\bar{Z}$ . From Euler's equations (4.1.2) with the torques (4.1.4) we see that this motion will exist if

$$\left( \frac{\partial U}{\partial \gamma'} \right)_0 = 0, \quad \left( \frac{\partial U}{\partial \gamma} \right)_0 = 0. \quad (4.2.3)$$

The subscript 0 indicates that the quantities are considered for the solution (4.2.1)–(4.2.2).

An analysis of the kinematic relations (4.1.4) and equations of motion of the mass center (4.1.1) in conjunction with conditions (4.2.3) shows [11] that the motion (4.2.1), (4.2.2) is possible if

$$\omega^2 = -\frac{1}{MR_0} \left( \frac{\partial U}{\partial R} \right)_0. \quad (4.2.4)$$

The following condition must be satisfied:

$$\left( \frac{\partial U}{\partial R} \right)_0 < 0. \quad (4.2.5)$$

Conditions (4.2.3)–(4.2.5) are the necessary and sufficient conditions for the existence of motion (4.2.1), (4.2.2). Note that equalities (4.2.3) constitute the conditions for a conditional extremum in  $U$  with respect to the variables  $\gamma, \gamma', \gamma''$ , constrained by the relation (4.1.10). Condition (4.2.5) shows that the force is attractive. Formula (4.2.4) defines the angular velocity of the mass center, so that the orbital period

$$T = \frac{2\pi}{\sqrt{-\frac{1}{MR_0} \left( \frac{\partial U}{\partial R} \right)_0}} \quad (4.2.6)$$

(a generalization of Kepler's third law).

For an approximate force function  $U$  (1.2.7), we have from (4.2.6)

$$T = T_k \left( 1 + \frac{3}{2} \frac{A+B-2C}{MR_0^2} \right)^{-\frac{1}{2}} \approx T_k \left( 1 - \frac{3}{4} \frac{A+B-2C}{MR_0^2} \right), \quad (4.2.7)$$

i.e., the period  $T$  differs from the Kepler period  $T_k$  by a term of the order of  $(\frac{l}{R_0})^2$ , where  $l$  is the size of the body. For small bodies, this difference is therefore very small, like all the other effects of translation—rotation coupling. For very large bodies, the deviation from the Kepler motion is naturally substantial. G.N.Duboshin observed in his paper at the Shternberg Astronomical Institute conference (1962) that the center of mass of a body moving in a circular orbit might have a velocity which would have been hyperbolic had the entire mass been concentrated at the mass center.

**Examples.** Let us consider the motion of a dumbbell-shaped body in a circular orbit. Let  $l$  be the halflength of the dumbbell,  $m$  the mass at one end; the mass of the rod is negligible. The mass center of the dumbbell may move in a circular orbit with the figure maintaining one of the three attitudes: the dumbbell axis points along the radius-vector, or along the tangent to the orbit, or along the normal to the orbital plane (to adopt Duboshin's terminology, a "spoke", an "arrow", and a "float"). If the cosine of the angle between the dumbbell axis and the radius-vector is  $\gamma$ , the force function is

$$U = \frac{\mu m}{R} \left\{ \frac{1}{\sqrt{1+2\bar{a}\gamma+\bar{a}^2}} + \frac{1}{\sqrt{1-2\bar{a}\gamma+\bar{a}^2}} \right\}, \quad \bar{a} = \frac{l}{R}.$$

Here  $R$  is the distance from the center of force to the center of mass of the dumbbell. Further,

$$\frac{\partial U}{\partial R} = -\frac{\mu m}{R^2} \left\{ \left[ \frac{1}{\sqrt{1+2\bar{a}\gamma+\bar{a}^2}} + \frac{1}{\sqrt{1-2\bar{a}\gamma+\bar{a}^2}} \right] - \bar{a} \left[ \frac{\gamma+\bar{a}}{(1+2\bar{a}\gamma+\bar{a}^2)^{3/2}} - \frac{\gamma-\bar{a}}{(1-2\bar{a}\gamma+\bar{a}^2)^{3/2}} \right] \right\}.$$

The principal central moments of inertia are as follows: the longitudinal moment is zero, the two lateral moments are  $2ml^2$  each.

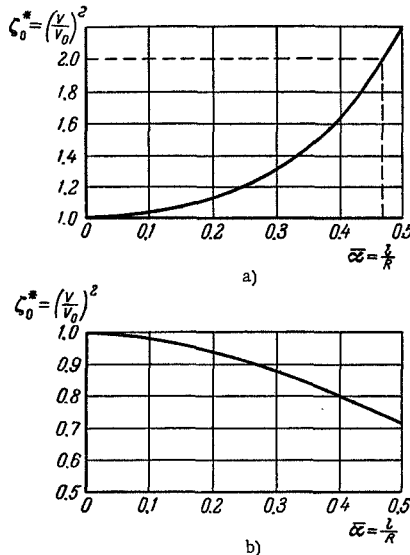


FIGURE 27. The squared ratio of the velocity  $V$  to the circular velocity  $V_0$  as a function of the parameter  $\bar{a} = l/R$ : a) "spoke"; b) "float" and "arrow".

Let us now consider the velocity  $V$  of the dumbbell mass center in a circular orbit. According to (4.2.4)  $V^2 = R_0^2\omega^2 = -R_0 \frac{1}{M} \left( \frac{\partial U}{\partial R} \right)_0$ , where  $M=2m$ . We shall examine the ratio of the square of the velocity  $V$  to the square of the circular velocity  $V_0$  in an orbit of radius  $R_0$ :

$$\zeta_0^* = \left( \frac{V}{V_0} \right)^2 = \frac{V^2}{\frac{\mu}{R_0}} = -\frac{R_0^2 \left( \frac{\partial U}{\partial R} \right)_0}{M\mu}.$$

i) "Spoke". Here  $\gamma = 1$ ,

$$\zeta_0^* = \frac{1 + \bar{a}^2}{(1 - \bar{a}^2)^2}.$$

First, we see that the deviation from the Kepler motion is not even of the order of  $\bar{a} = \frac{l}{R}$ , but of the order of  $\bar{a}^2 = \left( \frac{l}{R} \right)^2$ , which is negligibly small for

small bodies. On the other hand, we see that for fairly large bodies the velocities are considerably different from the circular. For  $\bar{a} = 0.47$ ,  $\zeta_0^* = 2$ , i.e., the velocity is parabolic. The size of the body, however, should be comparable with the dimensions of the orbit! Figure 27a plots the function  $\zeta(\bar{a})$ .

ii) "Float" and "arrow". Here  $\gamma = 0$ ,

$$\zeta_0^* = \frac{1}{(1 + \bar{a}^2)^{1/2}}$$

and the velocity is always less than circular (Figure 27b).

### § 3. ON BODIES SATISFYING THE CONDITIONS OF EXISTENCE OF RELATIVE EQUILIBRIUM

Note that conditions (4.2.3) are identically satisfied for the approximate force function  $U$  (1.2.7). If we consider the exact expression (1.2.3), (1.2.5) of the force function, conditions (4.2.3) reduce to the following (the integrals are taken over the entire volume of the body):

$$\left. \begin{aligned} \bar{J}_1 &= - \int \int \int \mu \frac{x' dm}{r^3} = 0, \\ \bar{J}_2 &= - \int \int \int \mu \frac{y' dm}{r^3} = 0, \\ r^2 &= R_0^2 + 2R_0 z' + x'^2 + y'^2 + z'^2. \end{aligned} \right\} \quad (4.3.1)$$

Conditions (4.3.1) are exactly satisfied for many different bodies (see below). If conditions (4.3.1) cannot be exactly satisfied, then surely they are satisfied approximately (which always holds true), and the inaccuracy involved for real small bodies is not large. This inaccuracy introduces small, continuous perturbations, whose order of smallness is clear from the derivation of the approximate expression (1.2.7) for the force function  $U$ .

Condition (4.2.5) is always satisfied in reality, since it holds true for the leading term in the expansion of  $U$ , and all the other terms being small in comparison with the leading component cannot violate the inequality (4.2.5). We shall not deal with condition (4.2.5) here, but proceed directly with the analysis of some bodies which exactly satisfy conditions (4.2.3) or, equivalently, (4.3.1).

We introduce spherical coordinates in the body's own system of axes  $x', y', z'$ :

$$x' = \rho' \sin \theta' \sin \varphi', \quad y' = \rho' \sin \theta' \cos \varphi', \quad z' = \rho' \cos \theta'.$$

Then

$$\begin{aligned} -\frac{1}{\mu} \bar{J}_{1,2} &= \\ &= \int_{\varphi'_1}^{\varphi'_2} d\varphi' \int_{\theta'_1(\varphi')}^{\theta'_2(\varphi')} d\theta' \int_{\rho'_1(\theta', \varphi')}^{\rho'_2(\theta', \varphi')} F(\rho', \theta') \tilde{\sigma}(\rho', \theta', \varphi') \frac{\sin \varphi'}{\cos \varphi'} d\rho'. \end{aligned}$$

Here  $F(\rho', \theta') = \frac{\rho'^3 \sin \theta'}{(R^2 + 2R\rho' \cos \theta' + \rho'^2)^{1/2}}$ ,  $\tilde{\sigma}(\rho', \theta', \varphi')$  a function specifying the density variation of the body. In particular, for a simply connected

"convex" body, we have  $\rho'_1 = 0$ ,  $\rho'_2 = \rho'_2(\theta', \varphi')$  — the equation of the surface of the body;  $\varphi'_1 = 0$ ,  $\varphi'_2 = 2\pi$ ,  $\theta'_1 = 0$ ,  $\theta'_2 = \pi$ .

We now assume that the body is "closed" in  $\varphi'$ , i.e., the integral with respect to  $\varphi'$  is taken over the entire interval from 0 to  $2\pi$  (a sphere, an ellipsoid, a torus, etc., also "horseshoe"-shaped bodies, with the axis  $z'$  meeting both legs of the "horseshoe"). The integrals are then transformed as follows:

$$\int_0^{2\pi} f(\varphi') d\varphi' = \int_0^\pi f(\varphi') d\varphi' + \int_\pi^{2\pi} f(\varphi') d\varphi' = \int_0^\pi f(\varphi') d\varphi' + \int_0^\pi f(\varphi'' + \pi) d\varphi'',$$

where  $\varphi'' = \varphi' - \pi$ . Then

$$\begin{aligned} -\frac{1}{\mu} \bar{J}_{1,2} &= \int_0^\pi d\varphi' \int_{\theta'_1(\varphi')}^{\theta'_2(\varphi')} d\theta' \int_{\rho'_1(\theta', \varphi')}^{\rho'_2(\theta', \varphi')} F(\rho', \theta') \tilde{\sigma}(\rho', \theta', \varphi') \frac{\sin \varphi'}{\cos \varphi'} d\rho' - \\ &- \int_0^\pi d\varphi'' \int_{\theta'_1(\varphi'' + \pi)}^{\theta'_2(\varphi'' + \pi)} d\theta' \int_{\rho'_1(\theta', \varphi'' + \pi)}^{\rho'_2(\theta', \varphi'' + \pi)} F(\rho', \theta') \times \tilde{\sigma}(\rho', \theta', \varphi'' + \pi) \frac{\sin \varphi''}{\cos \varphi''} d\rho'. \end{aligned}$$

From these expressions for  $J_1$  (with  $\sin \varphi'$  in the integrand) and for  $J_2$  (with  $\cos \varphi'$ ) it immediately follows that the shape of the body is such that

$$\theta_i(\varphi'' + \pi) = \theta_i(\varphi''), \quad \rho'_i(\theta', \varphi'' + \pi) = \rho'_i(\theta', \varphi''), \quad i = 1, 2, \quad (4.3.2)$$

and if the density is distributed according to a similar law, i.e., if

$$\tilde{\sigma}(\rho', \theta', \varphi'' + \pi) = \tilde{\sigma}(\rho', \theta', \varphi''), \quad (4.3.3)$$

we have  $\bar{J}_1 = 0$ ,  $\bar{J}_2 = 0$ , and conditions (4.3.1), or equivalently (4.2.4), are exactly satisfied. A body whose shape and density display a certain symmetry about the principal central axes of inertia thus satisfies conditions (4.2.4) for the existence of relative equilibrium. The symmetry conditions (4.3.2), (4.3.3) are fairly weak. Figure 28 is an example of a body satisfying the second condition in (4.3.2) (a section produced by a plane  $z' = \text{const}$  and a section containing the axis  $z'$  are shown). We see that the condition amounts to the requirement that the body should have an axis of symmetry. Any section through this axis is symmetric about this axis; different sections, however, are not identical, and the body in general is not a solid of revolution.

We can do without the geometrical conditions specifying the figure of the body. Indeed, the integrals may be taken over a certain region in space which a priori satisfies the conditions (4.3.2) and which encloses the entire volume occupied by the body being considered. The density of the new generated figure is  $\tilde{\sigma} \neq 0$  if the point belongs to the original rigid body, and  $\tilde{\sigma} = 0$  otherwise. If the distribution of the density defined in this way is consistent with (4.3.3), conditions (4.2.4) are satisfied for the rigid body being considered.

Physically, condition (4.3.3) implies that the density distribution in the body has an axis of symmetry (in the above sense)—the axis  $z'$ . According to the original definition of the system of axes  $x'y'z'$ , the axis of symmetry should coincide with one of the principal axes of inertia of the body. In relative equilibrium, this axis points along the radius-vector.

Various bodies with three different principal central moments of inertia ( $A \neq B \neq C$ ) can obviously satisfy this modified condition. Let us illustrate this by a simple example.

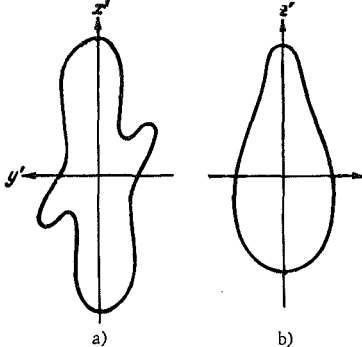


FIGURE 28. An example of a body satisfying the symmetry condition: a) section by a plane  $z' = \text{const}$ ; b) section through the axis  $z'$ .

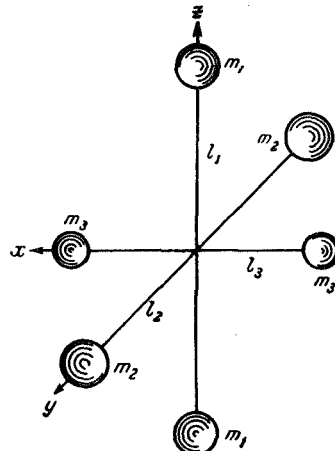


FIGURE 29. A body with unequal principal central moments of inertia satisfying the condition of existence of relative equilibrium.

**Example.** Consider a body consisting of three mutually perpendicular rods with halflengths  $l_1, l_2, l_3$ , each carrying two equal masses  $m_1, m_2, m_3$  at its respective ends: the masses at the two ends of one rod are equal to each other, but different from the masses attached to the other two rods. The rods meet at their midpoints;  $l_1$  points along the axis  $z$  of the body,  $l_2$  along  $y$ , and  $l_3$  along  $x$  (Figure 29). If the mass of the rods is neglected, this body may be treated as a system of discrete masses; the force function is therefore given by the following sum:

$$U = \frac{\mu}{R_0} \sum_{i=1}^{i=3} \left\{ \frac{1}{\sqrt{1 + 2\bar{a}_i \gamma^i + \bar{a}_i^2}} + \frac{1}{\sqrt{1 - 2\bar{a}_i \gamma^i + \bar{a}_i^2}} \right\} m_i, \quad (4.3.4)$$

where  $\bar{a}_i = \frac{l_i}{R_0}$ ;  $\gamma^1 = \gamma''$ ,  $\gamma^2 = \gamma'$ ,  $\gamma^3 = \gamma$ .

The principal central moments of inertia of this body are all different. Let  $B > A > C$ , i.e.,  $l_1^2 m_1 > l_3^2 m_3 > l_2^2 m_2$ . Clearly,  $l_i$  and  $m_i$  can always be chosen so as to justify this assumption. Conditions (4.2.3) for the existence of relative equilibrium are satisfied. Indeed,

$$\frac{\partial U}{\partial \gamma^i} = -\frac{\mu}{R_0} \left\{ \frac{1}{(1 + 2\bar{a}_i \gamma^i + \bar{a}_i^2)^{1/2}} - \frac{1}{(1 - 2\bar{a}_i \gamma^i + \bar{a}_i^2)^{1/2}} \right\} m_i \bar{a}_i. \quad (4.3.5)$$

For unperturbed motion  $\gamma^i=0$ ,  $i=2, 3$ , ( $\gamma^1=1$ ), so that  $\left(\frac{\partial U}{\partial \gamma^i}\right)_0 = 0$ , which was to be proved.

#### § 4. STABILITY OF RELATIVE EQUILIBRIUM

Unperturbed motion is assumed in the form (4.2.1), (4.2.2), and we proceed with an investigation of its stability. Perturbed motion is described by the parameters

$$\left. \begin{array}{l} R=R_0+\Delta, \quad \dot{\psi}_R=\omega+y, \quad \dot{R}, \quad \dot{\psi}_R, \\ p \quad r \quad q=\omega+x, \\ \tilde{\beta}_1 \quad \tilde{\beta}_3 \quad \tilde{\beta}_2=1+\eta, \\ \gamma \quad \gamma' \quad \gamma''=1+\zeta. \end{array} \right\} \quad (4.4.1)$$

Applying the spherical coordinates  $R$ ,  $\psi_R$ ,  $\varphi_R$  of the mass center, we obtain the following integrals of perturbed motion. From (4.1.5) we have

$$\begin{aligned} J_1^* = & \dot{R}^2 + 2R_0\omega^2\Delta + 2\omega R_0^2y + \omega^2\Delta^2 - \omega^2R_0^2\psi_R^2 + R_0^2y^2 + \\ & + 4\omega R_0\Delta y + R_0^2\dot{\psi}_R^2 + Ap^2 + 2B\omega x + Bx^2 + Cr^2 - \\ & - 2 \left\{ \frac{\partial U}{\partial R} \Delta + \frac{\partial U}{\partial \gamma} \gamma + \frac{\partial U}{\partial \gamma'} \gamma' + \frac{\partial U}{\partial \gamma''} \zeta + \frac{1}{2} \frac{\partial^2 U}{\partial R^2} \Delta^2 + \right. \\ & + \frac{1}{2} \frac{\partial^2 U}{\partial \gamma^2} \gamma^2 + \frac{1}{2} \frac{\partial^2 U}{\partial \gamma'^2} \gamma'^2 + \frac{1}{2} \frac{\partial^2 U}{\partial \gamma''^2} \zeta^2 + \frac{\partial^2 U}{\partial \gamma \partial \gamma'} \gamma \gamma' + \\ & + \frac{\partial^2 U}{\partial \gamma \partial \gamma''} \gamma \zeta + \frac{\partial^2 U}{\partial \gamma' \partial \gamma''} \gamma' \zeta + \frac{\partial^2 U}{\partial R \partial \gamma} \Delta \gamma + \\ & \left. + \frac{\partial^2 U}{\partial R \partial \gamma'} \Delta \gamma' + \frac{\partial^2 U}{\partial R \partial \gamma''} \Delta \zeta \right\} + o(3) = \text{const.} \end{aligned} \quad (4.4.2)$$

From (4.1.7)

$$\begin{aligned} J_2^* = & 2R_0\omega\Delta + \omega\Delta^2 - \omega R^2\psi_R^2 + R^2y + 2Ry\Delta + Ap\tilde{\beta}_1 + Bx + \\ & + B\omega\eta + Bx\eta + Cr\tilde{\beta}_3 + o(3) = \text{const.} \end{aligned} \quad (4.4.3)$$

The integrals (4.1.9) and (4.1.10) take the form

$$V_2 = \gamma^2 + \gamma'^2 + \zeta^2 + 2\zeta = 0, \quad V_3 = \tilde{\beta}_1^2 + \eta^2 + \tilde{\beta}_3^2 + 2\eta = 0. \quad (4.4.4)$$

The following simplified notations have been adopted in (4.4.2) and (4.4.3):

a)  $\frac{U}{M}$ ,  $\frac{A}{M}$ ,  $\frac{B}{M}$ ,  $\frac{C}{M}$  have again been replaced with  $U$ ,  $A$ ,  $B$ ,  $C$ ; we must henceforth keep in mind that these quantities stand for the force function and for the principal central moments of inertia related to the mass of the body;

b) all the derivatives of  $U$  correspond to the case of unperturbed motion,

i.e.,  $R=R_0$ ,  $\gamma=\gamma'=0$ ,  $\gamma''=1$ ; thus,  $\frac{\partial U}{\partial R}$  stands for  $\left(\frac{\partial U}{\partial R}\right)_{\substack{R=R_0 \\ \gamma''=1}}$ , etc.

c)  $o(3)$ ,  $\bar{o}(3)$  in the expressions for  $J_1^*$  and  $J_2^*$  stand collectively for terms above the second order of smallness.

According to well-known theorems /54, 74/, the existence of a non-alternant (fixed-sign) integral for the equations of perturbed motion is a sufficient condition for the stability of the unperturbed motion. We shall

seek this integral in the form of a quadratic combination of the integrals (4.4.2)–(4.4.4):

$$L = J_1^* - 2\omega J_2^* + gV_2 + fV_3 + \frac{k_0}{R_0^2} J_2^{*2}. \quad (4.4.5)$$

Here  $k_0$  is a constant,  $g$  and  $f$  are functions; the actual choice of  $k_0$ ,  $f$ , and  $g$  will be dealt with in what follows.

The Lyapunov function (4.4.5) is positive definite if it contains no terms of first order and if the quadratic form made up from the terms of second order is positive definite. Terms of third and higher orders do not influence the sign of  $L$ . Since

$$\frac{dL}{dt} = \dot{g}V_2 + \dot{f}V_3 = 0,$$

the conditions of  $L$  being positive definite are also sufficient conditions for the stability of the unperturbed motion (4.2.1), (4.2.2).

We now choose  $g$  and  $f$  as follows:

$$\left. \begin{aligned} g &= \frac{\partial U}{\partial \gamma''} + \frac{\partial^2 U}{\partial \gamma \partial \gamma''} \gamma + \frac{\partial^2 U}{\partial \gamma' \partial \gamma''} \gamma' + \\ &\quad + \frac{1}{2} \left( \frac{\partial^2 U}{\partial \gamma''^2} - \frac{\partial U}{\partial \gamma''} \right) \zeta + \frac{\partial^2 U}{\partial R \partial \gamma''} \Delta, \\ f &= \omega^2 B + \omega Bx - \frac{B\omega k_0}{R_0^2} (2R_0\omega\Delta + R_0^2 y + Bx). \end{aligned} \right\} \quad (4.4.6)$$

Having thus chosen  $f$  and  $g$  and applying condition (4.4.5), we see that the linear terms in the Lyapunov function (4.4.5) all vanish; all terms of second order containing  $\zeta$  and terms of second order containing  $\eta$ , with the exception of the term with  $\eta^2$ , also vanish; and last, on account of the particular choice of the functions  $g$  and  $f$ , the quadratic form entering  $L$  becomes nondegenerate and it can be made positive definite. In virtue of the preceding, we write for the Lyapunov function (4.4.5)

$$\begin{aligned} L = & Ap^2 - 2\omega A p \tilde{\beta}_1 + \omega^2 B \tilde{\beta}_1^2 + Cr^2 - 2\omega C r \tilde{\beta}_3 + \omega^2 B \tilde{\beta}_3^2 + \\ & + \omega^2 c_{33} \eta^2 + \dot{R}^2 + \omega^2 R_0^2 \dot{v}_R^2 + R_0^2 \dot{\psi}_R^2 + \\ & + c_{44} \gamma^2 + c_{55} \gamma'^2 + c_{11} \Delta^2 + c_{22} y^2 + c_{33} x^2 + 2c_{45} \eta \gamma' + 2c_{14} \Delta \gamma + \\ & + 2c_{15} \Delta \gamma' + 2c_{12} \Delta y + 2c_{13} \Delta x + 2c_{23} y x + o(3). \end{aligned} \quad (4.4.7)$$

Here  $o(3)$  contains only terms above the second order of smallness relative to perturbations, and the coefficients  $c_{ij}$  take the following values:

$$\left. \begin{aligned} c_{44} &= \frac{\partial U}{\partial \gamma''} - \frac{\partial^2 U}{\partial \gamma^2}, & c_{55} &= \frac{\partial U}{\partial \gamma''} - \frac{\partial^2 U}{\partial \gamma'^2}, & c_{45} &= - \frac{\partial^2 U}{\partial \gamma \partial \gamma'}, \\ c_{11} &= - \frac{\partial^2 U}{\partial R^2} + \omega^2 (4k_0 - 1), & c_{22} &= R_0^2 (1 + k_0), \\ c_{33} &= B \left( 1 + k_0 \frac{B}{R_0^2} \right), & c_{14} &= - \frac{\partial^2 U}{\partial R \partial \gamma}, & c_{15} &= - \frac{\partial^2 U}{\partial R \partial \gamma'}, \\ c_{12} &= 2R_0 \omega k_0, & c_{13} &= 2 \frac{\omega B k_0}{R_0}, & c_{23} &= B k_0. \end{aligned} \right\} \quad (4.4.8)$$

The quadratic form (4.4.7) can be divided into two parts. The first line in (4.4.7) contains two similar quadratic forms, which are positive definite if

$$B > A, \quad B > C. \quad (4.4.9)$$

The second line contains only nonzero positive terms (on the proviso that  $k_0$  is positive). Assuming a positive  $k_0$ , we also have  $c_{33} > 0$ . The other terms in (4.4.7) in general cannot be grouped into simpler quadratic forms, and they should therefore be analyzed jointly. The matrix of the quadratic form made up from these terms is

$$\begin{array}{cccccc} \Delta & y & x & \gamma & \gamma' \\ \Delta & c_{11} & c_{12} & c_{13} & c_{14} & c_{15} \\ y & c_{12} & c_{22} & c_{23} & 0 & 0 \\ x & c_{13} & c_{23} & c_{33} & 0 & 0 \\ \gamma & c_{14} & 0 & 0 & c_{44} & c_{45} \\ \gamma' & c_{15} & 0 & 0 & c_{45} & c_{55} \end{array} \quad (4.4.10)$$

The quadratic form in the variables  $\Delta, y, x, \gamma, \gamma'$  is positive definite if all the principal diagonal minors in (4.4.10) are positive. The requirement that the first three of these minors be positive is equivalent to the following conditions:

$$-\frac{\partial^2 U}{\partial R^2} + \omega^2(4k_0 - 1) > 0, \quad -\frac{\partial^2 U}{\partial R^2} + \omega^2 \frac{3k_0 - 1}{1 + k_0} > 0, \quad (4.4.11)$$

$$-\frac{\partial^2 U}{\partial R^2} + \omega^2 \frac{3k_0 - 1 - k_0 \delta_f^2}{1 + k_0 + k_0 \delta_f^2} > 0, \quad (4.4.12)$$

where  $\delta_f^2 = \frac{B}{R_0^2}$  is a dimensionless parameter.

It is easily seen that for any positive  $k_0$ ,

$$4k_0 - 1 > \frac{3k_0 - 1}{1 + k_0} > \frac{3k_0 - 1 - k_0 \delta_f^2}{1 + k_0 + k_0 \delta_f^2}.$$

Therefore, (4.4.11), (4.4.12) are satisfied if (4.4.12) holds true. Condition (4.4.12) is thus the only one required to decide whether all the first three diagonal minors of (4.4.10) are positive. The remaining conditions of stability will be obtained by examining the sign of the 4th and the 5th minors of (4.4.10) (the 5th minor coincides with the entire determinant). Writing out these minors and applying the previous inequalities, we obtain the following system of sufficient conditions for the stability of relative equilibrium:

$$\left. \begin{array}{l} a) \quad B > A, \quad B > C; \\ b) \quad c_{44} > \frac{c_{14}}{\Delta_3}, \quad c_{44}c_{55} - c_{45}^2 > \frac{c_{55}c_{14}^2 - c_{44}c_{15}^2}{\Delta_3}; \\ c) \quad \Delta_3 = BR_0^2 \left\{ -\frac{\partial^2 U}{\partial R^2} + \omega^2 \frac{3k_0 - 1 - k_0 \delta_f^2}{1 + k_0 + k_0 \delta_f^2} \right\} > 0, \\ \quad k_0 > 0. \end{array} \right\} \quad (4.4.13)$$

## § 5. ANALYSIS OF THE CONDITIONS OF STABILITY OF RELATIVE EQUILIBRIUM

Since in unperturbed motion the axis  $y'$  (with the moment of inertia  $B$ ) points along the normal to the orbital plane, the first condition in (4.4.13) implies that the axis with the largest moment of inertia, i.e., the least axis of the ellipsoid of inertia, should be directed at right angles to the orbital plane.

Conditions (b) and (c) contain some integrals over the volume of the body (i.e., the conditions of stability are specified in integral form). Let us first analyze condition (c). In what follows we shall show that this condition is satisfied for sufficiently large  $k_0$ . This condition is thus required only for the choice of the arbitrary constant  $k_0$ .

Applying (4.2.4) and the fact that we are dealing with quantities per unit mass (in other words, we may take  $M=1$ ), we write for condition (c)

$$\frac{\partial^2 U}{\partial R^2} + \frac{1}{R} \frac{\partial U}{\partial R} \frac{3k_0 - 1 - k_0 \delta_f^2}{1 + k_0 + k_0 \delta_f^2} < 0; \quad (4.5.1)$$

this inequality is not satisfied for  $k_0 = 0$ , since it does not hold true for the principal term  $U^* = \frac{\mu}{R}$  of the potential  $U$ :  $\frac{\partial^2 U^*}{\partial R^2} - \frac{1}{2} \frac{\partial U^*}{\partial R} = 3 \frac{\mu}{R^3} > 0$ . In reality, the additional terms in the potential  $U$  are small in comparison with the leading term, and are therefore unable to alter the sign of inequality. A nonzero  $k_0$  must be assumed (this in fact justifies the introduction of the quadratic term  $\frac{k_0}{R_0^2} J_2^2$  in the Lyapunov function (4.4.5)). For large  $k_0$ , condition (4.5.1) is satisfied. Indeed, for  $k_0 \rightarrow \infty$ , it reduces to the condition

$$\frac{\partial^2 U}{\partial R^2} + \frac{1}{R} \frac{\partial U}{\partial R} \frac{3 - \delta_f^2}{1 + \delta_f^2} < 0.$$

Since  $\delta_f$  is of the same order as the ratio of the body size to the distance from the center of force,  $\delta_f^2$  is very small in comparison with unity, and this condition approximately reduces to the well-known inequality for the Newtonian potential /31/:

$$\frac{\partial^2 U}{\partial R^2} + \frac{3}{R} \frac{\partial U}{\partial R} < 0.$$

This inequality obviously holds true for the principal term:

$$\frac{\partial^2 U^*}{\partial R^2} + \frac{3}{R} \frac{\partial U^*}{\partial R} = - \frac{\mu}{R^3} < 0.$$

The other terms in  $U$  and the terms with  $\delta_f^2$  cannot alter the sign of this inequality. Since in reality an arbitrarily large  $k_0$  may be taken, condition (4.5.1) can be always satisfied.

Let us now consider conditions (b) of (4.4.13). The parameters  $c_{14}$  and  $c_{15}$  entering these inequalities are defined by the following volume

integrals:

$$\left. \begin{aligned} c_{14} &= \bar{J}_1 + 3R_0 \int \int \int \frac{\mu x' (R_0 + z') dm}{[R_0^2 + 2R_0 z' + x'^2 + y'^2 + z'^2]^{3/2}}, \\ c_{15} &= \bar{J}_2 + 3R_0 \int \int \int \frac{\mu y' (R_0 + z') dm}{[R_0^2 + 2R_0 z' + x'^2 + y'^2 + z'^2]^{3/2}}, \end{aligned} \right\} \quad (4.5.2)$$

where  $\bar{J}_1$  and  $\bar{J}_2$  are determined from (4.3.1). In virtue of conditions (4.2.3) for the existence of a particular solution, we have  $\bar{J}_1 = \bar{J}_2 = 0$ . There are a great many bodies for which  $c_{14} = c_{15} = 0$  also. It is by no means obvious in the general case that the condition  $\bar{J}_1 = \bar{J}_2 = 0$  for the existence of relative equilibrium is equivalent to  $c_{14} = c_{15} = 0$ . However, for the class of bodies described in § 2, it can be easily verified by the same technique that the conditions  $\bar{J}_1 = \bar{J}_2 = 0$  and  $c_{14} = c_{15} = 0$  are simultaneous. Whenever  $c_{14} = c_{15} = 0$ , condition (b) of (4.4.13) reduces to the following:

$$\left. \begin{aligned} \frac{\partial U}{\partial \gamma''} - \frac{\partial^2 U}{\partial \gamma^2} &> 0, \\ \left( \frac{\partial U}{\partial \gamma''} - \frac{\partial^2 U}{\partial \gamma^2} \right) \left( \frac{\partial U}{\partial \gamma''} - \frac{\partial^2 U}{\partial \gamma'^2} \right) &> \left( \frac{\partial^2 U}{\partial \gamma \partial \gamma'} \right)^2. \end{aligned} \right\} \quad (4.5.3)$$

Conditions (4.5.3), in conjunction with condition (4.2.3), indicate that in unperturbed motion the force function has a conditional maximum with respect to the variables  $\gamma, \gamma', \gamma''$  constrained by relation (4.1.10). Now, since condition (a) in (4.4.13) implies that the centrifugal force function is maximal, the relative equilibrium is stable if the total force function of the Newtonian and the centrifugal forces is maximal in unperturbed motion with respect to the rotational parameters of the body.

If, however,  $c_{14} \neq c_{15} \neq 0$ , (4.5.3) must be replaced with the general condition (b) of (4.4.13).

Note that the integrals entering the existence conditions (4.2.3) and the stability conditions (4.4.13) of relative equilibrium are easily evaluated by series-expanding the integrands in powers of  $\frac{x'}{R_0}, \frac{y'}{R_0}, \frac{z'}{R_0}$  (terms above second order of smallness are ignored). This is equivalent to substituting the approximate force function (1.2.7), and not the exact expression (1.2.3), in conditions (4.2.3) and (4.4.13). The integrals evaluated in this way will differ from their exact values by terms of the order of  $\frac{l}{R_0}$ , which is negligible in reality (numerical estimates of this ratio are given in § 1 above).

This simplified form of conditions (4.4.13) gives the exact sufficient conditions of stability: if these conditions are satisfied, the Lyapunov function (4.4.5) is nonalternant, since a form with fairly small coefficients added to a form of the same order does not alter its sign /55/.

To this approximation, the existence conditions (4.2.3) are identically satisfied. In the stability condition (4.4.13) we moreover have

$$\begin{aligned} c_{14} &= c_{15} = c_{45} = 0, \\ c_{44} &= 3 \frac{\mu}{R_0^3} (A - C), \quad c_{55} = 3 \frac{\mu}{R_0^3} (B - C), \end{aligned}$$

and conditions (b) of (4.4.13) take the form  $A - C > 0, B - C > 0$ . These conditions, in conjunction with (a) in (4.4.13), give the following sufficient

condition of stability:

$$B > A > C, \quad (4.5.4)$$

which implies that in unperturbed motion the least axis of the ellipsoid of inertia points along the normal to the unperturbed orbital plane, while the largest axis of this ellipsoid is oriented along the radius-vector.

As we have just observed, condition (4.5.4) is one of the exact sufficient conditions of stability: if inequalities (4.5.4) are satisfied, the Lyapunov function (4.4.5) remains positive definite (for fairly small  $\frac{l}{R_0}$ ).

Furthermore, conditions (4.5.4) are the fundamental conditions of stability, since they correspond to the largest region of stability.

If  $\frac{l}{R_0}$  is not small enough, the more general conditions of stability (4.4.13) must be applied. For small  $\frac{l}{R}$  the generalized sufficient conditions (4.4.13) reveal new stable states of relative equilibrium, which are however secondary in comparison with the fundamental equilibria described by condition (4.5.4). The regions of stability corresponding to these new states are very small, being at most of the order of  $\frac{l}{R}$  relative to the fundamental region of stability.

The existence of these stable equilibria is nevertheless of some interest. Let us consider this case for the three-dimensional dumbbell introduced in § 3 (Figure 29).

Differentiating (4.3.5) with respect to  $R$ , we easily see that here  $c_{14}=c_{15}=0$ , and the stability conditions (b) of (4.4.13) therefore take the form (4.5.3). These conditions of stability can be written as

$$A - C > \delta^*, (A - C - \delta^*)(B - C - \delta_1^*) > \delta_2^*. \quad (4.5.5)$$

Here  $\delta^*$ ,  $\delta_1^*$ ,  $\delta_2^*$  are quantities of small absolute value:  $|\delta^*| \leq ml^2 \left( \frac{l}{R} + \frac{l^2}{R^2} + \dots \right)$ .

The right-hand side of the first inequality in (4.5.5) is exceedingly small in comparison with the left-hand side. If  $\delta^* > 0$ , the orientation of the axes of the ellipsoid of inertia in a stable equilibrium attitude is defined by condition (4.5.4). Conditions (4.5.5) in this case only impose additional restrictions on the magnitude of the principal central moments of inertia. If, however, the body configuration is such that  $\delta^* < 0$ , stable equilibrium is also possible for  $C > A$ , i.e., with the medium axis of the ellipsoid of inertia pointing along the radius-vector, and its largest axis lying along the tangent to the orbit. However, in virtue of the first condition in (4.5.5) the difference between the moments  $C$  and  $A$  should be very small, so that  $C > A > C - |\delta^*|$ . Furthermore, in virtue of the second condition in (4.5.5),

$$B > C + \delta_1^* + \frac{\delta_2^2}{A - C - \delta^*}. \quad (4.5.6)$$

For the three-dimensional dumbbell, we have

$$\begin{aligned}\tilde{\Delta} = & \left( \frac{\partial U}{\partial \dot{Y}''} - \frac{\partial^2 U}{\partial Y^2} \right)_{Y^*=\bar{Y}} = \frac{\mu}{R} m_1 \bar{a}_1 \left\{ \frac{1}{(1 - 2\bar{a}_1 + \bar{a}_1^2)^{3/2}} - \right. \\ & \left. - \frac{1}{(1 + 2\bar{a}_1 + \bar{a}_1^2)^{3/2}} \right\} - \frac{6\mu}{R} m_3 \bar{a}_3^2 \left\{ \frac{1}{(1 + \bar{a}_3^2)^{3/2}} \right\}. \end{aligned} \quad (4.5.7)$$

Condition (4.5.3) indicates that this expression should be positive. Since the quantity in the first braces is positive for any  $\bar{a}_1$ , the stability condition (4.5.3) can always be satisfied by an appropriate choice of  $\bar{a}_1$  and  $\bar{a}_3$ . The choice of  $\bar{a}_1$ , however, should be consistent with the condition  $B > C > A$ , which may be written as

$$l_3^2 m_3 > l_1^2 m_1 > l_2^2 m_2. \quad (4.5.8)$$

Series-expanding (4.5.7), we write the condition  $\tilde{\Delta} > 0$  in the form

$$m_1 l_1^2 > m_3 l_3^2 \left( 1 - \frac{5}{3} \bar{a}_1^2 + \tilde{\varphi} \right),$$

where  $\tilde{\varphi}$  incorporates terms above the second order of smallness in  $\bar{a}_1$  and  $\bar{a}_3$ . Since  $\bar{a}_1$  and  $\bar{a}_3$  are very small,  $\tilde{\varphi}$  may be ignored, and we see that the above condition is consistent with (4.5.8) only if

$$l_3^2 m_3 > l_1^2 m_1 > l_3^2 m_3 \left( 1 - \frac{5}{3} \bar{a}_1^2 \right),$$

i.e., stable equilibrium with the medium axis pointing at right angles to the orbital plane is possible only if the ellipsoid of inertia differs from an ellipsoid of revolution at most by terms of the order of  $(\frac{l_1}{R})^2$ .

It now remains to impose the stability condition (4.5.6), where  $A - C - \delta^* = \tilde{\Delta}$  is defined by (4.5.7), and  $\delta_1^*$  and  $\delta_2^*$  are small quantities, no less than of the order of  $\bar{a} ml^2$ ,  $\bar{a} = \frac{l}{R_0}$ . Condition (4.5.6) can obviously be satisfied by taking a sufficiently small  $C$ , without violating condition (4.5.8). Indeed, condition (4.5.6) is written as  $m_1 l_1^2 > m_2 l_2^2 + \delta_1^* + \frac{\delta_2^{*2}}{\tilde{\Delta}}$ , and we obtain a complete set of inequalities

$$\begin{aligned}l_3^2 m_3 &> l_1^2 m_1, \\ l_1^2 m_1 &> l_3^2 m_3 \left( 1 - \frac{5}{3} \bar{a}_1^2 \right), \\ l_1^2 m_1 &> m_2 l_2^2 + \delta_1^* + \frac{\delta_2^{*2}}{\tilde{\Delta}}, \\ l_1^2 m_1 &> m_2 l_2^2,\end{aligned}$$

which is always consistent for fairly small  $m_2 l_2^2$ , irrespective of the sign of  $\delta_1^* + \frac{\delta_2^{*2}}{\tilde{\Delta}}$ .

We should again emphasize that this attitude of stable relative equilibrium is secondary in comparison with the principal case (4.5.4).

The foregoing stability conditions apply to the orbital motion of the mass center, as well as to the motion around the center of mass. However, the permissible perturbations in the motion of the mass center, i.e., perturbations under which the motion remains stable, are very small. The permissible perturbations for the motion about the center of mass and for the orbital motion of the mass center can be estimated applying the Lyapunov function (4.4.7). Indeed,  $L=L_0=\text{const}$ , and since  $L$  is a sum of positive definite quadratic forms, each form separately is less than  $L$  (terms above the second order of smallness are ignored). The estimates can be made with an approximate force function  $U$ , so as to avoid manipulating with terms of high order of smallness. Then, for the direction cosines  $\gamma, \gamma', \tilde{\beta}_1, \tilde{\beta}_3$  we have

$$\begin{aligned}\gamma^2 &\leq \frac{L_0}{3\omega^2(A-C)}, \quad \gamma'^2 \leq \frac{L_0}{3\omega^2(B-C)}, \\ \tilde{\beta}_1^2 &\leq \frac{L_0}{\omega^2(B-A)}, \quad \tilde{\beta}_3^2 \leq \frac{L_0}{\omega^2(B-C)}.\end{aligned}$$

If  $\gamma^2 < 1$  and  $\gamma'^2 < 1$ , the motion (in  $\gamma$  and  $\gamma'$ ) will be oscillatory about a state of relative equilibrium. These conditions are equivalent to a single inequality

$$L_0 < 3\omega^2(A-C), \quad (4.5.9)$$

which defines the permissible magnitudes of the initial perturbations.  $\tilde{\beta}_1$  and  $\tilde{\beta}_3$  are analogously restricted by the condition  $L_0 < \omega^2(B-C)$ , and the combined condition of bounded oscillations about the center of mass is given by

$$L_0 < \min\{3\omega^2(A-C), \omega^2(B-C)\}$$

(the exact attitude of the satellite is more than fully defined by  $\gamma, \gamma', \tilde{\beta}_1, \tilde{\beta}_3$ ).

Let the initial perturbations be confined to the orbital plane, and let only the motion about the center of mass be perturbed. Then

$$L_0 = B \left( 1 + k_0 \frac{B}{R_0^2} \right) x_0^2 + 3\omega^2(A-C)y_0^2. \quad (4.5.10)$$

Since even for the very large  $k_0$  needed to ensure a positive definite  $L(k_0 \sim 10-100)$ , the quantity  $k_0 \frac{B}{R_0^2}$  of the real artificial satellites is small ( $10^{-4}-10^{-2}$ ), it may be easily ignored.

If  $\theta_0$  is the initial deviation of the satellite's axis from the equilibrium  $x_0 = \theta_0$ , condition (4.5.9) yields

$$|\dot{\theta}_0| \leq \omega \sqrt{3 \frac{A-C}{B}} |\cos \theta_0| \leq \omega \sqrt{3}$$

(since physically  $\frac{A-C}{B} < 1$ ). This estimate gives the order of magnitude of the permissible perturbations in this case. We see that  $\theta_0$  should be of the same order as the unperturbed orbital velocity of the satellite (i.e., from 0.01 deg/sec to 0.1 deg/sec for artificial satellites). These estimates are consistent with the figures obtained within the framework

of the limited problem (Chapter 2, § 1). The present approach, however, in distinction from the limited problem, makes it possible to estimate orbital perturbations as well. For example, for the same initial perturbations (4.5.10), we have from the Lyapunov function (4.5.7) the following estimate for the radial velocity perturbations:

$$\dot{R}^2 < B\dot{\theta}_0^2 + 3\omega^2(A - C)v_0^2.$$

Combining this condition with (4.5.9) (no pitch-over), we find

$$\dot{R}^2 < 3\omega^2(A - C). \quad (4.5.11)$$

(The moments of inertia are divided by the satellite's mass). Radial velocity perturbations result in an ellipticity of the orbit (the ellipticity should be understood in the osculating sense). To estimate this effect, we may approximately apply the formulas of the elliptical theory:  $\dot{R} = R^2 \frac{e \sin v}{P} \omega \approx R_0 \omega e \sin v$ ; here  $P$  is the focal parameter of the orbit,  $v$  the true anomaly,  $e$  the eccentricity. Inequality (4.5.11) is then written as

$$e^2 \sin^2 v < 3 \frac{A - C}{R_0^2};$$

this inequality should be satisfied at any point of the orbit, i. e., for any  $v$ , which leads to the following final estimate for eccentricity perturbations due to the translation—rotation coupling:

$$e^2 < 3 \frac{A - C}{R_0^2}. \quad (4.5.12)$$

If  $A$  and  $C$  are not exceedingly close to each other,  $A - C$  is of the order of  $l^2$ , where  $l$  is the size of the body, so that  $e < \sqrt{3} \left( \frac{l}{R_0} \right)^2$ . For a satellite moving at a height of 630 km above the surface of the Earth ( $R_0 = 7 \cdot 10^6$  m) and having the size  $l \sim 7$  m, the eccentricity perturbations are of the order of  $e \sim 10^{-6}$ .

If only  $\dot{R}_0$  is initially perturbed, we have  $L_0 = \dot{R}_0^2$ , and the condition of no pitch-over (4.5.9) provides us with an estimate of the permissible perturbation in radial velocity:

$$|\dot{R}_0| < \omega \sqrt{3(A - C)}.$$

For a  $\sim 10$  m satellite orbiting with a period of  $\sim 100$  min, we have from this estimate

$$|\dot{R}_0| < 10^{-2} \text{ m/sec} = 1 \text{ cm/sec},$$

which amounts to  $\sim 10^{-6} V_0$ , where  $V_0$  is the unperturbed orbital velocity of the satellite's mass center.

The translation—rotation coupling is thus very weak for real satellites. The permissible deviations from a circular orbit are of the order of the ratio of the satellite size to the distance from the center of attraction. Therefore, although the conditions of stability apply to perturbations in

translational, as well as rotational, motion, we should always keep in mind that the permissible perturbations in translational motion are exceedingly small.

The analysis of the present section leads to the conclusion that relation (4.5.4) is the principal condition of stability. In other possible stable attitudes, rigid restrictions are imposed on the body and on the region of stability (e.g., the body is dynamically symmetric apart from terms of the order of  $\frac{l}{R_0}$  and the regions of stability are of the order of  $\frac{l}{R_0}$ ). The sufficient conditions of stability (4.5.4) should therefore be regarded as fundamental, and this result can be stated as follows:

*The relative equilibrium of a rigid body in a circular orbit in a Newtonian central field is stable if, in unperturbed motion, the largest axis of the ellipsoid of inertia of the body points along the radius-vector of the orbit, the least axis along the normal to the orbital plane, and the medium axis along the tangent to the orbit.*

This sufficient condition of stability is fully consistent with the result obtained for the limited problem (Chapter 2, § 1).

## § 6. ONE PARTICULAR CASE OF TRANSLATIONAL—ROTATIONAL MOTION

Consider the motion of a body whose mass center describes a plane trajectory, the axis  $y'$  of the body pointing invariably along the axis  $\bar{Y}$  perpendicular to the orbital plane. It is easily seen that this motion is possible if  $\frac{\partial U}{\partial y'} \equiv 0$ . Then

$$y' = 0, \quad q = r = 0, \quad M_x = M_z = 0.$$

In the plane problem, we may take  $\gamma'' = \cos \Theta, \gamma = -\sin \Theta$ , where  $\Theta$  is the angle between the radius-vector of the mass center and the axis of the body. Then  $U = U(\Theta, R)$ . Equations (4.1.2) then reduce to a single equation

$$B \frac{d}{dt} (\dot{\Theta} + \dot{\varphi}_R) - \frac{\partial U}{\partial \Theta} = 0. \quad (4.6.1)$$

Here  $\dot{\varphi}_R$  is the orbital velocity of the satellite's mass center. This equation can be supplemented with two integrals of motion, (4.1.5) and (4.1.7). For the plane case, these integrals are written as

$$\frac{1}{2} M (\dot{R}^2 + R^2 \dot{\varphi}_R^2) + \frac{1}{2} B (\dot{\Theta} + \dot{\varphi}_R)^2 - U(R, \Theta) = h, \quad (4.6.2)$$

$$MR^2 \dot{\varphi}_R + B (\dot{\Theta} + \dot{\varphi}_R) = L_2. \quad (4.6.3)$$

The set (4.6.1)—(4.6.3) is closed in the unknown variables  $R, \Theta, \varphi_R$ . In certain bodies,  $U$  does not depend on  $\Theta$  (e.g., a body of revolution of uniform density which, in virtue of the condition  $\frac{\partial U}{\partial y'} = 0$ , is also symmetric about the orbital plane). Then  $\frac{\partial U}{\partial \Theta} = 0$ ; from (4.6.1) we have  $\dot{\Theta} + \dot{\varphi}_R = \text{const}$ , and then from (4.6.2) and (4.6.3),

$$\frac{1}{2} (\dot{R}^2 + R^2 \dot{\varphi}_R^2) - U(R) = h_0, \quad R^2 \dot{\varphi}_R = K_0. \quad (4.6.4)$$

The body rotates uniformly about the inertial axis perpendicular to the orbital plane; the orbit is not influenced by the spin, but it depends on the body shape via  $U$ . Equations (4.6.4) are integrated in the ordinary way: the trajectory is obtained by inverting the integral

$$\varphi_R - \varphi_{R0} = \int \frac{\frac{K_0}{R} dR}{\sqrt{2h_0 R^2 + 2U(R)R^2 - K_0^2}}, \quad (4.6.5)$$

and subsequent integration of the second equation in (4.6.4) gives the law of motion. To consider a particular case, take the approximate potential (4.2.7) ( $x'_0 = y'_0 = z'_0 = 0$ ). If  $A \neq B \neq C \neq A$ , equations (4.6.1)–(4.6.3) take the form

$$\left. \begin{aligned} & B \frac{d}{dt}(\dot{\theta} + \dot{\varphi}_R) + 3 \frac{\mu}{R^3}(A - C) \sin \theta \cos \theta = 0, \\ & \frac{1}{2} M(\dot{R}^2 + R^2 \dot{\varphi}_R^2) + \frac{1}{2} B(\dot{\theta} + \dot{\varphi}_R)^2 - \frac{\mu M}{R} - \\ & - \frac{1}{2} \frac{\mu}{R^3} (\sin^2 \theta (B+C-2A) + \cos^2 \theta (B+A-2C)) = h, \\ & MR^2 \ddot{\varphi}_R + B(\dot{\varphi}_R + \dot{\theta}) = L_2. \end{aligned} \right\} \quad (4.6.6)$$

In a dynamically symmetric case  $A = C$ , we have

$$\left. \begin{aligned} & \dot{\theta} + \dot{\varphi}_R = \text{const}, \\ & \frac{1}{2} M(\dot{R}^2 + R^2 \dot{\varphi}_R^2) - \frac{\mu M}{R} - \frac{1}{2} \frac{\mu}{R^3} (B - A) = h_0, \\ & MR^2 \dot{\varphi}_R = K_0. \end{aligned} \right\} \quad (4.6.7)$$

The equations are formally identical with the equations of motion of an equatorial satellite (see Appendix 2) and they are integrated by the same technique. The qualitative effects governing the orbital motion of the mass center of this body are therefore indistinguishable from the orbital effects of an equatorial satellite: the two differ only in the respective quantitative characteristics. The principal feature of an equatorial satellite, which is not observed in a Newtonian central field, is the secular motion of the perigee at a rate of

$$\Delta\omega_\pi = 2\pi \bar{\varepsilon} \frac{R_e^2}{P^2} \quad (4.6.8)$$

per one orbital revolution of the satellite.

In (4.6.8),  $R_e$  is the equatorial radius of the Earth,  $\bar{\varepsilon}$  a parameter determined by the Earth's flattening,  $P$  the focal parameter of the orbit. Formula (4.6.8) is an approximate expression to first order in  $\bar{\varepsilon}$ ; it is furthermore implied that  $\bar{\varepsilon} \ll e$ , where  $e$  is the eccentricity. (In a more general case, the motion should be calculated directly from the general formulas.)

For our particular problem, formula (4.6.8) is equivalent to

$$\Delta\omega_\pi = 3\pi \frac{B - A}{MP^2}. \quad (4.6.9)$$

Let us work out the following example. A satellite with a mass  $M = 1000 \text{ kg}$  and  $B - A = 49 \cdot 10^3 \text{ kg} \cdot \text{m}^2$  (e.g., a dumbbell with a halflength  $l = 7 \text{ m}$  and a halfmass  $\frac{M}{2} = 500 \text{ kg}$ ) moves in an orbit with a focal parameter  $P = 7 \cdot 10^6 \text{ m}$ . Then  $\Delta\omega_\pi = 3\pi \cdot 10^{-12}$  per one revolution of the satellite, which

approximately amounts to 2" in 100 years. We see that the orbital perturbations due to the particular shape of the satellite are so small that, say, Einstein's relativistic effects may be much greater. It is proved in the general theory of relativity (see, e.g., [68], p. 292), that the pericenters of heavenly bodies experience the following displacement per one orbital revolution:

$$\Delta\omega_{\text{er}} = \frac{6\pi\alpha_g}{P}, \quad \alpha_g = \frac{fM_0}{c^2}. \quad (4.6.10)$$

Here  $\alpha_g$  is the so-called gravitational radius,  $M_0$  the mass of the central body,  $c$  the velocity of light,  $f$  the gravitational constant;  $\alpha_g$  is small in comparison with the size of the body. For the Earth,  $\alpha_g = 0.443 \text{ cm} = 4.43 \cdot 10^{-3} \text{ m}$ . Comparing (4.6.10) with (4.6.9), we have

$$\frac{\Delta\omega_{\text{er}}}{\Delta\omega_{\text{R}}} = \frac{4\alpha_g MP}{B - A}. \quad (4.6.11)$$

For the purpose of estimates it suffices to take  $B - A \approx Ml^2$ , where  $l$  is the size of the satellite (this is exactly so for the dumbbell); then

$$\frac{\Delta\omega_{\text{er}}}{\Delta\omega_{\text{R}}} = 2 \frac{\alpha_g P}{l^2}.$$

For  $P = 7 \cdot 10^6 \text{ m}$  and  $l_0 = 7 \text{ m}$ , we have  $\frac{\Delta\omega_{\text{er}}}{\Delta\omega_{\text{R}}} \approx 1.3 \cdot 10^3$ , i.e., the relativistic effect is 1000 times as large as the shape effect; for these effects to be comparable, the gravitational radius  $\alpha_g$  must be in the same proportion to the size of the body  $l$  as the size of the body is to the dimensions of the orbit, i.e.,  $\frac{\alpha_g}{l} \sim \frac{l}{P}$ ; then  $l^2 \sim \alpha_g P$ . Let  $l^2 = 2\alpha_g P$ , and let  $P = 7 \cdot 10^6 \text{ m}$ . Then  $l \approx 250 \text{ m}$ . For satellites measuring a few hundreds of meters (orbiting stations), the relativistic effects are thus comparable with the shape effects (for the particular orbit used in the example). As the orbit increases, the body for which the relativistic and the shape effects are comparable also becomes larger.

For the Moon, the shape effect is several times greater than the relativistic effect. V.T. Kondurar' observed that the perturbations introduced in the lunar motion by its "shape effect" are of the same order of magnitude as some of the effects considered in the modern theory of the Moon.

## *Chapter 5*

### ***PERTURBED ROTATIONAL MOTION OF A SATELLITE AND EQUATIONS IN OSCULATING ELEMENTS***

#### **§ 1. PERTURBED ROTATIONAL MOTION AND A METHOD OF ITS ANALYSIS**

If the rotational kinetic energy of a satellite is much greater than the work done by the perturbing forces, the motion is nearly unperturbed over short periods of time. Over fairly long periods, however, the action of small perturbing torques may prove to be cumulative, so that the perturbation grows and a certain evolution of motion sets in. To permit effective analysis of the perturbed rotation of a satellite, it is best to apply the method of variation of constants (which is analogous to the method of osculating elements used in the analysis of orbital perturbations in celestial mechanics). The constant parameters — integrals of unperturbed motion — are regarded as variables in the perturbed case, and differential equations among these parameters are sought.

The unperturbed rotation of a satellite about its center of mass is described by Euler—Poinsot equations. Geometrically, this motion may be interpreted as the rolling of a triaxial ellipsoid of inertia around the angular momentum vector on a fixed plane perpendicular to this vector /1/.

The analysis is considerably simplified if the ellipsoid of inertia is an ellipsoid of revolution. This case of a dynamically symmetric space vehicle is often encountered in practice.

In the following we shall mainly deal with dynamically symmetric satellites, incidentally touching upon some results which apply to satellites without dynamic symmetry.

The unperturbed motion of a dynamically symmetric satellite is regular precession: the magnitude  $L$  of the angular momentum vector, its two angular coordinates  $\rho, \sigma$ , the nutation angle  $\theta$ , the angular velocities of precession and spin  $\dot{\psi}, \dot{\varphi}$ , and also the axial component  $r = \dot{\varphi} + \dot{\psi} \cos \theta$  of the angular velocity are all constant (the angles  $\rho, \sigma, \theta, \psi, \varphi$  are defined in § 1 of Chapter 1). These parameters can be conveniently adopted as the osculating elements of the perturbed motion.

The first three elements describe the variation of the angular momentum vector, the other elements describe the motion around the angular momentum vector. The angular velocities  $\dot{\psi}$  and  $\dot{\varphi}$  of precession and spin can be replaced with the angles  $\psi$  and  $\varphi$  as osculating elements, since in regular precession these angles vary linearly in time. If the external torques are  $\varphi$ -independent, the osculating element  $\varphi$  can be conveniently replaced with the projection  $r$  of the total angular velocity on the satellite's axis of symmetry.

## § 2. SOME PROBABILITY CHARACTERISTICS OF UNPERTURBED MOTION

A satellite, when released by the launching rocket, acquires a certain random angular velocity of spin relative to its center of mass due to the impulsive force applied by the injection mechanism. It would be interesting to consider the probability characteristics of the resulting regular precession of the orbiting satellite. The actual rotation is determined by the magnitude of the nutation angle  $\vartheta$ . If  $\vartheta$  is close to zero, the satellite spins about its symmetry axis; for  $\vartheta$  close to  $90^\circ$ , the satellite "tumbles".

Let the random angular momentum acquired by the satellite on injection have the components  $A p_0 = \xi$ ,  $A q_0 = \eta$ ,  $C r_0 = \zeta$  along the principal central axes of inertia. The angle  $\vartheta$  is a function of random variables:

$$\cos \vartheta = \frac{C r_0}{L}, \quad L = \sqrt{A^2 p_0^2 + A^2 q_0^2 + C^2 r_0^2}.$$

Let the random variables  $\xi$ ,  $\eta$ ,  $\zeta$  be independent, with normal distributions and zero mathematical expectations. The probability distribution densities of these random variables are written as

$$P_\xi(z) = \frac{1}{\sqrt{2\pi}\sigma_2} e^{-\frac{z^2}{2\sigma_2^2}}, \quad P_\eta(y) = \frac{1}{\sqrt{2\pi}\sigma_1} e^{-\frac{y^2}{2\sigma_1^2}},$$

$$P_\zeta(x) = \frac{1}{\sqrt{2\pi}\sigma_1} e^{-\frac{x^2}{2\sigma_1^2}}.$$

Here  $\sigma_1^2$ ,  $\sigma_2^2$  are the variances.

The probability that  $\cos \vartheta$  is not greater than a certain  $\tau$  is specified by the integral

$$P(\cos \vartheta < \tau) = \frac{1}{(2\pi)^{\frac{3}{2}}} \int_{z_1}^{\infty} \int_{y_1}^{\infty} \int_{x_1}^{\infty} e^{-\frac{x_1^2+y_1^2+z_1^2}{2}} dx_1 dy_1 dz_1.$$

$$\frac{\sqrt{(x_1^2+y_1^2)k^2+z_1^2}}{\sqrt{(x_1^2+y_1^2)k^2+z_1^2}} < \tau$$

Here

$$x_1 = \frac{x}{\sigma_1}, \quad y_1 = \frac{y}{\sigma_1}, \quad z_1 = \frac{z}{\sigma_2}.$$

Note that  $k = \frac{\sigma_1}{\sigma_2} = \frac{A[p_0]}{C[r_0]}$ , where  $[p_0]$  and  $[r_0]$  are the permissible spread of the transverse and the longitudinal angular velocities. This integral can be easily evaluated by writing the integrand in spherical coordinates. For the probability  $P$  and the probability distribution density  $p = \frac{dP}{d\tau}$  we have

$$P(\cos \vartheta < \tau) = \frac{1}{2} \left[ 1 + \frac{k\tau}{\sqrt{1-(1-k^2)\tau^2}} \right],$$

$$p(\tau) = \frac{1}{2} \frac{k}{[1-\tau^2(1-k^2)]^{\frac{3}{2}}}.$$

Let us consider the density graphs  $p(\tau)$  for various  $k$  (Figure 30). For  $k > 1$ , the graphs are peaked around  $\tau = 0$ . The probability that the angle  $\theta$  will lie in a certain interval near  $\theta = 90^\circ$  is therefore higher than the probability of this angle falling in the same interval near  $\theta = 0$ ; this preference becomes more pronounced as  $k$  increases. The probability is therefore high that the satellite will tumble, rather than spin. For  $k = 1$ , all values in the interval  $-1 < \tau < 1$  are equiprobable. For  $k < 1$ ,  $\tau$  with absolute values close to 1 are the more probable, which corresponds to spinning motion. Note that for comparable  $[p_0]$ ,  $[r_0]$ , the cases  $k \gg 1$  and

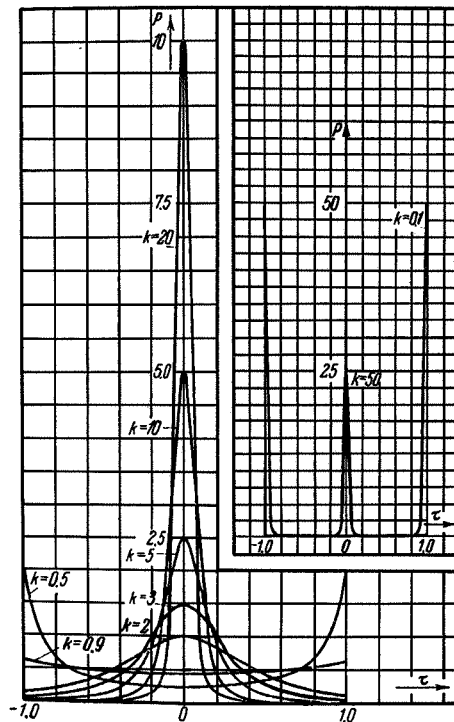


FIGURE 30. Probability distribution density of the random variable  $\tau = \cos \theta$ .

$k < 1$  correspond to the momental ratios  $\frac{A}{C} \gg 1$ ,  $\frac{A}{C} < 1$ . We may therefore say that a dynamically prolate satellite will probably tumble, while a dynamically oblate satellite will probably spin. Oblate satellites, as we shall show in the next chapters, are more stable than prolate bodies in the case of perturbed motion also: dissipative forces reduce the angle  $\theta$ , so that prolate satellites tend to pitch over.

Consider the graph (Figure 31) of the integrated characteristic  $P(\cos \theta < \cos 85^\circ)$ , i.e., the probability of the event  $85^\circ \leq \theta \leq 95^\circ$ . We see that for large  $k$  the tumble probability is close to unity. For  $k = 18$ , e.g., we have  $P = 0.73$ , and for  $k = 28$ , no less than  $P = 0.93$ . Figure 32 gives the values of the increment  $\Delta\theta(k)$ , defining the interval  $90^\circ - \Delta\theta < \theta < 90^\circ + \Delta\theta$ ,

where the angle  $\vartheta$  falls with a known probability  $P_0 = 0.95$ . We see that  $85^\circ \leq \vartheta \leq 95^\circ$  with this probability for  $k = 32.5$ .

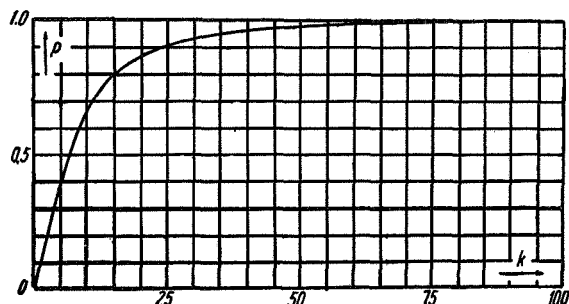


FIGURE 31. The probability  $P$  of the event  $85^\circ \leq \vartheta \leq 95^\circ$ .

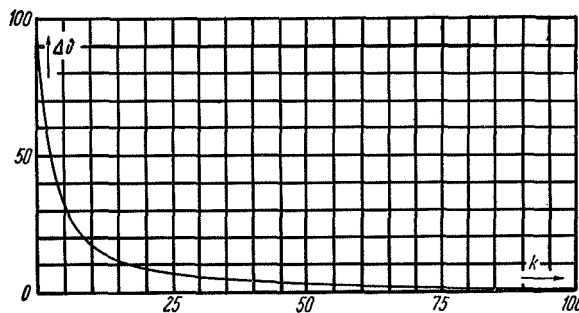


FIGURE 32. The values of the random variable  $\Delta\vartheta$  ( $\theta = 90^\circ \pm \Delta\vartheta$ ) with a probability  $P = 0.95$ .

The probability characteristics of other parameters may be calculated in the same way. It can be shown, e.g., that for  $\sigma_1^2 = \sigma_2^2$ , the mathematical expectation of the angular velocity of precession is given by  $M = \frac{4}{\sqrt{2\pi}} [p_0]$ .

### § 3. PERTURBED MOTION. EQUATIONS IN OSCULATING ELEMENTS

As we have observed in § 1 of this chapter, the following variables may be assumed as the osculating elements

$$L, \rho, \sigma, \vartheta, \psi(\dot{\psi}), \varphi(\dot{\varphi} \text{ or } r). \quad (5.3.1)$$

Consider a satellite acted upon by an external perturbing torque  $M$ . Then, according to the theorem of the angular momentum, we have for the components along the axes  $XYZ$  of the "perigee" system (see § 1, Chapter 1)

$$\frac{dL_X}{dt} = M_X, \quad \frac{dL_Y}{dt} = M_Y, \quad \frac{dL_Z}{dt} = M_Z. \quad (5.3.2)$$

Applying table (1.1.4), we write

$$L_x = L \sin \rho \sin \sigma, \quad L_y = L \cos \rho, \quad L_z = L \sin \rho \cos \sigma. \quad (5.3.3)$$

Differentiating (5.3.3) and applying (5.3.1), we solve the resulting set of equations for  $L$ ,  $\rho$ ,  $\sigma$  to obtain the first group of equations in osculating elements, namely the first three equations of the set (5.3.6) given below. The second group of equations is obtained proceeding from the following principle: the direction cosines of the body axes relative to the fixed axes and the time derivatives of these direction cosines should have the same expressions in terms of the osculating variables in cases of unperturbed and perturbed motion.

The position of the body axes  $Ox'y'z'$  relative to the fixed axes  $OXYZ$  is determined by a table of direction cosines from § 1 of Chapter 1.

Let  $z'$  be the axis of dynamic symmetry of the satellite, and let  $p$ ,  $q$ ,  $r$  be the projections of the absolute angular velocity of rotation of the satellite on the axes  $x'$ ,  $y'$ ,  $z'$ , respectively. Then we have Poisson's kinematic relations

$$\dot{a}_3 = qa_1 - pa_2, \quad \dot{\beta}_3 = q\beta_1 - p\beta_2, \quad \dot{\gamma}_3 = q\gamma_1 - p\gamma_2.$$

Seeing that the transverse moments of inertia are equal ( $A=B$ ), the right-hand sides of the Poisson relations can be expressed in terms of the components of the angular momentum  $L$  along the fixed axes  $X$ ,  $Y$ ,  $Z$ . After simple manipulations, we obtain

$$\left. \begin{aligned} \frac{da_3}{dt} &= \frac{1}{A} [L_y \gamma_3 - L_z \beta_3], & \frac{d\beta_3}{dt} &= \frac{1}{A} [L_z a_3 - L_x \gamma_3], \\ \frac{d\gamma_3}{dt} &= \frac{1}{A} [L_x \beta_3 - L_y a_3]. \end{aligned} \right\} \quad (5.3.4)$$

Substituting (5.3.3) and (1.1.6) in (5.3.4), and also inserting  $\dot{\sigma}$  and  $\dot{\rho}$  from the first group of equations in osculating elements, we obtain a set of three equations in two unknowns  $\dot{\psi}$ ,  $\dot{\phi}$ . The set is uniquely solvable, since only two of the three starting equations are independent. For  $\dot{\psi}$ , e.g., we find an equation which is included without modification in (5.3.6) below. The equation for  $\dot{\phi}$  has the form

$$\dot{\phi} = \frac{1}{L} [M_x (\cos \sigma \cos \psi - \sin \sigma \cos \rho \sin \psi) + M_y \sin \psi \sin \rho - M_z (\sin \sigma \cos \psi + \cos \sigma \cos \rho \sin \psi)]. \quad (5.3.5)$$

The osculating element  $\dot{\phi}$ , however, is more conveniently determined from the finite kinematic relation  $\cos \theta = \frac{Cr}{L}$ , which applies for perturbed, as well as unperturbed, motion; this relation can also be obtained by integrating the equations in osculating elements with the aid of (5.3.5). Then  $r$  is treated as an osculating element; the corresponding equation in (5.3.6) is simply one of Euler's dynamic equations for the case  $A=B$ .

Finally, if the torques depend on  $\varphi$ , the equations are closed by a kinematic relation which defines the projection  $r$  of the total angular velocity on the satellite's axis of symmetry. The complete system of equations in osculating elements for a dynamically symmetric satellite is thus written

in the form

$$\left. \begin{aligned} \dot{L} &= (M_X \sin \sigma + M_Z \cos \sigma) \cos \rho + M_Y \cos \rho, \\ \dot{\rho} &= \frac{1}{L} [(M_X \sin \sigma + M_Z \cos \sigma) \cos \rho - M_Y \sin \rho], \\ \dot{\sigma} &= \frac{1}{L \sin \rho} (M_X \cos \sigma - M_Z \sin \sigma), \\ \dot{\psi} &= \frac{L}{A} + \frac{1}{L} \{-M_X [\operatorname{ctg} \vartheta (\cos \sigma \sin \psi + \\ &\quad + \sin \sigma \cos \rho \cos \psi) + \operatorname{ctg} \rho \cos \sigma] + \\ &\quad + M_Y \sin \rho \operatorname{ctg} \vartheta \cos \psi + M_Z [\operatorname{ctg} \vartheta (\sin \sigma \sin \psi - \\ &\quad - \cos \sigma \cos \rho \cos \psi) + \operatorname{ctg} \rho \sin \sigma]\}, \\ \dot{\vartheta} &= r - \dot{\psi} \cos \vartheta - \dot{\sigma} (-\sin \psi \sin \vartheta \sin \rho + \\ &\quad + \cos \vartheta \cos \rho) + \dot{\rho} \cos \psi \sin \vartheta, \\ \dot{r} &= \frac{1}{C} [M_X \alpha_3 + M_Y \beta_3 + M_Z \gamma_3], \quad \cos \vartheta = \frac{Cr}{L}. \end{aligned} \right\} \quad (5.3.6)$$

Here  $\alpha_3, \beta_3, \gamma_3$  are defined by (1.1.6). Since in rotational motion we often have  $\frac{L}{A} \gg \frac{|M|}{L}$ , the following approximate formula can be applied for the rate of precession:  $\dot{\psi} \approx \frac{L}{A}$ ; this formula is exact in the case of unperturbed motion.

The set of equations in osculating elements can be differently assembled for different particular problems. For example, equations (5.3.2) are sometimes more convenient than the first three equations in (5.3.6); the last two equations in (5.3.6) are of course equivalent to a single equation (5.3.5) in  $\vartheta$ . The set (5.3.6) contains six differential equations and one finite relation and it is thus a system of sixth order. If the torques are  $\varphi$ -independent, the set (5.3.6) reduces to a system of fifth order and a separate equation for  $\varphi(t)$ . On the whole, this set of differential equations of motion of a satellite about its mass center in osculating elements is by no means simpler than the set of Euler's equations. The advantage of the set (5.3.6) is that it is eminently suitable for the application of approximate methods of analysis (asymptotic methods /22/, special numerical integration techniques /61/), permitting fairly simple and accurate investigation of the qualitative and quantitative characteristics of motion.

#### § 4. THE CASE OF PERTURBATIONS HAVING A FORCE FUNCTION

**1. Equations of motion and their first integrals.** It follows from the results of Chapter 1 that gravity torques have a force function which depends only on the attitude of the axis of symmetry of the body in space. This property also applies for the conservative part of the aerodynamic torques, for the magnetic torques, radiation torques, and some other torques. In this important particular case, equations (5.3.6) may be simplified, so that the approximate methods of analysis are directly applicable to the equations, without the introduction of particular expressions for the torques.

Consider perturbing torques described by the force function

$$U = U[\alpha_3, \beta_3, \gamma_3, v(t)]. \quad (5.4.1)$$

Here  $\nu$  is the true anomaly. The torque components along the fixed axes are

$$\left. \begin{aligned} M_x &= \frac{\partial U}{\partial \gamma_3} \beta_3 - \frac{\partial U}{\partial \beta_3} \gamma_3, & M_y &= \frac{\partial U}{\partial \alpha_3} \gamma_3 - \frac{\partial U}{\partial \gamma_3} \alpha_3, \\ M_z &= \frac{\partial U}{\partial \beta_3} \alpha_3 - \frac{\partial U}{\partial \alpha_3} \beta_3. \end{aligned} \right\} \quad (5.4.2)$$

Substituting (5.4.2) and (1.1.6) in equations (5.3.6) in osculating elements and seeing that

$$\frac{\partial \alpha_3}{\partial \rho} = \beta_3 \sin \sigma, \quad \frac{\partial \beta_3}{\partial \rho} = -\alpha_3 \sin \sigma - \gamma_3 \cos \sigma, \quad \frac{\partial \gamma_3}{\partial \rho} = \beta_3 \cos \sigma$$

etc., we obtain the following complete system of equations in osculating elements:

$$\left. \begin{aligned} \dot{L} &= \frac{\partial U}{\partial \psi}, & \dot{\rho} &= \frac{1}{L \sin \rho} \left\{ \frac{\partial U}{\partial \psi} \cos \rho - \frac{\partial U}{\partial \sigma} \right\}, & \dot{\sigma} &= \frac{1}{L \sin \rho} \frac{\partial U}{\partial \rho}, \\ \dot{\psi} &= \frac{L}{A} - \frac{1}{L} \left\{ \frac{\partial U}{\partial \rho} \operatorname{ctg} \rho + \frac{\partial U}{\partial \theta} \operatorname{ctg} \theta \right\}, & \dot{r} &= 0, & \cos \theta &= \frac{Cr}{L}. \end{aligned} \right\} \quad (5.4.3)$$

Since  $U$  is  $\varphi$ -independent, the equation for  $\varphi$  need not be written. The motion has a first integral

$$r = r_0 \quad (5.4.4)$$

so that (5.4.3) is a system of fourth order.

From (5.3.5) we have the obvious differential equation for  $\theta$ :

$$\dot{\theta} = \frac{1}{L} \operatorname{ctg} \theta \frac{\partial U}{\partial \psi}. \quad (5.4.5)$$

The set (5.4.3) may have other first integrals, aside from (5.4.4). Indeed, from (5.4.3) we have  $\frac{d}{dt}(L^2 - 2AU) = -\frac{\partial}{\partial t}(2AU)$ . In some problems, e.g., the motion of a gyroscope about a fixed point,  $U$  may be time-independent, and we directly obtain the energy integral in the form

$$L^2 - 2AU = \text{const.} \quad (5.4.6)$$

From the first two equations in (5.4.3), we have

$$\frac{d}{dt}(L \cos \rho) = \frac{\partial U}{\partial \sigma}. \quad (5.4.7)$$

Suppose that the dependence of  $U$  on the time  $t$  and the coordinate  $\sigma$  can be expressed in terms of a single parameter  $\kappa = \sigma - \omega_0 t$ , where  $\omega_0 = \text{const}$ . This particular case is encountered, e.g., in connection with the motion in a circular orbit ( $\omega_0$  being the angular velocity of the mass center in the circular orbit). An analogous case can be easily constructed for an elliptical orbit also. Then  $\frac{\partial U}{\partial t} = -\omega_0 \frac{\partial U}{\partial \sigma}$ , and from the foregoing formulas we have a Jacobi integral

$$L^2 - 2AU - 2A\omega_0 L \cos \rho = \text{const.} \quad (5.4.8)$$

Equations (5.4.3) are suitable for the analysis of oscillations, as well as spin. Let  $r_0 = 0$ , then  $\cos \vartheta = 0$  and  $U$  is  $\vartheta$ -independent. We may seek a solution such that  $\rho = 0$ ,  $\sigma = \sigma_0 = \text{const}$ ; this is possible if certain conditions are imposed on  $U$ , specifically, if  $\frac{1}{\sin \rho} \frac{\partial U}{\partial \rho} \Big|_{\substack{\rho=0 \\ \vartheta=\frac{\pi}{2}}} = 0$ . We are then left with the two equations  $\dot{\psi} = \frac{L}{A}$ ,  $\dot{L} = \frac{\partial U}{\partial \psi}$ , which give

$$\ddot{\psi} - \frac{1}{A} \frac{\partial U}{\partial \psi} = 0.$$

This is an equation of plane oscillations in the orbital plane.

**2. The analysis of equations in the case of fast spin.** The particular choice of the variables makes equations (5.4.3) highly convenient for the analysis of motion of a spinning satellite. Various approximate methods, e.g., the Bogolyubov-Krylov technique (Volosov's scheme /22/), can be easily applied to these equations. For fast spin, i.e., when  $L$  is large,  $\psi$  increases almost uniformly and fairly rapidly (not only in comparison with the rate of change in the osculating elements, but also, by assumption, in comparison with the orbital velocity  $v$  of the mass center). Therefore, to bring out the principal effects of motion (secular, long-periodic, and periodic), the equations of motion should be preferably averaged over the fast variable  $\psi$ . Averaging, say, in the first equation of (5.4.3) and seeing that, according to (5.4.1) and (1.1.6),  $U$  is a periodic function of  $\psi$ , with a period of  $2\pi$ , we obtain for the smoothed motion

$$\dot{L} = \frac{1}{2\pi} \int_0^{2\pi} \frac{\partial U}{\partial \psi} d\psi = \frac{1}{2\pi} [U(2\pi) - U(0)] = 0,$$

i.e.,  $L = L_0$  and therefore  $\cos \vartheta = \cos \vartheta_0$ . Moreover,

$$\dot{\rho} = -\frac{1}{L_0 \sin \rho} \frac{\partial \bar{U}}{\partial \sigma}, \quad \dot{\sigma} = \frac{1}{L_0 \sin \rho} \frac{\partial \bar{U}}{\partial \rho}, \quad \bar{U} = \frac{1}{2\pi} \int_0^{2\pi} U d\psi, \quad (5.4.9)$$

$$\dot{\psi} = \frac{L_0}{A} - \frac{1}{L_0} \left\{ \frac{\partial \bar{U}}{\partial \rho} \operatorname{ctg} \rho + \frac{\partial \bar{U}}{\partial \vartheta} \operatorname{ctg} \vartheta \right\} \approx \dot{\psi}_0. \quad (5.4.10)$$

In other words, *the satellite executes regular precession with an almost constant angular velocity (5.4.10) around the vector of angular momentum, which remains constant in magnitude, its direction in space varying according to equations (5.4.9).*

We see that the problem of the evolution of motion thus reduces to the investigation of the small set of two equations (5.4.9), which are easily written in the canonical form. Note that the averaging of the right-hand sides in the equations of motion (5.4.3) turned out to be equivalent to the averaging of the force function. Equations (5.4.9) are invariant under the transformation  $\rho, \sigma \rightarrow \theta, \lambda$  (the angles  $\theta, \lambda$  are defined in § 1 of Chapter 1) or under any similar transformation. We shall take the satellite to move in an unperturbed elliptical orbit, and applying (2.3.2), we change over from  $t$  to a new independent variable,  $v$ . Consider the function  $U_v$  and its

$\psi$ -average:

$$U_v = \frac{P^2}{\sqrt{\mu P} (1 + e \cos v)^2} U, \quad \bar{U}_v = \frac{1}{2\pi} \int_0^{2\pi} U_v d\psi. \quad (5.4.11)$$

Equations (5.4.9) are then written as

$$\frac{dp}{dv} = -\frac{1}{L_0 \sin \rho} \frac{\partial \bar{U}_v}{\partial \sigma}, \quad \frac{d\sigma}{dv} = \frac{1}{L_0 \sin \rho} \frac{\partial \bar{U}_v}{\partial p}. \quad (5.4.12)$$

Mechanically, averaging over  $\psi$  is equivalent to ignoring high-frequency oscillations of extremely small amplitude which are superimposed in the solution on the comparatively smooth oscillations described by (5.4.12). The high-frequency oscillations attributable to  $\psi$  will be called vibrational oscillations. Equations (5.4.12) in general are not integrable, since  $U$  depends on  $v$ . These equations describe extremely slow secular and long-periodic effects, as well as periodic effects attributable to  $v$ . The period of these oscillations is comparable with the orbital period of the satellite.

Secular and long-periodic terms vary extremely slowly in comparison with the orbital period of the satellite's mass center. To bring out these slow effects, the equations of motion must be averaged over  $v$ , as well as over  $\psi$ . Independent averaging over each phase variable ( $\psi, v$ ) separately is permissible if the frequencies of these two variables are incommensurate (which is assumed to apply in our case). This double averaging of equations (5.4.3) then reduces to the averaging of equations (5.4.12) over  $v$ . Thus

$$\left. \begin{aligned} \frac{dp}{dv} &= -\frac{1}{L_0 \sin \rho} \frac{\partial \bar{U}_v}{\partial \sigma}, & \frac{d\sigma}{dv} &= \frac{1}{L_0 \sin \rho} \frac{\partial \bar{U}_v}{\partial p}, \\ \bar{U}_v &= \frac{1}{(4\pi)^2} \int_0^{2\pi} \int_0^{2\pi} \frac{P^2}{\sqrt{\mu P} (1 + e \cos v)^2} U d\psi dv. \end{aligned} \right\} \quad (5.4.13)$$

In (5.4.13)  $\bar{U}_v$  is no longer dependent on  $v$ , and equations (5.4.13) therefore have the first integral

$$\bar{U}_v(\rho, \sigma) = \text{const}, \quad (5.4.14)$$

which describes the trajectory of the angular momentum vector (in its secular and long-periodic motion). Applying (5.4.14), we can complete the integration of equations (5.4.13), the final result being the law of motion of the angular momentum vector.

The solution of equations (5.4.12) is accurate at least to the next higher approximation than the solution of equations (5.4.13). There is an interesting particular case, which is sometimes encountered in practice, when equations (5.4.12) can also be integrated directly. Let the dependence of  $U_v$  on  $\sigma$  and  $v$  be expressible in terms of the parameter  $\kappa_v = \sigma - v$ , so that  $\bar{U}_v = \bar{U}_v(\rho, \kappa_v)$ . The coordinate  $\kappa_v$  is the angle between the current radius-vector  $r$  and the projection of the vector  $L$  on the orbital plane. The angles  $\rho, \kappa_v$  thus define the position of the vector  $L$  in the rotating system of axes  $n, \tau, r$  where  $n$  points along the normal to the orbital plane and  $\tau$  along the transversal. Equations (5.4.12) are written as

$$\frac{dp}{dv} = -\frac{1}{L_0 \sin \rho} \frac{\partial \Phi}{\partial \kappa_v}, \quad \frac{d\kappa_v}{dv} = \frac{1}{L_0 \sin \rho} \frac{\partial \Phi}{\partial p}, \quad \Phi = L_0 \cos \rho + \bar{U}_v. \quad (5.4.15)$$

Since  $\Phi$  is a function of  $\rho$  and  $\sigma$ , only and does not depend on  $v$ , equations (5.4.15) have a first integral which describes the trajectory of the vector  $L$  in the rotating system of axes:

$$\Phi = \text{const.} \quad (5.4.16)$$

This integral enables the integration of (5.4.15) to be completed. It may be regarded as a corollary of (5.4.8) for  $L=L_0$ . We shall show in the following that the equations of motion with gravity and aerodynamic perturbations (but only in a circular orbit), and the equations of motion with solar radiation perturbations for an arbitrary elliptical orbit around the Sun can all be reduced to the form (5.4.15).

The averaging technique is also useful in the general case of equations (5.3.6) (when the torques are arbitrary, without a force function). This method is applied in the following to analyze the secular perturbations due to the dissipative torques produced by aerodynamic friction and eddy currents.

## § 5. EQUATIONS FOR A DYNAMICALLY ASYMMETRIC BODY

We have until now dealt with equations in osculating elements for a dynamically symmetric body. In the general case of a triaxial ellipsoid of inertia ( $A \neq B \neq C$ ), fast spin is also conveniently treated in terms of the same variables  $L$ ,  $\rho$ ,  $\sigma$ ,  $\psi$ ,  $\theta$ ,  $\phi$ , which we have originally introduced for a dynamically symmetric body. The derivation of the corresponding equations is given by F. L. Chernous'ko /71/. Let

$$\left. \begin{aligned} M_1 &= (M_x \sin \sigma + M_z \cos \sigma) \cos \rho - M_y \sin \rho, \\ M_2 &= M_x \cos \sigma - M_z \sin \sigma, \\ M_3 &= (M_x \sin \sigma + M_z \cos \sigma) \sin \rho + M_y \cos \rho. \end{aligned} \right\} \quad (5.5.1)$$

$M_{1,2,3}$  are clearly the projections of the external torque  $M$  on the axes  $L_1$ ,  $L_2$ ,  $L$ , respectively (see Chapter 1, § 1). The orientation of the inertial body axes  $x'$ ,  $y'$ ,  $z'$  relative to the axes  $L_1$ ,  $L_2$ ,  $L$  is defined by the table of direction cosines  $a_{ij}$  (Chapter 1, § 1).

The first group of equations is obviously the same as for a dynamically symmetric body:

$$\frac{dL}{dt} = M_3, \quad \frac{d\rho}{dt} = \frac{M_1}{L}, \quad \frac{d\sigma}{dt} = \frac{M_2}{L \sin \rho}. \quad (5.5.2)$$

The components of the absolute angular velocity  $\omega$  of the satellite along the axes  $x'$ ,  $y'$ ,  $z'$  are

$$\left. \begin{aligned} p &= \dot{\rho} a_{21} + \dot{\sigma} (a_{31} \cos \rho - a_{11} \sin \rho) + \dot{\theta} \cos \varphi + \dot{\psi} a_{31}, \\ q &= \dot{\rho} a_{22} + \dot{\sigma} (a_{32} \cos \rho - a_{12} \sin \rho) - \dot{\theta} \sin \varphi + \dot{\psi} a_{32}, \\ r &= \dot{\rho} a_{23} + \dot{\sigma} (a_{33} \cos \rho - a_{13} \sin \rho) + \dot{\varphi} + \dot{\psi} a_{33}. \end{aligned} \right\} \quad (5.5.3)$$

On the other hand, the corresponding components of the vector  $\mathbf{L}$  are

$$\left. \begin{aligned} L_x &= Ap = L \sin \vartheta \sin \varphi, \\ L_y &= Bq = L \sin \vartheta \cos \varphi, \\ L_z &= Cr = L \cos \vartheta. \end{aligned} \right\} \quad (5.5.4)$$

Substituting  $p, q, r$  from (5.5.3),  $\dot{\rho}, \dot{\sigma}$  from (5.5.2), and  $\alpha_{ij}$  from (1.1.5), we solve the system for  $\dot{\vartheta}, \dot{\varphi}, \dot{\psi}$ :

$$\left. \begin{aligned} \dot{\vartheta} &= L \sin \vartheta \sin \varphi \cos \varphi \left( \frac{1}{A} - \frac{1}{B} \right) + \frac{M_2 \cos \psi - M_1 \sin \psi}{L}, \\ \dot{\varphi} &= L \cos \vartheta \left( \frac{1}{C} - \frac{\sin^2 \varphi}{A} - \frac{\cos^2 \varphi}{B} \right) + \frac{M_1 \cos \psi + M_2 \sin \psi}{L \sin \vartheta}, \\ \dot{\psi} &= L \left( \frac{\sin^2 \varphi}{A} + \frac{\cos^2 \varphi}{B} \right) - \frac{M_1 \cos \psi + M_2 \sin \psi}{L} \operatorname{ctg} \vartheta - \frac{M_2}{L} \operatorname{ctg} \rho. \end{aligned} \right\} \quad (5.5.5)$$

Equations (5.5.2) and (5.5.5) constitute the required closed system of equations in a form which is convenient for the application of asymptotic methods. For  $A=B$ , these equations reduce to equations (5.3.6) for  $\dot{\varphi}$  and  $\dot{\psi}$  and equation (5.3.5) for  $\dot{\vartheta}$ .

## Chapter 6

### GRAVITATIONAL PERTURBATIONS IN ROTATIONAL MOTION

#### § 1. PERMITTED AND FORBIDDEN MOTIONS OF A DYNAMICALLY SYMMETRIC SATELLITE. REGULAR PRECESSIONS IN A GRAVITATIONAL FIELD

1. Preliminary analysis of the permitted and the forbidden regions of motion. Let us consider the conditions for the libration and the rotation of a satellite. We assume a circular orbit. The integral (2.1.11) for a dynamically symmetric satellite ( $A = B, A \neq C$ ) takes the form

$$\frac{2T}{\omega^2(A-C)} = -k + 3\gamma''^2 - \beta''^2, \quad -k = \frac{2T_0}{\omega^2(A-C)} - 3\gamma_0''^2 + \beta_0''^2. \quad (6.1.1)$$

Here  $T$  is the kinetic energy of the satellite's relative rotation (relative to the system connected with the current radius-vector);  $\beta'' = \cos \theta_n$ ;  $\gamma'' = \cos \varepsilon_r$ , where  $\theta_n, \varepsilon_r$  are respectively the angles that the satellite's axis makes with the normal  $\mathbf{n}$  to the orbital plane and with the current radius-vector  $\mathbf{r}$ . The subscript 0 marks the initial values of the corresponding quantities. Since  $T > 0$ , (6.1.1) makes it possible to determine the permitted and the forbidden regions of motion of the satellite's axis.

**Case 1:**  $A > C$  (a dynamically prolate satellite). The permitted region of motion of the satellite's axis is defined by the inequalities

$$-\sqrt{-k + 3\gamma''^2} \leq \beta'' \leq \sqrt{-k + 3\gamma''^2}. \quad (6.1.2)$$

Seeing that  $\beta'' = \cos \theta_n = \cos \chi \sin \varepsilon_r$ , where  $\chi$  is the angular displacement of the satellite's axis around the radius-vector, reckoned from the meridian  $n\mathbf{r}$ , we have

$$-\sin \varepsilon_r < \beta'' < \sin \varepsilon_r, \quad 0 \leq \theta_n \leq \pi, \quad (6.1.3)$$

and the permitted regions of motion of the satellite's axis on the surface of a unit sphere for various  $k$  can be marked on the basis of inequalities (6.1.2)–(6.1.3) (Figure 33); these regions are symmetric about the satellite's orbital plane that they contain. If  $k > 0$ , the permitted motions are confined to a certain neighborhood of the direction  $\pm \mathbf{r}$ . The axis of the satellite as if seeks the radius-vector, and in the particular case  $k = 3$  it constantly points along the radius-vector. For  $0 > k > -1$ , the permitted region is a strip on the surface of the unit sphere in the vicinity of the orbital plane, with the exception of the "caps" near  $\pm \mathbf{n}$ . For  $k < -1$ , the permitted region of motion covers the entire sphere.

Case 2:  $A < C$  (a dynamically oblate satellite). The permitted regions of motion

$$\beta'' > \sqrt{-k+3\gamma''^2} \text{ and } \beta < -\sqrt{-k+3\gamma''^2}$$

are the forbidden regions of the previous case. For  $k=-1$ , the satellite's axis constantly points along the normal to the orbital plane. For  $-1 < k < 0$ , the axis moves near the normal; for  $k \geq 3$ , the permitted region covers the entire unit sphere.

We thus see that in a state of stable relative equilibrium a prolate satellite orients itself along the radius-vector, while an oblate satellite will point its axis along the normal to the orbital plane.

The foregoing analysis for the various possible values of  $k$  (6.1.1) is summarized in Table 5.

TABLE 5

Permitted regions of motion for various  $\frac{2T_0}{\omega^2 |A - C|} = \xi_T$  and constant  $e_r^0, \rho_n^0$

$A > C$		
$0 < \xi_T < 3 \cos^2 e_r^0 - \cos^2 \rho_n^0$	$3 \cos^2 e_r^0 - \cos^2 \rho_n^0 < \xi_T < 3 \cos^2 e_r^0 + \sin^2 \rho_n^0$	$3 \cos^2 e_r^0 + \sin^2 \rho_n^0 < \xi_T$
neighborhoods of $\pm r$	neighborhoods of $\pm n$ excluded	the entire sphere
$A < C$		
$0 < \xi_T < \cos^2 \rho_n^0 - 3 \cos^2 e_r^0 - 3 \cos^2 e_r^0$	$\cos^2 \rho_n^0 - 3 \cos^2 e_r^0 < \xi_T < 3 \sin^2 e_r^0 + \cos^2 \rho_n^0$	$3 \sin^2 e_r^0 + \cos^2 \rho_n^0 < \xi_T$
neighborhoods of $\pm n$	neighborhoods of $\pm r$ excluded	the entire sphere

We see from Table 5 that if  $\xi_T > 4$ , i.e.,

$$T_0 > 2\omega^2 |A - C|, \quad (6.1.4)$$

the permitted region of motion extends over the entire sphere, irrespective of the initial attitude of the axis; otherwise, the permitted regions are variously restricted. This suggests that if condition (6.1.4) does not hold true, the motion is oscillatory in a certain degree (or nearly oscillatory); on the other hand, if condition (6.1.4) is satisfied, the motion can be conveniently interpreted as the perturbation of the regular precession of the satellite. Inequality (6.1.4) therefore provides a certain criterion for the applicability of the approximate methods, e.g., the averaging technique, employed in this book.

If the constant projection  $r_0$  of the total angular velocity on the axis of symmetry identically vanishes ( $r_0 = 0$ ), the permitted regions of motion can be determined with a substantially higher accuracy /75/. Indeed, the

integral (6.1.1) takes the form

$$\frac{2T'}{(A-C)\omega^2} + \frac{C\beta''^2}{(A-C)} = -k + 3\gamma''^2 - \beta''^2, \quad T' > 0.$$

For  $A > C$ , say, the permitted regions are therefore described by the inequalities

$$-\sqrt{(1-\varepsilon)(3\gamma''^2 - k)} < \beta'' < \sqrt{(1-\varepsilon)(3\gamma''^2 - k)}, \quad \varepsilon = \frac{C}{A}.$$

These inequalities clearly define narrower regions than the analogous inequalities of (6.1.2) for  $r_0 \neq 0$ . The qualitative pattern, however, remains the same as in Figure 33.

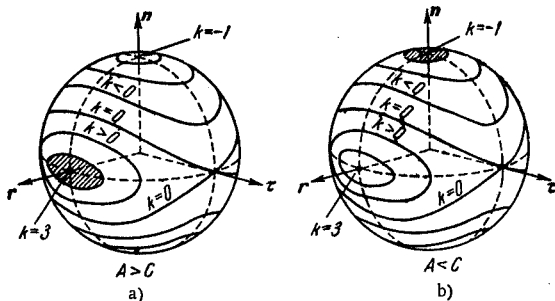


FIGURE 33. Permitted and forbidden regions of motion for the axis of a symmetric satellite in a field of gravity:  $r_0 \neq 0$ .

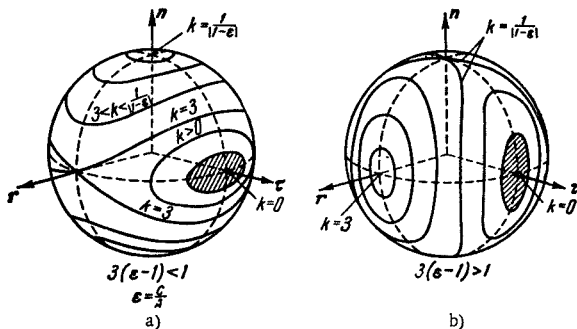


FIGURE 34. Permitted and forbidden regions of motion for the axis of a symmetric satellite in a field of gravity:  $r_0 = 0$ .

For a dynamically oblate satellite ( $A < C$ ), the change in the pattern of permitted motions is more substantial. Indeed, here  $k \geq 0$ , and the permitted regions are defined by the inequalities

$$-\sqrt{(\varepsilon-1)(k-3\gamma''^2)} \leq \beta'' \leq \sqrt{(\varepsilon-1)(k-3\gamma''^2)}. \quad (6.1.5)$$

These regions are marked in Figure 34. The outstanding feature in this case is the existence of a new point of stable equilibrium,  $\gamma'' = \beta'' = 0$ . In

other words, a dynamically oblate satellite in a state of relative equilibrium with its symmetry axis pointing along the tangent to the orbit is stable with respect to perturbations other than rotation about the axis of symmetry (i.e., conserving the condition  $r_0 = 0$ ). This constitutes an addition to the results of Chapter 2. In the plane  $\varepsilon, \delta$  (Figure 21), this conditionally stable relative equilibrium corresponds to the segment  $\varepsilon = \delta$ ,  $\varepsilon < 1$  which lies on the boundary of the region where the necessary conditions of stability are satisfied.\* Returning to conditions (6.1.5), we note that the permitted regions of motion vary according to the magnitude of the parameter  $3(\varepsilon - 1)$ .

(i).  $3(\varepsilon - 1) < 1$ . Then for  $k=0$  the axis points along the tangent; for

$0 < k < 3$  the axis moves around this direction; for  $3 < k < \frac{1}{|1-\varepsilon|}$  the axis moves near the orbital plane, excluding certain neighborhoods of the normal to this plane; for  $k > \frac{1}{|1-\varepsilon|}$  the permitted region covers the entire sphere.

(ii)  $3(\varepsilon - 1) > 1$ . The equilibrium is achieved for  $k=0$ ; for  $0 < k < \frac{1}{\varepsilon-1}$

the axis moves near this attitude (the permitted regions are elongated at right angles to the orbit, while in the previous case they are stretched along the orbit); for  $\frac{1}{\varepsilon-1} < k < 3$  the axis moves outside certain neighborhoods of the radius-vector; for  $k > 3$  the permitted region extends over the entire sphere.

For any  $k$ , these regions are substantially more accurate than the regions obtaining from Figure 33 for  $r_0 \neq 0$  (i.e.,  $k \geq 0$ ), and they therefore constitute a relevant addition to the previously considered pattern for  $r_0 \neq 0$  (regions with  $k < 0$  in Figure 33).

**2. Permitted and forbidden regions. Comprehensive analysis.** The foregoing analysis suggested a simple classification of the permitted regions of motion by means of curves of zero relative velocity. The regions that we have constructed are too broad, however, in the sense that they give no indication concerning the motion inside each region. A more detailed analysis can be carried out, bringing out the fine structure of the permitted regions in the general case  $r_0 \neq 0$  (in the previous subsection, we have established this fine structure for the particular case  $r_0 = 0$ ). In what follows, we partly proceed from the results of R. Pringle, obtained (by a different technique) in /88/.

Applying (2.1.6), we write for the integral (2.1.11)

$$\left. \begin{aligned} A(\bar{p}^2 + \bar{q}^2) &= 2h_0 - A\omega^2\beta''^2 + 2\omega Cr_0\beta'' - 3\omega^2(C-A)\gamma''^2 \geq 0, \\ 2h_0 &= A(\bar{p}_0^2 + \bar{q}_0^2) + A\omega^2\beta_0''^2 - 2\omega Cr_0\beta_0'' + 3\omega^2(C-A)\gamma_0''^2. \end{aligned} \right\} \quad (6.1.6)$$

The conditions of permitted motion are written in the form

$$\beta''^2 - 2\frac{Cr_0}{A\omega}\beta'' - \frac{3(A-C)}{A}\gamma''^2 - \tilde{k} \leq 0, \quad \tilde{k} = \frac{2h_0}{A\omega^2}. \quad (6.1.7)$$

\* The parameter  $\varepsilon = \frac{C}{A}$  has a different meaning here from Figure 21. In Figure 21 it is assumed that the moment of inertia  $A$  points along the tangent to the orbit, while in this section we are concerned with the various attitudes of the moment of inertia  $C$ , including the case of its being tangent to the orbit.

The equality corresponds to the bounding curves of the permitted regions. Considering the family of these curves (with  $\tilde{k}$  as the parameter) on the plane  $\beta'', \gamma''$  inside the circle

$$\gamma''^2 + \beta''^2 = 1 \quad (6.1.8)$$

is equivalent to considering a hemisphere of the unit sphere with the circle (6.1.8) as the symmetry meridian. Note the following characteristic points:

- $\beta''=0, \gamma''=1$ —the trace of the radius-vector;
- $\beta''=0, \gamma''=0$ —the trace of the transversal;
- $\beta''=1, \gamma''=0$ —the trace of the normal to the orbital plane.

The second-order curves (6.1.7) are hyperbolas for  $A>C$  (prolate satellite) and ellipses for  $A<C$  (oblate satellite); the common center of these two families of curves has the coordinates

$$\gamma''_1 = 0, \quad \beta''_1 = \frac{Cr_0}{A\omega}. \quad (6.1.9)$$

If the curve (6.1.7) meets the circle (6.1.8), the coordinates  $\gamma''_*, \beta''_*$  of the intersection points are defined by the equalities

$$\begin{aligned} \gamma''_* &= \pm \sqrt{1 - \beta''_*^2}, \\ \beta''_* &= \frac{\frac{Cr_0}{A\omega} \pm \sqrt{\frac{C^2 r_0^2}{A^2 \omega^2} - \frac{4A - 3C}{A} \left\{ \frac{3(C-A)}{A} - \tilde{k} \right\}}}{\frac{4A - 3C}{A}}. \end{aligned}$$

These points of intersection contract to the points

$$\gamma''_2 = \pm \sqrt{1 - \beta''_2^2}, \quad \beta''_2 = \frac{Cr_0}{\omega(4A - 3C)}. \quad (6.1.10)$$

If  $\left| \frac{Cr_0}{A\omega} \right| < 1$  and (or)  $\left| \frac{Cr_0}{\omega(4A - 3C)} \right| < 1$ , the points (6.1.9) and (or) (6.1.10) are singular points of the family of curves on the unit sphere.

Finally, let us introduce the curvatures  $K_1$  and  $K_2$  of this family of curves at the points  $\gamma''=0, \beta''=1$  and  $\gamma''=0, \beta''=-1$ , respectively:

$$K_1 = \frac{3(A-C)}{A\left(1 - \frac{Cr_0}{A\omega}\right)}, \quad K_2 = \frac{3(C-A)}{A\left(1 + \frac{Cr_0}{A\omega}\right)}. \quad (6.1.11)$$

By considering the parameters (6.1.9)—(6.1.11) together with inequality (6.1.7), we can fully classify the various permitted regions of motion. Without loss of generality, we take  $r_0>0$ .

The classification can be conveniently obtained for the plane  $\frac{r_0}{\omega}, \frac{C}{A}$  (Figure 35); the corresponding classes of regions are shown in Figure 36. We shall first consider the case  $A>C$ , so that  $\frac{Cr_0}{(4A-3C)\omega} < \frac{Cr_0}{A\omega}$ , i.e.,  $\beta''_2 < \beta''_1$ .

Type 1:  $\frac{Cr_0}{A\omega} < 1$ .

The permitted regions of motion contract to the points (6.1.10) which correspond to a direction in the plane through the radius-vector and the normal, making an angle  $\rho_2$  with the normal, where  $\cos \rho_2 = \beta''$ . The forbidden regions contract to the normals of the orbital plane. The points (6.1.10) thus correspond to a real stable motion of the satellite's axis of symmetry: the axis remains fixed in the orbital system (making an angle  $\rho_2$  with the normal to the orbital plane and an angle  $\pi/2$  (with the transversal). In the absolute space this motion amounts to a stable regular precession (see subsection 3 of this section).

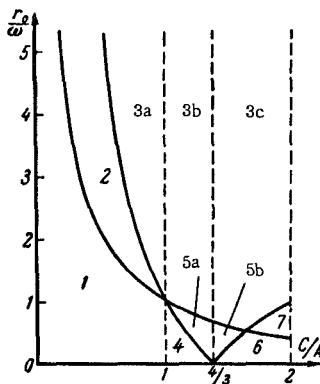


FIGURE 35. Classification of the permitted regions of motion in the plane  $\frac{r_0}{\omega}, \frac{C}{A}$ .

Type 2:  $1 < \frac{Cr_0}{A\omega} < \frac{4A - 3C}{A}$ .

Here  $|K_1| > 1$ , i.e., the curvature of the hyperbola is greater than the curvature of the circle (6.1.8); the permitted regions contract to the points (6.1.10), but the forbidden regions contract only to the direction of the negative normal ( $\beta'' = -1$ ) to the orbital plane.

Type 3a:  $\frac{4A - 3C}{A} < \frac{Cr_0}{A\omega}$ .

Then  $|K_1| < 1$  and the family of the curves has no singular points other than  $\beta'' = \pm 1$ ; the permitted regions contract to the point  $\beta'' = 1$ , while the forbidden regions contract to the point  $\beta'' = -1$ . (A prolate satellite may thus spin around an axis perpendicular to the orbital plane.)

No other cases are possible for a prolate satellite.

Let us now consider an oblate satellite ( $A < C < 2A$ ). The region  $1 < \frac{C}{A} < 2$  is divided into two subregions  $1 < \frac{C}{A} < \frac{4}{3}$  and  $\frac{4}{3} < \frac{C}{A} < 2$ . In the first subregion, the ellipses (6.1.7) are stretched along the axis  $\gamma''$ , and in the second subregion they are stretched along the axis  $\beta''$ . Here  $\frac{Cr_0}{A\omega} < \frac{Cr_0}{(4A - 3C)\omega}$ , i.e.,  $\beta'_1 < \beta'_2$ .

Let us consider the subregion  $1 < \frac{C}{A} < \frac{4}{3}$ .

$$\text{Type 4: } \frac{4A - 3C}{A} > \frac{Cr_0}{A\omega}.$$

$|K_1| < 1$  and the ellipse through the point  $\beta''=1$  lies partly outside the circle (6.1.8) and partly inside the circle. The permitted regions contract to the point (6.1.9), while the forbidden regions contract to the points  $\beta''=1$  and  $\beta''=-1$ . The point (6.1.9) in this case corresponds to a real stable motion of the satellite's axis of symmetry: the axis remains fixed in the orbital system making an angle  $\rho_1$ ,  $\cos \rho_1 = \beta_1''$ , with the normal to the orbital plane and an angle  $\pi/2$  with the radius-vector.

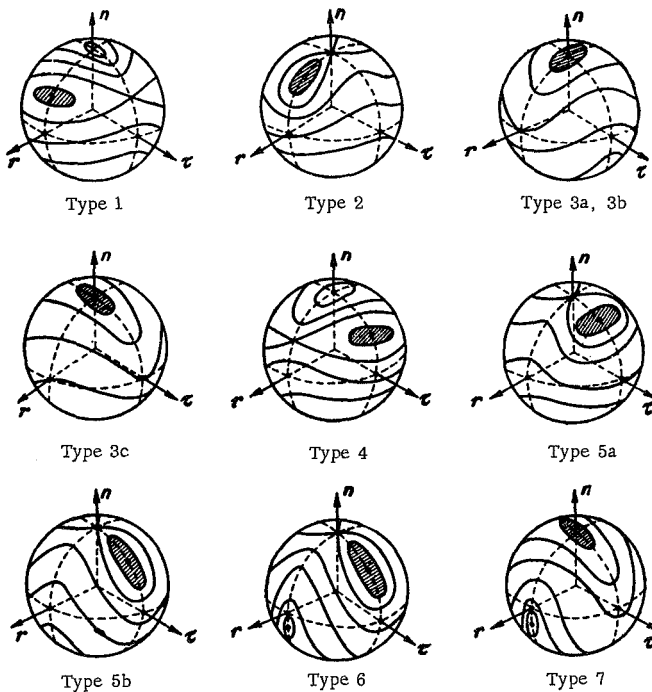


FIGURE 36. Permitted and forbidden regions of motion in the general case.

$$\text{Type 5 a: } \frac{4A - 3C}{A} < \frac{Cr_0}{A\omega} < 1.$$

$|K_1| > 1$  and the ellipse through the point  $\beta''=1$  lies entirely inside the circle (6.1.8). The permitted regions of motion contract to the point (6.1.9), and the forbidden regions to the point  $\beta''=-1$  only.

$$\text{Type 3 b: } \frac{Cr_0}{A\omega} > 1.$$

The permitted regions contract to the point  $\beta''=1$ , and the forbidden regions to the point  $\beta''=-1$ . The only difference between this case and 3a is that the boundaries of the regions here are elliptical arcs, while for type 3a these are arcs of hyperbolas.

Let us now consider the subregion  $\frac{4}{3} < \frac{C}{A} < 2$ . The ellipses (6.1.7) are stretched along the axis  $\beta''$ .

$$\text{Type 5b: } \left| \frac{4A-3C}{A} \right| < \frac{Cr_0}{A\omega} < 1.$$

It differs from type 5a only in that the ellipses are stretched along the axis  $\beta''$  (and not  $\gamma''$ , as in 5a); the permitted regions contract to the point (6.1.9), and the forbidden regions to the point  $\beta''=-1$ .

$$\text{Type 6: } \frac{Cr_0}{A\omega} < \left| \frac{4A-3C}{A} \right| < 1.$$

$K_2 > 1$ , i.e., the curvature of the ellipse tangent to the circle at the point  $\beta''=-1$  is greater than the curvature of the circle (in distinction from case 5b). The permitted regions contract to the point (6.1.9), and the forbidden regions contract to the points (6.1.10). (Pringle's analysis of this case in /88/ is in error and the drawing offered as an illustration does not apply.)

$$\text{Type 7: } 1 < \frac{Cr_0}{A\omega} < \left| \frac{4A-3C}{A} \right|.$$

The permitted regions contract to the points  $\beta''=\pm 1$ , and the forbidden regions to the points (6.1.10).

$$\text{Type 3c: } 1 < \left| \frac{4A-3C}{A} \right| < \frac{Cr_0}{A\omega}.$$

This case differs from 3b only in that the regions of motion here are bounded by arcs of ellipses stretched along the axis  $\beta''$  (and not  $\gamma''$ , as in 3b). The permitted regions contract to the point  $\beta''=1$ , and the forbidden regions to the point  $\beta''=-1$ .

In the particular case  $r_0 = 0$ , the preceding analysis reduces to the results of /75/ discussed at the end of subsection 1 of this section. It also points to the existence of stable equilibria for the axis of a spinning satellite in an orbital system. Let us consider these rotations in greater detail, following the approach of F. L. Chernous'ko /70/.

3. Regular precessions of a satellite in a field of gravity and their stability. The preceding analysis leads to the conclusion that the equilibria of the satellite's axis of symmetry in the orbital system, which correspond to regular precession in the system of fixed axes, can be of three types: 1) type (6.1.9); 2) type (6.1.10); 3) the satellite's axis of symmetry points along the normal to the orbital plane (the spin velocities about this axis being quite arbitrary). In /70/ it has been shown that no other regular precessions are possible. Thus,

$$r = \dot{\phi}_n + \omega \cos \theta_n,$$

where  $\dot{\phi}_n$  is the angular velocity of spin,  $\omega$  the angular velocity of precession, which is equal to the orbital velocity of the satellite's mass center, and  $\theta_n$  the angle between the satellite's axis and the normal to the orbital plane (the angle of nutation), so that  $\cos \theta_n = \beta''$ .

Using these notations, the various modes of regular precession can be conveniently written by three one-parametric families:

$$\theta_n = 0, \quad \alpha'' = \gamma'' = 0, \quad \beta'' = 1, \quad \dot{\phi}_n = \dot{\phi}_{n0}; \quad (6.1.12)$$

$$\theta = \theta_{n0} \neq 0, \quad \gamma'' = 0, \quad \beta'' = \cos \theta_{n0}, \quad \dot{\phi}_{n0} = (A-C)C^{-1}\omega \cos \theta_{n0}; \quad (6.1.13)$$

$$\theta = \theta_{n0} \neq 0, \quad \alpha'' = 0, \quad \beta'' = \cos \theta_{n0}, \quad \dot{\phi}_{n0} = 4(A-C)C^{-1}\omega \cos \theta_{n0}. \quad (6.1.14)$$

The parameter in (6.1.12) is  $\dot{\phi}_{n0}$ , while in (6.1.13) and (6.1.14) it is the angle  $\theta_{n0}$ , which by assumption ( $r_0 \geq 0$ ) lies in the first quadrant. The

solutions (6.1.13)–(6.1.14) have been obtained by an alternative technique by V. T. Konduraru' and G. N. Duboshin (see, e. g., /34, 46/).

Following Chetaev's method, we shall find sufficient conditions for the stability of the precessions (6.1.12)–(6.1.14). For a dynamically symmetric satellite, the first integral of relative motion in a circular orbit (2.1.11) takes the form

$$A(\bar{p}^2 + \bar{q}^2) + C\bar{r}^2 + 3\omega^2(C - A)\gamma^2 + \omega^2(A - C)\beta^2 = h.$$

Moreover, the condition of dynamic symmetry gives the first integral  $\bar{r} + \omega\beta = r_0$ . We shall choose the constants  $k_1^0, k_2^0$  so that the first integral  $V = h + k_1^0 r_0 + k_2^0 r_0^2$  has a proper minimum for the values of its arguments corresponding to one of the precessions (6.1.12–6.1.14). Note that in all these motions

$$p = q = 0, \quad \dot{r} = \dot{\varphi}_{n0}.$$

In case of perturbed motion,

$$\begin{aligned} p &= u_1, \quad q = u_2, \quad r = \dot{\varphi}_{n0} + u_3, \quad a'' = a''_u + u_4, \\ \gamma'' &= \gamma''_u + u_5, \quad \beta'' = \beta''_u + u_6, \end{aligned}$$

where  $a''_u, \beta''_u, \gamma''_u$  are the direction cosines in unperturbed motion; on substitution in Lyapunov's function  $V$ , one of the direction cosines should be eliminated using the relation  $a''^2 + \beta''^2 + \gamma''^2 = 1$ . Then it is easily seen that the first integral  $V$ , treated as a function of the variables  $u_i$ , has a proper minimum at the point  $u_i = 0$  if the following conditions are satisfied. For the unperturbed motion (6.1.12),

$$\left. \begin{aligned} k_1^0 &= -2C\dot{\varphi}_{n0}, \quad k_2^0 = 0 \\ \dot{\varphi}_{n0} &> (A - C)\omega/C \quad \text{for } A \leq C, \\ \dot{\varphi}_{n0} &> 4(A - C)\omega/C \quad \text{for } A \geq C. \end{aligned} \right\} \quad (6.1.15)$$

For the unperturbed motion (6.1.13),

$$\left. \begin{aligned} k_1^0 &= -2A\omega \cos \theta_{n0}, \quad k_2^0 = C^2/A \\ A &< C. \end{aligned} \right\} \quad (6.1.16)$$

For the unperturbed motion (6.1.14),

$$\left. \begin{aligned} k_1^0 &= -8(A - C)\omega \cos \theta_{n0}, \quad k_2^0 = 0 \\ A &> C. \end{aligned} \right\} \quad (6.1.17)$$

In virtue of the well-known theorem of stability, conditions (6.1.15)–(6.1.17) are sufficient conditions of stability of the motions (6.1.12)–(6.1.14), respectively.

Let us now compare the sufficient conditions with the necessary conditions of stability. These conditions are obtained by linearizing the equations of motion near the solutions (6.1.12)–(6.1.14), with the additional requirement of nonpositive real parts of the roots of the characteristic equation in the linear approximation.

An analysis of the stability of (6.1.12) leads to the following necessary conditions. Let  $\epsilon = C/A$ ,  $s = \varphi_{n0}/\omega$ . Then, for  $\epsilon \geq 1$ , one of the following two inequalities must be satisfied if the motion is stable:

$$\left. \begin{array}{l} s \geq \epsilon^{-1} - 1, \\ s \leq 4(\epsilon^{-1} - 1), \end{array} \right\} \quad (6.1.18)$$

and for  $\epsilon \leq 1$ , it is necessary either that

$$s \geq 4(\epsilon^{-1} - 1), \quad (6.1.19)$$

or that the following two inequalities are satisfied simultaneously:

$$\left. \begin{array}{l} s \leq \epsilon^{-1} - 1, \\ \sqrt{1 - \epsilon - es} + \sqrt{4 - 4\epsilon - es} \leq 2 - \epsilon - es. \end{array} \right\} \quad (6.1.20)$$

The sufficient conditions (6.1.15) differ from the first condition in (6.1.18) and from (6.1.19) only in that they are strict inequalities. Figure 37 plots the regions defined by inequalities (6.1.18)–(6.1.20) in the plane  $\epsilon, s$ . In

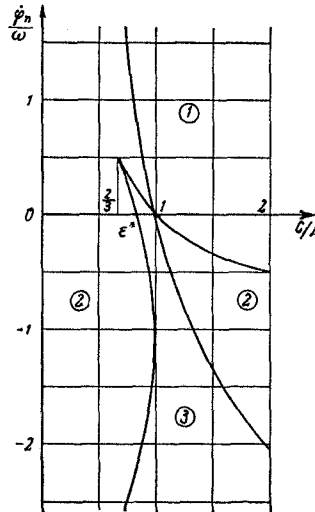


FIGURE 37. Region of stability (1), region of instability (2), and the region where the necessary conditions of stability are satisfied (3) for the rotation of a satellite around an axis perpendicular to the orbital plane.

the region 1 the motion is a priori stable (the sufficient conditions are satisfied), and in region 2 it is a priori unstable (the necessary conditions do not hold true); in region 3 only the necessary conditions of stability are satisfied. The boundaries of the regions 1, 2 and 2, 3 have an asymptote  $\epsilon = 0$ , and the boundary of the regions 2, 3, for  $\epsilon < 1$ , meets the axis  $\epsilon$  at the point  $\epsilon = \epsilon^* = (3\sqrt{5} - 5)/2 \approx 0.854$ . Note that in the region 3 some points ( $s \rightarrow -\infty$ , and also the straight line  $\epsilon = 1$ ) correspond to a priori stable modes of motion. Stability of this motion is also analyzed

in /93/, but the graph depicting the stable regions is in error, particularly near  $\epsilon = 1$ ; it does not show the region of instability for  $\epsilon > 1$ .

The necessary conditions of stability for the motions (6.1.13), (6.1.14) have been derived by Duboshin /34/. A necessary condition for the stability of (6.1.13) is  $A \leq C$ . The sufficient condition (6.1.16) differs from this necessary condition only in that it rules out the equality.

For the motion (6.1.14) to be stable, it is necessary either that  $A \geq C$  ( $\epsilon \leq 1$ ), or that the following two conditions are satisfied simultaneously /34/:

$$\epsilon \geq \frac{4}{3}, \quad \cos^2 \theta_{n0} \geq \frac{18\epsilon^2 - 27\epsilon + 8 + 2(3\epsilon - 2)\sqrt{(3\epsilon - 1)(3\epsilon - 4)}}{27\epsilon^2(\epsilon - 1)}. \quad (6.1.21)$$

In Figure 38, region 1 is the region of a priori stability of the motion (6.1.14), region 2 is the region where this motion is a priori unstable, and region 3 is the region where the necessary conditions (6.1.21) are satisfied. The curved boundary between regions 2 and 3 has a minimum at  $\theta_{n0} = \pi/4$  for  $\epsilon = C/A = 5/3$ .

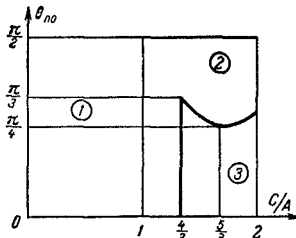


FIGURE 38. Region of stability (1), region of instability (2), and the region where the necessary conditions of stability are satisfied (3) for a satellite whose symmetry axis is perpendicular to the transversal.

Let us consider some particular cases. For  $\dot{\varphi}_{n0} = -\omega$  ( $s = -1$ ), the solution (6.1.12) describes the translational motion of a satellite whose axis of dynamic symmetry  $z'$  is perpendicular to the orbital plane ( $\dot{\varphi}_{n0}$  is the relative angular velocity). From the foregoing conditions it follows that this motion is stable only for a satellite having  $1 < C/A < 4/3$ .

For  $\dot{\varphi}_{n0} = 0$  ( $s = 0$ ), (6.1.12) represents a state of relative equilibrium of the satellite in a circular orbit, with the axis  $z'$  pointing at right angles to the orbital plane. Conditions (6.1.15), (6.1.20) show that this equilibrium is stable for  $A < C$  and unstable for  $C/A < \epsilon^* \approx 0.854$ . This result also follows from the analysis of Chapter 2 (Figure 21).

For  $\dot{\varphi}_{n0} = \pi/2$ , (6.1.13) and (6.1.14) represent the two other states of relative equilibrium of the satellite in a circular orbit: the axis  $z'$  points along the tangent or along the radius-vector  $R$ . It follows from the foregoing conditions that the orientation of the axis  $z'$  along the tangent is stable for  $A < C$  and unstable for  $A > C$ , which constitutes an addition to the results of Chapter 2 (Figure 21); the orientation along the radius-vector is stable for  $A > C$  and unstable for  $A < C$ .

## § 2. SECULAR GRAVITATIONAL PERTURBATIONS

The general theory of rotational motion of a dynamically symmetric satellite under perturbations with a force function (Chapter 5, § 4) is fully applicable to the case of gravitational perturbations.

From (1.2.7) and (5.4.11), making use of (1.1.8), we see that the motion of a dynamically symmetric satellite in a field of gravity is determined by the force function

$$U_v = \frac{3\sqrt{\mu}}{2P^{3/2}} (1 + e \cos v)(A - C)(\gamma_3 \cos v + \alpha_3 \sin v)^2. \quad (6.2.1)$$

From (5.4.11) and (5.4.13) we have the following expressions for the function  $U_v$  averaged over  $\psi$  and doubly averaged over  $\psi$  and  $v$ :

$$\bar{U}_v = \frac{3}{2} \frac{\sqrt{\mu}}{P^{3/2}} (1 + e \cos v)(A - C) \left[ 1 - \frac{3}{2} \sin^2 \vartheta \right] \sin^2 \rho \cos^2(\sigma - v), \quad (6.2.2)$$

$$\bar{U}_v = \frac{3}{4} \frac{\sqrt{\mu}}{P^{3/2}} (A - C) \left[ 1 - \frac{3}{2} \sin^2 \vartheta \right] \sin^2 \rho \quad (6.2.3)$$

(apart from an additive term which does not influence the motion).

We have shown in § 4 of Chapter 5 that the perturbed motion amounts to regular precession around the vector of angular momentum  $\mathbf{L}$ , which remains constant in magnitude making a constant angle  $\vartheta = \vartheta_0$  with the axis of symmetry; the secular motion of the vector  $\mathbf{L}$  is determined by equations (5.4.13), (6.2.3):

$$\rho = \rho_0, \quad \frac{d\sigma}{dv} = \frac{3}{2} \frac{\sqrt{\mu}}{P^{3/2}} \frac{(A - C)}{L_0} \left[ 1 - \frac{3}{2} \sin^2 \vartheta_0 \right] \cos \rho_0. \quad (6.2.4)$$

Secular motion of the angular momentum vector amounts to precession at a constant angular distance from the normal to the orbital plane.

*In secular motion, the vector of angular momentum precesses around the normal to the orbital plane, at a constant angular distance and with an angular velocity which is proportional (with a constant proportionality coefficient) to the angular velocity of the mass center in the elliptical orbit.*

In the particular case of a circular orbit, we have  $v = \omega_0 t$ ,  $\frac{\sqrt{\mu}}{P^{3/2}} = \omega_0$ , and the precession of  $\mathbf{L}$  is uniform in time. Changing over to  $v$  as the independent variable in (5.4.10) and averaging over  $v$ , we obtain an expression for the angular velocity of precession of the satellite's axis around the vector  $\mathbf{L}$ :

$$\bar{\psi}' = \frac{T}{2\pi} \frac{L_0}{A} + \frac{3}{2} \frac{\sqrt{\mu}}{P^{3/2}} \frac{A - C}{L_0} \left( \frac{1}{2} \cos^2 \rho + \frac{1}{2} \cos^2 \vartheta - 3 \cos^2 \rho \cos^2 \vartheta \right). \quad (6.2.5)$$

Here  $T$  is the orbital period of the satellite.

Formula (6.2.5) gives not only the principal term for the angular velocity of precession, but also a secular correction (which is constant here) due to gravitational perturbations. In reality, the secular term is very small in comparison with the principal term.

The right-hand sides of (6.2.4), (6.2.5), as it follows from the meaning of  $v$ -averages, give the change in the elements of motion when the true anomaly  $v$  has varied by 1 rad.

**Examples.** 1. Let us calculate the maximum increment of the angle  $\sigma$  when  $v$  varies by 1 rad, if the angle of nutation  $\theta=0$  ( $L=Cr_0$ , i.e., the satellite spins around the axis  $z'$  with an angular velocity  $r_0$ ) and the satellite's mass center travels in a circular orbit. Then  $\left[\frac{d\sigma}{dv}\right]_{\max} = \frac{3}{2} \frac{\omega_0}{r_0} \left(\frac{A}{C} - 1\right)$ . Table 6 lists  $\omega_0$  as a function of the orbit height  $h$ .

TABLE 6

$h$ , km	225	300	500	1000
$\omega_0$ , deg/sec	0.0675	0.0664	0.0635	0.0571

$\Delta\sigma$  as a function of  $\frac{\omega_0}{r_0}$  and  $\frac{A}{C}$  is listed in Table 7.

TABLE 7

$\frac{A}{C}$	0,5	2	11	101
$\frac{\omega_0}{r_0}$	-4.1	8.2	(82)	(820)
0,1	-0.41	0.82	8.2	(82)
0,01	-0.041	0.082	0.82	8.2

The values of  $\Delta\sigma$  outlined in the upper right-hand corner of the table show that the averaged formulas do not apply in this region, since here the motion of the angular momentum vector is not slow in comparison with the orbital velocity of the satellite's mass center.

2. Let us calculate the maximum increment of the angle  $\sigma$  as  $v$  varies by 1 rad, for a nutation angle  $\theta=90^\circ$  ( $L=Ap_0$ , i.e., the satellite spins around a lateral axis with an angular velocity  $p_0$ ); the satellite moves in a circular orbit. Then  $\left[\frac{d\sigma}{dv}\right]_{\max} = \Delta\sigma = -\frac{3}{4} \frac{\omega_0}{p_0} \left(1 - \frac{C}{A}\right)$ . The results are listed in Table 8.

TABLE 8

$\frac{A}{C}$	0,5	2	11	101
$\frac{\omega_0}{p_0}$	4.1	-2.05	-3.85	-4.0
0.1	0.41	-0.205	-0.385	-0.4
0.01	0.041	-0.0205	-0.0385	-0.04

The approximate parameters of Sputnik III were  $\frac{A}{C}=2.5$ ;  $\rho_0 \approx 2.5 \text{ deg/sec}$ ,  $\theta \approx 90^\circ$ . Then  $\Delta\sigma \approx 0.7 \text{ deg/rad}$ , and for an arbitrary  $\rho = \rho_0$ , we have  $\Delta\sigma = 0.7 \cos \rho_0 \text{ deg/rad}$ .

3. The period  $T_E$  of the luni-solar precession of the Earth's axis is calculated using the following formula, which is easily derived from (6.2.4):

$$T_E = \frac{1}{\Delta\sigma}; \quad \Delta\sigma = \frac{3}{2} \frac{A-C}{Cr_0} \cos \rho_0 \left( \sqrt{\frac{\omega_M}{1 + \frac{M_E}{M_M}}} + \omega_E \right).$$

where  $M_E/M_M = 81$  is the Earth to Moon mass ratio,  $\omega_E = \frac{360}{365} \text{ deg/day}$  and  $\omega_M = \frac{360}{28} \text{ deg/day}$  are the angular velocities of the Earth around the Sun and of the Moon around the Earth, respectively;  $r_0 = 360 \text{ deg/day}$  is the angular velocity of the Earth's spin;  $\rho_0 = 23^\circ.5$  is the inclination of the Earth's equator to the ecliptic;  $\frac{A-C}{C} = 0.0033$ . Calculations give  $T_E \approx 26,000 \text{ years}$ .

### § 3. GENERAL PROPERTIES OF MOTION

When the appropriate  $\bar{U}_v$  is inserted from (6.2.2) in (5.4.12), we have

$$\left. \begin{aligned} \frac{d\rho}{dv} &= N_0 (1 + e \cos v) \cos(\sigma - v) \sin(\sigma - v) \sin \rho, \\ \frac{d\sigma}{dv} &= N_0 (1 + e \cos v) \cos^2(\sigma - v) \cos \rho, \end{aligned} \right\} \quad (6.3.1)$$

$$N_0 = 3 \frac{\sqrt{\mu}}{P^3 h} \frac{A-C}{L_0} \left( 1 - \frac{3}{2} \sin^2 \theta_0 \right). \quad (6.3.2)$$

According to the general theory (Chapter 5, § 4), the motion around the angular momentum vector is an almost regular precession, the parameters  $L=L_0$ ,  $r=r_0$ ,  $\theta=\theta_0$  remaining constant; the velocity of precession  $\dot{\psi}$  according to (5.4.10) and (6.2.2) is

$$\begin{aligned} \dot{\psi} &= \frac{L_0}{A} - \frac{1}{L_0} \frac{3(A-C)\sqrt{\mu}}{P^3 h} (1 + e \cos v) \cos^2(\sigma - v) \times \\ &\times \left\{ \left( 1 - \frac{3}{2} \sin^2 \theta \right) \cos^2 \rho - \frac{3}{2} \sin \theta \cos \theta \sin^2 \rho \right\} \approx \frac{L_0}{A}. \end{aligned} \quad (6.3.3)$$

The analysis of perturbed motion reduces to the investigation of the equations of motion (6.3.1) of the vector  $L$ . In the solution of these equations, periodic oscillations in  $\sigma$  and  $\rho$  having a small (for small  $N_0$ ) amplitude and a period comparable with  $2\pi$  are superimposed on the secular motion (6.2.4). Since  $v$  varies fairly fast, while the variation in  $\sigma$  is slow, the difference  $\sigma - v$  fluctuates rapidly, repeatedly passing through successive extrema (at points where  $\kappa = \sigma - v$  takes the values  $\pm n\pi/2$ ,  $n = 0, 1, 2, \dots$ ).

The angle  $V$  between the tangent to the trajectory and the meridian of a unit sphere is given by the expression

$$\operatorname{tg} V = \frac{d\sigma \sin \rho}{d\rho} = \operatorname{ctg}(\sigma - v) \cos \rho. \quad (6.3.4)$$

For  $\sigma - v = 0$  and  $\sigma - v = \pm\pi$ , we have  $\operatorname{tg} V = \infty$ , and the trajectory is thus tangent to the parallel (and has a point of extremum). For  $\sigma - v = \pm\pi/2$  and  $\sigma - v = \pm 3\pi/2$ , we have  $\operatorname{tg} V = 0$ : the trajectory has a turning point. From (6.3.4) it also follows that the trajectory may pass through  $\rho = 90^\circ$  only at right angles to the equator of the unit sphere, and that for  $\rho < 90^\circ$ , the turning points are the points of minimum  $\rho$ , while the tangent points are the points of maximum  $\rho$  (Figure 39). For  $\rho > 90^\circ$ , the pattern is reversed, so

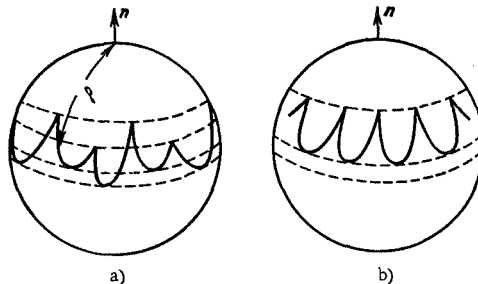


FIGURE 39. The motion of the angular momentum vector under gravitational perturbations: a) elliptical orbit; b) circular orbit.

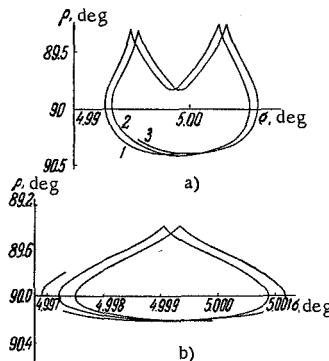


FIGURE 40. The motion of the angular momentum vector near the orbital plane (gravitational perturbations).

that the cusps of the trajectory  $\rho(\sigma)$  are turned facing the poles of the unit sphere. For  $\rho < 90^\circ$  the trajectory advances in a certain direction (in the direction of increasing  $\sigma$  if  $N_0 > 0$ ), and for  $\rho > 90^\circ$  it regresses in the opposite direction. We should also note that the amplitude of oscillations in  $\rho$  decreases, and the rate of change in  $\sigma$  increases, as  $\rho$  approaches 0 or  $\pi$ . Since the direction of motion is reversed at  $\rho = \pi/2$ , the trajectories are characteristically looped near  $\rho = \pi/2$ . The corresponding trajectories are plotted in Figure 40. Near  $\rho = \pi/2$  the rate of change in  $\sigma$ , as we see from the second equation in (6.3.1), is very small; the loops are therefore very narrow and drift very slowly. In particular, a periodic trajectory (with a stationary loop) may exist.

## § 4. THE CASE OF A CIRCULAR ORBIT. PRELIMINARY ANALYSIS

The near constancy of the angular momentum  $L$  in the case of a circular orbit can be proved by means of the Jacobi energy integral (2.1.5). After simple manipulations, this integral is written as

$$L^2 - 2\omega A(L \cos \rho - L_0 \cos \rho_0) + 3\omega^2 A(C - A)(\bar{v}''^2 - \bar{v}_0''^2) - L_0^2 = 0.$$

The subscript 0 marks the initial values of the corresponding quantities. Solving this quadratic equation for  $L$  (and taking the root with a plus sign in virtue of the conditions  $L = L_0$  and  $\rho = \rho_0$ ), we find

$$\begin{aligned} L &= \omega A \cos \rho + L_0 \left( 1 - 2 \frac{\omega A}{L_0} \cos \rho_0 - \right. \\ &\quad \left. - 3 \frac{\omega^2 A}{L_0^2} (C - A) (\bar{v}''^2 - \bar{v}_0''^2) + \frac{\omega^2 A^2}{L_0^2} \cos^2 \rho \right)^{\frac{1}{2}} = \\ &= L_0 \left\{ 1 + \frac{\omega A}{L_0} (\cos \rho - \cos \rho_0) + O \left[ \left( \frac{\omega A}{L_0} \right)^2 \right] \right\}, \end{aligned}$$

where  $O \left( \frac{\omega^2 A^2}{L_0^2} \right)$  contains terms of second and higher orders of smallness ( $\omega A \ll L_0$  in compliance with the basic assumption concerning rotational motion). Hence,  $L \approx L_0$ , at least to terms of the first order of smallness.

In fact, this equation is accurate to terms of second order:  $\frac{\omega A}{L_0} (\cos \rho - \cos \rho_0)$  is at least of second order of smallness, since  $\cos \rho - \cos \rho_0$ , as will be clear from what follows, is at least of the first order of smallness.

For a circular orbit,  $e = 0$ ,  $\frac{V\mu}{P^2} = \omega_0$ . We introduce a new variable  $\kappa_v = \sigma - v$ . Equations (6.3.1) then take the form (5.4.15):

$$\begin{aligned} \frac{d\rho}{dv} &= N_0 \sin \rho \sin \kappa_v \cos \kappa_v, \quad \frac{d\kappa_v}{dv} = 1 - N_0 \cos \rho \cos^2 \kappa_v, \quad (6.4.1) \\ N_0 &= 3 \frac{A - C}{L_0} \omega_0 \left( 1 - \frac{3}{2} \sin^2 \theta_0 \right), \end{aligned}$$

and have the first integral (5.4.16):

$$\cos^2 \kappa_v \sin^2 \rho + a^* \cos \rho = C, \quad a^* = \frac{2}{N_0}. \quad (6.4.2)$$

Since according to our basic assumption the rotational kinetic energy is fairly large, we may take  $N_0$  to be fairly small, and  $a^*$  fairly large (in absolute value). However, if the motion is being considered in a small range of  $v$  (of the order of one orbital revolution, which is of interest, say, in investigating the motion of a satellite around the Sun), the case  $|N_0| > 1$  is allowed.

Equation (6.4.2) may be written in the form

$$\cos \varepsilon_L = \sqrt{C - a^* \cos \rho}; \quad \cos e_L = \cos \kappa_v \sin \rho, \quad (6.4.3)$$

where  $\varepsilon_L$  is the angle between the angular momentum vector  $\mathbf{L}$  and the current radius-vector  $\mathbf{r}$ .

From (6.4.3) it follows that  $-\sin \rho \leq \cos \varepsilon_L \leq \sin \rho$ . This inequality, together with the integral (6.4.3), enable us to plot the trajectory traced by the tip of the vector  $\mathbf{L}$  on a unit sphere. The construction of these trajectories is described in detail in Chapter 8. It is found that the sine curves  $\pm \sin \rho$  give the meridian of the sphere about which all the trajectories are symmetric (the symmetry meridian). The poles 1, 2, 3, 4 of the trajectories lie on this meridian; one of these poles is unstable (Figure 41). The vector  $\mathbf{L}$  traces a closed curve in the rotating system of axes  $\mathbf{n}$ ,  $\mathbf{r}$ ,  $\mathbf{r}$  around one of the poles 2, 3, 4. Figure 41 represents the case  $\alpha^* > 0$ . For  $\alpha^* < 0$  the pattern is symmetric (relative to the equator of the sphere).

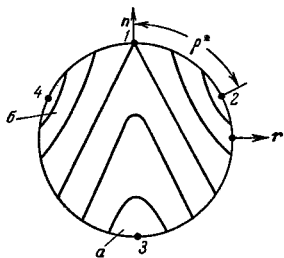


FIGURE 41. The motion of the angular momentum vector relative to the orbital system of axes:  $|N_0| > 1$ .

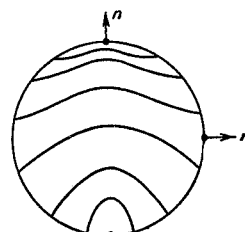


FIGURE 42. The motion of the angular momentum vector relative to the orbital system of axes:  $|N_0| < 1$ .

The poles 3 and 4 occur only when  $\alpha^*$  is sufficiently small. The coordinate  $\rho^*$  of these poles, as we see from (6.4.1), is given by the equality

$$\cos \rho^* = \frac{1}{N_0} \equiv \frac{1}{2} \alpha^*.$$

For large  $\alpha^*$ , these "skew poles" creep toward the  $\mathbf{n}$  pole, coinciding with it in the limit for  $|\alpha^*|=2$ . For  $|\alpha^*| \geq 2$ , i.e., for  $|N_0| \leq 1$ , the vector  $\mathbf{L}$  precesses around the normal  $\mathbf{n}$  to the orbital plane. The corresponding trajectories traced by the tip of the angular momentum vector in the orbital system are shown in Figure 42. In what follows we shall confine the analysis to this case of fairly small perturbations.

## § 5. THE CASE OF A CIRCULAR ORBIT. INTEGRATION OF THE EQUATIONS OF MOTION

Let us express  $\cos \alpha_v$  and  $\sin \alpha_v$  in terms of  $\rho$  from (6.4.2), inserting the result in the first equation of (6.4.1) and substituting the variable  $x=\cos \rho$ . We shall take  $0 < N_0 < 1$ . Without loss of generality, we may set  $\alpha_{v0}=0$  for  $v=0$ . Then  $C=\sin^2 \rho_0 + \alpha^* \cos \rho_0$ , and the first equation of (6.4.1) reduces

to a quadrature

$$\left. \begin{aligned} -x' &= \sqrt{2N_0} \sqrt{f(x)}, \quad f(x) = (x - x_1)(x - x_2)(x - x_3), \\ x_1 &= \cos \rho_0 + \frac{N_0}{2} \sin^2 \rho_0, \quad x_2 = \frac{2}{N_0} - \cos \rho_0, \quad x_3 = \cos \rho_0. \end{aligned} \right\} \quad (6.5.1)$$

We have  $x_2 > x_1 > x_3$ ,  $f(x) \rightarrow \pm \infty$  for  $x \rightarrow \pm \infty$ ; therefore, a positive maximum and a negative minimum occur in the intervals  $x_3 < x < x_1$  and  $x_1 < x < x_2$ , respectively; motion is thus permitted ( $f(x) > 0$ ) in the interval  $x_3 < x < x_1$ . Integrating (6.5.1) and inverting the elliptical integral, we find for  $x = \cos \rho$

$$\left. \begin{aligned} \cos \rho &= \cos \rho_0 + \frac{N_0}{2} \sin^2 \rho_0 \operatorname{sn}^2(u, k), \\ k &= \frac{N_0 \sin \rho_0}{2 \sqrt{1 - N_0 \cos \rho_0}}, \quad u = \sqrt{1 - N_0 \cos \rho_0} v. \end{aligned} \right\} \quad (6.5.2)$$

From (6.4.2) after simple manipulations we have

$$\cos \nu_v = \frac{\operatorname{cn}(u, k)}{\sqrt{1 - N_0 \cos \rho_0 \operatorname{sn}^2(u, k) - \frac{N_0^2}{4} \sin^2 \rho_0 \operatorname{sn}^4(u, k)}}. \quad (6.5.3)$$

From (6.4.3),

$$\cos \varepsilon_L = \cos \varepsilon_{L0} \operatorname{cn}(u, k); \quad \cos \varepsilon_{L0} = \sin \rho_0. \quad (6.5.4)$$

It can be easily shown that the modulus of the elliptical functions  $k < 1$  for  $N_0 < 1$ . If in (6.5.2)–(6.5.4) we substitute for  $\rho$  a new variable  $\bar{\rho} = \pi - \rho$ , and insert  $|N_0|$  for  $N_0$ , we obtain the corresponding formulas for the case  $N_0 < 0$ ,  $|N_0| < 1$ .

Applying (6.5.2)–(6.5.4), we can now proceed with the analysis of motion. By the period  $T_\rho$  of oscillations in  $\rho$  we shall mean the increment of the true anomaly  $\nu$  corresponding to one cycle of variation of the angle  $\rho$  from a certain  $\rho = \rho^*$  and back. It follows from (6.5.2) that

$$\begin{aligned} T_\rho &= \frac{2K(k^2)}{\sqrt{1 - N_0 \cos \rho_0}} \approx \\ &\approx \pi \left[ 1 + \frac{N_0}{2} \cos \rho_0 + \frac{N_0^2}{8} \left( 3 \cos^2 \rho_0 + \frac{1}{2} \sin^2 \rho_0 \right) \right]. \end{aligned} \quad (6.5.5)$$

Here  $K(k^2)$  is the complete elliptical integral of the first kind; the second part in (6.5.5) is obtained by series-expansion in  $N_0$ . From (6.5.2) we see that  $\frac{N_0}{2} \sin^2 \rho_0$  is the amplitude of oscillations in  $\cos \rho$ , which clearly approaches 0 for  $\rho_0 \rightarrow 0, \pi$ . The amplitude  $\Delta \rho$  of small oscillations in the angle  $\rho$  is thus easily seen to be  $|\Delta \rho| = \left| \frac{N_0}{2} \sin \rho_0 \right|$ . Using the parameters of Sputnik III, we have obtained in § 2 of this chapter the secular inequality  $\Delta \sigma = \frac{N_0}{2} \cos \rho_0 = 0.7 \cos \rho_0 \text{ deg/rad}$ ; for the amplitude  $\Delta \rho$  we correspondingly have  $\Delta \rho = 0.7 \sin \rho_0$ . Formula (6.5.2) shows that for an arbitrary  $\rho_0$ , the angle  $\rho$  does not vanish, since invariably  $\cos \rho_0 + \frac{N_0}{2} \sin^2 \rho_0 < 1$ , which is equivalent to the

obvious inequality  $N_0 \cos^2 \frac{\rho_0}{2} < 1$ . If  $\rho_0 = 0$ , then for any  $v$  the current value is  $\rho = 0$ , i.e., the vector  $L$  always points along the normal to the orbit.

It follows from (6.4.1) that the angle  $\kappa_v$  increases with some oscillations, and the period of  $\cos \kappa_v$  (see (6.5.3)) is twice the period of nutation:

$$T_\kappa = 2T_\rho = \frac{4K(k^2)}{\sqrt{1 - N_0 \cos \rho_0}}. \quad (6.5.6)$$

As the true anomaly  $v$  varies through the angle  $T_\kappa$ , the angle  $\kappa_v$  varies through  $2\pi$ ; the corresponding increment in the angle  $\sigma$  is therefore

$$\Delta\sigma = 2T_\rho - 2\pi \approx 2\pi \left[ \frac{N_0}{2} \cos \rho_0 + \frac{N_0^2}{8} \left( 3 \cos^2 \rho_0 + \frac{1}{2} \sin^2 \rho_0 \right) \right]. \quad (6.5.7)$$

Formula (6.5.7) gives the secular increment  $\Delta\sigma$  in the angle  $\sigma$  as  $v$  varies, not through  $2\pi$  (one orbital revolution of the satellite), but through the angle  $2T_\rho$ , equal to twice the period of nutation.

Formula (6.5.7), in distinction from (6.2.4), shows that the vector  $L$  displays a certain secular motion even when  $\rho_0 = 90^\circ$  (an effect of second order of smallness).

There is, however, a certain  $\rho_0 = \rho_0^*$  for which no secular motion is observed. Setting in (6.5.7)  $\Delta\sigma = 0$ , we have (approximately)

$$\cos \rho_0^* = -\frac{4}{5N_0} \left[ 1 - \sqrt{\left( 1 - \frac{5}{16} N_0^2 \right)} \right] \approx -\frac{N_0}{8}. \quad (6.5.8)$$

The required  $\rho_0^*$  is somewhat greater than  $90^\circ$  for a positive  $N_0$ , and somewhat less than  $90^\circ$  for a negative  $N_0$ . For  $\rho_0 = \rho_0^*$ , the trajectory  $\rho(\sigma)$  is closed (periodic). By definition,  $\rho_0^*$  is the exact solution of the transcendental equation  $T_\rho = \pi$ .

## § 6. THE CASE OF AN ELLIPTICAL ORBIT

The motion of the angular momentum vector in the case of an elliptical orbit ( $e \neq 0$ ) is described by equations (6.3.1). The factor  $N_0$  being small, we can solve (6.3.1), e.g., by the method of successive approximations or by other approximate techniques.

Equations (6.2.4) give the first-order solution

$$\rho = \rho_0, \quad \sigma = \sigma_0 + \frac{N_0}{2} \cos \rho_0 v. \quad (6.6.1)$$

Formulas (6.6.1) contain terms which describe secular motions only. To obtain the next higher approximation, (6.6.1) is inserted in the right-hand sides of (6.3.1) and the resulting equations are then integrated.  $N_0$  being small, the successive approximations can be terminated with the substitution of the zeroth approximation  $\rho = \rho_0$ ,  $\sigma = \sigma_0$ . Integration of (6.3.1)

then gives

$$\left. \begin{aligned} \rho &= \rho_0 + \frac{N_0}{4} \sin \rho_0 \left\{ [\cos 2(v - \sigma_0) - \cos 2\sigma_0] + \right. \\ &\quad \left. + e [\cos(v - 2\sigma_0) - \cos 2\sigma_0] + \right. \\ &\quad \left. + \frac{e}{3} [\cos(3v - 2\sigma_0) - \cos 2\sigma_0] \right\} \equiv \rho_0^* + \Delta\rho(v), \\ \sigma &= \sigma_0 + \frac{N_0}{2} \cos \rho_0 \left\{ v - e \sin v + \right. \\ &\quad \left. + \frac{1}{2} [\sin 2(v - \sigma_0) + 2 \sin 2\sigma_0] + \frac{e}{2} [\sin(v - 2\sigma_0) + \right. \\ &\quad \left. + \sin 2\sigma_0] + \frac{e}{6} [\sin(3v - 2\sigma_0) + \sin 2\sigma_0] \right\} \equiv \\ &\equiv \sigma_0^* + \frac{N_0}{2} \cos \rho_0 v + \Delta\sigma(v). \end{aligned} \right\} \quad (6.6.2)$$

Here  $\rho_0^*$ ,  $\sigma_0^*$  stand for sums of constant terms,  $\Delta\rho(v)$  and  $\Delta\sigma(v)$  are periodic increments which describe the oscillations of the angular momentum vector  $L$ , superimposed on the principal (secular) motion.

Let us now consider the periodic motions of the vector  $L$ . It is convenient to consider first the case of a circular orbit, previously discussed in §§ 4, 5. Then  $e = 0$ , and from (6.6.2) we have

$$\Delta\rho = \frac{1}{4} N_0 \sin \rho_0 \cos 2(v - \sigma_0), \quad \Delta\sigma = \frac{1}{4} N_0 \cos \rho_0 \sin 2(v - \sigma_0). \quad (6.6.3)$$

The angular displacements  $\Delta\rho$  and  $\Delta\sigma$  are made to correspond to linear displacements on the surface of a unit sphere,

$$\eta_\rho = \Delta\rho, \quad \delta_\sigma = \Delta\sigma \sin \rho_0.$$

Then, from (6.6.3)

$$\frac{\eta_\rho^2}{\left(\frac{N_0}{4} \sin \rho_0\right)^2} + \frac{\delta_\sigma^2}{\left(\frac{N_0}{4} \sin \rho_0 \cos \rho_0\right)^2} = 1. \quad (6.6.4)$$

In the case of a circular orbit, the tip of the angular momentum vector  $L$  is thus seen to move periodically tracing an ellipse (6.6.4). Since a secular motion is superimposed on this periodic mode, the ellipse (6.6.4) drifts over the sphere, so that its center travels along the parallel corresponding to  $\rho = \rho_0^*$ . The resultant trajectory of these two component motions is plotted in Figure 39: in § 3 we have shown that it has turning points.

In the case of an elliptical orbit,  $e \neq 0$ . The principal characteristic of motion in an elliptical orbit, which is not observed for circular orbits, is that the alternating maxima and minima of  $\rho$  are not equal to one another. From (6.3.1) we see that  $\rho$  is extremized for  $\sin 2(\sigma - v) = 0$ , or, approximately for  $\sin 2(\sigma_0 - v) = 0$ , i.e., for  $\sigma_0 - v = n\pi/2$ ,  $n = 1, 2, 3, \dots$ . Let  $\rho_i$ ,  $i = 1, 2, 3, 4$ , denote the extremal values of  $\rho$ ; then from (6.6.2)

$$\left. \begin{aligned} \rho_1 &= \rho_0 + N_0 \sin \rho_0 \left[ \frac{1}{2} \sin^2 \sigma_0 + \frac{e}{3} (\cos \sigma_0 - \cos 2\sigma_0) \right], \\ \rho_2 &= \rho_0 - N_0 \sin \rho_0 \left[ \frac{1}{2} \cos^2 \sigma_0 - \frac{e}{3} (\sin \sigma_0 - \cos 2\sigma_0) \right], \\ \rho_3 &= \rho_0 + N_0 \sin \rho_0 \left[ \frac{1}{2} \sin^2 \sigma_0 - \frac{e}{3} (\cos \sigma_0 + \cos 2\sigma_0) \right], \\ \rho_4 &= \rho_0 - N_0 \sin \rho_0 \left[ \frac{1}{2} \cos^2 \sigma_0 + \frac{e}{3} (\sin \sigma_0 + \cos 2\sigma_0) \right]. \end{aligned} \right\} \quad (6.6.5)$$

For  $N_0 \sin \sigma_0 > 0$ ,  $\rho_1$  and  $\rho_3$  are maxima,  $\rho_2$  and  $\rho_4$  are minima; the terms with  $e$  are in fact responsible for the two maxima and the two minima being different from each other ( $\rho_1 \neq \rho_3$ ,  $\rho_2 \neq \rho_4$ ). For  $N_0 > 0$ ,  $0 \leq \sigma_0 \leq 90^\circ$ , it is easily seen that  $\rho_1 > \rho_2$ ,  $\rho_2 < \rho_3$ ,  $\rho_2 > \rho_4$ ,  $\rho_1 > \rho_3$ , and the function  $\rho(v)$  is plotted in Figure 43. For  $\sigma_0 = 0$  the minima are equal ( $\rho_2 = \rho_4$ ), even though  $e \neq 0$ ; the maxima are also equal to each other,  $\rho_1 = \rho_3$ .

The graph of the periodic part of  $\sigma(v - \sigma_0)$  can be easily obtained in a similar way; in the interval  $0 \leq v - \sigma_0 \leq 2\pi$  this graph also has 4 extrema (2 minima and 2 maxima), the distinctive feature being the phase shift that it displays relative to the curve  $\rho(v - \sigma_0)$ .

Combining the graphs of  $\rho(v - \sigma_0)$  and  $\sigma(v - \sigma_0)$ , we can plot the trace of the angular momentum vector  $\mathbf{L}$  on the surface of a unit sphere. As it follows from the preceding, these loci of the vector  $\mathbf{L}$  are attributable to the periodic terms, and are thus analogous to the ellipse (6.6.4) for a circular orbit; the secular displacement of the locus center is ignored.

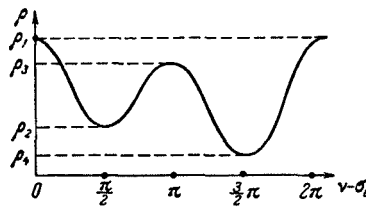


FIGURE 43. Illustrating the function  $\rho(v)$  for an elliptical orbit.

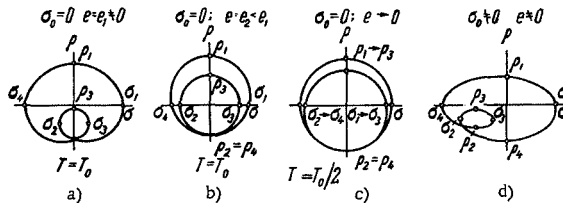


FIGURE 44. The trace of the angular momentum vector in periodic motion (secular motion ignored).

Figure 44a gives the corresponding locus for the case  $\sigma_0 = 0$ ,  $e \neq 0$ . The minima are equal in this case ( $\rho_2 = \rho_4$ ). The complete period of revolution along the curve is equal to the orbital period  $T_0$  of the satellite's mass center. As the eccentricity decreases, the inner and the outer loops approach each other (Figure 44 b, c), so that in the limit, for  $e \rightarrow 0$ , the loops merge into a single ellipse (6.6.4); the vector  $\mathbf{L}$  traces this ellipse in a time  $T = T_0/2$  (Figure 44 c). The general case  $\sigma_0 \neq 0$ ,  $e \neq 0$  is illustrated in Figure 44 d. When the secular motion of the locus center is taken into consideration, we see that the trace of the vector  $\mathbf{L}$  on the surface of a unit sphere has cusp points (see § 3), and the trajectory corresponding to the general case depicted in Figure 44 d is shown in Figure 39. In the case of an elliptical orbit, the motion thus depends not only on the eccentricity  $e$ , but also on the initial position of the vector  $\mathbf{L}$  relative to the radius-vector of the perigee, i.e., on the parameter  $\sigma_0$ .

We should note that there is still another component motion superimposed on the vector  $\mathbf{L}$ : this is the motion of the satellite's axis precessing with a constant nutation angle  $\theta_0$  around the angular momentum vector  $\mathbf{L}$ .

In conclusion, let us consider some numerical examples illustrating the main features of the perturbation effects.

1. Periodic motion of the vector  $\mathbf{L}$ . Initial conditions as in (6.5.8). An Earth satellite moves in a circular orbit ( $e = 0$ ) at an altitude of  $h = 500$  km;  $\theta_0 = 0$ ;  $\frac{A}{C} = 2.5$ ;  $r_0 = 10$  deg/sec.

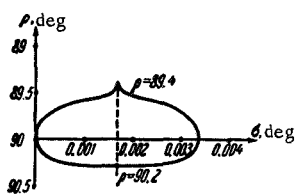


FIGURE 45. A periodic trajectory of the angular momentum vector.

The tip of the vector  $\mathbf{L}$  in this case traces the curve shown in Figure 45.  $\mathbf{L}$  is seen to oscillate slightly: the libration in  $\rho$  is fairly pronounced ( $\Delta\rho = 0^\circ.8$ ), the libration in  $\sigma$  is negligible ( $\Delta\sigma = 0^\circ.0036$ ).

2. Motion in a highly elliptical orbit. Apogee height  $h_a = 10,000$  km; perigee height  $h_p = 300$  km;  $e = 0.421$ ; orbital period  $T_0 = 205^m = 3^h 25^m$ . Satellite parameters:  $\theta_0 = 0^\circ$ ,  $r_0 = 10$  deg/sec,  $\frac{A}{C} = 2.5$ . Initial values:  $\sigma_0 = 45^\circ$ ,  $\rho_0 = 45^\circ$ .

The period in  $\rho$  is approximately equal to the orbital period of the satellite (Figure 46). Amplitude of oscillations  $[\Delta\rho]_{\max} = 0^\circ.5$ . The secular variation in  $\sigma$  constitutes the main effect: during one orbital revolution of the satellite, the vector  $\mathbf{L}$  rotates through  $\Delta\sigma = 2^\circ.7$  around the normal to the orbital plane.

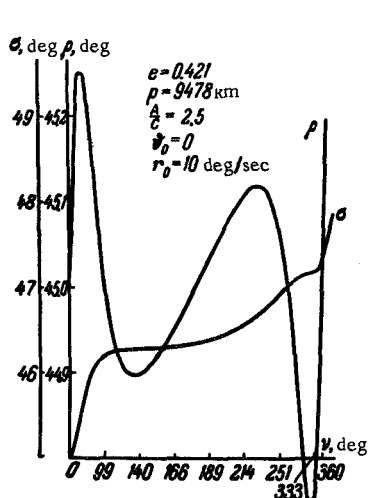


FIGURE 46. Specimen curves  $\rho(v)$  and  $\sigma(v)$ .

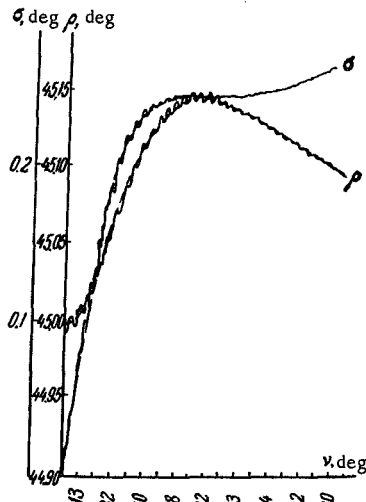


FIGURE 47. Specimen curves  $\sigma(v)$  and  $\rho(v)$  allowing for vibration terms (solid lines) and ignoring them (dashed lines).

3. Estimating the influence of the vibration terms (attributable to precession). The solution is obtained by numerical integration of the nonaveraged equations (5.4.3) (the solid curves in Figure 47), and also from the approximate relations of this chapter (dashed curves in Figure 47). The following parameters and initial values have been

assumed:  $A = 50 \text{ kgm} \cdot \text{sec}^2$ ,  $C = 20 \text{ kgm} \cdot \text{sec}^2$ ,  $L_0 = 3.49 \text{ kgm} \cdot \text{sec}$ ,  $\theta_0 = 70^\circ$ , which corresponds to an initial precessing velocity  $\dot{\psi} = 4 \text{ deg/sec}$  and angular velocity along the symmetry axis  $r_0 = 3.4 \text{ deg/sec}$ ; a highly elliptical orbit is assumed:  $h_n = 300 \text{ km}$ ,  $h_a = 10,000 \text{ km}$  ( $e = 0.421$ ,  $P = 9478 \text{ km}$ ). Initial values:  $\sigma_0 = 0$ ,  $\rho_0 = 45^\circ$ . We see from Figure 47 that the periodic increment in  $\rho$  is  $(\Delta\rho)_p \approx 0^\circ.15$ , whereas the increment due to vibrational oscillations is  $(\Delta\rho)_v \sim 0^\circ.001 - 0^\circ.005$ .

To sum up, the principal effects of motion are governed by the secular terms: their contribution must never be ignored. If higher precision is required, the secular effects may be supplemented with periodic terms. The vibrational terms need not be considered, since they are always negligible.

## § 7. GRAVITATIONAL PERTURBATIONS ON A SATELLITE WITH A TRIAXIAL ELLIPSOID OF INERTIA /71/

The method of averaging employed in previous sections is essentially the asymptotic method of N. M. Krylov and N. N. Bogolyubov /19/, as modified by V. M. Volosov /23, 24/, who considered a set of equations in the form

$$\dot{x} = \varepsilon X(x, y, t, \varepsilon), \quad \dot{y} = Y(x, y, t, \varepsilon), \quad \varepsilon \ll 1, \quad (6.7.1)$$

where  $x$ ,  $X$  are  $n$ -dimensional, and  $y$ ,  $Y$  are  $m$ -dimensional vector functions,  $\varepsilon$  is a small parameter;  $x$  are the "slow" variables, and  $y$  the "fast" variables. The general solution of the unperturbed (degenerate) system

$$x = \text{const}, \quad \dot{y} = Y(x, y, t, 0), \quad (6.7.2)$$

which obtains from (6.7.1) for  $\varepsilon = 0$ , is assumed to be known. Let  $y(x, y_0, t)$  be this general solution satisfying arbitrary initial conditions  $y(t_0) = y_0$ . An asymptotic solution of the set (6.7.1) to  $k$ -th approximation is sought in the form

$$\left. \begin{aligned} x &= \xi + \varepsilon u_1(\xi, \eta, t) + \dots + \varepsilon^{k-1} u_{k-1}(\xi, \eta, t), \\ y &= \eta + \varepsilon v_1(\xi, \eta, t) + \dots + \varepsilon^{k-2} v_{k-2}(\xi, \eta, t), \end{aligned} \right\} \quad (6.7.3)$$

where the variables  $\xi, \eta$  satisfy the  $k$ -th order equations

$$\left. \begin{aligned} \dot{\xi} &= \varepsilon A_1(\xi) + \varepsilon^2 A_2(\xi) + \dots + \varepsilon^k A_k(\xi), \\ \eta &= Y(\xi, \eta, t, 0) + \varepsilon B_1(\xi) + \dots + \varepsilon^{k-1} B_{k-1}(\xi), \end{aligned} \right\} \quad (6.7.4)$$

and  $A_i(\xi)$  is obtained by averaging the function  $X$  over the unperturbed solutions of (6.7.2):

$$A_i(\xi) = M_t \{X(\xi, y, t, 0)\}, \quad (6.7.5)$$

$$M_t \{f(x, y, t)\} = \lim_{T \rightarrow \infty} \frac{1}{T} \int_{t_0}^{t_0+T} f[x, y(x, y_0, t), t] dt. \quad (6.7.6)$$

The result of averaging in (6.7.5) is assumed to be independent of the initial values  $t_0, y_0$ , which holds true for a wide choice of cases.

In /23, 24/ an algorithm is given for constructing the functions  $u_i$ ,  $v_i$ ,  $A_i$ ,  $B_i$  and suitable substantiating theorems are proved. For some quite general assumptions, the  $k$ -th approximation (6.7.3) will deviate from the exact solution by terms of the order of  $\varepsilon^k$  in the variable  $x$ , and by terms of the order of  $\varepsilon^{k-1}$  in the variable  $y$ , for  $t$  varying in an interval of the order of  $\varepsilon^{-1}$ .

The set (6.7.4) is substantially simpler than the starting equations, since the equations for  $\xi$  are autonomous and can be integrated separately. The equations of perturbed motion (5.3.6), (5.4.3), (5.5.2), and (5.5.5) are all classified in one group with the general set (6.7.1). The "fast" variables, say, are the Eulerian angles, while the "slow" variables are the magnitude and the angular coordinates of the angular momentum vector. In previous sections the method of averaging was applied to analyze the equations of rotation of a dynamically symmetric satellite, (5.4.3). This method can also be successfully applied to investigate equations (5.5.2) and (5.5.5) for the rotation of a satellite with a triaxial ellipsoid of inertia.

This analysis was carried by F. L. Chernous'ko /71/. He considered two techniques for the introduction of the small parameter  $\varepsilon$ : 1) the ellipsoid of inertia is nearly spherical, so that  $A=J_0+\varepsilon A'$ ;  $B=J_0+\varepsilon B'$ ;  $C=J_0+\varepsilon C'$ ; 2) the relative angular velocity of the satellite is much higher than the mean

angular velocity  $\bar{\omega}_0 = \frac{2\pi}{T_0}$  of its orbital motion ( $T_0$  is the orbital period of the satellite), so that  $\varepsilon \sim \frac{A\bar{\omega}_0}{L_0} \ll 1$ ; arbitrary moments of inertia are assumed ( $A \geq B \geq C$ ). We shall adopt here the second technique, as it constitutes a direct generalization of the previous results and is of greater practical significance. This is the case of rotational kinetic energy which is large in comparison with the work of external forces.

The gravity torque components for a triaxial satellite can be written as

$$\left. \begin{aligned} M_1 &= 3\bar{\omega}_0^2(1+e \cos v)^3(1-e^2)^{-3} \sum_{j=1}^3 \bar{\beta}_j (\bar{\beta}_2 S_{3j} - \bar{\beta}_3 S_{2j}), \\ M_2 &= 3\bar{\omega}_0^2(1+e \cos v)^3(1-e^2)^{-3} \sum_{j=1}^3 \bar{\beta}_j (\bar{\beta}_3 S_{1j} - \bar{\beta}_1 S_{3j}), \\ M_3 &= 3\bar{\omega}_0^2(1+e \cos v)^3(1-e^2)^{-3} \sum_{j=1}^3 \bar{\beta}_j (\bar{\beta}_1 S_{2j} - \bar{\beta}_2 S_{1j}), \\ S_{ij} &= A a_{i1} a_{j1} + B a_{i2} a_{j2} + C a_{i3} a_{j3}. \end{aligned} \right\} \quad (6.7.7)$$

Here  $a_{ik}$  are defined by (1.1.5), and  $\bar{\beta}_j$  are the direction cosines of the radius-vector  $r$  relative to the axes  $L_1, L_2, L$ . It is easily seen that

$$\bar{\beta}_1 = \cos \rho \cos(v-\sigma), \quad \bar{\beta}_2 = \sin(v-\sigma), \quad \bar{\beta}_3 = \sin \rho \cos(v-\sigma).$$

The equations of motion are (5.5.2) and (5.5.5) with  $M_i$  inserted from (6.7.7). The unperturbed motion ( $\varepsilon = 0$ ) is an Euler-Poinsot motion, with constant  $L$ ,  $\rho$ ,  $\sigma$ , and a constant kinetic energy  $T$ . The function  $\psi(t)$  is representable as  $\psi = \psi_1(t) + \psi_2(t)$ ;  $\psi_1$ ,  $\psi_2$ ,  $\psi_3$  are  $t$ -periodic, with a period equal to the polhodic period  $\tau$  of the vector  $L$  (or acquire a constant increment  $2\pi$  in the time  $\tau$ );  $\psi_2 = \frac{2\pi t}{\tau}$ , where the periods  $\tau$  and  $\tau'$  depending on  $L$  and  $T$  are in general incommensurate. In the case of perturbed motion,  $T$  satisfies

the differential equation

$$\begin{aligned}\dot{T} = & \frac{2T}{L} M_3 + L \sin \vartheta \left[ \cos \vartheta \left( \frac{\sin^2 \varphi}{A} + \frac{\cos^2 \varphi}{B} - \frac{1}{C} \right) \times \right. \\ & \times (M_2 \cos \psi - M_1 \sin \psi) + \\ & \left. + \sin \varphi \cos \varphi \left( \frac{1}{A} - \frac{1}{B} \right) (M_1 \cos \psi + M_2 \sin \psi) \right].\end{aligned}\quad (6.7.8)$$

The "slow" variables ( $x$ ) of perturbed motion are  $L, \rho, \sigma, T$ , and the "fast" variables ( $y$ ) are  $\varphi$  and  $\psi$ . The angle  $\vartheta$  is expressed in terms of  $T$  and  $\varphi$  by the relation

$$T = \frac{L^2}{2} \left[ \left( \frac{\sin^2 \varphi}{A} + \frac{\cos^2 \varphi}{B} \right) \sin^2 \vartheta + \frac{\cos^2 \vartheta}{C} \right]. \quad (6.7.9)$$

Since

$$\dot{v} = \frac{\bar{\omega}_0 (1 + e \cos v)^2}{(1 - e)^{1/2}}, \quad (6.7.10)$$

and  $M_i \sim \omega_0^2$ , the equations of motion have the general structure

$$\dot{x} = \varepsilon^2 X(x, y, v), \quad \dot{y} = Y_0(x, y) + \varepsilon^2 Y_1(x, y, v), \quad \dot{v} = \varepsilon f(v). \quad (6.7.11)$$

When constructing a solution of the form (6.7.3) for the set (6.7.11), we find that  $u_1 = v_1 \equiv 0, A_1 = B_1 = A_3 \equiv 0, A_2 = M_1 \{X\}$ . The solution for the "slow" variables is sought in the form

$$x = \xi, \quad \dot{\xi} = \varepsilon^2 A_2(\xi, v) = \varepsilon^2 M_t \{X(\xi, y, v)\}. \quad (6.7.12)$$

The error in the solution for the slow variables is of the order of  $\varepsilon^2$  over time intervals of the order of  $\varepsilon^2$ , which corresponds to  $\varepsilon^{-1}$  orbital revolutions of the satellite (since  $\Delta v \sim \varepsilon^{-1}$ ).

To obtain a smoothed system (6.7.12), the right-hand sides of the equations of motion should be averaged (for fixed "slow" variables and  $v$ ) over the Euler—Poinsot motion. These right-hand sides are periodic functions of  $\vartheta, \varphi, \psi$  with a period of  $2\pi$  and incommensurate  $\tau$  and  $\tau'$ . It can be shown /71/ that in this case time-averaging is equivalent to independent averaging over  $\tau$  and  $\tau'$ , i.e.,

$$\begin{aligned}M_t \{f(\vartheta, \varphi, \psi)\} &= \frac{1}{\tau \tau'} \int_0^\tau \int_0^{\tau'} f \left[ \vartheta(t), \varphi(t), \psi_1(t) + \frac{2\pi t'}{\tau'} \right] dt dt' = \\ &= \frac{1}{2\pi\tau} \int_0^\tau \int_0^{2\pi} f(\vartheta(t), \varphi(t), \psi) d\psi dt = M_\psi M_t \{f(\vartheta, \varphi, \psi)\}.\end{aligned}\quad (6.7.13)$$

Here  $M_\psi$  denotes  $\psi$ -averaging, and  $M_t$  stands for averaging over  $\vartheta$  and  $\varphi$  (related by (6.7.9)) along the closed trajectories (polhodies) of the angular momentum vector in the Euler—Poinsot motion.

Averaging and changing over to a new independent variable — the true anomaly  $v$ , we find

$$\left. \begin{aligned} L &= L, \quad T = T_0, \\ \frac{d\theta}{dv} &= N(1 + e \cos v) \sin \rho \sin(\sigma - v) \cos(\sigma - v), \\ \frac{d\sigma}{dv} &= N(1 + e \cos v) \cos \rho \cos^2(\sigma - v), \\ N &= \frac{3}{2} \frac{\bar{\omega}_0}{(1 - e^2)^{3/2} L_0} \left\{ B + C - 2A + \right. \\ &\quad \left. + 3 \left( \frac{2T_0 A}{L_0^2} - 1 \right) \left[ C + (B - C) \frac{K(k) - E(k)}{k^2 K(k)} \right] \right\}. \end{aligned} \right\} \quad (6.7.14)$$

Here  $K(k)$ ,  $E(k)$  are the complete elliptical integrals of the first and the second kind, respectively,

$$k^2 = \frac{(B - C)(2T_0 A - L_0^2)}{(A - B)(L_0^2 - 2T_0 C)}. \quad (6.7.15)$$

This result holds true for polhodies around the axis  $x'$  ( $L^2 > 2TB$ ); for polhodies around the axis  $z'$  ( $L^2 < 2TB$ ),  $A$  and  $C$  in (6.7.14) and (6.7.15) should be switched. We see that equations (6.7.14) are formally identical with the previously investigated equations (6.3.1), but the constant coefficient  $N$  is more complex. It is easily verified that, in a case of dynamic symmetry ( $C = B$ ),  $N$  reduces to  $N_0$  from (6.3.1) (with suitably modified notations of the moments of inertia).

The perturbed motion of a satellite is thus made up from Euler—Poinsot motion around the angular momentum vector and proper motion of the angular momentum vector according to equations (6.7.14).

## Chapter 7

### AERODYNAMIC PERTURBATIONS IN ROTATIONAL MOTION

#### § 1. RESTORING AERODYNAMIC TORQUES. SECULAR EFFECTS

The restoring aerodynamic torque may be written in the form (1.3.11) (the first term only; the dissipative effects are ignored). Let  $\bar{c}(\delta_V) \equiv \bar{c}(\cos \delta_V)$ . The aerodynamic torque components on the axes of the perigee system are then written as

$$\left. \begin{aligned} M_x &= \frac{1}{2} \rho_a V \bar{c}(\cos \delta_V) [V_y \gamma_3 - V_z \beta_3], \\ M_y &= \frac{1}{2} \rho_a V \bar{c}(\cos \delta_V) [V_z \alpha_3 - V_x \gamma_3], \\ M_z &= \frac{1}{2} \rho_a V \bar{c}(\cos \delta_V) [V_x \beta_3 - V_y \alpha_3], \\ \cos \delta_V &= \frac{V_x \alpha_3 + V_y \beta_3 + V_z \gamma_3}{V}, \\ V_x &= \sqrt{\frac{\mu}{P}} (e + \cos v) - w \frac{P}{1+e \cos v} \cos i \cos v, \\ V_z &= -\sqrt{\frac{\mu}{P}} \sin v + w \frac{P}{1+e \cos v} \cos i \sin v, \\ V_y &= w \frac{P}{1+e \cos v} \sin i \cos (\omega_n + v). \end{aligned} \right\} \quad (7.1.1)$$

Here  $V_y$  and the second terms in the expressions for  $V_x$ ,  $V_z$  are attributable to the Earth's spin with an angular velocity  $w$ . The velocity contributed by the Earth's spin is some 1–5% of  $V$ , so that the terms with  $w$  can often be ignored. The torque (7.1.1) is produced by the force function

$$\begin{aligned} U &= -\frac{1}{2} \rho_a V^2 \int \bar{c}(\cos \delta_V) d(\cos \delta_V) = \\ &= -\frac{1}{2} \rho_a V^2 \left( a_0^b \cos \delta_V + \frac{1}{2} a_1^b \cos^2 \delta_V + \frac{1}{3} a_2^b \cos^3 \delta_V \right), \end{aligned} \quad (7.1.2)$$

where the last equality has been obtained by approximating  $\bar{c}(\cos \delta_V)$  in accordance with (1.3.19). The formulas of Chapter 5 can now be applied; in particular, the secular trajectory of the angular momentum vector is described by (5.4.14).

Let us first consider the motion neglecting the rotation of the atmosphere.

Then

$$\left. \begin{aligned} \cos \delta_V &= \frac{(e + \cos v) a_3 - \sin v \gamma_3}{\sqrt{1+e^2+2e \cos v}}, \\ V &= \sqrt{\frac{\mu}{P}} \sqrt{1+e^2+2e \cos v}, \\ U_v &= -\frac{1}{2} \bar{\rho}_a \sqrt{\mu P} \bar{\rho}_a \frac{1+e^2+2e \cos v}{(1+e \cos v)^2} \times \\ &\quad \times \left( a_0^\delta \cos \delta_V + \frac{a_1^\delta}{2} \cos^2 \delta_V + \frac{a_2^\delta}{3} \cos^3 \delta_V \right). \end{aligned} \right\} \quad (7.1.3)$$

The following symbols are used:  $\bar{\rho}_a$  the density of the atmosphere in perigee,  $\bar{\rho}_a = \frac{\rho_a(h)}{\rho_a}$  a nondimensional density function,  $\bar{\rho}_a(0)=1$ . We may take, e.g.,  $\bar{\rho}_a = \exp\left(-\frac{h}{H}\right)$ , where  $h=r-r_\pi=\frac{P}{1+e \cos v}-\frac{P}{1+e}$  is the elevation of a current point of the orbit above the perigee, and  $H$  the so-called density scale height (a constant quantity). Let

$$\left. \begin{aligned} J_1 &= \frac{1}{2\pi} \int_0^{2\pi} \bar{\rho}_a \frac{\sqrt{1+e^2+2e \cos v}}{(1+e \cos v)^2} (e + \cos v) dv, \\ J_2 &= \frac{1}{2\pi} \int_0^{2\pi} \bar{\rho}_a \frac{(e + \cos v)^2}{(1+e \cos v)^2} dv, \\ J_3 &= \frac{1}{2\pi} \int_0^{2\pi} \bar{\rho}_a \frac{\sin^2 v}{(1+e \cos v)^2} dv, \\ J_4 &= \frac{1}{2\pi} \int_0^{2\pi} \bar{\rho}_a \frac{(e + \cos v)^3 dv}{(1+e \cos v)^2 \sqrt{1+e^2+2e \cos v}}, \\ J_5 &= \frac{1}{2\pi} \int_0^{2\pi} \bar{\rho}_a \frac{(e + \cos v) \sin^2 v dv}{(1+e \cos v)^2 \sqrt{1+e^2+2e \cos v}}. \end{aligned} \right\} \quad (7.1.4)$$

For a constant perigee height  $h_\pi$ , these quantities depend on the apogee height  $h_a$  and on  $H$  (Figure 48). The aerodynamic perturbations in the

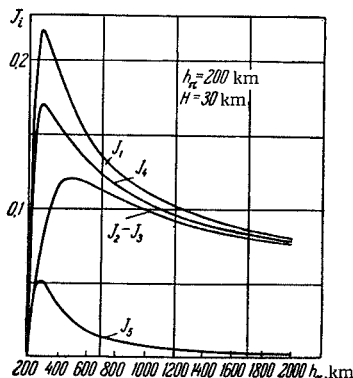


FIGURE 48. The integrals  $J_i$  vs. apogee height  $h_a$  for a constant perigee height  $h_\pi$ .

motion of the vector  $L$  can be conveniently considered in the coordinates  $\theta, \lambda$  (Chapter 1, § 1), applying relation (1.1.4a). In deriving the averaged expression (5.4.13) of the force function (7.1.3), we shall also make use of (1.1.7). Then from (5.4.14) we obtain the secular trajectory of the vector  $L$ :

$$\bar{U}_v = \bar{U}_{v1} + \bar{U}_{v2} = \bar{U}_v^0 \quad (7.1.5)$$

$$\begin{aligned} \bar{U}_{v1} = -\frac{\sqrt{\mu P}}{2} \rho_n \left\{ \cos \theta \cos \vartheta \left[ a_0^b J_1 + \frac{a_2^b}{2} J_4 \sin^2 \vartheta + \right. \right. \\ \left. \left. + a_2^b J_5 \left( \frac{\sin^2 \vartheta}{2} + \left( 1 - \frac{5}{2} \sin^2 \vartheta \right) \cos^2 \lambda \right) \right] + \right. \\ \left. + \frac{a_1^b}{2} (J_2 - J_3) \left( 1 - \frac{3}{2} \sin^2 \vartheta \right) \cos^2 \theta + \right. \\ \left. + \left( 1 - \frac{5}{2} \sin^2 \vartheta \right) \left[ \frac{a_2^b}{3} J_4 - a_2^b J_5 \cos^2 \lambda \right] \cos^3 \theta \cos \vartheta \right\}, \end{aligned} \quad (7.1.6)$$

$$\bar{U}_{v2} = -\frac{1}{4} \rho_n \sqrt{\mu P} a_1^b J_3 \left( 1 - \frac{3}{2} \sin^2 \vartheta \right) \sin^2 \rho. \quad (7.1.7)$$

$\bar{U}_{v2}$  is formally identical with the secular part of the force function of the gravity torques (6.2.3). The sum of the two functions gives

$$\begin{aligned} \bar{U}_v = \frac{1}{4} \left( 1 - \frac{3}{2} \sin^2 \vartheta \right) \left[ 3 \frac{\sqrt{\mu}}{P^{1/2}} (A - C) - \right. \\ \left. - \rho_n \sqrt{\mu P} a_1^b J_3 \right] \sin^2 \rho = k_0^* \sin^2 \rho. \end{aligned} \quad (7.1.8)$$

The term  $\bar{U}_{v2}$  thus introduces a certain quantitative correction in the previously considered gravitational effects; in the analysis of the combined effect of gravitational and aerodynamic perturbations (see Chapter 8),  $\bar{U}_{v2}$  is not treated as a term of independent qualitative significance; the main aerodynamic perturbation term is therefore  $\bar{U}_{v1}$  (7.1.6). The equations of perturbed motion for the perturbations  $\bar{U}_{v1}$ , according to the results of § 4 of Chapter 5, are

$$\frac{d\lambda}{dv} = \frac{1}{L_0 \sin \theta} \frac{\partial \bar{U}_{v1}}{\partial \theta}, \quad \frac{d\theta}{dv} = -\frac{1}{L_0 \sin \theta} \frac{\partial \bar{U}_{v1}}{\partial \lambda}. \quad (7.1.9)$$

and hence

$$\begin{aligned} \frac{d\lambda}{dv} = \frac{\rho_n}{2} \frac{\sqrt{\mu P}}{L_0} \left\{ \cos \vartheta \left[ a_0^b J_1 + \frac{a_2^b}{2} J_4 \sin^2 \vartheta + \right. \right. \\ \left. \left. + a_2^b J_5 \left( \frac{1}{2} \sin^2 \vartheta + \left( 1 - \frac{5}{2} \sin^2 \vartheta \right) \cos^2 \lambda \right) \right] + \right. \\ \left. + a_1^b (J_2 - J_3) \left( 1 - \frac{3}{2} \sin^2 \vartheta \right) \cos \theta + \right. \\ \left. + 3 \cos \vartheta \left( 1 - \frac{5}{2} \sin^2 \vartheta \right) \left[ \frac{a_2^b}{3} J_4 - a_2^b J_5 \cos^2 \lambda \right] \cos^2 \theta \right\}, \\ \frac{d}{dv} \cos \theta = \frac{\rho_n \sqrt{\mu P}}{L_0} a_2^b J_5 \cos \vartheta \left( 1 - \frac{5}{2} \sin^2 \vartheta \right) \times \\ \times \cos \theta \sin^2 \theta \cos \lambda \sin \lambda. \end{aligned} \quad (7.1.10)$$

Let us consider the principal properties of aerodynamic perturbations  $\bar{U}_{v1}$  in various particular cases.

1. All the integral coefficients in (7.1.6) (i.e.,  $J_2 - J_3, J_1, J_4, J_5$ ) vanish for  $e = 0$ ; circular orbits are therefore free from secular perturbations.

2.  $J_5$  is smaller by one order of magnitude than the other integral coefficients: this follows from Figure 48 and from the expression (7.1.4) for the integrals.  $J_5$  can therefore be ignored, setting  $J_5 \approx 0$ . From (7.1.10) we then have  $\theta \approx \theta_0$ , i.e., *aerodynamic perturbations produce precession of the vector L at a constant angular distance about the direction of the perigee tangent with a velocity  $\frac{d\lambda}{dv}$  from (7.1.10), where  $J_5=0, \theta=\theta_0$ .*

The contribution of the term  $J_5$  is considered at the end of this section.

3.  $a_1^b \neq 0$ , if the following two conditions are satisfied simultaneously:  
(a) the proportion of reflected molecules whose interaction with the satellite is other than ideally inelastic collision is fairly large, (b) the satellite does not possess bilateral symmetry (i.e., although the satellite has an axis of symmetry, it looks different from the nose and from the tail). Since condition (a) is fairly improbable, we may apparently take  $a_1^b \ll a_0^b, a_2^b$ , setting  $a_1^b = 0$ . For bilaterally symmetric satellites, this condition is satisfied irrespective of (a). Then, applying 2 and 3 above, we find

$$\left. \begin{aligned} \theta &= \theta_0, \quad \frac{d\lambda}{dv} = \frac{\rho_\pi}{2} \frac{\sqrt{\mu P}}{L_0} \cos \theta_0 [k_0^b + k_1^b \cos^2 \theta_0], \\ k_0^b &= a_0^b J_1 + \frac{a_2^b}{2} J_4 \sin^2 \theta_0, \quad k_1^b = \left(1 - \frac{5}{2} \sin^2 \theta_0\right) a_2^b J_4. \end{aligned} \right\} \quad (7.1.11)$$

In the simplest case (1.3.18),  $a_2^b = a_1^b = 0$  (the aerodynamic torque is a sinusoidal function of the angle of attack), and we have

$$\frac{d\lambda}{dv} = \frac{\rho_\pi}{2} \frac{\sqrt{\mu P}}{L_0} \cos \theta_0 a_0^b J_1. \quad (7.1.12)$$

It follows from (7.1.11) and (7.1.12) that for a tumbling satellite ( $\theta = 90^\circ$ ), the aerodynamic torque does not produce any secular effect. From the general formulas (7.1.10) we see that this proposition does not hold true if  $a_1^b \neq 0$ .

Let us consider the limiting case  $a_1^b \neq 0, a_2^b = a_0^b = 0$ , which corresponds to the hypothesis adopted in /79/. Then the trajectory

$$\bar{U}_{v1} + \bar{U}_{v2} = \text{const}$$

takes the form

$$(J_2 - J_3) \cos^2 \theta + J_3 \sin^2 \theta = \text{const.}$$

The family of trajectories for an elliptical orbit ( $e \neq 0, J_2 \neq J_3$ ) is plotted in Figure 49. The angular momentum vector will precess around the normal  $n$  to the orbital plane or around the perigee tangent  $V_\pi$  according as

$$|\cos \rho_0| \geq \sqrt{\frac{J_2 - J_3}{J_3}} \cos \theta_0,$$

where  $\rho_0, \theta_0$  are the initial coordinates of the angular momentum vector.

We should again emphasize that the case  $|a_1^b| \ll |a_0^b|, |a_2^b|$  is much more probable.

Let us consider the contribution of the small coefficient  $J_5$  which has been ignored in the derivation of the main formulas (7.1.11), (7.1.12). Inserting  $\theta = \text{const}$  in the right-hand side of the second equation in (7.1.10) and substituting the variable  $\lambda$  for  $v$ , we reduce the starting equation to quadratures. Its solution approximately describes the nutation of the vector  $L$ . Taking  $\theta \approx \theta_0 + \Delta\theta$ , we find

$$\Delta\theta = -\frac{\rho_\pi V \mu P a_2^\delta J_5}{2L_0 \lambda'} \left(1 - \frac{5}{2} \sin^2 \theta_0\right) \cos \theta \cos \theta_0 \sin \theta_0 \sin^2 \lambda, \quad (7.1.13)$$

where  $\lambda'$  is the approximate average velocity of secular precession, defined by (7.1.11). The contribution of  $J_5 \neq 0$  (the increment  $\Delta\theta$ ) thus slightly stretches the small circle  $\theta = \theta_0$  into an oval (Figure 50). Formula (7.1.13) shows that nutation in  $\theta$  is possible only if  $a_2^\delta \neq 0$ , i.e., if the aerodynamic torque coefficient is not constant and the aerodynamic torque is not a sinusoidal function of the angle of attack. For real satellites, these oscillations in  $\theta$  do not exceed  $2-3^\circ$ .

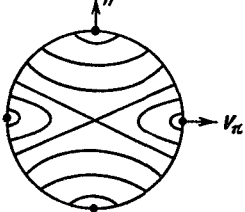


FIGURE 49. Secular trajectories of the angular momentum vector due to aerodynamic perturbations: the principal terms in the aerodynamic torque coefficient are zero ( $a_0^\delta = a_2^\delta = 0$ ;  $a_1^\delta \neq 0$ ).

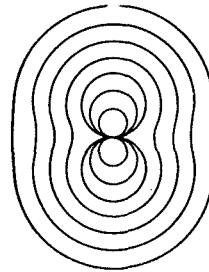


FIGURE 50. Curves traced by the tip of the angular momentum vector in a small neighborhood of the aeropoles for the case of aerodynamic torques dependent on the angle of attack.

These oscillations in  $\theta$  will distort the trajectory in a small neighborhood of the perigee. Let us approximately show how this happens. For simplicity, in the trajectory (7.1.5) we retain terms with  $\cos \theta$ , omitting all the terms with  $\cos^2 \theta$  and  $\cos^3 \theta$ . The integral of equations (7.1.5) is then written as

$$\cos \theta = \frac{C}{1 + \varepsilon_\lambda \cos^2 \lambda}, \quad (7.1.14)$$

where  $C$  is an integration constant,  $\varepsilon_\lambda$  a constant dependent on  $J_i$  and  $a_i^\delta$ . Let  $\varepsilon_\lambda > 0$ . The trajectories corresponding to the solution (7.1.14) are plotted in Figure 50. The curve  $\theta(\lambda)$  for  $C < 1$  is an oval, for  $C = 1$  it is a figure-of-eight tangent to the plane  $XY$ , and for  $C > 1$  it is a figure-of-eight not tangent to the plane  $XY$  (i.e., making a nonzero angle with  $Y$ ). For the curves

$C > 1$ , with  $\lambda = 0$  we have  $\cos \theta = \frac{C}{1 + \varepsilon_\lambda} < 1$ , i.e.,  $1 < C < 1 + \varepsilon_\lambda$ ;  $\lambda = 90^\circ$  cannot be achieved on these curves ( $\lambda$  oscillates between finite limits; the limiting

value  $\lambda^*$  is obtained for  $\theta = 0$ :  $\cos^2 \lambda^* = \frac{C-1}{\epsilon_1}$ ). This pattern is observed only in a small neighborhood of the perigee ( $\theta \sim 2 - 3^\circ$ ). When the region of motion is broadened, the tip of the vector  $L$  traces nearly circular ovals. For  $\epsilon_1 < 0$  the pattern is the same, but it is rotated through  $90^\circ$  about the axis  $X$ .

Let us consider some numerical examples.

**Example 1.** We assume the following numerical characteristics for the orbit, the satellite, and its spin:  $h_\pi = 225$  km,  $h_a = 900$  km,  $\rho_\pi = 3.28 \cdot 10^{-11} \text{ kg} \cdot \text{sec}^2 / \text{m}^4$ ,  $|L_0| = 500 \text{ kgm} \cdot \text{sec}^2 \cdot 10^\circ / \text{sec}$ ; characteristic area  $S = 6 \text{ m}^2$ ; center of mass to center of pressure distance  $z'_0 = 0.3 \text{ m}$ . The aerodynamic coefficient has the maximum and the minimum values  $c_{\max} = 18$ ,  $c_{\min} = 3$ . From these data we can calculate the coefficients  $a_0^b$  and  $a_2^b$ , and then, from (7.1.11), the velocity of secular precession. The results of

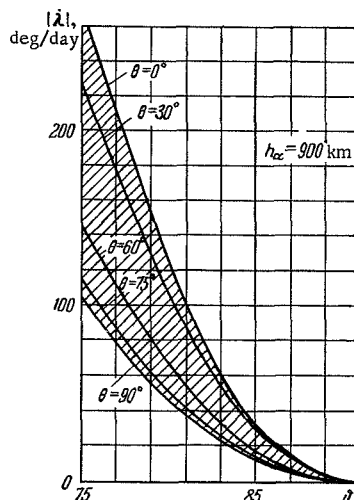


FIGURE 51. Angular velocity of secular precession of the angular momentum vector due to aerodynamic perturbations (for the parameters of Sputnik II).

these calculations are plotted in Figure 51, where the diagonally hatched region represents the permitted angular velocities of secular precession as a function of the angle of nutation  $\theta$  and the angle  $\theta$  between the vector  $L$  and the tangent at the perigee. We see that in the case of tumble ( $90^\circ > \theta > 80^\circ$ ), the angular velocity of secular precession may be as high as 50° per day. (Note that in one day the satellite completes 15—16 orbital revolutions.)

**Example 2.** For Sputnik III, we may take  $c_{\max} = 2.4$ ,  $c_{\min} = 2.1$ ,  $z'_0 = 0.3 \text{ m}$ . The dynamic parameters of Sputnik III will be found in the examples of Chapter 6. The orbital parameters are assumed the same as in the previous example. Then the rate of secular precession is  $\dot{\lambda} = 3 - 4^\circ$  per day ( $\sim 0^\circ.2$  per one orbital revolution), and the amplitude of the long-period nutation is  $\Delta\theta \sim 0^\circ.5$ .

## § 2. ATMOSPHERIC ROTATION AND ITS EFFECT ON SECULAR PERTURBATIONS

To bring out the main effects attributable to the rotation of the atmosphere, we adopt for  $\bar{c}(\delta_v)$  the simple approximation formula (1.3.18); then from (7.1.3)

$$U_v = -\frac{1}{2} \rho_\pi \sqrt{\mu P} \bar{a}_a \frac{1+e^2+2e \cos v}{(1+e \cos v)^2} a_0^\delta \cos \delta_v, \quad (7.2.1)$$

where  $\cos \delta_v$  is determined from (7.1.1). In (7.2.1) it suffices to retain terms of the first order of smallness relative to  $w$ . Then  $U_v$  is written as

$$\begin{aligned} U_v = & -\frac{1}{2} \rho_\pi \sqrt{\mu P} \frac{\bar{a}_a a_0^\delta}{(1+e \cos v)^2} \left\{ \left[ (e + \cos v) \times \right. \right. \\ & \times \sqrt{1+2e \cos v+e^2} - \frac{P^{1/2} w}{\sqrt{\mu}} \cos i \frac{e + \cos v}{\sqrt{1+e^2+2e \cos v}} \left. \right] a'' - \\ & - \left[ \sin v \sqrt{1+e^2+2e \cos v} - \frac{P^{1/2} w}{\sqrt{\mu}} \cos i \frac{\sin v}{\sqrt{1+e^2+2e \cos v}} \right] \gamma'' \left. \right\} - \\ & - \frac{1}{2} \rho_\pi P^2 w \bar{a}_a \frac{a_0^\delta}{1+e \cos v} \left\{ - \cos i \cos v a'' + \right. \\ & \left. + \sin i \cos (\omega_\pi + v) \beta'' + \cos i \sin v \gamma'' \right\}. \end{aligned} \quad (7.2.2)$$

Let

$$F_0 = J_1 - \frac{P^{1/2} w}{\sqrt{\mu}} \cos i \frac{1}{2\pi} \int_0^{2\pi} \frac{\bar{a}_a (e + \cos v) dv}{(1+e \cos v)^2 \sqrt{1+e^2+2e \cos v}}, \quad (7.2.3)$$

where  $J_1$  is defined by (7.1.4);

$$S_0 = \frac{1}{2\pi} \int_0^{2\pi} \bar{a}_a \frac{\sqrt{1+e^2+2e \cos v}}{(1+e \cos v)^3} dv. \quad (7.2.4)$$

Then  $U_v$  averaged over  $\psi$  and over  $v$  is written as

$$\begin{aligned} \bar{U}_v = & -\frac{1}{2} \rho_\pi \sqrt{\mu P} a_0^\delta F_0 \cos \theta \cos \theta + \\ & + \frac{1}{2} \rho_\pi w P^2 a_0^\delta S_0 \cos \theta (\cos i \cos \theta + \sin i \sin \omega_\pi \sin \theta \sin \lambda). \end{aligned} \quad (7.2.5)$$

Let also

$$\left. \begin{aligned} \sin \theta_w^* &= \frac{\sin i \sin \omega_\pi}{\sqrt{\cos^2 i + \sin^2 i \sin^2 \omega_\pi}}, \\ \cos \theta_w^* &= \frac{\cos i}{\sqrt{\cos^2 i + \sin^2 i \sin^2 \omega_\pi}}, \end{aligned} \right\} \quad (7.2.6)$$

$$\left. \begin{aligned} k_s &= \frac{1}{2} \rho_\pi w P^2 a_0^\delta S_0 \cos \theta \sqrt{\cos^2 i + \sin^2 i \sin^2 \omega_\pi}, \\ k_F &= \frac{1}{2} \rho_\pi \sqrt{\mu P} a_0^\delta F_0 \cos \theta, \end{aligned} \right\} \quad (7.2.7)$$

$$\cos \kappa_w = \cos \theta_w^* \cos \theta + \sin \theta_w^* \sin \theta \sin \lambda. \quad (7.2.8)$$

Then

$$\bar{U}_v = -k_F \cos \theta + k_s \cos \kappa_w = \bar{U}_v^0 \quad (7.2.9)$$

is the equation of the trajectory, which may also be written as

$$\cos \theta = C_0 - a_w \cos \nu_w. \quad (7.2.10)$$

Since

$$a_w = \frac{Pw \sqrt{\cos^2 i + \sin^2 i \sin^2 \omega_n}}{\sqrt{\frac{\mu}{P}}} \frac{S_0}{F_0} \sim \frac{Pw}{\sqrt{\frac{\mu}{P}}} \quad (7.2.11)$$

is small, the trajectory hardly differs from  $\cos \theta = \cos \theta_0$ , i.e., the contribution of atmospheric rotation is small in comparison with the main atmospheric effects.

Let us determine the poles of the trajectories. The equations of motion have the form (7.1.9) (with  $\bar{U}_v$  inserted from (7.2.5)), and we may write

$$\left. \begin{aligned} \frac{d\lambda}{dv} &= \frac{k_F}{L_0} - \frac{k_S}{L_0} \cos \theta_w^* + \frac{k_S}{L_0} \sin \theta_w^* \operatorname{ctg} \theta \sin \lambda, \\ \frac{d\theta}{dv} &= -\frac{k_S}{L_0} \sin \theta_w^* \sin \theta \cos \lambda. \end{aligned} \right\} \quad (7.2.12)$$

From these equations we find the pole coordinates  $\lambda_p, \theta_p$ :

$$\lambda_p = 90^\circ (270^\circ), \quad \pm \operatorname{tg} \theta_p = \frac{k_S \sin \theta_w^*}{k_F - k_S \cos \theta_w^*}. \quad (7.2.13)$$

Since  $k_S \ll k_F$ , the pole is close to  $\theta_p^* = 0, \pi$ , deviating by an estimated  $2-3^\circ$  from this point. The equation of the trajectory (7.2.9) (i.e., the force function) may be written as

$$\sqrt{k_F^2 + k_S^2 - 2k_F k_S \cos \theta_w^*} \cos \nu_L = \text{const}, \quad (7.2.14)$$

where  $\nu_L$  is the angular distance of the angular momentum vector from the pole of precession  $\lambda_p, \theta_p$ . Hence it follows that the angular momentum vector precesses around the pole whose coordinates  $\lambda_p, \theta_p$  are determined by relation (7.2.13), at a constant angular distance  $\nu_L$ , with the velocity

$$\begin{aligned} \frac{d\nu_L}{dv} &= -\frac{1}{L_0} \sqrt{k_F^2 + k_S^2 - 2k_F k_S \cos \theta_w^*} \approx \\ &\approx -\frac{k_F}{L_0} \left\{ 1 - \frac{k_S}{k_F} \cos \theta_w^* \right\}. \end{aligned} \quad (7.2.15)$$

The rotation of the atmosphere thus causes a slight displacement of the pole of precession of the angular momentum vector (in accordance with (7.2.13)) and a small change in the rate of precession of this vector (in accordance with (7.2.15)).

### § 3. PERIODIC PERTURBATIONS. ANALYSIS OF MOTION IN A CIRCULAR ORBIT

Until now we have only considered the secular effects attributable to the aerodynamic torques. Let us consider a more exact picture of motion, allowing for periodic (in  $v$ ) perturbations. This analysis is particularly

topical since secular aerodynamic perturbations occur in elliptical orbits only: they are absent in the case of circular orbits (on proviso that  $a^t \approx 0$ , which, as we have remarked, is highly probable). Consider the simple approximation (1.3.18) for the aerodynamic torque coefficient and the corresponding expression for  $U_v$ , (7.2.1); the rotation of the atmosphere is ignored. Averaging (7.2.1) over  $\psi$ , we apply expression (7.1.3) for  $\cos \delta_v$  and expression (1.1.6) for  $\alpha_3, \gamma_3$ . Then

$$\bar{U}_v = -\frac{1}{2} \sqrt{\mu P} \rho_n \bar{\theta}_a \frac{\sqrt{1+e^2+2e \cos v}}{(1+e \cos v)^2} \times a_0^6 \cos \theta \sin \rho [(e + \cos v) \sin \sigma - \sin v \cos \sigma]. \quad (7.3.1)$$

Substituting the variables  $\theta, \lambda$  according to (1.1.4a) we have

$$\bar{U}_v = -\frac{1}{2} \sqrt{\mu P} \rho_n \bar{\theta}_a \frac{\sqrt{1+e^2+2e \cos v}}{(1+e \cos v)^2} \times a_0^6 \cos \theta [(e + \cos v) \cos \theta - \sin v \sin \theta \cos \lambda]. \quad (7.3.2)$$

The equations of motion in the variables  $\rho, \sigma$  according to (5.4.12) have the form

$$\left. \begin{aligned} \frac{d\rho}{dv} &= P_v [(e + \cos v) \cos \sigma + \sin v \sin \sigma], \\ \frac{d\sigma}{dv} &= -P_v \operatorname{ctg} \rho [(e + \cos v) \sin \sigma - \sin v \cos \sigma], \end{aligned} \right\} \quad (7.3.3)$$

$$P_v = \frac{1}{2} \frac{\sqrt{\mu P} \rho_n a_0^6 \cos \theta}{L_0} - \bar{\theta}_a \frac{\sqrt{1+e^2+2e \cos v}}{(1+e \cos v)^2}, \quad (7.3.4)$$

and in the variables  $\theta, \lambda$

$$\frac{d\theta}{dv} = P_v \sin v \sin \lambda, \quad \frac{d\lambda}{dv} = P_v [(e + \cos v) + \sin v \operatorname{ctg} \theta \cos \lambda]. \quad (7.3.5)$$

From (7.3.5) we easily see that  $v$ -periodic oscillations of the angle  $\theta$  (and  $\lambda$ ) are superimposed in this case on the monotonic increase of the angle  $\lambda$  (the secular perturbation considered in § 1). For the particular case of a circular orbit ( $e = 0$ ), when no secular perturbations occur, equations (7.3.3), however, are more convenient: on substitution  $\sigma - v = \kappa_v$ , these equations are reduced to the form (5.4.15) and have the first integral (5.4.16):

$$\cos \rho - n^* \sin \rho \sin \kappa_v = \text{const}, \quad n^* = \frac{\frac{1}{2} \rho_n \sqrt{\mu P} a_0^6 \cos \theta}{L_0}, \quad (7.3.6)$$

which is in fact the trajectory of  $\mathbf{L}$  in a rotating (orbital) system of axes. Setting  $\Lambda$  for the angle between  $\mathbf{L}$  and the current velocity vector of the satellite's mass center, we have  $\sin \rho \sin \kappa_v = \cos \Lambda$ , and the trajectory of the vector  $\mathbf{L}$  is written as

$$\cos \rho - n^* \cos \Lambda = \text{const}. \quad (7.3.7)$$

Hence we easily see that on the surface of a unit sphere the vector  $\mathbf{L}$  describes a circle whose center is on the meridian through the trace of the normal to the orbital plane and the trace of the velocity vector of the center of mass; the center of the circle is located at an angular distance  $\rho^*$  from the normal to the orbital plane, and

$$\operatorname{tg} \rho^* = -n^*. \quad (7.3.8)$$

The angular momentum vector  $L$  moves in this circle with a constant velocity:

$$\frac{d\lambda_A}{dv} = -\sqrt{1+n^*}. \quad (7.3.9)$$

We see that if  $n^*$  is very small (i.e., the perturbations are negligible), then  $\rho^* \approx 0$ , and the angular momentum vector rotates around the normal to the orbital plane with an angular velocity  $\lambda'_A \approx -1$ , i.e., it is almost stationary in the absolute space. If now  $n^*$  is very large,  $\rho^*$  is close to  $\pi/2$ , and the angular momentum vector rotates around the oncoming stream. The aerodynamic torque thus has a certain attitude stabilizing influence on a spinning satellite.

Note that the singly averaged (i.e.,  $\psi$ -averaged) theory is sufficiently precise even for large perturbations which render the doubly averaged (over  $\psi$  and over  $v$ ) theory inaccurate. An approximate criterion for the applicability of the theory is as follows: the motion obtained on averaging should be substantially slower than the motion over which the averaging has been performed. In our case, this requirement reduces to  $\left| \frac{d\lambda_A}{dv} \right| \ll \left| \frac{d\psi}{dv} \right|$ . Let  $\dot{\psi} = 14$  deg/sec, the orbital velocity  $\frac{dv}{dt} = 0.07$  deg/sec; then the theory is sufficiently accurate for  $\left| \frac{d\lambda_A}{dv} \right| \ll 200$ , i.e., say, for  $n \leq 10-20$ . Double averaging is acceptable only for  $n \ll 1$ .

#### §4. THE EFFECT OF AERODYNAMIC DISSIPATIVE TORQUES

The aerodynamic dissipative torques have been derived in Chapter 1 in the form (1.3.11) (the second and subsequent terms). For the dissipation coefficient we have the approximate formulas (1.3.21).

We shall operate in the satellite's own system of axes. Let  $i'$ ,  $j'$ ,  $k'$  be the unit vectors of this inertial system,  $k'$  pointing along the axis of symmetry. Then

$$k = k', \quad j = j' \cos \varphi_0 + i' \sin \varphi_0, \quad i = -j' \sin \varphi_0 + i' \cos \varphi_0, \quad (7.4.1)$$

where  $i$ ,  $j$ ,  $k$  are the unit vectors of the semiconstrained system, and  $\varphi_0$  the angle of rotation of the satellite's inertial system relative to the semiconstrained system. It can be shown that

$$\cos \varphi_0 = \frac{\cos(\widehat{e_V i'})}{\sin \delta_V}, \quad \sin \varphi_0 = -\frac{\cos(\widehat{e_V j'})}{\sin \delta_V}. \quad (7.4.2)$$

Let  $p$ ,  $q$ ,  $r$  be the angular velocity components along the satellite's axes. Then

$$\bar{r} = r, \quad \bar{p} = -q \sin \varphi_0 + p \cos \varphi_0, \quad \bar{q} = q \cos \varphi_0 + p \sin \varphi_0. \quad (7.4.3)$$

Applying (7.4.2) and substituting (7.4.1) and (7.4.3) in the dissipative part of (1.3.11), we introduce the approximating values (1.3.21) of the functions

(1.3.12). The dissipative torque components along the satellite's axes are then written as

$$\begin{aligned} M_d = & \frac{1}{2} c\rho_a V_0 \{ I' [-pI_3 + r \cos(\hat{e}_v, \hat{i}') I_4] + \\ & + j' [-qI_3 + r \cos(\hat{e}_v, \hat{j}') I_4] + \\ & + k' [-rI_1 + (p \cos(\hat{e}_v, \hat{i}') + q \cos(\hat{e}_v, \hat{j}')) I_2] \}. \end{aligned} \quad (7.4.4)$$

Hence follows the meaning of  $I_i$ :  $I_1$  is the coefficient of dissipation along the axis of symmetry,  $I_3$  the coefficient of dissipation along the lateral axis. These terms damp the satellite's spin. The terms with  $I_2$  and  $I_4$  alter the orientation of the satellite.

The rotation of the atmosphere is ignored. Then

$$\left. \begin{aligned} \cos(\hat{e}_v, \hat{i}') &= \frac{1}{V_0} [V_x \alpha_1 + V_z \gamma_1], \\ \cos(\hat{e}_v, \hat{j}') &= \frac{1}{V_0} (V_x \alpha_2 + V_z \gamma_2), \\ V_0 &= \sqrt{\frac{\mu}{P}} \sqrt{1 + e^2 + 2e \cos v}, \\ V_x &= \sqrt{\frac{\mu}{P}} (e + \cos v), \\ V_z &= -\sqrt{\frac{\mu}{P}} \sin v, \\ p \cos(\hat{e}_v, \hat{i}') + q \cos(\hat{e}_v, \hat{j}') &= \\ &= \frac{1}{V_0} [V_x (p \alpha_1 + q \alpha_2) + V_z (p \gamma_1 + q \gamma_2)]. \end{aligned} \right\} \quad (7.4.5)$$

Here  $\alpha_i, \gamma_i$  are the direction cosines of the set  $\hat{i}', \hat{j}', \hat{k}'$  relative to the perigee system of axes  $XYZ$  (see § 1 of Chapter 1). Since

$$q\alpha_2 + p\alpha_1 = \frac{L_x - Cr\alpha_3}{A}, \quad q\gamma_2 + p\gamma_1 = \frac{L_z - Cr\gamma_3}{A}, \quad (7.4.6)$$

the equation of motion about the axis of symmetry  $k'$  is

$$C \frac{dr}{dt} = -\frac{1}{2} c\rho_a V_0 I_1 r + \frac{1}{2} c\rho_a \frac{I_2}{A} \{ V_x (L_x - Cr\alpha_3) + V_z (L_z - Cr\gamma_3) \}, \quad (7.4.7)$$

and the torque components along the perigee axes are

$$\left. \begin{aligned} M_X &= \frac{1}{2} c\rho_a V_0 \left\{ -\frac{I_3}{A} (L_x - Cr\alpha_3) - I_1 r \alpha_3 + \right. \\ &+ I_4 \frac{r}{V_0} [V_x (1 - \alpha_3^2) + V_z (-\alpha_3 \gamma_3)] + \\ &+ \frac{I_2}{V_0 A} \alpha_3 [V_x (L_x - Cr\alpha_3) + V_z (L_z - Cr\gamma_3)] \left. \right\}, \\ M_Y &= \frac{1}{2} c\rho_a V_0 \left\{ -\frac{I_3}{A} (L_y - Cr\beta_3) - I_1 r \beta_3 + \right. \\ &+ I_4 \frac{r}{V_0} [V_x (-\alpha_3 \beta_3) + V_z (-\beta_3 \gamma_3)] + \\ &+ \frac{I_2}{V_0 A} \beta_3 [V_x (L_x - Cr\alpha_3) + V_z (L_z - Cr\gamma_3)] \left. \right\}, \\ M_Z &= \frac{1}{2} c\rho_a V_0 \left\{ -\frac{I_3}{A} (L_z - Cr\gamma_3) - I_1 r \gamma_3 + \right. \\ &+ I_4 \frac{r}{V_0} [V_x (-\alpha_3 \gamma_3) + V_z (1 - \gamma_3^2)] + \\ &+ \frac{I_2}{V_0 A} \gamma_3 [V_x (L_x - Cr\alpha_3) + V_z (L_z - Cr\gamma_3)] \left. \right\}. \end{aligned} \right\} \quad (7.4.8)$$

The equations of motion of the angular momentum vector are written as

$$\dot{L}_x = M_x, \quad \dot{L}_y = M_y, \quad \dot{L}_z = M_z. \quad (7.4.9)$$

Let us investigate the secular inequalities of motion. Applying (2.3.2), we change over from  $t$  to a new independent variable  $v$  and average (7.4.7)–(7.4.9) over  $\psi$  and  $v$ . Let

$$\left. \begin{aligned} N_0^\theta &= \frac{1}{2} c \rho_\pi P \frac{1}{2\pi} \int_0^{2\pi} \frac{1}{\rho} \frac{\sqrt{1+e^2+2e \cos v}}{(1+e \cos v)^2} dv = \frac{1}{2} \rho_\pi P \bar{N}_0^\theta, \\ N_1^\theta &= \frac{1}{2} c \rho_\pi P \frac{1}{2\pi} \int_0^{2\pi} \frac{1}{\rho} \frac{e + \cos v}{(1+e \cos v)^2} dv = \frac{1}{2} \rho_\pi P \bar{N}_1^\theta. \end{aligned} \right\} \quad (7.4.10)$$

In the averaged combinations (1.1.7), the direction cosines of the vector  $L$  can be expressed as the ratios of its components to its magnitude ( $\cos \vartheta = \frac{L_y}{L}$ , etc.). We obtain the following equations of secular motion:

$$\left. \begin{aligned} L'_x &= -k_0^\theta L_x + k_1^\theta \cos \vartheta \frac{L_x^2}{L} + k_2^\theta \cos \vartheta L, \\ L'_y &= -k_0^\theta L_y + k_1^\theta \cos \vartheta \frac{L_x L_y}{L}, \\ L'_z &= -k_0^\theta L_z + k_1^\theta \cos \vartheta \frac{L_x L_z}{L}, \\ Cr' &= -N_0^\theta I_1 r + \frac{I_2 N_1^\theta}{A} \sin^2 \vartheta L_x, \quad \cos \vartheta = \frac{Cr}{L}. \end{aligned} \right\} \quad (7.4.11)$$

Here prime denotes differentiation by  $v$ , and  $k_0^\theta$ ,  $k_1^\theta$ ,  $k_2^\theta$  are defined by

$$\left. \begin{aligned} k_0^\theta(\vartheta) &= N_0^\theta \left( \frac{I_3}{A} \sin^2 \vartheta + \frac{I_1}{C} \cos^2 \vartheta \right), \\ k_1^\theta(\vartheta) &= \left[ -\frac{I_4 N_1^\theta}{C} \left( 1 - \frac{3}{2} \sin^2 \vartheta \right) + \frac{I_2 N_1^\theta}{A} \cdot \frac{3}{2} \sin^2 \vartheta \right], \\ k_2^\theta(\vartheta) &= \left[ \frac{I_4 N_1^\theta}{C} \left( 1 - \frac{1}{2} \sin^2 \vartheta \right) - \frac{I_2 N_1^\theta}{A} \cdot \frac{1}{2} \sin^2 \vartheta \right]. \end{aligned} \right\} \quad (7.4.12)$$

Note that in a circular orbit  $N_1^\theta = 0$ ,  $k_1^\theta = k_2^\theta = 0$ , and the motion is quite simple. We shall consider this case as we go on. In the general case of an elliptical orbit, from equations (7.4.11) for  $L'_x$  and  $L'_y$  we have

$$\frac{L_z}{L_y} = \text{const.} \quad (7.4.13)$$

This means that the plane through the vector  $L$  and the tangent at the perigee — the axis  $X$  — preserves a constant attitude in space, and the vector  $L$  may only move in this plane. From the first three equations in (7.4.11) we have

$$L' = -k_0^\theta L + \cos \vartheta (k_1^\theta + k_2^\theta) L_x. \quad (7.4.14)$$

Since

$$L_x = L \cos \theta, \quad -L \sin \theta \theta' = L'_x - L' \cos \theta, \quad (7.4.15)$$

we can substitute in the right-hand side of (7.4.15)  $L'$  from (7.4.14) and  $L'_x$  from (7.4.11); dividing through by  $L \sin \theta$ , we find

$$\dot{\theta}' = -k_2^\theta \cos \theta \sin \theta,$$

whence

$$\operatorname{tg} \frac{\theta}{2} = \operatorname{tg} \frac{\theta_0}{2} e^{-\int_{v_0}^v k_2^\theta \cos \theta dv} \quad (7.4.16)$$

where  $k_2^\theta(\theta)$  and  $\cos \theta$  in general vary slowly, in virtue of the equations of motion (7.4.11). To first approximation, we may take  $k_2^\theta(\theta) \cos \theta \approx k_2^\theta(\theta_0) \cos \theta_0$ . But even if the slow variation of  $k_2^\theta(\theta) \cos \theta$  is taken into consideration, the asymptotic behavior remains the same as with constant  $k_2^\theta \cos \theta$ : asymptotically,  $k_2^\theta \cos \theta$  has a definite constant sign. We see from (7.4.16) that if  $k_2^\theta \cos \theta > 0$ , then  $\theta \rightarrow 0$ ; if  $k_2^\theta \cos \theta < 0$ , then  $\theta \rightarrow \pi$  for  $v \rightarrow \infty$ . Either way, *the vector of angular momentum approaches the direction of the tangent to the orbit at its perigee*. We may approximately take

$$\operatorname{tg} \frac{\theta}{2} = \operatorname{tg} \frac{\theta_0}{2} \exp \{-k_2^\theta(\theta_0) \cos \theta_0\} (v - v_0). \quad (7.4.17)$$

For a circular orbit  $k_2^\theta = 0$ , and the vector  $\mathbf{L}$  invariably points in one direction.

Returning to (7.4.14), we have

$$\left. \begin{aligned} L' &= L \left\{ -k_0^\theta + \cos \theta \sin^2 \theta \cos \theta N_1^\theta \left( \frac{I_2}{A} + \frac{I_4}{C} \right) \right\}, \\ L &= L_0 \exp \int \left\{ -k_0^\theta + \right. \\ &\quad \left. + \cos \theta \sin^2 \theta \cos \theta N_1^\theta \left( \frac{I_2}{A} + \frac{I_4}{C} \right) \right\} dv. \end{aligned} \right\} \quad (7.4.18)$$

Since  $k_0^\theta > 0$  does not vanish in a circular orbit, and  $N_1^\theta = 0$  for  $e = 0$ , we see that  $N_1^\theta$  may be taken small in comparison with  $k_0^\theta$ ; furthermore, we shall later show that  $\theta \rightarrow 0$  or  $\theta \rightarrow \pi/2$ . In consequence of all this, the expression in braces is asymptotically a nonzero negative quantity, so that  $L \rightarrow 0$  for  $v \rightarrow \infty$ ; the angular velocity of precession  $\dot{\psi} \approx \frac{L}{A}$  also decreases. We may approximately take  $k_0^\theta = \text{const}$ , ignoring  $N_1^\theta$ ; then

$$L = L_0 \exp \{-k_0^\theta(v - v_0)\}. \quad (7.4.19)$$

We see from the last equation in (7.4.11) that the angular velocity component along the satellite's axis of symmetry can be written to the same approximation:

$$r = r_0 \exp \left\{ -\frac{N_0^\theta I_1}{C} (v - v_0) \right\}. \quad (7.4.20)$$

Let us consider the behavior of the angle  $\theta$ . We have  $\frac{d \cos \theta}{dv} = -\frac{Cr}{L^2} L' + \frac{C}{L} r'$ ; inserting  $L'$  and  $r'$  from (7.4.11), we find

$$\frac{d \cos \theta}{dv} = \cos \theta \sin^2 \theta \left( \frac{I_2}{A} - \frac{I_4}{C} \right) + N_1^\theta \cos \theta \sin^2 \theta \left\{ \frac{I_2}{A} \sin^2 \theta - \frac{I_4}{C} \cos^2 \theta \right\}.$$

Neglecting  $N_i^\theta$  in comparison with  $N_0^\theta$  and integrating, we find

$$\operatorname{tg} \vartheta = \operatorname{tg} \vartheta_0 \exp \left\{ \frac{I_1}{C} - \frac{I_3}{A} \right\} N_0^\theta (v - v_0). \quad (7.4.21)$$

Hence  $\vartheta \rightarrow 0$ , if  $\frac{I_1}{C} - \frac{I_3}{A} < 0$ , and  $\vartheta \rightarrow \pi/2$ , if  $\frac{I_1}{C} - \frac{I_3}{A} > 0$ . If we assume that the dissipation coefficients are approximately equal,  $I_1 \approx I_3$ , then  $\vartheta \rightarrow 0$  for  $A < C$  and  $\vartheta \rightarrow \pi/2$  for  $A > C$ . In other words, *a dynamically oblate satellite orients itself along the axis of symmetry ( $\vartheta \rightarrow 0$ ), and a dynamically prolate satellite tumbles ( $\vartheta \rightarrow \pi/2$ )*.

Remembering the asymptotic orientation of the angular momentum vector (see (7.4.17)), we arrive at the following general rule: *a satellite acted upon by aerodynamic dissipative forces orients itself so that the aerodynamic resistance is maximal*.

Indeed, the vector  $L$  tends to orient itself along the line of maximum aerodynamic head (the tangent at the perigee), and the angle  $\vartheta$  varies so that at the perigee the satellite turns its largest surface to the oncoming stream.

**Note 1.** The foregoing analysis does not apply for small angular velocities, since the method of averaging is valid for fairly large angular velocities of rotation only. The asymptotic expressions, however, give a correct description of the general tendencies of motion.

**Note 2.** The spin apparently decays at a faster rate than the motion of the vector  $L$  along the tangent: spin decay is determined by the parameter  $N_0^\theta$ , and the velocity of  $L$  by the parameter  $N_i^\theta$  which is of the order of  $\sim e N_0^\theta$ , where  $e$  is the eccentricity.

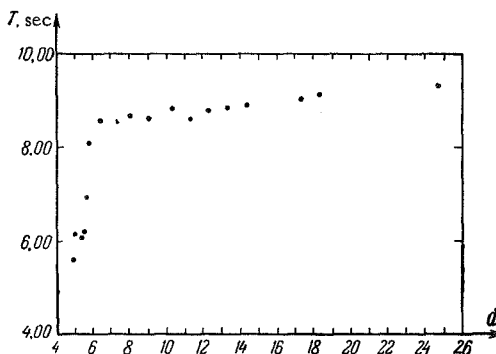


FIGURE 52. The period of rotation  $T$  of Sputnik I on various dates ( $d$ ) in October 1957.

**Example.** The spin decay of Sputnik I (Figure 52) is attributed by Warwick /95/ to atmospheric friction. The main effect is attributable to the friction with the satellite's long antennas. Since the antenna parameters are known, despin measurements give the density of the atmosphere at perigee ( $h_\pi = 220$  km), which according to Warwick is  $\rho_\pi = 3.8 \cdot 10^{-13}$  g/cm<sup>3</sup>; this result is in good agreement with other density determinations. The inverse problem is of some interest, namely the determination of the dissipation coefficients for known spin-fading rate

and atmospheric density. From (7.4.20), (7.4.19) we easily have for

$$\theta = 0 \text{ and } \theta = 90^\circ$$

$$T_\phi = T_\phi^0 \exp \frac{N_0^\theta I_1}{C} \Delta v, \quad T_\psi = T_\psi^0 \exp \frac{N_0^\theta I_3}{A} \Delta v,$$

where  $T_\phi$  and  $T_\psi$  are the periods of spin (for  $\theta=0$ ) or precession ( $\theta=90^\circ$ ). Setting  $N_0^\theta \approx \rho_\pi P$ ,  $\rho_\pi = 3.8 \cdot 10^{-13} \text{ g/cm}^3$ ,  $P = 6600 \text{ km}$ ,  $\Delta v = 320 \cdot 2\pi$  (which corresponds to  $\approx 20$  flight days),  $T^0 = 6 \text{ sec}$ ,  $T = 9.2 \text{ sec}$  (as in Figure 52), we obtain  $2.14 \cdot 10^{-4}$  for the decrement of damping  $\left( \frac{N_0^\theta I_3}{A} \text{ or } \frac{N_0^\theta I_1}{C} \right)$  and  $0.855 \text{ cm}^2/g$  for  $\frac{I_3}{A}$  (or  $\frac{I_1}{C}$ ). In Chapter 10 it is shown that the period of precession of Sputnik III increased from 135 sec to 195 sec in 280 orbital revolutions. This corresponds to a decrement of damping  $2.11 \cdot 10^{-4}$ .

## *Chapter 8*

### **ANALYSIS OF SECULAR PERTURBATIONS UNDER THE COMBINED INFLUENCE OF GRAVITY AND AERODYNAMIC TORQUES AND ORBIT EVOLUTION**

#### **§ 1. MOTION OF THE ANGULAR MOMENTUM VECTOR RELATIVE TO AN EVOLVING ORBIT**

Until now we have assumed that the satellite moves in a normal, unperturbed orbit. However, the actual orbits of artificial satellites evolve due to various perturbing factors. The effect of the atmosphere and the Earth's flattening are the two main causes of orbital perturbations. It is known /61/ that to first approximation, atmospheric effects do not alter the orientation of the orbit in space: they only change its shape. This evolution of the orbit can be introduced parametrically in the analysis of the rotational motion of a satellite (the  $P$  and the  $e$  in the corresponding formulas can be assumed to vary slowly in time). The Earth's flattening /61/ alters the orientation of the orbit in space, and its effect on the rotational motion of a satellite must be considered separately.

Indeed, if the rotational motion of the satellite is unperturbed, the angular momentum vector maintains a constant direction in space, and its attitude relative to the perturbed orbit clearly changes. Now, since perturbation of the satellite's spin depends on the position of the angular momentum vector relative to the orbit, orbit evolution must be considered simultaneously with the perturbations in the motion of the angular momentum vector relative to the orbit.

We shall limit the analysis to secular effects. They will be investigated in the coordinates  $\theta$  and  $\lambda$ —the "aerodynamic" coordinates of the angular momentum vector. Let us consider the infinitesimal increments of the angles  $\theta$  and  $\lambda$  produced by an infinitesimal change in the orbit's orientation in space due to the Earth's flattening. Adding these infinitesimal increments in  $\theta$  and  $\lambda$  with other infinitesimal increments produced by spin perturbations, and changing over to instantaneous angular velocities, we shall then obtain a system of differential equations for the motion of the angular momentum vector allowing for all the various effects jointly.

The Earth's flattening is known to produce secular inequalities in the longitude of the ascending node  $\Omega$  and in the longitude of perigee  $\omega_\pi$  /61/:

$$\left. \begin{aligned} k_\Omega &= \frac{d\Omega}{dv} = -\frac{\bar{e}R_e^2}{P^2} \cos i, \\ k_\omega &= \frac{d\omega_\pi}{dv} = \frac{\bar{e}R_e^2}{2P^2} (5 \cos^2 i - 1). \end{aligned} \right\} \quad (8.1.1)$$

Here  $R_e$  is the equatorial radius of the Earth,  $\bar{\epsilon} = 0.0016331$  a dimensionless quantity determined by the Earth's flattening.

The position of the angular momentum vector  $L$  relative to the perigee system of axes  $XYZ$  will be specified by the direction cosines  $m, n, k$  (1.1.4a). The mutual attitude of the perigee system  $XYZ$  and the fixed system  $\bar{XYZ}$  is defined by the same table of direction cosines from Chapter 1, § 1 as for the orbital system  $xyz$  and the system  $XYZ$ ; we should only take  $v=0$ , i.e.,  $u=\omega_\pi$ . The orientation of the vector  $L$  relative to the axes  $\bar{XYZ}$  is then given by the direction cosines  $\alpha_3^0, \beta_3^0, \gamma_3^0$  (1.1.9). If the satellite's spin is unperturbed,  $\alpha_3^0, \beta_3^0, \gamma_3^0$  are all constant, i.e., the vector  $L$  maintains a constant direction in space. If, however, the satellite's orbit moves in space according to (8.1.1), infinitesimal increments  $d\omega_\pi$  and  $d\Omega$  in the angles  $\omega_\pi$  and  $\Omega$  correspond to infinitesimal increments  $d\theta$  and  $d\lambda$  in the angles  $\theta$  and  $\lambda$ , which are determined from the equalities

$$\left. \begin{aligned} d\alpha_3^0 &= \frac{\partial \alpha_3^0}{\partial \theta} d\theta + \frac{\partial \alpha_3^0}{\partial \lambda} d\lambda + \frac{\partial \alpha_3^0}{\partial \Omega} d\Omega + \frac{\partial \alpha_3^0}{\partial \omega_\pi} d\omega_\pi = 0, \\ d\beta_3^0 &= 0, \quad d\gamma_3^0 = 0. \end{aligned} \right\} \quad (8.1.2)$$

The partial derivatives can be found without difficulty, but the expressions are somewhat unwieldy. We shall therefore omit the intermediate manipulations and give only the final result: eliminating  $d\lambda$  between the last two equations in (8.1.2), we find an expression for  $d\theta$ :

$$d\theta = [\cos i \cos \lambda + \sin \omega_\pi \sin i \sin \lambda] d\Omega + \cos \lambda d\omega_\pi. \quad (8.1.3)$$

Substituting (8.1.3) in any equation in (8.1.2) (e.g., the first equation), we obtain an expression for  $d\lambda$ :

$$\begin{aligned} -\sin \theta d\lambda &= -[-\sin \theta \cos \omega_\pi \sin i + \\ &\quad + \cos \theta (-\sin \lambda \cos i + \cos \lambda \sin \omega_\pi \sin i)] d\Omega + \\ &\quad + d\omega_\pi \cos \theta \sin \lambda. \end{aligned} \quad (8.1.4)$$

We can now write the complete equations of motion of the angular momentum vector relative to an evolving orbit, with spin perturbation by gravity and aerodynamic torques. In the present chapter we shall only consider the restoring aerodynamic torque, neglecting the aerodynamic dissipative effects investigated in Chapter 7, § 4.

## § 2. EQUATIONS OF SECULAR MOTION OF THE ANGULAR MOMENTUM VECTOR RELATIVE TO AN EVOLVING ORBIT WITH GRAVITY AND AERODYNAMIC PERTURBATIONS

To find the combined effect of aerodynamic and gravity forces in conjunction with the regression of the orbit, it suffices to introduce in the right-hand sides of (7.1.10) additional terms corresponding to the perturbations  $\bar{U}_n$  (7.1.8) (these perturbations are produced by gravity torques and by the gravity-similar part of the aerodynamic torques), where  $\sin^2 \rho = 1 - \sin^2 \theta \sin^2 \lambda$ ; terms corresponding to the displacements

(8.1.3) and (8.1.4) should also be introduced. Then

$$\left. \begin{aligned}
 \frac{d\lambda}{dv} &= \frac{\rho_\pi}{2} \frac{\sqrt{\mu P}}{L_0} \left\{ \cos \vartheta \left[ a_1^0 J_1 + \frac{a_2^0}{2} J_4 \sin^2 \vartheta + \right. \right. \\
 &\quad + a_2^0 J_5 \left( \frac{1}{2} \sin^2 \vartheta + \left( 1 - \frac{5}{2} \sin^2 \vartheta \right) \cos^2 \lambda \right) \left. \right] + \\
 &\quad + a_1^0 (J_1 - J_3) \left( 1 - \frac{3}{2} \sin^2 \vartheta \right) \cos \vartheta + \\
 &\quad + 3 \cos \vartheta \left( 1 - \frac{5}{2} \sin^2 \vartheta \right) \left[ \frac{a_2^0}{3} J_4 - a_2^0 J_5 \cos^2 \lambda \right] \cos^2 \theta \Big\} - \\
 &\quad - \frac{1}{2L_0} \left( 1 - \frac{3}{2} \sin^2 \vartheta \right) \left[ 3 \frac{\sqrt{\mu}}{P^{3/2}} (A - C) - \right. \\
 &\quad - \rho_\pi \sqrt{\mu P} a_1^0 J_3 \Big] \cos \theta \sin^2 \lambda + k_{\delta \lambda} [- \cos \omega_\pi \sin i + \\
 &\quad + \operatorname{ctg} \theta (- \sin \lambda \cos i + \cos \lambda \sin \omega_\pi \sin i)] - \\
 &\quad \left. \left. - k_\omega \operatorname{ctg} \theta \sin \lambda, \right. \right. \\
 \frac{d\theta}{dv} &= - \frac{\rho_\pi \sqrt{\mu P}}{L_0} a_2^0 J_5 \cos \vartheta \left( 1 - \frac{5}{2} \sin^2 \vartheta \right) \times \\
 &\quad \times \cos \theta \sin \theta \cos \lambda \sin \lambda + \frac{1}{2L_0} \left( 1 - \frac{3}{2} \sin^2 \vartheta \right) \times \\
 &\quad \times \left[ 3 \frac{\sqrt{\mu}}{P^{3/2}} (A - C) - \rho_\pi \sqrt{\mu P} a_1^0 J_3 \right] \sin \theta \sin \lambda \cos \lambda + \\
 &\quad + k_{\delta \theta} [\cos i \cos \lambda + \sin \omega_\pi \sin i \sin \lambda] + k_\omega \cos \lambda.
 \end{aligned} \right\} \quad (8.2.1)$$

Equations (8.2.1) allow for all the previously considered secular effects (with the exception of aerodynamic dissipation) plus orbit evolution. However, as in § 1 of Chapter 7, terms containing the small factors  $J_5$  and  $a_1^0$  can be neglected. Equations (8.2.1) are then substantially simplified. Let us consider some results of numerical integration of equations (8.2.1), setting  $a_1^0 = 0$  (but  $J_5 \neq 0$ ). These results will serve as a tentative introduction to the general problem of interaction of the various perturbations. A more detailed analysis will follow.

Let us first consider the combined influence of aerodynamic torques and orbital perturbations, ignoring for the meanwhile the gravitational perturbations. The results of analysis of numerical integration lead to the following conclusions. The precession angle  $\lambda$  of the angular momentum vector increases monotonically, the rate of rise oscillating about a certain mean value, which is close to the velocity of aerodynamic precession (7.1.11). The nutation angle  $\theta$  of the angular momentum vector oscillates almost periodically, and the period of oscillation in  $\theta$  is approximately equal to the time it takes the angle  $\lambda$  to increase by  $2\pi$ , i.e., the period of secular precession. The difference between the maximum and the minimum values of the angle  $\theta$  is close to  $10 - 30^\circ$ , i.e., the nutation is stronger than in the case of aerodynamic torques without orbit evolution. This means that orbit evolution (in fact, the regression of nodes, as will be shown in the following) somewhat displaces the precession-nutation pole of the angular momentum vector.

Figures 53 and 54 show typical specimen curves for the variation of  $\theta$ ,  $\lambda$ , and  $\dot{\lambda}$  in time (the abscissa gives  $n$  — the number of orbital circuits of the satellite). The calculations have been made for the parameters of Sputnik II. Figure 55 is a schematic diagram of motion, plotting the trajectory  $\theta(\lambda)$ . The origin of the coordinates is the trace of the perigee tangent on the unit sphere; the solid curve is described by the tip of the

angular momentum vector, the dashed circle is described by the tip of the satellite's axis when the angular momentum vector is fixed. It will be shown in the following that the trajectory  $\theta(\lambda)$  is open on account of the secular motion of the perigee. All the loops of this curve are close to one another, so that as  $\lambda$  goes through  $2\pi$ , the angle  $\theta$  approximately returns to its initial value. The angular momentum vector therefore traces almost the same curve in each period of the angle  $\lambda$ ; we see from Figure 55

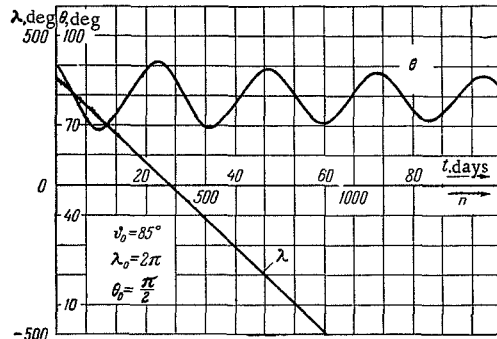


FIGURE 53. Secular variation in the angular coordinates of the angular momentum vector due to aerodynamic torques and orbit evolution (Sputnik II).

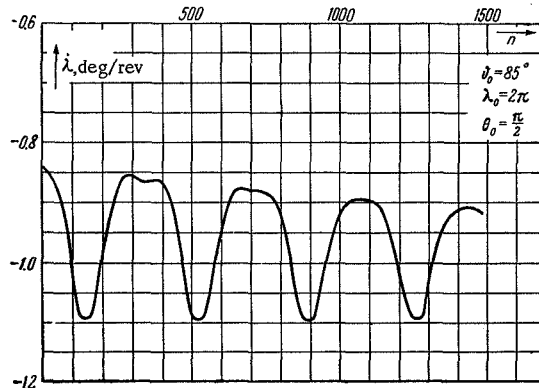


FIGURE 54. Variation in the angular velocity of secular precession of the angular momentum vector due to aerodynamic torques and orbit evolution.

that this curve is close to a circle with a center displaced relative to the trace of the perigee tangent. Figure 55 shows only one loop of this curve. Note that as it follows from Figures 53, 54, the amplitude of oscillations in the velocity of precession  $\dot{\lambda}$  and in the angle of nutation  $\theta$  varies gradually. This variation is attributable to a long-period effect connected with the motion of the perigee; eventually, however, the amplitude stops decreasing, and it rises again to the initial value.

The foregoing analysis brings out the characteristic gyroscopic attitude stabilization of the satellite relative to the direction of the perigee tangent, i.e., relative to the velocity vector of the center of mass at the point of maximum intensity of aerodynamic forces. Indeed, although the perigee tangent rotates in absolute space due to orbit evolution, the angular distance between the angular momentum vector and the perigee tangent hardly changes, so that the satellite's axis precesses and nutates about the rotating perigee tangent.

In this section we have not touched upon the subject of gravity torques. Their influence may be quite substantial for satellites of the type of Sputnik II, with characteristically large inertia parameters. Note that the axes of aerodynamic and gravitational precessions do not coincide: aerodynamic precession is executed around the perigee tangent, while the gravitational precession is around the normal to the orbital plane. The

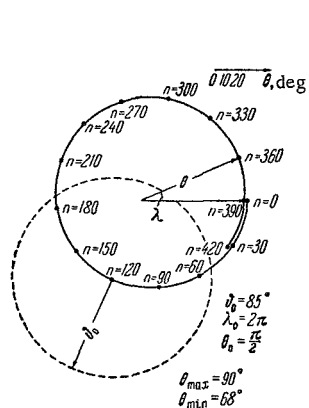


FIGURE 55. The secular trajectory of the angular momentum vector due to aerodynamic torques and orbit evolution.

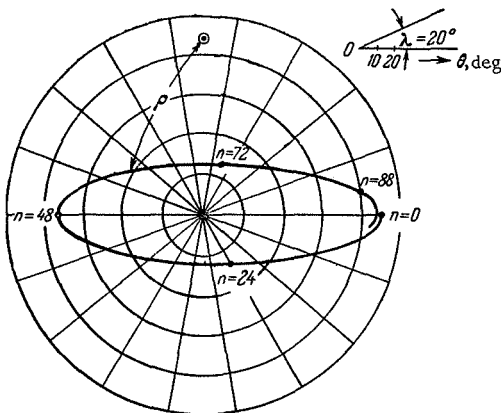


FIGURE 56. The secular trajectory of the angular momentum vector for a satellite of Sputnik II type (aerodynamic and gravity torques in conjunction with orbit evolution). The numbers  $n$  of orbital circuits are marked along the trajectory.

combined influence of aerodynamic and gravity torques will therefore result in a complex precession-nutation about a certain pole. This pole, in general, will move due to orbit evolution. A specimen trajectory  $\theta(\lambda)$  calculated from (8.2.1) is shown in Figure 56. The parameters and the initial conditions are the same as in the example depicted in Figures 53—55, the only addition being the introduction of gravity perturbations — a highly significant factor in this case. Here the precession-nutation pole coincides with the center of aerodynamic precession. This is so because for  $\rho = 90^\circ$  only the aerodynamic torques are effective, while the gravity precession velocity reverses its sign at  $\rho = 90^\circ$ . The strong influence of gravitational perturbations is manifested in the high "oblateness" of the trajectory, produced by the tendency of gravity torques to preserve a constant angle  $\rho$  between the angular momentum vector and the normal to the orbital plane.

Orbital perturbations produce the same effect as in Figure 55: the precession-nutation pole of the angular momentum vector is somewhat

displaced and the trajectory does not "close": the values of  $\theta$  for  $\lambda = 0$  and  $\lambda = 2\pi$  are slightly different (the difference being very small).

Calculations show that the motion relative to the orbit is characteristically stable in all the cases: all other conditions being constant, the motion relative to the evolving orbit does not differ much from the motion relative to the normal, stationary orbit.

Equations (8.2.1) also lend themselves to a direct analysis which helps to bring out all the principal features in the motion of the angular momentum vector. This analysis is presented in the following sections of the chapter.

### § 3. PRELIMINARY ANALYSIS. EQUATIONS OF SECULAR MOTION. INTEGRABLE CASES

Equations (8.2.1) for the secular motion of the angular momentum vector can be written as

$$\sin \theta \frac{d\lambda}{dv} = \frac{\partial \Phi}{\partial \theta}, \quad \sin \theta \frac{d\theta}{dv} = -\frac{\partial \Phi}{\partial \lambda}, \quad (8.3.1)$$

$$\begin{aligned} \Phi = & -k_0^* \sin^2 \theta \sin^2 \lambda - k_1^*(\lambda) \cos \theta - k_2^* \cos^2 \theta - k_3^*(\lambda) \cos^3 \theta + \\ & + k_{\eta}^* \{ \sin \theta (\cos \lambda \sin \omega_n \sin i - \sin \lambda \cos i) + \\ & + \cos \theta \cos \omega_n \sin i \} - k_{\omega}^* \sin \theta \sin \lambda. \end{aligned} \quad (8.3.2)$$

Here

$$\begin{aligned} k_0^* &= \frac{1}{4} \left( 1 - \frac{3}{2} \sin^2 \vartheta \right) \left[ 3 \frac{\sqrt{\mu P}}{P^{1/2}} (A - C) - \rho_n \sqrt{\mu P} a_1^6 J_3 \right], \\ k_1^*(\lambda) &= \frac{\sqrt{\mu P}}{2} \rho_n \cos \vartheta \left\{ a_0^6 J_1 + \frac{a_2^6}{2} J_4 \sin^2 \vartheta + a_2^6 J_5 \left[ \frac{\sin^2 \vartheta}{2} + \left( 1 - \frac{5}{2} \sin^2 \vartheta \right) \cos^2 \lambda \right] \right\}, \\ k_2^* &= (J_2 - J_3) \left( 1 - \frac{3}{2} \sin^2 \vartheta \right) \frac{\sqrt{\mu P}}{4} \rho_n a_1^6, \\ k_3^*(\lambda) &= \frac{\sqrt{\mu P}}{2} \rho_n \left( 1 - \frac{5}{2} \sin^2 \vartheta \right) \left[ \frac{a_2^6}{3} J_4 - a_2^6 J_5 \cos^2 \lambda \right] \cos \vartheta. \end{aligned}$$

In (8.3.1), (8.3.2), the term with  $k_0^*$  characterizes the secular effect of gravity torques and also part of the effect attributable to aerodynamic torques ( $a_i^6$ ). The main secular contribution of the aerodynamic torques is characterized by terms with  $k_1^*$ ,  $k_3^*$ , and also  $k_2^*$ .

The other terms in (8.3.2) are due to orbit evolution, namely the rotation of the perigee system of axes in the absolute space. We see that these terms are proportional to the rate of regression of the nodes  $k_{\eta}^*$  or to the rate of regression of the perigee point,  $k_{\omega}^*$ .

Note that  $-\sin \theta \sin \lambda = \cos \rho$ , where  $\rho$  is the angle between the angular momentum vector and the normal to the orbital plane; then, introducing the coordinates  $\theta^*$ ,  $\lambda^*$  of the celestial north pole, we have

$$\begin{aligned} \sin i \cos \omega_n &= \cos \theta^*, \quad \sin i \sin \omega_n = \sin \theta^* \cos \lambda^*, \\ \cos i &= -\sin \theta^* \sin \lambda^*, \\ \cos \theta \cos \theta^* + \sin \theta \sin \theta^* \cos(\lambda - \lambda^*) &= \cos \alpha^*, \end{aligned}$$

where  $\alpha^*$  is the angle between the angular momentum vector and the direction to the celestial north pole. The function  $\Phi$  (8.3.2) can be conveniently

written in the form

$$\Phi = -k_0^* \cos^2 \rho - k_1^* \cos \theta - k_2^* \cos^2 \theta - k_3^* \cos^3 \theta + k_{\delta} \cos \alpha^* + k_{\omega} \cos \rho. \quad (8.3.3)$$

Since  $\cos \alpha^*$  varies with  $\omega_n$ , and  $\omega_n = \omega_{n0} + k_{\omega} v$ , the function  $\Phi$  (8.3.2) depends on  $v$  (but only through  $\cos \alpha^*$ ); equation (8.3.1) is therefore not integrable by itself in the general case. For many Soviet satellites, the rate of regression of the perigee  $k_{\omega}$  is very small in comparison with the rate of regression of the node  $k_{\delta}$ , and is of course much smaller than any of the  $k_j^*$ ,  $j = 0, 1, 2, 3$ . On first approximation we may take  $k_{\omega} = 0$ ; then  $\omega_n = \omega_{n0}$ , the function  $\Phi$  is independent of  $v$ , and equations (8.3.1) have the first integral  $\Phi|_{k_{\omega}=0} = \Phi_0$ , i.e.,

$$-k_0^* \cos^2 \rho - k_1^* \cos \theta - k_2^* \cos^2 \theta - k_3^* \cos^3 \theta + k_{\delta} \cos \alpha^* = \Phi_0, \quad (8.3.4)$$

where the quantities  $\theta^*$ ,  $\lambda^*$  entering  $\cos \alpha^*$  are constant, since only the node regresses, so that the perigee axes remain at a constant angular distance from the direction to the celestial pole.

Equation (8.3.4) is the trace described by the tip of the angular momentum vector on the surface of a unit sphere with its origin at the satellite's mass center. Formula (8.3.4) allows for simultaneous influence of aerodynamic and gravity torques and the secular regression of the orbital node. Formula (8.3.4) gives a fairly accurate description of motion during one precession-nutation period of the angular momentum vector. Over longer times, the motion is gradually distorted by the secular regression of the perigee. This factor, however, may be allowed for by making use of the same formula (8.3.4), where  $\omega_n$  should be regarded as a slowly varying parameter. This approach amounts to the application of the method of osculating elements to the equation of trajectories. Here, according to (8.3.3), an additional term,  $\cos \rho$ , must be introduced in the left-hand side of (8.3.4).

Another limiting case obtains when the regression of the node is negligible in comparison with the regression of the perigee, i.e., when  $k_{\delta} = 0$ . The last equality is exact for a polar orbit,  $i = 90^\circ$ . The function  $\Phi$  (8.3.2) then does not depend on  $v$ , and equations (8.3.1) have the integral

$$-k_0^* \cos^2 \rho - k_1^* \cos \theta - k_2^* \cos^2 \theta - k_3^* \cos^3 \theta + k_{\omega} \cos \rho = \Phi_0. \quad (8.3.5)$$

Finally for an equatorial satellite,  $i = 0$ ,  $\cos \alpha^* = \cos \rho$ , regression of the node combines with the regression of the perigee, and equations (8.3.1) have the first integral

$$-k_0^* \cos^2 \rho - k_1^* \cos \theta - k_2^* \cos^2 \theta - k_3^* \cos^3 \theta + (k_{\omega} + k_{\delta}) \cos \rho = \Phi_0, \quad (8.3.6)$$

which is identical with (8.3.5), apart from the constant coefficient of  $\cos \rho$ . For nearly equatorial satellites (some American satellites), the motion around the center of mass can apparently be investigated from equation (8.3.6).

Let us outline another natural case when equations (8.3.1) have a first integral. After simple manipulations [8] it follows that in the absence of aerodynamic and gravitational perturbations, the following integral exists:

$$\cos \alpha^* = \text{const.} \quad (8.3.7)$$

The physical meaning of this integral is obvious. If the satellite is free from external torques, the angular momentum vector preserves a constant direction in the absolute space. In particular, the angle  $\chi^*$  that it makes with the direction to the celestial pole remains constant, and this statement is expressed in (8.3.7). Formula (8.3.7) enables us to consider the motion of the angular momentum vector relative to a regressing orbit in the torque-free case. The tip of the angular momentum vector traces a moving circle of constant radius  $\kappa^*$  on the surface of a unit sphere; the vector travels with an angular velocity  $k_0$  along the circle, while the center of the circle  $(\lambda^*, \theta^*)$  moves with an angular velocity  $k_\omega$  in a circle of constant radius  $i$  around the normal to the orbital plane (Figure 57).

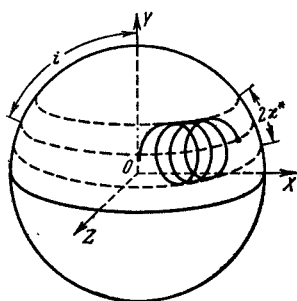


FIGURE 57. The path described by the tip of the angular momentum vector on the surface of a unit sphere in the torque-free case. The axis  $X$  points along the perigee tangent; the axis  $Y$  points along the normal to the orbital plane.

poles as an "aeropole" and a "gravipole", using the adjective "north" to denote the positive directions. In what follows we shall use the short term locus to denote the trajectory described by the tip of the angular momentum vector on the surface of a unit sphere.

We can now proceed with the analysis of motion in cases when the various factors interact.

#### § 4. INTERACTION OF AERODYNAMIC AND GRAVITATIONAL PERTURBATIONS. CLASSIFICATION OF MOTIONS

Following the arguments of Chapter 7, we shall henceforth take  $a_1^* = 0$ . This, in particular, leads to  $k_2^* = 0$  in (8.3.2) and other formulas. Furthermore, the coefficient  $k_0^*$  in this case is a function of gravitational terms only.

In (8.3.2) and in subsequent formulas,  $k_1^*$  and  $k_3^*$  were assumed to depend on  $\lambda$  according to (8.3.3). However, in Chapter 7 we have shown that this dependence is very weak, the coefficient  $J_5$  being small in comparison with  $J_1$ ,  $J_4$ . The terms with  $J_5$  only produce slight distortion of the locus, and they can be neglected putting  $J_5 = 0$ .

Note that the coefficients  $k_1^*$  and  $k_3^*$  are variable only because the aerodynamic torque coefficient is a function of the angle of attack  $\delta$ . If now  $C_m = \text{const} = a_2^b$ , we have  $a_2^b = 0$  and therefore  $k_3^* = 0$ ,  $k_1^* = \text{const}$ , and the foregoing effect vanishes. But even for  $C_m = f(\delta)$ , this effect, as shown in Chapter 7, is small. The loci outside a small neighborhood of the aeropole are close to the circles  $\theta = \text{const}$ , irrespective of whether the aerodynamic drag torque is constant ( $k_3^* = 0$ ) or varies with the angle of attack ( $k_3^* \neq 0$ ).

We may therefore put  $J_1 = 0$ , whence  $k_1^* = \text{const}$ ,  $k_3^* = \text{const}$ . It is in this approximation that we proceed to investigate the loci due to the combined influence of aerodynamic and gravity forces in nonregressing orbits. Since the contribution from regression is small, ignoring this effect we can nevertheless obtain the basic picture of the motion of a satellite about its center of mass. Having reconstructed the simplified pattern, we can easily allow for the regression of the orbit.

In our case, according to (8.3.4) ( $k_2^* = 0$ ,  $k_3^* = 0$ ), the equation of the locus is

$$\left. \begin{aligned} -k_0^* \cos^2 \rho - k_1^* \cos \theta - k_3^* \cos^3 \theta &= \Phi_0, \\ \cos \rho &= -\sin \theta \sin \lambda. \end{aligned} \right\} \quad (8.4.1)$$

In the system of coordinates  $\theta, \rho$ , each pair of values  $\theta, \rho$  corresponds to two points on the surface of a unit sphere which are placed symmetrically about the great circle through the gravi- and the aeropoles. This great circle will be called the symmetry meridian.

Since the case of aerodynamic torques without gravity (i.e., the case  $k_0^* = 0$ ) was discussed in Chapter 7, we shall now take  $k_0^* \neq 0$ .

The locus (8.4.1) is then written as

$$\cos \rho = \sqrt{C_0 - (\mu^* \cos \theta + \xi^* \cos^3 \theta)}, \quad (8.4.2)$$

and, in virtue of the second equation in (8.4.1), any real motion must satisfy

$$-\sin \theta \leq \cos \rho \leq \sin \theta. \quad (8.4.3)$$

All the loci are symmetric about the symmetry meridian. On this meridian, one of the inequalities in (8.4.3) reduces to a proper equality. The nature of the locus is determined by three parameters:  $C_0$ ,  $\mu^*$ ,  $\xi^*$ , where  $C_0$  is an arbitrary constant dependent on the initial conditions, while  $\mu^*$  and  $\xi^*$  are defined by

$$\left. \begin{aligned} \mu^* &= \frac{k_1^*}{k_0^*} = \frac{2P^2 \rho_{\pi} \cos \vartheta \left\{ a_0^b J_1 + \frac{a_2^b}{2} J_4 \sin^2 \vartheta \right\}}{3 \left( 1 - \frac{3}{2} \sin^2 \vartheta \right) (A - C)}, \\ \xi^* &= \frac{k_3^*}{k_0^*} = \frac{2P^2 \rho_{\pi} \left( 1 - \frac{5}{2} \sin^2 \vartheta \right) a_2^b J_4}{9 \left( 1 - \frac{3}{2} \sin^2 \vartheta \right) (A - C)}. \end{aligned} \right\} \quad (8.4.4)$$

If the aerodynamic torque coefficients are constant (independent of the angle of attack), we have  $a_2^b = 0$  and  $\xi^* = 0$ . The parameter  $\xi^*$  thus allows for the dependence of the aerodynamic torque coefficient on the angle of attack.

As an illustration, let us analyze the set of loci for the case  $\mu^* > 0$ ,  $\zeta^* > 0$ . We have

$$\cos \rho = \sqrt{C_0 - f(\theta)}, \quad \frac{df}{d\theta} = -\sin \theta (\mu^* + 3\zeta^* \cos^2 \theta) < 0,$$

i.e., in the relevant interval  $(0, \pi)$  of  $\theta$ -values, the function  $f$  monotonically decreases from  $f = \mu^* + \zeta^*$  to  $f = -(\mu^* + \zeta^*)$  (Figure 58 a). On this curve, we superimpose a family of straight lines  $f = C_0$ . Subtracting  $f$  from each  $C_0$ , we obtain the family  $C_0 - f$  (Figure 58 b). Real motion is permitted only in the region of positive  $C_0 - f$ . Extracting the square root (with + and - signs), we obtain the dependence  $\cos \rho(\theta, C_0)$  shown in Figure 58 c. Finally, in virtue of (8.4.3), the values of  $\cos \rho$  should in reality lie between the sine curves  $\sin \theta$  and  $-\sin \theta$  (Figure 58 d). It now remains to map this pattern on the

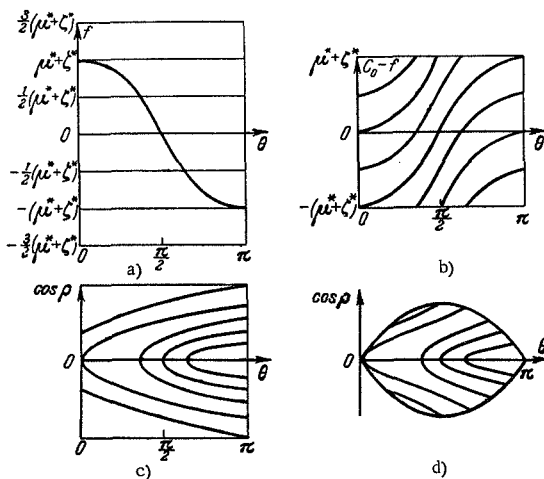


FIGURE 58. Illustrating the successive stages in the construction of the angular momentum locus.

surface of a unit sphere. Note that the sine curves  $\pm \sin \theta$  of the planar drawing (Figure 58 d) correspond to the symmetry meridian on the unit sphere; the points  $\cos \rho = 0, \theta = 0, \pi$  correspond to the aeropoles, and the points  $\cos \rho = \pm 1, \theta = \pi/2$  to the gravipoles. Since we are concerned with the interval  $[0, \pi]$  of  $\rho$ -values, where  $\cos \rho$  monotonically decreases, we may conclude that the locus on a unit hemisphere defined by the symmetry meridian is of the same character as the dependence  $\cos \rho(\theta, C_0)$  between the sine curves  $\pm \sin \theta$  in the planar drawing (Figure 58 d). We thus obtain a family of curves on the surface of the unit sphere, which is shown in Figure 59 a. Note that the loci are symmetric about the symmetry meridian.

Let us consider some peculiar features of this class of loci. We see that the loci fall into two groups: part of the loci are aerodynamic, namely closed curves centered at the aeropole. Gravitational perturbations produce a certain flattening of these loci, since gravity torques tend to conserve the angle  $\rho$  between the gravipole and the angular momentum vector. Another group comprises the "gravitational" loci: these are closed curves around certain points on the symmetry meridian, which approach the

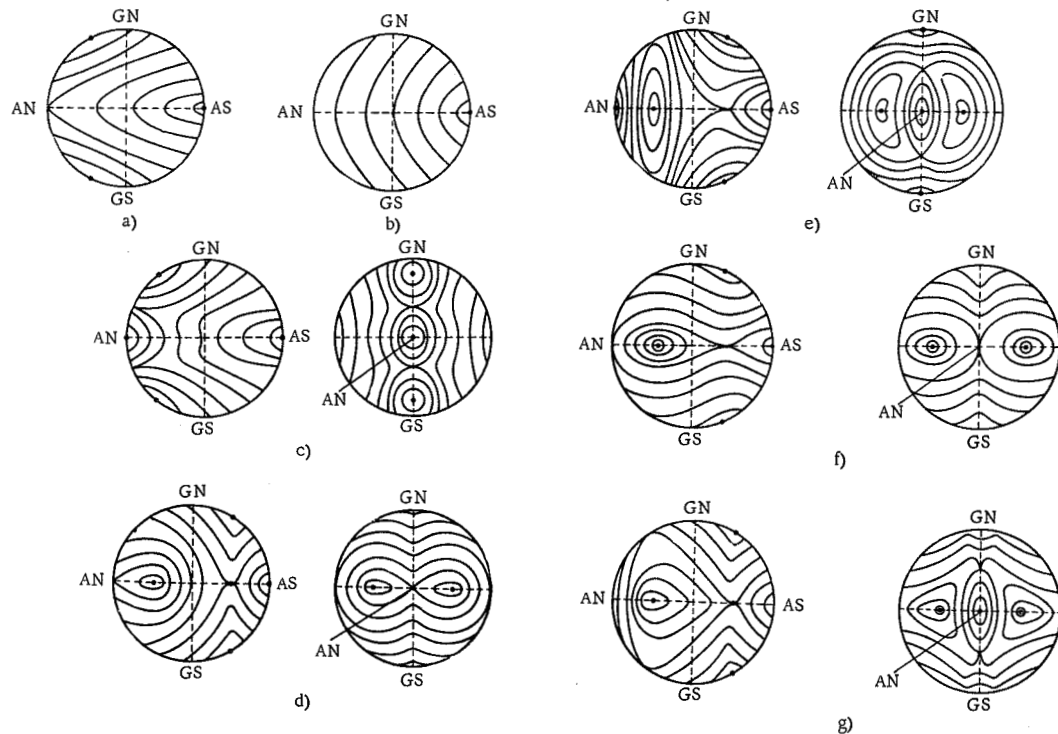


FIGURE 59. Various angular momentum loci for interacting aerodynamic and gravitational perturbations (secular motion):  
 a) three-pole; b) one-pole; c) four-pole; d) five-pole, first subclass; e) six-pole, first subclass; f) five-pole, second subclass;  
 g) six-pole, second subclass. Dots mark the position of the poles; AS — aerosouth, AN — aeronorth, GS — gravsouth, GN — gravnorth.

gravipoles as the magnitude of gravitational perturbations relative to aerodynamic perturbations increases. The region of "aerodynamic" loci will vary in breadth depending on the same factor, and in the limit, as the aerodynamic perturbations approach zero, it will contract to the "graviequator". The two groups are separated by the so-called asymptotic loci: the angular momentum vector moving along these paths approaches the perigee tangent. This is obviously a three-pole class of loci: there is one aerodynamic pole and two gravitational poles.

More detailed analysis is required in order to follow the evolution of the loci as the proportion of aerodynamic perturbations increases, and to establish other possible classes of loci.

To this end, let us find the poles of the loci. A pole is clearly a point  $\theta_i^*, \rho_i^*$  at which the locus corresponding to a certain constant  $C_0^*$  is tangent to the symmetry meridian (we have in mind the planar interpretation of the loci, as shown, e.g., in Figure 58 d). The analytical conditions corresponding to the case of a common tangent for the sine curve representing the symmetry meridian and for the locus of given  $C_0^*$  are written as

$$\cos \rho_i^* = \sin \theta_i^*, \quad \frac{d}{d\theta} \cos \rho_i^* = \cos \theta_i^*. \quad (8.4.5)$$

The set (8.4.5) defines the locus (the constant  $C_0^*$ ) which is tangent to the image of the symmetry meridian on the plane  $\theta, \cos \rho$ , and the point  $\theta_i^*$  at which the two curves have a common tangent; to find  $\theta_i^*$ , the set (8.4.5) is reduced to a quadratic equation in  $\cos \theta^*$  with the two roots

$$\cos \theta_{(1), (2)}^* = \frac{1}{3\zeta^*} (1 \pm \sqrt{1 - 3\mu^* \zeta^*}). \quad (8.4.6)$$

Each of these  $\theta_{(1), (2)}^*$  corresponds to a branch with the parameters  $C_{01}, C_{02}$ , one of the branches tangent to the sine curve from the inside, the other from the outside; for  $\zeta^* = 0, \cos \theta_i^* = \frac{\mu^*}{2}$ . (We consider one hemisphere only — the "gravinorthern" hemisphere. Everything is symmetric, however, in the gravisouthern hemisphere.) If  $\theta_{(1), (2)}^*$  are known, the corresponding constants  $C_{01}$  and  $C_{02}$  can be calculated from the first equation in (8.4.5); then

$$C_{01} - C_{02} = -\frac{4}{27\zeta^{*2}} (1 - 3\mu^* \zeta^*)^{\frac{1}{2}},$$

i.e., if the curves touch at two points, the  $C_{01}$  corresponding to  $\theta_{(1)}^*$  is less than the  $C_{02}$  corresponding to  $\theta_{(2)}^*$ , since from the last formula we have  $C_{01} - C_{02} < 0$ .

From (8.4.6), we clearly have  $0 < \cos \theta_{(2)}^* < \cos \theta_{(1)}^*$ , i.e.,

$$\frac{\pi}{2} > \theta_{(2)}^* > \theta_{(1)}^*. \quad (8.4.7)$$

If both points exist, the point  $\theta_{(2)}^*$  is the stable pole of the loci, whereas  $\theta_{(1)}^*$  is the unstable pole.

Let us consider the conditions for the simultaneous existence of the two points  $\theta_{(1)}^*$  and  $\theta_{(2)}^*$ . For the existence of the two points it is of course necessary that

$$\mu^* \zeta^* < \frac{1}{3}. \quad (8.4.8)$$

Note that according to (8.4.6) and (8.4.7), for the existence of the two points it is sufficient that  $\cos \theta_{(1)} < 1$ , which, in virtue of (8.4.6), yields

$$\mu^* + 3\xi^* - 2 > 0. \quad (8.4.9)$$

Thus, if conditions (8.4.8) and (8.4.9) are satisfied, the curves are tangent at two points. This corresponds to the class of loci depicted in Figure 59 c, i.e., the class of four-pole trajectories.

If now  $\mu^* + 3\xi^* - 2 < 0$ , there is a single point of tangency  $\theta_{(2)}^*$ , defining the previously considered class of three-pole trajectories (Figure 59 a). Elsewhere in the quadrant  $\mu^* > 0, \xi^* > 0$ , namely, in the region satisfying the inequalities

$$\left. \begin{array}{l} \mu^*\xi^* > \frac{1}{3}, \xi^* > \frac{1}{3} \\ \mu^* + 3\xi^* - 2 > 0, \xi^* < \frac{1}{3} \end{array} \right\} \quad (8.4.10)$$

and

the curves do not touch; in the planar interpretation, all the loci meet the symmetry meridian, so that they are all of aerodynamic character. The contribution of gravitational perturbations produces a certain "flattening" of the aerodynamic loci (Figure 59 e). This constitutes the so-called one-pole class.

We should emphasize that the aerodynamic loci are characteristically stable with respect to gravitational perturbations. The loci acquire a distinct aerodynamic character already for some finite values of  $\mu^*$  and  $\xi^*$  (we recall that  $\mu^*$  and  $\xi^*$  are proportional to the ratio of aerodynamic to gravitational perturbations). Conversely, if the region of aerodynamic loci is to be entirely eliminated,  $\mu^*$  and  $\xi^*$  must be made to approach zero, or in other words, the gravitational perturbations should be infinitely large in comparison with the aerodynamic perturbations. The presence of arbitrarily small aerodynamic perturbations is sufficient to produce a small, but finite, region which contains loci of aerodynamic character (having their pole at the aeropole).

Until now we have been discussing the quadrant  $\mu^* > 0, \xi^* > 0$ . Let us now consider other regions of  $\mu^*$  and  $\xi^*$ . In the quadrant  $\xi^* < 0, \mu^* < 0$ , the pattern is quite symmetric, but the main aeropole is in the aeronorth. The four-pole class obtains in the region

$$\mu^*\xi^* < \frac{1}{3}, \mu^* + 3\xi^* + 2 < 0, \quad (8.4.11)$$

the three-pole class in the region

$$\mu^* + 3\xi^* + 2 > 0, \quad (8.4.12)$$

and the one-pole class in the regions

$$\left. \begin{array}{l} \mu^*\xi^* > \frac{1}{3}, |\xi^*| > \frac{1}{3} \\ \mu^* + 3\xi^* + 2 < 0, |\xi^*| < \frac{1}{3} \end{array} \right\} \quad (8.4.13)$$

and

Let us now consider the case  $\mu^* < 0$ ,  $\zeta^* > 0$ . First let

$$3\zeta^* + \mu^* < 0. \quad (8.4.14)$$

Then  $f = -\sin \theta(\mu^* + 3\zeta^* \cos^2 \theta) > 0$ , and the problem is analogous to the previous case  $\mu^* < 0$ ,  $\zeta^* < 0$ , i.e., in general we should obtain the one-pole, three-pole, and four-pole classes. We shall show, however, that no four-pole class exists. Indeed, there are four poles only if the point  $\theta_{(1)}^*$  exists, in other words, according to (8.4.6), we must have  $\cos \theta_{(1)}^* < 1$ , or  $\frac{1}{3\zeta^*}(1 + \sqrt{1 + 3|\mu^*|\zeta^*}) < 1$ , which leads to inequality (8.4.9),  $\mu^* + 3\zeta^* > 2$ , in contradiction with inequality (8.4.14). As regards the three-pole case, it is permitted as long as

$$\cos \theta_{(2)}^* > -1. \quad (8.4.15)$$

In the quadrant being considered

$$\cos \theta_{(2)}^* = \frac{1}{3\zeta^*}(1 - \sqrt{1 + 3|\mu^*|\zeta^*}) < 0. \quad (8.4.16)$$

Inequality (8.4.15) thus reduces to (8.4.12),  $3\zeta^* + \mu^* + 2 > 0$ .

Thus, if  $\zeta^* > 0$ ,  $\mu^* < 0$  and  $0 > 3\zeta^* + \mu^* > -2$ , we have the three-pole class, and if  $3\zeta^* + \mu^* < -2$ , the one-pole class is obtained. The aeropole is in the aeronorth ( $\theta = 0$ ).

Let us now consider the case  $3\zeta^* + \mu^* > 0$ . Then  $f = 0$  for  $\cos^2 \theta = -\frac{\mu^*}{3\zeta^*}$ , i.e., the function is not monotonic: it has a minimum for  $\cos \theta = \sqrt{\frac{|\mu^*|}{3\zeta^*}}$  and a maximum for  $\cos \theta = -\sqrt{\frac{|\mu^*|}{3\zeta^*}}$ . The magnitudes of the minimum and the maximum are

$$f_{\min, \max} = \pm \frac{2}{3} |\mu^*| \sqrt{\frac{|\mu^*|}{3\zeta^*}}.$$

We shall now show that there always exists a point  $\theta_{(2)}^*$  at which the sine curve is externally tangent to the locus  $\sqrt{C_0 - f(\theta)}$ . Indeed, from (8.4.6) we see that in our case  $\cos \theta_{(2)} < 0$ , and the condition  $\cos \theta_{(2)} > -1$  leads to the inequality  $3\zeta^* + \mu^* + 2 > 0$ , which is satisfied in virtue of (8.4.16). The point of internal tangency  $\theta_{(1)}^*$  exists if  $\cos \theta_{(2)}^* < 1$ , i.e., if  $3\zeta^* + \mu^* - 2 > 0$ . Thus, if  $0 < 3\zeta^* + \mu^* < 2$ , the curves are tangent at one point only — the point of external tangency, and this, on account of the nonmonotonic variation of the function  $f(\theta)$ , leads to a five-pole class of trajectories (Figure 59).

If now  $3\zeta^* + \mu^* > 2$ , the curves are tangent both externally and internally, at two points; this fact, taken in conjunction with the nonmonotonic variation of the function  $f(\theta)$ , gives a six-pole class of trajectories (Figure 59). However, the behavior of the loci from these two classes near the poles varies depending on the parameters  $\mu^*$  and  $\zeta^*$ : each of the two classes (the five-pole and the six-pole) can be divided into two subclasses.

Let us consider the maximum and the minimum values of the function  $F(C_0, \theta) = \sqrt{C_0 - f}$  on the "boundary" locus, i.e., the locus where

$$\min F(\bar{C}_0, \theta) = F(\bar{C}_0, \theta_m) = \sqrt{\bar{C}_0 - f(\theta_m)} = 0.$$

Then

$$\bar{C}_0 = \frac{2}{3} |\mu^*| \sqrt{\frac{|\mu^*|}{3\zeta^*}}$$

and

$$\max F(\bar{C}_0, \theta) = F(\bar{C}_0, \theta_m) = \sqrt{\frac{4}{3} |\mu^*| \sqrt{\frac{|\mu^*|}{3\zeta^*}}}.$$

If  $F(\bar{C}_0, \theta_m) > 1$ , no real values of  $\cos \theta_{(t)}$  can be obtained, so that in the real region the boundary locus has a minimum only. The five- and the six-pole classes are then represented by the respective subclasses depicted in Figures 59 d, e. These two subclasses are characterized by a double pole (two closely adjoining poles) in the five-pole case and by a triple pole (three closely adjoining poles) in the six-pole case (near the aeronorth); a locus always exists enclosing these poles and clearing the antipodal aeropole (aerosouth). If, however,  $F(\bar{C}_0, \theta_m) < 1$ , the boundary locus has both a minimum and a maximum in the real region, so that the five- and the six-pole classes are represented by the subclasses in Figures 59 f, g, respectively. In these subclasses, there are no loci enclosing the double pole in the five-pole case or the triple pole in the six-pole case. There is, however, a locus surrounding three poles in each class. In the five-pole class, a certain locus encloses the double pole near the aeronorth together with the pole in the aerosouth. The corresponding locus in the six-pole class encloses the two poles near the aeronorth and the single pole in the aerosouth, while clearing the pole in the aeronorth.

As we have already observed, the different subclasses obtain according as  $F(\bar{C}_0, \theta_m) = \sqrt{\frac{4}{3} |\mu^*| \sqrt{\frac{|\mu^*|}{3\zeta^*}}}$  is greater or less than unity. The subclass corresponding to  $F(\bar{C}_0, \theta_m) > 1$  or, equivalently, to  $\zeta^* < \frac{16}{27} |\mu^*|^3$  will be called the first subclass, and that corresponding to  $\zeta^* > \frac{16}{27} |\mu^*|^3$ , the second subclass.

It now remains to consider the case  $\mu^* > 0, \zeta^* < 0$ . The pattern is entirely symmetric to that obtained in the previous case, but the aeronorth and the aerosouth are switched. A six-pole obtains if  $3\zeta^* + \mu^* + 2 < 0$ ; a five-pole if  $-2 < 3\zeta^* + \mu^* < 0$ ; a three-pole if  $0 < 3\zeta^* + \mu^*$ ; and a one-pole if  $2 < 3\zeta^* + \mu^*$ . The five-pole and the six-pole are divided each into two subclasses:  $|\zeta^*| > \frac{16}{27} \mu^*$  (second subclass) and  $|\zeta^*| < \frac{16}{27} \mu^*$  (first subclass).

This completes the classification of the trajectories described by the tip of the angular momentum vector on the surface of a unit sphere. The results are summarized in Table 9. Figure 60 shows the plane  $\mu^*, \zeta^*$  depicting the regions where the various classes of loci obtain.

It now remains to see what part of the  $\mu^*, \zeta^*$  plane corresponds to physically real values of aerodynamic and gravitational parameters of satellites.

We should first note that almost all the classes and trajectories are attributable to the variability of the aerodynamic drag coefficient. Indeed, if the coefficient is constant, we have  $a_0^* = 0$ , i.e.,  $\zeta^* = 0$ , so that the diversified pattern reduces to a single three-pole class for  $|\mu^*| < 2$  and a one-pole class for  $|\mu^*| > 2$ . The stability of aerodynamic trajectories with

TABLE 9

	Condition	Class	Subclass	Characteristic feature
$\mu^* > 0$	$3\zeta^* + \mu^* < 0$	Six-pole	$ \zeta^*  < \frac{16}{27} \mu^{*3}$	Triple pole near the aerosouth
			$ \zeta^*  > \frac{16}{27} \mu^{*3}$	A triple pole; aeronorth and two near the aerosouth
	$-2 < 3\zeta^* + \mu^* < 0$	Five-pole	$ \zeta^*  < \frac{16}{27} \mu^{*3}$	Double pole near the aerosouth
			$ \zeta^*  > \frac{16}{27} \mu^{*3}$	A triple pole; aeronorth and two near the aerosouth
	$0 < 3\zeta^* + \mu^* < 2$	Three-pole		Main aeropole in the aerosouth
	$\mu^*\zeta^* > \frac{1}{3}; \zeta^* > \frac{1}{3}$ $\mu^* + 3\zeta^* > 2; \zeta^* < \frac{1}{3}$	One-pole		
	$\mu^* + 3\zeta^* > 2; \mu^*\zeta^* < \frac{1}{3}$	Four-pole		Main aeropole in the aerosouth
$\mu^* < 0$	$3\zeta^* + \mu^* < 2$	Six-pole	$\zeta^* < \frac{16}{27}  \mu^* ^3$	Triple pole near the aeronorth
			$\zeta^* > \frac{16}{27}  \mu^* ^3$	A triple pole; aerosouth and two near the aeronorth
	$0 < 3\zeta^* + \mu^* < 2$	Five-pole	$\zeta^* < \frac{16}{27}  \mu^* ^3$	Double pole near the aeronorth
			$\zeta^* > \frac{16}{27}  \mu^* ^3$	A triple pole; aerosouth and two near the aeronorth
	$-2 < 3\zeta^* + \mu^* < 0$	Three-pole		Main pole in the aeronorth
	$\mu^*\zeta^* > \frac{1}{3}; \zeta^* < -\frac{1}{3}$ $3\zeta^* + \mu^* < -2; \zeta^* > -\frac{1}{3}$	One-pole		
	$\mu^*\zeta^* < \frac{1}{3}$ $3\zeta^* + \mu^* < -2$	Four-pole		Main aeropole in the aeronorth

respect to gravitational perturbations is particularly pronounced in this case: already for  $|\mu^*| > 2$ , i.e., with aerodynamic perturbations more than twice as large as gravitational perturbations, the loci are of aerodynamic character (the angular momentum vector precesses about the aeropoles), although the actual shape of the trajectories is somewhat distorted by gravitational perturbations.

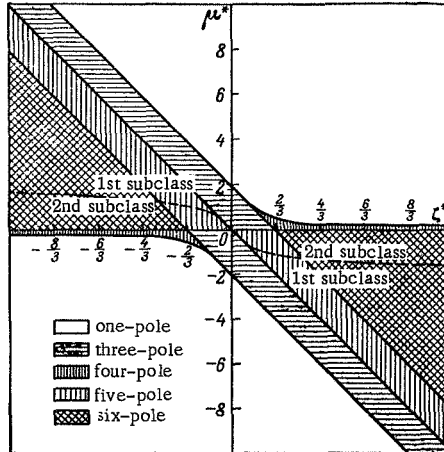


FIGURE 60. Regions corresponding to different classes of loci in the plane  $\mu^*, \xi^*$ .

Let us consider the general case  $\xi^* \neq 0, \mu^* \neq 0$ . From (8.4.4) we see that  $\mu^*$  may take arbitrarily large absolute values (for large  $a_0^\delta P^2 J_1$  and small  $A-C$ ); its sign may also change on account of the term  $1 - \frac{3}{2} \sin^2 \theta$  and, in general, on account of  $A-C$ . We may therefore consider the entire  $\mu^*$  axis. From (8.4.4) we moreover see that

$$\mu^* = K^* \xi^*, \quad K^* = \frac{\frac{a^\delta}{3} + \frac{1}{2} \sin^2 \theta}{1 - \frac{5}{2} \sin^2 \theta}, \quad a^\delta = \frac{a_0^\delta J_1}{a_2^\delta J_4}.$$

When  $a^\delta$  and  $\theta$  change, the slope  $K^*$  of this straight line to the  $\xi^*$  axis varies, and the line "sweeps" the region of real values of the parameters  $\mu^*$  and  $\xi^*$ . It is easily seen that for real values of  $a_0^\delta, a_2^\delta$ , and  $\theta$ , the straight line may make any angle with the  $\xi^*$  axis, with the exception of the region between the axis  $\xi^*$  and the line  $\mu^* = -\frac{1}{3} \xi^*$ . All the various classes of trajectories lie inside the region of real values of these parameters. In other words, all the classes of loci that we have considered are in fact realizable.

As we have observed, the character of the trajectory traced by the angular momentum vector is determined mainly by aerodynamic and gravitational perturbations, the contribution of orbital regression being negligible. In the present section we have therefore analyzed in some detail the interaction of aerodynamic and gravitational perturbations, and our principal conclusions can be summarized as follows:

1. *Aerodynamic perturbations are distinctly stable with respect to gravitational perturbations.* The aerodynamic-type loci are eliminated only if the gravitational perturbations are infinitely large in comparison with the aerodynamic perturbations. On the other hand, gravitational trajectories will vanish even if the aerodynamic to gravitational perturbations ratio is finite.

2. For interacting gravitational and aerodynamic perturbations, the character of the loci in some cases is decided in a considerable degree by the dependence of the aerodynamic torques on the angle of attack.

## § 5. THE INFLUENCE OF ORBITAL REGRESSION

Let us first consider the contribution due to the regression of the orbit's node, ignoring the regression of the perigee. The set of loci of the angular momentum vector is then described by equation (8.3.4); making use of the previous relations among  $\rho$ ,  $\pi^*$  and  $\theta$ ,  $\lambda$ , we see that when the effect of the regression of the node is added to aerodynamic and gravitational perturbations the loci remain closed, since  $\theta$  is a periodic function of  $\lambda$  (with a period of  $2\pi$ ). This means that perturbations due to the regression of the node will only distort the shape of the locus. This distortion is small if the rate of regression  $k_{\eta}$  is small in comparison with the velocities of aerodynamic and gravitational precessions.

*Thus, we may say that the loci are stable with respect to the regression of the node in the sense that the movement of the angular momentum vector relative to the regressing orbit under fairly large aerodynamic and gravitational perturbations nearly coincides with its movement relative to a nonregressing orbit.*

To study in greater detail the contribution from the regression of the node, and at a later stage the contribution from the regression of the perigee, let us consider the case of aerodynamic perturbations, without gravity torques.

We shall first investigate the combined effect due to the aerodynamic factors and the regression of the node, without any other perturbations. For simplicity, we take the aerodynamic torque coefficient to be independent of the angle of attack. Then, from (8.3.4) we obtain the following equation for the trajectory described by the angular momentum vector:

$$\cos \pi^* = C_0 + \varepsilon_{\eta} \cos \theta, \quad \varepsilon_{\eta} = \frac{k_2^*}{k_{\eta}} \quad (8.5.1)$$

From (8.5.1) and from the expression of  $\cos \pi^*$  in terms of  $\lambda$ ,  $\theta$  it follows that the loci are symmetric about the meridian  $\lambda=\lambda^*$  through the aeropoles and the poles of regression (the south and the north celestial poles). The family of loci is plotted according to the technique described in § 4. From the expression for  $\cos \pi^*$  we have

$$\cos(\theta + \theta^*) \leq \cos \pi^* \leq \cos(\theta - \theta^*). \quad (8.5.2)$$

From (8.5.1) we now plot the set of the curves  $\cos \pi^* = f(\theta, C_0)$  and the boundary curves  $\cos(\theta - \theta^*)$  and  $\cos(\theta + \theta^*)$  (Figure 61). From Figure 61 we can easily

map the trajectories on the surface of a unit sphere: the points  $(\cos \theta^*, 0)$ ,  $(-\cos \theta^*, \pi)$  correspond to the aeropoles; the points  $(1, \theta^*)$ ,  $(-1, \pi - \theta^*)$  correspond to the poles of regression. The boundary curves  $\cos(\theta + \theta^*)$  and  $\cos(\theta - \theta^*)$  correspond to the symmetry meridian of the loci; this meridian, as we have observed, passes through the aeropoles and the poles of regression.

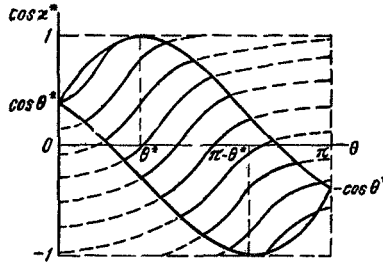


FIGURE 61. Illustrating the construction of the trajectories traced by the angular momentum vector in the case of regressing node. The maximum and the minimum of the function  $\cos \rho = f(\theta, C_0)$  occur at  $\theta^*$  and  $\pi - \theta^*$ , respectively.

The curves  $\cos \omega^*(\theta)$  (Figure 61) become steeper as the parameter  $\varepsilon_{\Omega}$  increases in absolute magnitude, i.e., as the relative magnitude of the aerodynamic precessing rate of the angular momentum vector rises in comparison with the rate of regression of the node. With  $\varepsilon_{\Omega} \rightarrow \infty$ , the curves degenerate into vertical straight lines  $\theta = \text{const}$ , which corresponds to a circle  $\theta = \text{const}$  on the surface of the unit sphere; for  $\varepsilon_{\Omega} = 0$  we have  $\cos \omega^* = \text{const}$ , i.e., a family of circles on the surface of the unit sphere centered at the pole of regression. In the general case, the trajectories on the unit sphere are closed curves, having certain two points on the symmetry meridian  $\lambda = \lambda^*$  as their poles. We shall now find these points. From the general equations of motion of the angular momentum vector (8.3.1) we see that, ignoring the regression of the perigee point and setting as before  $J_5 = 0$ ,  $a_i^* = 0$ , we can find the location of the pole  $\theta_0, \lambda_0$  ( $\theta_0 \neq \theta^*$ ) from the set of equations

$$\frac{\partial \Phi}{\partial \theta} \Big|_{\theta_0, \lambda_0} = 0, \quad \frac{\partial \Phi}{\partial \lambda} \Big|_{\theta_0, \lambda_0} = 0,$$

i.e.,

$$\left. \begin{aligned} & -k_{\Omega} \{ \sin \theta_0 \cos \theta^* - \cos \theta_0 \sin \theta^* \cos(\lambda_0 - \lambda^*) \} + \\ & + (k_1^* + 3k_3^* \cos^2 \theta_0) \sin \theta_0 - 2k_0^* \sin \theta_0 \cos \theta_0 \sin^2 \lambda = 0, \\ & -k_{\Omega} \sin \theta_0 \sin \theta^* \sin(\lambda^* - \lambda_0) + \\ & + 2k_0^* \sin^2 \theta_0 \sin \lambda_0 \cos \lambda_0 = 0. \end{aligned} \right\} \quad (8.5.3)$$

In our case  $k_0^* = 0$ ,  $k_3^* = 0$ ; the second equation in (8.5.3) then gives  $\lambda_0 = \lambda^*$ , so that from the first equation we have

$$\operatorname{ctg} \theta_0 = \operatorname{ctg} \theta^* - \frac{\varepsilon_{\Omega}}{\sin \theta^*} \quad (\lambda_0 = \lambda^*). \quad (8.5.4)$$

For example, for  $\theta^* = 60^\circ$  and  $\varepsilon_{\eta} = -3$ , we have  $\theta_0 = 13^\circ$ , while for  $\varepsilon_{\eta} = -10$ , we have  $\theta_0 = 5^\circ$ . Since in practice the rate of aerodynamic precession is several times as large as the rate of node regression, the displacement  $\theta_0$  of the pole relative to the aeropole is small, being of the order of  $5-10^\circ$ .

Let us consider the shape of the trajectories (8.5.1). To this end, we introduce  $\Delta$ , the arc of the great circle joining the pole  $\theta_0, \lambda_0$  of the loci with the current point  $\theta, \lambda$  of a locus. Then

$$\cos \Delta = \cos \theta \cos \theta_0 + \sin \theta \sin \theta_0 \cos(\lambda - \lambda^*). \quad (8.5.5)$$

Eliminating  $\cos(\lambda - \lambda^*)$  with the aid of  $\cos \pi^*$  ( $\S 3$ ), and applying (8.5.4), we have

$$\cos \Delta \sin \theta^* - \cos \pi^* \sin \theta_0 = -\cos \theta \varepsilon_{\eta} \sin \theta_0.$$

Inserting  $\cos \pi^*$  from (8.5.1), we obtain the final expression

$$\cos \Delta = \frac{C_0 \sin \theta_0}{\sin \theta^*}. \quad (8.5.6)$$

We see that the loci on the surface of a unit sphere constitute a family of concentric circles centered at the point  $\theta_0, \lambda_0$ , which is defined by relations (8.5.4).

In the case of pure aerodynamic perturbations, the loci are circles centered at the aeropole; we thus see that the contribution from the regression of the orbit's node amounts to the displacement of these loci as one whole along the meridian  $\lambda = \lambda^*$  and a certain alteration of the circle radii (for equal initial conditions), according to (8.5.5) and (8.5.6).

It now remains to consider the distortion of the locus (8.5.1), or equivalently (8.5.6), due to the regression of the perigee. Since the locus is a continuous function of the parameters, we see that for small aerodynamic perturbations the loci must nearly coincide with the "regressing" trajectory depicted in Figure 57. Conversely, if the aerodynamic perturbations are large, the orbital regression has but a negligible effect on the shape of the loci, and the trajectory should nearly coincide with a small circle on the unit sphere, centered at the aeropole.

Indeed, direct investigation of the loci by introducing a variable parameter  $\omega$  in (8.5.1), as well as numerical integration of the equations of motion show that if the aerodynamic precessing rate of the angular momentum vector is greater than the rate of orbital regression, the trajectory will pulsate (about the displaced aeropole), as in Figure 62 a. For the orbits of the early Soviet satellites, the radius of the locus during one complete revolution of the angular momentum vector around the pole of precession increased by amounts of  $0.5^\circ - 1^\circ$ .

If, conversely, the rate of orbital regression is large in comparison with aerodynamic perturbations, we have a trajectory which displays a secular movement of the pole of precession (Figure 62 b). The intermediate case is clearly a combination of simultaneous pulsation and regression (Figure 62 c).

Figures 53, 55, 56 show pronounced pulsation of the trajectories.

If gravitational perturbations are also taken into consideration, the regressions of the node and the perigee are seen to have similar effects. The regression of the node produces a constant displacement of the pole

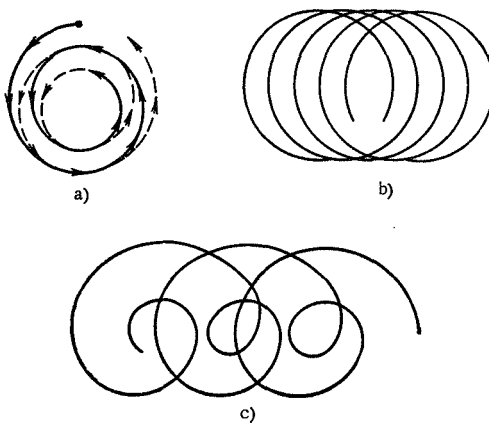


FIGURE 62. The trajectory of the angular momentum vector as distorted by the regression of the perigee (schematic):  
a) rate of regression much less than the aerodynamic precessing rate; b) rate of regression greater than the rate of precession;  
c) intermediate case.

of the gravi-aerodynamic locus. The regression of the perigee causes the locus to evolve (pulsation, movement of the pole of precession) without noticeably distorting the fundamental shape of the trajectory. The joint influence of the various factors will be considered further in Chapter 9.

## § 6. MEAN AERODYNAMIC DRAG COEFFICIENT

To determine the lifetime of a satellite when the atmospheric parameters are known or, conversely, to find the parameters of the atmosphere from satellite slow-down measurements, a certain mean drag coefficient is required. Indeed, on account of the fast precession of the satellite about its mass center and on account of the orbital motion of the satellite's mass center, the satellite may assume a random attitude relative to the oncoming stream; the drag coefficient will therefore vary rapidly in time, as a function of numerous parameters. This introduces considerable difficulties in the calculation of orbit evolution. It is obvious, however, that the fundamental trend of orbit evolution is decided by a certain mean atmospheric resistance, which can be allowed for by appropriately defining a mean aerodynamic drag coefficient. This coefficient should be a function, not only of the secular inequalities of motion, but also of the satellite's spin. The dependence of the aerodynamic drag coefficient  $C_R$  on the angle of attack  $\delta$  can be approximated with a formula analogous to expression (1.3.17) for the aerodynamic torque coefficient. We accordingly put

$$C_R = C_0 + C_2 \cos^2 \delta. \quad (8.6.1)$$

An elliptical orbit is assumed; the contribution of atmospheric rotation is ignored;  $\cos \delta$  is then determined from (7.1.3). To find the mean value of  $C_R$  for a single orbital circuit of the satellite, we should average (8.6.1) over the precessing and the orbital periods; averaging over the orbital

period is equivalent to averaging over  $v$  with the weight  $\frac{dt}{dv} = \frac{P^2}{V\mu P(1+e \cos v)^2}$ .

Also note that the mean drag coefficient should be consistent with the observed slow-down: it must therefore account not only for the attitude of the body relative to the oncoming stream, but also for the magnitude of the dynamic head in this stream. In an elliptical orbit, the dynamic head obviously differs at different points, in distinction from the situation obtaining with circular orbits: the averaging over the orbital period must therefore be carried out by assigning a certain weight to the dynamic head.

The contribution of variable dynamic head is illustrated by the following example. Consider a tumbling oblong satellite ( $\vartheta = 90^\circ$ ), which rotates in a certain "plane of precession", and let this plane be perpendicular to the orbital plane. If at the perigee the plane of precession is perpendicular to the oncoming stream, the satellite slow-down, and therefore the mean drag coefficient, are larger than in the case of an "edge-on" perigee passage. This distinction is irrelevant for circular orbits, since if at any point of the orbit the plane of precession is "face on" relative to the oncoming stream, there always exists a point where the plane meets the stream "edge on". Then, the dynamic head being constant at all points of the circular orbit, the mean drag coefficient will not depend on the attitude of the precession plane at any particular point of the orbit.

In virtue of the preceding, we define the mean aerodynamic drag coefficient  $\bar{C}_R$  by the formula

$$\bar{C}_R = \frac{\left(\frac{1}{2\pi}\right)^2 \int_0^{2\pi} \int_0^{2\pi} C_R \rho_a V^2 \frac{dt}{dv} dv d\psi}{\frac{1}{2\pi} \int_0^{2\pi} \rho_a V^2 \frac{dt}{dv} dv}. \quad (8.6.2)$$

Averaging over  $v$  and over  $\psi$ , as indicated in (8.6.2), we have

$$\left. \begin{aligned} \bar{C}_R &= C_0 + C_2 \left\{ n_1 + n_2 \sin^2 \theta \left( \frac{\tilde{J}_1}{J_0} - \frac{\tilde{J}_2}{J_0} \cos^2 \lambda \right) \right\}, \\ \tilde{J}_1 &= \frac{1}{2\pi} \int_0^{2\pi} \frac{\rho_a (e + \cos v)^2}{(1 + e \cos v)^2} dv, \\ \tilde{J}_2 &= \frac{1}{2\pi} \int_0^{2\pi} \frac{\bar{\rho}_a \sin^2 v}{(1 + e \cos v)^2} dv, \\ J_0 &= \frac{1}{2\pi} \int_0^{2\pi} \bar{\rho}_a \frac{1 + e^2 + 2e \cos v}{(1 + e \cos v)^2} dv, \quad \bar{\rho}_a = \frac{\rho_a}{\rho_\infty}, \\ n_1 &= \frac{J_1}{J_0} \cos^2 \theta_0 + \frac{1}{2} \frac{\tilde{J}_2}{J_0} \sin^2 \theta_0, \quad n_2 = \frac{3}{2} \sin^2 \theta_0 - 1. \end{aligned} \right\} \quad (8.6.3)$$

Figure 63 plots the ratios  $\frac{\tilde{J}_2}{J_0}$  and  $\frac{\tilde{J}_1}{J_0}$  calculated for an exponential density variation,  $H = 30$  km, perigee height  $h = 225$  km, and various apogee heights. We see that  $J_1 > J_2$ ; the equality  $J_1 = J_2$  obtains for circular orbits only.

From (8.6.3) we see that  $\bar{C}_R$  is a function of quasiconstant parameters only. During one circuit of the satellite,  $\theta$  and  $\lambda$  may be regarded constant. However,  $\theta$  and  $\lambda$  vary slowly from circuit to circuit, and the drag conditions change correspondingly. It follows from the results of this chapter that the interaction of aerodynamic and gravitational perturbations is sufficient to cause periodic oscillation in the angle  $\theta$  with an amplitude of a few tens of degrees; the satellite slow-down will also vary periodically.

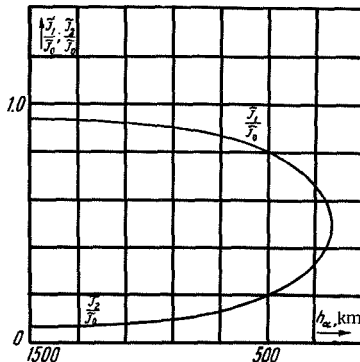


FIGURE 63. Integral quantities entering the expression for the mean aerodynamic drag coefficient.

Let us consider a particular case of tumble in a plane perpendicular to the orbital plane. Then  $\vartheta = 90^\circ$ ,  $\lambda = 0$  (the angular momentum vector lies in the orbital plane), and from (8.6.3) we have for  $\theta = 0$

$$\bar{C}_R = \bar{C}'_R = C_0 + C_2 \frac{1}{2} \frac{\bar{J}_2}{\bar{J}_0}, \quad (8.6.4)$$

and for  $\theta = \pi/2$

$$\bar{C}_R = \bar{C}''_R = C_0 + C_2 \frac{1}{2} \frac{\bar{J}_1}{\bar{J}_0}. \quad (8.6.4')$$

For an oblong satellite,  $C_0 > 0$ ,  $C_2 < 0$ . Now, since  $J_1 > J_2$ , we have  $\bar{C}'_R > \bar{C}''_R$ . Condition  $\theta = 0$  indicates that the precession plane is perpendicular to the oncoming stream at the perigee point, while  $\theta = \pi/2$  means that the precession plane meets the oncoming stream at the perigee "edge on". It is of course obvious that the "head-on" drag is on the average greater than the "edge-on" resistance.

Let us now consider more general values of the parameters. Figure 64 plots the dependence  $\bar{C}_R(\theta, \lambda)$  for a highly oblong satellite ( $C_0 = 18$ ;  $C_2 = -15.2$ ). We take  $\vartheta = 85^\circ$ ,  $h_r = 225$  km,  $h_a = 900$  km. It is seen that the amplitude of variation of  $\bar{C}_R$  in  $\lambda$  is small ( $|\Delta \bar{C}_R| < 1$ ), whereas the amplitude of  $\theta$ -variation is large. In § 2 of this chapter we considered an example (Figure 56) where the combined effect of gravitational and aerodynamic torques resulted in a change of  $60^\circ$  (from  $90^\circ$  to  $30^\circ$ ) in  $\theta$  during 25 circuits ( $\theta$  subsequently increased, approaching the original value by the time of the 48th circuit). We see from Figure 64 that this change in  $\theta$  will alter  $\bar{C}_R$  from  $\bar{C}_R = 10.8$

to  $\bar{C}_R = 15.6$ , i.e., the drag coefficient will increase nearly by 50%. The motion about the center of mass may thus considerably influence, in certain cases, the orbital motion of the satellite's mass center, causing periodic variation in slow-down.

Note that for  $e=0$   $\tilde{J}_1=\tilde{J}_2=\frac{1}{2}$ ,  $\tilde{J}_0=1$ , and as it follows from (8.6.3),  $\bar{C}_R$  depends on  $\cos^2 \rho = \sin^2 \theta \sin^2 \lambda$  only. Aerodynamic torques cause no secular perturbations, while secular gravitational perturbations conserve the angle  $\rho$ , so that  $\bar{C}_R$  remains constant as long as the angle  $\rho$  has not been changed by other perturbations. This angle can be altered, e.g., by magnetic perturbations, whose contribution is considered in the next chapter.

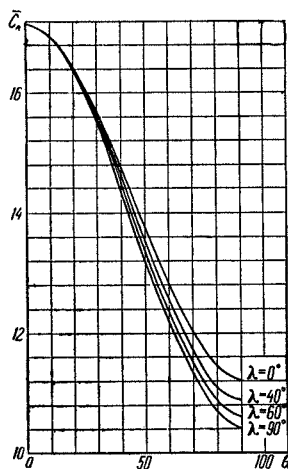


FIGURE 64. Mean aerodynamic drag coefficient.

To sum up, *the satellite slow-down is subject to long-period variations produced by the evolution of the satellite spin*. This fact must be taken into consideration in orbit analysis, in determination of atmospheric density from satellite slow-down [52], and in other related problems. (On this subject see also Chapter 10, Figure 87.)

## Chapter 9

### THE INFLUENCE OF MAGNETIC FIELDS AND OF SOLAR RADIATION TORQUES ON SATELLITE SPIN AND ATTITUDE

#### § 1. THE INTERACTION OF THE SATELLITE'S MAGNETIC FIELD WITH THE GEOMAGNETIC FIELD

Let us consider how the satellite spin is affected by the intrinsic magnetic field with a constant magnetic moment  $\mathbf{I}$  pointing along the satellite's axis of symmetry, as well as the contribution from the magnetization of the satellite shell. The torques on the satellite are defined by equations (1.4.1)–(1.4.4) in Chapter 1. We may write the force function  $U$  responsible for these torques:

$$U = -I_0 \left\{ H_{\bar{x}} \tilde{\alpha}_3 + H_{\bar{y}} \tilde{\beta}_3 + H_{\bar{z}} \tilde{\gamma}_3 + \right. \\ \left. + \frac{1}{2} k_H (H_{\bar{x}} \tilde{\alpha}_3 + H_{\bar{y}} \tilde{\beta}_3 + H_{\bar{z}} \tilde{\gamma}_3)^2 \right\}, \quad (9.1.1)$$

$$k_H = \frac{\mu_0 - 1}{4\pi} \frac{v}{I_0},$$

where  $\tilde{\alpha}_3, \tilde{\beta}_3, \tilde{\gamma}_3$  are the direction cosines of the satellite's axis of symmetry relative to the axes  $\bar{X}, \bar{Y}, \bar{Z}$  (see Chapter 1, § 1: the axis  $\bar{Y}$  points, by assumption, along the axis of the geomagnetic dipole; the axis  $\bar{Z}$  is directed in this chapter to the orbit's node, so that  $\Omega \equiv 0$ ); the field components  $H_{\bar{x}}, H_{\bar{y}}, H_{\bar{z}}$  are defined by (1.4.7).

The motion can of course be investigated with the aid of the theory presented in § 4 of Chapter 5. We introduce the function  $U_v$  (5.4.11) and perform double averaging, as in (5.4.13); we then easily write the equations of secular motion (5.4.13) of the angular momentum vector and the corresponding locus equation (5.4.14). We have

$$U_v = -\frac{I_0 P^2}{\sqrt{\mu D}} \frac{1}{(1 + e \cos v)^2} \left\{ H_{\bar{x}} \tilde{\alpha}_3 + H_{\bar{y}} \tilde{\beta}_3 + H_{\bar{z}} \tilde{\gamma}_3 + \right. \\ \left. + \frac{1}{2} k_H (H_{\bar{x}} \tilde{\alpha}_3 + H_{\bar{y}} \tilde{\beta}_3 + H_{\bar{z}} \tilde{\gamma}_3)^2 \right\}. \quad (9.1.2)$$

We now introduce the angular coordinates  $\rho_i, \sigma_i$  of the vector  $\mathbf{L}$  (Chapter 1, § 1). The direction cosines  $\tilde{\alpha}_3, \tilde{\beta}_3, \tilde{\gamma}_3$  have the form (1.1.6), with  $\rho_i$  and  $\sigma_i$  written for  $\rho$  and  $\sigma$  in the right-hand sides. Averaging (9.1.2) over  $\psi$  only and omitting the term  $\frac{1}{2} \sin^2 \theta$  in the averaged expressions for  $\tilde{\alpha}_3^2, \tilde{\beta}_3^2, \tilde{\gamma}_3^2$  (this term is irrelevant in the analysis of motion of the angular momentum

vector), we find the  $\psi$ -averaged  $U_v$  in the form

$$\begin{aligned} \bar{U}_v = & -\frac{I_0 P^2}{V \mu E} \frac{1}{(1+e \cos v)^2} \left\{ \cos \vartheta (H_{\bar{x}} a_3^0 + H_{\bar{y}} b_3^0 + H_{\bar{z}} c_3^0) + \right. \\ & \left. + \frac{1}{2} k_H \left(1 - \frac{3}{2} \sin^2 \vartheta\right) (H_{\bar{x}} a_3^0 + H_{\bar{y}} b_3^0 + H_{\bar{z}} c_3^0)^2 \right\}. \end{aligned} \quad (9.1.3)$$

Here  $a_3^0, b_3^0, c_3^0$  are the direction cosines of the angular momentum vector relative to the axes  $\bar{X}\bar{Y}\bar{Z}$ , defined by (1.1.10). Applying (1.1.10) and substituting (9.1.3) in (5.4.12), we obtain the equation of motion of the vector  $L$  to second approximation (i.e.,  $\psi$ -averaged, with  $\rho_1, \sigma_1$  substituted for  $\rho, \sigma$ ).

From (9.1.3) it follows, in particular, that if the satellite shell is nonmagnetic ( $k_H=0$ ), the vector  $L$  will nevertheless be perturbed by the intrinsic magnetic field with the moment  $I_0$ . The intrinsic magnetic moment  $I_0$  causes no perturbations only if  $\vartheta=\pi/2$ , i.e., when the satellite spins about a lateral axis. Note that

$$I_0 \cos \vartheta = I_L \quad (9.1.4)$$

is the projection of  $I$  on  $L$ , and it is this component of  $I$  which causes the perturbations. If, say,  $I$  does not point along the satellite's axis of symmetry,  $I_L \neq 0$  even when  $\vartheta=\pi/2$ , and perturbations do not vanish. The perturbations due to shell magnetization (when  $k_H \neq 0$ ) do not vanish for  $\vartheta=\pi/2$ , either.

Let us now try to bring out the perturbations in  $\rho_1, \sigma_1$ . To this end, (9.1.3) is again averaged, this time over the true anomaly  $v$ . We put

$$\left. \begin{aligned} J_s &= \frac{1}{2\pi} \int_0^{2\pi} \frac{H_s dv}{\frac{\mu_E}{P^2} (1+e \cos v)^2}, \\ J_{sh} &= \frac{1}{2\pi} \int_0^{2\pi} \frac{H_s H_k dv}{\frac{\mu_E^2}{P^6} (1+e \cos v)^2}, \\ s &= \bar{X}, \bar{Y}, \bar{Z}, \quad k = \bar{X}, \bar{Y}, \bar{Z}. \end{aligned} \right\} \quad (9.1.5)$$

Then

$$\left. \begin{aligned} J_{\bar{X}} &= -\frac{3}{2} \sin i \cos i, \quad J_{\bar{Y}} = \left(1 - \frac{3}{2} \sin^2 i\right), \\ J_{\bar{Z}} &= 0, \quad J_{\bar{X}\bar{X}} = 9 \sin^2 i \cos^2 i f_1(e, \omega_\pi), \\ J_{\bar{Y}\bar{Y}} &= \left(1 + 3e^2 + \frac{3}{8} e^4\right) - 6 \sin^2 i f_2(e, \omega_\pi) + \\ &\quad + 9 \sin^4 i f_1(e, \omega_\pi), \\ J_{\bar{Z}\bar{Z}} &= 9 \sin^2 i [f_2 - f_1], \\ J_{\bar{X}\bar{Y}} &= -3 \sin i \cos i [f_2 - 3 \sin^2 i f_1], \\ J_{\bar{Z}\bar{X}} &= 0, \quad J_{\bar{Z}\bar{Y}} = 0, \\ f_1(e, \omega_\pi) &= \frac{3}{8} + 6e^2 \left[ \frac{3}{16} \cos^4 \omega_\pi + \right. \\ &\quad \left. + \frac{18}{16} \cos^2 \omega_\pi \sin^2 \omega_\pi + \frac{5}{16} \sin^4 \omega_\pi \right] + \\ &\quad + e^4 \left[ \frac{9}{128} \cos^4 \omega_\pi + \frac{90}{128} \cos^2 \omega_\pi \sin^2 \omega_\pi + \frac{35}{128} \sin^4 \omega_\pi \right], \\ f_2(e, \omega_\pi) &= \frac{1}{2} + \frac{3}{4} e^2 [\cos^2 \omega_\pi + 3 \sin^2 \omega_\pi] + \\ &\quad + \frac{e^4}{16} [3 \cos^2 \omega_\pi + 5 \sin^2 \omega_\pi] \end{aligned} \right\} \quad (9.1.6)$$

The eccentricity enters these expressions in powers higher than the first, so that for low-eccentricity orbits the motion, with fairly high precision, is independent of  $e$ , and of course of  $\omega_\pi$ . In this case, ignoring the terms with  $e^2$  and  $e^4$ , we have

$$\left. \begin{aligned} J_{\bar{X}\bar{X}} &= \frac{27}{8} \sin^2 i \cos^2 i, \quad J_{\bar{Y}\bar{Y}} = 1 - 3 \sin^2 i + \frac{27}{8} \sin^4 i, \\ J_{\bar{Z}\bar{Z}} &= \frac{9}{8} \sin^2 i, \\ J_{\bar{X}\bar{Y}} &= -3 \sin i \cos i \left[ \frac{1}{2} - \frac{9}{8} \sin^2 i \right]. \end{aligned} \right\} \quad (9.1.7)$$

The doubly averaged  $U_v$  is now written in the form

$$\begin{aligned} \bar{U}_v = -\frac{I_0 \mu_E}{P^{3/2} \sqrt{\mu}} &\left\{ \cos \vartheta (J_{\bar{X}} \alpha_3^0 + J_{\bar{Y}} \beta_3^0) + \right. \\ &+ \frac{1}{2} k_H \left( 1 - \frac{3}{2} \sin^2 \vartheta \right) \frac{\mu_E}{P^3} (J_{\bar{X}\bar{X}} \alpha_3^{0^2} + J_{\bar{Y}\bar{Y}} \beta_3^{0^2} + \\ &\left. + J_{\bar{Z}\bar{Z}} \gamma_3^{0^2} + 2 J_{\bar{X}\bar{Y}} \alpha_3^0 \beta_3^0) \right\}. \end{aligned} \quad (9.1.8)$$

According to the general theory of Chapter 5, § 4, we write for the equation of the angular momentum locus (note that  $\gamma_3^{0^2} = 1 - \alpha_3^{0^2} - \beta_3^{0^2}$ )

$$\begin{aligned} \bar{U}_v = -\frac{I_0 \mu_E}{P^{3/2} \sqrt{\mu}} &\left\{ \cos \vartheta (J_{\bar{X}} \alpha_3^0 + J_{\bar{Y}} \beta_3^0) + \right. \\ &+ \frac{1}{2} k_H \left( 1 - \frac{3}{2} \sin^2 \vartheta \right) \frac{\mu_E}{P^3} [(J_{\bar{X}\bar{X}} - J_{\bar{Z}\bar{Z}}) \alpha_3^{0^2} + \\ &\left. + (J_{\bar{Y}\bar{Y}} - J_{\bar{Z}\bar{Z}}) \beta_3^{0^2} + 2 J_{\bar{X}\bar{Y}} \alpha_3^0 \beta_3^0] \right\} = \text{const.} \end{aligned} \quad (9.1.9)$$

The motion along this locus is then described by equations (5.4.13), in conjunction with (9.1.8); we thus have

$$\left. \begin{aligned} \frac{d\sigma_1}{dv} &= -\frac{I_0 \mu_E}{P^{3/2} \sqrt{\mu} L_0} \left\{ \cos \vartheta (J_{\bar{X}} \operatorname{ctg} \rho_1 \sin \sigma_1 - J_{\bar{Y}}) + \right. \\ &+ k_H \left( 1 - \frac{3}{2} \sin^2 \vartheta \right) \frac{\mu_E}{P^3} \left[ (J_{\bar{X}\bar{X}} - J_{\bar{Z}\bar{Z}}) \cos \rho_1 \sin^2 \sigma_1 - \right. \\ &\left. - (J_{\bar{Y}\bar{Y}} - J_{\bar{Z}\bar{Z}}) \cos \rho_1 + J_{\bar{X}\bar{Y}} \sin \sigma_1 \frac{\cos 2\rho_1}{\sin \rho_1} \right], \\ \frac{d\rho_1}{dv} &= \frac{I_0 \mu_E}{P^{3/2} \sqrt{\mu} L_0} \left\{ \cos \vartheta J_{\bar{X}} \cos \sigma_1 + \right. \\ &+ k_H \left( 1 - \frac{3}{2} \sin^2 \vartheta \right) \frac{\mu_E}{P^3} [(J_{\bar{X}\bar{X}} - J_{\bar{Z}\bar{Z}}) \times \\ &\times \sin \rho_1 \sin \sigma_1 \cos \sigma_1 + J_{\bar{X}\bar{Y}} \cos \rho_1 \cos \sigma_1] \left. \right\}. \end{aligned} \right\} \quad (9.1.10)$$

Let us consider some particular cases.

1.  $i = 0$  (equatorial orbit). Then  $J_{\bar{Y}} = 1$ ,  $J_{\bar{Y}\bar{Y}} \approx 1$ ,  $J_{\bar{X}} = J_{\bar{X}\bar{X}} = J_{\bar{Z}\bar{Z}} = J_{\bar{X}\bar{Y}} = 0$ . The vector  $\mathbf{L}$  precesses around the normal to the orbital plane (which points along the Earth's axis), at a constant angular distance  $\rho_1 = \rho_1^0$  and with a constant angular velocity

$$\frac{d\sigma_1}{dv} = \frac{I_0 \mu_E}{P^{3/2} \sqrt{\mu} L_0} \left\{ \cos \vartheta + k_H \left( 1 - \frac{3}{2} \sin^2 \vartheta \right) \frac{\mu_E}{P^3} \cos \rho_1^0 \right\}. \quad (9.1.11)$$

**Example.** Let  $\dot{\theta} = 0$  and  $k_H = 0$ ; we set  $P = 7000 \text{ km}$ ;  $\sqrt{\mu P} = V$ , where  $V$  is the velocity of the satellite's mass center (a circular orbit is assumed); let  $V \approx 8 \text{ km/sec}$ ,  $L_0 = Cr_0$ ,  $C = 500 \text{ kg} \cdot \text{m}^2$ ,  $r_0 = 0.1 \text{ rad/sec}$ ; also  $\mu_E = 8 \cdot 10^{25} \text{ G} \cdot \text{cm}^3$ , we take  $I_0 = 1200 \text{ G} \cdot \text{cm}^3$ . Then, according to (9.1.11), the secular regression of the vector  $\mathbf{L}$  during one orbital revolution of the satellite ( $\Delta\vartheta = 360^\circ$ ) is  $\Delta\sigma_i = 1^\circ.8$ .

2. The satellite shell is nonmagnetic,  $k_H = 0$ . The motion is induced by the constant intrinsic moment  $I_0$  only. Then it can be easily shown that *the angular momentum vector  $\mathbf{L}$  precesses at a constant angular distance  $x = x_0$  from a pole whose coordinates  $\sigma_i^*$ ,  $\rho_i^*$  are defined by*

$$\operatorname{ctg} \rho_i^* = \frac{J_{\bar{Y}}}{J_{\bar{X}}} = -\frac{1 - \frac{3}{2} \sin^2 i}{\frac{3}{2} \sin i \cos i}, \quad \sigma_i^* = \pm \frac{\pi}{2} \quad (9.1.12)$$

(i.e., the pole is in the plane  $\bar{XY}$  perpendicular to the line of nodes  $Z$  and through the Earth's axis  $\bar{Y}$ ). *The precessing velocity of the vector  $\mathbf{L}$  is constant:*

$$\frac{d\lambda_{\bar{X}}}{d\vartheta} = \frac{I_0 \mu_E}{2P^3 h \sqrt{\mu} L_0} \cos \dot{\theta} \sqrt{1 + 3 \cos^2 i}. \quad (9.1.13)$$

3.  $I_0 = 0$ , i.e., the initial magnetic field of the satellite is negligible. The only relevant factor is the magnetization of the satellite shell ( $k_H I_0 \neq 0$ ). Let  $\sigma_i^0 = \cos \tilde{\Phi}$ ,  $\rho_i^0 = \cos \sigma_i$ ;  $\tilde{\Phi}$  is thus the angle between the vector  $\mathbf{L}$  and the axis  $X$ . It follows from expression (9.1.9) for  $\bar{U}_v$  that the angular momentum loci are symmetric about the plane  $\bar{Y}\bar{X}$  (which is perpendicular to the line of nodes). Solving equation (9.1.9), which is a quadratic in  $\cos \tilde{\Phi}$ , we have

$$\cos \tilde{\Phi} = -\lambda_0 \cos \rho_i \pm \sqrt{C_0 + \zeta_0 \cos^2 \rho_i}. \quad (9.1.14)$$

Here  $C_0$  is an integration constant, and

$$\lambda_0 = \frac{J_{\bar{X}\bar{Y}}}{J_{\bar{X}\bar{X}} - J_{\bar{Z}\bar{Z}}}, \quad \zeta_0 = \frac{J_{\bar{X}\bar{Y}}^2}{(J_{\bar{X}\bar{X}} - J_{\bar{Z}\bar{Z}})^2} - \frac{J_{\bar{Y}\bar{Y}} - J_{\bar{Z}\bar{Z}}}{J_{\bar{X}\bar{X}} - J_{\bar{Z}\bar{Z}}}. \quad (9.1.15)$$

Depending on the orbital parameters (the angle  $i$ ), we may have  $\lambda_0 \leq 0$  and  $\zeta_0 \geq 0$ . Seeing that  $\cos \tilde{\Phi} = \sin \rho_i \sin \sigma_i$ , i.e.,  $-\sin \rho_i < \cos \tilde{\Phi} < \sin \rho_i$ , we can apply (9.1.14) to plot in the ordinary way the trajectories traced by the vector  $\mathbf{L}$  on the surface of a unit sphere. The corresponding loci are shown in Figure 65 for  $\lambda_0 < 0$ ; for  $\lambda_0 > 0$  the pattern is entirely symmetric, having been rotated around the axis  $\bar{Y}$ . The loci are arranged around two pairs of poles on the symmetry meridian (i.e., the  $\bar{Y}\bar{X}$  meridian), the traces of the axis  $Z$  ( $+Z$  and  $-Z$ ) constituting another pair of poles; one of these pairs is unstable. For  $\zeta_0 < 0$  the unstable poles (saddle points) are the traces of the  $\bar{Z}$  axis (i.e.,  $\sigma_i = 0, \pi; \rho_i = \pi/2$ ); for  $\zeta_0 > 0$  one of the pairs on the symmetry meridian is unstable.

The location of the poles  $\sigma_i^*, \rho_i^*$  on the symmetry meridian is best determined from the equations of motion (9.1.10), setting the right-hand sides equal to zero (note that in case on hand  $I_0 = 0$ ,  $I_0 k_H \neq 0$ ). Then

$$\sigma_i^* = \pm \frac{\pi}{2}, \quad \operatorname{tg} 2\rho_i^* = \pm \frac{2J_{\bar{X}\bar{Y}}}{J_{\bar{X}\bar{X}} - J_{\bar{Y}\bar{Y}}}. \quad (9.1.16)$$

Hence it follows, in particular, that for a polar orbit ( $i = 90^\circ$ ,  $J_{\bar{X}\bar{Y}} = 0$ ) we have  $\rho_1^* = 0, \pi/2, \pi$ ; now, for  $i = 90^\circ$ ,  $\zeta_0 > 0$ , so that the angular momentum vector will precess either around the  $\bar{X}$  axis (normal to the orbital plane) or around the  $\bar{Y}$  axis (Earth's axis, which in this case lies in the orbital plane), depending on the initial conditions. The precession is of course irregular: the motion is in fact a combination of precession and nutation with variable velocities (see (9.1.10)). Applying (9.1.9), we can reduce the problem to quadratures.

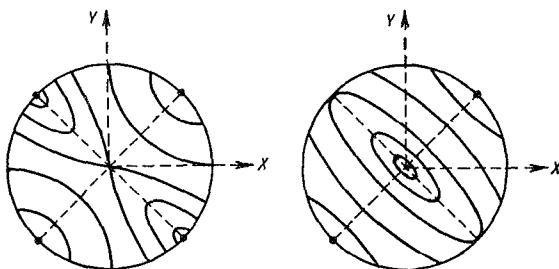


FIGURE 65. Secular paths described by the angular momentum vector due to the magnetization of the satellite shell (left  $\zeta_0 < 0$ , right  $\zeta_0 > 0$ ).

4. In the quite general case,  $I_0 \neq 0$ ,  $k_H \neq 0$ , the pattern depicted in Figure 65 is distorted: the poles shift (although the plane  $\bar{Y}\bar{X}$  remains the plane of symmetry), the regions of motion around the two poles in each pair are no longer equal (one of them becomes broader, while the other shrinks); the location of the poles now depends, not only on the orbital parameters, but also on the parameters of the satellite.

Note 1. We ignored the fact that the axis of the geomagnetic dipole does not coincide with the Earth's spin axis. This factor, however, can be introduced without any complications; the rotation of the dipole axis was considered, e.g., in /78/, where the equations were additionally averaged over the Earth's spin period.

Note 2. An analysis of the contribution from the transverse component  $I_{\perp}$  of the intrinsic magnetic moment  $I$  shows that under certain conditions the motion relative to the vector  $L$  may change qualitatively: continuous spin around the satellite's axis of symmetry may give way to oscillations about this axis /21/.

## § 2. THE INFLUENCE OF EDDY CURRENTS ON SATELLITE SPIN AND ATTITUDE

Let us consider the secular effects in the rotation of a satellite which are attributable to the induction of eddy currents as the satellite spins in the geomagnetic field. The torques on the satellite are assumed in the form (1.4.15) of Chapter 1. Averaging these expressions once (over  $\psi$ )

and putting  $k_s = k_{0s} = \text{const}$ , we have

$$\left. \begin{aligned} \bar{M}_{\bar{x}} &= -\Delta \{(H_{\bar{y}}^2 + H_{\bar{z}}^2) L_{\bar{x}} - H_{\bar{x}} H_{\bar{y}} L_{\bar{y}} - H_{\bar{x}} H_{\bar{z}} L_{\bar{z}}\}, \\ \bar{M}_{\bar{y}} &= -\Delta \{(H_{\bar{x}}^2 + H_{\bar{z}}^2) L_{\bar{y}} - H_{\bar{y}} H_{\bar{x}} L_{\bar{x}} - H_{\bar{y}} H_{\bar{z}} L_{\bar{z}}\}, \\ \bar{M}_{\bar{z}} &= -\Delta \{(H_{\bar{y}}^2 + H_{\bar{x}}^2) L_{\bar{z}} - H_{\bar{z}} H_{\bar{x}} L_{\bar{x}} - H_{\bar{z}} H_{\bar{y}} L_{\bar{y}}\}, \\ \Delta &= \frac{k_{0s}}{C} \cos^2 \vartheta + \frac{k_{0s}}{A} \sin^2 \vartheta. \end{aligned} \right\} \quad (9.2.1)$$

Double averaging (over  $\psi$  and over  $v$ ) gives (note that we have changed over from  $t$  to  $v$  as the independent variable)

$$\left. \begin{aligned} \bar{M}_{\bar{x}} &= -\frac{\mu_E^2 \Delta}{P^{1/2} \sqrt{\mu}} \{(J_{\bar{y}\bar{y}} + J_{\bar{z}\bar{z}}) L_{\bar{x}} - J_{\bar{x}\bar{y}} L_{\bar{y}}\}, \\ \bar{M}_{\bar{y}} &= -\frac{\mu_E^2 \Delta}{P^{1/2} \sqrt{\mu}} \{(J_{\bar{x}\bar{x}} + J_{\bar{z}\bar{z}}) L_{\bar{y}} - J_{\bar{x}\bar{y}} L_{\bar{x}}\}, \\ \bar{M}_{\bar{z}} &= -\frac{\mu_E^2 \Delta}{P^{1/2} \sqrt{\mu}} \{(J_{\bar{y}\bar{y}} + J_{\bar{x}\bar{x}}) L_{\bar{z}}\}. \end{aligned} \right\} \quad (9.2.2)$$

Here the coefficients  $J_{sk}$  are defined by (9.1.5)–(9.1.7).

The equations of secular motion of the angular momentum vector have the form

$$\frac{dL_{\bar{x}}}{dv} = \bar{M}_{\bar{x}}, \quad \frac{dL_{\bar{y}}}{dv} = \bar{M}_{\bar{y}}, \quad \frac{dL_{\bar{z}}}{dv} = \bar{M}_{\bar{z}}, \quad (9.2.3)$$

where  $\bar{M}_{\bar{x}}$ ,  $\bar{M}_{\bar{y}}$ ,  $\bar{M}_{\bar{z}}$  are defined by (9.2.2).

Since  $L_{\bar{x}}$ ,  $L_{\bar{y}}$ ,  $L_{\bar{z}}$  are not the only variables of (9.2.3) ( $\vartheta$  also enters these equations), an additional equation must be drawn up for  $\vartheta$ , like in § 4 of Chapter 7 in connection with aerodynamic dissipative torques.

For the secular evolution in  $\cos \vartheta$ , we have

$$\begin{aligned} \frac{d}{dv} \cos \vartheta &= \frac{1}{2} \left( \frac{k_{0s}}{A} - \frac{k_{0s}}{C} \right) \cos \vartheta \sin^2 \vartheta \left\{ J_{\bar{x}\bar{x}} \left( 1 + \frac{L_{\bar{x}}^2}{L^2} \right) + \right. \\ &\quad \left. + J_{\bar{y}\bar{y}} \left( 1 + \frac{L_{\bar{y}}^2}{L^2} \right) + J_{\bar{z}\bar{z}} \left( 1 + \frac{L_{\bar{z}}^2}{L^2} \right) + 2J_{\bar{x}\bar{y}} \frac{L_{\bar{y}} L_{\bar{x}}}{L^2} \right\} \frac{\mu_E^2}{P^{1/2} \sqrt{\mu}}. \end{aligned} \quad (9.2.4)$$

Equations (9.2.3) and (9.2.4) now constitute a closed set; if its solution is known, we can find  $r = \frac{L}{C} \cos \vartheta$  and  $\dot{\psi} \approx \frac{L}{A}$ ,  $L = \sqrt{L_{\bar{x}}^2 + L_{\bar{y}}^2 + L_{\bar{z}}^2}$ .

The principal features of motion can be investigated by approximate integration of (9.2.3), (9.2.4). We shall first consider some simple cases. Let the external field be plane-parallel, with a constant strength  $H = \text{const}$ . This holds true in the orbit of an equatorial satellite ( $i = 0$ ; the axis of the geomagnetic dipole points, by assumption, along the Earth's spin axis). Then, directly from the nonaveraged expressions (1.4.15) for the torque components, we have  $M_{\bar{y}} = 0$ , and hence  $L_{\bar{y}} = L_{\bar{y}}^0$ . In (9.2.2) all  $J_{sk}$ , with the exception of  $J_{\bar{y}\bar{y}}$ , will vanish. We may therefore average over  $\psi$  only. Taking (9.2.1), we put  $H_{\bar{y}} = H$ ,  $H_{\bar{x}} = H_{\bar{z}} = 0$ . The equations for  $L_{\bar{x}}$  and  $L_{\bar{y}}$  (with  $t$  as the independent variable) are written as

$$\dot{L}_{\bar{x}} = -\Delta H^2 L_{\bar{x}}, \quad \dot{L}_{\bar{y}} = -\Delta H^2 L_{\bar{y}}. \quad (9.2.5)$$

Hence it follows that  $\frac{L_X}{L_Y} = \operatorname{tg} \vartheta_1 = \text{const}$ , i.e., the vector  $L$  moves in a fixed plane  $\vartheta_1 = \text{const}$  through  $L$  and  $H$ .

Applying these integrals of motion, we can now find from (9.2.4) and (9.2.5) the following equations for  $L$ ,  $\vartheta$ ,  $\rho_1$ :

$$\left. \begin{aligned} \frac{dL}{dv} &= -a_E \left( \frac{k_0 s}{C} \cos^2 \vartheta + \frac{k_0 s}{A} \sin^2 \vartheta \right) L \sin^2 \rho_1, \\ \frac{d\rho_1}{dv} &= -a_E \left( \frac{k_0 s}{C} \cos^2 \vartheta + \frac{k_0 s}{A} \sin^2 \vartheta \right) \sin \rho_1 \cos \rho_1, \\ \frac{d \cos \vartheta}{dv} &= \frac{1}{2} a_E \left( \frac{k_0 s}{A} - \frac{k_0 s}{C} \right) \cos \vartheta \sin^2 \vartheta (1 + \cos^2 \rho_1), \\ a_E &= \frac{\mu_E^2}{P^{q_2} \sqrt{\mu}}. \end{aligned} \right\} \quad (9.2.6)$$

Here  $\rho_1$  is the angle between  $L$  and  $H$ . We see from (9.2.6) that  $L$  monotonically decreases; this, in conjunction with the integral  $L_Y = L_Y^0$ , implies that  $\rho_1 \rightarrow 0$ .

Equations (9.2.6) also have another integral [35]:

$$\left. \begin{aligned} (\sin \vartheta)^{\frac{2}{\varepsilon-1}} (\cos \vartheta)^{\frac{2\varepsilon}{1-\varepsilon}} &= D \operatorname{tg} \rho_1 \sin \rho_1, \\ \varepsilon &= \frac{C}{A}, \quad D = \text{const}. \end{aligned} \right\} \quad (9.2.7)$$

Since  $\rho_1 \rightarrow 0$ , it follows from this integral that  $\vartheta \rightarrow 0$  for  $\varepsilon > 1$  and  $\vartheta \rightarrow \pi/2$  for  $\varepsilon < 1$ .

To obtain explicit expressions for the time-variation of the functions, it suffices to perform approximate integration of the equations. Integrating (9.2.5) and putting  $\vartheta = \vartheta_0$  to first approximation, we find

$$\left. \begin{aligned} L_X &= L_X^0 \exp \left\{ -H^2 \left( \frac{k_0 s}{C} \cos^2 \vartheta_0 + \right. \right. \\ &\quad \left. \left. + \frac{k_0 s}{A} \sin^2 \vartheta_0 \right) \right\} (t - t_0), \\ L_Z &= L_Z^0 \exp \left\{ -H^2 \left( \frac{k_0 s}{C} \cos^2 \vartheta_0 + \right. \right. \\ &\quad \left. \left. + \frac{k_0 s}{A} \sin^2 \vartheta_0 \right) \right\} (t - t_0), \end{aligned} \right\} \quad (9.2.8)$$

whence, indeed,

$$L = \sqrt{L_X^2 + L_Y^2 + L_Z^2} \xrightarrow{t \rightarrow \infty} L_Y^0,$$

i.e., the vector  $L$  approaches the direction of the vector  $H$ , and its magnitude tends to a constant limit. The rate of precession thus also

approaches a constant limit,  $\dot{\psi} \approx \frac{L}{A} \rightarrow \frac{L_Y^0}{A}$ . Equation (9.2.4) is then integrated in the form

$$\operatorname{tg} \vartheta = \operatorname{tg} \vartheta_0 \exp H^2 \int \frac{1}{2} \left( \frac{L_Y^2}{L^2} + 1 \right) \left( \frac{k_0 s}{A} - \frac{k_0 s}{C} \right) dt. \quad (9.2.9)$$

Asymptotically, we have  $L_Y \approx L_Y^0$ , and then

$$\operatorname{tg} \vartheta \approx \operatorname{tg} \vartheta_0 \exp H^2 \left( \frac{k_0 s}{C} - \frac{k_0 s}{A} \right) (t - t_0), \quad (9.2.10)$$

i.e.,  $\theta \rightarrow 0$  if  $\frac{k_0 s}{C} - \frac{k_0 s}{A} < 0$  ( $A < C$ ) and, conversely,  $\theta \rightarrow \pi/2$  if  $\frac{k_0 s}{C} - \frac{k_0 s}{A} > 0$  ( $A > C$ ).

We have previously reached the same conclusion on the basis of (9.2.7) only. Thus,  $Cr \rightarrow L \rightarrow L_X^0 = \text{const}$  or  $Cr \rightarrow 0$ . In other words, a dynamically oblate satellite is stabilized so that it spins uniformly around its axis of symmetry, which tends to orient itself along the vector  $H$ ; a dynamically prolate satellite, on the other hand, tumbles and starts spinning with a

constant velocity  $\dot{\psi} = \frac{L_Y^0}{A}$  around a lateral axis, which also seeks the direction of the vector  $H$ .

The case of an equatorial orbit ( $H = \text{const}$ ), however, is exceptional. In an arbitrary orbit, on account of the rotation of the vector  $H$ , all the angular velocity components can be expected to decay, the vector  $L$  approaching zero (and not a finite constant limit), since the torque does not vanish relative to any preferred, fixed direction in space. This is obvious from the general expressions (9.2.2) for the torque components.

Let us consider, e.g., the case of a polar orbit, setting for simplicity  $e = 0$  (a circular orbit). The axis  $X$  of the fixed system  $X\bar{Y}\bar{Z}$  points along the normal to the orbital plane. From (9.1.7) we see that the coefficients  $J_{X\bar{Y}}$  and  $J_{\bar{X}\bar{X}}$  in (9.2.2) are both zero. Now, integrating (9.2.3) (we approximately take  $\theta = \theta_0$  and set  $\Delta_0 = \Delta(\theta_0)$ ), we find

$$\left. \begin{aligned} L_{\bar{X}} &= L_X^0 \exp \left\{ -\Delta_0 \frac{\mu_E^2}{P^3 h \sqrt{\mu}} (J_{\bar{Y}\bar{Y}} + J_{\bar{Z}\bar{Z}})(v - v_0) \right\}, \\ L_{\bar{Y}} &= L_Y^0 \exp \left\{ -\Delta_0 \frac{\mu_E^2}{P^3 h \sqrt{\mu}} J_{\bar{Z}\bar{Z}}(v - v_0) \right\}, \\ L_{\bar{Z}} &= L_Z^0 \exp \left\{ -\Delta_0 \frac{\mu_E^2}{P^3 h \sqrt{\mu}} J_{\bar{Y}\bar{Y}}(v - v_0) \right\}, \end{aligned} \right\} \quad (9.2.11)$$

i.e., all the components of  $L$  approach zero as  $v \rightarrow \infty$ . Hence,

$$L = \sqrt{L_{\bar{X}}^2 + L_{\bar{Y}}^2 + L_{\bar{Z}}^2} \xrightarrow[v \rightarrow \infty]{} 0, \quad \dot{\psi} \approx \frac{L}{A} \xrightarrow[v \rightarrow \infty]{} 0. \quad (9.2.12)$$

Let  $\bar{\lambda}$  be the angle between the axis  $\bar{Z}$  and the projection of the vector  $L$  on the orbital plane  $\bar{Z}\bar{Y}$ . Then, from (9.2.11),

$$\left. \begin{aligned} \operatorname{tg} \bar{\lambda} &= \frac{L_{\bar{Y}}}{L_{\bar{Z}}} = \operatorname{tg} \bar{\lambda}_0 \exp \Delta_0 \frac{\mu_E^2}{P^3 h \sqrt{\mu}} \frac{1}{4} (v - v_0), \\ \bar{\lambda} &\rightarrow \frac{\pi}{2} \text{ for } v \rightarrow \infty. \end{aligned} \right\} \quad (9.2.13)$$

If  $\bar{\theta}$  is the angle between the vector  $L$  and the axis  $\bar{X}$ , we have from (9.2.11) and (9.2.12)

$$\begin{aligned} \cos \bar{\theta} &= L_{\bar{X}}^0 \exp[-a_E(J_{\bar{Y}\bar{Y}} + J_{\bar{Z}\bar{Z}})(v - v_0)] \times \\ &\quad \times \left\{ L_{\bar{X}}^{0^2} \exp 2[-a_E(J_{\bar{X}\bar{X}} + J_{\bar{Z}\bar{Z}})(v - v_0)] + \right. \\ &\quad \left. + L_{\bar{Y}}^{0^2} \exp 2[-a_E J_{\bar{Z}\bar{Z}}(v - v_0)] + \right. \\ &\quad \left. + L_{\bar{Z}}^{0^2} \exp 2[-a_E J_{\bar{Y}\bar{Y}}(v - v_0)] \right\}^{-\frac{1}{2}}, \end{aligned} \quad (9.2.14)$$

where  $a_E = \frac{\mu_E^2}{P^h \sqrt{\mu}} \Delta_0$ . Hence, seeing that  $J_{\bar{Z}\bar{Z}} + J_{\bar{Y}\bar{Y}} > J_{\bar{Y}\bar{Y}}$  and  $J_{\bar{Z}\bar{Z}} + J_{\bar{Y}\bar{Y}} > J_{\bar{Z}\bar{Z}}$ , we find that  $\cos \bar{\theta} \rightarrow 0$  as  $v \rightarrow \infty$ ,  $\bar{\theta} \rightarrow \pi/2$  as  $v \rightarrow \infty$ . Relations (9.2.13) and (9.2.14) show that the angular momentum vector will orient itself parallel to the dipole axis (the axis  $\bar{Y}$ ).

Finally, integration of (9.2.4) yields

$$\operatorname{tg} \vartheta = \operatorname{tg} \vartheta_0 \exp \frac{1}{2} \left( \frac{k_{0s}}{C} - \frac{k_{0s}}{A} \right) \frac{\mu_E^2}{P^h \sqrt{\mu}} \int \left[ J_{\bar{Y}\bar{Y}} \left( 1 + \frac{L_Y^2}{L^2} \right) + J_{\bar{Z}\bar{Z}} \left( 1 + \frac{L_Z^2}{L^2} \right) \right] dv, \quad (9.2.15)$$

and it follows that the nutation angle  $\vartheta$  behaves as in the case of an equatorial orbit:  $\vartheta \rightarrow 0$  if  $\frac{k_{0s}}{C} - \frac{k_{0s}}{A} < 0$  and  $\vartheta \rightarrow \frac{\pi}{2}$  if  $\frac{k_{0s}}{C} - \frac{k_{0s}}{A} > 0$ .

Now, from (9.2.12) we see that the axial component  $r = \frac{L \cos \vartheta}{C}$  of the angular velocity approaches zero. The spin decays (in distinction from the case of an equatorial satellite). The secular rate of decay of the axial spin component  $r$  can be calculated by integrating the equation

$C \frac{dr}{dv} = \frac{dt}{dv} M_z$ . Here  $M_z$  is defined by (1.4.12), (1.4.14). After some manipulations, averaging over  $\psi$  and over  $v$  and integrating, we find

$$r = r_0 \exp \int \frac{\Re_E}{C} dv, \quad (9.2.16)$$

where

$$\begin{aligned} \Re_E = & - \frac{\mu_E^2}{P^h \sqrt{\mu}} k_{0s} \left\{ J_{\bar{X}\bar{X}} \left( 1 - \frac{L_X^2}{L^2} \right) + J_{\bar{Y}\bar{Y}} \left( 1 - \frac{L_Y^2}{L^2} \right) + \right. \\ & + J_{\bar{Z}\bar{Z}} \left( 1 - \frac{L_Z^2}{L^2} \right) - 2 J_{\bar{X}\bar{Y}} \frac{L_X L_Y}{L^2} \Big\} + \\ & + \frac{\mu_E^2}{2 P^h \sqrt{\mu}} k_{0s} \sin^2 \vartheta \left( 1 - \frac{C}{A} \right) \left\{ J_{\bar{X}\bar{X}} \left( 1 - 3 \frac{L_X^2}{L^2} \right) + \right. \\ & \left. + J_{\bar{Y}\bar{Y}} \left( 1 - 3 \frac{L_Y^2}{L^2} \right) + J_{\bar{Z}\bar{Z}} \left( 1 - 3 \frac{L_Z^2}{L^2} \right) - 6 J_{\bar{X}\bar{Y}} \frac{L_X L_Y}{L^2} \right\}. \end{aligned}$$

As an example, let us consider a spherical equatorial satellite. Then  $J_{\bar{Y}\bar{Y}} \neq 0$ , while the other  $J_h$  all vanish;  $A = C$ , and we therefore have from (9.2.4) that  $\vartheta = \vartheta_0$ ; furthermore,  $\dot{\vartheta}_0 = 0$ , since an unperturbed spherical satellite spins around a single axis which is fixed relative to the satellite and relative to the absolute space. Then

$$\Re_E = - \frac{\mu_E^2}{P^h \sqrt{\mu}} k_{0s} J_{\bar{Y}\bar{Y}} \left( 1 - \frac{L_Y^2}{L^2} \right) = - \frac{\mu_E^2}{P^h \sqrt{\mu}} k_{0s} J_{\bar{Y}\bar{Y}} \sin^2 \rho_1. \quad (9.2.17)$$

The coefficient  $k_{0s}$  for a spherical satellite is defined by (1.4.13). Formula (9.2.16) with  $\Re_E$  inserted from (9.2.17) is equivalent to the formula derived, say, in [38]; its distinctive feature, however, is that it allows for the change in the orientation of  $\rho_1$  of the spin axis relative to the magnetic field  $H$ . Indeed, from (9.2.6) it follows that in our case

$$\operatorname{tg} \rho_1 = \operatorname{tg} \rho_0^0 \exp \left\{ - \frac{a_E k_{0s}}{C} (v - v_0) \right\}$$

and that if  $\rho_i^0 = \frac{\pi}{2}$ , we invariably have  $\rho_i = \rho_i^0$ ; then, as we see from (9.2.16), (9.2.17),  $r$  decays at a constant rate. If now  $\rho_i^0 \neq \frac{\pi}{2}$ , we see that  $\rho_i \rightarrow 0$  and  $\frac{H_E}{C} \rightarrow 0$ , so that  $r$  decays at a slower rate than for  $\rho_i = \frac{\pi}{2}$ . Finally, for  $\rho_i^0 = 0$ , we have  $\rho_i = 0$ , and the spin does not decay.

**Example.** For a satellite with the parameters of Sputnik I we may take  $A = C = \frac{8}{15} a_{\text{sph}}^5 \rho_0 \pi$ , where  $\rho_0 = 836 \text{ kg/m}^3$  is the mean density of the satellite material,  $a_{\text{sph}} = 0.3 \text{ m}$  the radius of the satellite; in the coefficient (1.4.3) we put  $h_{\text{sph}} = 10^{-3} \text{ m}$ ;  $\mu = 2.8 \cdot 10^{-8} \text{ ohm} \cdot \text{m}$  (aluminum) ( $1 \text{ ohm} = 10^9 \text{ cm/sec}$ );  $H = 0.3 \text{ G}$ , and obviously  $\frac{J_{\bar{Y}\bar{Y}} \mu_E^2}{P^2 h_0 \sqrt{\mu}} dv = H^2 dt$ . Then, from (9.2.16), (9.2.17), setting  $\rho_i = \rho_i^0 = \frac{\pi}{2}$ , we see that the spin velocity  $r$  drops to  $1/e$  in 70 days [38]. According to the estimates of [38, 90], the equivalent spin-fading of the American Vanguard satellites takes 11 days.

Equations (9.2.3) (which are linear in  $L_{\bar{X}}, L_{\bar{Y}}, L_{\bar{Z}}$ ) with the torques (9.2.2) can be integrated in a quite general case (to the same approximation as the substitution  $\vartheta = \vartheta_0$  in (9.2.2)). An analysis of this solution indicates that the fundamental qualitative features are in general analogous to the case of motion in a polar orbit:

- 1) *the angular momentum vector asymptotically approaches a fixed direction in space* (e.g., the axis of the geomagnetic dipole in the particular cases of equatorial and polar orbits);
- 2) *the spin decays to zero* (with the exception of equatorial orbits);
- 3) *the spinning satellite stabilizes or tumbles ( $\dot{\vartheta} \rightarrow 0$  or  $\dot{\vartheta} \rightarrow \frac{\pi}{2}$ ), depending on the sign of  $\frac{k_{0S}}{C} - \frac{k_{0S}}{A}$ .*

As in the case of aerodynamic dissipative torques, the analysis no longer applies when the angular spin velocities become fairly small; the satellite then librates, while the formulas of this section describe rotational motion only.

### § 3. THE INFLUENCE OF SOLAR RADIATION TORQUES ON THE SPIN AND THE ATTITUDE OF AN ARTIFICIAL SUN SATELLITE

Consider an artificial satellite traveling in an elliptical orbit around the Sun, so that all the external torques, with the exception of solar radiation pressure, can be ignored. The solar radiation torques are approximated by expression (1.5.6). The torque (1.5.6) is equivalent to the force function

$$U(\cos \varepsilon_s) = -\frac{R_0^2}{R^2} \int a_r(\cos \varepsilon_s) d(\cos \varepsilon_s),$$

and, according to (5.4.11), for an arbitrary elliptical orbit

$$U_v(\cos \varepsilon_s) = -\frac{R_0^2}{\mu P} \int a_r(\cos \varepsilon_s) d(\cos \varepsilon_s). \quad (9.3.1)$$

Let us consider two cases:  $a_t = a_{0t}$  and  $a_t = a_{it} \cos \epsilon$ .

1)  $a_t = a_{0t}$ . Then

$$U_v = -\frac{a_{0t} R_0^2}{\sqrt{\mu P}} \cos \epsilon_s,$$

$$\cos \epsilon_s = \gamma_3 \cos v + \alpha_3 \sin v,$$

where  $v$  is the true anomaly,  $\gamma_3, \alpha_3$  are defined by (1.1.6). The  $\psi$ -averaged function  $U_v$  is written as

$$\bar{U}_v = -\frac{a_{0t} R_0^2}{\sqrt{\mu P}} \cos \theta \sin \rho \cos (\sigma - v),$$

which is the form leading to equations (5.4.15). Therefore, according to (5.4.16), the trajectory of the vector  $L$  is defined by

$$\left. \begin{aligned} \Phi &= L_0 \cos \rho - \frac{a_{0t} R_0^2}{\sqrt{\mu P}} \cos \theta \cos \epsilon_L = \text{const}, \\ \cos \epsilon_L &= \sin \rho \cos \chi_v, \quad \chi_v = \sigma - v. \end{aligned} \right\} \quad (9.3.2)$$

Here  $\epsilon_L$  is the angle between the angular momentum vector  $L$  and the current radius-vector  $R$ ; the locus (9.3.2) is a closed curve in a system of axes rotating with the radius-vector  $R$ . Substituting (9.3.2) in (5.4.15), we obtain the rate of change of the coordinates in the rotating system; however, the motion along the trajectory (9.3.2) admits of a simpler interpretation. We put

$$n_0 = \frac{a_{0t} R_0^2}{L_0 \sqrt{\mu P}} \cos \theta, \quad \operatorname{tg} \rho^* = -n_0. \quad (9.3.3)$$

Then we see that the trajectories (9.3.2) correspond, on the surface of a unit sphere, to a family of concentric circles

$$\cos \chi = C \quad (9.3.4)$$

with the poles

$$(a) \chi_{v(1)} = 0, \rho_{(1)} = \rho^*; \quad (b) \chi_{v(2)} = \pi, \rho_{(2)} = \pi - \rho^*, \quad (9.3.5)$$

where  $\rho^*$  is defined by (9.3.3); in (9.3.4)  $\chi$  stands for the angular distance of the vector  $L$  from the pole (a) of (9.3.5). The angular momentum loci  $n_0 > 0$  are depicted in Figure 66.

Let  $\lambda_\chi$  stand for the angle of rotation of the vector  $L$  around the pole (9.3.5). The vector  $L$  is then seen to rotate uniformly in  $v$ , with a velocity

$$\frac{d\lambda_\chi}{dv} = -\sqrt{1 + n_0^2}. \quad (9.3.6)$$

From (9.3.3) and (9.3.6) we see that if the radiation torques are very small ( $n_0 \approx 0$ ), the direction to the pole is nearly perpendicular to the orbital plane, and the velocity  $\frac{d\lambda_\chi}{dv}$  of the angular momentum vector in the rotating

system of axes is close to  $-1$ , i.e., in the fixed system the vector  $\mathbf{L}$  is almost at rest. Conversely, for large  $n_0$ , the stabilizing influence of the sunlight pressure becomes pronounced and the poles (9.3.5) shift in the direction of the current radius-vector  $\mathbf{R}$  ( $\rho^* \rightarrow \pi/2$ ), while the velocity (9.3.6) of the vector  $\mathbf{L}$  in the rotating system increases.

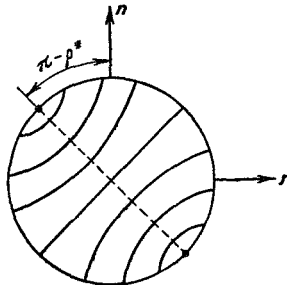


FIGURE 66. Angular momentum loci relative to the orbital system of axes due to solar radiation torques.

We now consider the second case.

2)  $a_r = a_{1r} \cos \varepsilon_s$ . Then

$$\begin{aligned} U_v &= -\frac{a_{1r} R_0^2}{2\sqrt{\mu P}} \cos^2 \varepsilon_s \\ \bar{U}_v &= -\frac{a_{1r} R_0^2}{2\sqrt{\mu P}} \left(1 - \frac{3}{2} \sin^2 \vartheta\right) \sin^2 \rho \cos^2(\sigma - v). \end{aligned} \quad (9.3.7)$$

The function  $\bar{U}_v$  again leads to equations (5.4.15), and according to (5.4.16) the trajectory of the vector  $\mathbf{L}$  in the rotating system of axes is written as

$$L_0 \cos \rho - \frac{a_{1r} R_0^2}{2\sqrt{\mu P}} \left(1 - \frac{3}{2} \sin^2 \vartheta\right) \cos^2 \varepsilon_L = \text{const.} \quad (9.3.8)$$

The equations of motion in the absolute coordinates  $\rho, \sigma$ , according to (9.3.7) and (5.4.12), have the form

$$\left. \begin{aligned} \frac{d\rho}{dv} &= -\frac{a_{1r} R_0^2}{L_0 \sqrt{\mu P}} \left(1 - \frac{3}{2} \sin^2 \vartheta\right) \sin \rho \cos(\sigma - v) \sin(\sigma - v), \\ \frac{d\sigma}{dv} &= -\frac{a_{1r} R_0^2}{L_0 \sqrt{\mu P}} \left(1 - \frac{3}{2} \sin^2 \vartheta\right) \cos \rho \cos^2(\sigma - v). \end{aligned} \right\} \quad (9.3.9)$$

Equations (9.3.9) are fully equivalent to the equations of motion (6.3.1) under gravity torques, provided we take  $e = 0$  in (6.3.1) and identify  $N_0$  with the constant factor in the right-hand sides of (9.3.9). All the results presented in § 4 of Chapter 6 for the case of a circular orbit therefore apply in our case of solar radiation torques on an artificial Sun satellite in an elliptical orbit, provided that

$$N_0 = n_1 \equiv -\frac{a_{1r} R_0^2}{L_0 \sqrt{\mu P}} \left(1 - \frac{3}{2} \sin^2 \vartheta\right).$$

The basic results of Chapter 6, § 4 refer to the case  $|n_1| < 1$ , when the loci have the shape depicted in Figure 42; the stabilizing influence of sunlight pressure is then negligible.

Let us consider the case  $|n_1| > 1$  in some detail. The loci have the form shown in Figure 41. The stabilizing effect of sunlight pressure is no longer negligible, and solar radiation torques produce new regions where the vector  $\mathbf{L}$  follows the radius-vector. The relevant times for artificial Sun satellites are comparatively small (roughly half the orbital period), and during these short periods fairly large values of the parameter  $n_1$  are admissible.

The poles of the solar radiation regions are defined by  $\kappa_v^* = 0, \pi; \cos \rho^* = 1/n_1$ . Let us consider the case  $n_1 > 0$  ( $n_1 < 0$  obtains without difficulty from the solution for  $n_1 > 0$ ). The angular momentum loci are then as shown in Figure 41. The first equation in (9.3.9) may be written as

$$\frac{d\rho}{dv} = n_1 \sin \rho \cos \kappa_v \sin \kappa_v, \quad (9.3.10)$$

and from (9.3.8)

$$\cos^2 \epsilon_L + \frac{2}{n_1} \cos \rho = C_0. \quad (9.3.11)$$

Hence, applying (9.3.2), we express  $\cos \kappa_v$  and  $\sin \kappa_v$  in terms of  $\rho$  and, on substitution in (9.3.10), we obtain

$$\left. \begin{aligned} \frac{dx}{dv} &= -\sqrt{2n_1} \sqrt{\left(x - \frac{n_1}{2} C_0\right) \left[x^2 - \frac{2}{n_1} x + C_0 - 1\right]}, \\ x &= \cos \rho. \end{aligned} \right\} \quad (9.3.12)$$

Seeing that in accordance with (9.3.11) and (9.3.2)  $C_0 = \cos^2 \kappa_{v_0} \sin^2 \rho_0 + \frac{2}{n_1} \cos \rho_0$ , and taking as the initial value of  $v$  a certain  $v_0$  for which  $\kappa_v = \kappa_{v_0} = 0$ , we obtain the following roots for the cubic in the radicand:

$$\begin{aligned} x_1 &= \cos \rho_0 + \frac{n_1}{2} \sin^2 \rho_0, \\ x_2 &= \frac{2}{n_1} - \cos \rho_0, \quad x_3 = \cos \rho_0. \end{aligned}$$

Three cases are possible:

$$\left. \begin{aligned} (a) \quad x_2 &> x_1 > x_3, \text{ when } -1 < \cos \rho_0 < \frac{2}{n_1} - 1, \\ (b) \quad x_1 &> x_2 > x_3, \text{ when } \frac{2}{n_1} - 1 < \cos \rho_0 < \frac{1}{n_1}, \\ (c) \quad x_1 &> x_3 > x_2, \text{ when } \frac{1}{n_1} < \cos \rho_0 < 1. \end{aligned} \right\} \quad (9.3.13)$$

In case (a), integrating equation (9.3.12) we find

$$\begin{aligned} \cos \rho &= \cos \rho_0 + \frac{n_1}{2} \sin^2 \rho_0 \operatorname{sn}^2(u, k), \\ u &= \sqrt{1 - n_1 \cos \rho_0} (v - v_0), \\ k &= \frac{n_1 \sin \rho_0}{2 \sqrt{1 - n_1 \cos \rho_0}}. \end{aligned}$$

This case corresponds to the motion of the angular momentum vector in the vicinity of the normal to the orbital plane (region a in Figure 41). The second coordinate  $\nu$ , is conveniently replaced, in accordance with (9.3.11), by the angular distance  $\varepsilon_L$  from the radius-vector. Then

$$\begin{aligned}\cos \varepsilon_L &= \cos \varepsilon_{L0} \operatorname{cn}(u, k), \\ \cos \varepsilon_{L0} &= \sin \rho_0.\end{aligned}$$

The period of motion of the vector  $L$  is

$$T = 4K(k^2)/\sqrt{1 - n_1 \cos \rho_0}.$$

In case (b), the angular momentum vector moves in the vicinity of the current radius-vector (region b in Figure 41), and integration of (9.3.12) yields

$$\begin{aligned}\cos \rho &= \cos \rho_0 + 2 \left( \frac{1}{n_1} - \cos \rho_0 \right) \operatorname{sn}^2(u, k), \\ u &= \frac{n_1}{2} \sin \rho_0 (\nu - \nu_0), \quad k = \frac{2\sqrt{1 - n_1 \cos \rho_0}}{n_1 \sin \rho_0}.\end{aligned}$$

The period of revolution of the vector  $L$  is

$$T = \frac{4K(k^2)}{n_1 \sin \rho_0},$$

and the angle  $\varepsilon_L$  is determined from

$$\cos \varepsilon_L = \cos \varepsilon_{L0} \operatorname{dn}(u, k), \quad \cos \varepsilon_{L0} = \pm \sin \rho_0.$$

The loci in case (c) are the same as in case (b), but they are reckoned from a different extremum point. These loci, however, are conveniently described by the independent equations

$$\begin{aligned}\cos \rho &= \cos \rho_0 - 2 \left( \cos \rho_0 - \frac{1}{n_1} \right) \operatorname{sn}^2(u, k), \\ u &= \sqrt{\frac{n_1^2}{4} \sin^2 \rho_0 + \cos \rho_0 (n_1 - 1)(\nu - \nu_0)}, \\ k &= \frac{2\sqrt{n_1 \cos \rho_0 - 1}}{\sqrt{n_1^2 \sin^2 \rho_0 + 4 \cos \rho_0 (n_1 - 1)}}, \\ T &= \frac{4K(k^2)}{\sqrt{n_1^2 \sin^2 \rho_0 + 4 \cos \rho_0 (n_1 - 1)}}, \\ \cos \varepsilon_L &= \cos \varepsilon_{L0} \operatorname{dn}(u, k), \quad \cos \varepsilon_{L0} = \pm \sin \rho_0.\end{aligned}$$

Substituting  $\cos \rho_0 \rightarrow \frac{2}{n_1} - \cos \rho_0$  and introducing a phase shift of  $\frac{T}{2}$ , we clearly reduce these expressions to the formulas of case (b).

Hitherto we have considered the case  $n_1 > 0$ . If now  $n_1 < 0$ , the required solution is obtained by substituting  $\rho = \pi - \rho$  for  $\rho$  and  $|n_1|$  for  $n_1$  in the foregoing formulas. To sum up, *solar radiation pressure has a certain attitude stabilizing influence (relative to the sunward direction) on a spinning satellite.*

**Example.** Let  $\frac{a_1}{2} = M_{\max} = 5 \cdot 10^{-7}$  kgm,  $\vartheta = 0$ ,  $L_0 = 1.5$  kgm·sec,  $\rho_0 = 90^\circ$ ; the initial data correspond to case (a) of (9.3.13). Then  $\rho^* = 73^\circ$ , i.e., the pole of precession of the vector  $L$  is displaced by  $17^\circ$  from the current radius-vector; the precession period  $T = 2.0$  rad =  $114^\circ$ , which is equivalent to  $\tilde{T} \approx 114$  days in the Earth's orbit.

In conclusion we should emphasize that the foregoing results are also applicable to a satellite with three unequal principal central moments of inertia, provided the torques can be written in the form (1.5.6), where  $k'$  is a unit vector along one of the principal central axes of inertia (the largest or the smallest). The nutation angle  $\vartheta$  should then be appropriately averaged before its introduction in the formulas. The results apply without any modification in the case of normal unperturbed motion ( $\vartheta = 0$ ), as is seen from a more rigorous analysis of the complete equations of motion for a triaxial satellite in the form (5.5.2), (5.5.5).

#### § 4. INTERACTION OF THE FUNDAMENTAL PERTURBATIONS

We shall refer to perturbations as being linear if a force function can be constructed which depends linearly on the direction cosines of the vector  $L$  relative to the coordinate axes. In the linear category we have the main part of aerodynamic perturbations (attributable to the sinusoidal dependence of the torque on the angle of attack), perturbations produced by the satellite's magnetic field with the intrinsic moment  $I$ , and also the effects due to orbital regression. Gravitational perturbations are nonlinear.

The above factors are often treated as the fundamental active perturbations. We shall therefore analyze the secular motion obtaining when these factors interact. The regression of the perigee, which is very slow for many of the Soviet satellites in comparison with the regression of the orbit's node, is henceforth ignored. In other words, we put  $k_\omega = 0$ ,  $k_\Omega \neq 0$ .

It follows from previous results that the secular motion of the angular momentum vector in this case is determined by the "force function"

$$\left. \begin{aligned} \Phi &= -k_I (J_X a_3^0 + J_Y b_3^0) + \\ &\quad + k_\Omega [k \sin \omega_n \sin i + n \cos i + m \cos \omega_n \sin i] - \\ &\quad - k_a m - k_g n^2, \\ n &= \cos \rho, \quad m = \sin \rho \sin \sigma, \quad k = \sin \rho \cos \sigma, \\ k_I &= \frac{I_0 \mu_E}{P^{n/2} \sqrt{\mu} L_0} \cos \vartheta, \quad k_a = \frac{\sqrt{\mu P} \rho_x}{2L_0} a_3^0 J_1 \cos \vartheta, \\ k_g &= \frac{3}{4} \frac{\mu}{P^{n/2}} \frac{A - C}{L_0} \left(1 - \frac{3}{2} \sin^2 \vartheta\right), \\ a_3^0 &= \bar{m} \bar{a}_1 + \bar{n} \bar{b}_1 + \bar{k} \bar{c}_1, \quad b_3^0 = \bar{m} \bar{a}_2 + \bar{n} \bar{b}_2 + \bar{k} \bar{c}_2. \end{aligned} \right\} \quad (9.4.1)$$

Here  $\bar{a}_i$ ,  $\bar{b}_i$ ,  $\bar{c}_i$  are defined by (1.1.1), where we take  $\Omega = 0$ ,  $u = \omega_n$ ;  $J_X$ ,  $J_Y$  are defined by (9.1.6). After some manipulations, we find

$$\left. \begin{aligned} \Phi &= m \left\{ \cos \omega_n \sin i \left( k_\Omega + \frac{1}{2} k_I \right) - k_a \right\} + n \cos i (k_\Omega - k_I) + \\ &\quad + k \sin \omega_n \sin i \left( k_\Omega + \frac{1}{2} k_I \right) - n^2 k_g \end{aligned} \right\} \quad (9.4.2)$$

Let

$$\left. \begin{aligned} \sin \rho^* \sin \sigma^* &= -\frac{\cos \omega_n \sin i \left( k_{\delta \zeta} + \frac{1}{2} k_I \right) - k_a}{k_\Sigma}, \\ \cos \rho^* &= -\frac{\cos i (k_{\delta \zeta} - k_I)}{k_\Sigma}, \\ \sin \rho^* \cos \sigma^* &= -\frac{\sin \omega_n \sin i \left( k_{\delta \zeta} + \frac{1}{2} k_I \right)}{k_\Sigma}, \end{aligned} \right\} \quad (9.4.3)$$

$$k_\Sigma^2 = \left\{ \cos \omega_n \sin i \left( k_{\delta \zeta} + \frac{1}{2} k_I \right) - k_a \right\}^2 + \cos^2 i (k_{\delta \zeta} - k_I)^2 + \sin^2 \omega_n \sin^2 i \left( k_{\delta \zeta} + \frac{1}{2} k_I \right)^2. \quad (9.4.4)$$

Then

$$\Phi = -k_\Sigma [\cos \rho \cos \rho^* + \sin \rho \sin \rho^* \cos (\sigma - \sigma^*)] - k_g \cos^2 \rho \equiv -k_\Sigma \cos \Delta - k_g \cos^2 \rho. \quad (9.4.5)$$

The expression in braces in (9.4.5) is the cosine of the angle  $\Delta$  between the angular momentum vector  $L$  and the direction defined according to (9.4.3) by the coordinates  $\rho^*, \sigma^*$ . Let  $\chi_\Delta$  be the angle through which the vector  $L$  rotates about the line  $\rho^*, \sigma^*$ . We shall only consider the linear part of (9.4.5), i.e., we put  $k_g = 0$ . Then clearly

$$\Delta = \Delta_0, \quad \frac{d\chi_\Delta}{dv} = k_\Sigma. \quad (9.4.6)$$

In other words, linear perturbations (here, the main parts of the aerodynamic and the magnetic perturbations, together with the regression of the node) cause secular precession of the angular momentum vector around the pole  $\rho^*, \sigma^*$  (9.4.3); the vector precesses uniformly in  $v$  with angular velocity  $k_\Sigma$  (9.4.4) at a constant angular distance  $\Delta_0$  from the pole. There is of course also an antipodal pole, with the coordinates  $\pi - \rho^*, \sigma^* + \pi$ .

When gravitational perturbations are introduced, the equations of motion take the form

$$\left. \begin{aligned} \frac{d\rho}{dv} &= -k_\Sigma \sin (\sigma - \sigma^*), \\ \frac{d\sigma}{dv} &= k_\Sigma [\cos \rho^* - \sin \rho^* \operatorname{ctg} \rho \cos (\sigma - \sigma^*)] + 2k_g \cos \rho \end{aligned} \right\} \quad (9.4.7)$$

and the path traced by the vector  $L$  is defined by the integral of these equations

$$\Phi = \Phi_0. \quad (9.4.8)$$

All the loci are symmetric about the meridian  $\sigma = \sigma^*$ . Their poles  $\sigma_p, \rho_p$  lie on this meridian ( $\sigma_p = \sigma^*, \sigma^* + \pi$ ), and they are defined by the solution of the equation

$$k_\Sigma [\cos \rho^* \mp \sin \rho^* \operatorname{ctg} \rho_p] + 2k_g \cos \rho_p = 0. \quad (9.4.9)$$

This equation is best solved for  $\cos \rho^*$ , and the function  $\cos \rho^*$  ( $\cos \rho_p$ ) is then inverted. We have

$$\left. \begin{aligned} \cos \rho^* &= \cos \rho_p \{ -2\tilde{\epsilon} \sin^2 \rho_p \pm \sqrt{1 - \tilde{\epsilon}^2 \sin^2 2\rho_p} \}, \\ \tilde{\epsilon} &= \frac{k_g}{k_x}. \end{aligned} \right\} \quad (9.4.10)$$

The graphs of  $\cos \rho^*$  ( $\cos \rho_p$ ) for various  $\tilde{\epsilon} > 0$  are shown in Figure 67.\* We see that for  $\tilde{\epsilon} < \frac{1}{2}$ , there are only two poles, as with pure linear perturbations;\*\* for  $\frac{1}{2} < \tilde{\epsilon} < 1$  there may be either two or four poles depending on  $\rho^*$ , and for  $\tilde{\epsilon} > 1$  there are always four poles. One of the four poles is unstable, while the other three are stable. On account of the asymmetric dislocation of the poles on the surface of the unit sphere, the paths are

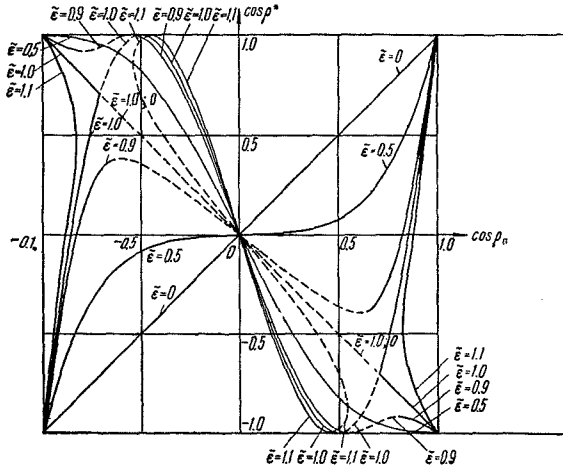


FIGURE 67. The location and the stability of the poles  $\rho_p$  of the secular paths of the angular momentum vector due to aerodynamic, magnetic, and gravitational perturbations and regression of the orbit's node:  $\rho^* \sigma^*$  pole coordinates without gravitational perturbations; bold lines—stable pole  $\rho_p \sigma_p = \sigma^*$ ; dashed lines—unstable pole  $\rho_p \sigma_p = \sigma^*$ ; fine lines—stable pole  $\rho_p, \sigma_p = \sigma^* \pi$ .

curiously curved. An analysis of the pole positions shows that the linear perturbations are relatively stable with respect to the nonlinear perturbations. Indeed, already when the linear perturbations are more than twice as large as the nonlinear ones ( $k_x > 2k_g$ ), the loci are distinctly "linear" (it is only the shape of the loci that is somewhat distorted, see Figure 68 a). Conversely, for any arbitrarily large  $k_g$ , there always exists a certain region which is exclusively influenced by the linear factors, where the loci are distinctly "nongravitational" (Figure 68 b). We have already encountered this state of things in the analysis of the combined influence of gravitational and aerodynamic perturbations (Chapter 8).

\* For  $\tilde{\epsilon}^* < 0$  the plot in Figure 67 goes into its mirror image relative to the axis  $\cos \rho_p$ .

\*\* In particular, for  $\tilde{\epsilon} = 0$ , the pole  $\rho_p$  "generates" itself ( $\cos \rho_p = \cos \rho^*$ ) and also its antipode:  $\cos \rho_p = -\cos \rho^*$ , i.e.,  $\rho_p = \pi - \rho^*$ ,  $\sigma_p = \sigma^* + \pi$ .

The angular momentum loci are plotted essentially by the same technique as in Chapter 8. According to (9.4.5), (9.4.8), we have

$$\cos \Delta = C_0 - \tilde{\varepsilon} \cos^2 \rho, \quad \cos(\rho + \rho^*) \leq \cos \Delta \leq \cos(\rho - \rho^*). \quad (9.4.11)$$

Applying (9.4.11), we can easily plot the family of loci  $\cos \Delta(C_0, \rho)$  on the plane  $(\cos \Delta, \rho)$  in the region enclosed by the cosine curves  $\cos(\rho + \rho^*)$  and  $\cos(\rho - \rho^*)$ .

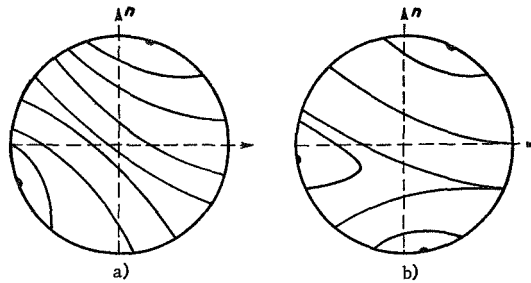


FIGURE 68. Secular paths of the angular momentum vector due to aerodynamic, magnetic, and gravitational perturbations and regression of the orbit's node.

subsequently mapping the pattern onto the surface of a unit sphere; it should be borne in mind that the boundary cosine curves are mapped into the symmetry meridians ( $\sigma = \sigma^* + \pi$  and  $\sigma = \sigma^*$ ), the extrema of these cosine curves corresponding to the linear poles  $\rho = \pi - \rho^*$ ,  $\rho = \rho^*$  and the points  $\cos \Delta = \pm \cos \rho^*$ ,  $\rho = 0, \pi$  to the gravitational poles. This mapping gives the patterns shown in Figure 68.

## *Chapter 10*

### **THE MOTION OF SOME ORBITED ARTIFICIAL EARTH SATELLITES AROUND THE CENTER OF MASS**

Information on the actual motion of an artificial space vehicle around its mass center is supplied by various probes and sensors in the payload, whose readings are telemetered to Earth bases. The instruments measure certain parameters which are indicatory of the satellite spin and attitude. These measurements can be made, say, with a magnetometer which senses the satellite attitude relative to the geomagnetic field; pressure gages and other instruments sensitive to the satellite's orientation relative to the oncoming air stream can also be used; sun trackers, horizon sensors, etc., are also suitable for this purpose. Satellite attitude is indirectly inferred from radio measurements (modulation of radio signals) and from optical data (satellite brightness variation, etc.).

In this chapter we discuss the actual spin and orientation of some orbited artificial satellites. The observed motions about the mass center are compared with the corresponding theory. Some methods used in obtaining experimental information on the motion of satellites around the center of mass are also described.

#### **§ 1. SPUTNIK III**

A self-orienting magnetometer /27/ measured the geomagnetic field strength from Sputnik III. The magnetometer comprises a rotating frame whose normal points at any time along the total magnetic field vector; this fixed orientation of the frame normal is maintained by special sensors and a tracker. The deflections of the frame relative to the satellite body are picked up by two sensors and the corresponding information is transmitted to the Earth. Given the time variation of the deflection angles, we can find the parameters of satellite motion about the mass center and its attitude in space.

Let us consider the technique for the determination of satellite spin and attitude and the results obtained for the corresponding parameters /9/.

1. **A method for the determination of spin and attitude parameters.**  
We shall show how the satellite spin and attitude can be recovered from the readings of magnetometer sensors.

During comparatively short times (e.g., during one circuit of revolution), the perturbations are negligibly small. To first approximation we may therefore assume that the motion of the satellite around its mass center is represented by the Euler—Poinsot case. In particular, for Sputnik III,

which had two equal principal central moments of inertia, the motion around the mass center in this case amounts to regular precession with a constant angular velocity  $\dot{\psi}$ , a constant nutation angle  $\theta$ , and a constant spin rate  $\dot{\varphi}$ . The system of fixed axes and the orientation of the angular momentum vector  $\mathbf{L}$  in this frame will be defined somewhat differently from the definition adopted in the previous chapters. Let  $XZY$  be the system of fixed axes: the axis  $Z$  points to the celestial pole, the axis  $X$  to the point of vernal equinox; let  $\rho_0$  be the angle between the vector  $\mathbf{L}$  and the axis  $Y$ ,  $\gamma_0$  the angle between the planes  $LY$  and  $XY$ . To find the satellite spin and attitude, we have to determine the orbital parameters  $\theta$ ,  $\dot{\varphi}$ ,  $\dot{\psi}$ ,  $\rho_0$ ,  $\gamma_0$ , for each circuit of revolution, and also to establish certain initial conditions for the satellite motion, e.g., the angles of spin and precession  $\varphi_0$  and  $\psi_0$  at some particular time. At least one set of these "initial values" is required for each circuit.

Figure 69 is a schematic diagram of the magnetometer. The rotation axis of the outer frame points along the satellite axis. The deflection angle  $\Delta$  of the outer frame about this axis

is picked up by a special sensor, whose readings will be denoted by  $q_1$ . The angle  $\Delta$  is reckoned from a certain fixed axis  $x'$  of the satellite, which is perpendicular to the satellite's axis of symmetry  $z'$ . For  $\Delta=0$ , the axis  $x'$  is at right angles to the outer frame.

The rotation axis of the inner frame is perpendicular to the outer frame axis. The normal to the inner frame always points along the magnetic field vector  $\mathbf{H}$ ; this fixed attitude is maintained by rotating the outer and the inner frames relative to the satellite body. The rotation angle of the inner frame is transmitted by a sensor, whose readings will be designated by  $q_2$ . A characteristic feature of the Sputnik III magnetometer is the dependence of  $q_2$  on  $q_1$  (while  $q_1$  is independent of  $q_2$ ): on account of the gear arrangement in the attitude control mechanism, one third of the readings of  $q_1$  is invariably added to the readings of  $q_2$ . The independent part of the readings of  $q_2$  is thus  $\Delta \sim q_2 - \frac{1}{3}q_1$ . Apart from a constant term representing the zero-point value of  $\Delta$ ,  $q_2 - \frac{1}{3}q_1$

is the angle between the satellite symmetry axis  $z'$  and the magnetic field vector  $\mathbf{H}$  (Figure 69). The angle  $\Delta$  is the angle between the plane  $z'H$  in which the angle  $\Lambda$  is reckoned and a fixed plane through the axis  $x'$  of the satellite. The angles  $\Lambda$  and  $\Delta$  thus completely define the satellite attitude relative to a magnetic line of force.

The orientation of the vector  $\mathbf{H}$  will be specified by the two coordinates  $\rho_H$  and  $\gamma_H$ , which are defined by analogy with  $\rho_0$  and  $\gamma_0$ . The satellite orbit is known, and the accuracy of the geomagnetic field data is sufficient for satellite attitude determinations, so that  $\rho_H$  and  $\gamma_H$  may be regarded as known functions of time (for more details, see [9]). The time dependences

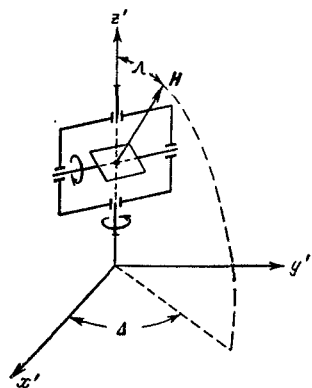


FIGURE 69. A schematic diagram of the magnetometer.

$\Lambda(t)$  and  $\Delta(t)$  are then determined by the dependence of the angles  $\Lambda$  and  $\Delta$  on spin and attitude parameters. The spin and attitude parameters can thus be found from the telemetered data.

For example, we have

$$\left. \begin{aligned} \cos \Lambda &= \cos \rho_H \cos \Lambda_y + \sin \rho_H \sin \Lambda_y \cos \alpha^\gamma, \\ \alpha^\gamma &= \gamma_H - \gamma_{0H} - \alpha^\gamma, \\ \cos \Lambda_y &= \cos \vartheta \cos \rho_0 + \sin \vartheta \sin \rho_0 \cos \bar{\psi}, \\ \bar{\psi} &= \bar{\psi}_0 + \dot{\psi}t, \\ \cos \alpha^\gamma &= \frac{\cos \vartheta - \cos \rho_0 \cos \Lambda_y}{\sin \rho_0 \sin \Lambda_y}, \\ \operatorname{ctg} \alpha^\gamma &= \frac{\sin \rho_0 \operatorname{ctg} \vartheta - \cos \rho_0 \cos \bar{\psi}}{\sin \bar{\psi}}, \\ 0 \leq \Lambda < 180^\circ, \quad 0 \leq \Lambda_y < 180^\circ, \\ \bar{\psi} &= \psi + 90^\circ, \end{aligned} \right\} \quad (10.1.1)$$

where  $\psi$  is the Eulerian angle of precession.

The set (10.1.1) gives the dependence

$$\Lambda = \Lambda(t, \rho_0, \gamma_0, \vartheta, \dot{\psi}, \bar{\psi}_0).$$

Spin parameters do not enter this formula, since  $\Lambda$  only describes the attitude of the satellite axis. On the other hand,  $\Delta$  is a function of spin. Here

$$\left. \begin{aligned} \Delta &= \varphi + \tilde{\nu}, \\ \tilde{\nu} &= \tilde{\nu}(\rho_0, \gamma_0, \rho_H, \gamma_H, \bar{\psi}_0 + \dot{\psi}t); \end{aligned} \right\} \quad (10.1.2)$$

$\tilde{\nu}$  is independent of  $\varphi$ , but it is a periodic function of  $\rho, \gamma, \psi + \dot{\psi}t$ . The angle  $\Delta$  is thus a linear function of the angle  $\varphi$  and of  $\varphi$  only; from  $\dot{\varphi} \sim \Delta$  we can thus find the spin rate  $\dot{\varphi}$  by isolating the linear component of these readings.

From (10.1.1) and (10.1.2) we see that the time dependences  $\Lambda(t)$  and  $\Delta(t)$  of the deflection angles obtained from magnetometer readings are described by fluctuating curves, where the oscillation period is equal in the first approximation to the period of precession  $T_\psi = \frac{2\pi}{\dot{\psi}}$  (provided the precession is fairly fast in comparison with the rotation of  $H$ ).

For Sputnik III, the corrections to the first-order  $T_\psi$  were small ( $1-2\%$ ), and they were determined by comparing the magnetometer readings with the readings of other instruments.

Having found  $\dot{\varphi}$  and  $\dot{\psi}$ , we can determine the angle of nutation  $\vartheta$  from the relation  $(\frac{A}{C} - 1)\dot{\psi} \cos \vartheta = \dot{\varphi}$ . The attitude parameters  $\rho_0$  and  $\gamma_0$  were calculated by the algorithm for the successive approximation of the parameters  $\rho_0, \gamma_0, \psi_0, \vartheta, \dot{\psi}$  which ensures the best fit between the theoretical and the experimental curves in the sense of the least-squares method /49/. Mathematically, the problem reduces to the solution of a set of algebraic linear inhomogeneous equations whose coefficients vary from approximation to approximation. Numerical values of the parameters obtained from various considerations can be applied as the first approximation for one circuit of revolution, or alternatively a whole range of parameters may be

tested. For each successive circuit, the first approximation is provided by the result obtained for the preceding circuit.

**2. Reduction of experimental results.** It follows from Subsection 1 that the parameters of precession can be determined in one of the two ways below: (i)  $\theta, \psi$  can be found by simultaneously selecting the constants which enter the expression for  $\Lambda(t)$  and the coordinates  $\rho_0, \gamma_0, \bar{\psi}_0$ ; (ii)  $\theta, \dot{\psi}$  are obtained directly from the readings of  $q_1$  and  $q_2$ , and the coordinates  $\rho_0, \gamma_0, \bar{\psi}_0$  are chosen at a later stage.

Both these techniques were used. The accuracy of the calculations was established by comparing the final values of the relevant parameters with the telemetered experimental curve. The fit between the theoretical and the experimental curves was quite satisfactory for all the treated circuits. Theoretical figures obtained by the two different techniques are also in satisfactory agreement with one another. The discrepancy in the angular coordinates as calculated by the two techniques is not greater than  $10-15^\circ$ . The only exception to this rule is the parameter  $\bar{\psi}_0$  (the initial attitude of the satellite axis). The values of this parameter obtained by the two methods differ by as much as  $30-40^\circ$  in some cases. This means that the calculated orientation of the instruments must be additionally corrected for  $\bar{\psi}_0$ . The variation in  $\bar{\psi}_0$  mainly displaces the extrema of the instrumental recordings; once these recordings are available, however, we can easily choose a particular  $\bar{\psi}_0$  for which the calculated attitude agrees with the readings of the corresponding instruments. It will be shown in Subsection 3 that this agreement can indeed be ensured by varying  $\bar{\psi}_0$  in a  $30^\circ$  range about the initial value.

Let us now consider the results of the reduction.

**Spin rate.** The dependence  $\dot{\phi}(N)$ , where  $N$  is the circuit number, is plotted in Figure 70.

We see that the spin rate decayed from  $0.375$  deg/sec during the third circuit to zero in the interval between the 17th and 42nd circuits. During the 42nd circuit,  $\dot{\phi} = -0.184$  deg/sec, i.e., the satellite now spins in the opposite direction about its symmetry axis. Then  $\dot{\phi}$  starts fluctuating about a mean value  $\dot{\phi}_m \approx -0.1$  deg/sec with an amplitude  $0 > \dot{\phi} > -0.2$  deg/sec.

This spin-rate variation is possibly attributable to the interaction of currents in the satellite payload with the Earth's magnetic field. Indeed, the magnetic field set up by the satellite currents is clearly asymmetric and time-variable, and its interaction with the geomagnetic field will vary, aiding or resisting the satellite spin according to its attitude relative to the Earth's field. Estimates show that for Sputnik III this effect could have been strong enough to produce the spin fading recorded in Figure 70

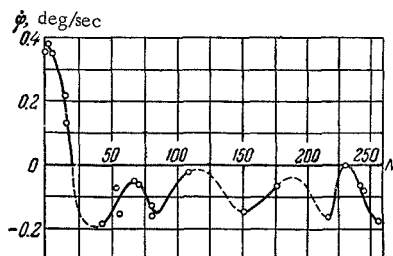


FIGURE 70. Spin rate of Sputnik III. The dashed line marks the extrapolated sections of the curve.

for the first orbital circuits. If the contribution from the payload currents is approximated by a certain fixed intrinsic magnetic field, the asymmetry of this field will make the satellite oscillate about its spin axis. We should also note that the satellite mass distribution, slightly deviating from the axisymmetric, may also cause (for  $\theta \sim \pi/2$ ) oscillations about the symmetry axis.

The interaction of eddy currents in the satellite shell with the Earth's field, as well as atmospheric friction, also have a certain spin-damping effect. Other factors (the change in the moments of inertia as the shutters were being opened and closed, micrometeorite impact, etc.) have but a negligible influence on the spin rate  $\dot{\varphi}$ .

**Precessing period.** Figure 71 plots the precessing period for each orbital circuit. These periods are derived directly from the magnetometer recordings. A correction of 2–5 sec should be introduced into these results to make them consistent with the readings of other instruments.

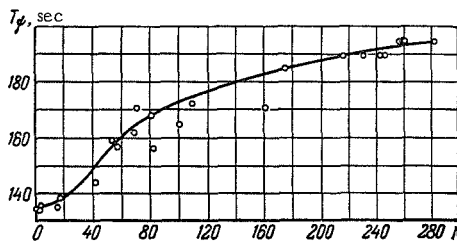


FIGURE 71. Precessing period of Sputnik III.

We see from Figure 71 that the period of precession increases from 135–136 sec during the first circuits to 195 sec during the 283rd circuit. The increase in the precessing period, i.e., decrease in the angular rate of precession  $\dot{\varphi}$ , is attributable to electromagnetic dissipative factors. The effect of these factors on  $\dot{\varphi}$  is smaller than on  $\dot{\psi}$ , since the initial rate of precession is several times as large as the initial spin rate. Note that the slight nonuniformity in the growth of the precessing period is due, not only to reduction errors, but apparently also to more or less significant fluctuations in the precessing rate, which are analogous to spin rate fluctuations.

Table 10 lists (in angular degrees per second) the rates of precession assumed as the constant parameter in method (i) for the determination of the attitude coordinates  $\rho_0, \gamma_0$ , and also the rates of precession obtained simultaneously with  $\rho_0, \gamma_0$  according to the five-parameter method (ii).

TABLE 10

N	1	3	5	15	17	42	54	56	68	70	81	82	109
(i) $\dot{\psi}$	2.65	2.52	2.57	2.56	2.51	2.50	2.30	2.30	2.14	2.18	2.14	—	2.14
(ii) $\dot{\psi}$	2.52	2.52	2.61	2.51	—	2.35	2.29	—	2.20	2.24	2.175	2.13	2.11

The maximum discrepancy between  $\psi$  (i) and  $\psi$  (ii) is very small ( $\sim 0.05 - 0.06$  deg/sec), which clearly shows that the precessing rate has been determined with satisfactory accuracy. This discrepancy corresponds to an error of 3–6 sec in the period of precession.

Nutation angle. For Sputnik III, the lateral-to-axial inertial ratio was  $\frac{A}{C} \approx 2.5$ . Given  $\frac{A}{C}$ ,  $\dot{\phi}$ ,  $\dot{\psi}$ , we can calculate the angle of nutation  $\theta$  from a formula in Subsection 1. The nutation angle was found to be close to  $90^\circ$ , departing from this value by no more than  $6^\circ$  during different circuits (Table 11). The satellite "tumbles".

TABLE 11

$N$	1	3	5	15	17	42	54	56	68	70	81	109
$ 90^\circ - \theta $	5°.5	5°.5	6°	3°	2°	3°	3°	3°	2°	3°	3°	2°

Absolute orientation of the angular momentum vector. The coordinates  $\rho_0$  and  $\gamma_0$  of the angular momentum vector  $L$  were determined by two techniques: by the three-parameter method (i) and by the five-parameter method (ii). Figure 72 plots the results obtained by the two methods.

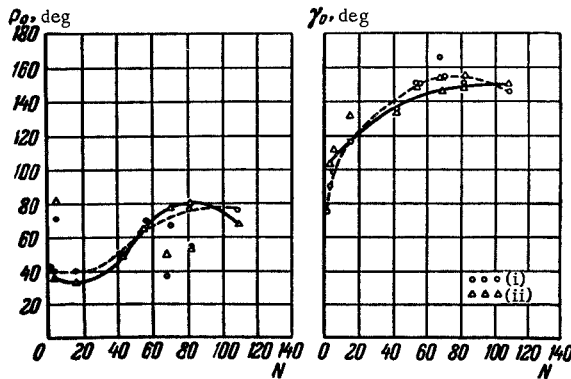


FIGURE 72. Absolute orientation of the angular momentum vector of Sputnik III.  
Dashed curve, method (i); solid curve, method (ii).

The two techniques are seen to be in satisfactory agreement. The largest discrepancy (in one case) is approximately  $15^\circ$ ; in other cases, the difference is close to  $5 - 10^\circ$ , and this figure can be assumed as the characteristic error in the attitude of the angular momentum vector. The variation in the coordinates from circuit to circuit is attributable to the slow motion of the angular momentum vector in space due to various perturbations. Figure 72 also gives the curves which describe, with an accuracy of  $5 - 10^\circ$  (ignoring the largely offset points of the 5th, 68th, and 82nd circuits), the corresponding dependences  $\rho_0(N)$  and  $\gamma_0(N)$ .

Orientation of the angular momentum vector relative to the orbit. The attitude of the vector  $L$  relative to the perigee system  $XYZ$  (see Chapter 1, § 1) is defined by the angle  $\theta$  between the vector  $L$  and the axis  $\bar{X}$  and by the angle  $\lambda$  between the orbital plane  $\bar{ZX}$  and the plane  $L\bar{X}$ . Using the tables of direction cosines (Chapter 1, § 1), we easily find  $\theta, \lambda$  from  $\rho_0, \gamma_0$ ; note that

$$\cos(L, \hat{\bar{X}}) = \cos(L, \hat{\bar{X}}) = \sin \rho_0 \cos \gamma_0,$$

$$\cos(L, \hat{\bar{Y}}) = \cos(L, \hat{\bar{Z}}) = \sin \rho_0 \sin \gamma_0,$$

$$\cos(L, \hat{\bar{Z}}) = \cos(L, \hat{\bar{Y}}) = \cos \rho_0.$$

The results of these calculations are plotted in Figures 73, 74. We see that in the mean,  $\lambda$  varies uniformly at a rate of  $\sim 0^\circ.76$  per revolution.

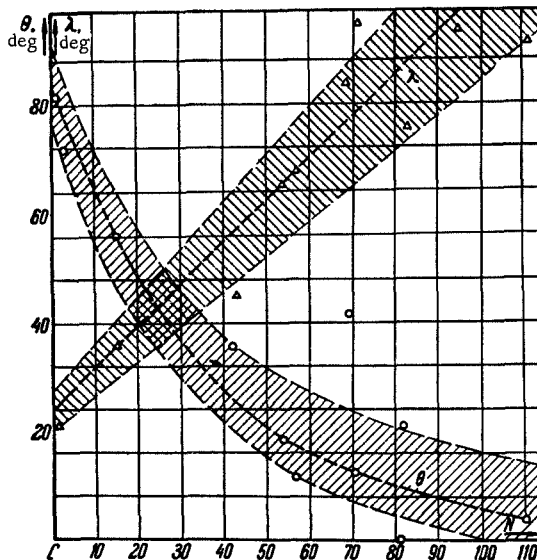


FIGURE 73. The orientation of the angular momentum vector relative to the orbit.

The angle  $\theta$  between the angular momentum vector and the perigee tangent varies monotonically from  $\sim 85^\circ$  during the first circuit to nearly zero after 100–110 circuits. The rate of change in  $\theta$  during the first 10–20 circuits is  $\sim 1^\circ.5$  per revolution, subsequently dropping almost to zero. The vector  $L$  eventually (by the time of the 109th circuit) orients itself along the tangent at the perigee point. In Figure 74, the movement of the vector  $L$  is plotted in polar coordinates  $\theta, \lambda$ ; the origin is the trace of the velocity vector of the satellite's mass center at the perigee point. The curve in Figure 74 has been plotted from the curves in Figure 73 which describe the mean movement of the angular momentum vector. The spread of the experimental points around the mean curve does not exceed  $10^\circ$  (the dashed regions in Figures 73, 74).

Since the nutation angle  $\theta$  between the satellite axis and the angular momentum vector is close to  $90^\circ$ , while during the late circuits the vector  $L$  points nearly along the velocity vector at the perigee point, the perigee passage during these circuits occurs in an attitude of maximum aerodynamic drag, and the satellite lifetime is correspondingly shortened.

Comparison of the actual movement of the vector with theory. Figure 74 plots the "mean" experimental path of the vector  $L$ , and also the theoretical paths (solid curves). In theoretical calculations, we only considered the secular motion of the vector  $L$ . The initial data were close to the experimental values. The satellite parameters, if known fairly accurately, were assumed as given; otherwise, they were chosen so as to ensure maximum fit of the mean experimental curve. The evolution of the orbit's node and perigee was taken into consideration. The perturbations included the torques produced by gravity, aerodynamic, and magnetic forces, eddy currents, and aerodynamic dissipative factors.

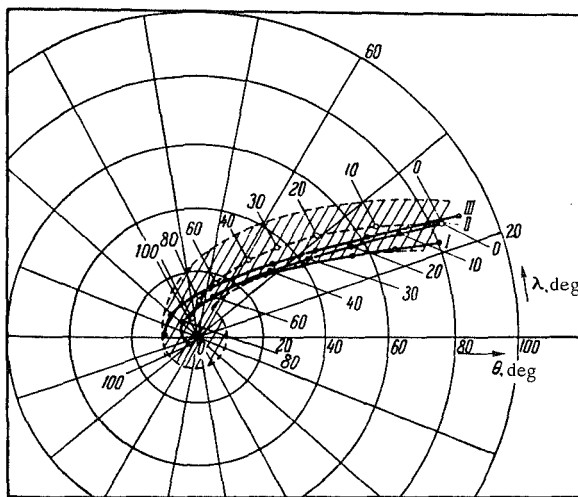


FIGURE 74. The paths of the angular momentum vector relative to the orbit. Circuit numbers are marked along the paths.

mean experimental path and the spread of experimental data;

— I, II, III — theoretical paths.

The divergence between the theoretical and the "mean" experimental curves is attributable to experimental errors (up to  $\pm 10^\circ$ , and even more in isolated points), to errors admitted in reduction and computation according to an approximate model of motion ("nearly regular" precession, which ignores the experimentally observed fluctuations in the spin rate  $\dot{\phi}$ ), to the approximate computational scheme used (allowing for the secular motion only), and to our particular interpretation of the external torques. Despite all this, however, the difference between the "mean experimental" attitude of the vector  $L$  and its calculated attitude is not greater than  $10^\circ$ . The general trend in the evolution of motion is also nearly identical in the experimental and the theoretical cases. These points suggest that

our model of motion gives a satisfactory, within the margin of experimental error, representation of the real motion.

On account of the foregoing errors and inaccuracies, it is advisable to compare the experimental data, not with a single theoretical curve, but with a bunch of curves generated by varying the initial values and the torque parameters. Some curves of this bunch are plotted in Figure 74. We see that a change by a factor of 1.2—1.5 in the external torque parameters qualitatively distorts the pattern of motion; the theoretical values of the parameters thus give a fairly reliable idea of the torque magnitudes and of the contribution from the external torques to the overall movement. Dissipative (aerodynamic and eddy-current) torques constitute an exception. During the comparatively brief period of 100—110 circuits, these torques

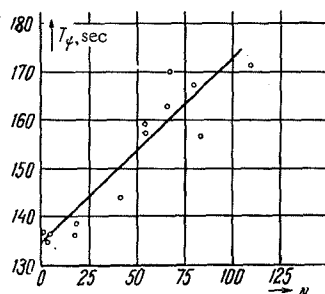


FIGURE 75. Precessing period.  
Dots — experimental results;  
solid line — theory.

degree to aerodynamic and magnetic torques also. It has been established that the projection  $I_L$  of the vector  $\mathbf{I}$  on  $\mathbf{L}$  points in the opposite direction relative to the vector  $\mathbf{L}$ . Formally, this factor is allowed for by introducing negative values of  $I_0 \cos \theta$ . Toward the end of the 110-circuit period (for  $\theta$  close to 0), the contribution from gravity torques diminishes in comparison with the contribution from aerodynamic torques, which remains fairly constant over the entire period.

The equations of secular motion were integrated in the "aerodynamic" variables  $\theta$ ,  $\lambda$ . Since in previous chapters we have considered the contribution from individual factors or the combined influence of some, but not all, factors, it now seems advisable to write the complete equations of secular motion. In these equations we introduce all the factors which have been considered in the previous chapters and which produce a certain effect on the secular evolution of the rotational motion (with the exception of solar radiation pressure). The general equations have the form

$$\left. \begin{aligned} \frac{d\lambda}{dv} &= \Lambda_a + \Lambda_g + \Lambda_H + \Lambda' + \Lambda^\theta, \\ \Lambda^\theta &= -\frac{1}{L \sin \theta} \{M_Y^\theta \cos \lambda + M_Z^\theta \sin \lambda\}, \\ \frac{d\theta}{dv} &= T_a + T_g + T_H + T' + T^\theta, \\ T^\theta &= \frac{1}{L} \{(M_Z^\theta \cos \lambda - M_Y^\theta \sin \lambda) \cos \theta - M_X^\theta \sin \theta\}, \\ \frac{dL}{dv} &= (M_Z^\theta \cos \lambda - M_Y^\theta \sin \lambda) \sin \theta + M_X^\theta \cos \theta, \\ \frac{d \cos \theta}{dv} &= f^{\partial a} + f^{\partial H}, \quad M_{X,Y,Z}^\theta = M_{X,Y,Z}^{\partial a} + M_{X,Y,Z}^{\partial H}. \end{aligned} \right\} \quad (10.1.3)$$

have a negligible influence on the motion of the vector  $\mathbf{L}$ , while their contributions to the variation in the magnitude of  $L$ , and therefore of  $\psi$ , are almost equal, so that it is virtually impossible to decide what particular dissipative factor prevails. In calculations we assumed that the dissipative effects due to eddy currents and aerodynamic drag have approximately equal influence on spin decay. Figure 75 plots the calculated variation of the precessing period  $T_\phi$  during the first 110 circuits (solid line) and the experimental values of  $T_\phi$  (dots) for some orbital circuits.

The motion of the vector  $\mathbf{L}$  is most sensitive to gravity torques, and in a considerable

The aerodynamic terms

$$\left. \begin{aligned} \Lambda_a &= \frac{\rho_\pi V \mu P}{2L} \cos \theta \left\{ a_0^a J_1 + \frac{a_2^a}{2} J_4 \sin^2 \theta + \right. \\ &\quad + a_2^a \left[ \frac{1}{2} \sin^2 \theta + \left( 1 - \frac{5}{2} \sin^2 \theta \right) \cos^2 \lambda \right] + \\ &\quad + 3 \left( 1 - \frac{5}{2} \sin^2 \theta \right) \left[ \frac{a_2^a}{3} J_4 - a_2^a J_5 \cos^2 \lambda \right] \cos^2 \theta \Big\} + \\ &\quad \left. + \frac{\rho_\pi V \mu P}{2L} a_1^a (J_2 - J_3) \left( 1 - \frac{3}{2} \sin^2 \theta \right) \cos \theta, \right. \\ T_a &= - \frac{\rho_\pi V \mu P}{L} a_2^a J_5 \cos \theta \left( 1 - \frac{5}{2} \sin^2 \theta \right) \times \\ &\quad \times \cos \theta \sin \theta \cos \lambda \sin \lambda. \end{aligned} \right\} \quad (10.1.4)$$

The coefficients  $J_i$  are defined by (7.1.4). For constant  $\bar{\rho}_a$  and  $e$ , the coefficients  $J_i$  are constant.

Gravity terms and the gravity-like part of the aerodynamic terms

$$\left. \begin{aligned} \Lambda_g &= - \frac{1}{2L} \left( 1 - \frac{3}{2} \sin^2 \theta \right) \left[ 3 \frac{V \mu}{P^2} (A - C) - \right. \\ &\quad \left. - \rho_\pi V \mu P a_1^g J_3 \right] \cos \theta \sin^2 \lambda, \\ T_g &= \frac{1}{2L} \left( 1 - \frac{3}{2} \sin^2 \theta \right) \left[ 3 \frac{V \mu}{P^2} (A - C) - \right. \\ &\quad \left. - \rho_\pi V \mu P a_2^g J_3 \right] \sin \theta \sin \lambda \cos \lambda. \end{aligned} \right\} \quad (10.1.5)$$

Terms attributable to orbit evolution

$$\left. \begin{aligned} \Lambda' &= k_\zeta [- \cos \omega_\pi \sin i + \operatorname{ctg} \theta (- \sin \lambda \cos i + \\ &\quad + \cos \lambda \sin \omega_\pi \sin i)] - k_\omega \operatorname{ctg} \theta \sin \lambda, \\ T' &= k_\zeta [\cos i \cos \lambda + \sin \omega_\pi \sin i \sin \lambda] + k_\omega \cos \lambda, \\ k_\zeta &= - \frac{\bar{\epsilon} R_e^2}{P^2} \cos i, \quad k_\omega = \frac{\bar{\epsilon} R_e^2}{2P^2} (5 \cos^2 i - 1), \\ \omega_\pi &= \omega_{\pi 0} + k_\omega y. \end{aligned} \right\} \quad (10.1.6)$$

Magnetic terms

$$\left. \begin{aligned} \Lambda_H &= - \frac{I_0 \mu_E}{LP \sqrt{\mu P}} \left\{ \cos \theta (J_{\bar{X}} a_\theta + J_{\bar{Y}} \beta_\theta) + \right. \\ &\quad + k_H \left( 1 - \frac{3}{2} \sin^2 \theta \right) [(J_{\bar{X}\bar{X}} - J_{\bar{Z}\bar{Z}}) \hat{\alpha} a_\theta + \\ &\quad + (J_{\bar{Y}\bar{Y}} - J_{\bar{Z}\bar{Z}}) \hat{\beta} \beta_\theta + J_{\bar{X}\bar{Y}} (\hat{\alpha} \beta_\theta + \hat{\beta} a_\theta)], \\ T_H &= \frac{I_0 \mu_E}{LP \sqrt{\mu P}} \left\{ \cos \theta (J_{\bar{X}} a_\lambda + J_{\bar{Y}} \beta_\lambda) + \right. \\ &\quad + k_H \left( 1 - \frac{3}{2} \sin^2 \theta \right) [(J_{\bar{X}\bar{X}} - J_{\bar{Z}\bar{Z}}) \hat{\alpha} a_\lambda + \\ &\quad + (J_{\bar{Y}\bar{Y}} - J_{\bar{Z}\bar{Z}}) \hat{\beta} \beta_\lambda + J_{\bar{X}\bar{Y}} (\hat{\alpha} \beta_\lambda + \hat{\beta} a_\lambda)] \Big\}. \end{aligned} \right\} \quad (10.1.7)$$

Here

$$\begin{aligned} \hat{\alpha} &= \cos \theta \cos \omega_\pi \cos i + \sin \theta \sin \lambda \sin i + \sin \theta \cos \lambda \sin \omega_\pi \cos i, \\ \hat{\beta} &= \cos \theta \cos \omega_\pi \sin i - \sin \theta \sin \lambda \cos i + \sin \theta \cos \lambda \sin \omega_\pi \sin i, \\ a_\theta &= - \cos \omega_\pi \cos i + \operatorname{ctg} \theta \sin \lambda \sin i + \operatorname{ctg} \theta \cos \lambda \sin \omega_\pi \cos i, \\ \beta_\theta &= - \cos \omega_\pi \sin i - \operatorname{ctg} \theta \sin \lambda \cos i + \operatorname{ctg} \theta \cos \lambda \sin \omega_\pi \sin i, \\ a_\lambda &= \cos \lambda \sin i - \sin \lambda \sin \omega_\pi \cos i, \\ \beta_\lambda &= - \cos \lambda \cos i - \sin \lambda \sin \omega_\pi \sin i. \end{aligned}$$

The coefficients  $J_s$ ,  $J_{hs}$ ,  $k$ ,  $s = \bar{X}, \bar{Y}, \bar{Z}$  are determined from (9.1.6); these coefficients are almost constant (slightly varying on account of  $\omega_\pi$ ).

Aerodynamic dissipative terms

$$\left. \begin{aligned} M_X^{\partial a} &= -k_0^\partial L_X + k_1^\partial \cos \theta \frac{L_X^2}{L} + k_2^\partial \cos \theta L, \\ M_Y^{\partial a} &= -k_0^\partial L_Y + k_1^\partial \cos \theta \frac{L_X L_Y}{L}, \\ M_Z^{\partial a} &= -k_0^\partial L_Z + k_1^\partial \cos \theta \frac{L_X L_Z}{L}, \\ L_X &= L \cos \theta, \quad L_Y = -L \sin \theta \sin \lambda, \\ L_Z &= L \sin \theta \cos \lambda, \\ k_0^\partial &= N_0^\partial \left( \frac{I_3}{A} \sin^2 \theta + \frac{I_1}{C} \cos^2 \theta \right), \\ k_1^\partial &= \left\{ -\frac{I_4 N_1^\partial}{C} \left( 1 - \frac{3}{2} \sin^2 \theta \right) + \frac{I_2 N_1^\partial}{A} \cdot \frac{3}{2} \sin^2 \theta \right\}, \\ k_2^\partial &= \left\{ \frac{I_4 N_1^\partial}{C} \left( 1 - \frac{1}{2} \sin^2 \theta \right) - \frac{I_2 N_1^\partial}{A} \cdot \frac{1}{2} \sin^2 \theta \right\}, \\ f^{\partial a} &= \cos \theta \sin^2 \theta \left( \frac{I_3}{A} - \frac{I_1}{C} \right) N_0^\partial + \\ &\quad + N_1^\partial \cos \theta \sin^2 \theta \left\{ \frac{I_2}{A} \sin^2 \theta - \frac{I_4}{C} \cos^2 \theta \right\}, \\ N_0^\partial &= \frac{1}{2} \rho_\pi P \bar{N}_0^\partial, \quad N_1^\partial = \frac{1}{2} \rho_\pi P \bar{N}_1^\partial. \end{aligned} \right\} \quad (10.1.8)$$

The coefficients  $N_0^\partial$  and  $N_1^\partial$  are defined by (7.4.10).

Terms attributable to eddy currents

$$\left. \begin{aligned} M_X^{eH} &= \cos \omega_\pi \cos i M_{\bar{X}} + \cos \omega_\pi \sin i M_{\bar{Y}} - \sin \omega_\pi M_{\bar{Z}}, \\ M_Y^{eH} &= -\sin i M_{\bar{X}} + \cos i M_{\bar{Y}}, \\ M_Z^{eH} &= \sin \omega_\pi \cos i M_{\bar{X}} + \sin \omega_\pi \sin i M_{\bar{Y}} + \cos \omega_\pi M_{\bar{Z}}, \\ M_{\bar{X}} &= -a^H \{(J_{YY} + J_{ZZ}) L_{\bar{X}} - J_{YX} L_{\bar{Y}}\}, \\ M_{\bar{Y}} &= -a^H \{(J_{XX} + J_{ZZ}) L_{\bar{Y}} - J_{ZX} L_{\bar{X}}\}, \\ M_{\bar{Z}} &= -a^H \{(J_{YY} + J_{XX}) L_{\bar{Z}}\}, \\ a^H &= \frac{\mu_E^2 k_0 s}{P^{3/2} \sqrt{\mu}} \left( \frac{\cos^2 \theta}{C} + \frac{\sin^2 \theta}{A} \right), \\ f^{eH} &= \frac{k_0 \Phi}{2} \left( \frac{1}{A} - \frac{1}{C} \right) \cos \theta \sin^2 \theta \left\{ J_{XX} \left( 1 + \frac{L_X^2}{L^2} \right) + \right. \\ &\quad \left. + J_{YY} \left( 1 + \frac{L_Y^2}{L^2} \right) + J_{ZZ} \left( 1 + \frac{L_Z^2}{L^2} \right) + \right. \\ &\quad \left. + 2 J_{XY} \frac{L_Y L_X}{L^2} \right\} \frac{\mu_E^2}{P^{3/2} \sqrt{\mu}}, \\ L_{\bar{X}} &= \cos \omega_\pi \cos i L_X - \sin i L_Y + \sin \omega_\pi \cos i L_Z, \\ L_{\bar{Y}} &= \cos \omega_\pi \sin i L_X + \cos i L_Y + \sin \omega_\pi \sin i L_Z, \\ L_{\bar{Z}} &= -\sin \omega_\pi L_X + \cos \omega_\pi L_Z. \end{aligned} \right\} \quad (10.1.9)$$

In calculations, we put

$$\begin{aligned} R_e &= 6371 \text{ km}; \quad \mu = 398602.0 \text{ km}^3/\text{sec}^2, \\ \mu_E &= 8.06 \cdot 10^{25} \text{ g}^{1/2} \cdot \text{cm}^{5/2}/\text{sec}; \\ \tilde{\epsilon} &= 0.0016331; \quad \rho_\pi = 2.12 \cdot 10^{-13} \text{ g/cm}^3; \\ P &= 6917 \text{ km}; \quad e = 0.0487. \end{aligned}$$

Table 12 lists the relevant data for one of the calculated curves of Figure 74 (curve II; the data for other curves are not much different). Some dimensional and nondimensional quantities characterizing the principal evolutionary effects attributable to various torques are given in the table.

TABLE 12

1	Initial data and moments of inertia	$\lambda_0 = 24^\circ$ $\theta_0 = 84^\circ$ $L_0 = 2.327 \cdot 10^8 \text{ g} \cdot \text{cm}^2/\text{sec}$ $\dot{\theta}_0 = 85^\circ$ $A = 5 \cdot 10^9 \text{ g} \cdot \text{cm}^2$ $C = 2 \cdot 10^9 \text{ g} \cdot \text{cm}^2$
2	a) Aerodynamic torque (maximum)  $\Lambda_a^{\max} \frac{L_0 \sqrt{\mu}}{P^{3/2}}$  b) $\Lambda_a^{\max}$	- 296.204 dyne · cm  - 0.001161
3	a) Gravity torque  $-\frac{3}{2} \frac{\mu}{P^3} (A - C) \left(1 - \frac{3}{2} \sin^2 \theta\right)$  b) $-\frac{1}{2L_0} \left(1 - \frac{3}{2} \sin^2 \theta\right) \cdot 3 \frac{\sqrt{\mu}}{P^{3/2}} (A - C)$	2648.13 dyne · cm  0.010369
4	a) Magnetic torque  $I_0 \mu_E \cos \theta / P^3$  b) $\frac{I_0 \mu_E}{L_0 P \sqrt{\mu P}} \cos \theta$	- 424.457 dyne · cm  - 0.001662
5	a) $k_\Omega$  b) $k_\omega$	- 0.000585  - 0.000074
6	a) Nondimensional decrement of damping for $N=110$ circuits  $\delta_3 \approx N_0 \frac{I_3}{A} + \frac{\mu_E^2}{P^{9/2} \sqrt{\mu}} \frac{k_0 s}{A}$  b) Initial value of the dissipative torque  $\left( \approx \delta_3 L_0 \frac{\sqrt{\mu}}{P^{3/2}} \right)$	$3.61 \cdot 10^{-4}$  92.280 dyne · cm

Solar attitude. Once  $\rho_0$ ,  $\gamma_0$  are known, we can calculate the orientation of the angular momentum vector relative to the Sun:

$$\begin{aligned}\cos \theta_0 &= \cos \rho_0 \cos \chi_0 + \\ &\quad + \sin \rho_0 \sin \chi_0 \cos \mu^*, \\ \cos \chi_0 &= \sin \Omega_0 \cos I^*, \\ 0 &\leq \chi_0 \leq 180^\circ, \\ \mu^* &= \gamma_0 - \gamma_0, \\ \sin \gamma_0 &= \frac{\sin I^*}{\sin \chi_0} \sin \Omega_0, \\ \cos \gamma_0 &= \frac{\cos \Omega_0}{\sin \chi_0}.\end{aligned}$$

Here  $\theta_0$  is the unknown angle between the angular momentum vector and the direction to the Sun,  $I^* \approx 23^\circ.5$  the inclination of the equator to the ecliptic,  $\Omega_0$  the longitude of the Sun from the point of vernal equinox. The results of this calculation are plotted in Figure 76. We see that  $\theta_0$  increases from

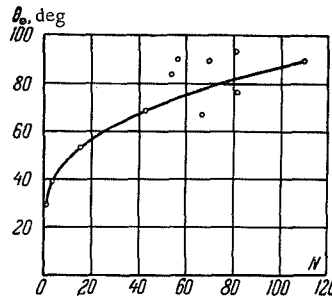


FIGURE 76. The orientation of the angular momentum vector relative to the Sun.

$30^\circ$  during the first circuit to  $90^\circ$  during the 100th circuit. Since the nutation angle is close to  $90^\circ$  (tumble), and since the satellite is also spinning, we come to the conclusion that the satellite is illuminated (and heated) by the Sun fairly uniformly.

3. Calculating the orientation of instruments in space. The attitude of the axis  $i$  of any instrument or the attitude of any one of the satellite's axes will be defined relative to the frame  $x'y'z'$  by the angle  $j$  between the axis  $l$  and the satellite's axis  $z'$  and by the angle  $\sigma$  reckoned counterclockwise from  $x'$  to  $y'$  (this is in fact the angle between the axis  $x'$  and the projection of  $l$  on the plane  $x'y'$ ). The attitude of the axis  $l$  is also defined by the direction cosines  $m_0$ ,  $n_0$ ,  $k_0$ , which refer to the axes  $x'$ ,  $y'$ ,  $z'$ , respectively:  $m_0 = \sin j \cos \sigma$ ,  $n_0 = \sin j \sin \sigma$ ,  $k_0 = \cos j$ .

Magnetic attitude. We are now in a position to specify fully the attitude of the satellite relative to the Earth's magnetic field. Indeed, the angle  $\Lambda$  between the axis  $z'$  and the magnetic field vector  $\mathbf{H}$  is supplied by the recording  $\Lambda = q_2 - \frac{1}{3}q_1$ , which is traced relative to a certain reference level that can be established for each circuit by analyzing the recording extrema;  $\Delta \equiv q_1$  is the angle between the plane in which the angle  $\Lambda$  is reckoned and the plane  $z'x$  (taken counterclockwise). The magnetic

attitude of the satellite is thus fully defined whenever the angles  $\Delta$  and  $\Lambda$  are recorded. Specimen recordings, showing the reference level for  $\Lambda$ , are depicted in Figures 77, 78 (here I is a recording of  $\Delta$ , II a recording of  $q_2$ , III a recording of  $\Lambda$ , IV the reference level from which  $\Lambda$  is reckoned).

If  $\Delta$  and  $\Lambda$  are known, we can easily compute the angle  $\kappa_{HI}$  between the vector  $H$  and the axis  $l$  of any instrument:

$$\cos \kappa_{HI} = \cos j \cos \Lambda + \sin j \sin \Lambda \cos (\Delta + \sigma). \quad (10.1.10)$$

Figure 79 shows a specimen curve calculated from (10.1.10): the angle between the axis of the photomultiplier /48/ ( $j = 90^\circ$ ,  $\sigma = 114^\circ$ ) and the

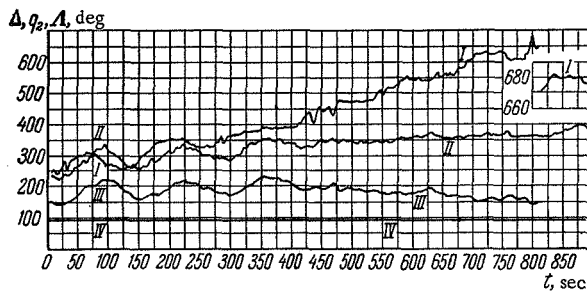


FIGURE 77. Magnetometer recording and the magnetic attitude of the satellite during the second circuit.

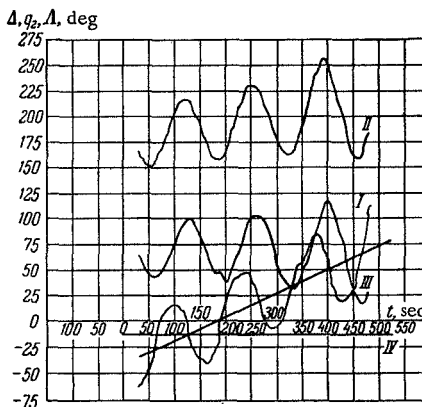


FIGURE 78. Magnetometer recording and the magnetic attitude of the satellite during the 15th circuit. The slanting line plots the linear part of  $\Delta$ .

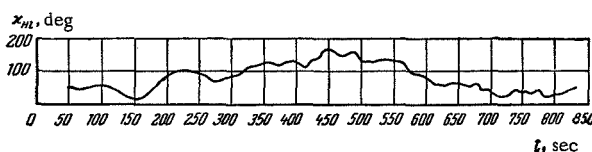


FIGURE 79. The angle between the magnetic line of force and the photomultiplier axis during the second circuit.

magnetic field vector during the second circuit. Note that from the recordings of  $q_1$  and  $q_2$  during the second circuit (Figure 77) we see that the angular momentum vector is close to the direction of a magnetic line of force (the angle  $\Lambda$  hardly fluctuates), i. e., the satellite axis is almost perpendicular to the vector  $H$ . The angle  $\kappa_m$  therefore displays no distinct short-period fluctuations connected with the satellite precession. Long-period fluctuations attributable to the satellite spin are well pronounced.

Orientation of a given satellite axis relative to a given direction in space. This quite general case is solved with the aid of the Eulerian angles  $\varphi = \varphi_0 + \dot{\varphi}t$ ,  $\psi = \psi_0 + \dot{\psi}t$ ,  $\theta = \theta_0$  and the absolute angular coordinates  $\rho_0$ ,  $\gamma_0$  of the angular momentum vector. The angle  $\tilde{\theta}$  between the given direction  $V$  in space and the instrument axis  $l$  is easily calculated using the following direction cosine matrices: 1) direction cosines of the frames  $XYZ$  and  $L_1L_2L$  (see Chapter 1, § 1; these direction cosines are expressible in terms of  $\rho_0$  and  $\gamma_0$ ); 2) direction cosines of the frames  $x'y'z'$  and  $L_1L_2L$  (expressible in terms of  $\varphi$ ,  $\psi$ ,  $\theta$ ); the matrix product of these two matrices defines the direction cosines of the satellite's axes relative to the fixed axes; 3) the  $m$ ,  $n$ ,  $k$  matrix defining the direction cosines of the given axis  $l$  in the satellite enables us to calculate the attitude of the axis  $l$  in space; 4) finally, the direction cosines of the vector  $V$  relative to the fixed axes give the angle  $\tilde{\theta}$  between  $l$  and  $V$ . As an example, let us calculate the angle  $\tilde{\theta}$  between a given axis in the satellite and the velocity vector of the satellite's center of mass.

Calculations show that satisfactory agreement between the theoretical results and the telemetered recordings is possible only after the introduction of appropriate corrections in the parameters obtained by reducing the magnetometer readings. The parameters  $\varphi_0$  and  $\psi_0$  had to be adjusted by as much as  $30^\circ$ . Inaccuracies in the determination of  $\psi_0$  produced a considerable discrepancy (20–30 sec) in the extremum positions obtained theoretically and observed on the recordings. The inaccuracies in  $\varphi_0$  are less critical: they mainly alter the magnitude of the extrema. Other parameters ( $\rho_0$ ,  $\gamma_0$ ,  $\varphi$ ,  $\psi$ ,  $\theta$ ) remained uncorrected; their variation has a

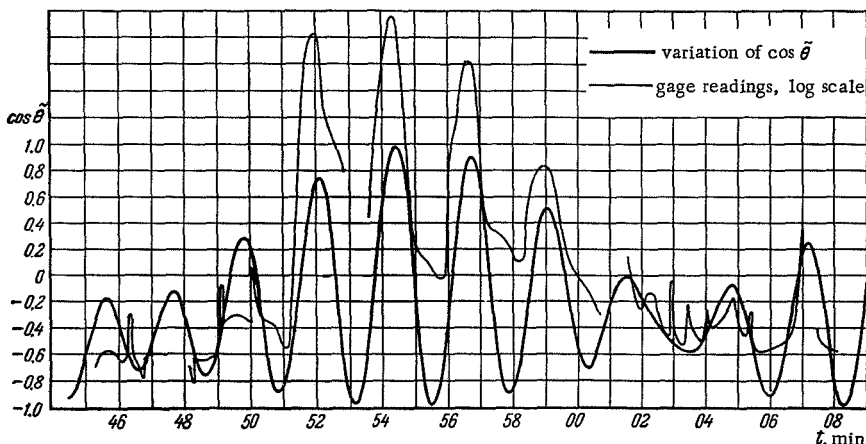


FIGURE 80. The orientation of the ionization pressure gage axis relative to the velocity vector during the 15th circuit compared to the pressure gage recording..

negligible influence on the results of calculations. Note that over large periods the errors in  $\dot{\psi}$  build up, introducing cumulative distortions in the extremum positions. If the rated  $\dot{\psi}$  was seen to produce extremum position displacement, suitable corrections were introduced in  $\dot{\psi}$ . The parameters  $\rho_0$  and  $\gamma_0$  were corrected only for those circuits whose  $\rho_0$  and  $\gamma_0$  were seen to be largely at variance with the set of  $\rho_0$  and  $\gamma_0$  values for other circuits.

The corrections were introduced from the recordings of the mass spectrometer /40/ and the ionization pressure gage /57/. Figure 80 is a specimen curve calculated for the angle  $\theta$  between the pressure gage axis and the velocity vector of the satellite's mass center. For comparison, this figure also shows the recording obtained with the corresponding instrument. Sputnik III attitude calculations were used in processing the readings of payload instruments from which various parameters of the upper atmosphere, the geomagnetic field, etc., were derived /28, 40, 48, 57/.

## § 2. EXPLORER XI AND EXPLORER IV

Radio signals provide an excellent tool for satellite attitude measurements. If the satellite is equipped, say, with a beamed antenna, the peak power is received in the direction of the axis of the antenna radiation pattern; there is a single-valued relation between the received radio power and the angle  $\alpha$  that the antenna axis makes with "base-to-satellite" line. If the satellite spins around the antenna pattern axis, the variation in the angle  $\alpha$  enables us to determine the attitude of the spin axis in space and the change of this attitude in time. There are also other radio techniques for establishing the spin axis attitude. For example, if the antenna pattern is "lobed", the signal length corresponding to a certain lobe divided by the total tumble period of the satellite gives the angle between the tumble axis and the "base-to-satellite" line. The analysis of radio signals served as the main tool in attitude measurements of several American satellites of the Explorer series. The most detailed and valuable data were published by Naumann and co-workers /84, 85/ and by others on Explorer XI. Some of the results of /84, 85/ are summarized in the following.

Explorer XI and Explorer IV were both elongated with a large lateral-to-axial inertial ratio (see Table 13). Satellites of this type, if spun about the longitudinal axis, tumble fairly rapidly (Explorer XI tumbled in 26 days) due to the influence of dissipative factors (external torques, elastic scattering, etc.).

Therefore, starting with a certain time, we may regard the satellite as spinning about the lateral axis (more precisely, the satellite's lateral axis makes a small angle with the angular momentum vector, so that the angle of nutation  $\theta$  is close to  $90^\circ$ ). Radio observations give the orientation of the angular momentum vector, as explained above. If there were no perturbations, this attitude would remain fixed, but since various external torques act on the satellite, the angular momentum vector moves slowly in space. This movement of the angular momentum vector is shown in Figure 81 for Explorer XI; the figure plots the observed variation in the two angular coordinates of the angular momentum vector, the right ascension  $\alpha$  and the declination  $\delta$  ( $d$  is time in days, after 27 April 1961).

TABLE 13  
Some parameters of Explorer satellites

Parameters	Explorer XI	Explorer IV
$A, \text{g} \cdot \text{cm}^2$	$1.627 \cdot 10^8$	$4.762 \cdot 10^7$
$C, \text{g} \cdot \text{cm}^2$	$0.040 \cdot 10^8$	$0.056 \cdot 10^7$
$A - C, \text{g} \cdot \text{cm}^2$	$1.587 \cdot 10^8$	$4.696 \cdot 10^7$
$\frac{4}{3} \frac{\mu}{r^8} (A - C), \text{dyne} \cdot \text{cm}$	111.92	31.78
$I_L \frac{\mu_E}{r^8} \approx I_x, \frac{\mu_E}{r^8}, \text{dyne} \cdot \text{cm}$	148.14	
$I_{z'} \frac{\mu_E}{r^8}, \text{dyne} \cdot \text{cm}$	450	-3500
$R, \text{km}$	7512	7616
$i, \text{deg}$	28.8	51.0
$\Delta\Omega, \text{deg/day}$	-5.0036	-3.6505
$L, \text{g} \cdot \text{cm}^2/\text{sec}$	$1.276 \cdot 10^8$	$4.568 \cdot 10^7$
$\Delta L (\text{diurnal}), \text{g} \cdot \text{cm}^2/\text{sec}$	$-0.223 \cdot 10^7 *$ $-0.0143 \cdot 10^7 **$	$-0.0076 \cdot 10^7$

\* First 20 days

\*\* After 26 days

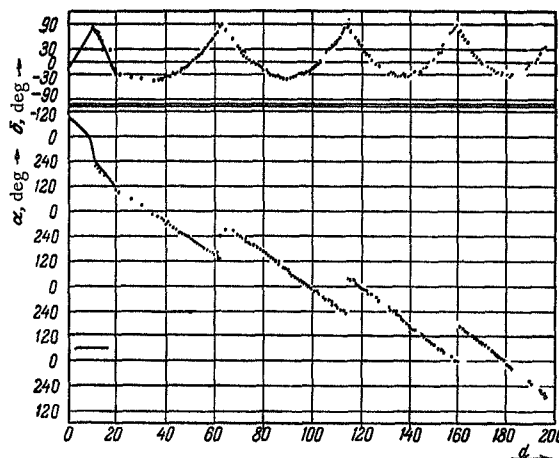


FIGURE 81. Observed orientation of the angular momentum vector of Explorer XI /85/.

Dots — observed orientation; solid curve — computed orientation assuming a longitudinal magnetic couple of 450 dyne · cm, a drag couple of 50 dyne · cm, and gravitational torques.

The magnitude of the angular momentum vector is known fairly accurately. It is equal to the product of the lateral moment of inertia by the angular velocity of tumble; the tumbling period is easily determined from the radio signal recordings. Given the magnitude of the vector  $\mathbf{L}$  and its two angular coordinates, we can easily calculate the observed components  $L_x, L_y, L_z$ ; differentiation gives the derivatives  $\dot{L}_x, \dot{L}_y, \dot{L}_z$  which are obviously equal to the components of the external torques on the satellite. These torques determined from the results of observations are then compared with the theoretically calculated torques.

The aerodynamic, gravity, and magnetic torques are assumed in the form of Chapter 1 and Chapters 6–9. Only the secular part of these torques is considered, i.e., torques averaged over two periods: the period of precession (tumble) and the period of orbital revolution.

If the aerodynamic torques vary sinusoidally with the angle of attack, then in accordance with Chapter 7, the mean secular aerodynamic torque vanishes for a tumbling satellite ( $\theta = \pi/2$ ). The aerodynamic torque is therefore considered only for the first 20 days after the launch of Explorer XI on 27 April 1961 (see Figure 81). After that, the satellite having tumbled ( $\theta = \pi/2$ ), zero aerodynamic torque is assumed. Only gravity torques and magnetic torques need be considered. The magnetic torques are made up from an induced component (i.e., torques attributable to the magnetization of the satellite shell) and a fixed component attributable to the satellite's intrinsic field. The fixed component vanishes in the mean for  $\theta = \pi/2$ , but since  $\theta$  is not precisely  $\pi/2$ , the effect of the fixed magnetic component is seen to be appreciable. An alternative explanation is that the constant magnetic moment of the satellite has both longitudinal and transverse components. The projection  $I_z$  of the magnetic moment  $I$  on  $\mathbf{L}$  does not vanish even when  $\theta = \pi/2$ . On the other hand, the calculated magnetization torque did not agree with the observed torque. This is seen from Figure 82.

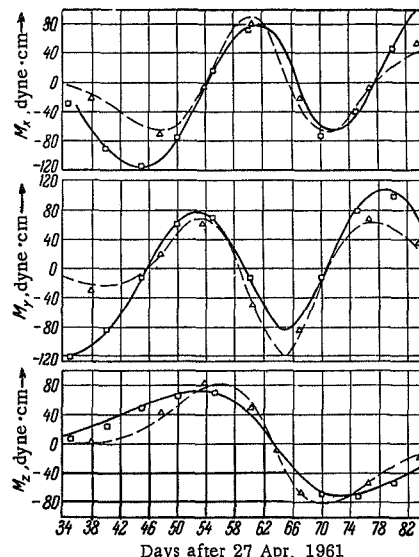


FIGURE 82. Analysis of torques on Explorer XI /85/.  
 ▲—▲ induced magnetic torque, detailed integration; .... induced  
 torque, approximate methods; ○—○ permanent magnetic torque;  
 — observed torque minus gravitational torque.

The solid line in the figure plots the difference between the observed torques and the gravity torques. Gravity torques may be calculated exactly, since the satellite's moments of inertia are known (Table 13). The "residual" torque observed in Figure 82 is thus attributable to the induced magnetic moment or the constant magnetic moment. The induced moment was chosen so that the calculated amplitude of torque fluctuations fitted the observed amplitude. To ensure this fit, we must take  $(\frac{\mu_E}{r^3})^2 (\mu_0 - 1) v = 384$  dyne · cm.

We see from Figure 82 that the calculated induced torque displays the same general trend as the observed component, but the correlation is not very

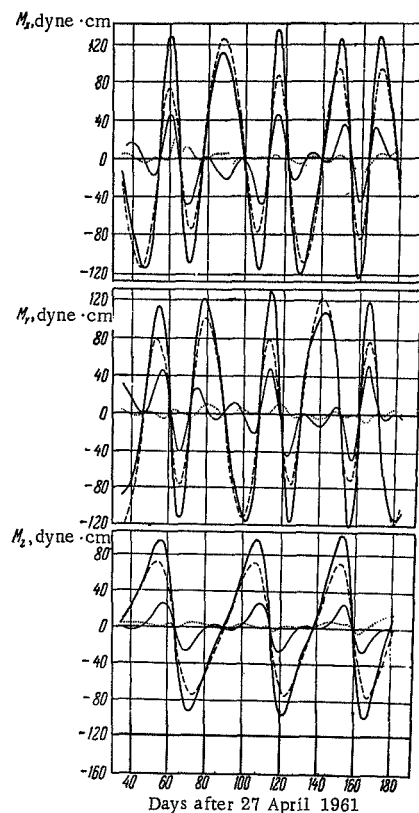


FIGURE 83. Analysis of torques on Explorer XI /85/.  
 — observed torque; --- permanent magnetic torques;  
 — gravitational torques; - - - residuals, observed minus  
 sum of magnetic and gravitational torques.

convincing. On the other hand, assuming a constant magnetic torque  $\frac{\mu_E}{r^3} I_L = 148.14$  dyne · cm, we obtain an excellent agreement between the calculated and the observed data (see Figure 82). This leads to the conclusion that the observed motion is governed by gravity torques and the torques attributable to the interaction of the Earth's magnetic field with the satellite's constant magnetic moment. Figure 83 plots the observed torques, together with gravity and magnetic torques, for days 35 through 180 after launch. A

separate curve plots the difference between the observed torque and the sum of gravity and magnetic torques. We see that the difference is not greater than 5 dyne · cm, while the maximum observed torques are close to 120 dyne · cm. This points to satisfactory agreement between the observed quantities and the theory.

The calculated movement of the angular momentum vector is compared with the observed movement in Figures 84, 85. During the first twenty days after launch (Figure 84), aerodynamic torques, as well as gravity and

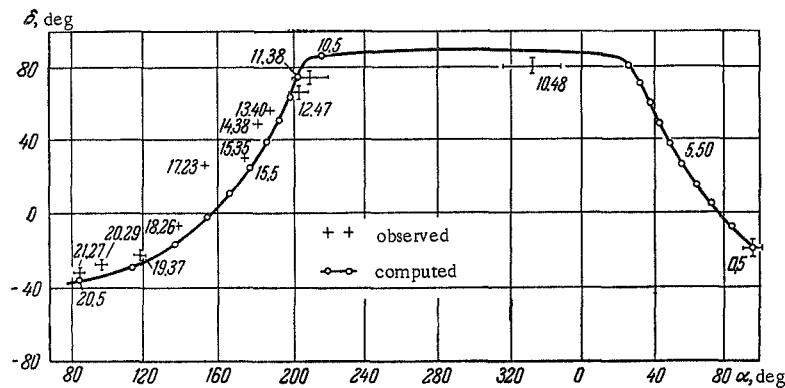


FIGURE 84. Orientation of the angular momentum vector for the first 20 days of Explorer XI /85/.

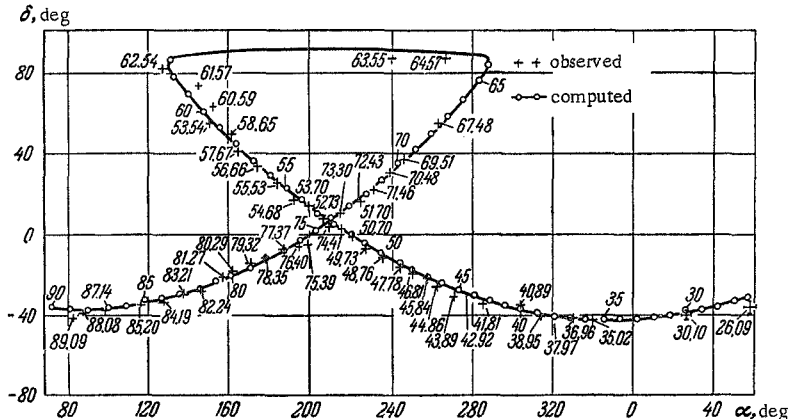


FIGURE 85. Orientation of the angular momentum vector of Explorer XI for day 26 to 90 /85/.

magnetic torques, were considered. To ensure satisfactory fit between the theory and the observations, we must take  $I_L \frac{\mu_E}{r^3} = 450$  dyne · cm and 50 dyne · cm for the aerodynamic torque. Starting with the 26th day after launch, the satellite tumbles, and the aerodynamic torques can be ignored; the magnetic effects are characterized, as before, by putting  $I_L \frac{\mu_E}{r^3} = 148.14$  dyne · cm

(Figure 85). We see from Figures 84 and 85 that the calculated and the observed motions are in excellent agreement.

The data on the orientation of Explorer IV are much less accurate than those for Explorer XI, but they can also be attributed to the effect of perturbation torques. The intrinsic value of these data, however, is in the fact that they provide satisfactory interpretation of some phenomena observed for Explorer IV. Figure 86, for example, plots the variation of temperature inside the satellite, obtained by telemetry. The solid curve in Figure 86 gives the variation of temperature calculated from the observed orientation of the angular momentum vector relative to the Sun. The recorded and the predicted temperatures are obviously in good agreement.

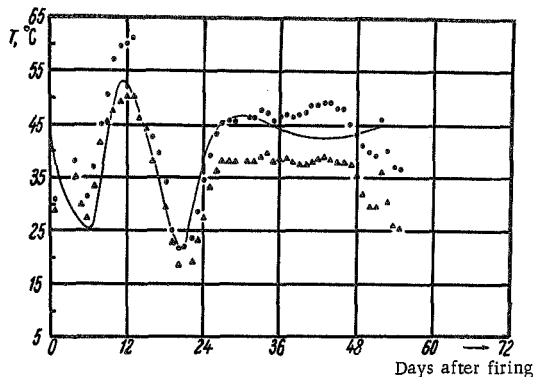


FIGURE 86. Temperature of Explorer IV /84/.  
Dots - telemetered data; solid curve - calculated  
from attitude measurements.

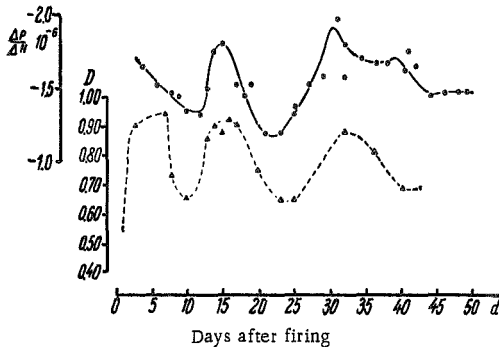


FIGURE 87. Orbital period of Explorer IV and effective drag area  
vs. days after firing /84/.  
—•—rate of change of orbital period; - - - - effective drag area.

Since the satellite attitude varies, the effective cross section (averaged over the tumbling period) is not constant, so that the drag forces and the orbital period are both variable. Figure 87 plots (solid curve) the observed variation of the orbital period of Explorer IV. This figure also records the variation in the effective surface during perigee passage. The effective surface variation has been calculated from the observed change in the

orientation of the angular momentum vector. A comparison of the two curves shows that the drag forces mainly vary with the satellite's effective cross-section area.

The results of his chapter indicate, first, that the existing theory of satellite spin provides satisfactory interpretation of various observed effects and, second, that these effects are quite general, influencing the satellite temperature, its orbital motion (i.e., period of revolution and lifetime), and other dynamic and physical characteristics.

In conclusion we should note that spin and attitude parameters can be determined from radio measurements, readings of magnetometers, solar trackers, ion traps and pressure gages, optical observations of satellite brightness variation, etc. Different techniques are generally established for recovering the orientation parameters applicable in each particular case. We shall not dwell on this subject in any detail, and the reader is referred to original publications. Various aspects of spin and attitude determination are considered, aside from the previously cited references, also in /25, 82, 86/, and other sources.

## *Chapter 11*

### **USES OF AN EARTH-ORIENTED SATELLITE IN SOLAR RESEARCH /59/**

Artificial Earth satellites employed in various scientific projects must be oriented in a certain way. Attitude control is essential in solar research, in particular, in measurements of solar radiation and corpuscular streams. The readings of spaceborne instruments in general are not indifferent to the satellite's solar attitude, and correct interpretation of extraterrestrial measurements is impossible without precise knowledge of the orientation of the instruments relative to the Sun.

A solar-research satellite should preferably be oriented so that one of the satellite's axes always points to the Sun. Solar measurements, however, can be made with differently oriented satellites, and even with satellites which are not oriented at all. This, of course, presupposes the introduction of a special solar tracker constantly pointing the optical axis of the instrument at the Sun; otherwise, we must accept the fact that the instrument is exposed to sunlight only when the angle between the instrument axis and the sunward direction is fairly small — less than the instrument's angle of view (the instrument angle).

We shall consider the insolation of instruments in a satellite with one axis pointing to the Earth, and the other axis along the normal to the orbital plane. This attitude is commonly employed in various Earth-oriented satellites. The results of the analysis show that narrow-angle instruments are sometimes exposed for a few tens of hours, which is quite sufficient for various scientific measurements.

#### **§ 1. INSOLATION TIME FOR A CONSTANT ORIENTATION OF THE ORBIT RELATIVE TO THE SUN**

The orientation of satellite orbits relative to the Sun is time-variable. The change in orientation is produced by the annual motion of the orbit with the Earth around the Sun, and also by the precession of the orbit around the Earth due to perturbations in the Earth's noncentral field. Orbit's orientation relative to the Sun has a substantial influence on the insolation time of spaceborne instruments. This factor cannot be ignored.

The orientation varies comparatively slowly, and during one revolution of the satellite around the Earth, the angle  $\nu$  between the normal to the orbital plane and the direction to the Sun (the obliquity or the inclination of the orbit) changes but little. Calculations show that the variation in  $\nu$  is not greater than  $0^{\circ}.5$  per revolution, whereas for orbits inclined at an

angle  $\approx 65^\circ$  to the Earth's equator, it is as low as  $0^\circ.25$ . The angle  $v$  may therefore be approximately regarded as constant during one revolution. The total insolation time is thus found in two stages: first, the insolation time is determined for a constant  $v$ , and then the time variation of the angle  $v$  is established. The insolation time for a constant orbital orientation ( $v = \text{const}$ ) is calculated in this section.

We shall consider an ideally oriented satellite, which does not oscillate about its equilibrium attitude. In the case of ideal terrestrial orientation, the axis of an instrument set at an angle  $\delta$  to the binormal will describe, during one orbital revolution, a circular conical surface around the binormal with an angle of opening  $\delta$ . For low-eccentricity orbits, the angular velocity of motion of the instrument axis relative to the binormal is nearly constant. The insolation time is defined as the time during which the Sun stays inside the instrument angle.

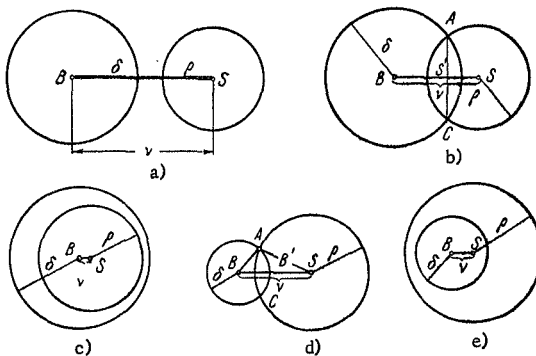


FIGURE 88. Illustrating the various possible relations between the parameters  $\rho$ ,  $\delta$ ,  $v$ : a)  $\delta > \rho$ ,  $v > \delta + \rho$ ; b)  $\delta > \rho$ ,  
 $\delta - \rho < v < \delta + \rho$ ; c)  $\delta > \rho$ ,  $v < \delta - \rho$ ; d)  $\delta < \rho$ ,  $\rho - \delta <$   
 $v < \rho + \delta$ ; e)  $\delta < \rho$ ,  $v < \rho - \delta$ .

During the satellite's lifetime, the Sun repeatedly enters and leaves the instrumental angle of view as the satellite moves in its orbit. We should therefore distinguish between the continuous insolation time, with the Sun staying without interruption inside the instrument angle, and the total insolation time, which is equal to the sum of all the continuous insolation times during the entire lifetime of a satellite.

Consider a unit sphere centered at the satellite's center of mass (Figure 88). The binormal of the satellite's orbit meets the sphere at the point  $B$ , and the line joining the satellite's mass center with the Sun intersects the sphere at the point  $S$ . The angular distance between the binormal and the sunward direction is measured in terms of the great-circle arc  $BS=v$ .

Let the instrument axis meet the unit sphere at some point  $A$ . Then during one orbital revolution of the satellite, the point  $A$  will trace a circle  $(B, \delta)$  on the unit sphere, having a radius  $\delta$  and centered at the point  $B$ . The instrument will function if the angular distance between the points  $A$  and  $S$  is not greater than the instrument angle  $\rho$ , i.e., if an arc of the

circle ( $B, \delta$ ) lies inside the circle ( $S, \rho$ ), centered at  $S$  and having a radius  $\rho$ . We always take  $\delta < \pi/2$ . A simple analysis gives the insolation conditions which are listed in Table 14 for various combinations of the parameters (the relations between the parameters are illustrated in Figure 88).

TABLE 14

	Relation between parameters	Insolation
$\delta > \rho$	$v > \delta + \rho$	No insolation (Figure 88 a)
	$\delta - \rho < v < \delta + \rho$	Insolation over part of the orbit (Figure 88 b)
	$v < \delta - \rho$	No insolation (Figure 88 c)
$\delta < \rho$	$v > \delta + \rho$	No insolation
	$\rho - \delta < v < \rho + \delta$	Insolation over part of the orbit (Figure 88 d)
	$v < \rho - \delta$	Insolation over entire orbit (Figure 88 e)

The insolation conditions in the table apply for  $v = \text{const}$ , and also for the general case  $v = v(t)$ . Note that these conditions do not allow for satellite eclipses, i.e., the immersion of the satellite in the Earth's shadow (this problem is considered separately in § 4 of this chapter). The insolation time is proportional to the length of the arc  $AB'C = 2\epsilon$ .

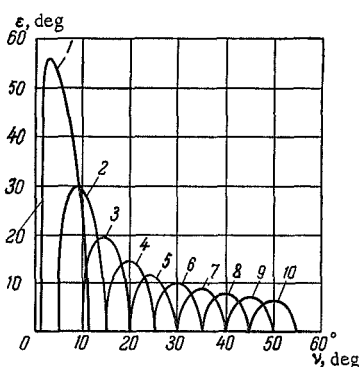


FIGURE 89. Insolation during one revolution vs. the angle  $v$  for  $\delta > \rho = 5^\circ$ : 1)  $\delta = 6^\circ$ , 2)  $\delta = 10^\circ$ , 3)  $\delta = 15^\circ$ , etc., ..., 10)  $\delta = 50^\circ$ .

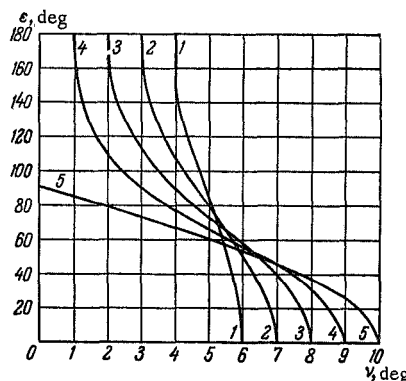


FIGURE 90. Insolation during one revolution vs. the angle  $v$  for  $\delta < \rho = 5^\circ$ : 1)  $\delta = 1^\circ$ , 2)  $\delta = 2^\circ$ , etc., ..., 5)  $\delta = 5^\circ$ .

Let  $T_0$  be the orbital period, and  $T$  the insolation time during one revolution, then

$$T = T_0 \frac{\epsilon}{\pi}. \quad (11.1.1)$$

From the spherical triangle  $BAS$  (Figure 88 d), we have

$$\cos \varepsilon = \frac{\cos \rho - \cos v \cos \delta}{\sin v \sin \delta}. \quad (11.1.2)$$

For given  $\rho$ ,  $v$ ,  $\delta$ , we can thus find from (11.1.1) and (11.1.2) the insolation time during one revolution. For a variable  $v$ , the length of the arc  $\varepsilon$  will change from circuit to circuit.

The graph in Figure 89 plots the dependence  $\varepsilon(v)$  for various  $\delta$  in the case  $\delta > \rho$ ,  $\rho = 5^\circ$ . We see from the graph that for this  $\rho$  it is advisable to have small  $v$ , since then, by choosing a suitable  $\delta$ , we can ensure longer insolation times than for large  $v$ .

Figure 90 plots the dependence  $\varepsilon(v)$  for various  $\delta$ ,  $\delta \leq \rho$ . Here the question of maximum insolation time during one circuit of revolution around the Earth is meaningless, since the maximum time is equal to the orbital revolution  $T_0$  of the satellite for all  $\delta < \rho$ . If now  $\delta > \rho$ , we see from Figure 89 that there exists a certain optimal  $v = v_{\max}$  ensuring maximum insolation time. In this case, we should clearly consider the choice of optimal parameters.

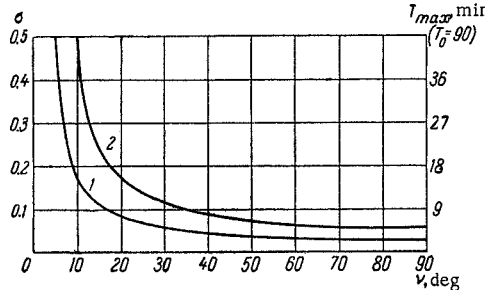


FIGURE 91. Maximum insolation time during one revolution  $T_{\max} = T_0 \sigma$  vs. angle  $v$  (in minutes):  
1)  $\rho = 5^\circ$ , 2)  $\rho = 10^\circ$ .

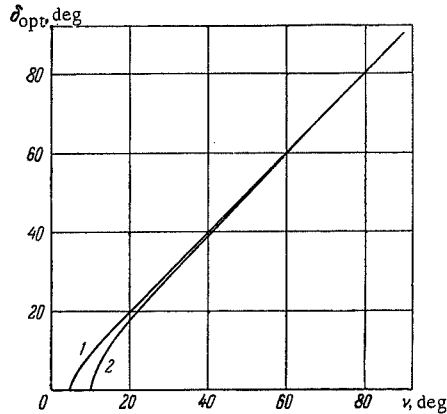


FIGURE 92. Optimal instrument setting angle vs.  $v$ :  
1)  $\rho = 5^\circ$ , 2)  $\rho = 10^\circ$ .

Let us investigate the following two problems.

1. The angle  $v$ , i.e., the orientation of the orbit relative to the Sun, is known. Find the instrument setting angle  $\delta$  which ensures maximum insolation  $T$ , and the magnitude of this maximum.

The formula

$$\cos \delta_{\text{opt}} = \frac{\cos v}{\cos \rho} \quad (11.1.3)$$

gives the optimal angle  $\delta$ . We see, in particular, that for  $v \gg \rho$ , we have  $\delta_{\text{opt}} \approx v$ . Inserting the optimal angle  $\delta_{\text{opt}}$  in (11.1.2), (11.1.1), we have

$$T_{\max} = \frac{T_0}{\pi} \arcsin \frac{\sin \rho}{\sin v}. \quad (11.1.4)$$

Figures 91, 92 plot  $\sigma = \frac{T_{\max}}{T_0}$  as a function of  $v$  and  $\delta_{\text{opt}}$  as a function of  $v$  for  $\rho = 5^\circ$  and  $\rho = 10^\circ$ .

2. Consider the inverse problem. The setting angle  $\delta$  is known. Find the angle  $v$  for which the insolation time is maximal, and calculate the magnitude of this maximum. We find

$$\cos v_{\text{opt}} = \frac{\cos \delta}{\cos \rho}, \quad T_{\max} = \frac{T_0}{\pi} \arcsin \frac{\sin \rho}{\sin v}.$$

In what follows, we shall often consider an orbit with  $i = 65^\circ$ , a revolution period  $T_0 = 90$  days, and a perigee height  $h_p = 225$  km. We shall refer to this as the typical orbit. The problem of the optimal orbit will be considered in § 3.

We have established that a reduction in  $v$  increases the insolation time. Therefore, for a given inclination of the orbit relative to the Earth's equator, it is advisable to choose the launch time (the hour of the day) so as to achieve a smallest possible  $v$ . Let a satellite be launched during vernal equinox (22 March). Then (see § 2), the smallest  $v$  attainable for the typical orbit is  $v \approx 25^\circ$ .

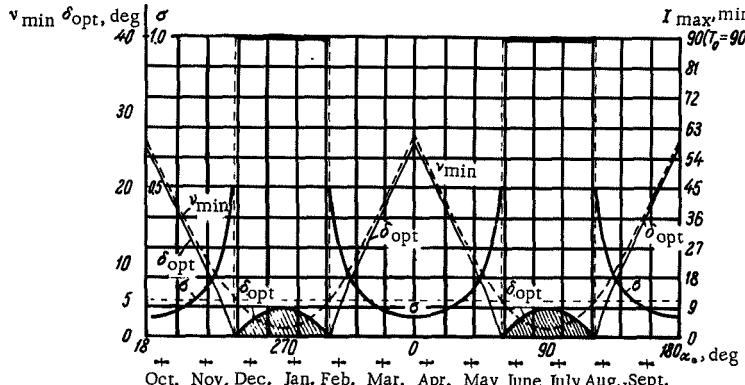


FIGURE 93. The maximum insolation time in orbit ( $\sigma = \frac{T_{\max}}{T_0}$ )

and the optimal setting angle  $\delta_{\text{opt}}$  vs. the day of the year (typical orbit,  $\rho = 5^\circ$ ).

We take the instrument angles  $\rho = 2^\circ 5$ ,  $\rho = 5^\circ$ ,  $\rho = 10^\circ$ . Then from (11.1.3) we find the respective optimal setting angles  $\delta_{\text{opt}} = 24^\circ 50'$ ,  $\delta_{\text{opt}} = 24^\circ 45'$ ,  $\delta_{\text{opt}} = 23^\circ 00'$  and the respective insolation times during one revolution  $T \approx 3$  min,  $T = 5.5$  min,  $T = 12$  min (for an orbital period  $T_0 = 90$  min).

Figure 93 plots the maximum insolation time during one revolution vs. the day of firing, for an optimal choice of the launch hour (bold solid line), and the optimal instrument setting angle vs. the day of firing (fine solid line) for  $\rho = 5^\circ$ .

The peculiar features of the graph are explained as follows. By choosing the optimal hour of launch, we ensure that the angle  $v$  takes the smallest possible value  $v_{\min}$  for that day of the year (dashed curve\*). This value, however, may be greater or smaller than the instrument angle (depending

\* The graph of  $v_{\min}$  vs. day of firing in Figure 93 is based on calculations which are reproduced at the end of the next section.

on the exact date). For an instrument angle  $\rho = 5^\circ$ ,  $v_{\min}$  is less than  $\rho$  if the satellite is launched in November—January or in May—July. During all the other months,  $v_{\min}$  is over  $5^\circ$ . But as we have shown before, for  $v < \rho$ , the satellite can be exposed to sunlight at all points of the orbit. To this end, it suffices to have the setting angle  $\delta$  smaller than the difference  $\rho - v$ .

The region  $\delta < \rho - v$  is cross hatched in the graph. In the months of November—January and May—July (for  $\rho = 5^\circ$ , or in other months for other  $\rho$ ), no single optimal  $\delta$  exists. By choosing any  $\delta$  from the cross hatched region, we ensure continuous illumination of the instrument during the entire revolution. The insolation time during one revolution is thus  $T = T_0 \approx 90$  min.

The situation is quite different for  $v > \rho$ , e.g., in January—April and in July—November for  $\rho = 5^\circ$ . Here each day is characterized by a single optimal setting angle  $\delta_{\text{opt}}$  defined by (11.1.3), which ensures the maximum insolation time (11.1.4). For  $v = \rho$  we have a singular case, since here  $\delta_{\text{opt}} = 0$ .

Note that for  $v < \rho$ ,  $\delta$  can be chosen uniquely if the requirement of maximum insolation time is supplemented by another requirement. For example, if  $\delta$  is chosen as follows:  $\delta = v$  for  $v < \frac{1}{2}\rho$  and  $\delta = \rho - v$  for  $\frac{1}{2}\rho < v < \rho$  then the instrument axis approaches the Sun to a minimum angular distance (as compared to other  $\delta$  with constant  $v$  and  $\rho$ ).

## §2. VARIATION OF ORBITAL ORIENTATION IN TIME

The diurnal variation in  $v$  may be as high as  $3^\circ$ , which is quite significant for our purposes. We proceed to derive the variation of  $v$  in time. Let (Figure 94)  $OAS$  be the plane of the ecliptic,  $OS$  the direction to the Sun,  $EAD$  the satellite's orbit,  $J$  the inclination of the orbit to the plane of the ecliptic,  $\bar{\Omega}$  the longitude of the orbit's ascending node from the point of vernal equinox,  $i$  and  $\Omega$  the corresponding elements relative to the equator,  $\alpha_0$  the longitude of the Sun from the point of vernal equinox,  $J^*$  the inclination of the Earth's equator to the ecliptic ( $J^* \approx 23^\circ.5$ ). Then

$$\left. \begin{aligned} \cos v &= -\sin(\alpha_0 - \bar{\Omega}) \sin J, \quad \alpha_0 = \alpha_0^0 + 2\pi \frac{t}{T_y}, \\ \cos J &= \cos J^* \cos i + \sin J^* \sin i \cos \Omega, \\ \sin \bar{\Omega} &= \frac{\sin i}{\sin J} \sin \Omega, \\ \Omega &= \Omega_0 - 2\pi k_0 \frac{t}{T_0}, \quad k_0 = \bar{\varepsilon} \left( \frac{\bar{a}}{a} \right)^2 \frac{\cos i}{(1 - e^2)^2}, \end{aligned} \right\} \quad (11.2.1)$$

where  $T_y$  is the length of the year,  $\alpha_0^0$  the initial value of  $\alpha_0$ ,  $T_0$  the period of orbital revolution,  $\bar{a}$  the Earth's radius,  $a$  the semimajor axis of the orbit,  $e$  the eccentricity of the orbit,  $\bar{\varepsilon} = 0.00163$ ,  $\Omega_0$  the initial longitude of the ascending node.

Time can be conveniently reckoned in units of  $\alpha_0$ , since

$$\Omega - \Omega_0 = -K(\alpha - \alpha_0^0),$$

$$K = \frac{k_0 T_y}{T_0}.$$

Substituting this expression in formulas for  $v$ , we find the dependence  $v(\alpha_0)$ , which describes the annual variation in the inclination  $v$ .

Calculations show that for the typical orbit  $K \approx 3.5$ . If the orbit passes through the poles ( $i = 90^\circ$ ), there is no precession:  $K=0, \Omega = \Omega_0$ . For an equatorial orbit ( $i = 0^\circ$ ), the precession is maximal, but it does not influence the time variation of the angle  $v$ , since here  $J=J^* = \text{const}$ ,  $\dot{\Omega} = 0$ , i.e., for an equatorial orbit, the variation in  $v$  does not depend on the hour of launch.

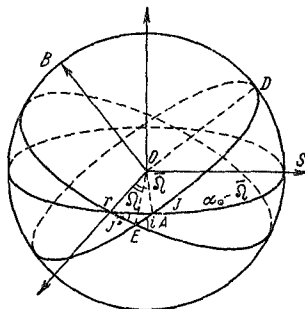


FIGURE 94. Relative position of the orbital plane  $AOD$ , the equatorial plane  $EOy$ , and the plane of the ecliptic  $OAS$ .

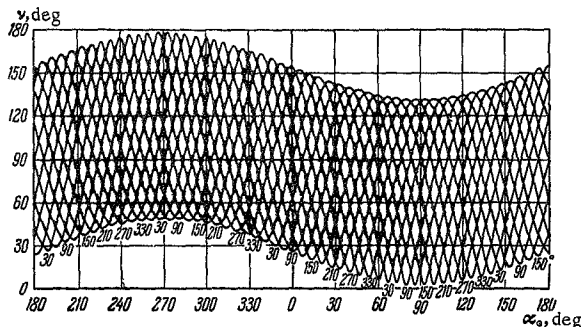


FIGURE 95. The angle  $v$  vs. the day of the year (typical orbit with  $i = 65^\circ$ ). The numerals near the curves give the corresponding values of  $\Omega_0$  (in degrees).

Figure 95 plots the curves  $v(\alpha_0)$  for  $i = 65^\circ$  as a function of  $\Omega_0$  ( $\Omega_0 = 0, 30, \dots, 330^\circ$ ) on 21 March ( $\alpha_0 = 0^\circ$ ).

From the angle  $\Omega$  and from the coordinates of the point of injection, we can easily calculate the launch hour. If the day of launch is known, we can always choose the hour of firing so that  $v$  should follow a desired curve.

The variation of  $v$  over the almost linear sections (Figure 95) at a rate of some  $3^\circ.5$  per day is attributable to the precession of the orbit. The effect produced by the annual motion is less pronounced for the typical orbit. The annual motion introduces a certain correction in the rate of change of  $v$ , and during the year the slope of the nearly linear sections to the axis  $\alpha_0$  varies so that  $\left| \frac{\Delta v}{\Delta \alpha_0} \right| \approx 3.5 \pm \delta^\circ$ , where  $\delta^\circ < 1^\circ$ . This clearly does not apply to the regions near the maxima and the minima of the  $v(\alpha_0)$  curves.

All the maxima and the minima fall on a single envelope, the curve  $\cos v_{\text{env}} = \pm \sin J$ . The best conditions for insolation in a given orbit are achieved near the summer and the winter solstices. On 21 December we have  $\max(v_{\text{max}}) \approx 179^\circ$ , i.e.,  $\min(180^\circ - v_{\text{max}}) \approx 1^\circ$ , and on 22 June we have  $\min(v_{\text{min}}) \approx 1^\circ$ . On any other day, the departure of  $v_{\text{min}}$  from zero is greater. Note that if the orbit is tangent to the polar circles ( $i = 66^\circ 30'$ ), the least  $v_{\text{min}}$  is zero.

The graph in Figure 95 shows that for almost two months in summer and in winter we can achieve  $v < 5^\circ$ , which for instrument angles  $\rho = 5^\circ$  ensures continuous illumination during one or several circuits of revolution.

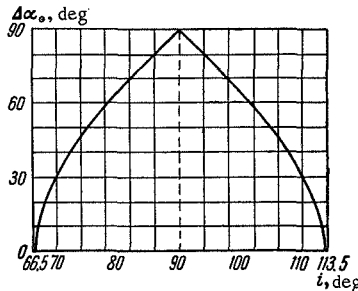


FIGURE 96. The longitude increment vs. orbital inclination.

The summer and the winter are by no means the best seasons for all types of orbits. This is true only for orbits with inclinations  $i \leq 90^\circ - J^*$  and  $i \geq 90^\circ + J^*$  to the equator, when the least  $v_{\text{min}}$  (or  $180^\circ - v_{\text{max}}$ ) are attained at the winter and the summer solstices.

For orbits with  $90^\circ + J^* > i > 90^\circ - J^*$  ( $i \neq 90^\circ$ ), the least  $v_{\text{min}}$  (or  $180^\circ - v_{\text{max}}$ ) can be attained at two points near the summer solstice and at two points near the winter solstice (and this least value will be zero); we thus have four minimum points  $\alpha_0^{(1,2)} = \alpha_0^{\text{sum}} \pm \Delta\alpha_0$ ;  $\alpha_0^{(3,4)} = \alpha_0^{\text{win}} \pm \Delta\alpha_0$ , where  $\alpha_0^{\text{sum}}$  and  $\alpha_0^{\text{win}}$  are the summer and the winter solstices, while  $\Delta\alpha_0$  is a function of  $i$  (Figure 96). For a polar orbit, the points  $\alpha_0^1$ ,  $\alpha_0^4$  and  $\alpha_0^2$ ,  $\alpha_0^3$  merge, and the best days of the year are two: the vernal and the autumnal equinoxes.

### § 3. DETERMINING THE TOTAL INSOLATION TIME

Since the orientation of the orbit varies in time, this factor must be taken into consideration in the analysis of insolation. The problem of greatest significance is how to ensure maximum continuous insolation, or alternatively, maximum total insolation.

Let us first consider the problem of maximum continuous insolation. It is simpler than the problem of maximum total insolation.

At a certain time ( $\alpha_0^*$ ,  $\Omega_k$ ) during the lifetime of a satellite which has been launched with the initial parameters  $\alpha_0^0$ ,  $\Omega_0$ , the normal to its orbital plane will make a minimum angle  $\nu = v_{\text{min}}$  with the sunward direction; after that, the angle  $\nu$  will start increasing. Let us find the continuous insolation time as a function of the attainable  $v_{\text{min}}$ . For  $v_{\text{min}} > \rho$ , continuous insolation

is possible only over part of the satellite's orbit. The maximum continuous insolation time is defined by (11.1.4), and in order to attain this insolation time, the instrument setting angle  $\delta$  must have the optimal value (11.1.3), where  $v=v_{\min}$ .

The case  $v_{\min} < \rho$  is, however, more interesting. Here,  $v$  may be smaller than the instrument angle  $\rho$ . In § 1 we showed that for  $v < \rho$ , continuous insolation is possible at all points of the orbit. Therefore, for a variable  $v$ , the continuous insolation time may be very large: it is in fact determined by the time that the angle  $v$  remains in the region  $v < \rho$ . We also showed that continuous illumination during the entire orbital period is possible for  $v < \rho - \delta$ . Hence it follows that the optimal setting angle needed to attain maximum continuous insolation is  $\delta_{\text{opt}} = 0$ .

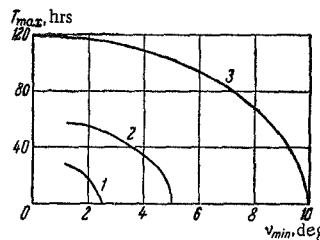


FIGURE 97. Maximum continuous insolation time vs.  $v_{\min}$  (typical orbit  $i = 65^\circ$  and setting angle  $\delta = 0$ ): 1)  $\rho = 2.5^\circ$ ; 2)  $\rho = 5^\circ$ ; 3)  $\rho = 10^\circ$ .

Figure 97 plots the continuous insolation time as a function of  $v_{\min}$  for  $v_{\min} < \rho$ , with  $\rho = 2.5^\circ, 5^\circ, 10^\circ$  and a setting angle  $\delta = 0$ , in an orbit with  $i = 65^\circ$ . We see that for  $\rho = 5^\circ$ , continuous insolation can be maintained for as long as 58 hours, i.e., almost for two and a half days. For  $\rho = 10^\circ$ , continuous insolation can be ensured almost for 120 hours. This is possible if the least  $v_{\min} \approx 1^\circ$ , as at the winter and the summer solstices (21 December and 22 June).

The graphs in Figure 97 show that if the least  $v_{\min}$  is not attained, the actual continuous insolation time in a certain neighborhood of this value is close to the maximum.

Note that an orbit with  $i = 65^\circ$  is the most convenient for prolonged insolation. In § 2 we showed that for orbits with  $113^\circ.5 \geq i \geq 66^\circ.5$ ,  $v = 0$  is attained four times a year, and not two times, as for orbits with  $i = 65^\circ$ . As  $i$  increases, the prospects of achieving maximum insolation time improve. Furthermore, the maximum insolation time increases with  $i$  on account of the reduction in the rate of precession of the orbit, and also because the least attainable  $v_{\min}$  for  $113^\circ.5 \geq i \geq 66^\circ.5$  is  $v_{\min} = 0$ , while for orbits with  $i = 65^\circ$ , the least  $v_{\min} \approx 1^\circ$ . For  $i > 90^\circ$ , the orbit precesses contrary to its precession for  $i < 90^\circ$ , and this partly compensates for the annual movement of the orbit. The angle  $v$  varies more slowly, which is beneficial for continuous insolation. For  $i$  close to  $113^\circ.5$ , however, the rate of precession is much greater than the rate of annual motion:  $v$  again changes at a faster rate and the conditions are not favorable for continuous insolation. There is consequently a certain optimal  $i_{\text{opt}} > 90^\circ$ , for which

the maximum continuous insolation can be attained. Figure 98 plots the continuous insolation time as a function of  $i$  for an orbit whose parameters (with the exception of  $i$ ) are those of the typical orbit. We see that  $i = 96^\circ.5$  is the optimal inclination which ensures continuous insolation for as long as  $T_{\max} \approx 605$  hours with  $\rho = 5^\circ$ ,  $T_{\max} = 309$  hours with  $\rho = 2^\circ.5$ , and  $T_{\max} = 186$  hours with  $\rho = 1^\circ.5$ . These insolation times are attainable in the neighborhood of 5 March and 6 April, 5 September and 7 October.

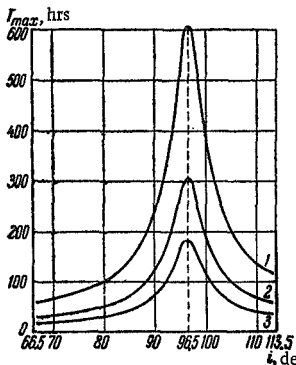


FIGURE 98. Maximum insolation time vs. orbit inclination: 1)  $\rho = 5^\circ$ , 2)  $\rho = 2^\circ.5$ , 3)  $\rho = 1^\circ.5$ .

In the following we shall show that the largest total insolation time is of the same order as the maximum continuous insolation time; orbits which are optimal as regards maximum continuous insolation are thus also optimal as regards maximum total insolation.

Let us now proceed with the determination of the total insolation time. The following three cases are distinguished, depending on the instrument setting angle  $\delta$  and the orbit inclination angle  $v$ :

(1) Insolation is possible only over part of the orbit. The total insolation time is the sum of insolation times during each revolution; this case obtains for  $\delta > \rho$ .

(2) Insolation is possible over part of the orbit and (after some time) at all points of the orbit; this case obtains for  $\delta < \rho$ .

(3) Only continuous insolation is possible; this case obtains for  $\delta = 0$  only (it has been analyzed in the preceding).

Let us consider cases (1) and (2). We shall first investigate the problem of the total insolation time  $T_2$  for arbitrary parameters.

In Figures 89, 90 we gave the insolation time vs.  $v$  for a given  $\delta$ . These graphs also apply in the case of variable  $v$ . Let  $v$  vary from  $v_0$  to  $v_{\min}$ , increasing again to  $v_0$ . This periodic variation in  $v$  ( $v_0 \rightarrow v_{\min} \rightarrow v_0$ ) can always be ensured if the launch time (the day and the hour) is suitably chosen and if the satellite lifetime is fairly long. Taking an appropriate  $v_{\min}$ , we thus achieve the maximum total insolation time attainable during the satellite's lifetime. Without loss of generality, let  $v_0$  be defined (for a given  $\delta$ ) by the equality  $v_0 = \delta + \rho$ , so that if  $v_0 > \delta + \rho$ , there is no insolation altogether, whereas if  $v_0 < \delta + \rho$ , we take another  $\delta$  which satisfies the equality. For  $v = v_0$ , we have  $s = 0$ , and the insolation time  $t_0 = 0$ . After one orbital

revolution of the satellite, we have  $v=v_0+\Delta v$ ,  $\varepsilon=\varepsilon_i$ , and insolation time  $t_i=T_0 \frac{\varepsilon_i}{\pi}$ , etc. The total insolation time is clearly

$$T_{\Sigma} = \frac{2T_0}{\pi} \sum_{v_{\min}}^{v_0} \varepsilon_i, \quad (11.3.1)$$

where the sum is taken over all the  $\varepsilon_i$  which occur during the variation of  $v$ .

A direct calculation based on (11.3.1) is fairly complicated since, first, the sum is taken over a great many and, second, the distance  $\Delta v$  between the terms of the sum is not constant; during one revolution, the orbital inclination changes by different amounts on different occasions. The sum (11.3.1) can be replaced approximately by some definite integral. Indeed,

the sum (11.3.1) may be written as  $T_{\Sigma} = \frac{2T_0}{\pi} \int_{v_{\min}}^{v_0} \varepsilon(v) \frac{dn}{dv} dv$ , where  $\Delta n_i$  is the increment

in the number of circuits corresponding to a change in  $v$  from  $v_i$  to  $v_{i+1}$  ( $\Delta n_i = 1$ ). Hence,

$$T_{\Sigma} \approx \frac{2T_0}{\pi} \int_{v_{\min}}^{v_0} \varepsilon(v) \frac{dn}{dv} dv = \frac{T_y}{\pi^2} \int_{v_{\min}}^{v_0} \varepsilon(v) \frac{da_{\odot}}{dv} dv. \quad (11.3.2)$$

The last equality follows from

$$\begin{aligned} a_{\odot} &= a_{\odot}^0 + 2\pi \frac{t}{T_y} = a_{\odot}^0 + 2\pi \frac{n T_0}{T_y}, \\ \frac{da_{\odot}}{dn} &= 2\pi \frac{T_0}{T_y}, \\ \frac{dn}{dv} &= \frac{dn}{da_{\odot}} \frac{da_{\odot}}{dv}. \end{aligned}$$

The integral (11.3.2) gives the total insolation time for the cases  $\delta > \rho$  only. For  $\delta < \rho$ , the insolation time is defined by (11.3.2) only if  $v_{\min} > \rho - \delta$ . If now  $v_{\min} < \rho - \delta$ , we have

$$T_{\Sigma} \approx \frac{T_y}{\pi^2} \int_{\rho-\delta}^{\rho+\delta} \varepsilon(v) \frac{da_{\odot}}{dv} dv + \Delta T. \quad (11.3.3)$$

Here  $\Delta T$  is the continuous insolation time. It is equal to the time it takes  $v$  to go from  $v=\rho-\delta$  to  $v=v_{\min}$  and back from  $v=v_{\min}$  to  $v=\rho-\delta$ . This time can be determined directly from the  $v=v(\alpha_{\odot})$  graphs (Figure 95).

The curves  $v(\alpha_{\odot})$  near the minima are approximated by the hyperbola

$$\frac{\bar{v}^2}{a^2} - \frac{\bar{a}_{\odot}^2}{a^2 \operatorname{tg}^2 \varphi} = 1, \quad \bar{v} = v - v_{\min} + a, \quad \bar{a}_{\odot} = a_{\odot} - a_{\odot}^m, \quad (11.3.4)$$

where  $a$  is the real semiaxis of the hyperbola,  $a_{\odot}^m$  the value of  $a_{\odot}$  corresponding to  $v=v_{\min}$ ;  $\varphi$  the opening half-angle of the asymptotes,

$$T_{\Sigma} \approx \frac{T_y}{\pi^2} |\operatorname{tg} \varphi| \int_{v_{\min}}^{v_0} \varepsilon(v) \frac{v + a - v_{\min}}{\sqrt{(v + a - v_{\min})^2 - a^2}} dv. \quad (11.3.5)$$

In calculations we may assume a constant  $|\operatorname{tg} \varphi|$  for all the  $v(\alpha_0)$  curves of Figure 95. The parameter  $a$  depends on  $v_{\min}$ . This dependence is determined from the following condition: for a certain  $\delta$  (which is common for all the curves), the true curve  $v(\alpha_0)$  merges with the asymptote of the hyperbola. The dependence  $a(v_{\min})$  is then approximated by the straight line shown in Figure 99 (for the curves of Figure 95, i.e., for the typical orbit). The dependence  $a(v)$  is defined by (11.1.2).

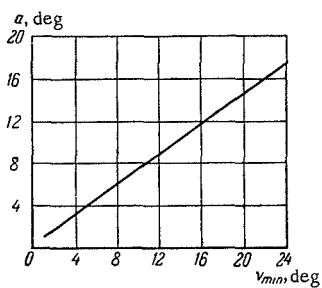


FIGURE 99. The approximate  $a(v_{\min})$  line.

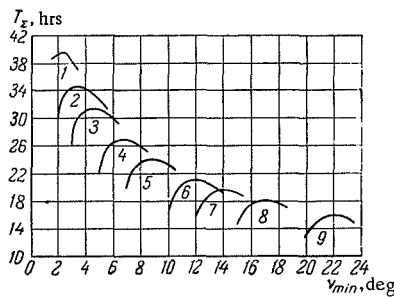


FIGURE 100. The total insolation time vs. the attainable  $v_{\min}$  (typical orbit,  $\rho = 5^\circ$ ):  
1)  $\delta = 6^\circ$ ; 2)  $\delta = 7^\circ$ ; 3)  $\delta = 8^\circ$ ; 4)  $\delta = 10^\circ$ ;  
5)  $\delta = 12^\circ$ ; 6)  $\delta = 15^\circ$ ; 7)  $\delta = 17^\circ$ ; 8)  $\delta = 20^\circ$ ; 9)  $\delta = 25^\circ$ .

Figure 100 plots the total insolation time as a function of the least attainable orbit inclination  $v=v_{\min}$  for  $\delta > \rho$ , with  $\rho = 5^\circ$ . We see from the graph that for each  $\delta$  there is a certain optimal  $v_{\min}$  which ensures a maximum insolation time. The dependence of the maximum insolation time  $T_{\max}$  on  $v_{\min}$  is plotted in Figure 101.

To attain this maximum insolation time, the instruments must be set at an optimal angle  $\delta_{\text{opt}}$ , whose dependence on  $v_{\min}$  (for  $\delta > \rho$ ) is plotted in Figure 102.

For  $\delta < \rho$  the insolation is qualitatively different (continuous insolation is possible during the entire revolution), and the dependence of the maximum insolation time  $T_{\max}$  on  $v_{\min}$  is therefore distinct. In some cases, calculations should be made according to (11.3.3). The dependence  $T_{\max}(v_{\min})$  for  $\delta < \rho$  is also plotted in Figure 101. We see that this curve meets the curve  $T_{\max}(v_{\min})$  for  $\delta > \rho$  at the point  $v_{\min} \approx 5^\circ$  (for  $\rho = 5^\circ$ ). Therefore, if for the particular time of year  $v_{\min} > 5^\circ$ , the optimal angle  $\delta_{\text{opt}} > \rho = 5^\circ$  should be chosen in accordance with Figure 102. If, however,  $v_{\min} < 5^\circ$ , the optimal angle  $\delta_{\text{opt}} < \rho = 5^\circ$ . Calculations show that for  $v_{\min} < 5^\circ$ ,

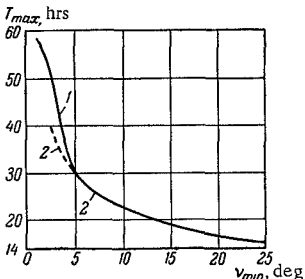


FIGURE 101. The maximum total insolation time vs.  $v_{\min}$  (typical orbit,  $\rho = 5^\circ$ ): 1) for  $\delta < \rho$ ; 2) for  $\delta > \rho$ ; the solid curve in the range  $v_{\min} > 5^\circ$  is the extension of the dashed curve 2 (curve 1, not shown in this interval, will pass below the solid line).

the angle  $\delta_{\text{opt}}$  can be selected between wide limits: a change of  $1-2^\circ$  in setting hardly affects the maximum insolation time  $T_{\max}$ . Figure 103 plots the maximum insolation time as a function of the setting angle  $\delta$  for  $\delta < \rho = 5^\circ$  and for various constant  $v_{\min}$ .

We see from the graph that if  $v_{\min} < 4^\circ$ , a change in  $\delta$  from 0 to  $3-4^\circ$  hardly affects the maximum insolation time. For the optimal  $\delta$  we may take  $\delta_{\text{opt}} = 0$ , since the insolation in this case is continuous.

For the typical orbit  $1^\circ < v_{\min} < 25^\circ$  (Figure 95), and we see from Figures 101 and 102 that in the best case the insolation time  $T_{\max} \approx 58$  hours for  $\rho = 5^\circ$  and similarly  $T_{\max} \approx 27$  hours for  $\rho = 2.5^\circ$ . In less favorable cases, the maximum insolation times are  $T_{\max} \approx 15$  hours for  $\rho = 5^\circ$  and  $T_{\max} \approx 6$  hours for  $\rho = 2.5^\circ$ .

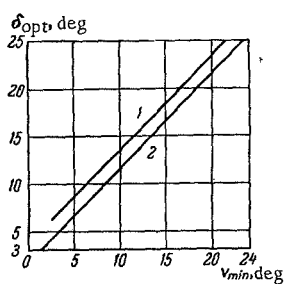


FIGURE 102. Optimal setting angle vs.  $v_{\min}$ : 1)  $\rho = 5^\circ$   
2)  $\rho = 2.5^\circ$ .

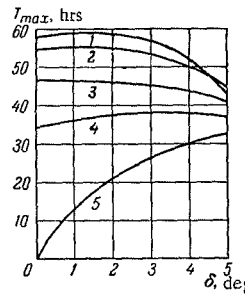


FIGURE 103. Maximum insolation time (for  $\delta < \rho = 5^\circ$ ) vs. instrument setting angle: 1)  $v_{\min} = 1^\circ$ ; 2)  $v_{\min} = 2^\circ$ ;  
3)  $v_{\min} = 3^\circ$ ; 4)  $v_{\min} = 4^\circ$ ; 5)  $v_{\min} = 5^\circ$ .

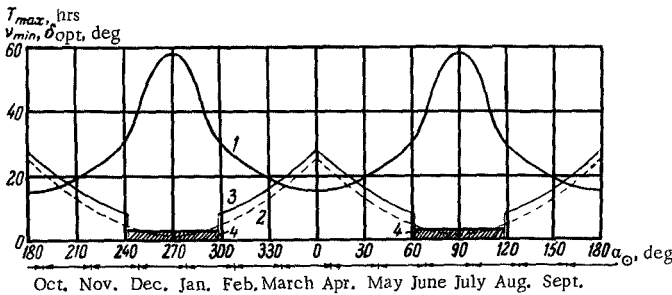


FIGURE 104. The maximum total insolation time attainable on a given date and the optimal setting angle of the instruments (typical orbit,  $\rho = 5^\circ$ ): 1)  $T_{\max}$  vs.  $a_0$ ; 2)  $v_{\min}$  vs.  $a_0$ ; 3)  $\delta_{\text{opt}}$  vs.  $a_0$ ; 4)  $\delta_{\text{opt}}$  regions for  $v_{\min} \leq \rho$ .

Since  $v_{\min}$  vs. the day of the year (Figure 95) and  $T_{\max}$  vs.  $v_{\min}$  (Figure 101) are known, we can plot the curve of  $T_{\max}$  vs. the day of the year. These graphs given in Figure 104 show that the maximum insolation time can be attained on any particular day if the optimal launch hour and the optimal setting angle are chosen. We see that the most favorable seasons are winter and summer: near the winter and summer solstices, insolation times of some 57-58 hours for  $\rho = 5^\circ$  and 27 hours for  $\rho = 2.5^\circ$  are attainable. The insolation will be continuous during the entire period if we take  $\delta = 0$ . These graphs also show that for two months every year, specifically during

the period 22 June  $\pm$  15 days and 21 December  $\pm$  15 days, a total insolation time of more than 50 hours can be attained for an instrument angle  $\rho = 5^\circ$ ; for instrument angles  $\rho = 2^\circ.5$ , the total insolation time during that period is over 16 hours. In the least favorable case, near the vernal and the autumnal equinoxes, the instruments with  $\rho = 5^\circ$  can be exposed to sunlight for 15 hours, and the instruments with  $\rho = 2^\circ.5$ , for 6 hours.

Figure 104 also plots the optimal setting angle  $\delta_{\text{opt}}$  of the instruments vs. the day of the year. It follows from the preceding that this dependence is not single-valued near the solstices: any  $\delta$  picked out from the cross hatched region in the graph ensures an insolation time which is approximately equal to that indicated in the plot. In particular, for  $\delta = 0$ , the insolation is continuous.

#### § 4. SUPPLEMENTS

Let us consider the influence of satellite eclipses (immersion in the Earth's shadow) on the conditions of insolation.

Let  $\theta$  be the angle between the lines joining the center of the Earth with the Sun and the satellite. Then

$$\cos \theta = \sin v \cos (\bar{u} - \psi),$$

$$\sin \psi = \frac{B}{\sin v},$$

$$\cos \psi = \frac{A}{\sin v},$$

$$A = \cos(a_O - \bar{\Omega}), \quad B = \sin(a_O - \bar{\Omega}) \cos J.$$

Here  $\bar{u}$  is the angle between the radius-vector and the intersection line of the orbit and the ecliptic.

Let  $R$  be the radius of the Earth,  $r$  the radius-vector of the orbit; it is easily shown that if  $\cos \theta < -\sqrt{1 - \left(\frac{R}{r}\right)^2}$ , the satellite is immersed in the Earth's shadow, and if  $\cos \theta > -\sqrt{1 - \left(\frac{R}{r}\right)^2}$ , the satellite is exposed to the Sun. In particular, if  $|\cos v| > \frac{R}{r_{\min}}$ , the satellite is illuminated by the Sun during the entire circuit ( $r_{\min}$  is the distance from the satellite's perigee point to the center of the Earth). Let the perigee height be  $h_* = 300$  km. Then  $|\cos v| > 0.9550$ , which implies that  $v < 17^\circ 40'$ . If  $h_* = 250$  km, the satellite is continuously insolated for  $v < 15^\circ 15'$ .

Hence it follows that for the principal cases of insolation, the occurrence of eclipses in no way affects the results of previous sections. Indeed, it is the noneclipsing region ( $v < 15^\circ$ ) which is of greatest significance, since the largest insolation times are attainable for these particular  $v$ . For example, to ensure continuous insolation for some 58 hours (with  $\rho = 5^\circ$ ), we must have  $v < 5^\circ$ . This is more than enough to prevent the satellite from eclipsing. The eclipsing region ( $v > 15^\circ$ ) is of secondary importance in connection with insolation problems. But even here the adverse effect of eclipses can be avoided by orienting the instrument not only relative to the binormal, but also relative to an axis which is perpendicular to the binormal (the setting angle with respect to this axis is determined in accordance with the initial conditions). Instruments oriented as indicated can be made to point to the Sun when the satellite is not eclipsed.

Let us evaluate the contribution from the nonuniform rotation of a satellite moving in an elliptical orbit. Since the angular velocity  $\omega$  in an orbit with eccentricity  $e$  ranges between the limits

$$\omega_m(1-e)^2 \leq \omega \leq \omega_m(1+e)^2$$

(where  $\omega_m = \sqrt{\frac{\mu P}{r^3}}$ ,  $P$  the focal parameter of the orbit,  $\mu$  the gravitational constant), the insolation time during one revolution varies between the limits

$$T_0 \frac{e}{\pi(1+e)^2} \leq T \leq T_0 \frac{e}{\pi(1-e)^2}.$$

Hence, the insolation time corrected for orbit ellipticity is  $T = T_0 \frac{e}{\pi}(1 \pm 2e)$ .

For  $e \leq 0.01$ , the correction is not greater than 2%. The variation in  $\omega$  is systematic, and it can be allowed for in calculations.

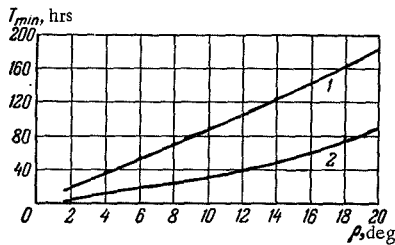


FIGURE 105. Minimum insolation time  $T_{\min}$  vs. instrument angle: 1) with programmed adjustment of the instrument axis; 2) without any corrections.

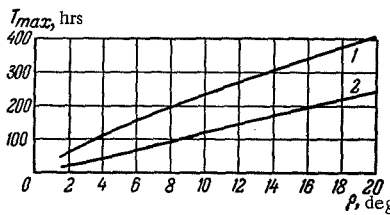


FIGURE 106. Maximum insolation time  $T_{\max}$  vs. instrument angle: 1) with programmed adjustment of the instrument axis; 2) without any corrections.

Trackers or programmed adjustment of the instrument axis permitting limited deviations from the mean attitude may increase the insolation time considerably (by a factor of 2–10). In practice, the introduction of these devices is equivalent to increasing the angle of view of the stationary instrument.

Figures 105 and 106 plot the minimum and the maximum insolation times as a function of the instrumental angle of view in two cases: for fixed setting of the instrument and for programmed adjustment of the instrument setting angle  $\delta$  between the limits  $\delta_{\min} < \delta < 90^\circ$ , where  $\delta_{\min} = \arccos \frac{\cos v_{\min}}{\cos p}$ ,  $\cos \delta = \frac{\cos v}{\cos p} = \cos \delta_{\text{opt}}$ .

## Appendix 1

### MOTION OF A RIGID BODY ABOUT A FIXED POINT IN A NEWTONIAN FORCE FIELD

Gravity torques have a substantial influence on the spin of artificial satellites. An analysis of these torques on a body with a fixed point will be very helpful in understanding the gravitational effects in the motion of satellites.

#### § 1. EQUATIONS OF MOTION. FIRST INTEGRALS

Let a fixed point  $O$  of the body be distant  $R$  from the center of attraction  $O^*$ . The point  $O$  is chosen as the origin of the system of fixed axes  $OXYZ$ , the axis  $OZ$  pointing away from the center of attraction. The origin of another, moving system of axes  $Ox'y'z'$  is also the point  $O$ ; the coordinate axes point along the principal axes of inertia of the body. Let  $\gamma, \gamma', \gamma''$  be the direction cosines of these inertial axes relative to the axis  $OZ$ . The Newtonian force function  $U$  on the rigid body is defined by (1.2.3).

The equations of motion of the rigid body about the fixed point  $O$  are

$$\left. \begin{aligned} A \frac{dp}{dt} + (C - B) qr &= \gamma'' \frac{\partial U}{\partial \gamma'} - \gamma' \frac{\partial U}{\partial \gamma''}, \\ B \frac{dq}{dt} + (A - C) rp &= \gamma \frac{\partial U}{\partial \gamma''} - \gamma'' \frac{\partial U}{\partial \gamma}, \\ C \frac{dr}{dt} + (B - A) pq &= \gamma' \frac{\partial U}{\partial \gamma} - \gamma \frac{\partial U}{\partial \gamma'}, \end{aligned} \right\} \quad (\text{A1.1.1})$$

$$\frac{d\gamma}{dt} = r\gamma' - q\gamma'', \quad \frac{d\gamma'}{dt} = p\gamma'' - r\gamma, \quad \frac{d\gamma''}{dt} = q\gamma - p\gamma' \quad (\text{A1.1.2})$$

Besides the exact equations of motion (A1.1.1), we shall also consider approximate equations consistent with the assumption that the distance  $R$  is large in comparison with the size of the body. The force function then has the form (1.2.7). Substituting this approximate expression of the force function in (A1.1.1), we obtain the equations of motion in the form /15/

$$\left. \begin{aligned} A \frac{dp}{dt} + (C - B) qr &= \\ &= -Mg(y'_0\gamma'' - z'_0\gamma') + 3 \frac{g}{R} (C - B) \gamma'\gamma'', \\ B \frac{dq}{dt} + (A - C) rp &= \\ &= -Mg(z'_0\gamma - x'_0\gamma'') + 3 \frac{g}{R} (A - C) \gamma''\gamma, \\ C \frac{dr}{dt} + (B - A) pq &= \\ &= -Mg(x'_0\gamma' - y'_0\gamma) + 3 \frac{g}{R} (B - A) \gamma\gamma'. \end{aligned} \right\} \quad (\text{A1.1.3})$$

Here  $g$  is the gravitational acceleration at a distance  $R$  from the center of attraction,  $x'_0, y'_0, z'_0$  are the coordinates of the body mass center. The equations of motion (A1.1.1), (A1.1.2) have three first integrals:

the energy integral

$$Ap^2 + Bq^2 + Cr^2 - 2U(\gamma, \gamma', \gamma'') = h, \quad (\text{A1.1.4})$$

the angular momentum integral

$$Ap\gamma + Bq\gamma' + Cr\gamma'' = k \quad (\text{A1.1.5})$$

and the relation between the direction cosines

$$\gamma^2 + \gamma'^2 + \gamma''^2 = 1. \quad (\text{A1.1.6})$$

When the approximate Newtonian force function is introduced, the integral (A1.1.4) is algebraic, having the form

$$Ap^2 + Bq^2 + Cr^2 + 2Mg(x'_0\gamma + y'_0\gamma' + z'_0\gamma'') + 3\frac{g}{R}(A\gamma^2 + B\gamma'^2 + C\gamma''^2) = h. \quad (\text{A1.1.6a})$$

A question of fundamental significance is whether or not the set (A1.1.1), (A1.1.2) or the set (A1.1.2), (A1.1.3) has a fourth integral. We shall consider three cases when a fourth integral exists and the equations are therefore integrable.

1. An analog of the Lagrange case for the motion of a heavy body. The exact equations of motion (A1.1.1), (A1.1.2) have the fourth integral

$$r = r_0, \quad (\text{A1.1.7})$$

if

$$A = B \quad (\text{A1.1.8})$$

and

$$\gamma' \frac{\partial U}{\partial \gamma} - \gamma \frac{\partial U}{\partial \gamma'} = 0. \quad (\text{A1.1.9})$$

The last condition is satisfied, in particular, if  $U$  is a function of  $\gamma''$  only, i.e.,  $U = U(\gamma'')$ . This holds true, e.g., for the approximate Newtonian force function (1.2.7) if the body mass center is on the axis of dynamic symmetry of the body, i.e., if  $x'_0 = y'_0 = 0$ .

2. The set (A1.1.2), (A1.1.3) has the fourth integral

$$x'_0 p + y'_0 q + z'_0 r = \text{const}, \quad (\text{A1.1.10})$$

if the body possesses complete dynamic symmetry ( $A = B = C$ ).

3. An analog of the Euler case for the motion of a heavy body. If the body is fixed at its center of mass, i.e.,

$$x'_0 = y'_0 = z'_0 = 0, \quad (\text{A1.1.11})$$

the equations of motion (A1.1.2), (A1.1.3) have the fourth integral

$$A^2 p^2 + B^2 q^2 + C^2 r^2 - 3\frac{g}{R}(BC\gamma^2 + AC\gamma'^2 + AB\gamma''^2) = l. \quad (\text{A1.1.12})$$

F. de Brun /76/ was the first to derive the integral (A1.1.12) in his analysis of the motion of a body, with each particle attracted to a certain fixed plane through the fixed point of the body with a force which is proportional to the distance from that plane. The equations of motion in this problem are formally identical with equations (A1.1.3), subject to the condition (A1.1.11); the only difference between the two cases is the meaning of the constant, which in (A1.1.3) is denoted by  $3\frac{g}{R}$ . The problem having the integral (A1.1.12) was reduced to quadratures in /81/, and by an alternative technique in /69/. E. I. Kharlamova /69/ also proposed a geometrical interpretation of motion for the particular case  $k=0$  in the integral (A1.1.5).

Yu. A. Arkhangel'skii /3, 4, 5/ has demonstrated that the problem being considered has no other single-valued general algebraic integrals, aside from those listed in this section.

## § 2. STABILITY OF STEADY-STATE SPIN /16/

**1. A body with a fixed mass center.** Let us consider the motion of a rigid body about its center of mass, using the approximate expression for the Newtonian force function. The equations of motion then have the integrals (A1.1.6a), (A1.1.5), (A1.1.12), (A1.1.6). By definition,  $\gamma''$  is the cosine of the angle made by the axis with the moment of inertia  $C$ ;  $\gamma'$  corresponds in the same sense to the moment  $B$ , and  $\gamma$  to the moment  $A$ .

The equations of motion in this case have the particular solution

$$r=r_0, \quad p=0, \quad q=0, \quad \gamma''=1, \quad \gamma=0, \quad \gamma'=0, \quad (\text{A1.2.1})$$

which describes the rotation of the body with a constant angular velocity  $r_0$  about a principal axis of inertia, the spin axis pointing to the center of attraction.

Let us investigate the stability of this motion.

The perturbed motion

$$r=r_0+\xi, \quad p, \quad q, \quad \gamma''=1+\delta, \quad \gamma, \quad \gamma' \quad (\text{A1.2.1a})$$

is described on first approximation by a linear system with a characteristic equation

$$\lambda^2 [\lambda^4 + m\lambda^2 + n] = 0, \quad (\text{A1.2.2})$$

$$m = -3\omega^2(a+b) + r_0^2(1+ab), \quad n = (3\omega^2 - r_0^2)^2 ab,$$

$$a = \frac{C-B}{A}, \quad b = \frac{C-A}{B}, \quad \omega^2 = \frac{g}{R}. \quad (\text{A1.2.3})$$

If at least one of the inequalities

$$n < 0, \quad m < 0, \quad m^2 - 4n < 0 \quad (\text{A1.2.4})$$

is satisfied, then among the roots of equation (A1.2.2) there is at least one root with a positive real part. The corresponding unperturbed motion is unstable.

Let the body spin about a central axis of inertia, i.e.,  $A > C > B$  or  $B > C > A$ . Then  $n < 0$ , and for any  $r_0$  the rotation about the central axis of inertia is unstable.

Let now the body spin about the largest axis of the ellipsoid of inertia. Then

$$C < A, \quad C < B. \quad (\text{A1.2.5})$$

From the integrals (A1.1.6a), (A1.1.12), (A1.1.6), we can easily derive the following integrals:

$$Ap^2 + Bq^2 + Cr^2 + 3\omega^2 \{(A - C)\gamma^2 + (B - C)\gamma'^2\} = V_1^0, \quad (\text{A1.2.6})$$

$$\begin{aligned} A(C - A)p^2 + B(C - B)q^2 + \\ + 3\omega^2(A - C)(C - B)(\gamma^2 + \gamma'^2) = V_2^0 \end{aligned} \quad (\text{A1.2.7})$$

Here  $V_1^0, V_2^0$  are constants. The quadratic form  $V_2^0$ , in virtue of condition (A1.2.5), is symmetric (nonalternant) in the variables  $p, q, \gamma, \gamma'$ . The motion is thus stable with respect to these variables. But then, from (A1.2.6) follows stability with respect to  $r$ , and from (A1.1.8) stability with respect to  $\gamma''$ . The spin about the axis with the least moment of inertia is thus stable for any  $r_0$ .

Let now

$$C > A, \quad C > B, \quad (\text{A1.2.8})$$

i.e., the body spins about the axis with the largest moment of inertia (about the least axis of the ellipsoid of inertia). Then  $a > 0, b > 0$ . We shall find a sufficient condition for the stability of rotation. The perturbed motion (A1.2.1a) has the following integrals:

$$\begin{aligned} Ap^2 + Bq^2 + C\zeta^2 + 2Cr_0\zeta + 3\omega^2 \{(A - C)\gamma^2 + (B - C)\gamma'^2\} = V_1, \\ 2Ap\gamma + 2Bq\gamma' + 2C\zeta - Cr_0(\gamma^2 + \gamma'^2 + \delta^2) - \\ - 2C\zeta(\gamma^2 + \gamma'^2 + \delta^2) = V_2, \\ A^2p^2 + B^2q^2 + C^2\zeta^2 + 2C^2r_0\zeta - \\ - 3\omega^2 \{B(C - A)\gamma^2 + A(C - B)\gamma'^2\} = V_3. \end{aligned}$$

We shall seek a Lyapunov function in the form

$$L = V_1 - r_0(1 + \kappa C)V_2 + \kappa V_3,$$

where  $\kappa$  is (meanwhile) an arbitrary factor. Then  $L = V + w$ , where  $V$  is a quadratic form, and  $w$  incorporates terms of third order.

If the quadratic form  $V$  is nonalternant,  $L$  is also nonalternant. The quadratic form  $V$  is written as

$$\begin{aligned} V = (1 + \kappa A)Ap^2 - 2r_0(1 + \kappa C)Ap\gamma + \\ + \gamma^2 \{3\omega^2(A - C)(1 + \kappa B) + Cr_0^2(1 + \kappa C)\} + \\ + (1 + \kappa B)Bq^2 - 2r_0(1 + \kappa C)Bq\gamma' + \\ + \gamma'^2 \{3\omega^2(B - C)(1 + \kappa A) + Cr_0^2(1 + \kappa C)\} + \\ + (1 + \kappa C)C\zeta^2 + Cr_0^2(1 + \kappa C)\delta^2 \end{aligned}$$

and it is positive definite if

$$\kappa > -\frac{1}{C}, \quad r_0^2 > 3\omega^2 \frac{(1+\kappa A)(1+\kappa B)}{(1+\kappa C)}.$$

The curve

$$\psi(\kappa) = \frac{(1+\kappa A)(1+\kappa B)}{(1+\kappa C)}$$

has a minimum  $\psi(\kappa_1) = \left\{ \frac{\sqrt{a} + \sqrt{b}}{1 + \sqrt{ab}} \right\}^2$  at the point  $\kappa_1 = -\frac{1}{C}(1 - \sqrt{ab}) > -\frac{1}{C}$ . If now  $\kappa_1$  is substituted for  $\kappa$  in the function  $L$ , we come to the following conclusion: the spin about the axis with the largest moment of inertia is stable if

$$r_0^2 > 3\omega^2 \left\{ \frac{\sqrt{a} + \sqrt{b}}{1 + \sqrt{ab}} \right\}^2. \quad (\text{A1.2.9})$$

We shall now show that the motion is unstable if the inequality is reversed.

Since invariably  $a < 1$  and  $b < 1$ , we have  $\frac{a+b}{1+ab} < \left\{ \frac{\sqrt{a} + \sqrt{b}}{1 + \sqrt{ab}} \right\}^2$ . Let us first consider the case  $r_0^2 < 3\omega^2 \frac{a+b}{1+ab}$ . Then  $m < 0$  and the motion is unstable. Let now

$$3\omega^2 \frac{a+b}{1+ab} < r_0^2 < 3\omega^2 \left\{ \frac{\sqrt{a} + \sqrt{b}}{1 + \sqrt{ab}} \right\}^2.$$

Then

$$r_0^2(1+ab) > 3\omega^2(a+b). \quad (\text{A1.2.10})$$

Reversing the inequality in (A1.2.9) and seeing that  $a < 1$ ,  $b < 1$ , we have  $r_0^2 < 3\omega^2$ ; then, from (A1.2.10),

$$r_0^2(1 - \sqrt{ab})^2 > 3\omega^2(\sqrt{a} - \sqrt{b})^2. \quad (\text{A1.2.11})$$

But it is easily seen that the expression  $m^2 - 4n$  entering one of the inequalities in (A1.2.4) can be written as

$$m^2 - 4n = \{r_0^2(1 - \sqrt{ab})^2 - 3\omega^2(\sqrt{a} - \sqrt{b})^2\} \{r_0^2(1 + \sqrt{ab})^2 - 3\omega^2(\sqrt{a} + \sqrt{b})^2\}.$$

From (A1.2.11) and from (A1.2.9) with a reversed inequality, we have  $m^2 - 4n < 0$ , i.e., the unperturbed motion is unstable.

The spin about the least axis of the ellipsoid of inertia is thus stable if and only if condition (A1.2.9) is satisfied. The angular velocity

$$r_* = \sqrt{3}\omega \frac{\sqrt{a} + \sqrt{b}}{1 + \sqrt{ab}}$$

may be termed the critical angular velocity.

Note that if  $r_0^2 \geq 3\omega^2$ , the stability condition (A1.2.9) is satisfied a fortiori. Let us estimate the spin velocities required for stable motion. On the Earth's surface, we have  $g = 9.81 \text{ m/sec}^2$ ,  $R = 6,371,000 \text{ m}$ ,

$r_0 \geq \sqrt{3 \frac{g}{R}} = 0.00215$  rad/sec; the spin is thus stable already for angular velocities of the order of 0.1 deg/sec, the motion becoming unstable for very low spin rates indeed.

In our problem, the spin about the major axis of the ellipsoid of inertia is thus stable irrespective of the angular velocity, whereas the spin about the least axis of the ellipsoid of inertia is stable only if the angular velocity is greater than a certain critical value. Otherwise, the spin is unstable. No stable rotation about the medium axis of inertia is possible.

It also follows from the preceding that a body fixed at its mass center in a Newtonian central field is in equilibrium only if one of the axes of the ellipsoid of inertia points to the center of attraction. This equilibrium, however, is unstable if the least or the medium axis points in this direction; stability is achieved only if the largest axis of the ellipsoid of inertia is oriented as specified. In our symbols, the condition of stable equilibrium is thus (A1.2.5).

Also note that the axes of permanent rotations of the body can be found, their stability being investigated by the same technique. This was done by G. K. Pozharitskii /62/.

2. Stability of steady-state spin in the case  $A=B$ ,  $U=U(\gamma')$ . The equations of motion (A1.1.1), (A1.1.2) in the case  $A=B$ ,  $U=U(\gamma')$  have the particular solution

$$p=0, \quad q=0, \quad r=r_0, \quad \gamma=0, \quad \gamma'=0, \quad \gamma''=1, \quad (\text{A1.1.12})$$

which describes spin with a constant angular velocity around the axis of kinetic symmetry, provided this axis points to the center of attraction.

The perturbed motion  $p$ ,  $q$ ,  $r=r_0+\zeta$ ,  $\gamma$ ,  $\gamma'$ ,  $\gamma''=1+\delta$  possesses the integrals

$$V_1 = A(p^2+q^2) + C(\zeta^2+2\zeta) - 2 \left( \frac{\partial U}{\partial \gamma''} \right)_{\gamma''=1} \delta - 2 \left( \frac{\partial^2 U}{\partial \gamma''^2} \right)_{\gamma''=1} \delta^2 + w(\delta^3, \dots),$$

$$V_2 = A(p\gamma + q\gamma') + C(\zeta\delta + \zeta + r_0\delta),$$

$$V_3 = \gamma^2 + \gamma'^2 + \delta^2 + 2\delta = 0, \quad V_4 = \zeta.$$

In the expression for  $V_1$ , the function  $U(1+\delta)$  has been series-expanded in  $\delta$ , so that  $w$  incorporates terms above the second order of smallness.

Following N. G. Chetaev's method /73/, we shall seek a Lyapunov function  $L$  as a quadratic combination of the integrals:

$$L = V_1 + 2\alpha V_2 - \left[ - \left( \frac{\partial U}{\partial \gamma''} \right)_{\gamma''=1} + Cr_0\alpha \right] V_3 - 2C(r_0+\alpha)V_4 + \frac{C(C-A)}{A} V_4^2 + \left( \frac{\partial^2 U}{\partial \gamma''^2} \right)_{\gamma''=1} V_3 \delta.$$

In virtue of the equations of motion, the derivative of  $L$  is

$$\frac{dL}{dt} = \left( \frac{\partial^2 U}{\partial \gamma''^2} \right)_{\gamma''=1} V_3 \frac{d\delta}{dt} = 0,$$

since  $V_3 = 0$ . The unperturbed motion is therefore stable if  $L$  is a non-alternant function.

The function  $L$  may be written as  $L = V + w^*$ , where  $V$  is a quadratic form,  $w^*$  incorporating terms above the second order of smallness. The function  $L$  is nonalternant, if the quadratic form  $V$  preserves a constant

sign. This quadratic form is written as

$$V = Ap^2 + 2\alpha Ap\gamma - \left[ -\left( \frac{\partial U}{\partial \gamma''} \right)_{\gamma'=1} + Cr_0x \right] \gamma^2 + \\ + Aq^2 + 2\alpha Aq\gamma' - \left[ -\left( \frac{\partial U}{\partial \gamma'''} \right)_{\gamma'''=1} + Cr_0x \right] \gamma'^2 + \\ + \frac{C}{A} \zeta^2 + 2\alpha C\zeta\delta - \left[ -\left( \frac{\partial U}{\partial \gamma''''} \right)_{\gamma''''=1} + Cr_0x \right] \delta^2.$$

If

$$C^2r_0^2 + 4A \left( \frac{\partial U}{\partial \gamma''} \right)_{\gamma'=1} > 0, \quad (\text{A1.2.13})$$

there exists a  $\alpha$  such that  $V$  is a positive definite quadratic form.

Condition (A1.2.13) is thus a sufficient condition for the stability of the

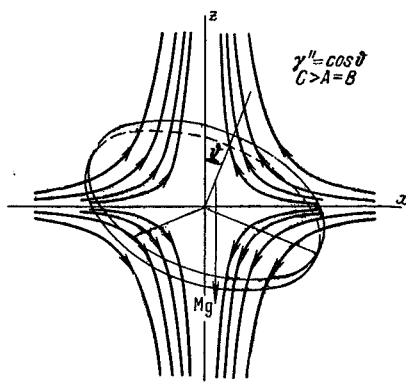


FIGURE 107. An oblate ellipsoid of inertia in a perturbation force field.

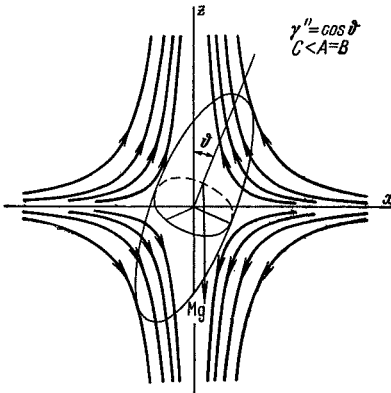


FIGURE 108. A prolate ellipsoid of inertia in a perturbation force field.

unperturbed motion (A1.2.12). An analysis of the first-order equations readily shows that for

$$C^2r_0^2 + 4A \left( \frac{\partial U}{\partial \gamma''} \right)_{\gamma'=1} < 0$$

the unperturbed motion is unstable. Indeed, (A1.2.13) is a necessary and sufficient condition of stability in an arbitrary force field  $U(\gamma')$  (a Newtonian field, in particular).

If  $U = -Mgz'_0\gamma'$ , condition (A1.2.13) reduces to the well-known condition for the stability of the steady-state motion of a heavy rigid body in the Lagrange case /73/:

$$C^2r_0^2 > 4AMgz'_0. \quad (\text{A1.2.14})$$

If the Newtonian field is approximately represented as  $U = -Mgz'_0\gamma'' - \frac{3}{2} \frac{g}{R} (C - A)\gamma'^2$ , condition (A1.2.13) is written in the form

$$C^2r_0^2 > 4A \left\{ Mgz'_0 + \frac{3}{2} \frac{g}{R} (C - A) \right\}. \quad (\text{A1.2.15})$$

For  $C > A$ , this condition is more rigid than condition (A1.2.14), while for  $C < A$  it is less demanding; this is not unexpected, since for  $C > A$  the perturbation forces produce a destabilizing effect (Figure 107), whereas for  $C < A$  they act as a restoring factor (Figure 108).

For  $r_0 = 0$  and  $z'_0 = 0$ , we have a sufficient condition of stability for the equilibrium of a body with a fixed mass center.

For  $z'_0 = 0$ ,  $r_0 \neq 0$ , we have a stability condition for a body spinning about its mass center  $r_0^2 > 4 \frac{A}{C} \frac{C-A}{C} 3 \frac{g}{R}$ , which reduces to condition (A1.2.9) for  $A=B$ .

### § 3. SOME CASES OF INTEGRABLE EQUATIONS AND ANALYSIS OF MOTION

1. The case of planar motion. This case obtains if

$$\left( \frac{\partial U}{\partial \gamma'} \right)_{\gamma'=0} = 0. \quad (\text{A1.3.1})$$

The equations of motion then have the particular solution  $p=0$ ,  $r=0$ ,  $\gamma'=0$ ,  $q=-\dot{\theta}$ ,  $\gamma''=\cos \theta$ ,  $\gamma=\sin \theta$ , where  $\theta$  is determined from the easily integrable equation  $B \frac{d^2 \theta}{dt^2} - \frac{\partial U}{\partial \theta} = 0$ . We have

$$\left. \begin{aligned} t - t_0 &= \int_{\theta_0}^{\theta} \frac{d\theta}{\sqrt{h + \frac{2}{B} U(\theta)}}, \\ h &= \dot{\theta}_0^2 - \frac{2}{B} U(\theta_0), \quad \dot{\theta}_0 = \left( \frac{d\theta}{dt} \right)_{t=t_0}. \end{aligned} \right\} \quad (\text{A1.3.2})$$

The motion of the body for various initial values can be determined by the conventional energy-balance technique frequently adopted in the theory of oscillations /20/.

When an approximate Newtonian force field is introduced, condition (A1.3.1) reduces to  $y'_0 = 0$ , and solution (A1.3.2) takes the form

$$t - t_0 = \int_{\theta_0}^{\theta} \frac{d\theta}{\sqrt{h + \frac{2Mga}{B} \cos(\theta + \delta) + \frac{3}{2} \frac{g}{R} \frac{A-C}{B} \cos 2\theta}}, \quad (\text{A1.3.3})$$

where

$$a = \sqrt{x_0^2 + z_0^2}, \quad \delta = \arcsin \frac{z'_0}{a} = \arccos \left( -\frac{z'_0}{a} \right),$$

$$h = \omega_0^2 - \frac{2Mga}{B} \cos(\theta_0 + \delta) - \frac{3}{2} \frac{g}{R} \frac{A-C}{B} \cos 2\theta_0,$$

$$\theta_0 = \theta(t_0), \quad \omega_0 = \dot{\theta}(t_0).$$

Inverting the integral (A1.3.3), we obtain the required solution.

Let the body be fixed at its mass center, i.e.,  $a=0$ . The motion is then entirely equivalent to the planar motion of a satellite in a circular orbit under gravity torques, and it is therefore described by the formulas in Chapter 2, § 2.

2. The case  $A=B$ ,  $U=U(\gamma'')$ . The first integrals of motion have the form

$$p^2 + q^2 - \frac{2U}{A} = h, \quad p\gamma + q\gamma' + br_0\gamma'' = k,$$

$$\gamma^2 + \gamma'^2 + \gamma''^2 = 1, \quad r = r_0.$$

Here  $b = \frac{C}{A}$ . Let  $\theta$ ,  $\psi$ ,  $\phi$  be the Eulerian angles, where  $\theta$  is the angle between the body axis of symmetry and the direction from the center of attraction to the fixed point,  $\psi$  the angle of precession. The energy and the angular momentum integrals take the form

$$\left. \begin{aligned} \sin^2 \theta \dot{\psi}^2 + \dot{\theta}^2 &= h + \frac{2U(\cos \theta)}{A}, \\ \sin^2 \theta \dot{\psi} &= k - br_0 \cos \theta. \end{aligned} \right\} \quad (\text{A1.3.4})$$

The variables can be easily separated in this set, and the problem reduces to quadratures:

$$\begin{aligned} \left( \frac{du}{dt} \right)^2 &= (1-u^2) \left[ h + \frac{2U(u)}{A} \right] - [k - br_0 u]^2 \equiv f(u), \\ u &= \cos \theta \equiv \gamma'', \\ \frac{d\psi}{dt} &= \frac{k - br_0 u}{1 - u^2}. \end{aligned}$$

Separating the variables and integrating, we find

$$t + C = \int \frac{du}{\sqrt{f(u)}}. \quad (\text{A1.3.5})$$

Inversion of the integral (A1.3.5) gives the corresponding time dependence, and all the unknown quantities may then be written as functions of time.

In the particular case

$$U = -Mgz'_0\gamma'',$$

we have the solution of the classical Lagrange problem on the motion of a heavy rigid body.

If

$$U = -Mgz'_0\gamma'' - \frac{3}{2} \frac{g}{R} (C - A) \gamma''^2,$$

we have the solution for the motion of a rigid body in a Newtonian force field (approximate representation) which is the analog of the Lagrange case.

3. One case of motion of a rigid body about a fixed point in a Newtonian force field /17/. Let us consider the following motion of a body about a fixed point in a Newtonian force field. The body is dynamically symmetric ( $A=B$ ), the fixed point is its center of mass; the initial conditions are as follows: the transverse spin components are zero ( $p_0=q_0=0$ ), and the axial component is arbitrary ( $r_0 \neq 0$ ). If there were no Newtonian forces, the body axis, as we know, would preserve a constant orientation in space. The movement of the body axis in this case is therefore entirely attributable to the presence of the Newtonian field. The contribution of the Newtonian field in this example emerges unobstructed by secondary factors connected

with the introduction of complex, general initial conditions. It is for this reason that this case merits special investigation.

This problem on the motion of a rigid body about a fixed point is integrable in quadratures as a particular case of two more general integrable instances that we have considered before (analogs of the Euler and the Lagrange cases).

The quadratures (A1.3.4) take the form

$$\left(\frac{du}{dt}\right)^2 = (1 - u^2)[h + m\omega^2 u^2] - [k - br_0 u]^2 \equiv f(u),$$

$$\text{where } \frac{d\psi}{dt} = \frac{k - br_0 u}{1 - u^2},$$

$$m = 3 \frac{A - C}{C}, \quad \omega^2 = \frac{g}{R}, \quad u = \cos \theta.$$

With our initial conditions ( $p_0 = q_0 = 0$ ), we have

$$h = -m\omega^2 u_0^2, \quad k = br_0 u_0$$

and thus

$$\left. \begin{aligned} \left(\frac{du}{dt}\right)^2 &= f(u), \\ f(u) &= (u_0 - u) \{ -(1 - u^2)(u + u_0)m\omega^2 - \\ &\quad - (u_0 - u)b^2 r_0^2 \}, \end{aligned} \right\} \quad (\text{A1.3.6})$$

$$\frac{d\psi}{dt} = br_0 \frac{u_0 - u}{1 - u^2}. \quad (\text{A1.3.7})$$

The motion can be analyzed without inverting the elliptical quadratures (A1.3.6), (A1.3.7). From (A1.3.6) it follows that the real motion occurs in a certain  $u$  interval between the following limits: the initial  $u_0$  and some  $u_1$  related with  $u_0$  by the expression

$$u_0 = u_1 \frac{b^2 r_0^2 - (1 - u_1^2)m\omega^2}{b^2 r_0^2 + (1 - u_1^2)m\omega^2}. \quad (\text{A1.3.8})$$

The body axis will thus trace a curve lying between the parallels  $u_0$  and  $u_1$  on the surface of a unit sphere centered at the mass center of the body.

Let  $V$  be the angle between the curve traced by the body axis and a meridian on the unit sphere; then

$$\operatorname{tg} V = -(1 - u^2) \frac{d\psi}{du} = -br_0 \frac{u - u_0}{Vf(u)}.$$

Hence,  $\operatorname{tg} V = 0$  for  $u = u_0$ , i.e., a turning point occurs on the parallel  $u = u_0$ . For  $u = u_1$ ,  $\operatorname{tg} V = \infty$ , i.e., the locus is tangent to the parallel  $u_1$ .

The precessing rates are clearly maximal on the parallel  $u_1$ :  $\dot{\psi}(u_1) = \dot{\psi}_{\max}$ . We introduce a mean rate of precession

$$\langle \dot{\psi} \rangle = \frac{1}{2} [\dot{\psi}(u_0) + \dot{\psi}(u_1)] = \frac{1}{2} \dot{\psi}(u_1). \quad (\text{A1.3.9})$$

Inserting (A1.3.8) in (A1.3.7) and applying (A1.3.9), we find

$$\langle \dot{\psi} \rangle = -3\omega^2 \frac{A - C}{Cr_0} \frac{\cos \theta_1}{1 + 3 \sin^2 \theta_1 \left( \frac{\omega}{r_0} \right)^2 \left( \frac{A - C}{C} \right) \frac{A}{C}}. \quad (\text{A1.3.10})$$

Here  $\theta_1$  is expressed in terms of  $\theta_0$  and the problem parameters in accordance with (A1.3.8). If  $\frac{\omega}{r_0} \ll 1$ , i.e., the perturbations are small, then to terms of first order of smallness,

$$\langle \dot{\psi} \rangle \approx -3\omega^2 \frac{A-C}{Cr_0} \cos \theta_0. \quad (\text{A1.3.11})$$

Let us consider expression (A1.3.8). This dependence for various values of the parameter

$$\zeta = \frac{b^2 r_0^2}{m \omega^2} \quad (\text{A1.3.12})$$

is schematically shown in Figure 109. These curves are highly useful in grasping the general pattern of motion. We shall first consider the region  $\zeta > 0$  or, equivalently,  $m > 0$  (a prolate body). This region lies between the

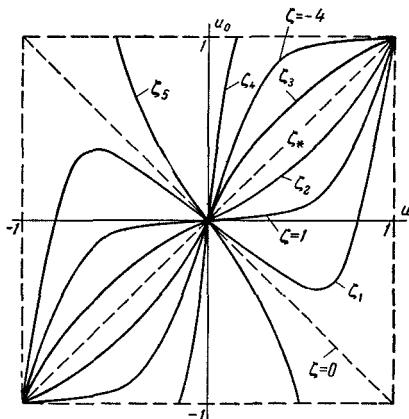


FIGURE 109. The boundaries  $u_0$ ,  $u_1$  of motion.

bisectors  $u_0 = \pm u_1$  and contains the  $u_1$  axis. If  $\zeta = \zeta_2 > 1$ , for each  $u_0$  there is a single  $u_1$ , which approaches  $u_0$  as  $\zeta$  increases; here  $|u_1| > |u_0|$ ,  $u_1$  and  $u_0$  having like signs. The curve for  $\zeta = 1$  is tangent to the  $u_1$  axis. With  $\zeta = \zeta_1 < 1$ , for each  $u_0$  there is either one or three  $u_1$  (the polynomial  $f(u_1)$  together with  $u_0$  has two or four real roots). But in permitted motion,  $u_1$  and  $u_0$  have like signs (this easily follows from expression (A1.3.6) for  $f(u)$  in this case). We again have the condition  $|u_1| > |u_0|$ .

In the case  $\zeta > 0$  the motion has the following trend: the parallel  $u_1$  is nearer to the pole of the unit sphere than the parallel  $u_0$ ; the locus curve is tangent to the parallel  $u_1$  and has a turning point on  $u_0$  (Figure 110a).

For an oblate body  $m < 0$ , and therefore  $\zeta < 0$ . In this case, for each  $u_0$  there is always one  $u_1$  (Figure 109). If now  $\zeta < -1$ , e.g.,  $\zeta = \zeta_3$  or  $\zeta = \zeta_4$  in Figure 109,  $u_1$  and  $u_0$  have like signs and  $|u_1| < |u_0|$ . The turning points lie on the initial parallel  $u_0$  which is nearer to the pole than  $u_1$  (Figure 110b). If  $\zeta = \zeta_0 > -1$ ,  $u_1$  and  $u_0$  have unlike signs, the satellite axis moving across the equator of the unit sphere; qualitatively, the locus is the same as in Figure 110b.

Note that the curve  $\zeta = -4$  (Figure 109) is tangent to the horizontal lines  $u_0 = \pm 1$  at the points  $u_1 = \pm 1$ . Hence it follows that the motion  $u_0 = u_1 = \pm 1$  (spin around an axis pointing to the center of attraction) is stable if  $|\zeta| = |\zeta_s| \geq 4$  and unstable if  $|\zeta| = |\zeta_s| < 4$ : in the former case, an infinitesimal departure of  $u_0$  from unity produces an infinitesimal departure of  $u_1$  from unity, whereas in the latter case, as we see from Figure 109,  $u_1$  displays a finite deviation from unity for any arbitrarily small deviation of  $u_0$ . For  $\zeta > 0$ , i.e., for a prolate body, we see from Figure 109 that the motion  $u_0 = u_1 = \pm 1$  is always stable. The necessary and sufficient conditions for the stability of spin about the vertical axis are thus

$$\zeta > 0, \quad \zeta < -4.$$

This result is identical with one of the relations of § 2, where the stability conditions have been derived by the Lyapunov—Chetaev technique.

Note that for  $\zeta \rightarrow +0$ ,  $u_1 \rightarrow \pm 1$ , which corresponds to the reduction of space motion to planar motion with  $r_0 \rightarrow 0$ . In this case  $\langle \dot{\psi} \rangle \rightarrow 0$ , as we see from (A1.3.10), and the symmetry axis of a prolate body oscillates across the

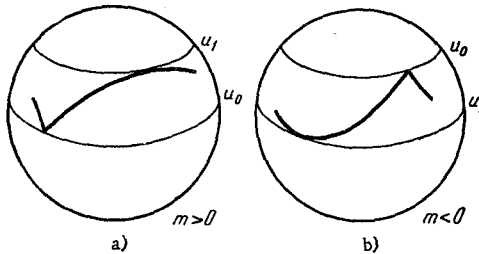


FIGURE 110. The path of a body axis on a unit sphere.

pole ( $u_1 = +1$  or  $-1$ , depending on the sign of  $u_0$ ) in the range bounded by the parallel  $\theta_0 = \arccos u_0$ . If  $\zeta \rightarrow -0$ ,  $u_1 \rightarrow -u_0$ , and the symmetry axis of an oblate body oscillates across the equator between two equidistant parallels.

If  $r_0$  is close to zero, or at least  $r_0 \ll \omega$ , then (for an oblate body)

$$\langle \dot{\psi} \rangle \approx \frac{C}{A} r_0 \frac{\cos \theta_0}{\sin^2 \theta_0}$$

and the period of precession is

$$T_\psi = \frac{2\pi}{r_0} \frac{A}{C} \frac{\sin^2 \theta_0}{\cos \theta_0}.$$

The nutation period is close to the period of plane oscillations,

$$T_0 = \sqrt{\frac{4K(k^2)}{3\theta^2 \frac{C-A}{C}}}, \quad k^2 = \cos^2 \theta_0;$$

$K$  is the complete elliptical integral of the first kind.

Take the nutation-to-precession ratio

$$\frac{T_0}{T_\psi} = \frac{2K(\cos^2 \theta_0)}{\pi \sqrt{3 \frac{C-A}{C}}} \frac{C}{A} \frac{r_0}{\omega} \frac{\cos \theta_0}{\sin^2 \theta_0}. \quad (\text{A1.3.13})$$

Since

$$\frac{2}{\pi} K(\cos^2 \theta_0) = 1 + \left(\frac{1}{2}\right)^2 \cos^2 \theta_0 + \left(\frac{1}{2} \cdot \frac{3}{4}\right)^2 \cos^4 \theta_0 + \dots$$

then in the case of small oscillations in a narrow equatorial belt ( $\theta_0=90^\circ - \theta^*$ , a small  $\theta^*$ ) we approximately have

$$\frac{T_0}{T_\psi} \approx \frac{\frac{C}{A} \sin \theta^*}{\sqrt{3 \frac{C-A}{C}}} \frac{r_0}{\omega}.$$

Since by assumption  $r_0 \ll \omega$  and  $\theta^*$  is small, a great many nutations are contained in a single period of precession, so that a small segment of the locus on the surface of a unit sphere is made up from numerous "lobes". As the initial point moves away from the equator, however, both the nutation amplitude and the "lobe" width grow due to the increase of  $K(\cos^2 \theta_0)$  in the numerator and the decrease of  $\sin^2 \theta_0$  in the denominator of (A1.3.13).

In a general case, the difference  $\Delta = u_1 - u_0$  in the cosines of the boundary latitudes, as it follows from (A1.3.8), is

$$\Delta = 2 \cos \theta_1 \sin^2 \theta_1 \frac{x_*}{1+x_* \sin^2 \theta_1}; \quad x_* = \frac{1}{\xi}. \quad (\text{A1.3.14})$$

For a fast spinning body, we have  $\frac{\omega}{r_0} \ll 1$ ,  $x_* = \frac{1}{\xi} \ll 1$ , and as we see from Figure 109,  $\theta_1 = \theta_0 + \delta$ , where  $\delta$  is small. Then from (A1.3.8)

$$\Delta = 2x_* u_0 (1 - u_0^2),$$

i.e.,

$$\Delta = 6 \left(\frac{\omega}{r_0}\right)^2 \left(\frac{A-C}{C}\right) \frac{A}{C} \cos \theta_0 \sin^2 \theta_0. \quad (\text{A1.3.15})$$

The precession period, according to (A1.3.11), is a large quantity of the order of  $\frac{r_0}{\omega}$ :

$$T_\psi = \frac{2\pi}{3 \frac{A-C}{C} \cos \theta_0 \omega} \left(\frac{r_0}{\omega}\right).$$

Let us now estimate the nutation period of a fast spinning body.

We take  $u=u_0+x$ , where  $x$  is a small quantity. Then from (A1.3.6), retaining under the radical terms of first and second order of smallness only, we have

$$\frac{dx}{dt} = \sqrt{x [2m\omega^2 u_0 (1 - u_0^2) - xb^2 r_0^2]}.$$

Hence the nutation halfperiod

$$\frac{\tau}{2} = \int_0^{\Delta} \frac{dx}{\sqrt{x[2m\omega^2 u_0(1-u_0^2) - xb^2 r_0^2]}} = \frac{\pi}{br_0}.$$

We see that the nutation is extremely rapid. The locus traced on a unit sphere contains numerous fine "lobes".

In conclusion we note that for  $A \gg C$  the motion is close to plane oscillations (in the same sense as for  $r_0 \rightarrow 0$ ), since in the limit ( $C=0$ ) expressions (A1.3.6) and (A1.3.7) reduce to the equations of plane oscillations.

## Appendix 2

### THE ORBIT OF AN EQUATORIAL EARTH SATELLITE

The solution of the equations of motion for a point in the equatorial plane of an oblate spheroid which has been used in Chapters 2 and 4 is based on the existence of two integrals of motion in the field of any distance-dependent central force; with the aid of these two integrals, the problem can be reduced to quadratures /80/ or analyzed qualitatively /47/. It is of course interesting to consider this solution in application to the particular case of an artificial Earth satellite traveling in an equatorial orbit. The solution of this problem in polar coordinates is expressed in terms of elliptical functions. Seeing that the general problem of satellite movement is best solved in osculating elements /61/, we should first establish their variation in a case which lends itself to exact solution. In this way we shall be able to trace the relation between the properties of motion and the behavior of the osculating elements.

In this Appendix we investigate the properties of the trajectory and the variation of the osculating orbital elements of an equatorial satellite.

For the potential  $V$ , to terms of first order of smallness with respect to the Earth's flattening, we have

$$V = \frac{\mu}{R} + \bar{\varepsilon} \frac{R_e^2 \mu}{3R^3}, \quad (\text{A2.1})$$

where  $R$  is the satellite's distance from the center of gravitation,  $\bar{\varepsilon}$  a dimensionless coefficient, which in accordance with /39/ is defined as  $\bar{\varepsilon} = \alpha_R - \frac{m}{2}$ ,  $m = \frac{\Omega^2 R_e}{g_e}$ ,  $R_e$  the equatorial radius of the Earth,  $\Omega$  angular velocity of the Earth's spin,  $g_e$  gravitational acceleration at the equator;  $\alpha_R$  is the Earth's flattening,  $\alpha_R = \frac{R_e - R_p}{R_e}$ , where  $R_p$  is the Earth's polar radius, numerically,  $\bar{\varepsilon} = 0.0016331$ . Furthermore,  $\mu = fM$ , where  $f$  is the gravitational constant,  $M$  the Earth's mass.

The motion will be regarded as planar; it possesses the areal integral and the energy integral:

$$R^2 \frac{d\varphi_R}{dt} = C, \quad (\text{A2.2})$$

$$v^2 - \frac{2\mu}{R} - \bar{\varepsilon} \frac{2\mu R_e^2}{3R^3} = h, \quad (\text{A2.3})$$

where

$$h = v_0^2 - \frac{2\mu}{R_0} - \bar{\varepsilon} \frac{2\mu R_e^2}{3R_0^3}, \quad C = r_0 v_0 \sin \varphi^*. \quad (\text{A2.4})$$

Here  $\varphi^*$  is the angle between the initial directions of the radius-vector  $r$  and of the velocity vector  $v$ ,  $\varphi_R$  is the polar angle reckoned from a fixed direction.

The motion is determined by the roots of the polynomial

$$P(u) = u^3 - \frac{3C^3}{2\bar{\epsilon}\mu R_e^2} u^2 + \frac{3C^2}{\bar{\epsilon}R_e^2} u + \frac{3hC^3}{2\bar{\epsilon}\mu R_e^2}, \quad u = \frac{C}{R}. \quad (\text{A2.4})$$

Let  $h < 0$ . This condition, unlike the case  $h \geq 0$ , gives trajectories which do not recede to infinity.

For  $h < 0$ , the polynomial (A2.4) has either one or three real positive roots. The actual initial velocities of artificial Earth satellites correspond to the case of the three real roots  $0 < u_3 < u_2 < u_1$ ; in permitted motion,  $P(u) > 0$ ,  $u$  ranges in one of the two intervals  $u_3 \leq u \leq u_2$  or  $u_1 \leq u \leq \infty$ . The second interval represents periodic motion through the center of gravitation. In reality, the initial data are such that the  $u$  of the artificial Earth satellite falls in the first of the two permitted intervals.

The roots  $u_1, u_2, u_3$  may be expressed in terms of the coefficients of the polynomial (A2.4) by solving the cubic  $P(u)=0$ . Integration of the equations of motion then yields the trajectory of the equatorial satellite

$$R(\varphi_R) = \frac{\frac{C}{u_3}}{1 + \left(\frac{u_2}{u_3} - 1\right) \operatorname{sn}^2 [\sqrt{(u_1 - u_3) A} (\varphi_R - \varphi_{R1}), k^2]}, \quad (\text{A2.5})$$

$$k^2 = \frac{u_2 - u_3}{u_1 - u_3} < 1, \quad A = \frac{\bar{\epsilon}_1 R_e^2}{6C^3}. \quad (\text{A2.6})$$

The radius-vector is thus a periodic function of  $\varphi_R$ , with a period  $T_R$ :

$$T_R = \frac{2}{\sqrt{(u_1 - u_3) A}} K(k^2). \quad (\text{A2.7})$$

Here  $K$  is the complete elliptical integral of the first kind. Since  $T_R \neq 2\pi$ , the distance to the satellite does not assume the initial value as the radius-vector rotates through  $2\pi$ . The initial distance is attained when the radius-vector rotates through  $T_R$ . This implies that the satellite's trajectory, in general, is not closed, tracing a curve schematically shown in Figure 111.

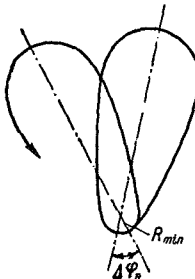


FIGURE 111. A schematic trajectory of the equatorial satellite.

From (A2.5) we see that at the points

$$\theta_{\max} = \theta_1 \text{ and } \theta_{\min} = \theta_1 + \sqrt{\frac{1}{A(u_1 - u_3)}} 2K$$

the distance  $R$  is respectively maximal and minimal:  $R_a = \frac{C}{u_3}$ ,  $R_\pi = \frac{C}{u_2}$ . The roots  $u_2$  and  $u_3$  thus have the following meaning:

$$u_2 = \frac{C}{R_\pi}, \quad u_3 = \frac{C}{R_a},$$

where  $R_a$  and  $R_\pi$  are respectively the apogee and the perigee distances,  $R_a$  and  $R_\pi$  are known with fair accuracy from the theory of satellite motion in elliptical orbits, and we can thus avoid resorting to the complicated formulas for the solution of the cubic  $P(u)=0$ . We shall henceforth assume that  $R_a$  and  $R_\pi$  are exactly known. Putting

$$\tilde{P} = \frac{2R_\pi R_a}{R_\pi + R_a}, \quad \tilde{e} = \frac{R_a - R_\pi}{R_a + R_\pi}, \quad \tilde{a}_* = \sqrt{(u_1 - u_3)A}$$

and reckoning the motion from the perigee point (in perigee  $\varphi_R = \varphi_{R\pi} = 0$ ), we may write the equation of the trajectory (A2.5) in the form

$$R(\varphi_R) = \frac{\tilde{P}}{1 + \tilde{e} [\operatorname{cn}^2 \psi_R - \operatorname{sn}^2 \psi_R]}, \quad \psi_R = \tilde{a}_* \varphi_R. \quad (\text{A2.5a})$$

In the limit, for  $\tilde{e} \rightarrow 0$ ,  $\operatorname{cn} \psi = \cos \frac{\varphi_R}{2}$ ,  $\operatorname{sn} \psi = \sin \frac{\varphi_R}{2}$ , and (A2.5a) reduces to an elliptical orbit.

During the time between two successive perigee passages, the radius-vector of the perigee will have rotated through the angle  $\Delta\varphi_R = T_R - 2\pi$ . Let us find a relation between  $\Delta\varphi_R$  and the orbital parameters. Since according to one of Vieta's relations  $u_1 + u_2 + u_3 = \frac{3C^3}{2\tilde{e}\mu R_e^2} = \frac{1}{4A}$ , we have

$$\Delta\varphi_R = \frac{4K(k^2)}{\sqrt{1 - 4A(u_2 + 2u_3)}} - 2\pi, \quad (\text{A2.8})$$

where on account of (A2.6)

$$k^2 = \frac{4A(u_2 - u_3)}{1 - 4A(u_2 + 2u_3)}. \quad (\text{A2.9})$$

In the case of no perturbations,  $A=0$  and from (A2.8) we have  $\Delta\varphi_R=0$ . In general, however,  $\Delta\varphi_R \neq 0$ .

We now express (A2.8) in terms of  $\tilde{P}$  and  $\tilde{e}$ . We have

$$\left. \begin{aligned} 1 - 4A(u_2 + 2u_3) &= 1 - \frac{2}{3}\tilde{e} \frac{R_e^2}{\tilde{P}^2} (3 - \tilde{e}), \\ 4A(u_2 - u_3) &= \frac{4}{3}\tilde{e} \frac{R_e^2}{\tilde{P}^2} \tilde{e}. \end{aligned} \right\} \quad (\text{A2.9a})$$

Since moreover

$$\tilde{P} = R_\pi(1 + \tilde{e}), \quad (\text{A2.10})$$

expressions (A2.8) and (A2.10) give the required dependence of  $\Delta\varphi_R$  on the parameters of the orbit:

$$\Delta\varphi_R = f(R_\pi, \tilde{e}).$$

Figure 112 plots this dependence for  $R_\pi = R + h_\pi$ , with  $h_\pi = 320$  km. We see that the rate of regression of the perigee does not exceed  $0^\circ.6$  per revolution. For an orbit with a greater perigee height, the rate of regression is even smaller. The rate of regression is a nearly linear function of the orbit's elongation parameter  $\tilde{e}$ .

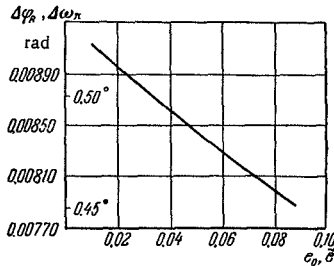


FIGURE 112. Secular regression of the perigee point for the orbit of an equatorial satellite ( $h_\pi = 320$  km).

The curvature  $\kappa_a$  of the trajectory in apogee (i.e., for  $\varphi_R = \varphi_{R1}$ ) is not equal to the perigee curvature  $\kappa_\pi$  (i.e., for  $\varphi_R = \varphi_{R\min}$ ):

$$\kappa_\pi = \frac{1}{\tilde{P}} [1 + \tilde{e} - 4\tilde{e}\tilde{a}_*^2(1 - k^2)], \quad \kappa_a = \frac{1}{\tilde{P}} [1 - \tilde{e} + 4\tilde{e}\tilde{a}_*^2],$$

$$\tilde{a}_*^2 = \frac{1}{4} \left\{ 1 - \frac{2}{3} \tilde{e} \frac{R^2}{\tilde{P}^2} (3 - \tilde{e}) \right\}, \quad k^2 = \frac{4\tilde{e} \frac{R^2}{\tilde{P}^2} \tilde{e}}{3 - 2\tilde{e} \frac{R^2}{\tilde{P}^2} (3 - \tilde{e})}.$$

It is easily seen that always  $\kappa_a < \kappa_\pi$ . Hence, the trajectory may be regarded as a certain oval figure rotating in its own plane which is sharper in perigee and blunter in apogee (Figure 111).

If the trajectory of the satellite is known, integration of (A2.2) gives the time dependence of motion.

This problem can also be solved by the conventional celestial-mechanical method of osculating elements. The equations in osculating elements for the case of a central perturbing force have the form (see /32/)

$$\frac{d\theta}{dt} = S_1 \sin v, \quad (A2.11)$$

$$\frac{d\omega_\pi}{dt} = -\frac{1}{e} S_1 \cos v, \quad (A2.12)$$

$$\frac{dP}{dt} = 0. \quad (A2.13)$$

Here  $S_1 = \sqrt{\frac{P}{\mu}} S(R)$ , and  $S(R)$  is the perturbation acceleration,  $e$  the eccentricity of the osculating ellipse,  $P$  its focal parameter; the absolute

magnitude of the radius-vector is given by the relation  $R = \frac{P}{1+e \cos v}$ . The angle  $v$  is reckoned from the line joining the center of gravitation with the perigee point; this line is not stationary in space, making a variable angle  $\omega_\pi$  with a certain fixed direction. The perturbation being central, the equations in osculating elements do not contain an equation for the angle  $i$  of the orbit's inclination to the equator and for the longitude  $\Omega$  of the ascending node; the angle  $i$  remains constant ( $i=0$ ), whilst the movement of the node is combined with the movement of the orbit's perigee to produce the overall effect of in-plane orbital rotation described by equation (A2.12).

From (A2.13) we have  $P=P_0$ , i.e., the focal parameter of an equatorial orbit remains constant. This property obtains for arbitrary central perturbations /32/, and in a certain degree it implies that the figure of the orbit is not altered in the rotating system of axes.

We now change over to the true anomaly  $v$  as the independent variable in equations (A2.11) and (A2.12).

The substitution-of-variables formula for the general case will be found, e.g., in /36/ and /61/. In our case, the relation between  $dt$  and  $dv$  can be obtained as follows. The forces being central, we have the areal integral  $R^2 \frac{d\varphi_R}{dt} = C = \sqrt{\mu P}$ . But since the polar angle  $\varphi_R$  is given by  $\varphi_R = v + \omega_\pi$ , then  $\frac{dv}{dt} = \frac{C}{R^2} - \frac{d\omega_\pi}{dt}$ , where  $\frac{d\omega_\pi}{dt}$  is determined from (A2.12). Hence

$$\left. \begin{aligned} \frac{dv}{dt} &= \frac{\sqrt{\mu P}}{R^2} + \frac{1}{e} \sqrt{\frac{P}{\mu}} S \cos v, \\ dt &= \frac{R^2 dv}{\sqrt{\mu P} + \frac{R^2}{e} \sqrt{\frac{P}{\mu}} S \cos v}. \end{aligned} \right\} \quad (\text{A2.14})$$

Equations (A2.14) relate the differentials  $dt$  and  $dv$ . Note that, in accordance with (A2.14),  $v$  is not necessarily a monotonic function of time, and it is therefore not always a suitable independent variable.

The equations in osculating elements for the case of the central perturbation acceleration  $S(R)$  take the form

$$\frac{d\omega_\pi}{dv} = \frac{-R^2 S \sqrt{\frac{P}{\mu}} \cos v}{\sqrt{\mu P} e + \sqrt{\frac{P}{\mu}} R^2 S \cos v}, \quad (\text{A2.15})$$

$$\frac{de}{dv} = \frac{\sqrt{\frac{P}{\mu}} R^2 S e \sin v}{\sqrt{\mu P} e + \sqrt{\frac{P}{\mu}} R^2 S(R) \cos v}. \quad (\text{A2.16})$$

We have assumed that  $\frac{dv}{dt} \neq 0$ .

The solution of equations (A2.15), (A2.16) for any  $S(R)$  is reduced to quadratures. Putting

$$R^2 S(R) = f(R) \equiv F(1 + e \cos v),$$

we substitute new variables  $e=y$ ,  $e \cos v=u$ . The integral of equation (A2.16) is then written as

$$y^2 + \frac{2}{\mu} \int F(1+u) du = \text{const.} \quad (\text{A2.17})$$

Hence  $e$  can be found as a function of  $v$ , and then, by taking the quadrature of (A2.15), we find  $\omega_n = \omega_n(v)$ . In the particular case of a satellite orbiting in the Earth's equatorial plane, we have

$$S = -\frac{\bar{\epsilon} \mu R_e^2}{R^4}.$$

Then from (A2.17) we obtain the following equation for  $e(v)$ :

$$\frac{3}{2}(e^2 - e_0^2) = \bar{\epsilon} \frac{R_e^2}{P_0^2} [(1 + e \cos v)^3 - (1 + e_0)^3], \quad e_0 = e(0). \quad (\text{A2.18})$$

Having thus found  $e(v)$ , we obtain from (A2.15) the following formula for the regression of the perigee:

$$\omega_n - \omega_{n0} = \int \frac{\bar{\epsilon} \frac{R_e^2}{P_0^2} (1 + e \cos v)^2 \cos v dv}{e - \bar{\epsilon} \frac{R_e^2}{P_0^2} (1 + e \cos v)^2 \cos v}. \quad (\text{A2.19})$$

To find the regression of the perigee  $\Delta\omega_n$  per one circuit of revolution, formula (A2.19) should be integrated from 0 to  $2\pi$ . The function  $\Delta\omega_n(e_0)$  obtained in this way is plotted in Figure 112.

In the scale of Figure 112, the lines plotting  $\Delta\varphi_R(\bar{\epsilon})$  and  $\Delta\omega_n(e_0)$  virtually coincide. The results of (A2.8) and (A2.19) are identical to within  $\bar{\epsilon}$ :

$$\Delta\varphi_R = 2\pi \bar{\epsilon} \frac{R_e^2}{P_0^2}, \quad \Delta\omega_n = 2\pi \bar{\epsilon} \frac{R_e^2}{P_0^2}. \quad (\text{A2.20})$$

Figures 113, 114 give the variation of the osculating elements with  $v$  for various initial conditions. Figure 113 brings out the periodic and the secular regressions of the perigee argument  $\omega_n$ . For low-eccentricity orbits, the periodic fluctuations in  $\omega_n$  are fairly large (for  $e_0 = 0.01$ , the

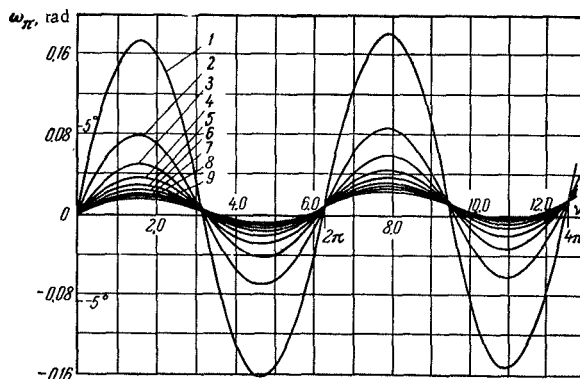


FIGURE 113. Variation of the osculating perigee argument (for  $h_x = 320$  km):

1) initial eccentricity  $e_0 = 0.01$ ; 2)  $e_0 = 0.02$ , etc., 9)  $e_0 = 0.09$ .

amplitude of these oscillations is as large as  $10^\circ$ . The eccentricity  $e$ , however, remains fairly constant, the slight fluctuations in this parameter being hardly dependent on the initial  $e_0$  (see Figure 114).

From (A2.18) it follows that for  $v=0$ ,  $e=e_{\max}=e_0$ , and for  $v=\pi$ ,  $e_{\min} \approx e_0 - 2\varepsilon \left(\frac{R_e}{P_0}\right)^2$ , providing that  $e_0$  is sufficiently large to ensure  $e_{\min} > 0$ . The fact that the osculating eccentricity is less in apogee than in perigee implies that the curvature of the trajectory at the apogee point is greater than in perigee (as we have already observed). For very small  $e_0$  (comparable with  $\varepsilon$  and even smaller), the dependence  $e(v)$  is different from that plotted in Figure 114; invariably  $e(v) > 0$ .

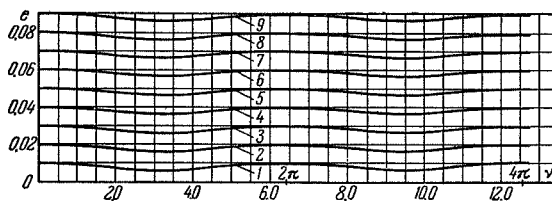


FIGURE 114. Variation of the osculating eccentricity.  
Notations as in Figure 113.

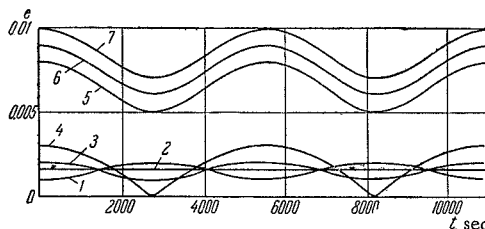


FIGURE 115. Variation of the osculating eccentricity for orbits with a small initial eccentricity:

- 1)  $e_0 = 0.001$ ; 2)  $e_0 = 0.0016$ ; 3)  $e_0 = 0.002$ ; 4)  $e_0 = 0.003$ ;
- 5)  $e_0 = 0.008$ ; 6)  $e_0 = 0.009$ ; 7)  $e_0 = 0.010$ .

Figure 115 plots  $e(t)$  for small  $e_0$ . Note that for small  $e_0 < \varepsilon \frac{R^2}{R_0^2}$ ,  $v$  is no longer a monotonic function of time, and, as we have previously observed, it cannot be used as an independent variable. In particular, for a circular orbit  $v = \text{const}$ , which is obviously a disqualifying property for a prospective independent variable. Indeed, equations (A2.11), (A2.12), (A2.14) have a solution  $v=0, e=e_0 = \varepsilon \frac{R_e^2}{R_0^2}, P=P_0, R=R_0, \omega_\pi = \frac{\sqrt{\mu P_0}}{R_0^2} (t - t_0) + \omega_{\pi 0}$  which shows that in osculating elements the circular orbit is described by an ellipse which rotates with an angular velocity  $|\dot{\omega}_\pi| = \frac{\sqrt{\mu P_0}}{R_0^2}$ , the satellite constantly occupying the perigee point of this osculating ellipse ( $v=0$ ). We are indebted to T.M. Eneev for this example. We see that sometimes in perturbed motion  $\frac{dv}{dt} \equiv 0$  for arbitrarily small perturbations ( $S \neq 0$ ).

## BIBLIOGRAPHY

1. APPELL, P. *Traité de Mécanique Rationnelle*, Vol. II. — Paris, Gauthier-Villars. 1953.
2. ARNOL'D, V. I. *Malye znamenateli i problemy ustoichivosti dvizheniya v klassicheskoi i nebesnoi mehanike* (Small Denominators and the Stability of Motion in Classical and Celestial Mechanics). — *Uspekhi Matematicheskikh Nauk*, 18(6) : 91 — 192. 1963.
3. ARKHANGEL'SKII, Yu. A. *Ob odnoznachnykh integralakh v zadache o dvizhenii tverdogo tela v n'yutonovskom pole sil* (On Single-Valued Integrals for the Motion of a Rigid Body in a Newtonian Force Field). — *Prikladnaya Matematika i Mekhanika*, 26(3) : 568 — 571. 1962.
4. ARKHANGEL'SKII, Yu. A. *Ob odnoi teoreme Puankare, otnosyashcheisya k zadache o dvizhenii tverdogo tela v n'yutonovskom pole sil* (On a Theorem by Poincaré Relating to the Motion of a Rigid Body in a Newtonian Force Field). — *Prikladnaya Matematika i Mekhanika*, 26, No. 6. 1962.
5. ARKHANGEL'SKII, Yu. A. *Ob algebraicheskikh integralakh v zadache o dvizhenii tverdogo tela v n'yutonovskom pole sil* (On Algebraic Integrals for the Motion of a Rigid Body in a Newtonian Force Field). — *Prikladnaya Matematika i Mekhanika*, 27, No. 1. 1963.
6. BELETSKII, V. V. *Dvizhenie iskusstvennogo sputnika Zemli otносitel'no tsentra mass* (Motion of an Artificial Earth Satellite About Its Mass Center). — In: "Iskusstvennye sputniki Zemli", Vol. 1, pp. 25 — 43. Izdatel'stvo AN SSSR. 1958.
7. BELETSKII, V. V. *O libratsii sputnika* (Librations of a Satellite). — In: "Iskusstvennye sputniki Zemli", Vol. 3, pp. 13 — 32. Izdatel'stvo AN SSSR. 1959.
8. BELETSKII, V. V. *Klassifikatsiya dvizhenii iskusstvennogo sputnika Zemli okolo tsentra mass* (Classification of Motions of an Artificial Earth Satellite About Its Mass Center). — In: "Iskusstvennye sputniki Zemli", Vol. 6, pp. 11 — 32. Izdatel'stvo AN SSSR. 1961.
9. BELETSKII, V. V. and Yu. V. ZONOV. *Vrashchenie i orientatsiya tre'tego sovetskogo sputnika* (Sputnik III Spin and Attitude). — In: "Iskusstvennye sputniki Zemli", Vol. 7, pp. 32 — 35. Izdatel'stvo AN SSSR. 1961.
10. BELETSKII, V. V. *Libratsiya sputnika na ellipticheskoi orbite* (Librations of a Satellite in an Elliptical Orbit). — In: "Iskusstvennye sputniki Zemli", Vol. 16, pp. 46 — 56. Izdatel'stvo AN SSSR. 1963.
11. BELETSKII, V. V. *Nekotorye voprosy postupatel'novo-vrashchatel'nogo dvizheniya tverdogo tela v n'yutonovskom pole sil* (Some Aspects of Translational—Rotational Motion of a Rigid Body in a Newtonian Force Field). — In: "Iskusstvennye sputniki Zemli", Vol. 16, pp. 68 — 93. Izdatel'stvo AN SSSR. 1963.
12. BELETSKII, V. V. *Nekotorye voprosy dvizheniya iskusstvennykh sputnikov otносitel'no tsentra mass* (Some Aspects of the Motion of Artificial Satellites About the Mass Center). — In: "Problemy dvizheniya iskusstvennykh nebesnykh tel", pp. 218 — 228. Izdatel'stvo AN SSSR. 1963.
13. BELETSKII, V. V. *Evolyutsiya vrashcheniya dinamicheski simmetrichnogo sputnika* (Spin Evolution in a Dynamically Symmetric Satellite). — *Kosmicheskie Issledovaniya*, 1(3) : 389 — 385. 1963.
14. BELETSKII, V. V. *Dvizhenie iskusstvennykh sputnikov otносitel'no tsentra mass* (Motion of Artificial Satellites About the Mass Center). — Second All-Union Conference on Theoretical and Applied Mechanics, Moscow, 29 January — 5 February 1964.
15. BELETSKII, V. V. *Ob integriruemosti uravnenii dvizheniya tverdogo tela okolo zakreplennoi tochki pod deistviem tsentral'nogo n'yutonovskogo polya sil* (Integrability of the Equations of Motion of a Rigid Body Around a Fixed Point in a Newtonian Central Field). — *Doklady Akademii Nauk SSSR*, 113(2) : 287 — 290. 1957.
16. BELETSKII, V. V. *Nekotorye voprosy dvizheniya tverdogo tela v n'yutonovskom pole sil* (Some Aspects of the Motion of a Rigid Body in a Newtonian Force Field). — *Prikladnaya Matematika i Mekhanika*, 21(6) : 749 — 758. 1957.
17. BELETSKII, V. V. *Ob odnom sluchae dvizheniya tverdogo tela okolo zakreplennoi tochke v n'yutonovskom pole sil* (A Case of Motion of a Rigid Body About a Fixed Point in a Newtonian Force Field). — *Prikladnaya Matematika i Mekhanika*, 27(1) : 175 — 178. 1963.

18. BELETSKII, V. V. Orbita ekvatorial'nogo sputnika Zemli (The Orbit of an Equatorial Earth Satellite). – In: "Iskusstvennye sputniki Zemli", Vol. 13, pp. 53–60. Izdatel'stvo AN SSSR. 1962.
19. BOGOLYUBOV, N. N. and Yu. A. MITROPOL'SKII. Asimptoticheskie metody v teorii nelineinikh kolebanii (Asymptotic Methods in the Theory of Nonlinear Vibrations). – Fizmatgiz. 1958.
20. BULGAKOV, B. V. Kolebaniya (Oscillations), Vol. 1. – Gostekhizdat. 1949.
21. VDOVIN, V. A. Vliyanie vzaimodeistviya magnitnogo polya sputnika s magnitnym polem Zemli na dvizhenie sputnika okolo ego tsentra inertsii (Interaction of Satellite's Magnetic Fields with the Earth's Magnetic Fields and Its Influence on the Motion of the Satellite About the Center of Inertia). Dissertation, Moscow Physico-Technical Institute. 1963.
22. VOLOSOV, V. M. Usrednenie v sistemakh obyknovennykh differentsiyal'nykh uravnenii (Averaging in Systems of Ordinary Differential Equations). – Uspekhi Matematicheskikh Nauk, 17(6):3–126. 1962.
23. VOLOSOV, V. M. O metode usredneniya (On a Method of Averaging). – Doklady Akademii Nauk SSSR, 137(1):21–24. 1961.
24. VOLOSOV, V. M. O vyssikh priblizheniyakh pri usrednenii (On Higher Approximations in Averaging). – Doklady Akademii Nauk SSSR, 137(5):1022–1025. 1961.
25. GRIGOREVSKII, V. M. O bystrykh izmeneniyakh perioda vrashcheniya otnositel'no poperechnoi osi vtorogo sovetskogo iskusstvennogo sputnika Zemli (On Fast Changes in the Spin of Sputnik II About a Lateral Axis). – Doklady Akademii Nauk SSSR, 137(3):572–575. 1961.
26. GURKO, O. V. and L. I. SLABKII. Ispol'zovanie silovyh vliyanii gravitatsionnogo i svetovogo polei Solntsa dlya orientatsii kosmicheskikh apparatov (Attitude Control of Space Vehicles by Solar Gravity and Radiation Pressure Forces). – In: "Iskusstvennye sputniki Zemli", Vol. 16, pp. 34–45. Izdatel'stvo AN SSSR. 1963.
27. DOLGINOV, S. Sh., L. N. ZHUGOV, and N. V. PUSHKOV. Predvaritel'noe soobshchenie o geomagnitnykh izmereniyakh na tret'em sovetskem iskusstvennom sputnike Zemli (A Preliminary Report on Geomagnetic Measurements on Sputnik III). – In: "Iskusstvennye sputniki Zemli", Vol. 2, pp. 50–53. Izdatel'stvo AN SSSR. 1958.
28. DOLGINOV, S. Sh., L. N. ZHUGOV, N. V. PUSHKOV, L. O. TYURMINA, and I. V. FRYAZINOV. Nekotorye rezul'taty izmereniya postoyannogo magnitnogo polya Zemli s tret'ego iskusstvennogo sputnika Zemli nad territoriei SSSR (Some Results of Measurements of the Constant Geomagnetic Fields over USSR Territory from Sputnik III). – Geomagnetizm i Aeronomiya, 2(6):1061; 1075. 1962.
29. DUBOSHIN, G. N. O differentsiyal'nykh uravneniyakh postupatel'no-vrashchatel'nogo dvizheniya vzaimno prityagivayushchikhsya tel (Differential Equations of the Translational–Rotational Motion of Mutually Attracted Bodies). – Astronomicheskii Zhurnal, 35(2):265–276. 1958.
30. DUBOSHIN, G. N. O vrashchatel'nom dvizhenii iskusstvennykh nebesnykh tel (Rotational Motion of Artificial Heavenly Bodies). – Byulleten' ITA AN SSSR, 7:511–520. 1960.
31. DUBOSHIN, G. N. O periodicheskikh dvizheniyakh v sisteme sputnikov Saturna (Periodic Motions in the System of Saturn Satellites). – Trudy GAISh, 15:158–250. 1945.
32. DUBOSHIN, G. N. Nebesnaya mehanika (osnovnye zadachi i metody) (Celestial Mechanics, Principal Problems and Methods). – Fizmatgiz. 1963.
33. DUBOSHIN, G. N. Osnovy teorii ustochivosti dvizheniya (Fundamentals of the Theory of Stability of Motion). – Izdatel'stvo Moskovskogo Universiteta. 1952.
34. DUBOSHIN, G. N. O vrashchatel'nom dvizhenii iskusstvennykh nebesnykh tel (Rotational Motion of Artificial Celestial Bodies). – Byulleten' ITA AN SSSR, 7(7):511–520. 1960.
35. EGOROV, S. S. Vliyanie vikhrevykh tokov v obolochke sputnika na ego vrashchenie i orientatsiyu (The Influence of Eddy Currents in the Shell of a Satellite on Its Spin and Attitude). Dissertation, Moscow State University. 1963.
36. EGOROV, V. A. Ob opredelenii istinnoi anomalii v vozmušchennom dvizhenii (The Determination of True Anomaly in Perturbed Motion). – Astronomicheskii Zhurnal, 35(1):166–168. 1958.

37. ZLATOUSTOV, V. A., D. E. OKHOTSIKII, V. A. SARYCHEV, and A. P. TORZHEVSKII. Periodicheskie resheniya v zadache o ploskikh kolebaniyakh sputnika na ellipticheskoi orbite (Periodic Solutions in the Problem of Plane Oscillations of a Satellite in an Elliptical Orbit). – Kosmicheskie Issledovaniya, 2(5) : 658 – 666. 1964.
38. ZONOV, Yu. V. K voprosu o vzaimodeistvii sputnika s magnitnym polem Zemli (The Interaction of a Satellite with the Geomagnetic Field). – In: "Iskusstvennye sputniki Zemli", Vol. 3, pp. 118 – 124. 1959.
39. IDEL'SON, N. I. Teoriya potentsiala i ee prilozhenie k teorii figury Zemli i geofizike (Potential Theory and Its Application to the Theory of Earth's Figure and Geophysics). – GTTI, 1986.
40. ISTOMIN, V. G. Izmenenie kontsentratsii polozhitel'nykh ionov s vysotoi po dannym mass-spektrometricheskikh izmerenii na tret'em sputnike (Vertical Variation in the Concentration of Positive Ions according to Mass-Spectrometric Measurements of Sputnik III). – In: "Iskusstvennye sputniki Zemli", Vol. 6, pp. 127 – 131. Izdatel'stvo AN SSSR. 1961.
41. KARYMOV, A. A. Opredelenie sil i momentov sil svetovogo davleniya, deistvuyushchikh na telo pri dvizhenii v kosmicheskem prostranstve (Solar Radiation Pressure and Torques on a Space Vehicle). – Prikladnaya Matematika i Mekhanika, 26(5) : 867 – 876. 1962.
42. KARYMOV, A. A. Ustoichivost' vrashchatel'nogo dvizheniya geometricheski simmetricheskogo iskusstvennogo sputnika v pole sil svetovogo давления (Stability of Spin of a Dynamically Symmetric Artificial Satellite in a Field of Radiation Pressure Forces). – Prikladnaya Matematika i Mekhanika, 28(5) : 923 – 930. 1964.
43. KILL', I. D. O periodicheskem reshenii odnogo nelineinogo uravneniya (Periodic Solution of a Certain Nonlinear Equation). – Prikladnaya Matematika i Mekhanika, 27(6) : 1107 – 1110. 1963.
44. KONDURAR', V. T. Problema dvizheniya dvukh ellipsoidov pod deistviem vzaimnogo prityazheniya (The Motion of Two Mutually Attracted Ellipsoids), Part II. – Trudy GAISh, 9(2) : 307 – 369. 1939.
45. KONDURAR', V. T. O vozmušcheniyakh postupatel'no-vrashchatel'nogo dvizheniya sputnika i planety, vyzyvaemykh ikh szhatiem (Perturbations of Translational–Rotational Motion of a Satellite and a Planet Due to their Oblateness). – Astronomicheskii Zhurnal, 39(3) : 516 – 526. 1962.
46. KONDURAR', V. T. Chastnye resheniya obshchei zadachi o postupatel'no-vrashchatel'nom dvizhenii sferoida pod deistviem prityazheniya shara (Particular Solutions for the General Problem of Translational–Rotational Motion of a Spheroid Attracted by a Sphere). – Astronomicheskii Zhurnal, 36(5) : 890 – 901. 1959.
47. KONDURAR', V. T. Problema dvizheniya dvukh ellipsoidov pod deistviem vzaimnogo prityazheniya (The Motion of Two Mutually Attracted Ellipsoids), Part I. – Astronomicheskii Zhurnal, 13 : 563 – 588. 1936.
48. KRASOVSKII, V. I., K. S. SHKLOVSKII, Yu. I. GAL'PERIN, E. M. SVETLITSKII, Yu. M. KUSHNIR, and G. A. BORDOVSKII. Obnaruzhenie v verkhnei atmosfere elektronov s energiei okolo 10 kev (The Discovery of 10 keV Electrons in the Upper Atmosphere). – In: "Iskusstvennye sputniki Zemli", Vol. 6, pp. 113 – 126. Izdatel'stvo AN SSSR. 1961.
49. KRYLOV, A. M. Lektsii o priblizhennykh vychisleniyakh (Lectures on Approximate Calculations). – Gostekhizdat. 1950.
50. LANDAU, L. D. and E. M. LIFSHITZ. Elektrodinamika sploshnykh sred (Electrodynamics of Continuous Media). – Gostekhizdat. 1957.
51. LANDAU, L. D. and E. M. LIFSHITZ. Teoriya polya (Field Theory). – Fizmatgiz. 1960.
52. LIDOV, M. L. Opredelenie plotnosti atmosfery po nablyudaemomu tormozheniyu pervykh iskusstvennykh sputnikov Zemli (Atmospheric Density from Observed Deceleration of the First Artificial Earth Satellites). – In: "Iskusstvennye sputniki Zemli", Vol. 1, pp. 9 – 20. Izdatel'stvo AN SSSR. 1958.
53. LUR'E, A. I. Moment gravitatsionnykh sil, deistvuyushchikh na sputnik (Gravity Torques on a Satellite). – Prikladnaya Matematika i Mekhanika, 27(2) : 377 – 378. 1963.
54. LYAPUNOV, A. M. Obshchaya zadacha ob ustoichivosti dvizheniya (The General Problem of the Stability of Motion). – Gostekhizdat. 1950.
55. MALKIN, I. G. Teoriya ustoichivosti dvizheniya (The Theory of Stability of Motion). – Gostekhizdat. 1952.

56. MITRA, S. K. The Upper Atmosphere. — [Russian translation. 1955.]
57. MIKHNEVICH, V. V., B. S. DANILIN, A. I. REPNEV, and V. A. SOKOLOV. Nekotorye rezul'taty opredeleniya strukturnykh parametrov atmosfery s pomoshch'yu tret'ego sovetskogo iskusstvennogo sputnika Zemli (Some Results on the Structural Parameters of the Atmosphere Obtained by Sputnik III). — In: "Iskusstvennye sputniki Zemli", Vol. 3, pp. 84 – 97. Izdatel'stvo AN SSSR. 1959.
58. MAUSER, J. A New Method for Constructing Solutions of Nonlinear Differential Equations. — Russian translation in "Matematika", 6(4) : 3 – 10. 1962.
59. OKHOTSIMSKII, D. E. and V. V. BELETSKII. Ispol'zovanie orientirovannogo na Zemlyu sputnika dilya issledovanii, svyazannykh s Solntsem (The Application of an Earth-Oriented Satellite in Solar Research). — In: "Iskusstvennye sputniki Zemli", Vol. 16, pp. 94 – 123. Izdatel'stvo AN SSSR. 1963.
60. OKHOTSIMSKII, D. E. and V. A. SARYCHEV. Sistema gravitatsionnoi stabilizatsii iskusstvennykh sputnikov (Gravity Stabilization System for Artificial Satellites). — In: "Iskusstvennye sputniki Zemli", Vol. 16, pp. 5 – 9. Izdatel'stvo AN SSSR. 1963.
61. OKHOTSIMSKII, D. E., T. M. ENEEV, and G. P. TARATYNOVA. Opredelenie vremeni sushchestvovaniya iskusstvennogo sputnika Zemli i issledovanie vekovykh vozmushchenii ego orbitы (Determining the Lifetime of an Artificial Earth Satellite and Secular Orbital Perturbations). — Uspekhi Fizicheskikh Nauk, 13(1a) : 34 – 50. 1957.
62. POZHARITSKII, G. K. Ob ustoichivosti permanentnykh vrashchenii tverdogo tela s zakreplennoi tochkoi, nakhodyashchegosya v n'yutonovskom tsentral'nom pole sil (Stability of Permanent Rotations of a Rigid Body with a Fixed Point in a Newtonian Central Field). — Prikladnaya Matematika i Mekhanika, 23(4) : 722 – 793. 1959.
63. SARYCHEV, V. A. Vliyanie szhatiya Zemli na vrashchatel'noe dvizhenie sputnika (The Influence of Earth's Flattening on the Rotational Motion of a Satellite). — In: "Iskusstvennye sputniki Zemli", Vol. 6, pp. 3 – 11. Izdatel'stvo AN SSSR. 1961.
64. SARYCHEV, V. A. Issledovanie dinamiki sistemy gravitatsionnoi stabilizatsii (The Dynamics of a Gravity Stabilization System). — In: "Iskusstvennye sputniki Zemli", Vol. 16, pp. 10 – 33. 1963.
65. SARYCHEV, V. A. Vliyanie soprotivleniya atmosfery na sistemu gravitatsionnoi stabilizatsii ISZ (The Influence of Atmospheric Drag on Gravity Attitude Stabilization of Artificial Earth Satellites). — Kosmicheskie Issledovaniya, 2(1) : 23 – 32. 1964.
66. TORZHEVSKII, A. P. Sushchestvovanie nechetnykh periodicheskikh reshenii nelineinogo differentialsial'nogo uravneniya vtorogo poryadka (The Existence of Odd Periodic Solutions for a Second-Order Nonlinear Differential Equation). — Kosmicheskie Issledovaniya, 2(5) : 667 – 678. 1964.
67. FILIPPOVICH, I. V. Vliyanie aerodinamiki na kolebaniya sputnika v gravitatsionnom pole (The Influence of Aerodynamic Factors on Satellite Vibrations in a Gravitation Field). — Dissertation, Moscow State University. 1962.
68. FOK, V. A. Teoriya prostranstva, vremeni i tyagoteniya (Theory of Space, Time, and Gravitation). — Gostekhizdat. 1958.
69. KHARLAMOVA, E. I. O dvizhenii tverdogo tela vokrug nepodvizhnoi tochki v tsentral'nom n'yutonovskom pole sil (The Motion of a Rigid Body About a Fixed Point in a Newtonian Central Field). — Izvestiya Sibirskogo Otdeleniya AN SSSR, No. 6. 1959.
70. CHERNOUS'KO, F. L. Ob ustoichivosti regul'arnoi precessii sputnika (Stability of Satellite Regular Precession). — Prikladnaya Matematika i Mekhanika, 28(1) : 155 – 157. 1964.
71. CHERNOUS'KO, F. L. O dvizhenii sputnika otmositel'no tsentra mass pod deistviem gravitatsionnykh momentov (The Motion of a Satellite About the Mass Center under Gravity Torques). — Prikladnaya Matematika i Mekhanika, 27(3) : 474 – 483. 1963.
72. CHERNOUS'KO, F. L. Rezonansnye yavleniya pri dvizhenii sputnika otmositel'no tsentra mass (Resonance Phenomena in the Motion of a Satellite About Its Mass Center). — Zhurnal Vychislitel'noi Matematiki i Prikladnoi Fiziki, 3(3) : 528 – 538. 1963.

73. CHETAEV, N. G. Ob ustoichivosti vrashcheniya tverdogo tela s odnoi nepodvizhnou tochkoi v sluchae Lagranzha (The Stability of Rotation of a Rigid Body with a Fixed Point in the Lagrange Case). — Prikladnaya Matematika i Mekhanika, 18(1) : 123—125. 1954.
74. CHETAEV, N. G. Ustoichivost' dvizheniya (Stability of Motion). — Gostekhizdat, 1955.
75. AUELmann, R. R. Regions of Librations for a Symmetrical Satellite. — AIAA Journal, 1(6) : 1445—1447. 1963.
76. de BRUN, F. Rotation kring en fix punkt. — *Ofversigt af Kongl. Svenska Vetenskaps-Akademiens Värhhandlingar*. Stockholm. 1893.
77. CLANCY, T. F. and T. P. MITCHELL. Effects of Radiation Forces on the Attitude of an Artificial Earth Satellite. — AIAA Journal, 2(3) : 517—524. 1964.
78. COLOMBO, G. On the Motion of Explorer XI around its Center of Mass. — Preprint Amer. Astronaut. Soc., No. 45. 1962.
79. HAGIHARA, Y. Rotation of an Earth Satellite in Flight along its Orbit. — Smithsonian Contrbs. Astrophys., 5(9) : 113—143. 1961.
80. JILDEN, H. — Comptes Rendus, 91 : 957—959. 1880.
81. KOBB, G. Sur le problème de la rotation d'un corps autour d'un point fixe. — Bulletin de la Société Mathématique, — 23. 1895.
82. LUNDQUIST, C. Spatial Orientation of the Explorer Satellites. — Space J., 1(3) : 15—20. 1958.
83. MORAN, J. P. Effect of Plane Librations on the Orbital Motions of a Dumbbell Satellite. — ARS Journal, 31(8) : 1089—1096. 1961.
84. NAUMANN, R. J. Recent Information Gained from Satellite Orientation Measurements. — Planetary and Space Science, 7 : 445—453. 1961.
85. NAUMANN, R. J. Observed Torque—Producing Forces Acting on Satellites. — Dynamics of Satellites Symposium, Paris, 28—30 May, 1962, pp. 238—256. Springer—Verlag, Berlin—Göttingen—Heidelberg. 1963.
86. NOTNI, P. and H. OLEAK. Der Lichtwechsel der Trägerrakete von Sputnik III. — Monatsber. Deutsch. Akad. Wiss., Berlin, 1(7—10) : 394—396. 1959.
87. NOTNI, P. and H. OLEAK. Die Bewegung eines rotierenden zylinderförmigen Satelliten in der Atmosphäre. — Veröff. Sternwarte Babelsberg, 13, No. 3. 1959.
88. PRINGLE, R. Jr., Bounds of the Librations of a Symmetrical Satellite. — AIAA Journal, 2(5) : 909—913. 1964.
89. ROBERSON, R. E. Gravitational Torque on a Satellite Vehicle. — Journ. Franklin Inst., 265 : 13—22. 1958.
90. ROSENSTOCK, H. B. The Effect of the Earth's Magnetic Field on the Spin of the Satellite. — *Astronautica acta*, 3(3) : 215—226. 1957.
91. SCHRELLO, D. M. Aerodynamic Influences on Satellite Libration. — ARSJ, 31(3) : 442—444. 1961.
92. SCHINDLER, G. M. Satellite Librations in the Vicinity of Equilibrium Solutions. — *Astronautica acta*, 6(5) : 233—240. 1960.
93. THOMSON, W. T. Spin Stabilization of Attitude Against Gravity Torque. — Journal of the Astronaut. Sciences, 9 : 31—33. 1962.
94. TISSERAND, F. *Traité de Mécanique Céleste*, Vol. 2, Paris. 1891.
95. WARWICK, I. W. Decay of Spin in Sputnik I. — *Planetary and Space Sci.*, 1(1) : 43—49. 1959.
96. WEGGINS, L. E. Relative Magnitudes of Space—Environment Torques on a Satellite. — AIAA Journal, 2(4) : 232—233. 1964.